Characterization of Reservoir Fluids based on Perturbation from n-Alkanes

by

Ashutosh Kumar

A thesis submitted in partial fulfillment of the requirements for the degree of

Doctor of Philosophy

in
Petroleum Engineering

Department of Civil and Environmental Engineering
University of Alberta

Abstract

Reliable design of gas and/or steam injection for enhanced oil recovery requires compositional reservoir simulation, in which phase behavior of reservoir fluids is represented by an equation of state (EOS). Various methods for reservoir fluid characterization using an EOS have been proposed in the literature. Conventional characterization methods addressed the challenge of the reliable prediction of the condensation/vaporization mechanisms in gas injection processes. It is even more challenging to characterize reservoir fluids for multiphase behavior consisting of three hydrocarbon phases. Complex multiphase behavior was observed experimentally for many gas floods. The importance of considering multiphase behavior in gas flooding simulation was also demonstrated in the literature. However, no systematic method has been proposed, especially for three-phase characterization.

The main objective of this research is to develop a reliable method for multiphase fluid characterization using an EOS. The Peng-Robinson EOS is used with the van der Waals mixing rules in this research. The fluid types considered are gas condensate, volatile oil, black oil, heavy oil, and bitumen.

The most important difference from the conventional methods is that, in this research, reservoir fluids are characterized by perturbation of the EOS model that has been calibrated for n-alkanes, in the direction of increasing level of aromaticity. This methodology is referred to as perturbation from n-alkanes (PnA), and used consistently throughout the dissertation.

The experimental data required for the characterization methods presented in this dissertation are the saturation pressure and liquid densities at a given temperature, in addition to compositional information. Other types of experimental data, such as minimum miscibility pressures, liquid dropout curves, and three-phase envelopes, are used to test the predictive capability of the PR EOS models resulting from the PnA method.

First, the PnA method is applied to simpler phase behavior that involves only two phases of vapor and liquid. The Peng-Robinson EOS is calibrated for vapor pressures and liquid densities

for n-alkanes from C_7 to C_{100}. Two different characterization methods are developed for two-phase characterization using the PnA method. In one of them, fluid characterization is performed by adjusting critical pressure, critical temperature, and acentric factor. In the other, fluids are characterized by directly adjusting the attraction and covolume parameters for each pseudocomponent.

Then, the PnA method is extended to three phases. Unlike for two phases, the Peng-Robinson EOS is calibrated for three-phase data measured for n-alkane/n-alkane and CO_2/n-alkane binaries. A new set of binary interaction parameters (BIPs) is developed for these binaries, and applied for reservoir fluid characterization.

The PnA method applied for two and three phases results in three different methods of fluid characterization. They are individually tested for many different reservoir fluids to demonstrate their reliability. The validation of the methods is based on experimental data for 110 fluids in total (50 gas condensates, 15 volatile oils, 35 black oils, 4 heavy oils, and 6 bitumens).

Results consistently show that the use of the PnA method with the PR EOS yields a systematic, monotonic change in phase behavior predictions from n-alkanes. The two characterization methods developed for two phases do not require volume shift to obtain accurate predictions of compositional and volumetric phase behavior. However, they may not give reliable predictions for three phases. The three-phase characterization presented in this research is the most comprehensive method that can predict reliably two and three phases. However, volume shift is required for matching density data in this last method. Therefore, it should be used with a proper understanding of the relationship among different EOS-related parameters and their effects on phase behavior predictions.

Dedication

ॐ सह नाववतु, सह नौ भुनक्तु, सह वीर्यं करवावहै। तेजस्वि नावधीतमस्तु मा विद्विषावहै ॥

Ohm Saha nāvavatu, Saha nau bhunaktu, Saha vīryaṁ karavāvahai ǀ Tejasvinā vadhītam astu mā vidviṣāvahai ॥

ॐ शान्तिः शान्तिः शान्तिः ॥

Ohm Shāntiḥ Shāntiḥ Shāntiḥ ॥

- कृष्ण यजुर्वेद तैत्तिरीय उपनिषद (2.2.2) से
  From the Krishna Taitiriya Upanishad (2.2.2)

(Meaning: Ohm, May we all be protected. May we all be nourished. May we work together with great energy. May our intellect be sharpened. Let there be no animosity amongst us. Ohm, Let there be peace (in me) ! Let there be peace (in nature) ! Let there be peace (in divine forces) !)

I dedicate this work to my father who is no more to see my success. I miss his silent love, friendly guidance, and motivation to achieve greater heights in life.

Acknowledgements

Table of Content

List of Tables

List of Figures

xiii

xiv

Chapter 1: Introduction

In this section, the area of oil and gas industry relevant to present research is recognized in the subsection "Background". Conventional practices in the relevant area described in "Background" are briefly described in the subsection "Conventional Characterization Methods for Reservoir Fluid". The area of issues is also recognized in this subsection. Issues related to conventional characterization are discussed in the subsection "Issues Related to Conventional Characterization". The subsection "Problem Statement" recognizes the issues that the present research aims to address. Finally, "objective of the research" is explained.

1.1.   Background

Hydrocarbons are major source of world energy. Hydrocarbons are present in different forms in the reservoir, such as gas, gas condensates, oil, and bitumen. Reservoir fluids are recovered from reservoirs using various enhanced oil recovery methods after primary recovery methods are insufficient for economic recovery. Miscible gas injection is an important enhanced recovery method used as secondary or tertiary recovery mechanism as shown in **Figure 1.1**, which presents a summary of different enhanced recovery projects around the world for the years 2010, 2012, and 2014 from oil and gas journal worldwide survey (Moritis 2010; Koottungal 2012, 2014).

Miscible gas injection is one of several enhanced recovery methods that is applied to reservoir containing wide gravity range fluids such as gas condensates, volatile oils, normal oils, heavy oils. Sänger and Hagoort (1998); Taheri et al. (2013), Abdrakhmanov (2013) studied the miscible gas injection to recover gas condensates. Clark et al. (2008) studied the miscible gas injection for volatile oil of Tirrawarra field of Australia. Solvent injection has been successfully implemented in West Texas (Mizenko 1992; Stein et al. 1992; Tanner et al. 1992), the Powder River Basin (Fulco 2000), Alaska (McGuire et al. 2001), Canada (Malik and Islam 2000), and the North Sea (Varotsis et el. 1986). For the recovery of heavy oils and bitumen, solvent is coinjected with steam to take synergic benefit of thermal and compositional mechanism (Gupta et al. 2005; Gupta and Gittins 2006; Dickson et al. 2011).

Reservoir fluids are held back in pore spaces because of capillary pressure resulting from interfacial tension between two different phases. The interfacial tension can be reduced by achieving miscibility of the injected fluid and in-situ hydrocarbon. Holm (1986) defined miscibility for reservoir fluids as the physical condition for two or more fluids that will permit them to mix in all proportions. Miscibility at given pressure-temperature conditions for injectant and reservoir fluid system can be either first contact miscibility (FCM) or multi contact miscibility (MCM). In first contact miscibility, injectant and reservoir fluids are miscible at first contact in all proportion. However, for systems that are not miscible at first contact, miscibility can be achieved by multiple contacts between the injectant gas and reservoir fluids either by pressure adjustment or by composition change of injection gas. At a given temperature, minimum pressure at which miscibility through multiple contact can be achieved between a given injection gas and a reservoir fluid is called minimum miscibility pressure (MMP) (Pedersen and

Christensen 2007). If reservoir pressure and reservoir temperature are kept constant, miscibility between injection gas and reservoir fluid depends on the composition of the injection gas. Minimum enrichment of injection gas for which miscibility can be achieved at a given pressure and a given temperature is called minimum miscibility enrichment (MME). Enrichment gases usually contain CO_2, CH_4, C_2H_6 and liquefied petroleum gases (C_3 and C_4) (Whitson and Brulè 2000), however composition of components such as C_3, C_4, and higher carbon number components significantly affects the miscibility conditions. Techno-economic feasibility of a miscible gas injection project depends on MMP and MME factors.

Once miscibility is achieved, theoretically, 100% hydrocarbon recovery is possible, which leads to highest possible local displacement efficiency. However, field scale implementation of miscible gas injection does not result in such high recovery because of poor sweep efficiency from reservoir heterogeneity and gravity override. Even though, displacement efficiency can be as high as 70-90%, due to poor sweep efficiency, a typical additional recovery after water-flooding may be only 10-20% of original oil in place (Sheng 2013). Nevertheless, gas flooding is well-developed technology and has demonstrated good economic recoveries in the world (Manrique et al. 2007, Sheng 2013), and good recovery from miscible gas injection will depend on proper understanding of the impact of key factors on sweep and displacement efficiency (Sheng 2013).

Conventionally, enhanced oil recovery from miscible gas injection process refers to enhanced recovery from the miscibility of liquid and vapor hydrocarbon phases for injected gas/solvent and reservoir fluid mixture. The definitions of MMP and MME hitherto consider the miscibility of liquid and vapor hydrocarbon phases present for a solvent and oil mixture, and these terms for miscibility may not be suitable for use when three hydrocarbon phases are present. Experiments have confirmed the presence of three hydrocarbon phases (oil rich liquid phase L_1, solvent rich liquid phase L_2, and vapor phase V) for light gases' (carbon dioxide, methane, ethane, propane, and butane) mixtures with heavier n-alkanes, and with reservoir fluid.

For binary mixtures, CO_2, methane, ethane, propane, and butane were studied as the solvent component mixed with a heavier n-alkane component (Rodrigues and Kohn 1967; Kulkarni et al. 1974; Hottovy et al. 1981a; Enick et al. 1985; Fall and Luks 1985; Fall et al. 1985; Estrera and Luks 1987; Peters et al. 1987a, 1987b; Peters et al. 1989; Van der Steen et al. 1989; Peters 1994; Secuianu et al. 2007). For these binary mixtures, three hydrocarbon phases have been observed at extremely low temperature (close to critical temperature of methane) to high temperature (close to critical temperature of butane) as shown in **Figure 1.2**. Presence of three hydrocarbon phases for ternary mixtures has been confirmed by Chang et al. (1966), Lin et al. (1977), Hottovy et al. (1981), Hottovy et al. (1982), Merrill et al. (1983), Llave et al. (1986), Estrera and Luks (1988), Jangkamolkulchal and Luks (1989), Iwade et al. (1992), and Gregorowicz et al. (1993a, 1993b).

With the presence of the components showing three hydrocarbon-phase behavior in binary or ternary mixture (described in previous paragraph) in reservoir fluids, three hydrocarbon-phase behavior

is expected from its mixture with solvents. Three hydrocarbon phases have been observed for reservoir fluids (light oil, heavy oil, bitumens) and solvents mixtures by various researchers (Shelton and Yarborough 1977; Henry and Metcalfe 1983; Turek et al. 1988; Roper 1989; Sharma et al. 1989; Okuyiga 1992; Creek and Sheffield 1993; DeRuiter et al. 1994; Mohanty et al. 1995; Godbole et al. 1995, Badamchi-Zadeh et al. 2009; Li et al. 2013) in temperature range of 291 K to 316 K. Multiphase behavior (number of hydrocarbon phases ≥ 3) at very high temperature (<613 K) has been observed by Zou et al. (2007) for Athabasca Vacuum Bottom and pentane mixture.

Discussions in previous paragraphs indicate presence of three hydrocarbon phases during oil recovery with gas injection in practical reservoir temperature ranges. These multiple hydrocarbon phases present complex recovery mechanism as they have different mobility and inter-phase miscibility conditions. Miscibility in presence of three hydrocarbon phases may not be like two hydrocarbon phase miscibility where miscibility is achieved by merging of liquid and vapor phase. Experimental studies (Shelton and Yarborough 1977; Henry and Metcalfe 1983; Okuyiga 1992; Creek and Sheffield 1993; DeRuiter et al. 1994; Mohanty et al. 1995) have confirmed efficient oil recoveries when two or more than two hydrocarbon phases are present in the solvent and oil mixture.

Oil recovery amounting to 90±5% has been experimentally observed with CO_2 or rich gases as injectant gas (Shelton and Yarborough 1977; Creek and Sheffield 1993). Similar experimental observation was made in case of displacement of the West Sak oil with gas mixture (methane, ethane, propane, and butane). Unlike two hydrocarbon phase oil recovery where oil recovery is monotonic function of dilution i.e. recovery decreasing with increasing dilution, researchers such as Okuyiga (1992), DeRuiter et al. (1994), and Mohanty et al. (1995) observed non-monotonic oil recovery with increased methane dilution in the injection gas (**Figure 1.3**). They observed 93% recovery at 1.2 pore volume of injection gas with 62% methane, whereas recovery was 85% for injection gas with 51% methane.

Mohanty et al. (1995) explained the non-monotonicity of oil recovery on the degree of closeness of density/composition of the L_2 phase with V phase and with L_1 phase on upstream and downstream of the three-phase respectively. The study by Okuno and Xu (2014) has shown high displacement efficiency in the presence of three hydrocarbon phases, when composition path approached to critical end points of oil and solvent mixture. The local displacement efficiency depends on the components' redistribution in the transition zone between two phases and three phases (upstream and downstream of three-phase). For efficient displacement of oil, L_2 and V phases from three-phases should merge with non-oleic phase on upstream side, and L_2 phase on downstream side should appear from oleic phase.

Experimental and analytical studies on three hydrocarbon phases and non-monotonic oil recovery, discussed in previous paragraphs, indicate to potential use of those understandings for more efficient oil recovery from in-situ three hydrocarbon phases' flow conditions with proper design and simulation of partially miscible gas injection process. Simulation of oil recovery from the miscible gas injection in presence of two/three hydrocarbon phases is function of two important parts: phase behavior and flow behavior. Phase behavior, which determines the miscibility of injectant fluid with the reservoir fluid at a

given pressure-temperature conditions, is function of fluid characterization, whereas flow behavior depends on the properties of flow medium. Phase behavior for a given overall composition at a given pressure-temperature condition determines some key information, such as number of phases, and composition and amount of these phases. Combination of phase and flow behavior makes the simulation of oil recovery complex, as overall composition becomes function of time and location between injector and producer.

Simulating correct number of phases, their composition and volumes is important for a reliable recovery simulation. Commonly used commercial simulators do not allow more than two hydrocarbon phases (liquid and vapor). Although, presence of three phases depends on temperature-pressure conditions, and asymmetric nature of injection gas and reservoir hydrocarbons; ruling out the possibility of presence of three phases during dynamic miscibility process can lead to unreliable hydrocarbon recovery simulation. Khan (1992) has shown the difference between simulated recoveries from two-phase and three-phase simulators. Experimental data can be helpful to some extent but it may not be possible to conduct experiments at all possible temperature-pressure points and compositions that may appear during miscibility process as overall composition along the composition path from injection to production point keeps on changing with time and place.

A reliable and robust reservoir fluid characterization is therefore, needed to simulate the number of phases, its compositional and volumetric properties in the miscible or partially miscible displacement process correctly. The subject of the present research is the reservoir fluid characterization, where issues related to conventional characterization approaches are discussed and resolved by proposing a new characterization algorithm for reliable multiphase behavior simulation.

1.2.   Conventional Characterization Methods for Reservoir Fluids

Characterization of reservoir hydrocarbons is the process of representing reservoir hydrocarbons compounds by a suitable number of pure, lumped and/or pseudocomponents and assigning them with suitable EOS parameters so that EOS simulated phase behaviors match with experiments satisfactorily. Reservoir fluids are characterized using conventional approaches (Pedersen and Christensen 2007) with cubic equations of states (EOS) in commercial simulators, because of their simplicity and accuracy. Commonly used two-parameter cubic equations of state are PR EOS (Peng and Robinson 1976, 78), SRK EOS (Soave 1982). A typical characterization process consists of four main steps (Whitson and Brulè 2000; Pedersen and Christensen 2007) as follows:

Step 1. Estimation of a molar distribution with respect to molecular weight (MW) or carbon   number (CN) to split the plus fraction into detailed components.

Step 2. Estimation of properties for the detailed components such as critical temperature (T_C), critical pressure (P_C), critical volume (V_C), acentric factor (ω), and volume-shift parameters (Peneloux et al. 1982).

Step 3. Grouping of the detailed components into fewer pseudocomponents.

Step 4. Regression of pseudocomponents' properties to match experimental data available.

At step 1, a probability distribution function is fitted to the composition analysis data available to split plus fractions. Gamma distribution (Whitson 1983) is the most general form of probability distribution function, its other commonly used forms are chi-square (Quiñones-Cisneros et al. 2003), logarithmic (Pedersen et al. 1983, 1984).

Step 2 uses correlations to estimate critical properties and acentric factors of the split components. These correlations include Edmister (1958), Cavett (1962), Lee and Kesler (1975), Kesler and Lee (1976), Twu (1984), Riazi and Daubert (1980, 1987), Riazi and Al-Sahhaf (1996), and Korsten (2000). The correlations of Pedersen et al. (1989, 1992, 2004), and Kredjbjerg and Pedersen (2006) are functions of MW and density at atmospheric conditions, which are in turn functions of CN. These correlations are developed for an EOS to reproduce vapor pressures and the critical point for the pseudocomponent of a given CN. However, the PR and SRK EOSs with these correlations cannot accurately model densities of heavy hydrocarbons unless volume-shift parameters (Peneloux et al. 1982; Jhaveri and Youngren 1988) are used. Volume shift parameters are assigned to single carbon number fractions at this step.

Step 3 reduces the number of components used in the fluid model and calculates properties of each pseudocomponent by averaging over its member components. Use of fewer components can make EOS calculations more efficient, but it may also result in erroneous predictions of phase behavior due to reduced dimensionality in composition space. Grouping procedures in the literature include the ones of Pedersen et al. (1984), and Whitson and Brulè (2000). The former uses the equal mass grouping with mass-weighted averaging of properties, while the latter uses the equal mole grouping with mole-weighted averaging. Alternately, probability distribution functions are used to create desired number of pseudocomponents directly, in which case lumping is not required; for such approaches step 3 is not relevant.

Step 4 is often needed because each of steps 1-3 has certain assumptions resulting in deviations of predictions from actual phase behavior. Hence, parameters such as T_C, P_C, ω, constant terms of the attraction and covolume parameters of a cubic EOS (Ω_a and Ω_b), volume-shift parameters, and binary interaction parameters (BIPs) for pseudocomponents are regressed either manually or semi-automatically. These adjustment parameters offer flexibility that may be required to match various types of PVT data such as saturation pressure, constant mass expansion, constant volume depletion, differential liberation, separator tests, swelling tests, minimum miscibility pressures, and viscosity data. Manual approach of regression for conventional oil characterization is discussed in detail in Whitson and Brulè (2000), and Pedersen and Christensen (2007). Unlike manual regression in which selection and amount of adjustment in regression parameters depend of the individual, in automatic regression (Agarwal et al. 1990) selection of regression parameter is done based on sensitivity of parameters to the data to be matched, however amount of adjustment is provided manually.

1.3. Issues Related to Conventional Characterization

Conventional characterization methods have been used by various researchers (Nghiem and Li 1986; Sharma et al. 1989; Negahban and Kremesec 1989; Okuyiga 1992; Khan et al. 1992; Creek and Sheffield 1993; Reid 1994; Mohanty et al. 1995; Godbole et al. 1995; Guler et al. 2001; Aghbash and Ahmadi 2012) to develop EOS models to predict three hydrocarbon phases behavior for solvent-injection cases for numerical simulation of hydrocarbon recovery. Two important observations can be made from these approaches. First, these approaches were same as approaches for fluid characterization for liquid-vapor phase behavior predictions, except for data type and amount of data used in regression. This indicates that conventional approaches may not reliable for three-phase behavior prediction if three-phase data are not used in regression. Second, these characterization procedures were specific to the fluids studied and may not be applied to different fluid or fluid type; for example, a characterization approach used for heavy oil may not be used for another heavy oil or a gas condensate. These observations indicate to some fundamental issues with the conventional characterization that need to be identified and resolved. Issues related to conventional characterization can broadly be categorized in two sub-sections as shown below.

(1) Algorithm: Conventional characterization methods lack reliable framework, as there are no well-defined and justified guidelines for estimation of default values for EOS parameters, selection of regression parameters and approaches for adjustment of the selected regression parameters. These issues are explained in the following paragraphs.

- Estimation of Default Values for EOS Parameters: Default values are starting values for EOS parameters such as T_C, P_C, ω, binary interaction parameters (BIPs), volume shift parameters. The default values for parameters are estimated using several correlations as enumerated at step 2 of conventional characterization methods for reservoir fluids. Commonly used correlations to estimate critical properties of single carbon number fractions are empirical in nature and are functions of experimentally measurable physical parameters such as boiling point (T_b), specific gravity (γ) or molecular weight. These correlations represent different trends of parameters with carbon number. Rodriguez and Hamouda (2010) have shown different trends of parameters, such as molecular weight, T_b, T_C, P_C, ω, and γ, with carbon number estimated from different correlations.

  Some correlations are fluid type specific and number of phases specific, for example: Pedersen et al. (2002) used in PVTsim (2011), Pedersen et al. (2002), Krejbjerg, and Petersen (2006) present correlations for normal oils, highly aromatic fluids, and heavy oils respectively. However, in the absence of any universal approach for identifying boundaries separating different fluid types, and lack of continuity of such correlations at the boundaries, it is difficult to make selection of correlations for a given fluid. Pedersen et al. (2006) provide two sets of correlations, one for simulating L-V type phase behavior and other to simulate L_1-L_2-V type

phase behavior. Application of these correlations is subject to availability of experimental phase behavior data in larger P-T-x space.

In absence of any justifiable guideline, the issue of different default values from different correlations presents difficult task of selecting a suitable correlation.

- Selection of Regression Parameters: Conventional characterization has several potential regression parameters such as T_C, P_C, ω, Ω_a, Ω_b, BIPs and volume shift parameters. Selection criteria for regression parameters are not known; hence, set of selected regression parameters is subjective and may vary from user to user.

- Regression: After selection of regression parameter, next important issue relates to order, direction, and amount of regression. Order of regression determines the order in which different parameters are to be regressed. The direction of regression indicates increase or decrease in the regression parameter and amount of regression determines the amount of adjustment.

Conventional characterization does not provide well-defined and justified guidelines and leaves these aspects for individuals to decide. Hence, conventional characterization can result in multiple EOS models that have similar correlative capabilities at P-T-x points represented by data used in regression, but different predictive capabilities at other P-T-x points.

An example to demonstrate the issues related to the selection of regression parameters and regression approach is presented in **Figure 1-4.** The composition of fluid F2 and other experimental data presented in Jaubert et al. (2002) are used in this example. The fluid is characterized using the conventional characterization with the PR EOS (1976,1978) in PVTsim (2011). The heptane plus fraction of the fluid split into four pseudocomponents using a logarithmic distribution function (Pedersen et al. 1983, 1984). The saturation pressure of this fluid is 117.70 bars at 372.05 K. Starting with the same default T_C, P_C, and ω for pseudocomponents, the saturation pressure was matched by adjusting different sets of regression parameters. The BIPs used are default values in PVTsim, and they are not adjusted for matching the saturation pressure. Hydrocarbon-hydrocarbon BIPs are zero. The BIPs for N_2-hydrocarbons, CO_2-hydrocarbons, and N_2-CO_2 are fixed to be non-zero values. They are -0.017 for N_2-CO_2, 0.0311 for N_2-C_1, 0.0515 for N_2-C_2, 0.0852 for N_2-C_3, 0.08 for N_2-C_4, 0.1 for N_2-C_5, 0.08 for N_2-C_i, where $i \geq 6$, 0.12 for CO_2-C_j, where $1 \leq j \leq 6$, and 0.1 for CO_2-pseudo-components.

Four different sets of regression parameters were considered for adjustment, each resulting in a PR EOS model. Regression was carefully performed to maintain the physical trend of EOS parameters with molecular weight of pseudocomponents. The EOS parameters for these models are listed in **Tables 1.1, 1.2, 1.3**, and **1.4**. Figure 1-4 shows the P-T phase envelopes from four different EOS models (shown as EOS model 1, 2 ,3, and 4). It also shows the P-T phase envelope from the EOS model with pseudocomponents having default values for EOS parameters. From the figure, it is evident that all EOS models have same prediction at the temperature 372.05 K; however, at different temperature points, predictions in P-T space are different for different EOS models. Even though all EOS models at 372.05 K have the same pressure prediction, they have different predictions in pressure-composition

7

space. Minimum miscibility pressure (MMP) calculations are performed using all EOS models with an injection gas (mole fractions for components N_2, CO_2, CH_4, C_2H_6, C_3H_8, C_4H_{10}, C_5H_{12}, and C_6H_{14} are 0.005, 0.050, 0.0582, 0.171, 0.120, 0.050, 0.017, and 0.005, respectively) at 372.05 K. The MMPs from EOS models 1, 2, and 3 are 322.10 bars, 274.15 bars, and 295.80 bars, respectively. The MMP calculation for EOS model 4 could not be not done due to the presence of three hydrocarbon phases. The slim-tube MMP measured for the fluid is 235 bars, which shows that none of the EOS models are reliable in P-x space at the temperature.

(2) Binary Interaction Parameters:

For multi-phase fluid characterization, BIP plays significant role in conventional characterization as it controls attraction parameters (Kredjbjerg and Pedersen 2006). However, conventional characterization does not have systematic approach to develop BIPs for multiphase behavior simulation. Reliability and robustness of BIPs depend on two important aspects, (i) the default BIP values, and (ii), the approach of regression to match data.

Conventionally, default values of BIPs are estimated with correlations that are functions of critical volume (Chueh and Prausnitz 1967) or critical temperatures (Gao et al. 1992) of components, and then indexes in these expressions used as regression parameters to match the experimental data. These correlations were developed for L-V phase behavior predictions, but later were used for multiphase behavior fluid characterization without modification. The approach of achieving default BIPs does not appear to be reliable and robust as the default BIPs do not conform to basic phase behavior expected for solvent and component mixture.

Regression of default BIPs is arbitrary and subjective in absence of well-defined guidelines on binary interaction parameter regression. This presents difficult task of selection of components' pairs for BIP regression, order of regression and amount of regression; practically there is no restriction on these aspects. Approaches adopted to adjust binary interaction parameters are guided by immediate objective of matching the available data ignoring the impact of such BIPs in P-T-x space. This necessitates use of multiphase behavior data at regression step of EOS model development for simulation of multiphase behavior; however, such EOS models may not be reliable in P-T-x space other than that represented by data used in regression.

These issues listed in previous paragraphs

1.4. Problem Statement

Issues related to conventional characterization methods were discussed in the previous section in details. In this section, those issues in context of defining research objectives are summarised as problem statement.

Multiphase behavior simulation using conventional characterization with PR EOS may not be reliable and robust for numerical simulation of hydrocarbon recovery with gas injection process. Conventional characterization correlates the EOS parameters to the data in limited P-T-x space with unsystematic algorithm and unreliable approach for BIP development. Three-phase behavior prediction

may not be reliable from EOS model developed using two-phase data. These fundamental issues may render the EOS models unreliable in the P-T-x space other than that defined by the data used in the regression. The EOS model developed from conventional characterization is fluid or fluid type or number of phases specific, and subjective. Although, composition space for reservoir fluids is continuous, conventional characterization lacks the capability of characterizing fluid irrespective of fluid type or number of phases.

1.5. Research Objectives

In order to address the issues with the conventional characterization, this research aim to find a new method for reservoir fluid characterization with following features:

1. Compatible with Peng and Robinson (1976, 1978) EOS and van der Waals mixing rule. Although there are several modifications to the attraction and covolume parameters of the PR EOS, the original PR EOS (1976, 78) is used without any modification throughout this research. This is to facilitate easy implementation in PVT and hydrocarbon recovery simulators.

2. The characterization method should be applicable to hydrocarbon system irrespective of reservoir fluid types such as gas condensates, volatile oils, normal oils, heavy oils, bitumens.

3. Characterization method should be systematic with well-defined and physically justifiable initial values and search direction for regression parameters. The algorithm of EOS parameters optimization should be simple, robust, and reliable.

4. Binary interaction parameters used should be reliable for multiple hydrocarbon phase prediction for mixture of solvent and hydrocarbon system.

5. The EOS model should be capable of reliable multiphase PVT simulation using minimum amount of phase behavior data such as composition of fluid, saturation pressure and density at reservoir temperature.

1.6. Structure of the Thesis

This is paper-based thesis, which presents the research work in four published journal papers and two under review papers. Introduction, problem statement, and objective of the research on the title of the thesis were presented in the introduction section. Each paper has its own literature search, research objective, research, discussion, conclusion, nomenclature, and references as part of research on title of the thesis. Understanding of organization of thesis is made easier by presenting fundamental of research in following three paragraphs.

As outlined in research objective, for systematic characterization of reservoir fluid, default values of EOS parameters for pseudocomponents need to be well defined. Normal alkanes, among the three prominent hydrocarbon groups i.e. paraffins, naphthenes, and aromatics, has well-defined homologous series and has lowest critical temperature and pressure for same carbon number hydrocarbons. This also means that the lowest value, a single carbon fractions of a reservoir fluid can have, is its n-alkane equivalent critical parameters. Hence, PT phase envelope for a mixture of a light n-alkane with a

pseudocomponent changes systematically with its aromatic conent, as demonstrated in **Figure 1-5**. Vapor pressure curves for propane and carbon-number-16 components (n-alkane $C_{16}H_{34}$ and aromatic $C_{16}H_{10}$) are shown in this figure. The PT phase envelopes for the equimolar mixture of propane and a pseudocomponent (with carbon number 16) are shown in the figure. The pseudocomponent is assumed to be a mixture of n-$C_{16}H_{34}$ and $C_{16}H_{10}$; different cases of aromatic contents (i.e., 0, 10, 40, 50, 80 and 100%) in the pseudocomponent are considered to create PT phase envelopes. A systematic change in the phase envelope with the aromatic content is clearly observed. The phase envelope corresponding to the case when the pseudocomponent is totally n-alkane (i.e., 0% aromatic component) is the inner most phase envelope. The phase envelope expands with increasing aromatic content for the pseudocomponent. This indicates that PT phase envelope for a reservoir fluid with all of heptane plus fractions assumed as n-alkanes may be considered as the limiting phase envelope, and actual phase envelope of the reservoir fluid should be outside this. In this research, pseudocomponents of reservoir fluids are first assigned n-alkane equivalent critical parameters and then higher critical parameters for each pseudocomponent are searched that can match the experimental data such as saturation pressure. This approach of characterization is named as perturbation from n-alkanes (PnA).

Kelser et al. (1979), Twu (1984), and Nji (2008, 2009) have presented perturbation from n-alkane based correlations to estimate T_C, P_C, and ω for pseudocomponents as function of perturbation parameters; these perturbation parameters were themselves functions of other parameters such as boiling point, specific gravity, molecular weight. Perturbation parameters as adjustable parameters to optimize critical pressure for pseudocomponents was used by Quiñones-Cisneros et al. (2003); however, their objective was limited to estimating PR EOS attraction and covolume parameters for use in their friction theory based viscosity model. In this research, PnA approach treats perturbation parameters as adjustable parameters for all PR EOS parameters to characterize reservoir fluid to simulate multiphase behavior for reservoir fluids.

The PnA method is applied to characterize reservoir fluid in two ways, with/without use of volume shift parameter. When volume shift parameters are not used, saturation pressure and density, both data are matched by regression of PR EOS; this has been used in papers presented in Chapter 2 to 6. In Chapter 7, PnA method is applied to characterize reservoir fluids by matching saturation pressure by regressing on PR EOS parameter and density data is matched by regressing on volume shift parameters; however, this approach requires well-designed binary interaction parameters for three hydrocarbon-phase predictions. All the journal papers support the reliability and efficiency of the PnA method for multi-phase reservoir fluid characterization. **Table 1.5** presents the arrangement of different papers in the thesis.

Chapter 2: This chapter presents the content of first published paper on component level characterization for n-alkane homologous group. Critical temperature, critical pressure, and acentric factor for n-alkanes from n-C_7 to n-C_{100} are optimized for Peng-Robinson EOS to match vapor pressure and density data. These optimized parameters are used to estimate n-alkane equivalent (i.e.

pseudocomponents as 100% n-alkanes) PR EOS parameters for pseudocomponents in perturbation from n-alkane (PnA) approach of reservoir fluid characterization presented in Chapter 3 to 6.

Chapter 3: The PnA approach in this research for the first time is applied mainly to heavy oils for multiphase behavior prediction for solvent injection process. This chapter presents the paper where algorithm has been developed for regression of EOS parameters (T_C, P_C, and ω) to match saturation pressure and density data. Resulting EOS model is then used to predict phase behavior for oils. This paper also presents difference in phase behavior predictions from EOS models developed with/without volume shift parameters.

Chapter 4: The paper presented in Chapter 3 has limited application of PnA method to heavy oils. Content of the Chapter 4 presents the application of PnA characterization for reservoir fluids in general including gas condensates, volatile oils, light oils, and heavy oils. The algorithm used in Chapter 3 is special case of algorithm used for regression of EOS parameters (T_C, P_C, and ω) in Chapter 4. Wherever data are available for comparison, the PnA method has been validated by predicting three hydrocarbon phases for heavy oils.

Chapter 5: Attraction and covolume parameters are basic units of a cubic EOS. Using attraction and covolume parameters as regression parameters can simplify the regression algorithm and reduce the computation time by virtue of small number of regression parameters. Numerical simulation efficiency can improve by characterizing fluids in terms of attraction and covolume parameters for components. Chapter 5 presents the PnA method for characterization of reservoir fluids including gas condensates, volatile oils, light oils, and heavy oils using a new algorithm for regression of PR EOS attraction and covolume parameters for saturation pressure and density data match.

Chapter 6: This chapter presents the characterization of bitumen by regression of PR EOS attraction and covolume parameters. The algorithm presented in Chapter 5 is simplified further for bitumen characterization. This algorithm successfully characterizes bitumen as single pseudocomponent, which has similar predictive capability as multiple pseudocomponent conventional characterization. The paper develops a mechanism, which is to be used before running the simulation, to estimate the sensitivity of recovery simulation to bitumen characterization methods. This helps in selecting reliable and efficient characterization method for simulation.

Chapter 7: The chapter uses PnA method of reservoir fluid characterization where saturation pressure is matched by regression of EOS parameters (T_C, P_C, and ω) and density matching is done by volume shift parameters. The approach uses well-developed binary interaction parameter for multiphase behavior prediction. The method has been validated by successful prediction of multiphase behavior for 90 reservoir fluids including gas condensates, volatile oils, light oils, heavy oils, and bitumens.

Chapter 8: This chapter presents an overview of the research activities presented in Chapter 2-7 in context of research objective. Conclusion and recommendation for future research are also presented in this chapter.

11
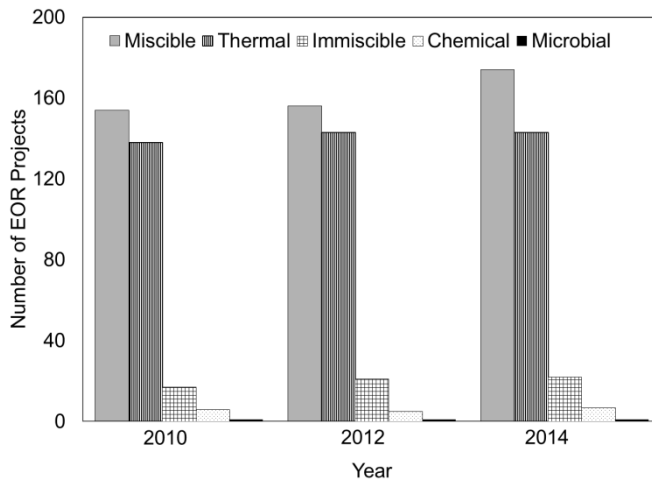
Figure 1-1. Trend of different enhanced oil recovery (EOR) projects (miscible, thermal, immiscible, chemical and microbial).
The data are from Moritis (2010) and Koottungal (2012, 2014).
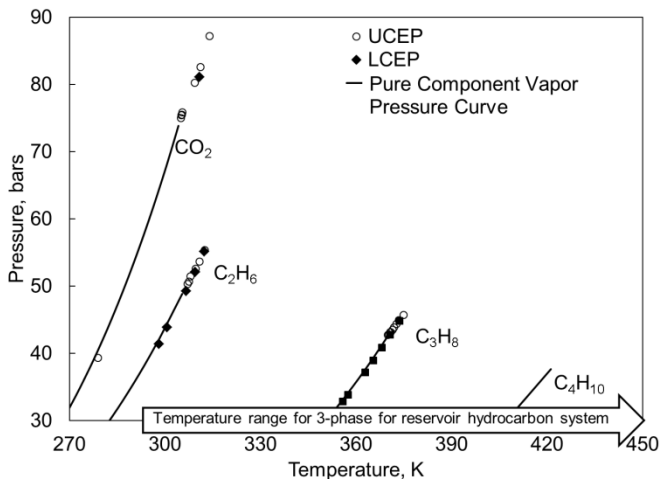
Figure 1-2. Temperature ranges for three hydrocarbon phases' presence for binary mixtures and for solvent and reservoir fluid mixture.
Solid curves depict the vapor pressure curves for carbon-dioxide, methane, propane, and butane. Upper Critical End Point (UCEP) where L_2 phase merges with vapor in presence L_1 and Lower Critical End Point (LCEP) where two liquid phases (L_1 and L_2) merge in presence of vapor phase form the upper and lower bounds of three-phase region in pressure-temperature space. Absence of LCEP in some cases (CO_2) for binary mixture indicates continuity of three-phase with decreasing temperature. Three-phase temperatures for binary mixtures for CO_2, C_2H_6, C_3H_8, and C_4H_{10} with n-alkanes are close to their respective critical temperature points. Temperature range for three hydrocarbon phases shown by arrow is for reservoir hydrocarbon and solvent mixture.

12
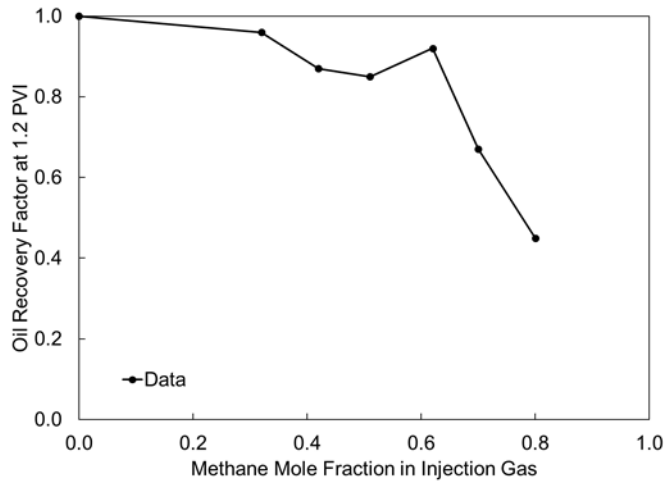
Figure 1-3. Non-monotonic trend for oil recovery from slim tube experiment (Mohanty et al. 1995) for the West Sak oil.

The oil is displaced by gas mixture of methane, ethane, propane, and butane at 291.50 K. Seven gas mixtures with different methane mole % (0, 32, 42, 51, 62, 70, and 80) are used in the slim tube oil displacement. The phase behavior observed in the slim tube for oil and gas mixture changes from first contact miscible at 0% methane gas mixture to multicontact miscible to three-phase immiscible to two phase immiscible with increasing methane concentration in the injection gas. Monotonic recovery is observed for reservoir oil and gas system with presence of two hydrocarbon phases. Non-monotonicity is accounted for the presence of three hydrocarbon phases.
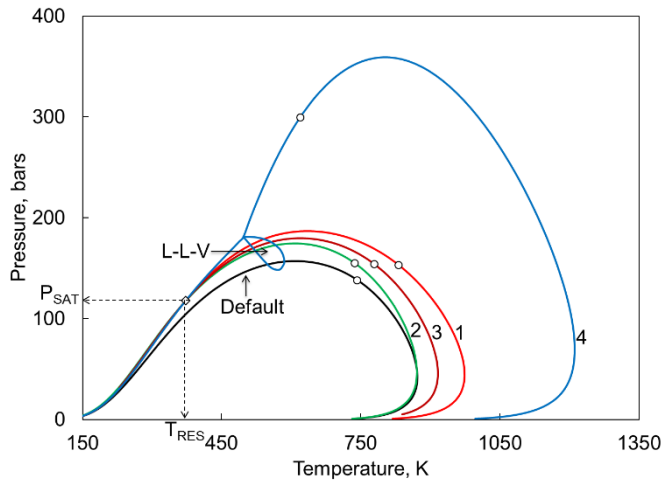
Figure 1-4. Comparison of PT envelopes from four PR EOS models developed using conventional characterization.

All the EOS models have same predictive capability at data point (saturation pressure used to regress T_C, P_C, and ω); however, they have different predictions at other pressure-temperature points.
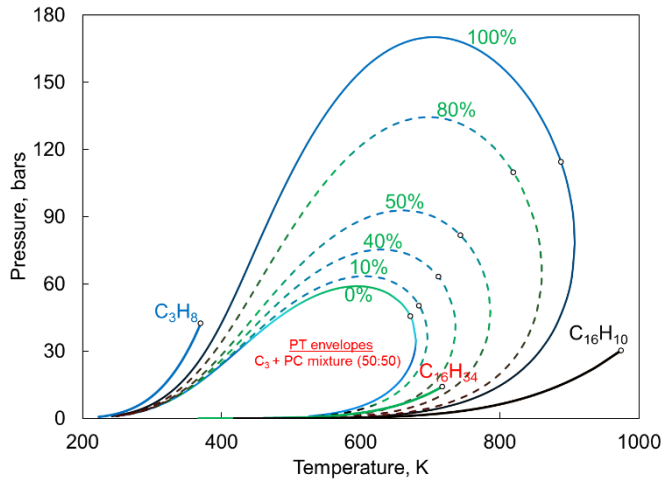
Figure 1-5.   Systematic change in PT phase envelope with increasing aromatic contents in pseudocomponents.

Pseudocomponent has carbon number of 16 and is assumed be binary mixture of n-alkane ($C_{16}H_{34}$) and aromatic ($C_{16}H_{10}$) components. The PT phase envelope is for equimolar binary mixture of propane and pseudocomponent. Percentage on PT phase envelope shows the mole % of aromatic content in pseudocomponent.

14

Table 1.1: PR EOS model 1 from conventional characterization.					
Components	Z	MW (g/mol)	T_C (K)	P_C (bars)	ω
N_2	0.0020	28.01	126.20	33.94	0.0400
CO_2	0.0134	44.01	304.20	73.76	0.2250
CH_4	0.2364	16.04	190.60	46.00	0.0080
C_2H_6	0.0856	30.07	305.40	48.84	0.0980
C_3H_8	0.0668	44.10	369.80	42.46	0.1520
C_4H_{10}	0.0530	58.12	425.20	38.00	0.1930
C_5H_{12}	0.0445	72.15	469.60	33.74	0.2510
C_6H_{14}	0.0403	86.18	507.40	29.69	0.2960
PC-1	0.2214	135.61	680.11	23.09	0.4843
PC-2	0.1146	250.30	833.78	16.04	0.7892
PC-3	0.0772	381.17	977.11	13.62	1.0364
PC-4	0.0448	634.24	1231.07	12.02	1.0276

Table 1.2: PR EOS model 2 from conventional characterization.					
Components	Z	MW (g/mol)	T_C (K)	P_C (bars)	ω
N_2	0.0020	28.01	126.20	33.94	0.0400
CO_2	0.0134	44.01	304.20	73.76	0.2250
CH_4	0.2364	16.04	190.60	46.00	0.0080
C_2H_6	0.0856	30.07	305.40	48.84	0.0980
C_3H_8	0.0668	44.10	369.80	42.46	0.1520
C_4H_{10}	0.0530	58.12	425.20	38.00	0.1930
C_5H_{12}	0.0445	72.15	469.60	33.74	0.2510
C_6H_{14}	0.0403	86.18	507.40	29.69	0.2960
PC-1	0.2214	135.61	611.45	26.18	0.4843
PC-2	0.1146	250.30	749.60	18.19	0.7892
PC-3	0.0772	381.17	878.47	15.44	1.0364
PC-4	0.0448	634.24	1106.78	13.63	1.0276

Table 1.3: PR EOS model 3 from conventional characterization.					
Components	Z	MW (g/mol)	T_C (K)	P_C (bars)	ω
N_2	0.0020	28.01	126.200	33.94	0.0400
CO_2	0.0134	44.01	304.200	73.76	0.2250
CH_4	0.2364	16.04	190.600	46.00	0.0080
C_2H_6	0.0856	30.07	305.400	48.84	0.0980
C_3H_8	0.0668	44.10	369.800	42.46	0.1520
C_4H_{10}	0.0530	58.12	425.200	38.00	0.1930
C_5H_{12}	0.0445	72.15	469.600	33.74	0.2510
C_6H_{14}	0.0403	86.18	507.400	29.69	0.2960
PC-1	0.2214	135.61	642.024	24.66	0.4843
PC-2	0.1146	250.30	787.081	17.13	0.7892
PC-3	0.0772	381.17	922.390	14.54	1.0364
PC-4	0.0448	634.24	1162.119	12.83	1.0276

Table 1.4: PR EOS model 4 from conventional characterization.					
Components	Z	MW (g/mol)	T_C (K)	P_C (bars)	ω
N_2	0.0020	28.01	126.20	33.94	0.0400
CO_2	0.0134	44.01	304.20	73.76	0.2250
CH_4	0.2364	16.04	190.60	46.00	0.0080
C_2H_6	0.0856	30.07	305.40	48.84	0.0980
C_3H_8	0.0668	44.10	369.80	42.46	0.1520
C_4H_{10}	0.0530	58.12	425.20	38.00	0.1930
C_5H_{12}	0.0445	72.15	469.60	33.74	0.2510
C_6H_{14}	0.0403	86.18	507.40	29.69	0.2960
PC-1	0.2214	135.61	611.45	23.09	0.4843
PC-2	0.1146	250.30	749.60	16.04	0.7892
PC-3	0.0772	381.17	993.90	13.62	1.0364
PC-4	0.0448	634.24	1502.66	12.02	1.0276

Table 1.5. Organisation of papers as chapters and features of papers		
Chapter No.	Title	Features
1	Introduction	
2	Critical Parameters Optimized for Accurate Phase Behavior Modeling for Heavy n-Alkanes up to C_{100} using the Peng-Robinson Equation of State. (*Published in Fluid Phase Equilibria*)	[1] Optimization of T_C, P_C, and ω for homologous series of n-alkanes up to C_{100} to match saturation pressure and density data. [2] Volume shift not used to match density.
3	Reservoir Oil Characterization for compositional Simulation of Solvent Injection Processes (*Published in Industrial and Engineering Chemistry Research*)	[1] Characterization of oils for by direct perturbation of T_C, P_C, and ω. [2] Three regression parameters. [3] Volume shift not used for density match. [4] Comparison of phase behavior predictions and simulated oil recoveries for oil characterized with and without using volume shift parameters.
4	Characterization of Reservoir Fluids using an EOS based on Perturbation from n-Alkanes (*Published in Fluid Phase Equilibria*)	[1] Characterization of reservoir fluids such as gas condensates, volatile oil, light oils, heavy oils by direct perturbation of T_C, P_C, and ω). [2] Three regression parameters. [3] Volume shift not used for density match.
5	Direct Perturbation of the Peng-Robinson Attraction and Covolume Parameters for Reservoir Fluid Characterization (*Published in Chemical Engineering Science*)	[1] Characterization of reservoir fluids such as gas condensates, volatile oil, light oils, heavy oils by direct perturbation of attraction and covolume parameters [2] Two regression parameters [3] Volume shift not used for density match.
6	Systematic Characterization of Bitumen-Solvent Interactions in Steam-Solvent Coinjection Simulation (*Submitted to Fuel*)	[1] Characterization of bitumens by direct perturbation of attraction and covolume parameters [2] Two regression parameters [3] Volume shift not used for density match [4] Mechanism is developed to study the sensitivity of simulation to bitumen characterization.
7	A New Algorithm for Multiphase Fluid Characterization for Solvent Injection. (*Submitted to Society of Petroleum Engineering Journal*)	[1] Reservoir fluid such as gas condensate, volatile oils, light oil, heavy oil, bitumen by direct perturbation of T_C, P_C, and ω. [2] Single regression parameter [3] BIPs developed for three hydrocarbon phase predictions. [4] Volume shift used for density match.
8	Conclusion and Future Research	

1.7. References

Abdrakhmanov, A. 2013. Modeling and Optimization of the Rich Gas-Condensate Reservoir. Master Thesis. Norwegian University of Science and Technology, Norwey.

Agarawal, R.K., Li, Y-K., and Nghiem, L. 1990. A Regression Technique with Dynamic Parameter Selection for Phase-behavior Matching. *SPE Res Eng* **5** (1): 115-120.

Aghbash, V.N. and Ahmadi, M. 2012. Evaluation of CO_2-EOR and Sequestration in Alaska West Sak Reservoir Using Four-Phase Simulation Model. Presented at the SPE Western Regional Meeting, Bakers-field, California, 21-23 March.

Ambrose, D. and Tsonopoulos, C. 1995. Vapor-Liquid Critical Properties of Elements and Compounds. 2. Normal Alkanes. *J. Chem. Eng. Data* **40** (3): 531-546.

Badamchi-Zadeh, A., Yarranton, H. W., Svrcek, W. Y. et al. 2009. Phase Behavior and Physical Property Measurements for VAPEX Solvents: Part I. Propane and Athabasca Bitumen. *J Can Pet Technol* **48** (1): 54-61.

Cavett, R.H. 1962. Physical Data for Distillation Calculations, Vapor-Liquid Equilibria. *Proc. Am. Pet. Inst. Div. Refining.* **42** (3): 351-357.

Chang, L.C., Hurt, L.J., and Kobayashi, R. 1966. Vapor-Liquid Equilibria of Light Hydrocarbons at Low Temperatures and High Pressure: The Methane-n-Heptane System. *AIChE J.* **13** (6): 1099-1107.

Chueh, P.L. and Prausnitz, J.M. 1967. Vapor-Liquid Equilibria at High Pressures: Calculation of Partial Molar Volumes in Non-Polar Liquid Mixtures. *AIChE J.* **13** (6): 1107-1113.

Clark, P., Toulekima, S., Sarma, H., 2008. A Miscibility Scoping Study for Gas Injection into a High-Temperature Volatile Oil Reservoir in the Cooper Basin, Australia. Presented at the SPE Asia Pacific Oil and Gas Conference and Exhibition, Perth, Australia. 20-22 Oct.

Creek, J.L. and Sheffield, J.M. 1993. Phase Behavior, Fluid Properties, and Displacement Characteristics of Permian Basin Reservoir Fluid/ CO_2 Systems. *SPE Res Eval & Eng* **8** (1): 34-42. SPE-20188-PA.

DeRuiter, R.A., Nash, L.J., and Singletary, M.S. 1994. Solubility and Displacement Behavior of a Viscous Crude with CO_2 and Hydrocarbon Gases. *SPE Res Eval & Eng* **9** (2): 101-106. SPE-20523-PA.

Dickson, J.L., Clingman, S., Dittaro, L.M. et al. 2011. Design Approach and Early Field Performance for a Solvent-Assisted SAGD Pilot at Cold Lake, Canada. Presented at the SPE Heavy Oil Conference and Exhibition, Kuwait City, Kuwait, 12-14 December. SPE-150639-MS.

Edmister, W.C. 1958. Applied Hydrocarbon Thermodynamics, Part 4: Compressibility Factors and Equations of State. *Pet. Refiner.* **37**: 173-179.

Enick, R., Holder, G.D., and Morsi, B.I. 1985. Critical and Three Phase Behavior in the Carbon Dioxide/Tridecane System. *Fluid Phase Equilib.* **22** (2): 209-224.

Estrera, S.S. and Luks, K.D. 1987. Liquid-Liquid-Vapor Equilibrium Behavior of Certain Ethane + n-Paraffin Mix. *J. Chem. Eng. Data.* **32** (2): 201-204.

Fall, D.J. and Luks, K.D. 1985. Liquid-Liquid-Vapor Phase Equilibria of the Binary System Carbon Dioxide + n-Tridecane. *J. Chem. Eng. Data.* **30** (3): 276-279.

Fulco, G.J. 1999. Case History of Miscible Gas Flooding in the Powder River Basin North Buck Draw Unit. Presented at the SPE Rocky Mountain Regional Meeting, Gillette, Wyoming, 15-18 April. SPE-55634-MS.

Gao., G., Daridon, J-L., Saint-Guirons, H. et al. 1992. A Simple Correlation to Evaluate Binary Interaction Parameters of the Peng-Robinson Equation of State: Binary Light Hydrocarbon Systems. Fluid Phase Equilib. **74**: 85-93.

Godbole, S.P., Thele, K.J., and Reinbold, E.W. 1995. EOS Modeling and Experimental Observations of Three-Hydrocarbon-Phase Equilibria. *SPE Res. Eng.* **10** (2): 101-108. SPE-24936-PA.

Gregorowicz, J., De Loos, T.W., and De Swaan Arons, J. 1993a. Liquid-Liquid-Vapour Phase Equilibria in the System Ethane + Propane + Eicosane: Retrograde Behaviour of the Heavy Liquid Phase, *Fluid Phase Equilib.* **84**: 225-250.

Gregorowicz, J., Smits, P.J., de Loos, T.W. et al. 1993b. Liquid-Liquid-Vapour Phase Equilibria in the System Methane + Ethane + Eicosane: Retrograde Behaviour of the Heavy Liquid Phase. *Fluid Phase Equilib*. **85**, 225-238.

Gupta, S.C. and Gittins, S.D. 2006. Christina Lake Solvent Aided Process Pilot. *J Can Pet Technol* **45** (9): 15-18. PETSOC-06-09-TN.

Gupta, S.C., Gittins, S., and Picherack, P. 2005. Field Implementation of Solvent Aided Process. *J Can Pet Technol* **44** (11): 8-13. PETSOC-05-11-TN1.

Guler, B., Wang, P., Delshad, M. et al. 2001. Three- and Four- Phase Flow Compositional Simulations of CO_2/NGL EOR. Presented at the SPE Annual Technical Conference and Exhibition, New Orleans, Louisiana, 30 September-3 October.

Henry, R.L. and Metcalfe, R.S. 1983. Multiple-Phase Generation During Carbon Dioxide Flooding. *SPE J.* **23** (4): 595-601.

Holm, L.W. 1986. Miscibility and Miscible Displacement. *J Pet Technol* **38** (8):817-818.

Hottovy, J.D., Kohn, J.P., and Luks, K.D. 1981. Partial Miscibility Behavior of the Methane-Ethane-n-Octane System. *J. Chem. Eng. Data.* **26** (2): 135-137.

Hottovy, J.D., Kohn, J.P., and Luks, K.D. 1982. Partial Miscibility Behavior of the Ternary Systems Methane-Propane-n-Octane, Methane-n-Butane-n-Octane, and Methane-Carbon Dioxide-n-Octane. *J. Chem. Eng. Data.* **27** (3): 298-302.

Hottovy, J.D., Luks, K.D., and Kohn, J.P. 1981a. Three-phase liquid-liquid-vapor equilibriums behavior of certain binary carbon dioxide-n-paraffin systems. *J. Chem. Eng. Data* **26** (3): 256-258.

Iwade, S., Katsumura, Y., and Ohgaki, K. 1992. High-Pressure Phase Behavior of Binary Systems of Heptadecane and Octadecane with Carbon Dioxide or Ethane. *J. Chem. Eng. Jpn*. **26** (1): 74-79.

Jangkamolkulchai, A. and Luks, K.D. 1989. Partial Miscibility Behavior of the Methane + Ethane + n-Docosane and the Methane + Ethane + n-Tetradecylbenzene Ternary Mixtures. *J. Chem. Eng. Data*. **34** (1): 92-99.

Jhaveri, B.S. and Youngren, G.K. 1988. Three-Parameter Modification of the Peng-Robinson Equation of State to Improve Volumetric Predictions. *SPE J*. **3** (3): 1033-1040.

Kesler, M.G. and Lee, B.I. 1976. Improve Prediction of Enthalpy of Fractions, Hydrocarbon Processing. *Hydrocarb Process* **55** (3): 153-158.

Khan, S.A., Pope, G.A., and Sepehrnoori, K. 1992. Fluid Characterization of Three-Phase CO_2/Oil Mixtures. Presented at the SPE/DOE Enhanced Oil Recovery Symposium, Tulsa, Oklahoma, 22-24 April. SPE-24130-MS.

Koottungal, Leena. 2012. Worldwide EOR Survey, *Oil Gas J.* **110** (4).

Koottungal, Leena. 2014. Worldwide EOR Survey, *Oil Gas J.* **112** (5).

Korsten, H. 2000. Internally Consistent Prediction of Vapor Pressure and Related Properties. *Ind. Eng. Chem. Res.* **39** (3): 813-820.

Krejbjerg, K. and Pedersen, K.S. 2006. Controlling VLLE Equilibrium with a Cubic EoS in Heavy Oil Modeling. Presented at 57th Annual Technical Meeting of the Petroleum Society (Canadian International Petroleum Conference), Calgary. 13-15 June. PETSOC-2006-052.

Kukarni, A.A., Zarah, B.Y., Luks, K.D. et al. 1974. Phase-Equilbriums Behavior of System Carbon Dioxide-n-Decane at Low Temperatures. *J. Chem. Eng. Data*   **19** (1), 92-94.

Lee, B.I. and Kesler, M.G. 1975. A Generalized Thermodynamic Correlation Based on Three-Parameter Corresponding States. *AIChE J.* **21** (3): 510-527.

Li, H., Zheng, S., and Yang. D. 2013. Enhanced Swelling Effect and Viscosity Reduction of Solvent(s)/CO_2/Heavy-Oil Systems. *SPE J*. **18** (4): 695-707. SPE-150168-PA.

Lin, Y-N., Chen, R.J.J., Chappelear, P.S. et al. 1977. Vapor-Liquid Equilibrium of the Methane-n-Hexane System at Low Temperature. *J. Chem. Eng. Data* **22** (4): 402-408.

Llave, F.M., Luks, K.D., and Kohn, J.P. 1987. Three-Phase Liquid-Liquid-Vapor Equilibria in the Nitrogen-Methane-Ethane and Nitrogen-Methane-Propane Systems. *J. Chem. Eng. Data.* **32** (1): 14-17.

Lolley, C.S. and Richardson, W.C. 1997. Compositional Input for Thermal Simulation of Heavy Oils with Application to the San Ardo Field. Presented at International Thermal Operation & Heavy Oil Symposium, Bakersfield, California, 10-12 Dec. SPE-37538-MS.

Malik, Q.M. and Islam, M.R. 2000. CO_2 Injection in the Weyburn Field of Canada: Optimization of Enhanced Oil Recovery and Greenhouse Gas Storage with Horizontal Wells. Presented at the SPE/DOE Improved Oil Recovery Symposium, Tulsa, Oklahoma, 3-5 April. SPE-59327-MS.

Manrique, E.J., Muci, V.E., and Gurfinkel, M.E. 2007. EOR Field Experiences in Carbonate Reservoirs in the United States. *SPE Res Eval & Eng* **10** (6): 667-686.

McGuire, P.L., Spence, A.P., and Redman, R.S. 2001. Performance Evaluation of a Mature Miscible Gasflood at Prudhoe Bay. *SPE Res Eval & Eng* **4** (4): 318-326. SPE-72466-PA.

Merrill, R.C., Luks, K.D., and Kohn, J.P. 1983. Three-Phase Liquid-Liquid-Vapor Equilibrium in the Methane + n-Pentane + n-Octane, Methane + n-Hexane + n-Octane, and Methane + n-Hexane + Carbon Dioxide Systems. *J. Chem. Eng. Data* **28** (2): 210-215.

Mizenko, G.J. 1992. North Cross (Devonian) Unit CO_2 Flood: Status Report. Presented at the SPE/DOE Enhanced Oil Recovery Symposium, Tulsa, Oklahoma, 22-24 April. SPE-24210-MS.

Mohanty, K.K., Masino, W.H. Jr., Ma, T.D. et al. 1995. Role of Three-Hydrocarbon-Phase Flow in a Gas-Displacement Process. *SPE Res Eng* **10** (3): 214-221. SPE-24115-PA.

Moritis, Guntis. 2010. Worldwide EOR Survey, *Oil Gas J.* **102** (14).

Negahban, S. and V. J. Kremesec Jr. 1989. Development and Validation of Equation-of-State Fluid Descriptions for CO_2-Reservoir Oil Systems. SPE 19637. Presented at the 64th Annual Technical Conference and Exhibition, San Antonio, 8-11 March.

Nghiem, L. X. and Li, Y.K. 1986. Effect of Phase Behavior on CO_2 Displacement Efficiency at Low Temperatures: Model Studies With an Equation of State. *SPE Res Eng* **1** (4): 414-422.

Okuno, R. and Xu, Z. 2014. Efficient Displacement of Heavy Oil by Use of Three Hydrocarbon Phases. *SPE J.* **19** (5): 956-973. SPE-165470-PA.

Okuyiga, M.O. 1992. Equation of State Characterization and Miscibility Development in a Multiple Phase Hydrocarbon System. Presented at the SPE Annual Technical Conference and Exhibition, Washington, DC, 4-7 Oct. SPE-24937-MS.

Pedersen, K. S. and Christensen, P. L. 2007. Phase Behavior of Petroleum Reservoir Fluids. CRC Press, Taylor & Francis Group, Boca Raton, FL, USA.

Pedersen, K.S., Thomassen, P., and Fredenslund, Aa. 1983. SRK- EOS Calculation for Crude Oil. *Fluid Phase Equilib.* **14:** 209–218.

Pedersen, K.S., Thomassen, P., and Fredenslund, Aa. 1984. Thermodynamics of Petroleum Mixture Containing Heavy Hydrocarbons. 1. Phase Envelope Calculation by Use of the Soave-Redlich-Kwong Equation of State. *Ind. Eng. Chem. Proc. Des. Dev.* **23** (1): 163–170.

Pedersen, K.S., Thomassen, P., and Fredenslund, Aa. 1984. Thermodynamics of Petroleum Mixture Containing Heavy Hydrocarbons. 1. Phase Envelope Calculation by Use of the Soave-Redlich-Kwong Equation of State. *Ind. Eng. Chem. Proc. Des. Dev.* **23** (1): 163–170.

Pedersen, K.S., Blilie, A.L., and Meisingset, K.K. 1992. Calculations on Petroleum Reservoir Fluids Using Measured and Estimated Compositional Data for the Plus Fraction. *Ind. Eng. Chem. Res.* **31** (5): 1378-1384.

Pedersen, K.S., Milter, J., and Sørensen, H. 2004. Cubic Equations of State Applied to HT/HP and Highly Aromatic Fluids. *SPE J.* **9** (2): 186-192.

Pedersen, K.S., Thomassen, P., and Fredenslund, Aa. 1989. Characterization of Gas Condensate Mixtures. *Advances in Thermodynamics*, Taylor and Francis, New York, 1, 137-152.

Peneloux, A., Rauzy, E., and Fréze, R. 1982. A Consistent Correction for Redlich-Kwong-Soave Volume. *Fluid Phase Equilib*. **8** (1):7-23.

Peng, D.-Y. and Robinson, D.B. 1976. A New Two-Constant Equation of State. *Ind. Eng. Chem. Fund.* **15** (1): 59-64.

Peng, D.-Y. and Robinson, D.B. 1978. The Characterization of the Heptanes and Heavier Fractions for the GPA Peng-Robinson Programs. *GPA Research Report RR-28*.

Peters, C.J. 1994. Multiphase Equilibria in Near-Critical Solvents. In Supercritical Fluids, ed. E. Kiran and J.M.H. Levelt Sengers, 117-145. Dordrecht, The Netherlands: Springer Netherlands,

Peters, C.J., De Roo, J.L., and De Swaan Arons, J. 1987b. Three-Phase Equilibria in (Ethane + Pentacosane). *J. Chem. Thermodyn*. **19** (3): 265-272.

Peters, C.J., Van der Kooi, H.J., and De Swaan Arons, J. 1987a. Measurements and Calculations of Phase Equilibria for (Ethane + Tetracosane) and (p, V_m^*, T) of Liquid Tetracosane. *J. Chem. Thermodyn.* **19** (4): 395-405.

Peters, C.J., Van Der Kooi, H.J., De Roo, J.L. et al. 1989. The Search for Tricriticality in Binary Mixtures of Near-Critical Propane and Normal Paraffins. *Fluid Phase Equilib*. **51:** 339-351.

PVTsim 20.0. 2011. Calsep A/S, Lyngby, Denmark.

Quiñones -Cisneros, S.E., Zéberg-Mikkelsen, C.K., and Stenby, E.H. 2003. Friction Theory Prediction of Crude Oil Viscosity at Reservoir Conditions Based on Dead Oil Properties. *Fluid Phase Equilib*. **212** (1-2): 233–243.

Reid, T. 1994. Study of Hydrocarbon Miscible Solvent Slug Injection Process for Improved Recovery of Heavy Oil From Schrader Bluff Pool, Milne Point Unit, Alaska. Annual Report for DE-FG22-93BC14864 for the US Department of Energy. University of Alaska Fairbanks, Alaska.

Riazi, M.R. and Al-Sahhaf, T.A. 1996. Physical Properties of Heavy Petroleum Fractions and Crude Oils*. Fluid Phase Equilib*. **117** (1-2): 217-224.

Riazi, M.R. and Daubert, T.E. 1980. Simplify Property Predictions. *Hydrocarb. Process.* **59** (3): 115-116.

Riazi, M.R. and Daubert, T.E. 1987. Characterization Parameters for Petroleum Fractions. *Ind. Eng. Chem. Res.* **26** (4): 755-759.

Rodriguez, I. and Hamouda, A.A. 2010. An Approach for Characterization and Lumping of Plus Fractions of Heavy Oil. *SPE Res Eval Eng* **13** (2): 283-295.

Rodrigues, A.B. and Kohn, J.P. 1967. Three Phase Equilibria in the Binary Systems Ethane-n-Docosane and Ethane-n-Octacosane. *J. Chem. Eng. Data*. **12** (2): 191-193.

Roper, M. 1989. An Experimental Study of CO_2/West-Sak-Crude-Oil Phase Behavior. MS thesis, University of Alaska Fairbanks, Fairbanks, Alaska.

Sänger, P. and Hagoort, J. 1998. Recovery of Gas Condensate by Nitrogen Injection Compared with Methane Injection. *SPE J.* **3** (1): 26-33.

Secuianu, C., Feroiu, V., and Geana, D. 2007. Investigation of Phase Equilibria in the Ternary System Carbon Dioxide + 1-Heptanol + n-Pentadecane. *Fluid Phase Equilib.* **261** (1-2): 337-342.

Sharma, A.K., Patil, S.L., Kamath, V.A. et al. 1989. Miscible Displacement of Heavy West Sak Crude by Solvents in Slim Tube. Presented at the SPE California Regional Meeting, Bakersfield, California, 5-7 April. SPE-18761-MS.

Shelton, J.L., and Yarborough, L. 1977. Multiple Phase Behavior in Porous Media During CO_2 or Rich-Gas Flooding. *J. Pet. Technol.* **29** (9):1171-1178.

Sheng, J. 2013. Enhanced Oil Recovery Field Case Studies, Gulf Professional Publishing.

Soave, G. 1972. Equilibrium Constants from a Modified Redlich-Kwong Equation of State. *Chem. Eng. Sci.* **27** (6): 1197-1203.

Stein, M.H., Frey, D.D., Walker, R.D. et al. 1992. Slaughter Estate Unit CO_2 Flood: Comparison between Pilot and Field-Scale Performance. *J Pet Technol* **44** (9): 1026-1032. SPE-19375-PA.

Tanner, C.S., Baxley, P.T., Crump III, J.G. et al. 1992. Production Performance of the Wasson Denver Unit CO_2 Flood. Presented at the SPE/DOE Enhanced Oil Recovery Symposium, Tulsa, Oklahoma, 22-24 April. SPE-24156-MS.

Taheri, A., Høier, L., and Torsæter, O. 2013. Miscible and Immiscible Gas Injection for Enhancing of Condensate Recovery in Fractured Gas Condensate Reservoir. Presented at the EAGE Annual Conference and Exhibition incorporating SPE Europe, London, UK, 10-13 June.

Turek, E.A., Metcalfe, R.S., and Fishback, R.E. 1988. Phase Behavior of Several CO_2/ West Texas-Reservoir-Oil Systems. *SPE Res Eng* **3** (2): 505-516. SPE-13117-PA.

Twu, C.H. 1984. An Internally Consistent Correlation for Predicting the Critical Properties and Molecular Weights of Petroleum and Coal-Tar Liquids. *Fluid Phase Equilib.* **16** (2): 137-150.

Van der Steen, J., De Loos, T.W., and de Swaan, A.J. 1989. The Volumetric Analysis and Prediction of Liquid-Liquid-Vapor Equilibria in Certain Carbon Dioxide + n-Alkane Systems. *Fluid Phase Equilib.* **51:** 353-367.

Varotsis, N., Stewart, G., Todd, A.C. et al. 1986. Phase Behavior of Systems Comprising North Sea Reservoir Fluids and Injection Gases. *J Pet Technol* **38** (11): 1221-1233. SPE-12647-PA.

Whitson, C.H. 1983. Characterizing Hydrocarbon Plus Fractions. *SPE J.* **23** (4): 683-694.

Whitson, C.H. and Brulè, M.R. 2000. Phase Behaviour. SPE Henry L. Doherty Series, Vol. 20, SPE, Richardson, Texas.

Chapter 2: Critical Parameters Optimized for Accurate Phase Behavior Modeling for Heavy n-Alkanes up to C$_{100}$ using the Peng-Robinson Equation of State

A version of this has been published in Fluid Phase Equilibria, Year: 2012, Volume: 335, Pages: 46–59.

2.1. Introduction

Cubic equations of state (EOSs) are widely used in the petroleum industry to model volumetric and compositional phase behavior of petroleum reservoir fluids. Since the original research of van der Waals 0 in 1873, many cubic EOSs have been developed including the Peng-Robinson (PR) EOS (Peng and Robinson 1976; 1978) and the Soave-Redlich-Kwong (SRK) EOS (Soave 1972). These cubic EOSs are used in compositional reservoir simulation to design enhanced oil recovery (EOR) using solvents. With recent advances in the EOS compositional reservoir simulation technology, it is now possible to robustly simulate complex gas/CO_2 injection processes that involve critical endpoint behavior (Okuno et al. 2011).

Reliable predictions of EOR using compositional reservoir simulation require accurate characterization of reservoir fluids using a cubic EOS. Such characterization methods have been developed, and implemented in commercial software for conventional oils (Pedersen et al. 1992; Neau and Jaubert 1993; PVTsim 2011; Riazi 2005; Pedersen and Christensen 2007; Whitson and Brule 2000). Characterization of heavy oils using an EOS, however, is more difficult than that of conventional oils. Firstly, compositions of heavy oils are highly uncertain in terms of the concentration of each carbon number (CN) group and the paraffins-naphthenes-aromatics (PNA) distribution within each CN group. Secondly, critical parameters required in EOS fluid characterization are unknown for hydrocarbons heavier than tetracosane, n-C_{24} (Ambrose and Tsonopoulos 1995). Thirdly, accurate prediction of heavy oil densities is difficult using two-parameter cubic EOSs with a constant critical compressibility factor such as the PR and SRK EOSs (Peng and Robinson 1976, 1978; Soave 1972). A cubic EOS with more than two parameters can improve density predictions for heavy oils (Klara and Hemanth-Kumar 1987), but at the expense of computational efficiency.

In the literature, a few different sets of correlations were proposed for critical temperature (T_C), critical pressure (P_C), and acentric factor (ω) extrapolated for hydrocarbons heavier than C_{24} (Voulgaris et al. 1991; Rodríguez and Hamouda 2008). These correlations, however, were developed based on reservoir oil samples, and do not explicitly account for effects of the PNA distribution on critical parameters. Since a heavier CN group can contain a wider variety of compounds, more uncertainties in phase behavior predictions arise when such generic correlations are used for heavy oil characterization.

Cubic EOSs are incapable of accurate prediction of densities and vapor pressures for heavy hydrocarbons even when accurate critical parameters are known and used. The volume shift approach of Péneloux et al. (1982) (Jhaveri and Youngren (1988) for the PR EOS) is widely used to improve density predictions with cubic EOSs. The volume shift approach, however, does not improve compositional phase behavior predictions. Use of volume shift in EOS fluid characterization can cause erroneous oil recovery predictions in simulation of miscible gas injection, where mass transfer among phases is significant (Kumar and Okuno 2014).

Another approach for improving the PR EOS is to modify the alpha function (Mathias 1983; Stryjek

and Vera 1986; Melhem et al. 1989; Li and Yang 2011; Nji et al. 2008, 2009). These modified alpha functions can improve vapor pressure predictions for heavy hydrocarbons. However, they change the functional form of the PR EOS, which does not allow for direct application with commercial reservoir simulators.

Ting et al. (2003) and Voutsas et al. (2006) fitted the critical parameters for the PR EOS to density and vapor pressure predictions for selected hydrocarbons and their binary mixtures. They considered n-alkanes C_1, C_2, C_3, C_4, C_6, C_7, C_{10}, C_{16}, C_{18}, C_{20}, C_{24}, C_{30}, C_{36}, and C_{40} for their critical parameter optimization. They presented that the PR EOS with the fitted critical parameters exhibits accurate phase behavior predictions for the fluids studied. This approach keeps the functional form of the PR EOS, and minimizes use of volume shift. However, no attempt has been made to optimize the critical parameters for the PR EOS for a wide CN range that is common for reservoir oils.

In this research, we develop optimized values and new correlations for T_C, P_C, and ω for accurate phase behavior predictions for heavy n-alkanes up to C_{100} using the PR EOS. Our development is focused on a homologous series of n-alkanes mainly because more data are available for n-alkanes than for the other types of hydrocarbons. For characterization of actual oils, the effects of N and A components on phase behavior predictions can be considered by perturbations from n-alkanes' critical parameters as proposed by Quiñones-Cisneros et al. (2003).

The subsequent sections present our development of optimized T_C, P_C, and ω along with experimental data used. We then develop new correlations based on the optimized values for T_C, P_C, and ω. The new set of critical parameters is used to demonstrate improved predictions of densities and vapor pressures of n-alkanes and their mixtures. We also present application of the optimum critical parameters for characterizing 25 different reservoir oils.

2.2. Optimization of Critical Parameters

The PR EOS is one of the most widely used cubic EOSs in the petroleum industry. It uses two parameters as given below in **Equations 2-1** to **2-5**.

$$p = \frac{RT}{v-b} - \frac{a_c \alpha(T)}{v^2 + 2bv - b^2} \tag{2-1}$$

$$\text{where} \quad a_c = 0.457235529 \frac{(RT_c)^2}{P_c} \tag{2-2}$$

$$\sqrt{\alpha(T)} = \left[1 + m\left(1 - \left(\frac{T}{T_c}\right)^{0.5}\right)\right] \tag{2-3}$$

$$m = 0.37464 + 1.54226\omega - 0.26992\omega^2 \quad \text{for } \omega < 0.49 \tag{2-4}$$

$$m = 0.379642 + 1.48503\omega - 0.164423\omega^2 + 0.016666\omega^3 \quad \text{for } \omega \geq 0.49 \tag{2-5}$$

Equations 2-4 and 2-5 indicate that the m(ω) function is one-to-one as shown in **Figure 2-1**; i.e., a given positive real value for ω results in a unique value for m, and vice versa. Our optimization is performed in terms of T_C, P_C, and m. It is easy to derive ω corresponding to an optimized m.

26

2.2.1. Experimental Data Used for Optimization

Our optimization uses experimental data for vapor pressure and liquid density of n-alkanes. **Table 2-A1 and 2-A2** summarize the sources and T-P ranges of data used for the optimization. **Table 2-1** lists the n-alkanes for which experimental data are available for liquid densities and vapor pressures, and data uncertainties for each of the compounds.

Saturated liquid densities estimated in Yaws (2010) are used for n-alkanes that have no liquid density data available in the literature (Table 2-A1 shows for which n-alkanes the estimations of Yaws (2010) are used). The estimation of saturated liquid densities is based on a modified form of the Rackett equation (1970) using four parameters (Daubert et al. 1997). The quality of the estimations in Yaws (2010) is difficult to judge owing to the lack of experimental data. However, the modified Rackett equation represents experimental data very well (Poling et al. 2001). Poling et al. (2001) recommended the modified Rackett equation for estimation of saturated liquid densities.

Vapor pressure data for many n-alkanes are not available in the literature. Therefore, vapor pressure data for such n-alkanes are supplemented by the correlation of Riazi and AlQaheem (2010) given by **Equation 2-6**. This correlation has been developed using updated (Dykyj et al. 1997) vapor pressure data available for n-alkanes between C_7 to C_{100}.

$$\ln P_r^{vap} = (a_1 + a_2 r + a_3 r^3) + (b_1 + b_2 r + b_3 r^2)T_r^{-2} + (c_1 + c_2 r)T_r \qquad (2\text{-}6)$$

In Equation 2-6, $P_r^{vap} = \frac{P^{vap}}{P_c}$ and $T_r = \frac{T}{T_c}$. Coefficients a_1, a_2, a_3, b_1, b_2, b_3, c_1 and c_2 are given in **Table 2-2**. The r values for some hydrocarbons between C_2 to C_{40} are available in Riazi (2005). For other hydrocarbons up to C_{100}, the procedure recommended by Riazi and AlQaheem (2010) has been used to estimate the value for r. Equation 2-6 results in less than 2% deviation in vapor pressure predictions for the CN range shown in Table 2-2. Table 2-A2 indicates n-alkanes for which the correlation of Riazi and AlQaheem (2010) is used. For all the n-alkanes considered in our optimization, C_7-C_{100}, we ensure use of vapor pressure data points both for $T_r \leq 0.7$ and $T_r \geq 0.7$. This is to ensure the accuracy of vapor pressure predictions around T_r of 0.7, which is used in Pitzer's definition of ω in **Equation 2-7**.

$$\omega = -\log_{10}\left[\frac{P_{SAT}}{P_C}\right]_{\left(\frac{T}{T_C} = 0.7\right)} - 1 \qquad (2\text{-}7)$$

2.2.2. Optimization Method

T_C, P_C, and ω are optimized considering reduction of

- Average absolute deviations (AAD) in density predictions
- AAD in vapor pressure predictions
- Deviations of T_C and P_C from physical critical points,

while keeping smooth variations of T_C, P_C, and ω with respect to molecular weight (MW), and the consistency with Pitzer's definition for ω, Equation 2-7. The minimization of AADs for both density and vapor pressure predictions can be challenging. A set of T_C, P_C, and ω that gives a minimum for the sum

of the two types of AADs does not necessarily result in a minimum for each of the AADs. When a change in P_C decreases AAD in density predictions, it can increase AAD in vapor pressure predictions. For this reason, our optimization also considers that AAD in vapor pressure predictions should be similar to that in density predictions.

Minimization of the AADs can have many local minima, and it is unlikely that the global minimum always exists for this minimization. Smoothness of T_C, P_C, and ω with respect to MW is considered when the minimization needs an additional criterion due to multiple local minima close to each other.

2.2.2.1. Initialization

We optimize T_C, P_C, and ω using the exhaustive search method, for which initial estimates are provided using the solver function within the Excel software. The initialization using the Excel solver function starts with T_C, P_C, and ω from the correlations developed for n-alkanes by Gao et al. (2001). Predictions of vapor pressures and saturated liquid densities are sensitive to T_C and P_C, respectively (Voulgaris et al. 1991). Therefore, T_C and P_C are primarily used to reduce AADs in vapor pressure and density predictions. The initialization steps for a given n-alkane are as follows:

Step 1. AAD in vapor pressure predictions is reduced using T_C only.

Step 2. AAD in vapor pressure predictions is reduced using m only. The m parameter is defined in Equations 2-4 and 2-5.

Step 3. AAD in liquid density predictions is reduced using P_C only.

Step 4. The sum of AADs for vapor pressure and liquid density predictions is reduced using T_C and P_C.

Step 5. The sum of AADs for vapor pressure and liquid density predictions is reduced using T_C, P_C, and m.

Steps 1-5 are repeated until reduction of the AADs becomes marginal. During the iteration, we confirm that T_C, P_C, and m with respect to MW are smooth for 94 n-alkanes from C_7 through C_{100}. The values for T_C, P_C, and m that do not follow the smooth trends are replaced with values interpolated between the neighboring CNs.

The values for T_C and P_C initialized above are generally greater than physical values given in the literature. For example, the initialized critical point for C_{100} is (T_C, P_C) = (1094.0 K, 4.34 bars), and the physical critical point is (T_C, P_C) = (1038.2 K, 2.71 bars) from DECHEMA (see reference). The deviation from the physical values is reduced in the subsequent optimization using the exhaustive search method.

2.2.2.2. Exhaustive Search for Optimum T_C, P_C, and ω

An algorithm was developed for our optimization using the exhaustive search method. The algorithm allows for simultaneous adjustment of T_C, P_C, and m, unlike the initialization described in Section 2.2.2.1.

The exhaustive search method defines its search domain to be (-5%, +1%) from the initial value for T_C and (-8%, +2%) from the initial value for P_C for each n-alkane. This rectangular domain in T-P space is then discretized into 6,000 grids allowing for a unit change of 0.1% in each of T_C and P_C. We use the asymmetric search domain with respect to the initial point in T and P directions. This is because we search for optimum values that are lower than the initial values set in Section 2.2.2.1.

28

For each set of T_C and P_C, we calculate m by minimizing AAD in vapor pressure predictions. In this optimization of m, we consider the consistency with Pitzer's definition of ω. For a given set of T_C, P_C, and m, the PR EOS can provide a saturation pressure at T_r of 0.7 (P_{SAT} in Equation 2-7). Equation 2-7 can then give a value for ω. However, this ω value does not necessarily match another ω value that can be calculated from either Equation 2-4 or 2-5 with the current m value. The consistency is satisfied when the absolute difference between these two ω values becomes smaller than a tolerance (e.g., 10^{-3}).

The resulting set of T_C, P_C, and m is then used to calculate AAD in liquid density predictions. The AADs in vapor pressure and liquid density predictions are recorded for 6,000 sets of T_C, P_C, and m. Selection of the optimum set of T_C, P_C, and m for each n-alkane is, in general, based on the total of the AADs in vapor pressure and liquid density predictions. It is observed that the optimum set results in vapor pressure and liquid density AADs that are similar to each other. Smooth curves are usually observed for optimum T_C, P_C, and m with respect to MW. If a set of T_C, P_C, and m that gives the minimum AADs deviates from the overall trends, it is replaced by another set of T_C, P_C, and m while minimizing AADs.

2.3.   Optimum T_C, P_C, m, and ω

The method discussed in Section 2.2 gives T_C, P_C, and m optimized for vapor pressure and liquid density predictions using the PR EOS for 94 n-alkanes from C_7 through C_{100}. Optimized values for ω are calculated using Equations 2-4 and 2-5. The final values for T_C, P_C, m, and ω are presented in **Table 2-B** along with T_C, P_C, and ω based on the correlations of Gao et al. (2001), which are given in **Equations 2-8 to 2-10**.

$$T_C = \left[6573.87 - 4680.77\exp\left(-0.1831(CN^{0.6667} - 2.08)\right)\right]^{\frac{1}{1.276}} \tag{2-8}$$

$$P_C = 42.44\exp\left(-0.3757(CN^{0.5684} - 1.8672)\right) \tag{2-9}$$

$$\omega = \left[3.212102 - 2.937628\exp\left(-0.04699(CN^{0.6667} - 2.08)\right)\right]^{\frac{1}{0.6851}} \tag{2-10}$$

In the above equations, CN is carbon number. T_C and P_C are in Kelvin and bar, respectively. The accuracy (AAD) of the above correlations for T_C, P_C, and ω is 0.2, 0.8, and 0.4%, respectively, for n-alkanes from C_3 to C_{36}.

Use of our optimized T_C, P_C, and ω with the PR EOS gives significantly improved calculations of liquid density and vapor pressure for n-alkanes from C_7 through C_{100} as shown in Table 2-A1 and 2-A2 respectively. Using the optimized values, the AAD is 2.8% for 3583 density data points and 1.6% for 1525 vapor pressure data points. These data points include n-alkanes from C_7 to C_{100}. **Figures 2-2 and 2-3** present the comparisons of density and vapor pressure predictions using our optimized T_C, P_C, and ω with those using Equations 2-8 to 2-10. Using the optimized T_C, P_C, and ω, AADs for both density and vapor pressure predictions are consistently small for the wide range of CN from C_7 to C_{100}. A reason for the smaller variation of the AADs for CN greater than 40 is the relatively consistent T_r-P_r ranges and

29

sources for the data used (see Table 2-A1 and 2-A2). When Equations 2-8 to 2-10 are used, AADs for density and vapor pressure predictions increase with CN. The AAD for C_{100} is 86.9% for density prediction and 60.9% for vapor pressure prediction when the correlations of Gao et al. (2001), Equations 2-8 to 2-10, are used.

As mentioned before, the objective of our optimization is to develop T_C, P_C, and ω that give accurate phase behavior predictions for n-alkanes up to C_{100} using the PR EOS. That is, the values for T_C and P_C presented in Table 2-B are not physical critical points. There are a few different proposals for T_C, P_C, and ω correlations for heavy n-alkanes in the literature. Gao et al. (2001) developed correlations for T_C, P_C, and ω for n-alkanes up to C_{100}, which are given in Equations 2-8 to 2-10. Riazi and Al-Sahhaf (1996) developed their correlations that are recommended for n-alkanes up to C_{20}. Although efforts have been made to minimize the deviation from physical values in our optimization (see Section 2.2), **Figures 2-4 to 2-6** show that T_C, P_C, and ω developed in this research deviate from values available in the literature. In these figures, Riazi and Al-Sahhaf's correlations are extrapolated up to C_{100}. Yaws (2010) also gives values for T_C and P_C for n-alkanes, but they are not shown in Figures 2-4 to 2-6 because their trends are not smooth at C_{30}.

Equations 2-11 to 2-13 present new correlations developed for T_C, P_C, and m using the optimized values given in Table 2-B. These correlations (**Equations 2-11, 2-12,** and **2-13)** are recommended for use with the PR EOS only.

$$T_C = 1154.35 - 844.83[1.0 + 1.7557 \times 10^{-3}MW]^{-2.0} \tag{2-11}$$

$$P_C = 559.93MW^{-0.638} - 1.49 \tag{2-12}$$

$$m = 0.4707 + 2.4831MW^{-\left(\frac{39.933}{MW}\right)} \tag{2-13}$$

These correlations accurately represent the optimized T_C, P_C, and m. The R^2 values are 0.99975, 0.99970, and 0.99949 for T_C, P_C, and m, respectively. Maximum absolute deviations for Equations 2-11, 2-12, and 2-13 are 7.35 K for n-$C_{15}H_{32}$, 0.24 bars for n-$C_{21}H_{64}$, and 0.0022 for n-$C_{31}H_{64}$, respectively. Standard deviations are 1.74 K for Equation 2-11, 0.07 bars for Equation 2-12, and 0.005 for Equation 2-13. Equation 2-11 shows an asymptotic value of 1154.35 K for T_C. An asymptote of 2.9538 for m can be found in Equation 2-13. Equation 2-12 gives P_C of 1.0 bar for MW of 4856 gm/mol, which is close to the MW of n-C_{347}.

Figure 2-7 shows a sensitivity analysis for Equation 2-11 in terms of AADs in density and vapor pressure predictions. The AADs here consider all data points (3583 density and 1525 vapor pressure data) for n-alkanes from C_7 to C_{100}. The AAD is 3.0% for density predictions and is 3.4% for vapor pressure prediction using Equations 2-11 to 2-13. The AAD in density predictions exhibit a monotonic trend with respect to T_C near the optimum values given by Equation 2-11. Figure 2-7 also indicates that vapor pressure predictions are more sensitive to T_C than density predictions. Equation 2-11 gives a minimum in the density AAD and the total AAD.

Figure 2-8 presents a similar sensitivity analysis for Equation 2-12. The density AAD exhibits a minimum with a small positive change in P_C, while the vapor pressure AAD exhibits a minimum with a

small negative change in P_C. Equation 2-12 gives a minimum for the sum of the two AADs.

Figure 2-9 shows the sensitivity of the AADs to the m parameter near the optimum values given in Equation 2-13. The vapor pressure AAD is sensitive to the m parameter, but the density AAD is nearly constant for ±10% changes from Equation 2-13. Equation 2-13 gives a minimum for the vapor pressure AAD and the total AAD. Figures 2-7, 2-8, and 2-9 also show that density predictions are more sensitive to P_C than to T_C and the m parameter.

2.4.   Application of Optimized Critical Parameters to Mixtures

In Section 2.3, we developed a new set of critical parameters for the PR EOS that can accurately predict liquid densities and vapor pressures of n-alkanes up to C_{100}. This section is to show that the PR EOS with the critical parameters developed also improves phase behavior predictions for mixtures. We first demonstrate improved phase behavior predictions for various n-alkane mixtures. Application of our critical parameters is then presented for characterization of 25 different reservoir oils. All phase behavior calculations in this section use the PR EOS with the van der Waals mixing rules, and zero binary interaction between hydrocarbons.

2.4.1. Phase Behavior Predictions for n-Alkane Mixtures

We make comparisons between the PR EOS with our correlations for critical parameters (i.e., Equations 2-10 to 2-12) and the PR EOS with the correlations of Gao et al. (2001) (i.e., Equations 2-8 to 2-10). No attempts are made to adjust parameters to obtain a better match between experimental data and predictions.

Table 2-3 shows use of our correlations gives improved accuracy for density predictions for various n-alkane mixtures. AADs in density predictions become greater for heavier hydrocarbons when the correlations of Gao et al. (2001) are used. Use of our correlations for the PR EOS exhibits consistently small AADs in density predictions for all mixtures studied.

The two sets of the correlations are also compared in terms of bubble point pressure predictions for six different mixtures, C_1-C_{16}, C_1-C_{20}, C_2-C_{16}, C_2-C_{20}, C_2-C_{22}, and C_2-C_{24}. For C_2-C_{22} and C_2-C_{24} mixtures, bubble point pressures at two different temperatures are considered for the comparisons. Predictions of bubble and dew points are compared for three n-alkane binaries C_6-C_{16}, C_6-C_{24}, and C_6-C_{36}. As shown in **Figures 2-10 to 2-20**, use of our correlations gives more accurate predictions for bubble and dew points pressures for most of the mixtures studied. Our correlations ensure that bubble point and dew point pressures near the end points (i.e., 0.0 and 1.0 on the x axis) of the figures are accurately predicted using the PR EOS.

Deviations from experimental data are observed for middle-range mixing ratios. Such deviations are attributed mainly to the van der Waals mixing rules used to estimate the attraction and covolume parameters for mixtures. The deviations can be significantly improved if a binary interaction parameter is adjusted for each n-alkane binary. We developed the optimized critical parameters considering their application for characterization of reservoir oils. In reservoir oil characterization, the main challenge

comes from uncertainties in properties and amounts of non-identifiable compounds. Adjustment of binary interaction parameters for such a case can result in physically absurd predictions Pedersen and Christensen (2007). That is, we do not show adjustment of binary interaction parameters to fit EOS predictions to data in this research.

2.4.2. Density Prediction for Reservoir Oils

Different reservoir oils have different distributions of CN groups and PNA components within a given CN group. Even for a given reservoir oil, the concentrations of PNA components likely vary with CN. Characterization of heavy oils is more difficult than that of conventional oils because heavy oils contain a larger amount of heavy fractions, for which CN and PNA distributions are highly uncertain.

In a typical fluid characterization using an EOS, a distribution of CN groups is estimated based on composition analysis data available. Once a CN group distribution is specified, critical parameters are assigned to each CN group. Correlations for critical parameters proposed in the literature are generic in that they do not explicitly consider the concentrations of PNA components. Use of these generic correlations is unsuitable for heavy oil characterization because a heavier CN group can have a wider variety of compounds in it.

A potential method to address the uncertainties is to consider a PNA distribution in a reservoir oil as perturbation from n-alkane mixtures. The critical parameters developed in this research for a homologous series of n-alkanes can serve as a well-defined reference for the perturbation consideration. Since T_C and P_C for N and A components are in general greater than those for P components within a given CN group, T_C and P_C for n-alkanes developed in this research provide the lower bounds of critical parameters for pseudocomponents for actual oils.

Quiñones-Cisneros et al. (2003, 2004a, 2005) proposed a novel fluid characterization method. In their method, P_C for a pseudocomponent is expressed as $P_{Ci} = f \cdot P_{CPi}$, where i is a component index, P_{CP} is P_C for paraffinic components, and f is a perturbation factor that represents deviation from P_{CP}. So, the f factor is 1.0 for P_{CPi}.

In this section, we apply the critical parameters developed in this research for characterizing 25 reservoir oils (**Table 2-4**) on the basis of Quiñones-Cisneros et al.'s characterization method. Measured saturation pressures are used to adjust P_C through the perturbation factor f as in Quiñones-Cisneros et al. (2003, 2004a, 2005). No other parameters are adjusted. Density predictions are then compared with experimental data.

The characterization steps given below are applied to 25 different reservoir oils presented in Table 2-4.

Step 1. Composition. Heavy fractions are split into detailed components using a chi-square distribution. The detailed components are then grouped into 10 components consisting of N_2, CO_2, C_1, C_{2-3}, C_4, C_5, and four heavy pseudocomponents.

Step 2. Critical parameters. For the well-defined components (i.e., N_2, CO_2, and C_1-C_5), physical critical parameters available in the literature are used. For the four pseudocomponents, two sets of

correlations are used; Equations 2-11 to 2-13 developed in this research and the correlations of Quiñones-Cisneros et al. (2005) as given by **Equations 2-14, 2-15,** and **2-16.**

$$T_C = -423.587 + 210.152\ln(\text{MW}) \qquad\qquad (2\text{-}14)$$

$$P_C = \text{Exp}(9.67283 - 4.05288\text{MW}^{0.1}) \qquad\qquad (2\text{-}15)$$

$$\omega = \text{Exp}(8.50471 - \frac{15.1665}{\text{MW}^{0.1}}) \qquad\qquad (2\text{-}16)$$

Step 3. Perturbation of P_C. Adjust the perturbation factor f to match the experimental saturation pressure at the reservoir temperature.

For all reservoir oils characterized, binary interaction parameters between non-hydrocarbon and hydrocarbon components are 0.02 for N_2-C_1, 0.06 for N_2-$C_{2\text{-}3}$, 0.08 for N_2-$C_{i>3}$, 0.12 for CO_2-C_1, and 0.15 for CO_2-$C_{i>1}$ (Quiñones-Cisneros et al. 2005). Volume-shift parameters are zero for all components. In the above, two fluid models are created for each of 25 reservoir oils; i.e., one using Equations 2-11 to 2-13 and the other using Equations 2-14 to 2-16 for T_C, P_C, and ω. Equations 2-14 and 2-16 are generic correlations that do not consider the PNA distribution, while Equation 2-15 is the correlation for P_{CP} proposed by Quiñones-Cisneros et al. (2005). The two fluid models are compared in terms of density predictions for each of the reservoir oils studied (Table 2-4).

Table 2-4 lists the resulting perturbation factors for the 25 reservoir oils. The critical parameters developed in this research result in systematically reduced perturbation required to match saturation pressures. All perturbation factors are calculated to be greater than 1.0 using Equations 2-11 to 2-13 except for the heavy oil oil-6. This observation is consistent with the fundamental concept of the perturbation; i.e., the perturbation factor represents deviation from P_{CP}, and P_C is lower for the P components than for the N and A components within a given CN group. The variation of the resulting perturbation factors is small for oils lighter than 25°API. A wider variation of the resulting perturbation factors is observed for heavier oils, which likely results from higher uncertainties in heavier oils' compositions.

Table 2-4 lists AADs in density predictions for the 25 reservoir oils using Equations 2-11 to 2-13 developed in this research and Equations 2-14 to 2-16 taken from Quiñones-Cisneros et al. (2005). As shown in **Figure 2-21**, use of Equations 2-11 to 2-13 results in more accurate density predictions for most of the reservoir oils studied. The correlations developed in this research require less perturbation from P_{CP} to obtain more accurate density predictions for oils lighter than 25°API. For such lighter oils, it is likely that the concentration of paraffinic components is relatively high.

Figure 2-21 also show that AADs in density predictions for five oils heavier than 25°API (22.6, 13.38, 11.98, 11.63, and 9.5°API) are larger when Equations 2-11 to 2-13 are used. Using these equations, however, smaller perturbations of P_C are required to match measured saturation pressures even for these five heavy oils as given in Table 2-4. Reliable characterization for these low-API reservoir oils using the PR EOS were recently developed based on a new perturbation method with the critical parameters developed in this research (Kumar and Okuno 2014).

2.5. Conclusions

We developed correlations for critical temperatures (T_C), critical pressures (P_C), and acentric factors (ω) that are optimized for phase behavior modeling of n-alkanes from C_7 to C_{100} using the Peng-Robinson (PR) EOS. Density and vapor pressure data available in the literature were used for the optimization. The new set of T_C, P_C, and ω satisfies Pitzer's definition of ω. The optimum T_C, P_C, and ω values were applied to predict phase behavior of n-alkane mixtures and 25 different reservoir oils using the PR EOS. The conclusions are as follows:

- Critical parameters and acentric factors for n-alkanes from C_7 to C_{100} are optimized using 3583 density and 1525 vapor pressure data for use with PR EOS. These optimized parameters results in 2.8% AAD in density prediction and 1.6% vapor pressure prediction.

- The PR EOS with our correlations for T_C, P_C, and ω gives 3.0% and 3.4% AADs in density and vapor pressure predictions, respectively, for n-alkanes from C_7 to C_{100}. When conventional correlations are used for critical parameters, the PR EOS exhibits less accurate predictions for heavier n-alkanes, and AADs can be as high as 61% for vapor pressure prediction and 87% for density prediction for n-C_{100}.

- The critical parameter correlations developed in this research significantly improve phase behavior predictions for n-alkane mixtures. Use of conventional correlations for critical parameters available in the literature results in larger AADs in density prediction and bubble-and dew-point predictions. The errors are more significant for heavier n-alkane mixtures using the conventional correlations.

- The critical parameters for n-alkanes developed provide useful initial values for characterization of reservoir oils using the PR EOS. Results showed that, when perturbation of P_C from the n-alkane values is used to match experimental data, resulting values for P_C are greater than the n-alkane values. This is because aromatic and naphthenic components have higher critical pressures than n-alkanes for a given carbon number group. The new set of T_C and P_C correlations for a homologous series of n-alkanes can serve as the lower bounds for T_C and P_C of pseudocomponents of reservoir fluids characterized using the PR EOS.

- The PR EOS with the critical parameters developed in this research exhibits improved predictive capability for oils lighter than 25°API, where concentrations of aromatic and naphthenic components are typically insignificant.

2.6. Nomenclature

Roman symbols

b	Covolume parameter in a cubic EOS
f	Perturbation factor defined in Section 2.4.2
m	$m(\omega)$ function in the PR EOS given in Equations 2-4 and 2-5
P	Pressure, bar
P_C	Critical pressure, bar
P_{CP}	Critical pressure for a paraffinic component, bar
P_r	Reduced pressure
P_r^{vap}	Reduced vapor pressure
T	Temperature, K
T_C	Critical temperature, K
T_r	Reduced temperature
v	Molar volume

Greek letters

$\alpha(T)$	Alpha function in the PR EOS
ω	Acentric factor

Abbreviations

AAD	Average absolute deviation
CN	Carbon number
EOS	Equation of state
MW	Molecular weight
NBP	Normal boiling point, K
PNA	Paraffins, naphthenes, and aromatics
PR	Peng-Robinson
SRK	Soave-Redlich-Kwong

2.7.   References

Ambrose, D. and Tsonopoulos, C. 1995. Vapor-Liquid Critical Properties of Elements and Compounds. 2. Normal Alkanes. *J. Chem. Eng. Data* **40** (3): 531-546.

Aucejo, A., Burguet, M.C., Muñoz, R. et al. 1995. Viscosities and Refractive Indices of Some n-Alkane Binary Liquid Systems at 298.15 K. *J. Chem. Eng. Data* **40** (1): 141-147.

Banipal, T.S., Garg, S.K., and Ahluwalia, J.C. 1991. Heat Capacities and Densities of Liquid n-Octane, n-Nonane, n-Decane, and n-Hexadecane at Temperatures from 318.15 K to 373.15 K and at Pressures up to 10 MPa. J. Chem. Thermodyn. **23** (10): 923-931.

Coats, K.H. and Smart, G. T. 1986. Application of a Regression Based EOS PVT Program to Laboratory Data. *SPE Res Eng* **1** (3): 277-299. SPE-11197-PA.

Cullick, A.S., Pebdani, F.N., and Griewank, A.K. 1989. Modified Corresponding States Method for Predicting Densities of Petroleum Reservoir Fluids. *Ind. Eng. Chem. Res.* **28** (3): 340-347.

Daridon, J.L., Carrier, H., and Lagourette, B. 2002. Pressure Dependence of the Thermophysical Properties of n-Pentadecane and n-Heptadecane. *Int. J. Thermophys*. **23** (3): 697-708.

Daubert, T.E., Danner, R.P., Sibel, H.M. et al. 1997. Physical and Thermodynamic Properties of Pure Chemicals: Data Compilation, Taylor & Francis, Washington, D.C., 1997.

DECHEMA Gesellschaft für Chemische Technik und Biotechnologie http://i-systems.dechema.de/detherm/mixture.php

Doolittle, A.K. 1964. Specific Volumes of n-Alkanes. *J. Chem. Eng. Data* **9** (2): 275-279.

Dutour, S., Daridon, J.L., and Lagourette, B. 2000. Pressure and Temperature Dependence of the Speed of Sound and Related Properties in Normal Octadecane and Nonadecane. *Int. J. Thermophys*. **21** (1): 173-184.

Dutour, S., Lagourette, B., and Daridon, J.L. 2001. High-Pressure Speed of Sound and Compressibilities in Heavy Normal Hydrocarbons: n-$C_{23}H_{48}$ and n-$C_{24}H_{50}$. *J. Chem. Thermodyn.* **33** (7): 765-774.

Dutour, S., Lagourette, B., and Daridon, J.L. 2002. High-pressure speed of sound, density and compressibility of heavy normal paraffins: $C_{28}H_{58}$ and $C_{36}H_{74}$. *J. Chem. Thermodyn*. **34** (4): 475-484.

Dykyj, J., Svoboda, J., Wilhoit, R. et al. 1997. Vapor Pressure of Chemicals. Landolt-Börnstein: Berlin, Sub-volume A.

Elizalde-Solis, O., Galicia-Luna, L.A., and Camacho-Camacho, L.E. 2007. High-Pressure Vapor–Liquid Equilibria for CO_2 + Alkanol Systems and Densities of n-Dodecane and n-Tridecane. *Fluid Phase Equilib*. **259** (1): 23-32.

Ewing, M.B. and Ochoa, J.C.S. 2005. Vapor Pressures of n-Heptane Determined by Comparative Ebulliometry. *J. Chem. Eng. Data* **50** (5): 1543-1547.

Gao, W., Robinson Jr., R.L., and Gasem, K.A.M. 2001. Improved Correlations for Heavy n-Paraffin Physical Properties. *Fluid Phase Equilib*. **179** (1-2): 207-216.

Goodwin, A.R., Bradsell, C.H., and Toczylkin, L.S. 1996. (p,ρ,T) of Liquid n-Octane Obtained with a Spherical Pycnometer at Temperatures of 298.03 K and 313.15 K and Pressures in the Range 0.7

MPa to 32 MPa. *J. Chem. Thermodyn*. **28** (6): 637- 646.

Gregorowicz, J., Kiciak, K., and Malanowski, S. 1987. Vapour Pressure Data for 1-Butanol, Cumene, n-Octane and n-Decane and Their Statistically Consistent Reduction with the Antoine Equation. *Fluid Phase Equilib*. **38** (1-2): 97-107.

J. D. van der Waals, Over de Continuiteit van den Gas-en Vloeistoftoestand, Ph.D. dissertation (excerpt), Leiden, The Netherlands, 1873.

Jhaveri, B.S. and Youngren, G.K. 1988. Three-Parameter Modification of the Peng-Robinson Equation of State to Improve Volumetric Predictions. *SPE J.* **3** (3): 1033-1040.

Joyce, P.C. and Thies, M.C. 1998. Vapor-Liquid Equilibria for the Hexane + Hexadecane and Hexane + 1-Hexadecanol Systems at Elevated Temperatures and Pressures. *J. Chem. Eng. Data* **43** (5): 819-822.

Joyce, P.C., Gordon, J., and Thies, M.C. 2000. Vapor−Liquid Equilibria for the Hexane + Tetracosane and Hexane + Hexatriacontane Systems at Elevated Temperatures and Pressures. *J. Chem. Eng. Data* **45** (3): 424-427.

Khasanshin, T.S. and Shchemelev, A.P. 2002. The Thermodynamic Properties of n-Tetradecane in Liquid State. *High Temp*. **40** (2): 207-211.

Klara, S.M. and Hemanth-Kumar, K. 1987. Comparisons of Computational Efficiencies of Different Equations of State and Transport Property Correlations in a Compositional Simulator. Presented at SPE Annual Technical Conference and Exhibition, Dallas, Texas, 27-30 September. SPE-16942-MS.

Krejbjerg, K. and Pedersen, K. S. 2006. Controlling VLLE Equilibrium with a Cubic EoS in Heavy Oil Modeling. Presented at Canadian International Petroleum Conference, Calgary, Alberta, 13-15 June. PETSOC-2006-052.

Kumar, A. and Okuno, R. 2014. Reservoir Oil Characterization for Compositional Simulation of Solvent Injection Processes. *Ind. Eng. Chem. Res.* **53** (1): 440-455.

Li, H. and Yang, D. 2011. Modified α Function for the Peng-Robinson Equation of State To Improve the Vapor Pressure Prediction of Non-hydrocarbon and Hydrocarbon Compounds. *Energy Fuels* **25** (1): 215-223

Mathias, P. M. 1983. A Versatile Phase Equilibrium Equation of State. *Ind. Eng. Chem., Process Des. Dev*. **22** (3): 385–391.

Melhem, G.A., Saini, R., and Goodwin, B.M. 1989. A Modified Peng-Robinson Equation of State. *Fluid Phase Equilib*. **47**: 189-237

Morgan, D.L. and Kobayashi, R. 1994. Direct Vapor Pressure Measurements of Ten n-Alkanes m the 10-C_{28} Range. *Fluid Phase Equilib*. **97**: 211-242.

Neau, E., Jaubert, J.N., and Rogalski, M. 1993. Characterization of Heavy Oils. *Ind. Eng. Chem. Res.* **32** (6): 1196-1203.

Nji, G.N., Svrcek, W.Y. and Yarranton, H. et al. 2008. Characterization of Heavy Oils and Bitumens. 1.

Vapor Pressure and Critical Constant Prediction Method for Heavy Hydrocarbons. *Energy Fuels* **22** (1): 455-462.

Nji, G.N., Svrcek, W.Y. and Yarranton, H. et al. 2009. Characterization of Heavy Oils and Bitumens 2. Improving the Prediction of Vapor Pressures for Heavy Hydrocarbons at Low Reduced Temperatures Using the Peng−Robinson Equation of State. *Energy Fuels* **23** (1): 366-373.

Okuno, R., Johns, R.T., and Sepehrnoori, K. 2011. Mechanisms for High Displacement Efficiency of Low-Temperature CO_2 Floods. *SPE J.* **16** (4): 751-767.

Patil, S., Dandekar, A., Khataniar, S. 2008. Project Report, DOE Award No. DE-FC26-01NT41248. http://www.osti.gov/bridge/purl.cover.jsp?purl=/963365-YrCq8p/963365.pdf.

Pedersen, K.S., and Christensen, P.L., 2007. Phase Behavior of Petroleum Reservoir Fluids. CRC Press, Taylor & Francis Group, Boca Raton, FL, USA.

Pedersen, K.S., Blilie, A.L., and Meisingset, K.K. 1992. Calculations on Petroleum Reservoir Fluids Using Measured and Estimated Compositional Data for the Plus Fraction. *Ind. Eng. Chem. Res.* **31** (5): 1378-1384.

Peneloux, A., Rauzy, E., and Fréze, R. 1982. A Consistent Correction for Redlich-Kwong-Soave Volume. *Fluid Phase Equilib*. **8** (1): 7-23.

Peng, D.-Y. and Robinson, D.B. 1976. A New Two-Constant Equation of State. *Ind. Eng. Chem. Fund.* **15** (1): 59-64.

Peng, D.-Y. and Robinson, D.B. 1978. The Characterization of the Heptanes and Heavier Fractions for the GPA Peng-Robinson Programs. *GPA Research Report RR-28*.

Perry, R.H. and Green, D.W. 2007. Perry's Chemical Engineers' Handbook, 8th Edition, The McGraw Hill Companies, Inc., New York, USA.

Peter, C.J., Spiegelaar, J., and   De Arons, J.S. 1988. Phase Equilibria in Binary Mixtures of Ethane + Docosane and Molar Volumes of Liquid Docosane. *Fluid Phase Equilib*. **41** (3): 245-256.

Peters, C.J., De Arons, J.S., Sengers, J.M.H.L. et al. 1988. Global Phase Behavior of Mixtures of Short and Long n-Alkanes. *AIChE J.* **34** (5): 834–839.

Poling, B.E., Prausnitz, J.M., and   O'Connell, J.P. 2001. The Properties of Gases and Liquids, The McGraw-Hill, New York, NY, 2001.

PVTsim, 20.0, 2011. CALSEP International Consultants, Copenhagen, Denmark.

Queimada, A.J., Marrucho, I.M., Coutinho, J.A.P. et al. 2005. Viscosity and Liquid Density of Asymmetric n-Alkane Mixtures: Measurement and Modeling. *Int. J. Thermophys.* **26** (1): 47-61.

Quiñones-Cisneros, S.E., Andersen, S.I., and Creek, J. 2005. Density and Viscosity Modeling and Characterization of Heavy Oils. *Energy Fuels* **19** (4): 1314-1318.

Quiñones-Cisneros, S.E., Dalberg, A., and Stenby, E.H. 2004b. PVT Characterization and Viscosity Modeling and Prediction of Crude Oils. *Pet. Sci. Technol.*, **22** (9-10): 1309–1325.

Quiñones-Cisneros, S.E., Zéberg-Mikkelsen, C.K., and Stenby, E.H. 2003. Friction Theory Prediction of Crude Oil Viscosity at Reservoir Conditions Based on Dead Oil Properties. *Fluid Phase Equilib*.

212 (1-2): 233–243.

Quiñones-Cisneros, S.E., Zéberg-Mikkelsen, C.K., Baylaucq, A. et al. 2004a. Viscosity Modeling and Prediction of Reservoir Fluids: From Natural Gas to Heavy Oils. *Int. J. Therm.* **25** (5): 1353-1366.

Rackett, H.G. 1970. Equation of State for Saturated Liquids. *J. Chem. Eng. Data* **15** (4): 514-517.

Riazi M.R. and Al-Sahhaf, T.A. 1996. Physical Properties of Heavy Petroleum Fractions and Crude Oils. *Fluid Phase Equilib.* **117** (1-2): 217-224.

Riazi, M.R. 2005. Manual 50, Characterization and Properties of Petroleum Fractions; ASTM International: West Conshohocken, PA.

Riazi, M.R. and AlQaheem, Y.S. 2010. Predicting Vapor Pressure of Heavy Hydrocarbons from Molar Refraction and Its Applications to Petroleum Mixtures. *Ind. Eng. Chem. Res.* **49** (15): 7104-7112.

Rodríguez, I. and Hamouda, A. A. 2008. An Approach for Characterization and Lumping of Plus Fractions of Heavy Oil. Presented at SPE International Thermal Operations and Heavy Oil Symposium, Calgary, 20-23 October. SPE-117446.

Schilling, G., Kleinrahm, R., and Wagner, W., 2008. Measurement and Correlation of the (p, ρ, T) Relation of Liquid n-Heptane, n-Nonane, 2,4-Dichlorotoluene, and Bromobenzene in the Temperature Range from (233.15 to 473.15) K at Pressures up to 30 MPa for Use as Density Reference Liquids. *J. Chem. Thermodyn*. **40** (7), 1095-1105.

Soave, G. 1972. Equilibrium Constants from a Modified Redlich-Kwong Equation of State. *Chem. Eng. Sci.* **27**:1197-1203.

Stryjek, R. and Vera, J. H. 1986. PRSV: An improved peng—Robinson equation of state for pure compounds and mixtures. *Can. J. Chem. Eng*. **64** (2): 323-333.

Susnar, S.S., Budziak, C.J., Hamza, H.A. et al. 1992. Pressure Dependence of the Density of n–Alkanes. *Int. J. Thermophys.* **13** (3), 443-452.

Ting, P.D., Joyce, P.C., Jog, P.K. et al. 2003. Phase Equilibrium Modeling of Mixtures of Long-Chain and Short-Chain Alkanes Using Peng–Robinson and SAFT. *Fluid Phase Equilib*. **206** (1-2), 267-286.

Voulgaris, M., Stamatakis, S. and Tassios, D. 1991. Prediction of Physical Properties for Non-Polar Compounds, Petroleum and Coal Liquid Fractions. *Fluid Phase Equilib*. **64**: 73-106.

Voutsas, E.C., Pappa, G.D., Magoulas, K. et al. 2006. Vapor Liquid Equilibrium Modeling of Alkane Systems with Equations of State: "Simplicity versus Complexity. *Fluid Phase Equilib.* **240** (2): 127-139.

Whitson, C.H. and Brulè, M.R. 2000. Phase Behaviour. SPE Henry L. Doherty Series, Vol. 20, SPE, Richardson, Texas.

Yaws, C.L. 2010. Yaws' Thermo Physical Properties of Chemicals and Hydrocarbons (Electronic Edition), Knovel, 2010.

Table 2-1. Uncertainties in experimental data that are used in our optimization in section 2.2		
n-Alkanes	Density Data Uncertainty	Vapor Pressure Data Uncertainty
C_7H_{16}	0.020 %	0.025 %
C_8H_{18}	0.036 %	±0.000066 bar
C_9H_{20}	0.020 %	0.200 %
$C_{10}H_{22}$	0.020 %	±0.000066 bar
$C_{11}H_{24}$	0.200 %	
$C_{12}H_{26}$	0.200 %	0.200 %
$C_{13}H_{28}$	±0.0002 (gm/cc)	
$C_{14}H_{30}$	0.100 %	±[0.0015P +0.000048] bar*
$C_{15}H_{32}$	0.100 %	
$C_{16}H_{34}$	±0.00003 (gm/cc)	±[0.0015P +0.000048] bar*
$C_{17}H_{36}$	0.200 %	
$C_{18}H_{38}$	0.100 %	±[0.0015P +0.000048] bar*
$C_{19}H_{40}$	0.100 %	±[0.0015P +0.000048] bar*
$C_{20}H_{42}$	0.200 %	±[0.0015P +0.000048] bar*
$C_{22}H_{46}$		±[0.0015P +0.000048] bar*
$C_{23}H_{48}$	0.100 %	
$C_{24}H_{50}$	0.100 %	±[0.0015P +0.000048] bar*
$C_{28}H_{58}$	0.070 %	±[0.0015P +0.000048] bar*
$C_{30}H_{62}$	0.200 %	
$C_{36}H_{74}$	0.070 %	
$C_{40}H_{82}$	0.200 %	
*Uncertainty is pressure dependent and is given as ±[0.0015P +0.000048] bar, where P is pressure in bar.		

Table 2-2. Coefficients in the correlations of Riazi and AlQaheem (2010) given in Equation 2-6.								
Carbon number	a_1	a_2	a_3	b_1	b_2	b_3	c_1	c_2
C_1-C_{50}	-3.0337	0.3265	-0.0018060	-1.0097	-0.2056	0.001702	4.0519	-0.1216
C_{51}-C_{100}	0.9948	0.1581	-0.0006864	-2.5795	-0.1275	0.0008085	1.5701	-0.03715

Table 2-3. AADs in density predictions for n-alkane mixtures using the PR EOS. AADs using Equations 2-11 to 2-13 developed in this research are compared to those using Equations 2-8 to 2-10 of Gao et al. (2001).

Components	No. of Data	Reference	AAD This Research	AAD Gao et al.
Heptane (C_7) + Octane (C_8)	11	Aucejo et al. (1995)	0.3	1.7
Heptane (C_7) + Nonane (C_9)	11	Aucejo et al. (1995)	0.7	2.9
Heptane (C_7) + Decane (C_{10})	11	Aucejo et al. (1995)	1.2	4.1
Heptane (C_7) + Undecane (C_{11})	11	Aucejo et al. (1995)	0.6	5.3
Heptane (C_7) + Dodecane (C_{12})	10	Aucejo et al. (1995)	1.7	6.5
Heptane (C_7) + Hexadecane (C_{16})	11	Aucejo et al. (1995)	3.1	12.6
Octane (C_8) + Nonane (C_9)	11	Aucejo et al. (1995)	0.9	3.8
Octane (C_8) + Decane (C_{10})	11	Aucejo et al. (1995)	1.2	4.8
Octane (C_8) + Undecane (C_{11})	11	Aucejo et al. (1995)	0.7	5.9
Octane (C_8) + Dodecane (C_{12})	11	Aucejo et al. (1995)	1.9	7.3
Octane (C_8) + Hexadecane (C_{16})	11	Aucejo et al. (1995)	3.2	12.8
Nonane (C_9) + Decane (C_{10})	11	Aucejo et al. (1995)	1.4	5.6
Nonane (C_9) + Undecane (C_{11})	11	Aucejo et al. (1995)	0.9	6.7
Nonane (C_9) + Dodecane (C_{12})	11	Aucejo et al. (1995)	1.9	7.8
Nonane (C_9) + Hexadecane (C_{16})	11	Aucejo et al. (1995)	3.3	15.2
Decane (C_{10}) + Undecane (C_{11})	11	Aucejo et al. (1995)	1.3	7.6
Decane (C_{10}) + Dodecane (C_{12})	11	Aucejo et al. (1995)	2.3	8.7
Decane (C_{10}) + Hexadecane (C_{16})	11	Aucejo et al. (1995)	3.4	13.5
Undecane (C_{11}) + Dodecane (C_{12})	11	Aucejo et al. (1995)	1.8	9.5
Undecane (C_{11}) + Hexadecane (C_{16})	11	Aucejo et al. (1995)	3.0	14.1
Dodecane (C_{12}) + Hexadecane (C_{16})	11	Aucejo et al. (1995)	3.7	14.7
Decane (C_{10}) + Eicosane (C_{20})	24	Queimada et al. (2005)	4.2	18.0
Decane (C_{10}) + Docosane (C_{22})	20	Queimada et al. (2005)	4.6	20.7
Decane (C_{10}) + Tetracosane (C_{24})	16	Queimada et al. (2005)	4.9	23.5
Decane (C_{10}) + Docosane (C_{22}) + Tetracosane (C_{24})	23	Queimada et al. (2005)	4.8	21.8

Table 2-4. Comparisons of density predictions using the correlations developed in this research (Equations 2-11 to 2-13) and those using the correlations of Quiñones-Cisneros et al. (Equations 2-14 to 2-16). Volume shift parameters are not used for these comparisons.

Oils	API Gravity*	Molecular Weight	No. of Data	Reference	Perturbation Factor[#]	AAD [%][§]
Oil-1	60.18	86.57	13	Quiñones-Cisneros et al. (2004b)	1.1201(1.2655)	4.8(7.8)
Oil-6	55.73	83.31	20	Coats and Smart (1986)	1.2639(1.4330)	12.0(14.9)
Oil-2	47.63	89.83	11	Quiñones-Cisneros et al. (2004b)	1.3033(1.4537)	13.3(16.2)
Oil-7	47.09	113.60	20	Coats and Smart (1986)	1.2064(1.3515)	7.2(10.0)
Light Oil	43.68	105.26	7	Cullick et al. (1989)	1.2158(1.3424)	5.8(7.5)
Oil-3	40.46	87.80	5	Quiñones-Cisneros et al. (2004b)	1.4226(1.6044)	18.2(22.1)
Fluid-1	35.73	124.57	8	Pedersen et al. (1992)	1.3327(1.4845)	12.6(16.6)
Oil-6	35.67	118.18	5	Quiñones-Cisneros et al. (2004b)	1.2828(1.4482)	7.7(11.7)
Oil-3	34.24	114.65	12	Quiñones-Cisneros et al. (2003)	1.4056(1.5612)	15.7(18.9)
Oil-1	34.04	123.79	8	Coats and Smart (1986)	1.3869(1.5594)	12.5(16.1)
Oil-4	33.35	114.57	6	Quiñones-Cisneros et al. (2004b)	1.3827(1.5497)	14.6(19.0)
Oil-7	29.24	159.99	16	Quiñones-Cisneros et al. (2004b)	1.2658(1.4123)	5.0(9.4)
Oil-5	28.90	130.55	3	Quiñones-Cisneros et al. (2004b)	1.3984(1.5610)	14.3(18.8)
Oil†	22.60	296.90	13		1.0697(1.1659)	10.2(8.2)
Oil-4	25.70	167.03	11	Quiñones-Cisneros et al. (2003)	1.4204(1.5624)	14.0(16.9)
Oil-8	24.25	182.05	16	Quiñones-Cisneros et al. (2004b)	1.3625(1.5149)	9.3(13.6)
Oil-1	20.81	170.59	16	Quiñones-Cisneros et al. (2004a)	1.2869(1.4230)	7.3(10.9)
Oil-5	20.19	240.24	15	Quiñones-Cisneros et al. (2003)	1.3031(1.4217)	1.9(3.7)
Oil-G	17.01	237.92	12	Patil et al. (2008)	1.5368(1.7087)	17.9(23.1)
Oil-H	13.84	232.17	15	Patil et al. (2008)	1.3395(1.4655)	2.1(4.6)
Oil-6	13.38	377.88	13	Quiñones-Cisneros et al. (2004a)	1.0126(1.0943)	21.6(20.3)
Oil-5	11.98	422.94	13	Quiñones-Cisneros et al. (2004a)	1.1124(1.1970)	14.7(13.7)
Oil-7	11.63	431.59	12	Quiñones-Cisneros et al. (2005)	1.0854(1.1671)	16.9(15.9)
Heavy Oil	10.00	421.35	8	Krejbjerg and Pedersen (2006)	1.6511(1.7762)	24.9(26.4)
Oil-8	9.50	443.06	13	Quiñones-Cisneros et al. (2005)	1.1255(1.2089)	15.1(14.2)

Total number of data = 291
Overall AAD for this research =11.20%
Overall AAD for Quiñones-Cisneros et al. = 13.48%

*API gravity calculated except for Oil† and Heavy Oil.
†This is an actual oil, but the source is not mentioned due to confidentiality.
[#] Number inside brackets shows the perturbation factor from Quiñones-Cisneros et al.
[§] Number inside brackets shows the AAD from Quiñones-Cisneros et al.
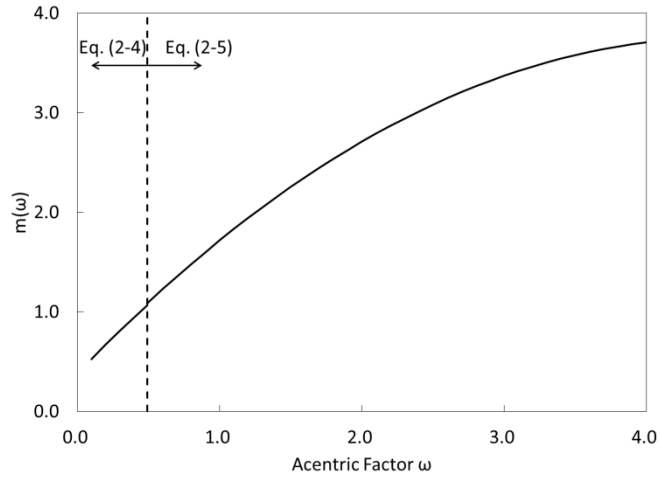
Figure 2-1. The m(ω) function for the Peng-Robinson EOS as defined in Equations 2-4 and 2-5.
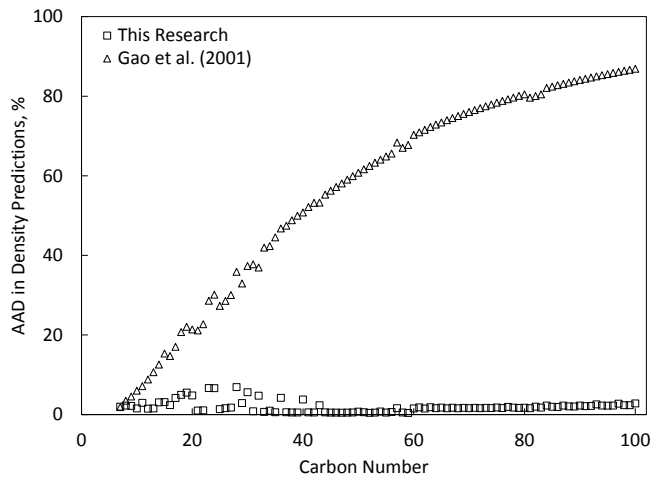
Figure 2-2. Average absolute deviation (AAD) in density predictions for n-alkanes from C_7 to C_{100} using the correlations developed in this research and the correlations of Gao et al. (2001).
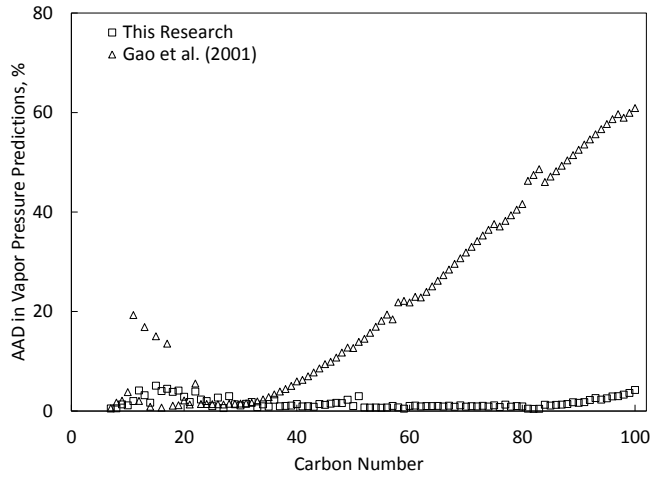
Figure 2-3. Average absolute deviation (AAD) in vapor pressure predictions for n-alkanes from C_7 to C_{100} using the correlations developed in this research and the correlations of Gao et al. (2001).
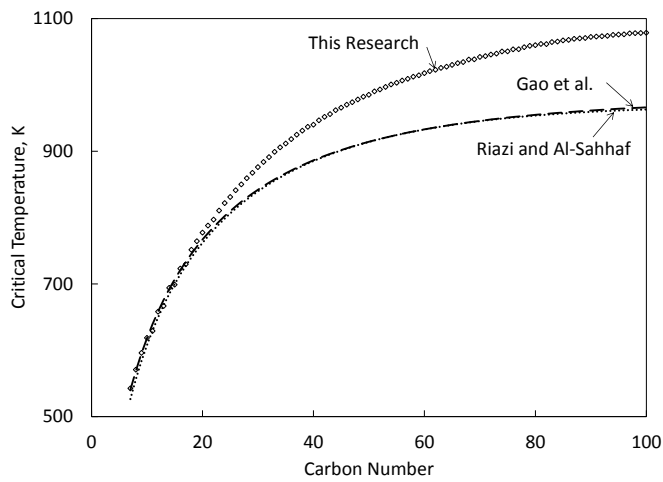
Figure 2-4. Optimum critical temperature (T_C) developed for the PR EOS in this research, and the T_C correlations of Gao et al. (2001) and Riazi and Al-Sahhaf (1996).
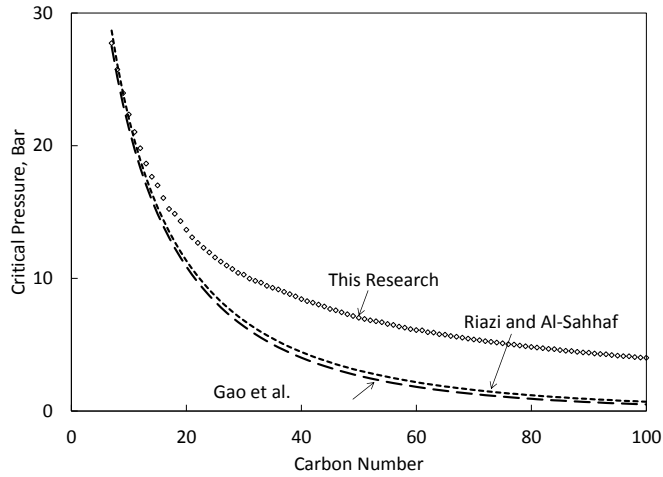
Figure 2-5. Optimum critical pressure (P_C) developed for the PR EOS in this research, and the P_C correlations of Gao et al. (2001) and Riazi and Al-Sahhaf (1996).
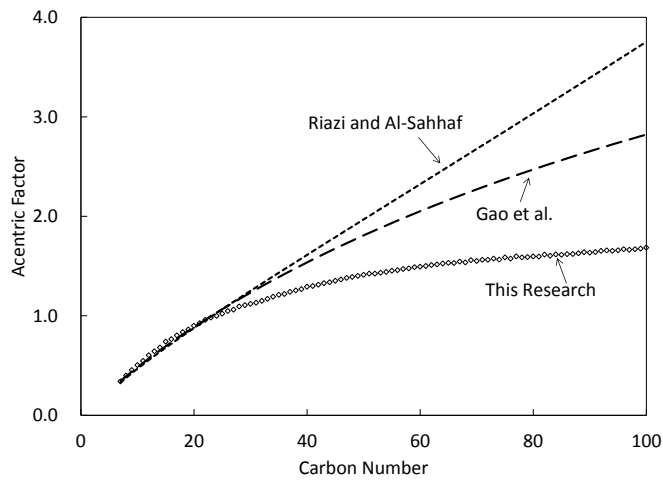
Figure 2-6. Optimum acentric factor (ω) developed for the PR EOS in this research, and the ω correlations of Gao et al. (2001) and Riazi and Al-Sahhaf (1996).
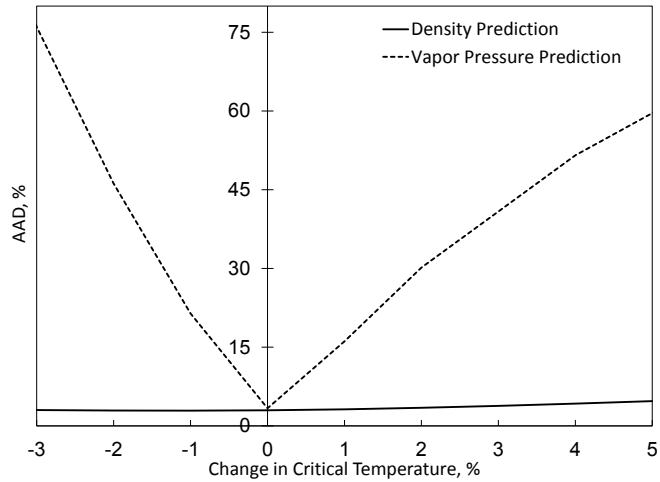
Figure 2-7. Sensitivity of density and vapor pressure predictions to T_C around the optimum values given in Equation 2-11.
The 0% change in T_C corresponds to use of Equation 2-11, which gives a minimum in the sum of the AADs in density and vapor pressure predictions.
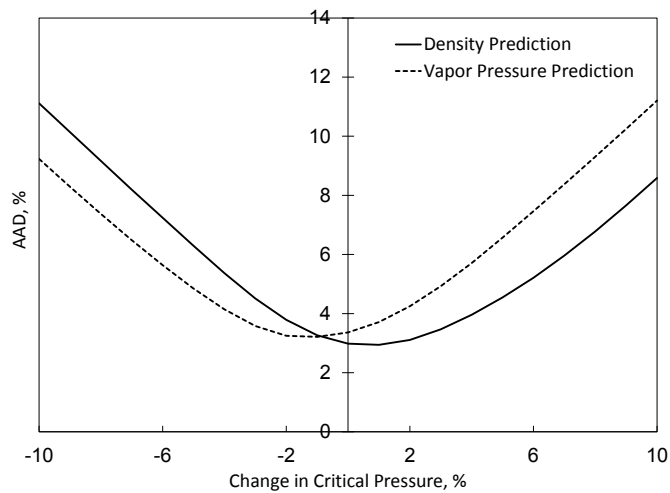
Figure 2-8. Sensitivity of density and vapor pressure predictions to PC around the optimum values given in Equation 2-12.
The 0% change in PC corresponds to use of Equation 2-12, which gives a minimum in the sum of the AADs in density and vapor pressure predictions.
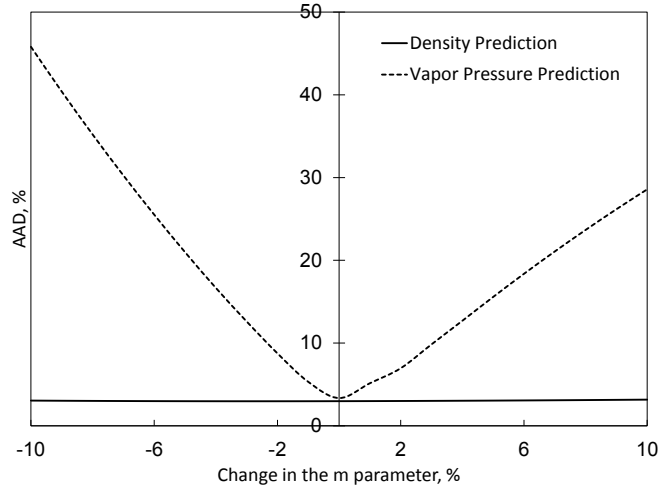
Figure 2-9. Sensitivity of density and vapor pressure predictions to the m parameter around the optimum values given in Equation 2-13.

The 0% change in m corresponds to use of Equation 2-13, which gives a minimum in the sum of the AADs in density and vapor pressure predictions.
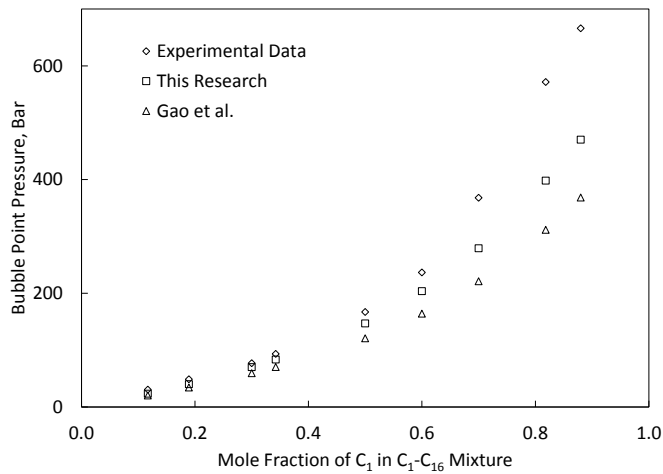
Figure 2-10. Comparison of bubble point pressure predictions with experimental data (Peters et al. 1988) for C_1-C_{16} mixtures at 300 K.

For the predictions, the PR EOS is used with the critical parameters developed in this research and those by Gao et al. (2001).
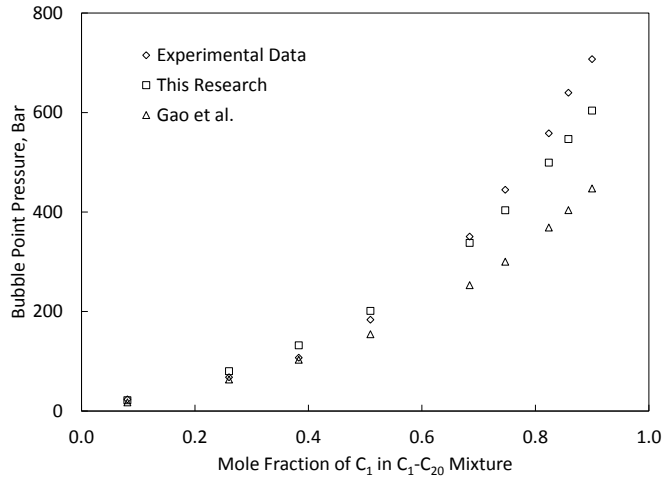
Figure 2-11. Comparison of bubble point pressure predictions with experimental data (Peters et al. 1988) for C_1-C_{20} mixtures at 363.15 K.
For the predictions, the PR EOS is used with the critical parameters developed in this research and those by Gao et al. (2001).
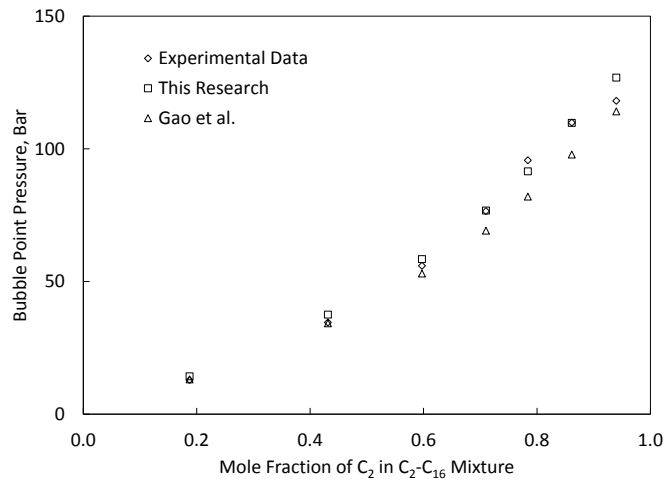
Figure 2-12. Comparison of bubble point pressure predictions with experimental data (Peters et al. 1988) for C_2-C_{16} mixtures at 363.15 K.
For the predictions, the PR EOS is used with the critical parameters developed in this research and those by Gao et al. (2001).
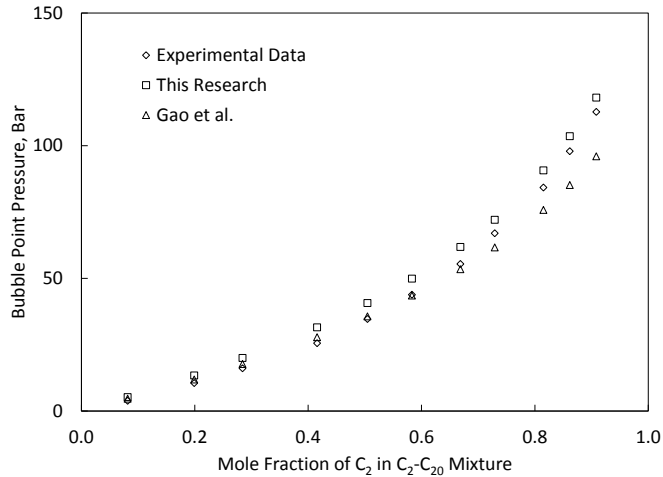
Figure 2-13. Comparison of bubble point pressure predictions with experimental data (Peters et al. 1988) for C_2-C_{20} mixtures at 350 K.
For the predictions, the PR EOS is used with the critical parameters developed in this research and those by Gao et al. (2001).
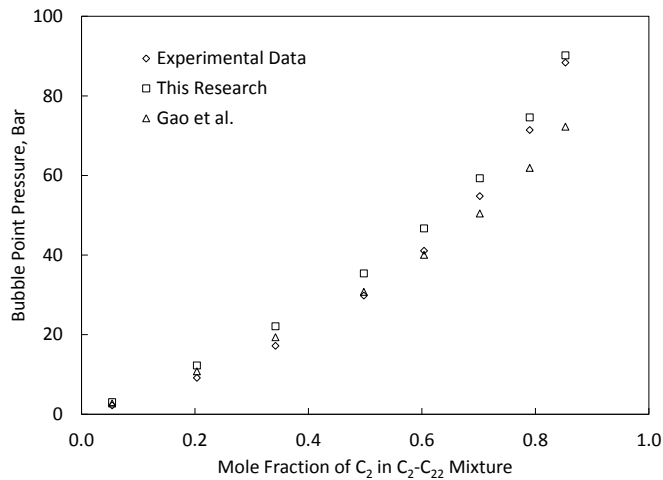
Figure 2-14. Comparison of bubble point pressure predictions with experimental data (Peters et al. 1988) for C_2-C_{22} mixtures at 340 K.
For the predictions, the PR EOS is used with the critical parameters developed in this research and those by Gao et al. (2001).
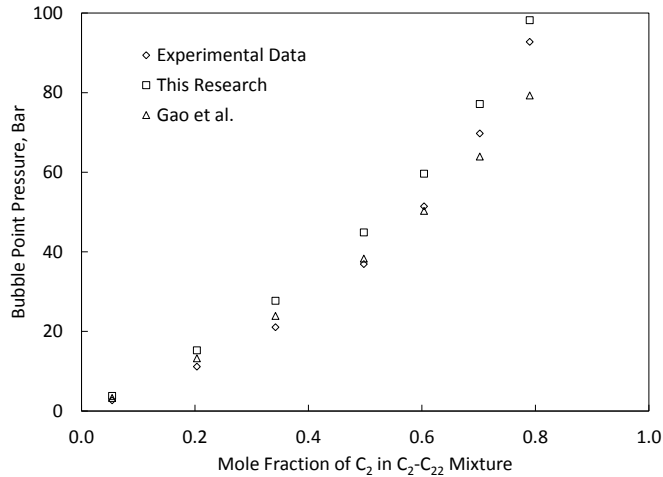
Figure 2-15. Comparison of bubble point pressure predictions with experimental data (Peters et al. 1988) for C_2-C_{22} mixtures at 360 K.
For the predictions, the PR EOS is used with the critical parameters developed in this research and those by Gao et al. (2001).
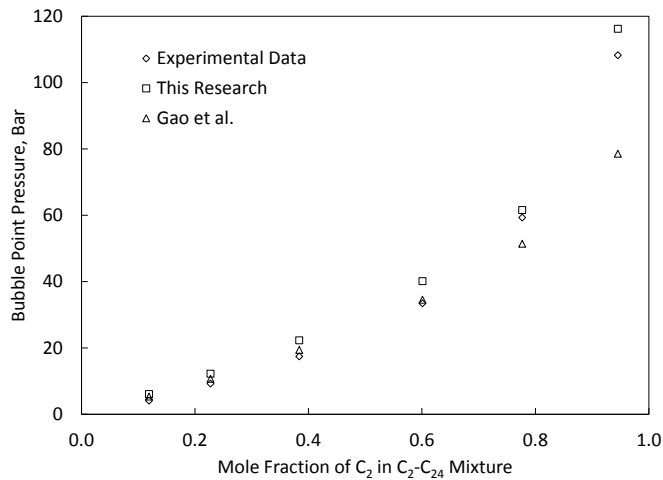
Figure 2-16. Comparison of bubble point pressure predictions with experimental data (Peters et al. 1988) for C_2-C_{24} mixtures at 330 K.
For the predictions, the PR EOS is used with the critical parameters developed in this research and those by Gao et al. (2001).
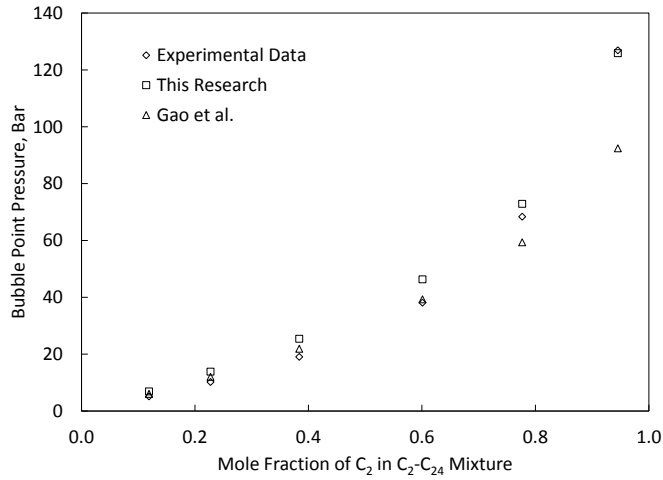
Figure 2-17. Comparison of bubble point pressure predictions with experimental data (Peters et al. 1988) for C_2-C_{24} mixtures at 340 K.

For the predictions, the PR EOS is used with the critical parameters developed in this research and those by Gao et al. (2001).
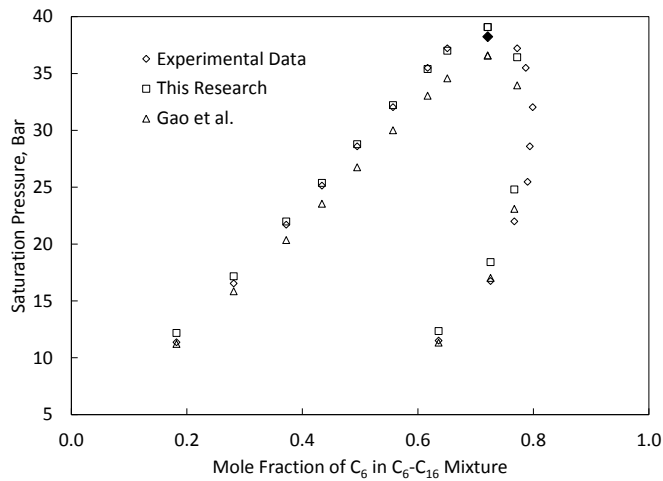
Figure 2-18. Comparison of bubble and dew point predictions with experimental data (Joyce and Thies 1998) for C_6-C_{16} mixture at 623K.

The critical point is given as ♦. For the predictions, the PR EOS is used with the critical parameters developed in this research and those by Gao et al. (2001).
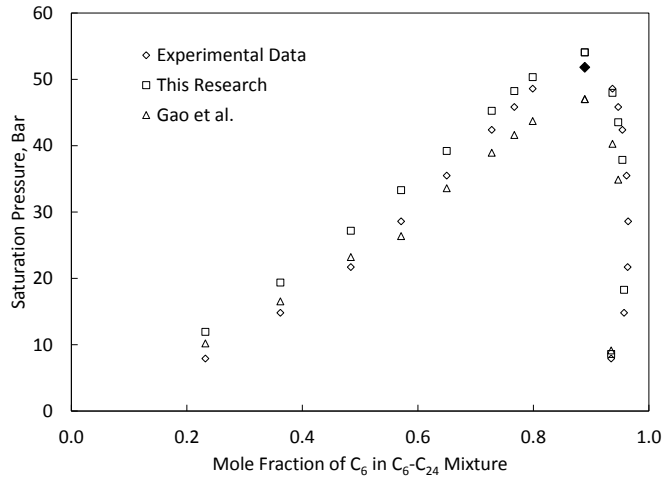
Figure 2-19. Comparison of bubble and dew point predictions with experimental data (Joyce et al. 2000) for C_6-C_{24} mixture at 622.9K.
The critical point is given as ♦. For the predictions, the PR EOS is used with the critical parameters developed in this research and those by Gao et al. (2001).
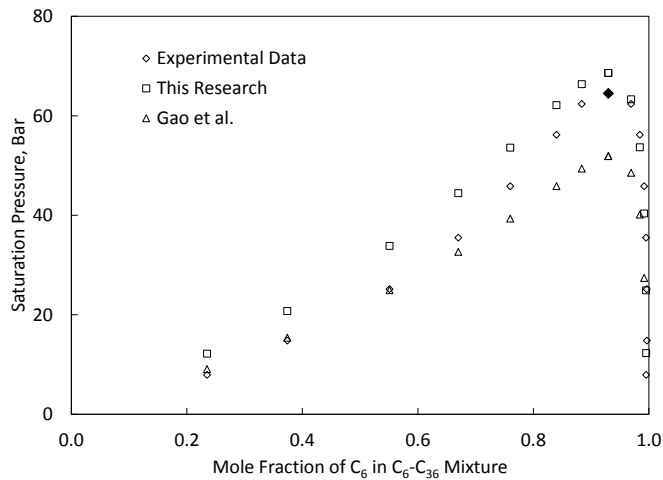
Figure 2-20. Comparison of bubble and dew point predictions with experimental data (Joyce et al. 2000) for C_6-C_{36} mixture at 621.8K.
The critical point is given as ♦. For the predictions, the PR EOS is used with the critical parameters developed in this research and those by Gao et al. (2001).
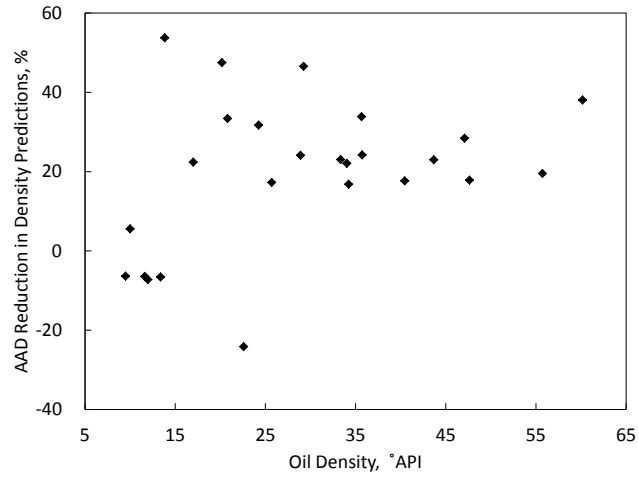
Figure 2-21. AAD reduction in density predictions for 25 different reservoir oils listed in Table 2-3. AAD reduction in density predictions is defined as AAD using Equations 2-14 to 2-16 less AAD using Equations 2-11 to 2-13 divided by AAD using Equations 2-14 to 2-16.

Chapter 3: Reservoir Oil Characterization for Compositional Simulation of Solvent Injection Processes

3.1. Introduction

Solvent methods for enhanced oil recovery and heavy-oil recovery have been studied and implemented in oil fields (e.g., Mohanty et al. 1995; DeRuiter et al. 1994). Various steam/solvent coinjection schemes are also proposed in the literature (Hornbrook et al. 1991; Nasr et al. 2003; Gupta et al. 2003; Li et al. 2011; Gate and Chakrabarty 2008) to improve efficiency of the conventional steam-assisted gravity drainage. Reliable design of such oil recovery processes requires compositional reservoir simulation to model mass transfer among phases using a cubic equation of state (EOS).

Cubic EOSs are widely used in the petroleum industry to model volumetric and compositional phase behavior of conventional oils. The most widely used cubic EOSs are the Peng-Robinson (PR) EOS (Peng and Robinson 1976, 1978) and the Soave-Redlich-Kwong (SRK) EOS (Soave 1972). These EOSs together with the van der Waals mixing rules are suitable for computationally efficient representation of vapor-liquid equilibrium for hydrocarbon mixtures at a wide range of pressures (Okuno et al. 2010).

However, application of these EOSs for modeling heavy-oil recovery is not straightforward. For heavy-oil recovery, a typical operation range in pressure-temperature-composition (P-T-x) space is much wider than that for enhanced recovery of conventional oil. When steam and solvent are coinjected for heavy-oil recovery, reservoir temperatures lie between an initial reservoir temperature and steam temperatures; e.g., between 290 K and 530 K for a typical solvent-steam-assisted gravity drainage. Also, mixtures of solvent and heavy oils are highly size-asymmetric, resulting in a wider variety of composition conditions. The wide operation range in P-T-x space provides technical challenges for the traditional use of cubic EOSs with the van der Waals mixing rules.

Fluid characterization using an EOS is conducted based on experimental data available, which typically consist of composition analysis and pressure-volume-temperature (PVT) data. However, it can be difficult to take reliable downhole fluid samples for heavy oil (Memon et al. 2010; Zabel et al. 2010). Even when a reliable sample is available for a heavy oil, its detailed composition is uncertain because of high concentrations of non-identifiable compounds. Availability of experimental data in P-T-x space, especially at different composition conditions, is often limited for heavy oil mainly because of its high viscosity and highly uncertain composition. Laboratory measurements are performed at certain P-T-x conditions. It is difficult to measure phase behavior along the compositional path for a given solvent injection in the laboratory. Use of a reliable fluid characterization method is as important as use of reliable experimental data to predict phase behavior during solvent injection processes in compositional simulation. Heavy-oil PVT data that are measurable include saturation pressures (P_{SAT}) and densities at different conditions. It is not unusual that they are the only reliable PVT data for a heavy oil.

Characterization of conventional oils using an EOS has been developed, and implemented in commercial software (Whitson and Brulè 2000; Pedersen and Christensen 2007). A typical characterization process consists of four main steps as follows:

Step 1. Estimation of a molar distribution with respect to molecular weight (MW) or carbon number (CN) to split the plus fraction (e.g., C_{7+}) into detailed components.

Step 2. Estimation of properties for the detailed components such as critical temperature (T_C), critical pressure (P_C), critical volume (V_C), acentric factor (ω), and volume-shift parameters.

Step 3. Grouping of the detailed components into fewer pseudocomponents.

Step 4. Regression of pseudocomponents' properties to match experimental data available.

In step 1, a distribution function is fitted to the composition analysis data available. Forms of distribution functions proposed in the literature include the gamma (Whitson 1983), chi-squared (Quiñones-Cisneros et al. 2003), and logarithmic distributions (Pedersen et al. 1983, 1984). The gamma distribution is the most general form among the three, and reduces to the other two when certain assumptions are used. The logarithmic distribution is a widely used form for conventional oil characterization, where composition analysis can provide composition information for a large fraction of the fluid. Heavy oils often require more flexible distribution functions, like the gamma and chi-squared ones, to match their composition analysis data (Ghasemi et al. 2011). Regardless of the type of the distribution function used, however, the reliability of the resulting molar distribution depends primarily on how much uncertainty is left as a plus fraction in composition analysis.

Step 2 uses correlations to estimate properties of the split components because critical properties measured for hydrocarbons heavier than C_{24} are not available (Ambrose and Tsonopoulos 1995). These correlations include Cavett (1962), Edmister (1958), Kesler and Lee (1976), Riazi and Al-Sahaff (1996), Korsten (2000), Riazi and Daubert (1980, 1987), Twu (1984), and Lee and Kesler (1975). The correlations of Pedersen et al. (1989, 1992, 2004) are functions of MW and density at atmospheric conditions, which are in turn functions of CN. These correlations are developed for an EOS to reproduce vapor pressures and the critical point for the pseudocomponent of a given CN. However, the PR and SRK EOSs with these correlations cannot accurately model densities of heavy hydrocarbons unless volume-shift parameters (Peneloux et al. 1982; Jhaveri and Youngren 1988) are used. Krejbjerg and Pedersen (2006) developed new correlations for T_C, P_C, and ω for heavy-oil characterization. Their correlations do not attempt to model three-hydrocarbon-phase behavior, although such phase behavior often occurs for highly asymmetric mixtures of heavy oil with solvent (Polishuk et al. 2004).

Step 3 reduces the number of components used in the fluid model and calculates properties of each pseudocomponent by averaging over its member components. Use of fewer components can make EOS calculations more efficient, but it can also result in erroneous predictions of phase behavior due to reduced dimensionality in composition space. Common grouping procedures in the literature include the ones of Pedersen et al. (1984) and Whitson and Brulè (2000). The former uses the equal mass grouping with mass-weighted averaging of properties, while the latter uses the Gaussian quadrature grouping method with mole-weighted averaging.

In the equal mass grouping approach, detailed split components are grouped into fewer pseudocomponents that have an approximately same mass. The critical properties for a

56

pseudocomponent are estimated by taking the mass-weighted average of the critical properties of member components for that pseudocomponent. In the Gaussian quadrature grouping method of Whitson and Brulè (2000), each pseudocomponent has a wider range of molecular weights, and a component may be present in multiple pseudocomponents (Pedersen and Christensen 2007). Representative critical properties for a pseudocomponent are estimated by taking the mole-weighted average of critical properties of member components for that pseudocomponent. Jørgensen and Stenby (1995) conducted a comparative study of 12 different grouping methods and concluded that it was difficult to single out the best grouping method.

As mentioned before, simulation of solvent methods for heavy-oil recovery requires reliable representation of phase behavior at a wide range of composition conditions. Therefore, a reliable fluid model for solvent/heavy-oil mixtures often requires more components than that for solvent/conventional-oil mixtures.

Step 4 is often needed because each of steps 1-3 makes certain assumptions resulting in deviations of predictions from actual phase behavior. Regression procedures for conventional oil characterization are discussed in detail in Whitson and Brulè (2000), and Pedersen and Christensen (2007). Typical parameters adjusted in this step include T_C, P_C, ω, volume-shift parameters, and binary interaction parameters (BIPs) for pseudocomponents. The constant terms of the attraction and covolume parameters of a cubic EOS, Ω_a and Ω_b, are sometimes adjusted, but this is not recommended as explained by Wang and Pope (2001). These adjustment parameters offer flexibility that may be required to match various types of PVT data such as P_{SAT}, constant mass expansion, constant volume depletion, differential liberation, separator tests, swelling tests, minimum miscibility pressures, and viscosity data. Different EOS fluid models can result depending on which parameters are adjusted and how much they are adjusted (Lolley and Richardson 1997).

As described above, each of steps 1-4 is more difficult for heavy oil than for conventional oil. The main reason for the difficulties is that heavy-oil characterization is conducted under high uncertainties in oil composition, components' properties (e.g., T_C, P_C, and ω), and phase behavior in P-T-x space. Also, considering direct use of EOS fluid models in compositional simulation, it is undesirable that modeling heavy-oil/solvent mixtures often requires many components to accurately model their phase behavior.

In this research, a new characterization method is developed for simulation of enhanced oil recovery and heavy-oil recovery. The uncertainty issues discussed above are addressed by incorporating physical observations into our procedures for critical parameter estimation, step 2, and regression, step 4. Since density data are easier to obtain than composition data, our method effectively uses density data to improve phase behavior predictions in P-T-x space; i.e., volume-shift parameters are not required in our characterization method. In the following section, the conventional characterization method used in this research is defined. We then present a new characterization method and its application to 22 different reservoir oils. Comparisons are made between the new and conventional

57

characterization methods in terms of phase behavior predictions in P-T-x space for actual reservoir oils and their mixtures with solvents.

3.2. Conventional Characterization Method Used in This Research

The conventional characterization method used in this research is based mainly on Pedersen and Christensen (2007) and Wang and Pope (2001). The method of Pedersen and Christensen (2007) has been implemented in the PVTsim software of Calsep (2011). Descriptions are given below for the conventional characterization steps 1-4 (see the introduction section for the definitions of the steps). All characterizations in this research assume that PVT data available include the oil composition, the oil P_{SAT} at the reservoir temperature, and liquid densities and viscosities at different pressures at the reservoir temperature. All EOS calculations in this research use the PR EOS, **Equation 3-1** to **3-3**, with the van der Waals mixing rules.

$$p = \frac{RT}{v-b} - \frac{a_c\alpha(T)}{v^2+2bv-b^2} ,$$ (3-1)

where $a_c = 0.457235529 \frac{(RT_c)^2}{P_c}$

$$\sqrt{\alpha(T)} = \left[1 + m\left(1 - \left(\frac{T}{T_c}\right)^{0.5}\right)\right]$$

$m = 0.37464 + 1.54226\omega - 0.26992\omega^2$ for $\omega < 0.49$ (3-2)

$m = 0.379642 + 1.48503\omega - 0.164423\omega^2 + 0.016666\omega^3$ for $\omega \geq 0.49$ (3-3)

Step 1 of the conventional method assumes a logarithmic distribution for splitting a plus fraction. In step 2, critical properties, such as T_C, P_C, and ω, are estimated using Krejbjerg and Pedersen (2006). Step 3 uses the equal-mass grouping with mass-weighted averaging of properties.

Although there is no well-defined regression scheme for step 4 due to its high flexibility in the conventional method, **Figure 3-S1** in the supporting information depicts the conventional regression scheme used in this research, which is based on Pedersen and Christensen (2007) and Christensen (1999). Adjustments are made for T_C, P_C, and ω of pseudocomponents to match the P_{SAT} at the reservoir temperature. Adjustment parameters are selected based on their sensitivities to P_{SAT} calculation (Voulgaris et al. 1991).

After matching the P_{SAT}, density data at different pressures at the reservoir temperature are matched. We consider two options here; one is to adjust T_C, P_C, and ω, and the other to adjust volume-shift parameters (the temperature independent C_{PEN} parameters in the PVTsim software). The second option is widely used in the literature. In this paper, the conventional methods with the first option and with the second option are referred to as the $CM_{w/o}V$ and CM_wV, respectively. The $CM_{w/o}V$ and CM_wV are collectively called the CM. The CM_wV will be compared with our new method (NM) developed in the next section, both with 11 components. The $CM_{w/o}V$ will be used with 30 components to generate pseudodata for the comparisons. The regression step confirms that T_C and P_C have physically correct trends with respect to MW; i.e., T_C monotonically increases and P_C monotonically decreases with increasing MW. V_C for pseudocomponents are also adjusted to match viscosity data using the Lohrenz-

Bray-Clark (LBC) model (Lohrenz et al. 1964). BIPs are not adjusted in this research. These two notes also apply for the NM described in the next section.

The PVTsim software is used as part of the CM because its flexibility enables to apply the most prevalent characterization procedure in the literature (see Figure 3-S1 in the supporting information). It requires step-wise manual adjustment of parameters based on engineering judgments, which can be done with PVTsim. In the CM, T_C, P_C, and ω for each pseudocomponent are tuning parameters. For example, use of four pseudocomponents results in 12 adjustment parameters. Parameter values resulting from a regression process depend on the weights assigned to sets of experimental data, the ranges of variation allowed for parameters, and the order of parameter adjustments. Special care must be taken by experienced engineers to ensure smooth and physically justifiable curves for T_C, P_C, and ω with respect to MW. Automated robust characterization is possible when the automatic regression keeps physically justifiable trends of parameters, which is achieved in the NM as will be discussed. Note that the NM also satisfies Pitzer (1955) and Pitzer et al. (1955)'s definition of acentric factor for each component.

3.3.   New Characterization Method Based on Perturbation from n-Alkanes

The new characterization method (NM) developed in this section addresses two major issues that the CM can pose when applied for heavy-oil characterization. These issues, which are described below, come essentially from the fact that heavy-oil characterization must be conducted under high uncertainties in oil composition, components' properties (e.g., T_C, P_C, and ω), and phase behavior in P-T-x space. In the following subsections, we first describe the issues of the CM. Our development of the NW is then presented in detail.

3.3.1. Issues of the Conventional Method

One of the two major issues is in step 2, estimation of pseudocomponents' properties. Conventional correlations for pseudocomponents' properties in the literature are typically functions of two parameters; e.g., MW and specific gravity. The fundamental reason for use of two types of parameters is that a CN group contains a wide variety of compounds. One way to categorize hydrocarbon compounds is paraffins, naphthenes, and aromatics (PNA). T_C and P_C of paraffins are in general lower than those of aromatics within a given CN group (Kumar and Okuno 2012). The trend is the other way around for ω. That is, one of the two parameters, specific gravity, is required to consider the effects of a PNA distribution within a CN group on critical properties of the CN group. However, specific gravities of pseudocomponents in a plus fraction are unknown. They are then estimated using a function of CN in Pedersen and Christensen (2007). In this way, a certain PNA distribution is implicitly assumed in the CM for property estimation, and the PNA distribution assumed is not well defined for users.

The PNA distribution implicitly set is coupled with a shortcoming of cubic EOSs in the CM. That is, even when T_C, P_C, and ω of a well-defined hydrocarbon (e.g., a n-alkane compound) are given, cubic EOSs are inaccurate in predicting its liquid densities unless a volume-shift parameter is used (Ting et

al. 2003; Voutas et al. 2006; Yakoumis et al. 1997). This shortcoming of cubic EOSs is more serious for heavier hydrocarbons (Kumar and Okuno 2012). Regression in step 4 then attempts to decrease errors caused by the coupled problem mentioned above, where adjustments of T_C, P_C, and ω must be performed with little justification in a physical sense.

Another major issue addressed in this research is the separation of volumetric and compositional behaviors using volume-shift parameters in the CM_wV. For heavy oil, available experimental data are mostly volumetric ones, instead of compositional ones. Volume-shift parameters are typically needed when the CM is used with a small number of components to match heavy-oil density data. In such a case, compositional behavior predictions of the resulting fluid model depend significantly on how much one relies on volume-shift parameters to match density data.

Thermodynamically, however, volumetric phase behavior, including densities, is a consequence of compositional phase behavior; i.e., compositional and volumetric phase behaviors should not be modeled separately. Density data for a given fluid contain its composition information. The CM_wV does not effectively use density data to improve compositional phase behavior predictions. Although composition analysis is often difficult for heavy oils, density data can supplement compositional data for heavy-oil characterization by minimizing use of volume-shift parameters. Thus, our NM does not use volume-shift parameters, which can also reduce the number of adjustment parameters. Section 3-S2 in the supporting information presents the effects of volume shift parameters on the Gibbs free energy when used as regression parameters in reservoir oil characterization.

3.3.2. Characterization Steps in the New Method

The most important novelties of the NM lie in steps 2 and 4 as will be described below. For steps 1 and 3, the NM is based on Quiñones-Cisneros et al. (2003. 2004a, 2004b, 2005); i.e., the chi-squared distribution is used for step 1, and the equal-mass grouping with mass-weighted averaging of properties is used for step 3.

Step 2, estimation of T_C, P_C, and ω for pseudocomponents, in the NM is based on the correlations of Kumar and Okuno (2012). The PR EOS with the correlations gives accurate predictions of liquid densities and vapor pressures for n-alkanes from C_7 to C_{100} without using volume-shift parameters. These correlations were developed using the optimized critical parameters and *m* parameters for the PR EOS for n-alkanes from C_7 to C_{100}. The optimized critical values do not represent the physical critical points. In reservoir oil characterization, however, physical critical points of pseudocomponents are not well defined at first. Only n-alkane compounds can form a well-defined homologous hydrocarbon series. There are sufficient experimental data for the homologous series of n-alkane compounds in the literature, which were used in Kumar and Okuno (2012).

The NM considers a PNA distribution of a plus fraction as perturbation from a limiting distribution of 100% n-alkanes. Considering the trends of T_C, P_C, and ω with respect to the PNA distribution, T_C and P_C of a pseudocomponent should be higher than the n-alkane values from the correlations of Kumar and Okuno (2012). Similarly, ω of a pseudocomponent should be lower than the n-alkane values. The

amounts of perturbations in T_C, P_C, and ω from the n-alkane values are related to the concentration of components other than n-alkanes, especially aromatic components, in the plus fraction. Step 2 of the NM combines the perturbation concept and the correlations of Kumar and Okuno (2012) as given in **Equations 3-4, 3-5, and 3-6.**

$$T_c = 1154.35 - 844.83(1.0 + 1.7557 \times 10^{-3} f_T MW)^{-2.0} \tag{3-4}$$

$$P_c = 559.93 \left(\frac{MW}{f_P}\right)^{-0.638} - 1.49 \tag{3-5}$$

$$m = 0.4707 + 2.4831(f_m\ MW)^{-\left(\frac{39.933}{f_m\ MW}\right)} \tag{3-6}$$

The *m* parameter in Equation 3-6 is defined in Equations 3-2 and 3-3 as a one-to-one function of ω. The perturbation factors for T_C, P_C, and *m* are expressed as f_T, f_P, and f_m, respectively. These perturbations are qualitative deviation of pseudocomponents from n-alkane behavior. The perturbed values are valid only with the cubic EOS used. Equations 3-4 to 3-6 reduce to the correlations of Kumar and Okuno (2012) for n-alkanes when the perturbation factors are 1.0. As a pseudocomponent deviates from the n-alkane with the same MW, f_T and f_P increase, and f_m decreases from the value of 1.0.

Equations 3-4 to 3-6 also consider another physical trend that can be derived from the correlations of Riazi and Al-Sahhaf (1996) and Pan et al. (1997). Using their correlations, the differences between aromatics and paraffins in terms of T_C and P_C decrease with increasing MW **(Figures 3-1 and 3-2).** In terms of *m*, the difference exhibits a maximum around MW of 500 gm/mol as shown in **Figure 3-3.** These curves indicate that the effects of non-alkane compounds on T_C, P_C, and *m* vary with MW.

Figures 3-1 to 3-3 also show how T_C, P_C, and *m* in our Equations 3-4 to 3-6 deviate from their n-alkane values as the perturbation factors (f_T, f_P, and f_m) change from unity. Figures 3-1 to 3-3 present that Equations 3-4 to 3-6 qualitatively represent the physical trends mentioned above. Figure 3-1 shows that the sensitivity of T_C to f_T in Equation 3-4 exhibits a maximum around MW of 200 gm/mol, which is not observed from the correlations of Riazi and Al-Sahhaf (1996). However, the behavior of T_C with respect to f_T in the MW range of 100-200 gm/mol does not affect practical fluid characterization because most of pseudocomponents are out of this MW range, especially for heavy oils.

Step 4 of the NM uses Equations 3-4 to 3-6 to regress T_C, P_C, and *m* of pseudocomponents for matching P_{SAT} and density data. **Figure 3-S2** and the summary of step 4 given in **Section 3-S1 (**in the supporting information) present the algorithm to adjust f_T, f_P, and f_m. There are three main iteration loops, the P_{SAT}, density, and ω loops. The P_{SAT} loop is the innermost loop contained by the density loop. The ω loop contains the other two loops.

The initial values for f_T and f_P are 1.0. The f_m parameter is initialized by solving **Equation 3-7,**

$$0.6 = 0.4707 + 2.4831(f_m MW_1)^{-\left(\frac{39.933}{f_m\ MW_1}\right)}, \tag{3-7}$$

where MW_1 is the MW of the lightest pseudocomponent in a fluid model. The value on the left side of Equation 3-7, i.e. 0.6, is lower than the *m* for benzene, 0.6866 (see Equation 3-2 with ω = 0.21). Use

of Equation 3-7 assumes all pseudocomponents are heavier than C_6. The value 0.6 can be unduly low if MW_1 is much greater than the MW of benzene. However, this value is recommended for robustness.

In the P_{SAT} loop, f_P is adjusted by Δf_P (e.g., $+10^{-6}$) per iteration to match the P_{SAT} by decreasing the ψ function **(Equation 3-8).** Once the ψ function becomes smaller than a tolerance (e.g., 10^{-4}), the density loop decreases the δ function **(Equation 3-9)** by adjusting f_T and f_P. In the density loop, f_P is set to 1.0 at the beginning of each iteration, and f_T is adjusted by Δf_T (e.g., $+10^{-5}$) per iteration. If the f_T exceeds 3.5 or the δ function at the current iteration is greater than that at the previous iteration, then the algorithm moves to the ω loop. The f_T value can be greater than the upper bound of 3.5 when MW_1 is much greater than the MW of benzene in Equation 3-7. The accuracy of density predictions is less than 1% in AAD for all the oils tested in the next section.

$$\psi = \frac{\text{abs}(\text{Experimental } P_{SAT} - \text{Calculated } P_{SAT}) * 100}{\text{Experimental } P_{SAT}} \tag{3-8}$$

$$\delta = \sum_{i=1}^{k} \frac{1}{k} \left[\frac{\text{abs}(\text{Experimental Density} - \text{Calculated Density}) * 100}{\text{Experimental Density}} \right]_i \tag{3-9}$$

The ω loop is to satisfy the internal consistency of T_C, P_C, and ω; i.e., the definition of ω given by Pitzer (1955) and Pitzer et al. (1955) and in **Equation 3-10. Equations 3-11 and 3-12** are used to back calculate ω from the current m for each pseudocomponent. These ω values are then used in Equation 3-10 to obtain saturation pressures for pseudocomponents (P_{SATI}) at $0.7 T_C$.

$$(P_{SAT})_{\text{at } T_r = 0.7} = 10^{-(1+\omega)} P_C \tag{3-10}$$

$$m = 0.37464 + 1.54226\omega - 0.26992\omega^2 \quad \text{for } \omega \leq 0.3984 \tag{3-11}$$

$$m = 0.379642 + 1.48503\omega - 0.164423\omega^2 + 0.016666\omega^3 \quad \text{for } \omega \geq 0.3984 \tag{3-12}$$

Use of the PR EOS with the current T_C, P_C, and ω yields another saturation pressure at $0.7 T_C$ (P_{SATII}) for each pseudocomponent. The average absolute deviation ε for P_{SATI} and P_{SATII} for all pseudocomponents is then calculated using **Equation 3-13**

$$\varepsilon = \frac{1}{n} \sum_{i=1}^{n} \text{Abs}(P_{SATI} - P_{SATII}), \tag{3-13}$$

where n is the number of pseudocomponents. If f_T is greater than 3.5 or the ε function at the current iteration is smaller than that at the previous iteration, f_m is increased by Δf_m (e.g., $+10^{-3}$) to continue on the ω loop. For each ω iteration, f_T and f_P start with 1.0. The final values for f_T, f_P, and f_m are determined when the ε function becomes greater than that at the previous iteration. The final set of f_T, f_P, and f_m gives the first minimum of the ε function encountered in the calculation.

In the regression algorithm, the initial value is 1.0 for f_T and f_P, corresponding to the n-alkane values in Kumar and Okuno (2012). The search direction for f_T and f_P is the increasing direction from their initial values because pseudocomponents' T_C and P_C should be higher than n-alkane's value for a given MW. Therefore, Δf_T and Δf_P are positive to be physically justified. We set a lower bound for f_m in Equation 3-

7, which is used as the initial f_m value. Thus, Δf_m should also be positive. If the converged f_m is smaller than 1.0, it is consistent with the ω perturbation concept that pseudocomponents' ω should be lower than n-alkane's value for a given MW.

The regression algorithm in the NM provides a unique set of T_C, P_C, and m unlike the CM, where the resulting T_C, P_C, and m depend on the selection of adjustment parameters and adjustment amounts for them. Our regression algorithm can work with fewer adjustment parameters, compared to the CM, because of the physical observations incorporated in its development.

Equations 3-11 and 3-12 are different from Equations 3-2 and 3-3 in terms of their ω ranges. Equations 3-2 and 3-3 give the same value for m at ω = 0.39839, but not at the boundary ω = 0.49. The value of 0.39839 falls in the ω range 0.20-0.49 that is recommended for both Equations 3-2 and 3-3 by Peng and Robinson (1978). Therefore, the value of 0.3984 is chosen as the boundary value for Equations 3-11 and 3-12.

In general, the PR EOS overpredicts the molar volume for hydrocarbons heavier than heptane (Søreide 1989). The values for the critical parameters must be increased to match densities and vapor pressures regardless of the hydrocarbon compound type (i.e., P or N or A). Also, the density of an aromatic hydrocarbon is higher than that of n-alkane for a given MW. Although the correlations used for n-alkanes do not represent physical critical points, the search directions described above are still valid as will be demonstrated in the next section.

The NM developed in this section uses the PR EOS. However, it can also be used with other cubic EOSs if a new set of critical parameters is developed for the selected cubic EOS as Kumar and Okuno (2012) did for the PR EOS. The regression algorithm assumes that densities, viscosities, and P_{SAT} data are the only PVT data used in characterization. More adjustment parameters may be used when more PVT data are available, especially at different composition conditions. The regression algorithm can be extended for such a case by using molar distribution parameters as variables and creating additional loops. For example, the chi-squared distribution has two parameters, which influence mole fractions and MWs of pseudocomponents. These adjustment parameters will be effective especially for heavy oils, considering the importance of molar distributions of pseudocomponents in EOS calculations. BIPs for pseudocomponent/non-hydrocarbon (e.g., CO_2) pairs can significantly affect phase behavior calculations. We, however, recommend that the regression step should minimize the number of adjustment parameters to avoid physically absurd adjustment of parameters.

3.4.   Characterization of Reservoir Oils Using the New Method

In this section, the NM is applied to 22 different reservoir oils ranging from 9.5°API to 60.18°API. The oils are actual reservoir oils, for which data are available in the literature as shown in **Table 3-1.** The number of pseudocomponents is fixed to be four for the 22 oils. Mole fractions and MWs of pseudocomponents for oils 1-13 and 18-20 are taken directly from the corresponding references, which are based on the chi-squared distribution. P_{SAT} and reservoir temperature data are available in the

references as numerical values for the 22 oils. Many of the density data used have been obtained by digitizing density plots in the references. The number of density data points used is given for each oil in Table 3-1.

Figure 3-4 shows how the ε function varies with f_m for oils 5, 6, and 9. Step 4 of the NM converges to the final set of f_T, f_P, and f_m (and corresponding T_C, P_C, and m) at a minimum ε value for each oil. The same behavior of f_m occurs for the other oils studied in this research.

Table 3-1 lists the converged f_T, f_P, and f_m values for the 22 oils studied. Figures 3-5, 3-6, and 3-7 show the relationship between the API gravity and the converged f_T, f_P, and f_m values, respectively. For all the oils, the converged f_T and f_P values are greater than 1.0, and the converged f_m values are smaller than 1.0. These results indicate that the regression algorithm successfully found the solutions that are consistent with the perturbation concept described in the previous section.

Figures 3-5 to 3-7 also show a trend that f_T, f_P, and f_m are converging toward 1.0 as the API gravity becomes larger. This is likely because the paraffinic portion of the PNA distribution for a lighter oil is greater than that for a heavier oil. The PNA distribution of a heavy oil in general can deviate significantly from the reference distribution of 100% n-alkanes because a heavier CN group allows for a wider variety of compounds in it.

Unlike manual adjustments performed in the CM, the regression process in the NM can be easily codified for automation and takes only 1-3 minutes per oil using our code written in FORTRAN on the Intel Core i7-960 processor at 3.20 GHz and 8.0 GB RAM. The algorithm presented is based on the exhaustive search method of optimization for robustness. More rapid convergence would be achieved if a gradient method is used with initial guesses for f_T, f_P, and f_m based on the previous iteration steps.

3.5.   Comparison Between the New and Conventional Methods

We now make comparisons between the NM and CM in terms of various types of phase behavior predictions in P-T-x space for the oils in Table 3-1. PVT data for heavy oils are scarce as described in the introduction section and in the literature (Kokal and Sayegh 1993; Yazdani and Maini 2010). Data types used in this research are oil compositions; oil P_{SAT} at reservoir temperatures, and liquid densities and viscosities at different pressures at reservoir temperatures. Other than these measured data, pseudo data (Merrill and Newley 1993) were generated using the $CM_{w/o}V$ with 30 components (see Figure 3-S1 in the supporting information) because a complete set of data suitable for comparisons in a wide P-T-x range is not available for heavy oils. The 30 components consist of N_2, CO_2, C_1, C_2, C_3, C_4, C_5, C_6, and 22 pseudocomponents for the C_{7+} fraction.

Fluid characterization using a cubic EOS can result in deviation between predictions and data for a few fundamental reasons; (1) the functional form of the EOS used, (2) the characterization of the attraction ("a") and covolume ("b") parameters based on critical parameters, (3) the critical parameters used, and (4) the number of components used. The focus of the comparisons in this section is on items (3) and (4). Thus, the comparisons are made among different fluid models that have different critical

64

parameters and numbers of components for the PR EOS (i.e., for a fixed cubic EOS and a characterization method for a and b).

If the number of components in the fluid of interest was known and used in the fluid model, there should be no errors caused solely by reduction in composition space. We have conducted a sensitivity analysis for the effects of the number of components used on phase behavior predictions **(Figures 3-8 and 3-9).** The results indicate that use of 22 pseudocomponents is appropriate for generating pseudo data in this research. The differences in predictions are diminishing as the number of pseudocomponents used becomes more than 16. This result is consistent with other papers in the literature (Lolley and Richardson 1997; Egwuenu et al. 2008; Pedersen et al. 1985). Also, the $CM_{w/o}V$ method used for generating pseudo data follows the method of Pedersen et al. (Pedersen et al. 1989, 1992, 2004). It has been found that this method generally has a high predictive capability (Zuo and Zhang 2000) when properly used (see Figure 3-S1 in the supporting information).

Given the above, the pseudo data generated can be interpreted as phase behavior data for a PR fluid, a fluid that behaves as described by the PR EOS. Global phase diagrams of binary (Mushrif 2004; Yang 2004; Mushrif and Phoenix 2008) and ternary (Gauter 1999, Gauter et al. 1999) mixtures have been successfully represented using the PR EOS. Their results show that the PR EOS is capable of predicting at least qualitatively accurate phase behavior for reservoir fluids. When experimental data are not available or measurable, use of synthetic or pseudo data has been recommended for developing thermodynamic fluid models (Satyro et al. 2013). In the present research, the validation of the NM is made against pseudo data for PR fluids. We believe this is a reasonable approach in the absence of reliable experimental data other than oil compositions, densities, saturation pressures, and viscosities. There is also an important benefit using the pseudo data. Meaningful comparisons in any conditions in P-T-x space, particularly along the composition path for a given displacement at a given dispersion level, may be possible only with the pseudo data.

Separately from the 30-component models created for pseudo data, two fluid models are created for each oil using the NM and CM_wV with 11 components (see Figures 3-S1 and 3-S2 in the supporting information for the CM_wV and NM algorithms, respectively). The 11 components consist of N_2, CO_2, C_1, C_2, C_3, C_{4-5}, C_6, and four pseudocomponents for the C_{7+} fraction.

BIPs are not adjustment parameters in this research. Fixed BIP values are used for the 22 oils. BIPs are zero for hydrocarbon-hydrocarbon pairs. Non-zero values are used for non-hydrocarbon-hydrocarbon and non-hydrocarbon-non-hydrocarbon pairs; i.e., N_2-hydrocarbons, CO_2-hydrocarbons, and N_2-CO_2.

We adjust no BIPs, and set BIPs of hydrocarbon-hydrocarbon pairs to zero for the following reasons:

(1) The number of regression parameters should be minimized (Wang and Pope 2001; Egwuenu et al. 2008). Use of BIPs as regression parameters can damage the predictive capability of the resulting fluid model (Wang and Pope 2001).

(2) Non-zero BIPs for hydrocarbon-hydrocarbon pairs may lead to non-physical liquid-phase split (Pedersen et al. 1988).

(3) Use of zero BIPs can improve computational efficiency (Egwuenu et al. 2008; Michelsen 1986). It has also been shown that fluid properties can be better predicted when most of BIPs are set to zero (Pedersen and Christensen 2007).

(4) Use of negative BIPs, which may occur after regression, can cause non-convergence in successive substitution for flash calculations (Heidemann and Michelsen 1995).

The BIPs for N_2-hydrocarbons, CO_2-hydrocarbons, and N_2-CO_2 are fixed to be some non-zero values. The CM uses the default values from PVTsim as they would be the most suitable values for PVTsim. They are -0.017 for N_2-CO_2, 0.0311 for N_2-C_1, 0.0515 for N_2-C_2, 0.0852 for N_2-C_3, 0.08 for N_2-C_4, 0.1 for N_2-C_5, 0.08 for N_2-C_i, where $i \geq 6$, 0.12 for CO_2,-C_j, where $1 \leq j \leq 6$, and 0.1 for CO_2-pseudocomponents. These BIPs in the NM are based on Peng and Robinson (1976, 1978), who properly considered effects of hydrocarbon types on BIPs for the PR EOS. They recommended 0.1 for N_2-paraffins and N_2-napthenes, 0.18 for N_2-aromatics, and 0.1 for CO_2-hydrocarbons. Since pseudocomponents are mixtures of PNA compounds, we use the average values in the NM, which is [0.1 + 0.1 + 0.18] / 3 = 0.12666 ≈ 0.13 for N_2-pseudocomponents, and 0.1 for CO_2-pseudocomponents. The NM uses 0.0 for N_2-CO_2, 0.1 for N_2-C_i, where $1 \leq i \leq 6$, 0.13 for N_2-pseudocomponents, and 0.1 for CO_2-hydrocarbons.

In the following subsections, phase behavior predictions based on the NM and CM_wV are compared with the pseudo data. **Tables 3-S1, 3-S2, 3-S3, and 3-S4** (in the supporting information) give the resulting fluid models for oil 3 (13.38°API) and oil 6 (24.25°API) using the NM and CM_wV. These models are used in many of the comparisons presented below.

3.5.1. P-T Predictions

We first present the comparisons in terms of P-T predictions. Heavy-oil/solvent mixtures often exhibit three hydrocarbon-phases near the vapor pressures of the solvent components. The three phases consist of the gaseous (V), oleic (L_1), and solvent-rich liquid (L_2) phases (e.g., Mohanty et al. 1995; Polishuk et al. 2004). **Figures 3-10 and 3-11** show the 2-phase and 3-phase envelopes for a mixture of 10% oil 6 and 90% C_2. The CM_wV gives the V-L_1 and V-L_1-L_2 regions that are much smaller than those predicted by the NM. The NM predictions are in good agreement with the pseudo data points. The NM predictions are more accurate for lower temperatures. The three-phase envelope predicted by the NM almost coincides with data.

The deviation of the CM_wV predictions from the pseudo data is more significant for a mixture of 10% oil 6 and 90% C_3. **Figure 3-12** shows that the CM_wV results in an erroneous two-phase envelope for this mixture. The NM correctly generates the phase behavior predictions. **Figure 3-13** shows that the NM predicts a three-phase envelope that is close to the data points. The three-phase behavior predicted by the CM_wV occurs in a much smaller P-T region apart from the correct three-phase region based on the pseudo data and the NM.

The accuracy of the NM for L_1-L_2-V phase behavior is remarkable considering that the complex phase behavior characteristic of highly asymmetric hydrocarbon mixtures is predicted using only four pseudocomponents for the C_{7+} fraction. The reduced dimensionality in composition space does not damage phase behavior predictions using the NM.

3.5.2. P-x Predictions

A P-x prediction presents a cross section of isothermal phase behavior between two compositions. This subsection shows P-x predictions for the oil-6/C_1, oil-6/C_2, and oil-6/CO_2 pairs at the oil-6 reservoir temperature 333.15 K. Figure 3-14 shows the P-x predictions along with pseudo data for the oil-6/C_1 pair. The NM and CM_wV are accurate at low mixing ratios of C_1. This is because the 11-component models are fitted to P_{SAT} at the reservoir temperature at the oil composition. As the mixture composition goes away from the oil composition, the CM_wV predictions deviate from the pseudo data. The NM accurately predicts the bubble-point pressures along the mixing line.

The advantage of the NM over the CM_wV becomes more significant for P-x predictions for the oil-6/C_2 pair as shown in Fig. 15. At the C_2 mixing ratio of 90%, the CM_wV predicts a bubble point at 137.44 bars, which is approximately 39 bars lower than the pseudo data and the prediction by the NM.

Mixtures of CO_2 and reservoir oil often exhibit continuous transition between L_1-V and L_1-L_2 phase equilibria (Okuno et al. 2011) at low temperatures. Figure 3-16 presents such phase behavior for oil 6 and CO_2 at 333.15 K. The NM accurately predicts the upper boundary of the two-phase region in P-x space. The CM_wV erroneously gives a smaller region for the immiscible two liquid phases.

Figure 3-17 shows saturated liquid densities predicted along the mixing line between oil 6 and the equimolar C_1-C_2 mixture at 333.15 K. The density at the oil composition was used to create the EOS fluid models. Therefore, the CM_wV and NM are both accurate at lower mixing ratios of the solvent. As the mixture composition goes away from the oil composition, however, the CM_wV predictions deviate from the NM predictions and the pseudo data. The results indicate that the fluid models based on the CM_wV cannot accurately represent phase equilibrium and volumetric properties at compositions away from the oil composition.

3.5.3. T-x Predictions

A T-x diagram presents another important cross section of phase behavior, particularly when coinjection of solvent and steam is considered for heavy-oil recovery. **Figure 3-18** shows T-x predictions for oil-3/C_6 mixtures at 34.47 bars. The CM_wV overpredicts saturation temperatures except for low C_6 mixing ratios, while the NM accurately predicts them along the mixing line. If the fluid model based on the CM_wV is used in reservoir simulation of solvent/steam coinjection, propagation of the solvent in the reservoir can be significantly underestimated, resulting in erroneous reservoir performance forecasts.

The overprediction of saturation temperatures by the CM_wV becomes more significant for higher pressures. **Figure 3-19** shows T-x predictions at 60.00 bars. The NM still predicts accurately the saturation temperatures at all mixing ratios tested. However, the CM_wV predicts much higher saturation temperatures even at low C_6 mixing ratios. The deviation at the C_6 mixing ratio of 0.3 is 139 K. At C_6

mixing ratios higher than 0.3, there are no saturation temperatures predicted by CM_wV because the cricondenbar becomes lower than 60.00 bars as can be seen in **Figure 3-20.**

3.5.4. Thermodynamic Minimum Miscibility Pressure (MMP) Calculation

The thermodynamic MMP is the minimum displacement pressure at which complete miscibility is developed along the composition path from the injectant to the reservoir oil for one-dimensional flow in the absence of dispersion (John and Orr 1996). The thermodynamic MMP is a widely used parameter for design of solvent injection. In this subsection, the thermodynamic MMPs are calculated for 18 oils in Table 3-1 at their reservoir temperatures. Two different injectants are considered; pure C_1 and pure CO_2. For the C_1 cases, the MMP calculations are performed based on the method of characteristics using PVTsim. For the CO_2 cases, the mixing-cell method within PennPVT (Ahmadi and John 2011; PennPVT) is used. MMP calculations are not shown for oils 1, 2, 4, and 18 because three phases are present during the MMP calculations using the EOS fluid models for these oils based on the $CM_{w/o}V$ with 30 components.

Figure 3-21 compares the MMPs based on the NM with the pseudo data for 18 oils with C_1. Although the C_1-MMPs presented are calculated at different temperatures, the plots show that the calculated C_1-MMPs are higher for heavier oils. The accuracy of the MMPs observed for the wide variety of oils indicates that the NM successfully retains compositional phase behavior using only four pseudocomponents for the C_{7+} fraction. **Figure 3-22** shows that the C_1-MMPs predicted based on the CM_wV are lower than the pseudo data. The deviation is more significant for heavier oils. The maximum deviation of the C_1-MMPs is 5.3% for the NM, but it is 34% for the CM_wV. **Figures 3-23 and 3-24** show the comparisons of the NM with the CM_wV in terms of the CO_2-MMP. The maximum deviations of the CO_2-MMPs are 6.1% and 62% for the NM and the CM_wV, respectively.

Figures 3-20 and 3-22 indicate that compositional phase behavior predictions are more erroneous for heavier oils using the CM_wV. This is because the CM_wV uses density corrections through volume-shift parameters. A larger amount of volume correction is required and performed for heavier oils in the CM_wV as shown in Tables 3-S2 and 3-S4 in the supporting information (see also the Issues of the Conventional Method subsection). However, the thermodynamic MMP considered here is a parameter representing primarily compositional phase behavior, instead of volumetric phase behavior, of the fluid system considered. Therefore, the separation of volumetric from compositional phase behavior predictions causes errors in MMP predictions.

3.5.5. 1-D Displacement Simulation Case Study

Solvent injection for heavy-oil recovery is typically conducted under partially miscible conditions. In such displacements, the oil recovery history depends on how components propagate with the throughput of injectant. Fluid characterization can significantly affect oil recovery predictions because interaction of phase behavior and fluid flow determines components' propagation in a reservoir. This simulation case study aims to compare predictions of components' propagation using the NM and CM.

We present 1-D isothermal displacement of oil 6 with the equimolar C_1/C_2 mixture under partially miscible conditions. The MMP calculated for this case is 412.23 bars using the $CM_{w/o}V$ with 30 components. Using 11 components, it is 413.34 bars and 327.23 bars based on the NM and the CM_wV, respectively (see Tables 3-S3 and 3-S4 in the supporting information for the fluid models). Input data for the simulations using the GEM simulator of Computer Modelling Group (CMG 2011) are given in **Table 3-2. Figures 3-25 and 3-26** present predictions of density and viscosity using the NM, CM_wV and $CM_{w/o}V$ along with experimental data. Viscosity was matched using PVTsim by adjusting only V_C of pseudocomponents using the LBC method (Lohrenz et al. 1964). The injection and production pressures are fixed at 203.45 bars and 200 bars, respectively. The small pressure difference is used to make pressure variation in the reservoir small. Simulation results based on the $CM_{w/o}V$ with 30 components are used as pseudo data. Simulation results based on the NM and CM_wV are then compared.

Figure 3-27 shows oil recovery predictions compared to the pseudo data. The recovery curves for 0.0-0.3 hydrocarbon pore-volumes injected (HCPVI) are not shown because they nearly coincide. Oil recovery based on the NM is almost identical to the pseudo data. However, the CM_wV results in oil recovery simulation that is significantly overpredicted by approximately 8%. The overprediction is consistent with other comparisons made in previous subsections, where the fluid models based on the CM_wV exhibit more miscibility in their phase diagrams and MMP calculations. To see the effect of numerical dispersion on oil recovery simulation, the number of gridblocks is decreased from 250 to 50. Figure 3-23 shows the same advantage of the NM over the CM_wV under more dispersive conditions (The previous subsection showed comparisons for the dispersion-free case). The number of gridblocks is fixed to be 250 for further comparisons.

The different oil recovery histories are predicted because the NM and CM_wV predict different saturation profiles as shown in **Figure 3-28. Figure 3-29** shows that the C_1 fronts based on the NM and CM_wV deviate from each other, resulting in different predictions of gas breakthrough as can be seen in Figure 3-23. Figure 3-24 also indicates the CM_wV erroneously predicts faster propagation of heavy components. Since the deviation of the CM_wV shown in Figure 3-24 increases with the injectant throughput, the simulation based on the CM_wV becomes more erroneous later.

3.6. Conclusions

We developed a new method for fluid characterization using the PR EOS with the van der Waals mixing rules. The method characterizes reservoir fluids using perturbations of T_C, P_C, and ω from n-alkane values. T_C, P_C, and ω for n-alkanes used are based on our previous research, which are optimized for the PR EOS for predictions of vapor pressures and liquid densities without volume shift. The optimized reference values allow for robust regression using three perturbation factors f_T, f_P, and f_m for T_C, P_C, and ω, respectively. In our regression, Pitzer's definition of ω is properly satisfied for each component. The new characterization method was applied to 22 different reservoir oils. Comparisons were made between the new and conventional characterization methods in terms of predictions of various phase

diagrams, thermodynamic minimum miscibility pressures (MMPs), and 1-D oil displacement. The conclusions are as follows:

o The new method (NM) exhibits significant insensitivity of phase behavior predictions to the number of components used for a plus fraction. Two- and three-phase behavior predictions in P-T-x space using the NM with 11 components are almost identical to those using the conventional method without volume shift ($CM_{w/o}V$) with 30 components.

o The reliability of the NM is also observed for MMP calculations and 1-D oil displacement simulations. Oil displacement predictions based on the NM with 11 components are nearly identical to those based on the $CM_{w/o}V$ with 30 components. This is true even at different dispersion levels tested. Results indicate that the NM can reduce the dimensionality of composition space while keeping accurate phase behavior predictions along composition paths at different dispersion levels.

o The NM does not require volume-shift parameters to accurately predict compositional and volumetric phase behaviors. The conventional method with volume shift (CM_wV) separates volumetric phase behavior predictions from compositional phase behavior predictions. This separation should be carefully used especially for heavy-oil characterization. Our results show that the CM_wV with 11 components yields erroneous phase behavior predictions, which typically show significantly smaller two- and three-phase regions in P-T-x space. The advantage of the NM over the CM_wV in phase behavior predictions is more significant for P-T-x conditions away from those used for parameter regression.

o The new regression algorithm developed searches for an optimum set of T_C, P_C, and ω for pseudocomponents using physically justified search directions starting from the well-defined initial values. Unlike in the CM, robust convergence of T_C, P_C, and ω does not require step-wise manual adjustments of parameters. The automatic regression process in the NM took only a few minutes per oil for the 22 oils characterized.

o The perturbation factors f_T, f_P, and f_m developed in this research are unity for n-alkanes. The perturbation factors capture physical trends that can be derived from the literature; e.g., for a given molecular weight, T_C and P_C are lower and ω is larger for paraffins compared to other types of hydrocarbon compounds. For the 22 oils characterized in this research, the converged f_T and f_P values are all greater than 1.0, and the converged f_m values are all smaller than 1.0. Deviations of f_T, f_P, and f_m from unity can be physically interpreted as deviations of the plus fractions from n-alkane mixtures.

o The NM requires no changes in the current compositional simulation formulation because it uses the PR EOS with the van der Waals mixing rules.

3.7. Nomenclature

Roman Symbols

a   = Attraction parameter in a cubic equation of state

A   = Aromatic

A_{mix} = Attraction parameter for a mixture in a cubic equation of state

b   = Covolume parameter in a cubic equation of state

B_{mix} = Covoulme parameter for a mixture in a cubic equation of state

C_{PEN} = Peneloux volume-shift parameter

m   = Parameter in the Peng–Robinson EOS (1978) defined in Equation 3-2 and 3-3

D   = Dimension

f_m = Perturbation factor for the *m* parameter

f_P = Perturbation factor for critical pressure

f_T = Perturbation factor for critical temperature

Δf_m = Step size for f_m

Δf_P = Step size for f_P

Δf_T = Step size for f_T

m_A = Acentric factor for aromatics

k   = Number of density data

m_P = Acentric factor for paraffins

n   = Number of pseudocomponents

N   = Napthenes

p   = Pressure, bar

P   = Paraffins

P_C = Critical pressure, bar

P_{CA} = Critical pressure of aromatics, bar

P_{CP} = Critical pressure of paraffins, bar

R   = Universal gas constant

T   = Temperature, K

T_C = Critical temperature, K

T_{CA} = Critical temperature of aromatics, K

T_{CP} = Critical temperature of paraffins, K

TOL   = Tolerance

v = Molar volume, gm/mol

V_C = Critical volume, gm/mol

Abbreviations

^oAPI = API (American Petroleum Institute) gravity

BIP   = Binary interaction parameter

CM   = Conventional (characterization) method

CM_wV = Conventional (characterization) method using volume shift

$CM_{w/o}V$ = Conventional (characterization) method without using volume shift

CN   = Carbon number

EOR   = Enhanced oil recovery

EOS   = Equation of state

HCPVI   = Hydrocarbon pore-volume injected

MMP   = Minimum miscibility pressure, bar

MW   = Molecular weight, gm/mol

NM   = New (characterization) method

PC   = Pseudocomponent

PNA   = Paraffin-napthene-aromatic

PR   = Peng-Robinson

P-T-x   = Pressure-temperature-composition

SRK   = Soave-Redlich-Kwong

Greek symbols

δ = Average absolute deviation for density given by Equation 3-9

ε = Average absolute deviation for saturation pressure given by Equation 3-13

Ω_a = Constant term in the attraction parameter of a cubic EOS

Ω_b = Constant term in the covolume parameter of a cubic EOS

ψ = Absolute % deviation given by Equation 3-8

ω = Acentric factor

3.8. References

Ahmadi, K. and Johns, R.T. 2011. Multiple Mixing-Cell Model for MMP Determination. *SPE J.* **16** (4): 733-742.

Ambrose, D. and Tsonopoulos, C. 1995. Vapor-Liquid Critical Properties of Elements and Compounds. 2. Normal Alkanes. *J. Chem. Eng. Data* **40** (3): 531-546.

Cavett, R.H. 1962. Physical Data for Distillation Calculations, Vapor-Liquid Equilibria. *Proc. Am. Pet. Inst. Div. Refining.* **42** (3): 351-357.

Christensen, P.L. 1999. Regression to Experimental PVT Data. *J Can Petro Technol* 38 (13): 1-9.

CMG, Computer Modeling Group, Calgary, Canada, 2011.

Coats, K.H. and Smart, G.T. 1986. Application of a Regression Based EOS PVT Program to Laboratory Data. *SPE Res Eng* **1** (3): 277-299.

Cullick, A.S., Pebdani, F.N., and Griewank, A.K. 1989. Modified Corresponding States Method for Predicting Densities of Petroleum Reservoir Fluids. *Ind. Eng. Chem. Res.* **28** (3): 340-347.

DeRuiter, R.A., Nash, L.J., and Singletary, M.S. 1994. Solubility and Displacement Behavior of a Viscous Crude With CO_2 and Hydrocarbon Gases. *SPE Res Eng* **9** (2): 101-106.

Edmister, W.C. 1958. Applied Hydrocarbon Thermodynamics, Part 4: Compressibility Factors and Equations of State. *Pet. Refiner.* **37**: 173-179.

Egwuenu, A.M., Johns, R.T., and Li, Y. 2008. Improved Fluid Characterization for Miscible Gas Floods. *SPE Res Eval Eng* 11 (4): 655-665.

Gates, I.D. and Chakrabarty, N. 2008. Design of the Steam and Solvent Injection Strategy in Expanding Solvent Steam-Assisted Gravity Drainage. *J Can Pet Technol* **47** (9): 12-20.

Gauter, K. 1999. Fluid Multiphase Behavior in Ternary Systems of Near-Critical CO_2. PhD dissertation, the Technical University of Berlin, Berlin, Germany.

Gauter, K., Heidemann, R.A., and Peters, C.J. 1999. Modeling of Fluid Multiphase Equilibria in Ternary Systems of Carbon Dioxide as the Near-Critical Solvent and Two Low-Volatile Solutes. *Fluid Phase Equilib.* **158-160**: 133-141.

Ghasemi, M., Alavian, S.A., and Whitson, C.H. 2011. C_7+ Characterization of Heavy Oil Based on Crude Assay Data. Presented at SPE Heavy Oil Conference and Exhibition held in Kuwait City, Kuwait, 12-24 Dec. SPE 148906-MS.

Gupta, S., Gittins, S., and Picherack, P. 2003. Insights into Some Key Issues with Solvent Aided Process. *J Can Pet Technol* **43** (2): 54-61.

Heidemann, R.A. and Michelsen, M.L. 1995. Instability of Successive Substitution. *Ind. Eng. Chem. Res.* **34** (3): 958-966.

Hornbrook, M.W., Dehghani, K., Qadeer, S. et al. 1991. Effects of CO_2 Addition to Steam on Recovery of West Sak Crude Oil. *SPE Res Eng* **6** (3): 278-286.

Jhaveri, B.S. and Youngren, G.K. 1988. Three-Parameter Modification of the Peng-Robinson Equation of State to Improve Volumetric Predictions. *SPE J.* **3** (3): 1033-1040.

Jørgensen, M. and Stenby, E.H. 1995. Optimization of Pseudo-components Selection for Compositional Studies of Reservoir Fluids. Presented at the Annual Technical Conference and Exhibition, Dallas, Texas, 22-25 Oct. SPE-30789-MS

Johns, R.T. and Orr, Jr. F.M. 1996. Miscible Gas Displacement of Multicomponent Oils. *SPE J.* **1** (1): 39-50.

Kesler, M.G. and Lee, B.I. 1976. Improve Prediction of Enthalpy of Fractions, Hydrocarbon Processing. *Hydrocarb Process* **55** (3): 153-158.

Kokal, S.L. and Sayegh, S.G. 1993. Phase Behavior and Physical Properties of CO_2-Saturated Heavy Oil and its Constitutive Fractions: Experimental Data and Correlations. *J. Pet. Sci. Eng.* **9** (4): 289-302.

Korsten, H. 2000. Internally Consistent Prediction of Vapor Pressure and Related Properties. *Ind. Eng. Chem. Res.* **39** (3): 813-820.

Krejbjerg, K. and Pedersen, K.S. 2006. Controlling VLLE Equilibrium with a Cubic EoS in Heavy Oil Modeling. Presented at 57th Annual Technical Meeting of the Petroleum Society (Canadian International Petroleum Conference), Calgary. 13-15 June. PETSOC-2006-052.

Kumar, A. and Okuno, R. 2012. Fluid Characterization Using an EOS for Compositional Simulation of Enhanced Heavy-Oil Recovery. Presented at SPE Annual Technical Conference and Exhibition, San Antonio, Texas, 8-10 Oct. SPE 159494-MS

Kumar, A. and Okuno, R. 2012. Critical Parameters Optimized for Accurate Phase Behavior Modeling for Heavy n-Alkanes up to C_{100} using the Peng-Robinson Equation of State. *Fluid Phase Equilib.* 335: 46-59.

Lee, B.I. and Kesler, M.G. 1975. A Generalized Thermodynamic Correlation Based on Three- Parameter Corresponding States. *AIChE J.* **21** (3): 510-527.

Li, W., Mamora, D.D., and Li. Y. 2011. Solvent-Type and –Ratio Impacts on Solvent-Aided SAGD Process. *SPE Res Eval & Eng* **14** (3): 320-331.

Lohrenz, J., Bray, B.G., and Clark, C.R. 1964. Calculating Viscosities of Reservoir Fluids from their Compositions. *J. Pet. Technol.* **16** (10): 1171-1176.

Lolley, C.S. and Richardson, W.C. 1997. Compositional Input for Thermal Simulation of Heavy Oils with Application to the San Ardo Field. Presented at International Thermal Operation & Heavy Oil Symposium, Bakersfield, California, 10-12 Dec. SPE-37538-MS

Memon, A.I., Gao, J., Taylor, S.D. et al. 2010. A Systematic Workflow Process for Heavy Oil Characterization: Experimental Techniques and Challenged. Presented at Canadian Unconventional Resources and International Petroleum Conference, Calgary, Alberta. 19-21 Oct. SPE-137006-MS

Merrill, R.C. and Newley, T.M.J. 1993. A Systematic Investigation into the Most Suitable Data for the Development of Equations of State for Petroleum Reservoir Fluids. *Fluid Phase Equilib*. **82**: 101-110.

Michelsen, M.L. 1986. Simplified Flash Calculation for Cubic Equation of State. *Ind. Eng. Chem. Proc. Des. Dev.* **25** (1): 184-188.

Mohanty, K.K., Masino, W.H., Ma, T.D. et al. 1995. Role of Three-Hydrocarbon-Phase Flow in a Gas-Displacement Process. *SPE Res Eng* **10** (3): 214-221.

Mushrif, S.H. 2004. Determining Equation of State Binary Interaction Parameters Using K- and L-Points. Master thesis, the University of Saskatchewan, Saskatoon, Canada.

Mushrif, S.H. and Phoenix, A.V. 2008. Effect of Peng-Robinson Binary Interaction Parameters on the Predicted Multiphase Behavior of Selected Binary Systems. *Ind. Eng. Chem. Res.* **47** (16): 6280-6288.

Nasr, T.N., Beaulieu, G., Golbeck, H. et al. 2003. Novel Expanding Solvent-SAGD Process "ES-SAGD". *J Can Pet Technol* **42** (1): 13.

Okuno, R., Johns, R.T., and Sepehrnoori, K. 2011. Mechanisms for High Displacement Efficiency of Low-Temperature CO_2 Floods. *SPE J.* 16 (4): 751-767.

Okuno, R., Johns, R.T., and Sepehrnoori, K., 2010. Three-Phase Flash in Compositional Simulation Using a Reduced Method, *SPE J.* **15** (3): 689-703.

Pan, H., Firoozabadi, A., and Fotland, E. 1997. Pressure and Composition Effect on Wax Precipitation: Experimental Data and Model Results. *SPE Prod & Fac* **12** (4): 250-258.

Pedersen, K.S. and Christensen, P. L. 2007. Phase Behavior of Petroleum Reservoir Fluids. CRC Press, Taylor & Francis Group, Boca Raton, FL, USA.

Pedersen, K.S., Blilie, A.L., and Meisingset, K.K. 1992. Calculations On Petroleum Reservoir Fluids Using Measured And Estimated Compositional Data for the Plus Fraction. *Ind. Eng. Chem. Res.* **31** (5): 1378-1384.

Pedersen, K.S., Milter, J., and Sørensen, H. 2004. Cubic Equations of State Applied to HT/HP and Highly Aromatic Fluids. *SPE J.* **9** (2): 186-192.

Pedersen, K.S., Thomassen, P., and Fredenslund, Aa. 1989. Characterization of Gas Condensate Mixtures. Advances in Thermodynamics, Taylor & Francis, New York.

Pedersen, K.S., Thomassen, P., and Fredenslund, Aa. 1983. SRK-EOS Calculation for Crude Oils. *Fluid Phase Equilib*. **14:** 209-218.

Pedersen, K.S., Thomassen, P., and Fredenslund, Aa. 1984. Thermodynamics of Petroleum Mixtures Containing Heavy Hydrocarbons. 1. Phase Envelope Calculations by Use of the Soave-Redlich-Kwong Equation of State. *Ind. Eng. Chem. Proc. Des. Dev.* **23** (1): 163170.

Pedersen, K.S., Thomassen, P., and Fredenslund, Aa. 1985. Thermodynamics of Petroleum Mixtures Containing Heavy Hydrocarbons. 3. Efficient Flash Calculation Procedures Using the SRK Equation of State. *Ind. Eng. Proc. Des. Dev.* 24 (4): 948-954.

Pedersen, K.S., Thomassen, P., and Fredenslund, Aa. 1988. On the Dangers of Tuning Equation of State Parameters. *Chem. Eng. Sci*. 43 (2): 269-278.

Peneloux, A., Rauzy, E., and Fréze, R. 1982. A Consistent Correction for Redlich-Kwong-Soave Volume. *Fluid Phase Equilib.* **8** (1): 7-23.

Peng, D.-Y. and Robinson, D.B. 1976. A New Two-Constant Equation of State. *Ind. Eng. Chem. Fund.* **15** (1): 59-64.

Peng, D.-Y. and Robinson, D.B. 1978. The Characterization of the Heptanes and Heavier Fractions for the GPA Peng-Robinson Programs. *GPA Research Report* RR-28.

PennPVT Toolkit, Gas Flooding Joint Industrial Project, Director: Dr. Russell T. Johns, EMS Energy Institute, The Pennsylvania State University, University Park, PA.

Pitzer, K.S. 1955. The Volumetric and Thermodynamic Properties of Fluids. I. Theoretical Basis and Viral Coefficients. *J. Am. Chem. Soc.* **77** (13): 3427-3433.

Pitzer, K.S., Lippmann, D.Z., Curl Jr, R.F. et al. 1955. The Volumetric and Thermodynamic Properties of Fluids. II. Compressibility Factor, Vapor Pressure, and Entropy of Vaporization. *J. Am. Chem. Soc.* **77** (13): 3433-3440.

Polishuk, I., Wisniak, J., and Segura, H. 2004. Estimation of Liquid-Liquid-Vapor Equilibria in Binary Mixtures of n-Alkanes. *Ind. Eng. Chem. Res.* **43** (18): 5957-5964.

PVTsim 20.0. 2011. Calsep A/S, Lyngby, Denmark.

Quiñones-Cisneros, S.E., Andersen, S.I., and Creek, J. 2005. Density and Viscosity Modeling and Characterization of Heavy Oils. *Energy Fuels* **19** (4): 1314-1318.

Quiñones-Cisneros, S.E., Dalberg, A., and Stenby, E.H. 2004b. PVT Characterization and Viscosity Modeling and Prediction of Crude Oils. *Pet. Sci. Technol.*, **22** (9-10): 1309–1325.

Quiñones-Cisneros, S.E., Zéberg-Mikkelsen, C.K., and Stenby, E.H. 2003. Friction Theory Prediction of Crude Oil Viscosity at Reservoir Conditions Based on Dead Oil Properties. Fluid Phase Equilib. 212 (1-2): 233–243.

Quiñones-Cisneros, S.E., Zéberg-Mikkelsen, C.K., Baylaucq, A. et al. 2004a. Viscosity Modeling and Prediction of Reservoir Fluids: From Natural Gas to Heavy Oils. *Int. J. Therm.* **25** (5): 1353-1366.

Riazi, M.R. and Al-Sahhaf, T.A. 1996. Physical Properties of Heavy Petroleum Fractions and Crude Oils. *Fluid Phase Equilib*. **117** (1-2): 217-224.

Riazi, M.R. and Daubert, T.E. 1980. Simplify Property Predictions. *Hydrocarb. Process.* **59** (3): 115-116.

Riazi, M.R. and Daubert, T.E. 1987. Characterization Parameters for Petroleum Fractions. *Ind. Eng. Chem. Res.* **26** (4): 755-759.

Satyro, M.A., Shaw, J.M., and Yarranton, H.W. 2013. A Practical Method for the Estimation of the Oil and Water Mutual Solubilities. *Fluid Phase Equilib.* 355: 12-25.

Soave, G. 1972. Equilibrium Constants from a Modified Redlich-Kwong Equation of State. *Chem. Eng. Sci.* **27**:1197-1203.

Søreide, I. 1989. Improved Phase Behavior Predictions of Petroleum Reservoir Fluids from a Cubic Equation of State, Ph.D. dissertation, Norwegian University of Science and Technology, Trondheim, Norway, 1989.

Ting, P.D., Joyce, P.C., Jog, P.K. et al. 2003. Phase Equilibrium Modeling of Mixtures of Long-Chain and Short-Chain Alkanes Using Peng–Robinson and SAFT. *Fluid Phase Equilib*. **206** (1-2), 267-286.

Twu, C.H. 1984. An Internally Consistent Correlation for Predicting the Critical Properties and Molecular Weights of Petroleum and Coal-Tar Liquids. *Fluid Phase Equilib.* **16** (2): 137-150.

Voulgaris, M., Stamatakis, S., and Tassios, D. 1991. Prediction of Physical Properties for Non-Polar Compounds, Petroleum and Coal Liquid Fractions. *Fluid Phase Equilib*. **64**: 73-106.

Voutsas, E.C., Pappa, G.D., Magoulas, K. et al. 2006. Vapor Liquid Equilibrium Modeling of Alkane Systems with Equations of State: "Simplicity versus Complexity. *Fluid Phase Equilib.* **240** (2): 127-139.

Wang, P. and Pope, G.A. 2001. Proper Use of Equations of State for Compositional Reservoir Simulation. *J. Petrol. Tech*. **53** (7): 74-81.

Whitson, C.H. 1983. Characterizing Hydrocarbon Plus Fractions. *SPE J.* **23** (4): 683-694.

Whitson, C.H. and Brulè, M.R. 2000. Phase Behaviour. SPE Henry L. Doherty Series, Vol. 20, SPE, Richardson, Texas.

Yakoumis, I., Kontogeorgis, G.M., Voutsas, E. et al. 1997. Vapor-Liquid Equilibria for Alcohol/Hydrocarbon Systems Using the CPA Equation of State. *Fluid Phase Equilib.* **130** (1-2): 31-47.

Yang, Q. 2004. Automatic Development of Global Phase Diagrams for Binary Systems in Pressure-Temperature Space. Master thesis, the University of Saskatchewan, Saskatoon, Canada.

Yazdani, A. and Maini, B.B. 2010. Measurements and Modeling of Phase Behaviour and Viscosity of a Heavy Oil/Butane System. *J Can Pet Technol* **49** (2): 9-14.

Zabel, F., Law, D.H.-S., Taylor, S. et al. 2010. Impact of Uncertainty of Heavy Oil Fluid Property Measurements. *J Can Pet Technol* **49** (3): 28-35.

Zuo, J.Y. and Zhang, D. 2000. Plus Fraction Characterization and PVT Data Regression for Reservoir Fluids near Critical Conditions. Presented at SPE Asia Pacific Oil and Gas Conference and Exhibition, Brisbane, Australia, 16-18 Oct. SPE 64520-MS

Table 3-1. Twenty two reservoir oils characterized in this research and converged f_T, f_P, and f_m values using the new characterization method								
Oil No.	References	MW (gm/mol)	°API	T_{RES} (K)	$k^\#$	f_T	f_P	f_m
1	Quiñones-Cisneros et al. (2005), Oil-8	443.08	9.50	322.05	13	2.12110	1.74580	0.359
2	Quiñones-Cisneros et al. (2005), Oil-7	431.59	11.63	322.05	12	1.71016	1.65705	0.368
3	Quiñones-Cisneros et al. (2004a), Oil-6	377.88	13.38	322.05	13	2.91379	1.83307	0.246
4	Quiñones-Cisneros et al. (2004a), Oil-5	422.94	11.98	322.05	13	1.81952	1.67153	0.379
5	Quiñones-Cisneros et al. (2004a), Oil-1	170.59	20.81	330.40	16	2.94230	1.78866	0.406
6	Quiñones-Cisneros et al. (2004b), Oil-8	182.05	24.25	333.15	16	2.81319	1.91049	0.429
7	Quiñones-Cisneros et al. (2004b), Oil-7	159.99	29.24	330.40	16	2.31276	1.74384	0.440
8	Quiñones-Cisneros et al. (2004b), Oil-6	118.18	35.61	346.15	5	2.08100	1.71149	0.434
9	Quiñones-Cisneros et al. (2004b), Oil-5	130.55	28.30	337.85	3	2.89841	1.84940	0.453
10	Quiñones-Cisneros et al. (2004b), Oil-4	114.57	33.35	337.85	6	2.46282	1.74305	0.493
11	Quiñones-Cisneros et al. (2004b), Oil-3	87.80	40.46	337.25	5	2.35278	1.64743	0.554
12	Quiñones-Cisneros et al. (2004b), Oil-2	89.83	47.63	366.45	11	2.09759	1.47213	0.540
13	Quiñones-Cisneros et al. (2004b), Oil-1	86.57	60.18	427.60	13	1.39453	1.18216	0.641
14	Oil*	296.90	22.60‡	357.50	13	2.19267	1.61825	0.309
15	Coats and Smart (1986), Oil-1	123.79	34.04	355.37	8	2.63596	1.84711	0.402
16	Coats and Smart (1986), Oil-6	83.31	55.73	385.37	20	2.06638	1.44575	0.453
17	Coats and Smart (1986), Oil-7	113.60	45.03	328.15	20	1.95919	1.47130	0.500
18	Quiñones-Cisneros et al. (2003), Oil-5	240.24	20.19	345.93	15	1.55725	1.57795	0.585
19	Quiñones-Cisneros et al. (2003), Oil-4	167.03	25.70	344.95	11	2.12027	1.68612	0.588
20	Quiñones-Cisneros et al. (2003), Oil-3	114.65	34.24	337.85	12	2.04203	1.60648	0.616
21	Cullick et al. (1989), Light Oil	105.28	43.68	377.59	8	1.99705	1.54570	0.414
22	Pedersen et al. (1992), Fluid-1	124.57	35.73	344.75	8	1.86796	1.54972	0.614

* This is an actual oil, but the source is not mentioned for confidentiality.
‡ As reported. All other densities are calculated values.
# k is number of density data in Equation 3-9.

Table 3-2. Input parameters used in the 1-D simulation case study			
No. of gridblocks	250	Reservoir pressure	200 bars
Grid dimensions	3.05 m × 3.05 m × 1.52 m	Reservoir temperature	333.15 K
Permeability	1500 mD	Production pressure	200 bars
Porosity	0.15	Injection pressure	203.45 bars
Initial oil saturation	0.8		
Initial water saturation	0.2	Injection gas	CH_4:C_2H_6 (50:50)
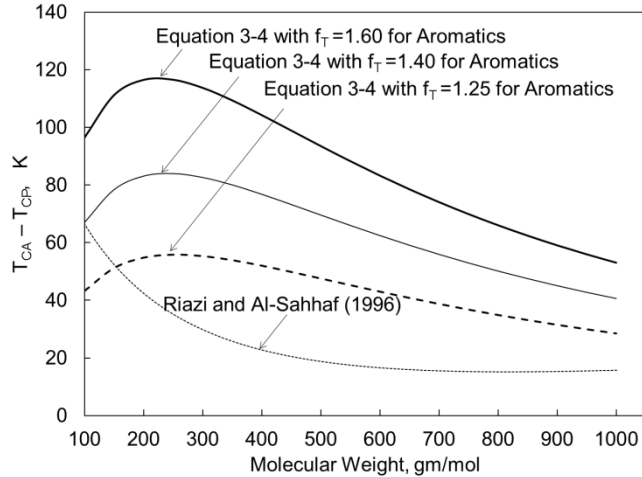
Figure 3-1. Differences between aromatics and paraffins for critical temperature, TCA-TCP, based on the correlations of Riazi and Al-Sahhaf (1996) and Equation 3-4.
 T_{CA} using Equation 3-4 assumes three different f_T values for aromatics, 1.25, 1.40, and 1.60. T_{CP} using Equation 3-4 uses f_T of 1.0.
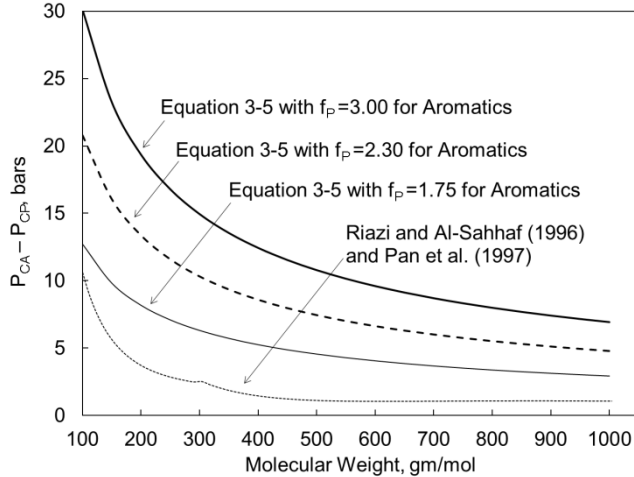
Figure 3-2. Differences between aromatics and paraffins for critical pressure, P_{CA}-P_{CP}, based on the correlations of Riazi and Al-Sahhaf (1996), Pan et al. (1997), and Equation 3-5.
P_{CA} using Equation 3-5 assumes three different f_P values for aromatics, 1.75, 2.30, and 3.0. P_{CP} using Equation 3-5 uses f_P of 1.0. The correlation of Pan et al. (1997) is used for molecular weight larger than 300 gm/mol.
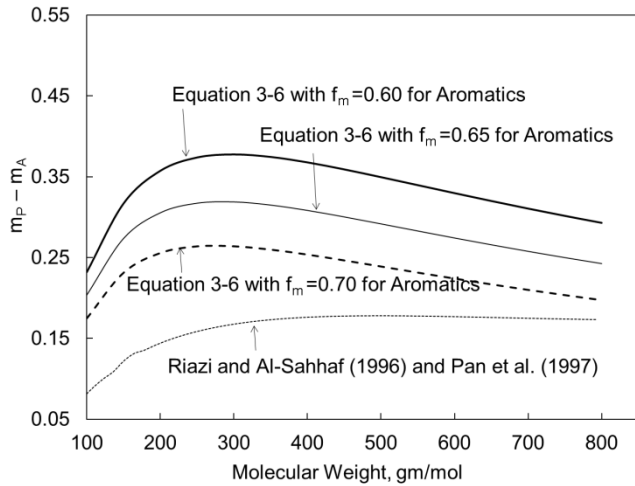
Figure 3-3. Differences between aromatics and paraffins for the m parameter, mP-mA, based on the correlations of Riazi and Al-Sahhaf (1996), Pan et al. (1997), and Equation 3-6.

The m parameter is defined in Equations 3-2 and 3-3. m_A using Equation 3-6 assumes three different f_m values for aromatics, 0.60, 0.65, and 0.70. m_P using Equation 3-6 uses f_m of 1.0. The correlation of Riazi and Al-Sahhaf (1996) is used for m_P, and the correlation of Pan et al. (1997) is used for m_A.
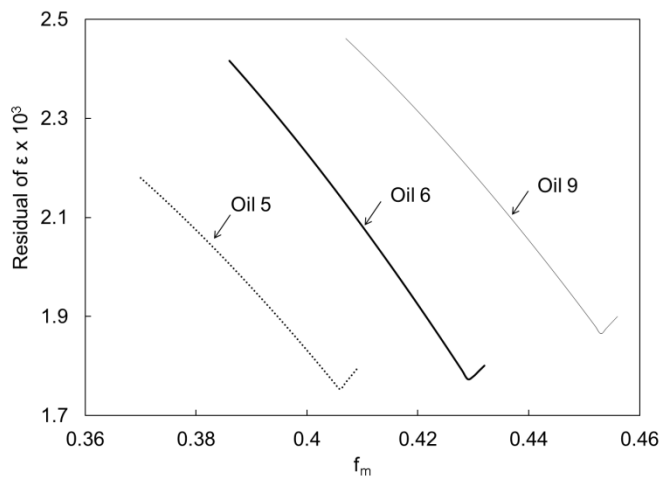
Figure 3-4. Convergence behavior for the ε function (Equation 3-13) with f_m for oils 5, 6, and 9 given in Table 3-1.

The regression algorithm (Figure 3-S2 in the supporting information) finds an optimum set of f_T, f_P, and f_m at the minimum shown for each oil.

80
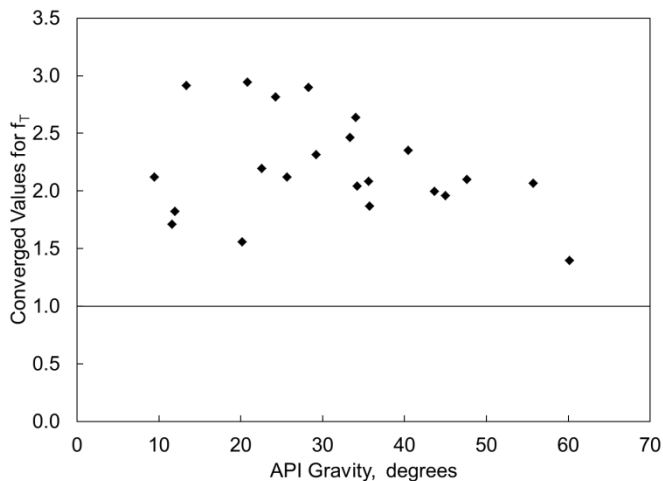
Figure 3-5. The converged f_T values for the 22 different oils in Table 3-1.
The regression algorithm (Figure 3-S2 in the supporting information) starts with f_T =1.0, and searches for an optimum f_T in the increasing direction. Perturbation of f_T from 1.0 qualitatively represents deviation of a plus fraction from a n-alkane mixture.
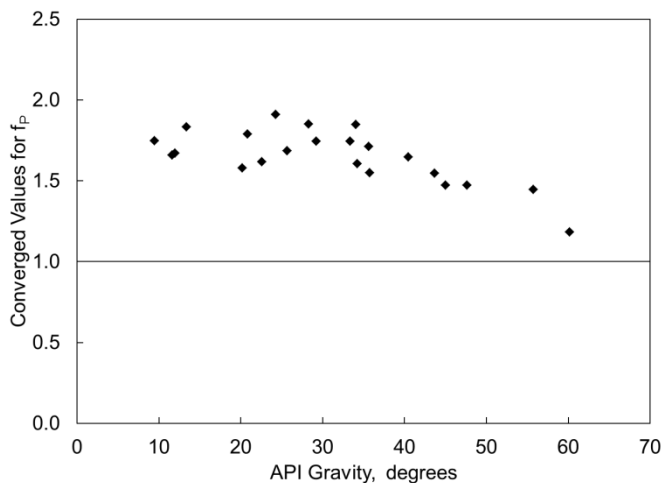
Figure 3-6. The converged f_P values for the 22 different oils in Table 3-1.
The regression algorithm (Figure 3-S2 in the supporting information) starts with f_P =1.0, and searches for an optimum f_P in the increasing direction. Perturbation of f_P from 1.0 qualitatively represents deviation of a plus fraction from an n-alkane mixture.

81
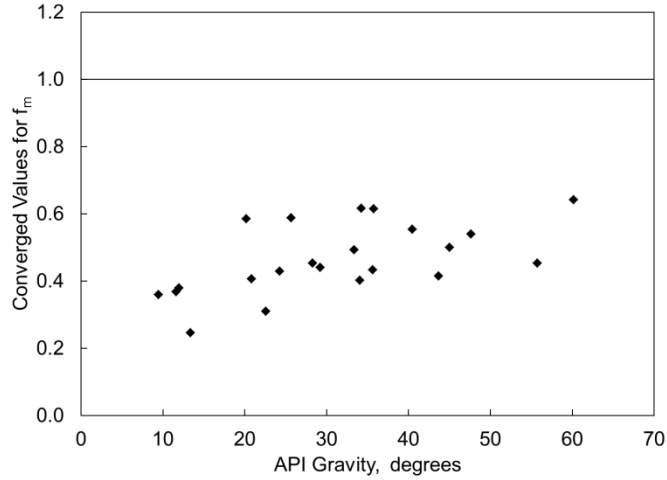
Figure 3-7. The converged f_m values for the 22 different oils in Table 3-1.
The regression algorithm (Figure 3-S2 in the supporting information) starts with f_m based on Equation 3-7, and searches for an optimum f_m in the increasing direction. Perturbation of f_m from 1.0 qualitatively represents deviation of a plus fraction from an n-alkane mixture.
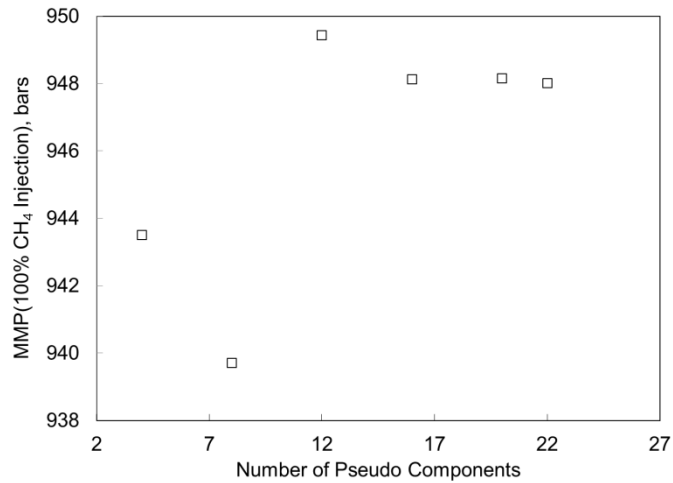
Figure 3-8. MMP calculated for Oil 6 with 100% methane at 333.15 K using $CM_{w/o}V$ with different numbers of pseudocomponents.
Eight pure components (N_2, CO_2, C_1, C_2, C_3, C_4, C_5, and C_6) are used with 4, 8, 12, 16, 20, and 22 pseudocomponents. The variation of calculated MMP becomes insignificant for more than 16 pseudocomponents.
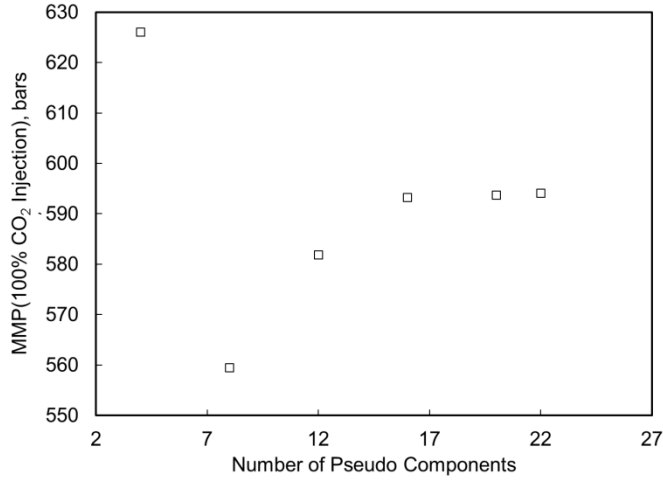
Figure 3-9. MMP calculated for Oil 6 with 100% CO_2 at 333.15 K using $CM_{w/o}V$ with different numbers of pseudo components.

Eight pure components (N_2, CO_2, C_1, C_2, C_3, C_4, C_5, and C_6) are used with 4, 8, 12, 16, 20, and 22 pseudocomponents. The variation of calculated MMP becomes insignificant for more than 16 pseudocomponents.
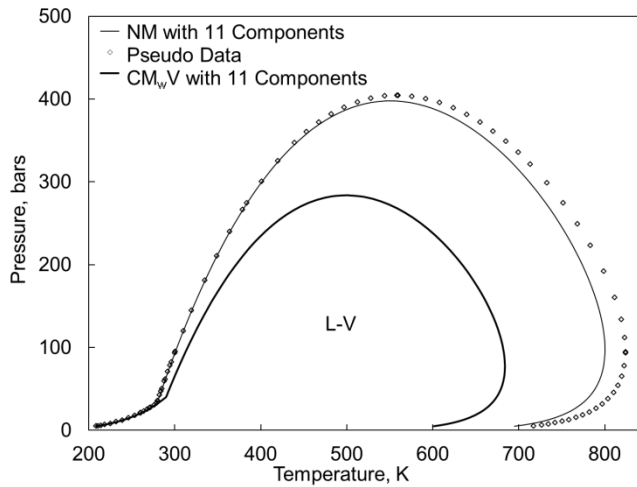
Figure 3-10. Two-phase P-T diagrams for a mixture of oil 6 10% and C_2 90% based on the NM and the CM_wV.

The 11-component models for oil 6 are given in Tables 3-S3 and 3-S4 in the supporting information. The pseudo data are generated using the conventional method without using volume shift parameters ($CM_{w/o}V$) with 30 components.
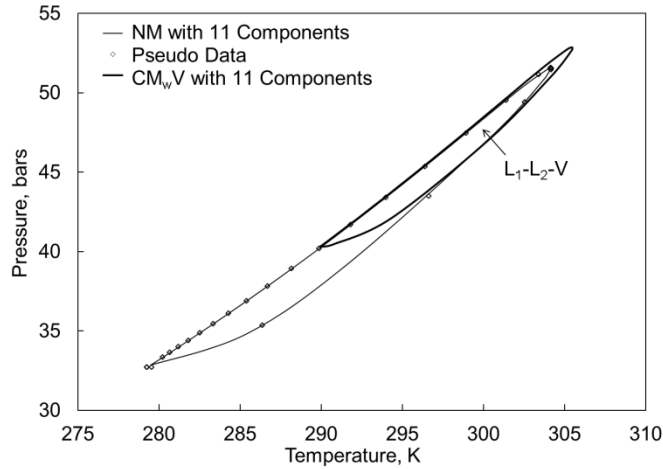
Figure 3-11. Three-phase P-T diagrams for a mixture of oil 6 10% and C_2 90% based on the NM and the CM_wV.
The 11-component models for oil 6 are given in Tables 3-S3 and 3-S4 in the supporting information. The pseudo data are generated using the $CM_{w/o}V$ with 30 components.
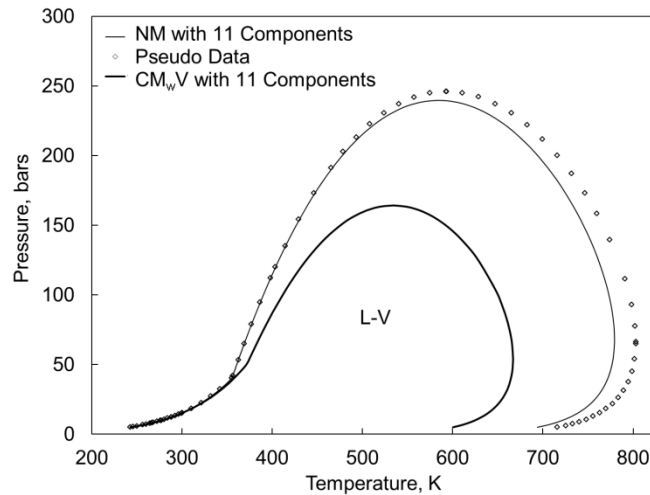
Figure 3-12. Two-phase P-T diagrams for a mixture of oil 6 10% and C_3 90% based on the NM and the CM_wV.
The 11-component models for oil 6 are given in Tables 3-S3 and 3-S4 in the supporting information. The pseudo data are generated using the $CM_{w/o}V$ with 30 components.
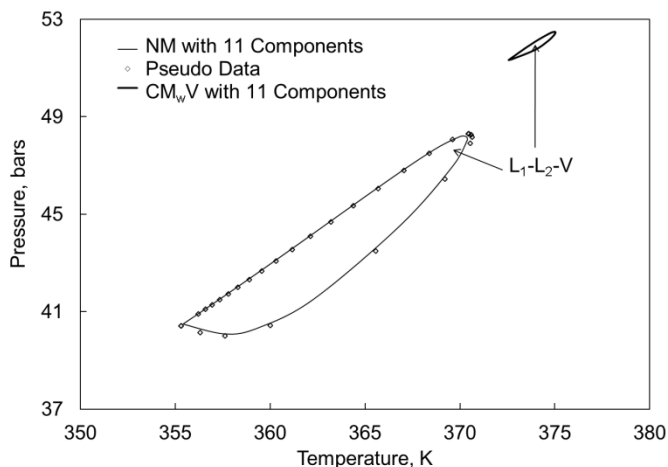
Figure 3-13. Three-phase P-T diagrams for a mixture of oil 6 10% and C_3 90% based on the NM and the CM_wV.
The 11-component models for oil 6 are given in Tables 3-S3 and 3-S4 in the supporting information. The pseudo data are generated using the $CM_{w/o}V$ with 30 components.
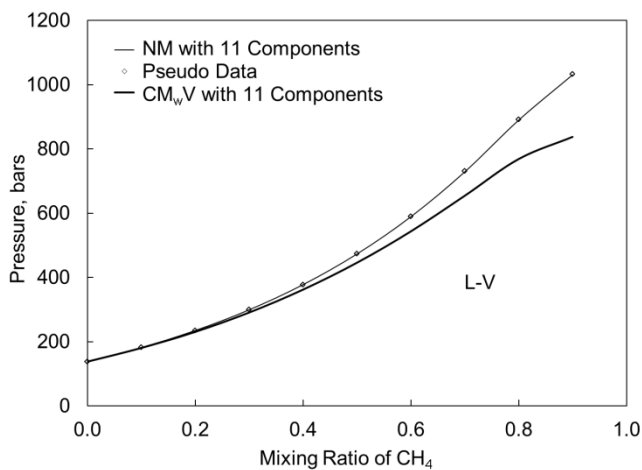
Figure 3-14. P-x diagrams for the oil-6/C_1 pseudo binary pair at 333.15 K based on the NM and CM_wV with 11 components.
The 11-component models are given in Tables 3-S3 and 3-S4 in the supporting information. The pseudo data are generated using the $CM_{w/o}V$ with 30 components.
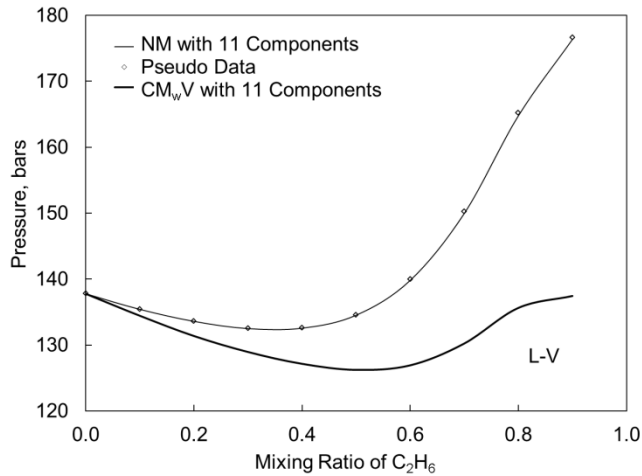
Figure 3-15. P-x diagrams for the oil-6/C_2 pseudo binary pair at 333.15 K based on the NM and CM_wV with 11 components.
The 11-component models are given in Tables 3-S3 and 3-S4 in the supporting information. The pseudo data are generated using the $CM_{w/o}V$ with 30 components.
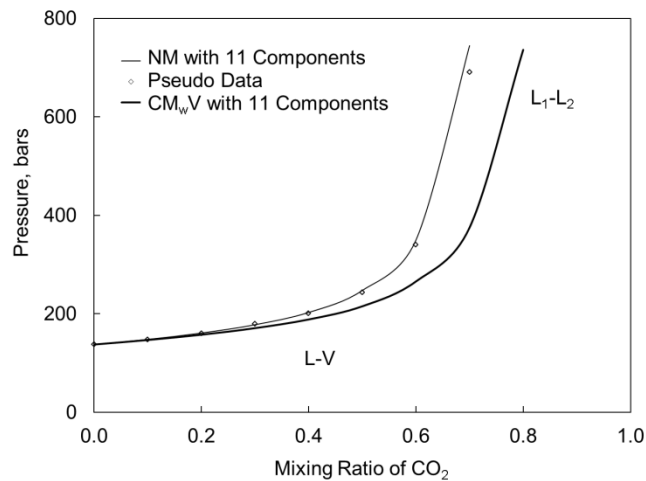
Figure 3-16. P-x diagrams for the oil-6/CO_2 pseudo binary pair at 333.15 K based on the NM and CM_wV with 11 components.
The 11-component models are given in Tables 3-S3 and 3-S4 in the supporting information. The pseudo data are generated using the $CM_{w/o}V$ with 30 components.
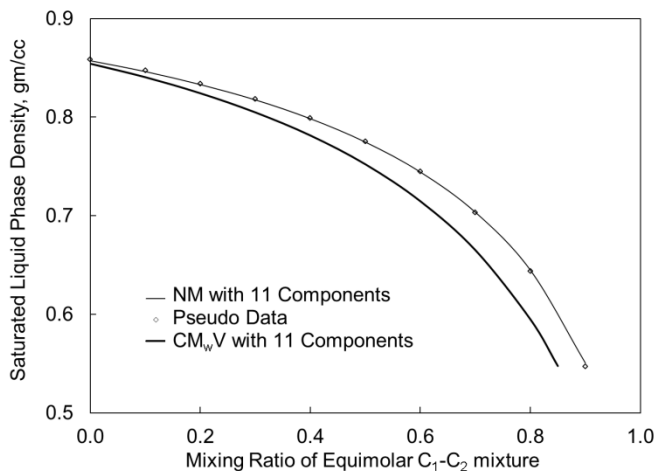
Figure 3-17. Saturated liquid densities for mixtures of oil 6 and the equimolar C_1-C_2 mixture at 333.15 K.
The 11-component models based on the NW and the CM_wV are given in Tables 3-S3 and 3-S4 in the supporting information, respectively. The pseudo data are generated using the $CM_{w/o}V$ with 30 components.
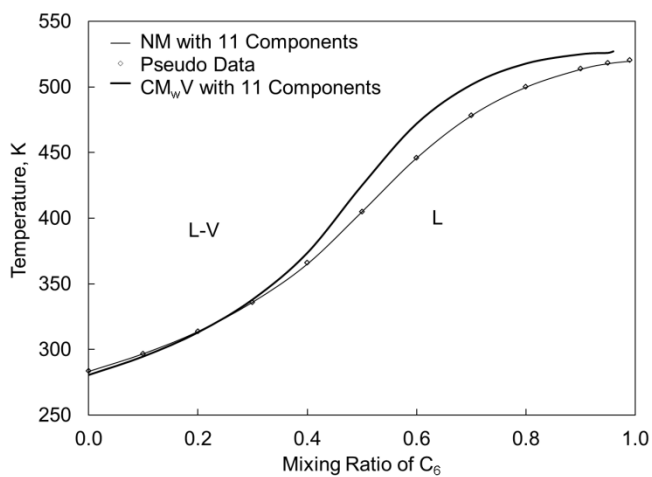
Figure 3-18. T-x diagrams for the oil-3/C_6 pseudo binary pair at 34.47 bars.
The 11-component models based on the NW and the CM_wV are given in Tables 3-S1 and 3-S2 in the supporting information, respectively. The pseudo data are generated using the $CM_{w/o}V$ with 30 components.
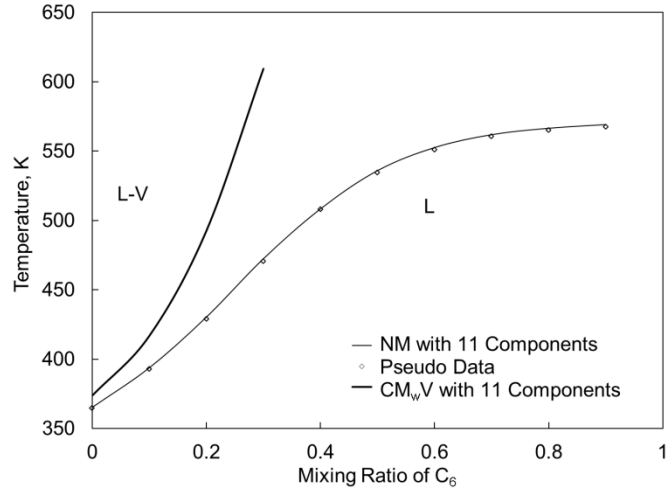
Figure 3-19. T-x diagrams for the oil-3/C_6 pseudo binary pair at 60.00 bars.
The 11-component models based on the NW and the CM_wV are given in Tables 3-S1 and 3-S2 in the supporting information, respectively. The pseudo data are generated using the $CM_{w/o}V$ with 30 components.
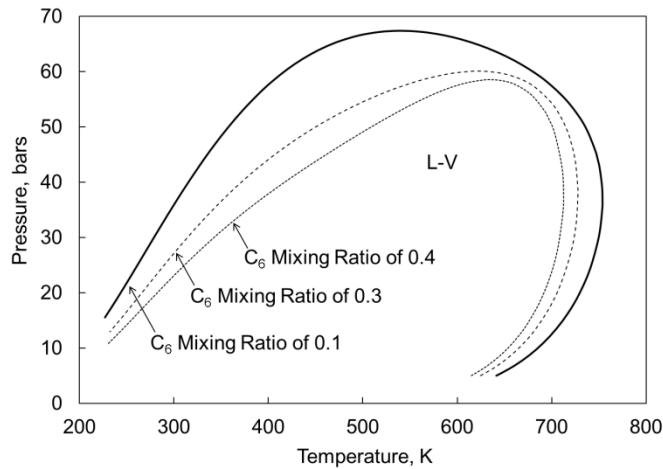
Figure 3-20. Two-phase PT diagrams for mixtures of oil 3 and C_6 at three different C_6 mixing ratios, 0.1, 0.3, and 0.4.
At the C_6 mixing ratio of 0.4, there is no two-phase region at 60.0 bars, which can be also seen in Figure 3-17.

88
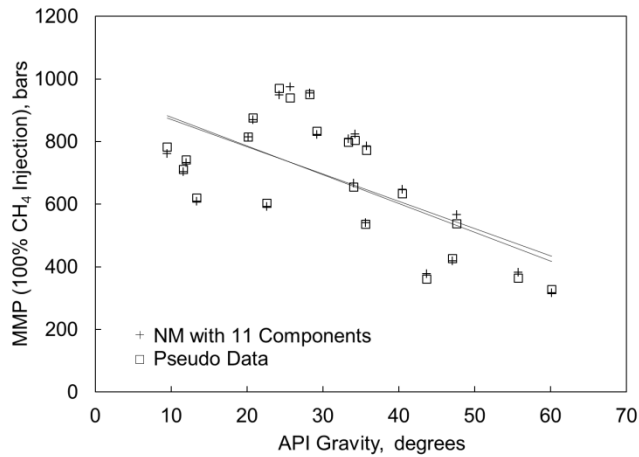
Figure 3-21. Comparison of MMP calculations for 22 oils in Table 3-1 based on the NM with 11 components and the $CM_{w/o}V$ with 30 components.
The injection gas is pure methane. The MMPs for 18 oils are calculated at their own reservoir temperatures, which are different from one another. The two trend lines for the NW with 11 components and the $CM_{w/o}V$ with 30 components almost overlap each other.
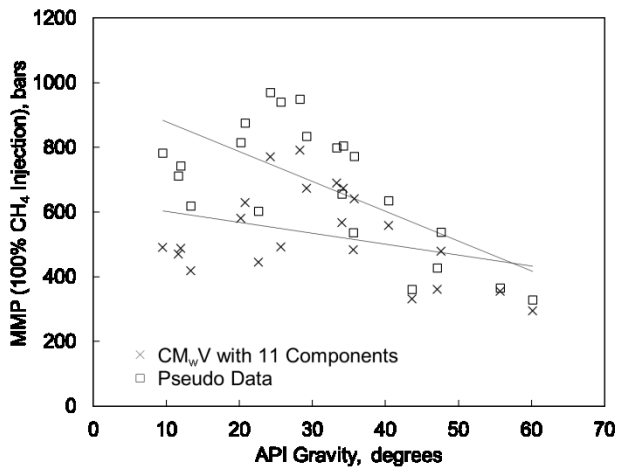
Figure 3-22. Comparison of MMP calculations for 22 oils in Table 3-1 based on the CM_wV with 11 components and the $CM_{w/o}V$ with 30 components.
The injection gas is pure methane. The MMPs for 18 oils are calculated at their own reservoir temperatures, which are different from one another. The two trend lines for the CMwV with 11 components and the CMw/oV with 30 components deviate from each other as the API gravity becomes smaller.
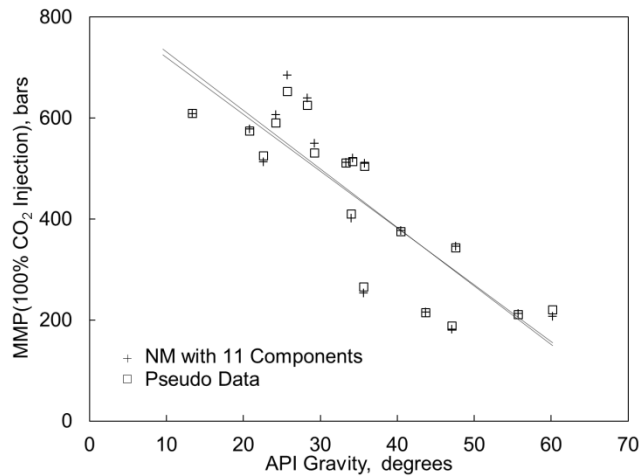
Figure 3-23. Comparison of MMP calculations for 18 oils in Table 3-1 based on the NM with 11 components and the $CM_{w/o}V$ with 30 components.

The injection gas is pure CO_2. The MMPs for 18 oils are calculated at their own reservoir temperatures, which are different from one another. The two trend lines for the NW with 11 components and the $CM_{w/o}V$ with 30 components are close to each other.
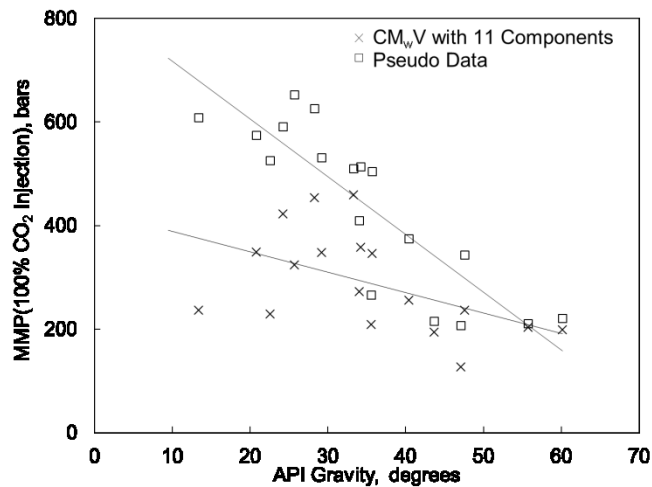
Figure 3-24. Comparison of MMP calculations for 18 oils in Table 3-1 based on the CM_wV with 11 components and the $CM_{w/o}V$ with 30 components.

The injection gas is pure CO_2. The MMPs for 18 oils are calculated at their own reservoir temperatures, which are different from one another. The two trend lines for the CM_wV with 11 components and the $CM_{w/o}V$ with 30 components deviate from each other as the API gravity becomes smaller.

90
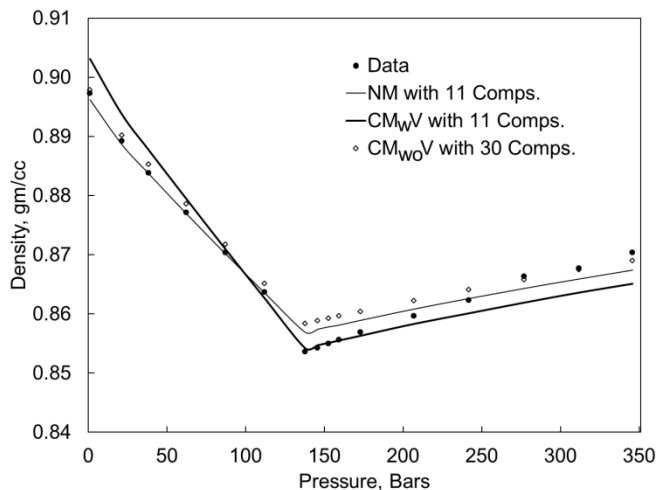
Figure 3-25. Measured and calculated densities for oil 6 at 333.15 K.
Adjustment of pseudocomponents' T_C, P_C, and ω is performed for the NM with 11 components, and the $CM_{w/o}V$ with 30 components. The CM_wV with 11 components adjusts only volume shift parameters of pseudocomponents to match densities.
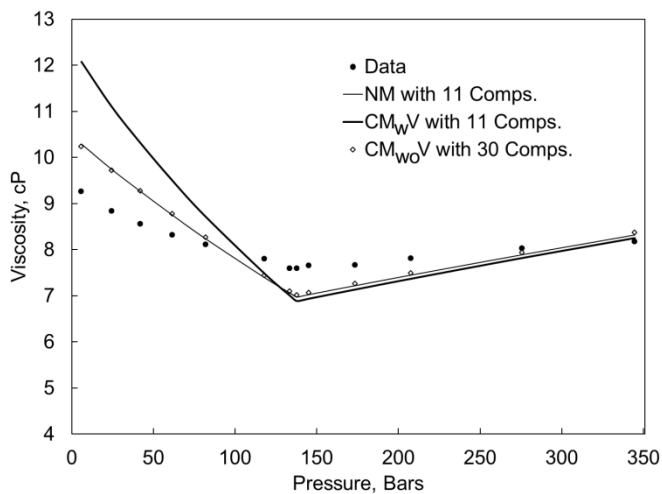
Figure 3-26. Measured and calculated viscosities for oil 6 at 333.15 K.
Adjustment of V_C was performed for pseudocomponents to match viscosities using the LBC method for the NM and CM_wV with 11 components, and the $CM_{w/o}V$ with 30 components.
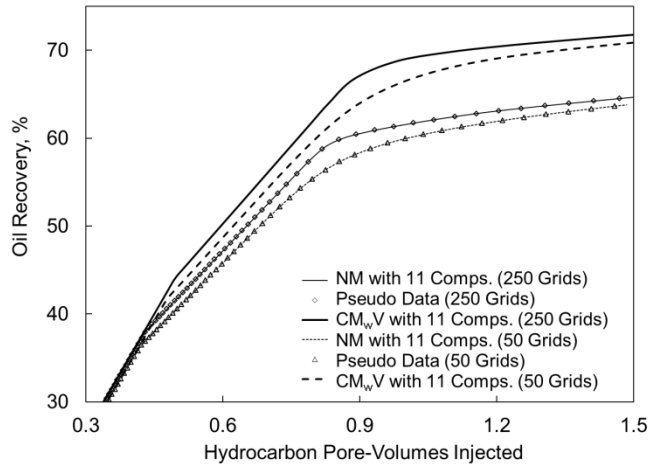
Figure 3-27. Oil recovery predictions in 1-D oil displacement simulations based on the NM and CM_wV with 11 components, along with pseudo data points generated from the $CM_{w/o}V$ with 30 components. Oil 6 is displaced by the equimolar C_1/C_2 mixture at 333.15 K at 200 bars, which is below MMP. Input parameters are given in Table 3-2. The recovery curves for 0.0-0.3 HCPVI nearly coincide, and they are not shown.
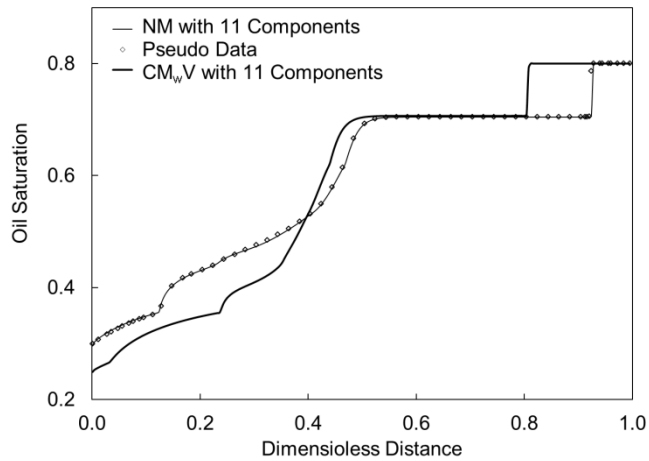
Figure 3-28. Oil saturation profiles at 0.4 HCPVI for the oil-6 displacement with the equimolar C_1/C_2 mixture at 333.15 K and 200 bars.
Predictions using the NM and CM_wV with 11 components are shown along with pseudo data generated from the $CM_{w/o}V$ with 30 components.
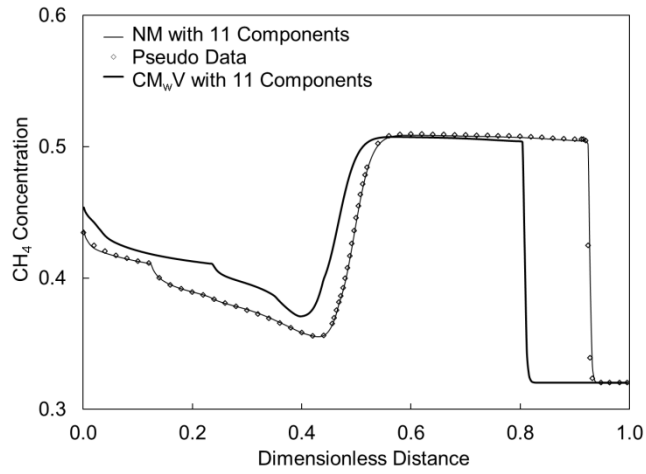
Figure 3-29. Concentration profiles for C_1 at 0.4 HCPVI for the oil-6 displacement with the equimolar C_1/C_2 mixture at 333.15 K and 200 bars.

Predictions using the NM and CM_wV with 11 components are shown along with pseudo data generated from the CMw/oV with 30 components.

Chapter 4: Characterization of Reservoir Fluids using an EOS based on Perturbation from n-Alkanes

A version of this has been published in Fluid Phase Equilibria, Year (2013), Volume: 358, Pages: 250-271.

4.1. Introduction

Compositional modeling is widely used to simulate enhanced oil recovery and recovery of gas condensates and volatile oils. Reliability of compositional simulation can depend significantly on the phase behavior model used in the simulation. Cubic equations of state (EOSs), such as the Peng-Robinson (PR) EOS (Peng and Robinson 1976, 1978), are used to calculate phase behavior in compositional simulation. These cubic EOSs along with the van der Waals mixing rules give reasonable accuracy and high computational efficiency for vapor-liquid equilibrium of reservoir fluids.

Characterization of reservoir fluids using a cubic EOS is conducted based on experimental data available, which typically consist of composition analysis and pressure-volume-temperature (PVT) data. Compositional analysis provides the concentrations of light components (e.g., up to C_6) and a plus fraction (e.g., C_{7+}), and the density of the plus fraction at atmospheric conditions. The compositional uncertainty left as a plus fraction becomes higher for heavier fluids (Kumar and Okuno 2012a). PVT measurements are performed at selected pressure-temperature-composition (P-T-x) conditions. It is difficult to predict and cover reservoir P-T-x conditions, which result from fluid and energy flow in a heterogeneous reservoir, in laboratory measurements. Thus, reservoir fluid characterization is performed under unavoidable uncertainties in composition and phase behavior data in P-T-x space. However, theory has not been established, based on which engineers can perform reliable fluid characterization using a cubic EOS under such uncertainties.

A typical characterization process consists of four main steps (Whitson and Brulè 2000; Pedersen and Christensen 2007) as follows:

Step 1. Estimation of a molar distribution with respect to molecular weight (MW) or carbon number (CN) to split the plus fraction into detailed components.

Step 2. Estimation of properties for the detailed components such as critical temperature (T_C), critical pressure (P_C), critical volume (V_C), acentric factor (ω), and volume-shift parameters.

Step 3. Grouping of the detailed components into fewer pseudocomponents.

Step 4. Regression of pseudocomponents' properties to match experimental data available.

The parameter regression in step 4 is often needed because steps 1-3 make certain assumptions causing deviations of predictions from actual phase behavior. For example, various correlations used in step 2 were developed for an EOS to reproduce the critical point and vapor pressure for the pseudocomponent of a given CN. Use of such correlations implicitly assumes a certain distribution of hydrocarbon types within that CN group (e.g., paraffins, naphthenes, and aromatics, or PNA distribution). Furthermore, unless volume shift is used, a cubic EOS is inaccurate in prediction of liquid densities even if accurate critical parameters and acentric factor are known and used (Peneloux et al. 1982; Jhaveri and Youngren 1988; Søreide 1989).

Current best practice for step 4 is step-wise manual adjustment of parameters to match experimental data available. Simultaneous regression of various parameters using software as a black box is not recommended (Kumar and Okuno 2012a). The adjustment parameters often used include T_C, P_C, V_C,

ω, volume-shift parameters, and binary interaction parameters (BIPs) for pseudocomponents. Special care must be taken by experienced engineers to ensure physically acceptable trends of adjustment parameters with respect to MW or CN (Wang and Pope, 2001). Even with this best practice, different fluid models are created depending on selection of adjustment parameters and the adjustment amounts (Lolley and Richardson 1997). Since parameter adjustments are conducted with little physical justification, it is unclear whether the resulting fluid model is reliable when used in compositional simulation to predict oil and gas recovery.

The various issues described above indicate that theory should be developed for reliable fluid characterization using a cubic EOS under uncertainties in composition and phase behavior data in P-T-x space. One of the main reasons for the lack of theory is likely the unknown, implicit, non-linear relationship between phase behavior predictions and adjustment parameters such as T_C, P_C, V_C, ω, volume-shift parameters, and BIPs.

Different characterization methods have been proposed for different reservoir fluids (Whitson 1983; Stamataki and Magoulas 2001; Montel and Gouel 1984; Leibovici 1984; Lomeland and Harstad 1995); for example, gas condensates (Yarborough 1979; Lawal et al. 1985; Pedersen et al. 1988; Guo and Du 1989), volatile oils (Peneloux et al. 1979; Whitson and Torp 1983), near-critical fluids (Zuo and Zhang 2000; Al-Meshari and McCain 2006; Hosein and Dawe 2011; Hosein et al. 2013), and heavy oils (Krejbjerg and Pedersen 2006; Ghasemi et al. 2011). However, P-T-x space that phase behavior spans is continuous. Although size-asymmetric mixtures can be difficult to model using a cubic EOS with the van der Waals mixing rules (Gregorowicz and De Loos 2011; Harismiadis et al. 1991), it will substantially benefit the petroleum industry if continuous modeling of all types of reservoir fluids becomes possible using a simple cubic EOS.

In our previous research, a method was developed for heavy-oil characterization using the PR EOS with the van der Waals mixing rules without volume shift (Kumar and Okuno 2012a). Uncertainty issues in heavy-oil characterization were addressed based on the concept of perturbation from n-alkanes (the PnA method). Pseudocomponents were initially assigned T_C, P_C, and ω that were optimized for n-alkanes in terms of liquid densities and vapor pressures using the PR EOS (Kumar and Okuno 2012b). The optimized reference values allowed for well-defined directions for perturbation of pseudocomponents' T_C, P_C, and ω to match PVT data available. We presented that robust regression using the PnA method required only three perturbation parameters to match volumetric and compositional phase behaviors with no volume shift. Important physical considerations used in the development of this PnA method include the following:

(1) A PNA distribution of a plus fraction is interpreted as a perturbation from the limiting distribution of 100% n-alkanes.

(2) T_C and P_C of n-alkane are lower than those of other types of hydrocarbons (e.g., aromatics) within a given CN group. The trend is the other way around for ω.

(3) Without using volume shift, compositional and volumetric phase behaviors are properly coupled, and density data are effectively used.

(4) Pitzer's definition of ω (Pitzer 1955; Pitzer et al. 1955) is satisfied for all pseudocomponents.

In this paper, we extend the PnA method to lighter fluids, such as gas condensates, volatile oils, and near-critical fluids. The main novelty of the new PnA method is that it considers proper variations of the attraction and covolume parameters of pseudocomponents based on the component distribution determined in the first characterization step. This physical consideration added is more important for lighter fluids. The new PnA method naturally reduces to the previous PnA method for heavy oils.

In the subsequent sections, we first discuss effects of volume shift on the Gibbs free energy and phase behavior predictions. The extension of the PnA method is then discussed in detail, where the importance of considering the interrelationship between the attraction and covolume parameters is explained. After that, the extended PnA method is applied to 77 different reservoir fluids, consisting of 34 heavy and black oils, 12 volatile oils, and 31 gas condensates. Six fluids are near critical among them. The universal applicability of the PnA method is conclusively shown in these applications.

4.2.   Effect of Volume-Shift Parameter Regression on Gibbs Free Energy

Volume-shift parameters are widely used to correct volumetric predictions from a cubic EOS. Volume-shift parameters alter the form of a cubic EOS, but not the form of the fugacity equations. Therefore, volume shift can be performed separately from compositional behavior predictions (Peneloux et al. 1982; Jhaveri and Youngren 1988). Volume shift, however, affects compositional behavior predictions when used as regression parameters in fluid characterization.

Kumar and Okuno (2012a) conducted comparisons of phase behavior predictions from two characterization methods using the PR EOS; one without volume shift and the other with volume shift. Although the two characterizations were equally accurate at the P-T-x conditions used in the regression, the latter gave erroneous phase behavior predictions at other P-T-x conditions. The deviation between the two characterizations was more significant for heavier oils since heavier oils tend to require more volume correction using the PR EOS.

In this section, we discuss the effects of volume shift in fluid characterization on phase behavior predictions. Volumetric phase behavior predictions are solved for in solution of a cubic equation, which contains volume-shift parameters (if used), T_C, P_C, ω, and BIPs. Thus, two different characterizations that give the same volumetric predictions have different sets of T_C, P_C, ω, BIPs, and volume-shift parameters.

Compositional phase behavior predictions are determined by the parameters that form the single-phase Gibbs free energy (i.e., the Gibbs free energy calculated assuming a stable single-phase state even in multiphase regions). Let us consider two characterizations for a given fluid that yield the same volumetric predictions; one without volume shift and the other with volume shift. The parameter set is $(\underline{T}_C, \underline{P}_C, \underline{\omega}, \underline{k})^{wo}$ for the former, and is $(\underline{T}_C, \underline{P}_C, \underline{\omega}, \underline{k}, \underline{c})^{w}$ for the latter. The underlines for $\underline{T}_C$, $\underline{P}_C$, $\underline{\omega}$, and $\underline{c}$ indicate vectors consisting of N_C elements, where N_C is the number of components. $\underline{c}$ is a vector for

N_C volume-shift parameters. $\underline{k}$ is a BIP matrix consisting of k_{ij} ($i = 1, 2,\ldots, N_C$, and $j = 1, 2,\ldots, N_C$). For the two cases, the dimensionless molar Gibbs free energy change on mixing, g, at a given T, P, and overall composition ($\underline{z}$) is the following:

$$g^{wo} = \left(\frac{\Delta_{mix}G}{RT}\right)^{wo} = \sum_{i=1}^{N_C} z_i \ln\left[\frac{z_i\overline{\varphi}_i(\underline{T}_C,\underline{P}_C,\underline{\omega},\underline{k},T,P,\underline{z})^{wo}}{\varphi_i(T_{Ci},P_{Ci},\omega_i,T,P)^{wo}}\right] \tag{4-1}$$

$$g^{w} = \left(\frac{\Delta_{mix}G}{RT}\right)^{w} = \sum_{i=1}^{N_C} z_i \ln\left[\frac{z_i\overline{\varphi}_i(\underline{T}_C,\underline{P}_C,\underline{\omega},\underline{k},T,P,\underline{z})^{w}\exp\left(\frac{c_iP}{RT}\right)}{\varphi_i(T_{Ci},P_{Ci},\omega_i,T,P)^{w}\exp\left(\frac{c_iP}{RT}\right)}\right] = \sum_{i=1}^{N_C} z_i \ln\left[\frac{z_i\overline{\varphi}_i(\underline{T}_C,\underline{P}_C,\underline{\omega},\underline{k},T,P,\underline{z})^{w}}{\varphi_i(T_{Ci},P_{Ci},\omega_i,T,P)^{w}}\right] \tag{4-2}$$

where φ_i is the fugacity coefficient for pure component i, and $\overline{\varphi}_i$ is the fugacity coefficient of component i in a mixture of overall composition $\underline{z}$. A single phase is assumed. **Equations 4-1** and **4-2** show that two different sets of parameters give two different single-phase Gibbs free energy surfaces in P-T-x space.

For example, an oil is characterized as a ternary fluid using the PR EOS with and without volume shift as shown in **Table 4-1.** Actual compositional simulation studies often require a larger number of components. Use of only three components in this case study is to visually demonstrate the volume-shift effects in a simple manner. The ternary fluid consists of the L, I, and H components. All BIPs are zero for the two characterizations without loss of generality of the discussion. The two characterizations are equally accurate in calculation of the saturation pressure, 196.48 bars, at the reservoir temperature 330.4 K and oil densities at 276.3, 258.5, 223.6, 196.5, 175.2, 144.6, 103.0, 62.3, 41.0, and 7.1 bars at 330.4 K. However, the two characterizations have different properties for the H component.

Figures 4-1 and 4-2 show g^{wo} and g^{w}, respectively, in composition space at 196.48 bars and 330.4 K based on the parameters given in Table 4-1 and Equations 4-1 and 4-2. The contour lines are equally spaced. The difference between g^{wo} and g^{w} is not obvious in the figures, but g^{wo} exhibits a deeper valley than g^{w} in this case. Although volume shift does not change the form of fugacity equations, different set of parameters (the w and wo cases) results in different phase equilibria. For the two cases, the fugacity equations for liquid-vapor (L-V) equilibrium at a given T, P, and overall composition is the following:

$$x_i^{wo}\overline{\varphi}_i^{L}\left(\underline{T}_C, \underline{P}_C, \underline{\omega}, \underline{k}, T, P, \underline{x}\right)^{wo} = y_i^{wo}\overline{\varphi}_i^{V}\left(\underline{T}_C, \underline{P}_C, \underline{\omega}, \underline{k}, T, P, \underline{y}\right)^{wo} \tag{4-3}$$

$$x_i^{w}\overline{\varphi}_i^{L}\left(\underline{T}_C, \underline{P}_C, \underline{\omega}, \underline{k}, T, P, \underline{x}\right)^{w} = y_i^{w}\overline{\varphi}_i^{V}\left(\underline{T}_C, \underline{P}_C, \underline{\omega}, \underline{k}, T, P, \underline{y}\right)^{w} \tag{4-4}$$

for all i, where i = 1, 2,.., N_C, and $\underline{x}$ and $\underline{y}$ are the liquid and vapor phase composition vectors, respectively. **Equations 4-3** and **4-4** are solved on the Gibbs free energy shown in Figures 4-1 and 4-2. Results are presented in **Figures 4-3 and 4-4.** The two-phase envelope without volume shift is larger than that with volume shift at 196.48 bars and 330.4 K in this case. The two characterizations give similar predictions near the oil composition. However, the difference becomes significant in the region away from the oil composition.

The different immiscibilities predicted can result in a large difference in the minimum miscibility pressure (MMP) for the two characterizations. For example, the MMP calculated at 330.4 K for the injection gas of 40% L and 60% I is 351.86 bars without volume shift and 250.75 bars with volume shift. This simple case study clearly shows that the effects of volume shift can be quite significant on oil recovery predictions. Since P-T-x conditions used in laboratory measurements cannot cover actual reservoir conditions encountered in reservoir processes, the volume-shift effects in P-T-x space should be considered in fluid characterization. The PnA method does not require volume shift to accurately predict volumetric and compositional phase behaviors. Therefore, the PnA method uses no volume shift, and properly couples the two types of phase behavior.

4.3. Extension of the Perturbation from n-Alkanes (PnA) method

The PnA method previously presented in Kumar and Okuno (2012a) successfully characterized heavy oils with the PR EOS as described in the introduction section. It required only three adjustment parameters f_T, f_P, and f_m to perturb T_C, P_C, and ω of pseudocomponents, respectively. The f_m perturbation parameter was used for the m parameter, a one-to-one function of ω used in the temperature-dependent term in the attraction term of the PR EOS. The perturbations were performed in well-defined directions from the n-alkane values of Kumar and Okuno (2012b). A single value for each of the three adjustment parameters was successfully applied for all pseudocomponents for heavy-oil characterization.

In this section, the PnA method is extended to characterize other types of reservoir fluids without loss of simplicity. A fourth adjustment parameter is introduced to consider proper trends of the attraction and covolume parameters of the PR EOS with respect to MW (or CN) depending on the overall composition of the fluid to be characterized. The main novelty of this research lies in here.

4.3.1. Overall Composition

The chi-squared distribution function is used in the composition characterization step in the PnA method. More complicated functions like the gamma (Γ) distribution function can also be used. However, the chi-squared distribution function can characterize the degree of skew, which is the key information required in the new PnA method, using the p parameter in

$$f_{dis} = \frac{2^{-\frac{p}{2}} e^{-\frac{S}{2}} S^{\left(\frac{p}{2}-1\right)}}{\Gamma\left(\frac{p}{2}\right)}$$ (4-5)

Equation 4-5 expresses the probability density for the S variable, which is MW or CN in the context of composition characterization. The p parameter increases with decreasing API gravity in general. Its practical values range between 2 and 10 (Quiñones-Cisneros et al. 2004a, 2004b). **Figure 4-5** shows chi-squared distributions for different p values. The compositional characterization method using Equation 4-5 is described in detail in Quiñones-Cisneros et al. (2004b), and is not duplicated here.

4.3.2. Critical Parameters for n-Alkanes and Their Internal Consistency

A plus fraction contains a variety of compounds, such as paraffins, naphthenes, and aromatics (PNA). Conventional characterization methods assume implicitly a certain PNA distribution in their critical parameter estimation as described in the introduction section. In the PnA method, the PNA distribution of a plus fraction is initially set to be the limiting distribution of 100% n-alkanes, and then characterized explicitly in the regression algorithm. Thus, pseudocomponents are initially assigned the n-alkane values for T_C, P_C, and m based on the correlations of Kumar and Okuno (2012b). The MW in the correlations was adjusted by perturbation parameters f_T, f_P, and f_m in Kumar and Okuno (2012a) (**Equations 4-6 to 4-8**);

$$T_C = 1154.35 - 844.83(1.0 + 1.7557 \times 10^{-3} f_T MW)^{-2.0} \tag{4-6}$$

$$P_C = 559.93 \left(\frac{MW}{f_P}\right)^{-0.638} - 1.49 \tag{4-7}$$

$$m = 0.4707 + 2.4831(f_m\ MW)^{-\left(\frac{39.933}{f_m\ MW}\right)} \quad . \tag{4-8}$$

The m parameter is function of ω as shown in **Equations 4-9** and **4-10**:

$$m = 0.37464 + 1.54226\omega - 0.26992\omega^2 \quad \text{for } \omega < 0.3984 \tag{4-9}$$

$$m = 0.379642 + 1.48503\omega - 0.164423\omega^2 + 0.016666\omega^3 \quad \text{for } \omega \geq 0.3984. \tag{4-10}$$

Equations 4-6 to 4-8 reduce to the original correlations of Kumar and Okuno (2012b) for n-alkanes when the perturbation parameters are 1.0. These correlations were developed using T_C, P_C, and m optimized for n-alkanes from C_7 to C_{100} in terms of the vapor pressure and liquid density using the PR EOS without volume shift. These correlations yield 3.0% and 3.4% AAD for density and vapor pressure predictions, respectively.

Use of the correlations of Kumar and Okuno (2012b) with the PR EOS satisfies Pitzer's definition of ω for each n-alkane. That is, the vapor pressure (P_{VAPI}) calculated at $0.7T_C$ using the PR EOS with T_C, P_C, and ω is equal to the vapor pressure (P_{VAPII}) from **Equation 4-11**.

$$(P_{VAP})_{at\ T_r=0.7} = 10^{-(1+\omega)} P_C \tag{4-11}$$

using P_C and ω. This internal consistency of T_C, P_C, and ω was also satisfied for each pseudocomponent in the regression algorithm of Kumar and Okuno (2012a) by minimizing the ε function as shown in **Equation 4-12**.

$$\varepsilon = \frac{1}{n}\sum_{i=1}^{n} \text{abs}(P_{VAPI} - P_{VAPII}) \tag{4-12}$$

where n is the number of pseudocomponents. A minimum in ε typically occurs when the m parameter for one of the pseudocomponents falls in a range between 0.94 and 0.96. The internal consistency is satisfied when one of the pseudocomponents has an m parameter value of 0.946 in the new algorithm presented later.

4.3.3. Attraction and Covolume Parameters

Equations 4-6 to 4-8 use a single value for each of the three perturbation parameters for all pseudocomponents. This uniform perturbation was successful in the previous PnA method for characterizing heavy oils. In this research, the PNA distribution of a plus fraction is characterized more mechanistically.

Yarborough (1978) presented trend curves for specific gravity (SG) at 288.15 K and 1.01325 bars as a function of CN and "aromaticity". The aromaticity parameter was defined as the percentage of total carbon atoms in a molecule, which are within the benzene ring. In our opinion, however, aromaticity in his presentation should be interpreted as deviation from n-alkanes. For example, naphthenes cannot be well-defined using aromaticity, but their standard SG trend was shown to be much higher than that of n-alkanes. Nevertheless, the term "aromaticity", instead of deviation from n-alkane, is used for brevity in this paper. In Yarborough's presentation, CN ranged from 7 to 40, and aromaticity from 0 to 80. The standard SG trend curves for the aromaticity levels of 10 and 60 are reproduced in **Figure 4-6**. The standard SG increases with CN and aromaticity. Although the trend curves of Yarborough are based on the standard SG, we use them here to show qualitatively how perturbation should be done in different regions of composition space.

Figure 4-6 also shows the standard SG calculated for the aromaticity levels of 10 and 60 using the PR EOS with uniformly perturbed critical parameters. The uniform perturbations for the two aromaticity levels were conducted by matching the standard SG of C_7. Results show that the uniform perturbation gives deviation from Yarborough's trend curves for higher CN. However, the deviation levels off at a certain CN as shown in **Figure 4-7.**

We then match the SG trend curves for CNs from 8 to 40 using variable perturbation. **Figure 4-8** shows the resulting perturbation parameters for CNs from 7 to 40 for the aromaticity level of 10. Uniform perturbation is appropriate for the higher CN range, while sharply increasing perturbation is required for the lower CN range. This explains why uniform perturbation can be used for heavy-oil characterization, where CNs of all pseudocomponents are typically higher than 20. For lighter reservoir fluids, however, a few pseudocomponents usually fall in the region of composition space where perturbation should be increased with CN or MW.

Perturbations of critical parameters directly affect the attraction (a) and covolume (b) parameters of a cubic EOS, which in turn affect the Gibbs free energy and volumetric predictions in P-T-x space. **Figures 4-9 and 4-10** show the a and b parameters, respectively, for three levels of aromaticity 0, 10, and 60. The original correlations of Kumar and Okuno (2012b) are used for n-alkanes (i.e., zero aromaticity). The f_T, f_P, and f_m values fitted to Yarborough's trend curves are used for the aromaticity levels 10 and 60. The a parameter increases with CN for a fixed aromaticity level. The effect of aromaticity on the a parameter is not systematic; i.e., the a parameter increases with aromaticity for light hydrocarbons, and the trend is the other way around for heavier hydrocarbons. The trend of the b parameter is more systematic. The b parameter for n-alkane is higher than those for aromatic

hydrocarbons for a given CN. Also, n-alkanes exhibit the largest gradient of the b parameter with respect to CN.

Figure 4-11 shows a parameter group a/b^2 (ψ) based on the values for the a and b parameters in Figures 4-9 and 4-10. The ψ parameter for each component can be calculated using the PR EOS as follows:

$$\psi = \frac{\Omega_a}{\Omega_b^2} P_C \alpha(T).$$
(4-13)

The ψ parameter is a function of T_C, P_C, ω, and T as shown in **Equation 4-13**. The ψ parameter is sensitive to the level of aromaticity for light and intermediate hydrocarbons, where variable perturbation is required (see Figure 4-11). This is also true at a realistic reservoir temperature of 370.15 K as shown in **Figure 4-12**. We therefore use the ψ parameter to control variable perturbation in different regions of composition space. The ψ parameter monotonically decreases with CN for high aromaticity levels, but exhibits a maximum for low aromaticity levels including n-alkanes. van Konynenburg and Scott (1980) used the ψ parameter in their pioneering research on classification of binary phase diagrams using the van der Waals EOS. The ψ parameters for two components (i.e., ψ_i, where i = 1, 2.) were used to characterize size-asymmetric binary mixtures.

Figure 4-12 is useful in considering qualitatively how the ψ parameter should be characterized depending on the fluid composition of interest. In general, heavier fractions are relatively more naphthenic and aromatic than lighter fractions (Yarborough 1979; Nagy and Colombo 1967). This physical trend is plausible considering that a larger number of carbon atoms allow for more variations of hydrocarbon molecular structures; e.g., if the uniform distribution of molecular structures is considered within individual CN groups, the concentration of n-alkane becomes lower for higher CN.

The ψ parameter changes its sensitivity to aromaticity around CN 20 as shown in Figures 4-11 and 4-12. In the CN range higher than approximately 20, the ψ parameter decreases with CN regardless of the level of aromaticity. In the lower CN range, the ψ parameter typically increases with CN because of the increasing aromaticity trend with respect to CN within a given fluid as just discussed in the previous paragraph. Two trend curves for the ψ parameter are presented for these two model fluids in Figure 4-12.

The ψ parameter typically increases with CN (like the lighter model fluid in Figure 4-12), if all pseudocomponents are within the range of C_7-C_{20}. For some heavy oils, the lightest pseudocomponent can be around C_{20}, and the ψ parameter is expected to decrease almost linearly with CN (like the heavier model fluid in Figure 4-12). For many fluids, however, the CN range of pseudocomponents contains the boundary of the two distinct regions, which is approximately C_{20}. For these fluids, the ψ parameter exhibits combinations of these two model trends depending on the CN range of their pseudocomponents and their average aromaticity. The two model trends in Figure 4-12 are shown to be linear for simplicity. Actual trends of characterized fluids are non-linear in general as shown in the next section.

We assume use of four pseudocomponents based on the chi-squared compositional characterization for discussion here. CN ranges observed for various fluids in our research can be summarized as follows: 7-30 for gas condensates, 9-45 for light oils, 11-60 for intermediate oils, and 13-85 for heavy oils. Light gas condensates, for which the C_{7+} fraction is less than 2%, can have all four pseudocomponents within the CN range from 7 to 20. Their ψ trends can be strongly influenced by the n-alkane curve, which exhibits a convex trend (see Figure 4-12).

The overall composition information can be obtained by the distribution function fitted to the composition data available. The PnA method considers an expected trend of ψ in the regression process depending on the p parameter value obtained from the fitted chi-squared distribution. Uniform perturbation is suitable for heavy oils as presented in Kumar and Okuno (2012a). Hence, the p parameter value of 10 corresponding to extra heavy oils is considered as the limiting value, for which perturbation is uniform. With increasing API gravity, the p parameter value decreases below 10, and variable perturbation is required according to the ψ trends discussed above.

4.3.4. Regression Algorithm

In this subsection, we discuss briefly how the current PnA method implements the new concept regarding the ψ parameter presented in the previous subsection. The main difference from the regression algorithm of Kumar and Okuno (2012a) is that the perturbation parameters f_T, f_P, and f_m in Equations 4-6 to 4-8 are augmented by a fourth adjustment parameter γ. We measure a deviation of the fluid of interest from the limiting fluid with the p parameter value of 10 using constants d_j, where j is the component index for pseudocomponents. The d constants are calculated specifically to a given fluid, and collectively serve as a fluid type indicator. Then, the d constants and the fourth adjustment parameter γ are combined to have a desired trend of the ψ parameter.

The algorithm uses four adjustment parameters f_T, f_P, f_m, and γ to match the saturation pressure at the reservoir temperature and liquid densities at different pressures and the reservoir temperature. Volume shift parameters are not used in the PnA method. BIPs are constant as described in Kumar and Okuno (2012a). The BIPs used in the PnA method are 0.0 for N_2-CO_2, 0.1 for N_2-C_i, where $1 \leq i \leq 6$, 0.13 for N_2-pseudocomponents, and 0.1 for CO_2-hydrocarbons. BIPs are zero for hydrocarbon-hydrocarbon pairs. A step-wise description of the algorithm is presented below.

Step 1. Composition characterization: Using the composition data available, the plus fraction is split into n pseudocomponents using the chi-squared distribution function (Equation 4-5; see Quiñones-Cisneros et al. 2004b). This step gives the mole fractions and MWs of n pseudocomponents and the p value of the fluid.

Step 2. Calculation of gradation constants d_j: The mole fractions and MWs of n pseudocomponents are calculated assuming that the fluid p value is 10. We calculate the ratios of the MWs from step 1 to the MWs with the assumption of p equal to 10. The resulting ratios are normalized with respect to the ratio for the lightest pseudocomponent. These normalized ratios are the d_j constants, where j = 1, 2, …, n. That is, d_1 is always 1.0.

Step 3. Check for the necessity of using density data. Characterize the fluid assuming that f_T, f_P, and f_m are equal to 1.0 in Equations 4-6 to 4-8. Compare density calculations using the PR EOS to the experimental density data. If the average density deviation indicates overprediction of the densities, than go to step 5. Otherwise, continue to step 4 below.

Step 4. Characterization using density and saturation pressure data.

    i. $f_T = 1.0$, $f_P = 1.0$, $\gamma = 0.0$, and $k = 1$, where k is the iteration index.

    ii. Find f_m with which T_C, P_C, and m are internally consistent using **Equation 4-14.**

$$m_j = 0.4707 + 2.4831 \left(f_{mk} MW_j d_j^{\gamma k}\right)^{-\left(\frac{39.933}{f_{mk} MW_j d_j^{\gamma k}}\right)} \tag{4-14}$$

In each iteration, f_m is adjusted until one of the pseudocomponents has an m parameter value equal to 0.946.

    iii. Calculate critical parameters using **Equations 4-15** and **4-16.**

$$T_{Cjk} = 1154.35 - 844.83 \left(1.0 + 1.7557 \times 10^{-3} f_{Tk} d_j^{\gamma k} MW_j\right)^{-2.0} \tag{4-15}$$

$$P_{Cjk} = 559.93 \left(\frac{MW_j}{f_{Pk} d_j^{\gamma k}}\right)^{-0.638} - 1.49 \tag{4-16}$$

    iv. Adjust f_T and f_P to match the saturation pressure and density data.

    v. Update γ using **Equation 4-17**.

$$\gamma_k = 0.5\left[\gamma_{k-1} + z_I(3.464 + h)\left(f_{T,k-1}^{2\theta} + f_{P,k-1}^{2\theta} + f_{m,k-1}^{2\theta}\right)/\left(f_{T,k-1} + f_{P,k-1} + f_{m,k-1}\right)\right], \tag{4-17}$$

where $\theta = (3.0 + h)/h$, h is the harmonic mean of z_L, z_I, and z_H, and

z_L: Mole fraction of methane in the overall composition

z_I: Sum of the mole fractions of N_2, CO_2, and C_i, where i = 2, 3,…, 6.

z_H: Mole fraction of C_{7+}.

f_T and f_P are set to 1.0, and go to step 4-ii until the difference of the γ values between two consecutive iterations becomes below a tolerance; e.g., 10^{-3}.

Step 5. Characterization using only saturation pressure data.

    i. $f_T = 0.98$, $f_P = 0.98$, $\gamma = 0.0$ (for bubble point search), $\gamma = 1.5$ (for dew point search), and k = 1, where k is the iteration index.

    ii. Find f_m with which T_C, P_C, and m are internally consistent using Equation 4-14.

    iii. Calculate critical parameters using Equations 4-15 and 4-16.

    iv. Adjust γ until the saturation pressure is matched.

    Figure 4-13 shows an example trend of the four adjustment parameters f_T, f_P, f_m, and γ during iteration when oil 2 (39.89°API) in **Table 4-2** is characterized using the above algorithm. As γ increases from the starting value of zero, f_T, f_P, and f_m decrease. Convergence is achieved when the rate of increase in γ or the rate of decrease in f_T, f_P, and f_m becomes negligible. The internal consistency of T_C, P_C, and m is evaluated by the ε function given in Equation 4-12. **Figure 4-14** shows that the ε function decreases with increasing γ and is sufficiently small on convergence. The algorithm is written in

FORTRAN, and takes less than two minutes on average per fluid using the Intel Core i7-960 processor at 3.20 GHz and 8.0 GB RAM.

Gas condensates and light volatile oils behave like n-alkane mixtures due to low concentrations of the C_{7+} fraction. For these fluids, density data are not required in the PnA method. The next section shows that the correlations of Kumar and Okuno (2012b) enable the PR EOS to accurately predict densities in such cases.

The key parameter in the PnA method is γ, which controls the ψ gradient with respect to CN (or MW) of pseudocomponents. Hence, adjustment of γ can be carried out using more data, instead of using Equation 4-17. For example, liquid saturation data from constant volume depletion (CVD) and constant composition expansion (CCE), slim-tube MMPs, and three-phase data can be used to adjust γ. For solubility data, BIPs may be adjusted for methane and heavier pseudocomponents to change phase behavior predictions locally in composition space. As is shown in the next section, the PnA method systematically and monotonically adjusts phase behavior predictions using a few adjustment parameters, unlike the conventional methods.

4.4. Application of the PnA method

In this section, the PnA method is applied to 77 reservoir fluids, ranging from 9.5°API to 71.1°API, where 12 components are used altogether; N_2, CO_2, C_1, C_2, C_3, C_4, C_5, C_6, and four pseudocomponents. Data available and used for characterization are (i) overall compositions, (ii) saturation pressures at reservoir temperatures, and (iii) liquid densities at different pressures at reservoir temperatures, unless otherwise stated. Other types of data available, such as MMPs, CVD, and CCE, are not used in characterization, but are used to evaluate the reliability of characterized fluid models.

The significance of considering the ψ parameter is first presented using oils listed in Table 4-2. Predictions from the PR EOS with the PnA characterization are then compared with data for various fluids in the case studies subsection.

4.4.1. Significance of the ψ Parameter

In the previous section, we discussed that perturbation from n-alkanes should consider the CN range of the pseudocomponents used. Uniform perturbation is appropriate for heavy oils since all pseudo components usually fall in the higher CN range where the ψ parameter is insensitive to the level of aromaticity. For lighter fluids, some of pseudocomponents are in the lower CN range where the ψ parameter is sensitive to the level of aromaticity (see Figure 4-12). Variable perturbation should be considered to obtain appropriate trends of the ψ parameter for these fluids.

The ψ parameter for the PR EOS is a function of T_C, P_C, and m at a given temperature as shown in Equation 4-13. Obviously, different characterization schemes result in different trends of the ψ parameter. To see this, oil 1 (35.22°API) in Table 4-2 is characterized using four different schemes; Case 1. The PnA method with uniform perturbation (i.e., γ is fixed at zero)

Case 2.   The PnA method with variable perturbation (i.e., the algorithm presented in the previous section)

Case 3.   The conventional method using the PVTsim software without volume shift ($CM_{w/o}V$)

Case 4.   The conventional method using the PVTsim software with volume shift (CM_wV).

Case 1 corresponds to the previous PnA method presented in Kumar and Okuno (2012a).   Cases 3 and 4 are based on step-wise manual adjustment of T_C, P_C, and ω as described in detail in Kumar and Okuno (2012a).   The number of components used is 12 for all cases.   The CMs use the default BIP values from PVTsim as they would be the most suitable values for PVTsim.   They are -0.017 for N_2-CO_2, 0.0311 for N_2-C_1, 0.0515 for N_2-C_2, 0.0852 for N_2-C_3, 0.08 for N_2-C_4, 0.1 for N_2-C_5, 0.08 for N_2-C_i, where $i \geq 6$, 0.12 for CO_2,-C_j, where $1 \leq j \leq 6$, and 0.1 for CO_2-pseudocomponents.   As in the PnA method, BIPs are zeros for hydrocarbon-hydrocarbon pairs in the CMs.   For a fair comparison, the same composition characterization based on the chi-squired distribution is used for the four cases.   Saturation pressure and density data are matched by adjusting T_C, P_C, and ω for cases 1-3.   For case 4, volume shift is conducted to match density data, and saturation pressure is matched using T_C, P_C, and ω.   Then, we calculate the MMPs for the oil with injection gas (0.48% N_2, 4.97% CO_2, 58.22% C_1, 17.14% C_2, 12.10% C_3, 4.97% C_4, 1.66% C_5, and 0.53% C_6) at the reservoir temperature 374.85 K.   The corresponding slim-tube MMP is reported to be 220 bars in Jaubert et al. (2002).

The resulting trend of ψ along with the AD on the MMP is shown for each case in **Figure 4-15**.   The CN range of the pseudocomponents is approximately from 11 to 40, which is similar to the entire CN range presented in Figure 4-12.   Case 1 with uniform perturbation exhibits a monotonically decreasing trend of ψ with respect to CN for the four pseudocomponents.   The calculated MMP has a large AD of +19% compared to the slim-tube MMP.   Considering the approximate CN of 11 for the lightest pseudocomponent, the negative slope of ψ is not expected.   Cases 3 and 4 present an obvious minimum in the trend of ψ with respect to CN.   Even though the MMP calculated for case 3 is relatively accurate, it may be difficult to justify such ψ trends, considering the CN range of the pseudocomponents and that heavier pseudocomponents are more naphthenic and aromatic than lighter pseudocomponents in general (Yarborough 1979).   Use of volume shift in case 4 makes the calculated MMP less accurate due to the fundamental reasons presented in the section on Effect of Volume-Shift Parameter Regression on Gibbs Free Energy.   Case 2 shows a monotonically increasing trend of ψ with respect to CN.   The converged γ is 1.23.   Considering the inevitable dispersion effects in slim-tube tests, the AD of -6.0% is acceptable in this case.

Matching MMP data in fluid characterization has been proposed in the literature (e.g., Egwuenu et al. (2008).   It will be easy to implement this proposal in the PnA method.   **Figure 4-16** shows the MMPs calculated for different γ values.   A monotonic change in the calculated MMP is observed with respect to γ.   The slim-tube MMP of 220 bars can be predicted with γ of 1.08, and the corresponding ψ trend is shown by a dashed line in Figure 4-15.   Although matching a slim-tube MMP without considering dispersion effects has little practical importance, this exercise shows that phase behavior predictions

can be adjusted systematically and monotonically with the PnA method. Similar control over phase behavior predictions is difficult with the CM.

Figures 4-17 and 4-18 show the a and b parameters for the four pseudocomponents for each of the four cases. The dashed curves correspond to the case for γ of 1.08. Case 4 deviates significantly from the other cases in the a and b parameters. However, it is case 1 that has the largest error in the MMP calculation as shown in Figure 4-15. The a and b parameters are interdependent in fluid characterization, and the ψ parameter properly captures the interrelationship between the a and b parameters. Cases 1-3 are similar in the trends of the a and b parameters. However, the ψ parameter effectively makes the differences among the cases more marked.

For all oils in Table 4-2, slim-tube tests and measured MMPs are reported in the literature. **Table 4-3** lists slim-tube and calculated MMPs for eight oils from Table 4-2, one of which is oil 1 discussed above. A small amount of C_{7+} contained in some of the injection gases is discarded for the MMP calculations (their C_{7+} concentrations are less than 0.3%). Two cases are considered for these MMP calculations; one with variable perturbation and the other with uniform perturbation. The AAD on the MMP calculations is 6.7% for the former case and 26.7% for the latter case. These results further indicate the significance of considering the ψ parameter in perturbation using γ. The AAD from the new PnA method is similar to the result of Jaubert et al. (2002), who conducted MMP calculations for the same oils. Unlike the PnA method, they developed fluid models using various data from standard PVT measurements, swelling tests, and multicontact tests.

4.4.2. Case Studies

The 77 different fluids considered here are 34 heavy and black oils, 12 volatile oils (including one near-critical fluid), and 31 gas condensates (including three near-critical fluid). These fluids are listed in Table 4-2 and **Tables 4-4, 4-5, and 4-6.**

For oils 1-22 listed in Table 4-4, available data are limited to overall compositions, saturation pressures, and liquid densities that are used in characterization. Most of them are heavy oils, for which data are in general scarce in literature (Kokal and Sayegh 1993; Yazdani and Maini 2010). Therefore, pseudo data (Merrill and Newley 1993) are generated for MMPs with pure CO_2 and pure C_1 and some three-phase envelopes using 30 components (including 22 pseudocomponents) based on the $CM_{w/o}V$ (Pedersen and Christensen 2007; Krejbjerg and Pedersen 2006; Pedersen et al. 1983, 1984, 1989, 1992, 2004) as explained in detail in Kumar and Okuno (2012a). Using the $CM_{w/o}V$, the effects of the number of components on phase behavior predictions diminish when more than 16 components are used (Kumar and Okuno 2012a). Thus, use of 22 pseudocomponents is appropriate to avoid errors caused by reduction of composition space. We directly use the compositions characterized by Quiñones-Cisneros et al. (2004b) for oils 1-13, 18, and 22 in Table 4-4.

Tables 4-5 and 4-6 list volatile oils and gas condensates, respectively, for which PVT data are available, such as CVD and CCE data. MMP data are unavailable for the volatile oils. Tables 4-2, 4-4, 4-5, and 4-6 present converged γ values and corresponding f_T, f_P and f_m values, which are plotted with

respect to the API gravity in **Figures 4-19 to 4-22**. The converged f_T and f_P values are greater than 1.0, and the converged f_m values are smaller than 1.0. The overall trends indicate that heavier fluids tend to require more perturbation from n-alkanes. This is consistent with the physical trend that heavier fractions are relatively more naphthenic and aromatic than lighter fractions (Nagy and Colombo 1967; Yarborough 1979).

The γ parameter plays an important role in the extended PnA method. It controls the gradient of ψ with respect to MW or CN for pseudocomponents. Figure 4-22 shows that the γ parameter becomes greater for lighter fluids. This is because a lighter fluid contains pseudocomponents lighter than C_{20} at higher concentrations. The ψ parameter is sensitive to aromaticity for such lower CNs as shown in Figure 4-12. For heavy oils, variable perturbation from n-alkanes is less significant; the importance of the ψ and γ parameters diminishes as the API gravity becomes lower as shown in Figure 4-22. For extra heavy oils, the PnA method reduces to the previous PnA method developed in Kumar and Okuno (2012a).

Figure 4-23 depicts the average gradient of ψ with respect to MW of pseudocomponents (Δψ/ΔM). This average gradient is calculated using ψ's and MWs for the lightest and heaviest pseudocomponents. The gradient is small for heavy fluids, and gradually increases as the API gravity increases. This is consistent with the trends of ψ for the two model fluids presented in Figure 4-12. **Figure 4-24** shows the variation of the ψ gradient with respect to γ. As γ increases, the gradient also increases. These figures indicate that the algorithm successfully converged as designed in the previous section. The ψ parameter is effectively controlled by adjusting γ.

4.4.2.1. MMP Calculations

We showed that the extended PnA method gives better MMP predictions than the previous PnA method for eight oils in Table 4-2. Here, we further test the extended PnA method for oils 1-22 in Table 4-4. MMPs at reservoir temperatures are calculated for 100% C_1 using PVTsim (2011) and for 100% CO_2 using PennPVT (Ahmadi and Johns 2011; PennPVT). CO_2-MMP for oils 1, 2, 4, and 18 in Table 4-4 are not considered because of the presence of three phases during the MMP calculations.

Figures 4-25 and 4-26 compare the MMPs from the PnA method and those from pseudo data. Good agreement is observed between them for heavy oils and light oils. Some oils in the range of 30-40°API, however, have AD of 20% (encircled in Figures 4-25 and 4-26). This is because of the discontinuity in the $CM_{w/o}V$ used to generate the pseudo data. PVTsim used in the $CM_{w/o}V$ gives two different characterization options, normal and heavy characterizations, based on an oil gravity criterion of 30°API. We observed that there can be significant differences in phase behavior predictions between these two characterization options around 30°API. Such a discontinuity in fluid characterization is undesirable considering the continuity of phase behavior (or, more fundamentally, the single-phase Gibbs free energy) in P-T-x space. The PnA method avoids the discontinuity by incorporating various physical considerations in the development as explained in the previous sections; the most important

one is variable perturbation from n-alkanes for application to a wide variety of fluids. The AAD in C_1-MMPs and CO_2-MMPs for the 22 oils is approximately 7% using the extended PnA method.

4.4.2.2. Volatile Oils

We characterize the 12 volatile oils given in Table 4-5. The types of phase behavior predicted for the oils are presented in the table; liquid saturation in CVD and CCE, and relative volume in CCE are indicated as 1, 2, and 3, respectively, in Table 4-5. Table 4-5 also lists the limits of measured values in the experiments along with deviations of the predictions from data. Since these are volatile oils, liquid saturation is 100% at the bubble points. Liquid saturation data at lowest measured pressures are listed for data types 1 and 2. Relative volume data at lowest measured pressures are listed for data type 3. Using the PnA method, the AD is 3.7% in CVD liquid saturation prediction, and predictions of CCE relative volume are nearly perfect.

Figures 4-27 and 4-28 compare the CVD liquid saturation curves for volatile oils 1 and 5, respectively. These oils were characterized using only saturation pressure data (see step 5 in the regression algorithm subsection). The PnA method yields the small AADs given in Table 4-5 for these oils even without using density data. The γ parameter converges to 0.62 using the algorithm given in section 4.3.4. Figure 4-27 also shows the CVD liquid saturation with the following γ values: 0.3, 0.4, 0.5, and 0.6. The liquid saturation curve varies monotonically with the γ parameter. As an example for CCE predictions, **Figure 4-29** compares the CCE relative volume for volatile oil 6. Nearly perfect prediction for the CCE relative volume is observed from the figure.

Figure 4-27 also shows the liquid saturation curve using the $CM_{w/o}V$ with 12 components. The CN ranges for pseudocomponents in the PnA and $CM_{w/o}V$ are almost the same. For a fair comparison, density matching is not conducted for both cases (Density matching actually deteriorates the CVD liquid saturation prediction using the $CM_{w/o}$ in this case). A large deviation is observed in the $CM_{w/o}V$ case for pressures between 250 bars and 455 bars.

To see the fundamental difference between the PnA and $CM_{w/o}V$ for volatile oil 1, **Figure 4-30** compares the a_i and b_i parameters for the four pseudocomponents in the two characterizations. It is difficult to find any abnormality in Figure 4-30. However, **Figure 4-31** presents an important difference between the two characterizations in the ψ parameter, which was defined as a_i/b_i^2 before. The ψ trend for the PnA method exhibits a combined trend of the two model fluids in Figure 4-12. The $CM_{w/o}V$ method results in the ψ trend that exhibits a minimum for the second lightest pseudocomponent. With this range of pseudocomponents' CNs, the ψ value for the second lightest pseudocomponent should not be less than that for the lightest pseudocomponent. A large deviation in the liquid saturation curve prediction around the saturation pressure is likely attributed to this ψ behavior for the $CM_{w/o}V$.

Volatile oil 12 in Table 4-5 is a near-critical fluid, for which CCE liquid saturation is predicted in **Figure 4-32.** This oil is characterized at temperature of 371.6 K, and the critical temperature of the oil is 388.1 K. The PnA method is able to reproduce quantitatively the substantial sensitivity of liquid saturation to pressure.

4.4.2.3. Gas Condensates

The 31 gas condensates listed in Table 4-6 include a wide MW range from 19.75 to 54.92. Gas condensates 6, 7, 8, 11, and 12 are near critical. As indicated in Table 4-6, CVD liquid saturation curves (data type 1) are predicted for 26 gas condensates. CCE tests (data types 2 and 3) are predicted for the other five gas condensates. Characterization of the gas condensates does not use density data in regression due to low C_{7+} fractions. These gas condensates behave like light n-alkane mixtures, for which the PR EOS predicts densities accurately with the correlations of Kumar and Okuno (2012b). The AAD for density predictions is less than 4% for the gas condensates given in Table 4-6.

Table 4-6 summarizes results for phase behavior predictions using the PnA method. For gas condensates, liquid saturation is zero at dew point. Hence, the maximum value in the experimental data is listed for each gas condensate, along with the AAD. The PnA method is successful for these gas condensates as indicated by the low AADs. As sample results, **Figures 4-33 and 4-34** depict CVD liquid saturation for gas condensates 20 and 5, respectively. The former exhibits low liquid saturation with a maximum of 1.89% at the lowest measured pressure. The latter exhibits a maximum saturation of 30.40% at a relatively high pressure in the two phase region. These results for gas condensates and volatile oils indicate that the PnA method is quantitatively accurate in prediction of quality lines and densities.

Figure 4-35 shows the ψ trends for gas condensates 4, 12, 20, and 26, for which the maximum liquid saturations are 25.00%, 40.90%, 1.89%, and 69.81%, respectively. The CN range of pseudocomponents is typically narrow for gas condensates, and the ψ parameter increases with CN as shown in Figure 4-12. In general, the slope of ψ becomes smaller as the CN range of pseudo components becomes wider. The four pseudocomponents for gas condensate 20 are lighter than C_{20}. Hence, the sharply increasing trend is conceivable since the ψ parameter is sensitive to aromaticity in this CN region. Gas condensates 4 and 12 have CN ranges of C_8-C_{22} and C_8-C_{26}, respectively. The ψ parameters for these fluids exhibit convexity in the low CN region, which can be seen for n-alkanes in Figure 4-12. Gas condensate 26 has the pseudocomponents in the CN range of C_9-C_{30}. Because of the wide CN range, the ψ parameter shows a combined trend of the two model fluids in Figure 4-12.

Matching liquid saturation data can be difficult using the conventional fluid characterization methods. This is true especially when liquid saturation is sensitive to pressure and temperature (e.g., see Figures 4-27, 4-32, and 4-34). Matching such liquid saturation data requires accurate prediction of dense quality lines and liquid densities (i.e., compositional and volumetric phase behaviors) along the experimental pressure path at a fixed temperature. However, the PR EOS is quite accurate in liquid density prediction for light fluids using the correlations of Kumar and Okuno (2012b). Thus, adjustment of compositional phase behavior for the small C_{7+} fraction is crucial for reliable prediction of condensation/vaporization behavior of these fluids.

To show this, we characterize near-critical gas condensate 7 in Table 4-6 using the PnA and CM_wV methods. CVD liquid saturation curves from the two characterizations are compared with data points in

Figure 4-36. The CM_wV results in large deviations near the dew point. However, the two methods result in similar phase behavior for the C_{7+} fraction as shown in **Figure 4-37.** The converged γ value for the PnA method is 0.820 as given in Table 4-6. The best match of the PnA characterization results in γ of 0.930. Figure 4-37 shows that the two values of γ give essentially the same phase behavior of the C_{7+} fraction. These results indicate the significant sensitivity of liquid saturation to C_{7+} characterization in this case. PVT measurements for C_{7+} at the reservoir temperature 424.82 K and lower would not help because the three phase-envelopes nearly coincide there as shown in Figure 4-37.

The PnA method is able to control gas condensate behavior by adjusting only one parameter (γ) to match the dew point. The adjustment changes phase behavior predictions systematically as shown in Figures 4-36 and 4-37. Figure 4-36 shows the CVD liquid saturation curves for different γ values. It is evident that the predicted curve changes monotonically with varying γ and systematically in pressure space. Gas condensate 6 is another near-critical fluid, for which **Figure 4-38** shows quality lines (β is the vapor phase mole fraction). The calculated critical point is 402.0 K and 339.2 bars. The reservoir temperature and pressure are 422.6 K and 339.4 bars, respectively. **Figure 4-39** shows that the PnA method accurately predicts CVD liquid dropout, which results from the dense quality lines near the critical point.

4.4.2.4. Heavy Oils

Oils heavier than 30°API listed in Table 4-4 are considered as heavy oils (Krejbjerg and Pedersen 2006). The present PnA method reduces to the previous PnA method developed for heavy oils (Kumar and Okuno 2012a) when γ is zero. As can be seen in Figure 4-22, the γ values for extra-heavy oils of 10°API are nearly zero. The present PnA method performs similarly to the previous one for heavy oils. Our focus here is on the West Sak oil (oil 23 in Table 4-4), for which gas solubility data are available in the literature, and predictions of three hydrocarbon phases.

4.4.2.4.1. P-V Predictions

For oil 23, the oleic phase saturations for two mixtures (60% CO_2 and 40% oil, and 80% CO_2 and 20% oil) are predicted at 299.81 K using the PnA method. Reasonable accuracy of the PnA method is observed in **Figures 4-40 and 4-41.** The AAD is 2.7% for the 60% CO_2 mixture, and 5.6% for the 80% CO_2 mixture. Figure 4-41 shows predictions with different γ values; 0.048, 0.8, 1.0, and 1.2. The converged γ value is 0.048 using the algorithm given in section 4.3.4. A systematic change in predictions in pressure space is observed. The change is also monotonic with the γ parameter. With available phase saturation data, the optimum γ value can be easily selected using the PnA method.

Aghbash and Ahmadi (2012) developed a 10-component fluid model for this oil. They used all non-zero BIPs. The PnA method does not require non-zero BIPs for hydrocarbon pairs to obtain similar phase behavior predictions. **Figure 4-42** compares the ψ parameters for pseudocomponents from Aghbash and Ahmadi (2012) with those from the PnA method. The ψ parameter monotonically decreases with CN for the two cases, which is in line with our discussion for heavy oils in Figure 4-12. The non-zero BIPs used in Aghbash and Ahmadi (2012) likely did not cause absurd behavior of the

Gibbs free energy in P-T-x space in this case. However, special care must be taken when BIPs are used in regression (Pedersen and Christensen 2007; Wang and Pope 2001; Egwuenu et al. 2008).

4.4.2.4.2. Three-Phase Predictions

Mixtures of oil and solvent can present complex three-hydrocarbon-phase behavior (Mohanty et al. 1995; Polishuk et al. 2004; Okuno et al. 2011). The three phases are the gaseous (V), oleic (L_1), and solvent-rich liquid (L_2) phases. Here, we compare three-phase predictions from the PnA method with pseudo data. **Figure 4-43** shows the three-phase envelope for a mixture of 80% CO_2 and 20% West Sak oil. **Figures 4-44 and 4-45** show the three-phase envelopes for two mixtures with oil 5 in Table 4-4; 90% C_2 and 10% oil 5, and 90% C_3 and 10% oil 5. Three-phase predictions from the PnA method nearly coincide with the pseudo data.

4.5.   Conclusions

We first presented the effects of volume shift on phase behavior in P-T-x space when volume-shift parameters are used as regression parameters in fluid characterization. Then, the PnA method developed for heavy oils in our previous research was extended to characterize lighter fluids, such as gas condensates, volatile oils, and near-critical fluids. Extensive case studies using 77 different reservoir fluids demonstrated the universal applicability, reliability, robustness, and efficiency of the new PnA method. The PR EOS with the van der Waals mixing rules was used throughout the research. Conclusions are as follows:

o Volume-shift parameters affect compositional phase behavior predictions when used as regression parameters in fluid characterization. P-T-x conditions used in laboratory measurements are only a small part of actual P-T-x conditions encountered in reservoir processes. Therefore, volume shift should be carefully performed in regression since it can substantially affect oil recovery predictions through altered phase behavior predictions in P-T-x space. The PnA method uses no volume shift, and properly couples volumetric and compositional phase behaviors.

o T_C, P_C, and ω were perturbed to match the density trend curves with respect to CN for different levels of aromaticity presented in Yarborough (1979). Results show that uniform perturbation is appropriate for the CN range approximately higher than 20. Sharply increasing perturbation with CN is required for the lower CN range. This explains why the previous PnA method successfully used uniform perturbation for characterizing heavy oils, for which pseudocomponents' CNs are typically higher than 20. Case studies demonstrated that perturbation from n-alkanes depends on the CN range of pseudocomponents in the new PnA method.

o The ψ parameter defined in Equation 4-13 for the PR EOS is more sensitive to the level of aromaticity in the lower CN range than in the higher CN range. The ψ parameter increases with CN for fluids that have all pseudocomponents in the lower CN range, where sharply increasing perturbation with CN is required. The trend is the other way around for fluids that have all pseudocomponents in the higher CN range, where variable perturbation is less important. Mixed

trends of the ψ parameter with respect to CN are expected for fluids that have pseudocomponents in the two CN ranges. Case studies confirmed this point. Conventional characterization methods can exhibit unexpected trends of the ψ parameter with respect to CN.

o The regression algorithm developed in this research controls the trend of the ψ parameter with respect to CN using a fourth adjustment parameter γ. The algorithm also considers the size of composition space using the distribution function fitted to the composition data of the fluid to be characterized. Case studies showed the reliability and robustness of the algorithm for all fluids tested in this research. The algorithm written in FOTRAN takes less than two minutes on average per fluid using the Intel Core i7-960 processor at 3.20 GHz and 8.0 GB RAM.

o The importance of the ψ and γ parameters diminishes as the API gravity decreases. For extra heavy oils, the new PnA method naturally reduces to the previous PnA method, where γ is zero.

o The PnA method controls phase behavior predictions monotonically with parameter adjustments and systematically in P-T-x space. This was demonstrated by quantitative prediction of condensation/vaporization behavior of gas condensates and light oils and MMPs for various oil displacements, which can be difficult using conventional fluid characterization. Unlike the conventional methods, the PnA method uses only four adjustment parameters and incorporates physical considerations in parameter adjustment.

o The PnA method requires no change in the thermodynamic model used; i.e., it can be readily implemented in existing software based on the PR EOS with the van der Waals mixing rules.

4.6.   Nomenclature

Roman Symbols

a   Attraction parameter in a cubic equation of state

A   Aromatic

b   Covolume parameter in a cubic equation of state

$\underline{c}$ Peneloux volume-shift parameter for N_C components

d   Gradation constants

f_{dis} Chi-squared distribution function defined in Equation 4-5

f_m Perturbation factor for the *m* parameter

f_P Perturbation factor for critical pressure

f_T Perturbation factor for critical temperature

$\Delta_{mix}\underline{G}$ Molar Gibbs free energy change on mixing

g   Dimensionless molar Gibbs free energy change on mixing

k_{ij} Binary interaction parameter for components i and j

m   Parameter in the Peng–Robinson EOS (1978) defined in Equations 4-9 and 4-10

N_C Number of components

P   Pressure, bar

p   Parameter in the chi-squared distribution

P_C Critical pressure, bar

$\underline{P}_C$ Critical pressure vector for N_C components

R   Universal gas constant

S   Parameter in the chi-squared distribution

T   Temperature, K

T_C Critical temperature, K

$\underline{T}_C$ Critical temperature vector for N_C components

$\underline{T}_{RES}$ Reservoir temperature

$\underline{x}$ Mole fraction vector for the liquid phase

$\underline{y}$ Mole fraction vector for the gaseous phase

$\underline{z}$ Overall composition vector

z_L Mole fraction of methane in fluid

z_I Sum of mole fractions of non C_{7+} excluding methane

z_H Mole fractions of C_{7+}

Abbreviations

°API   API (American Petroleum Institute) gravity

BIP   Binary interaction parameter

CN   Carbon number

CM$_{w/o}$V	Conventional (characterization) method without volume shift
CM$_w$V	Conventional (characterization) method with volume shift
EOS	Equation of state
MMP	Minimum miscibility pressure, bars
MW	Molecular weight, gm/mol
PC	Pseudocomponent
PNA	Paraffin-napthene-aromatic
PR	Peng-Robinson
P-T-x	Pressure-temperature-composition

Greek symbols

β	Vapor molar phase fraction
ε	T_C, P_C, and ω consistency function defined in Equation 4-12
Γ	Gamma function
$\bar{\phi_\iota}$	Fugacity coefficient of component i in a mixture
ϕ_i	Fugacity coefficient of pure component i
γ	Gradation parameter
Ω_a	Constant term in the attraction parameter of a cubic EOS
Ω_b	Constant term in the covolume parameter of a cubic EOS
ψ	a_i/b_i^2 defined in Equation 4-13 for the PR EOS
θ	Parameter as defined in Equation 4-17
ω	Acentric factor

Subscripts/Superscript symbols

w	With (volume shift)
w/o	Without (volume shift)
L	Liquid phase
V	Gaseous phase

4.7.   References

Aghbash, V.N. and Ahmadi, M. 2012. Evaluation of CO2-EOR and Sequestration in Alaska West Sak Reservoir Using Four-Phase Simulation Model. Presented at the Western North American Regional Meeting, Bakersfield, California. 19-23 March. SPE-153920-MS.

Ahmadi, K. and Johns, R.T. 2011. Multiple Mixing-Cell Model for MMP Determination. *SPE J.* **16** (4): 733-742.

Al-Ajmi, M.F., Tybjerg, P., Rasmussen, C.P. et al. 2011. EoS Modeling for Two Major Kuwaiti Oil Reservoirs. Presented at the SPE Middle East Oil and Gas Show and Conference, Manama, Bahrain, 25-28 Sept. SPE-141241-MS.

Al-Meshari, A. 2004. New Strategic Method to Tune Equation of State to Match Experimental Data for Compositional Simulation. PhD dissertation, Texas A&M University, Texas.

Al-Meshari, A.A. and McCain, W.D. 2006. An Accurate Set of Correlations for Calculating Critical Properties and Acentric Factors for Single Carbon Number Groups. Presented at SPE Technical Symposium of Saudi Arabia Section, Dhahran, Saudi Arabia, 21-23 May. SPE-106338-MS.

Coats, K.H. 1985. Simulation of Gas Condensate Reservoir Performance. *J Petrol Tech* **37** (10): 1870-1886.

Coats, K.H. and Smart, G.T. 1986. Application of a Regression Based EOS PVT Program to Laboratory Data. *SPE Res Eng* **1** (3): 277-299.

Cullick, A.S., Pebdani, F.N., and Griewank, A.K. 1989. Modified Corresponding States Method for Predicting Densities of Petroleum Reservoir Fluids. *Ind. Eng. Chem. Res.* **28** (3): 340-347.

Danesh, A. 1998. PVT and Phase Behavior of Petroleum Reservoir Fluids, Elsevier Science & Technology Books.

Drohm, J.K., Trengove, R.D., and Goldthrope, W.H. 1988. On the Quality of Data from Standard Gas-Condensate PVT Experiments. Presented at the SPE Gas Technology Symposium, Dallas, Texas, 13-15 June. SPE-17768-MS.

Egwuenu, A.M., Johns, R.T., and Li, Y. 2008. Improved Fluid Characterization for Miscible Gas Floods. *SPE Res Eval Eng* **11** (4): 655-665.

Ghasemi, M., Alavian, S.A., and Whitson, C.H. 2011. C$_7$+ Characterization of Heavy Oil Based on Crude Assay Data. Presented at SPE Heavy Oil Conference and Exhibition held in Kuwait City, Kuwait, 12-24 Dec. SPE 148906-MS.

Gregorowicz, J. and De Loos, T.W. 2011. Prediction of Liquid−Liquid−Vapor Equilibria in Asymmetric Hydrocarbon Mixtures. *Ind. Eng. Chem. Res*. **40** (1): 444-451.

Guo, T.M. and Du, L. 1989. A New Three-Parameter Cubic Equation of States for Reservoir Fluids: Part 3- Application to Gas Condensates. SPE e-library, Paper SPE-19374-MS.

Harismiadis, V.I., Koutras, N.K., Tassios, D.P. et al. 1991. How Good is Conformal Solutions Theory for Phase Equilibrium Predictions?: Gibbs Ensemble Simulations of Binary Lennard-Jones Mixtures. *Fluid Phase Equilib*. **65**: 1-18.

Hosein, R. and Dawe, R.A. 2011. Characterization of Trinidad Gas Condensates. *J Pet Sci Technol* **29** (8): 817-823.

Hosein, R., Jagai, T., and Dawe, R.A. 2013. A Method for Predicting the Phase behavior of Trinidad Gas Condensates. *The West Indian Journal of Engineering* **35** (2): 22-30.

Imo-Jack, O. 2010. PVT Characterization of a Gas Condensate Reservoir and Investigation of Factors Affecting Deliverability. Presented at the Annual SPE International Conference and Exhibition, Tinapa-Calabar, Nigeria, 31 July-7 Aug. SPE-140629-MS.

Jaubert, J-N., Avaullee, L., and Souvay, J.F. 2002. A Crude Oil Data Bank Containing more than 5000 PVT and Gas Injection Data. *J Pet Sci Technol* **34** (1): 65-107.

Jaubert, J-N., Avaullee, L., and Pierre, C. 2002. Is it still necessary to measure the minimum miscibility pressure? *Ind. Eng. Chem. Res.* **41** (2): 303-310.

Jhaveri, B.S. and Youngren, G.K. 1988. Three-Parameter Modification of the Peng-Robinson Equation of State to Improve Volumetric Predictions. *SPE J.* **3** (3): 1033-1040.

Kokal, S.L. and Sayegh, S.G. 1993. Phase Behavior and Physical Properties of CO_2-Saturated Heavy Oil and its Constitutive Fractions: Experimental Data and Correlations. *J. Pet. Sci. Eng.* **9** (4): 289-302.

Krejbjerg, K. and Pedersen, K.S. 2006. Controlling VLLE Equilibrium with a Cubic EoS in Heavy Oil Modeling. Presented at 57th Annual Technical Meeting of the Petroleum Society (Canadian International Petroleum Conference), Calgary. 13-15 June. PETSOC-2006-052.

Kumar, A. and Okuno, R. 2012a. Fluid Characterization Using an EOS for Compositional Simulation of Enhanced Heavy-Oil Recovery. Presented at SPE Annual Technical Conference and Exhibition, San Antonio, Texas, 8-10 Oct. SPE 159494-MS

Kumar, A. and Okuno, R. 2012b. Critical Parameters Optimized for Accurate Phase Behavior Modeling for Heavy n-Alkanes up to C_{100} using the Peng-Robinson Equation of State. *Fluid Phase Equilib.* **335**: 46-59.

Lawal, A.S., Van derLaan, E.T. and Thambynaygam, R.K.M. 1985. Four-Parameter Modification of the Lawal-Lake-Silberberg Equation of State for Calculating Gas-Condensate. Presented at Annual Technical Conference and Exhibition of the Society of Petroleum Engineers, Las Vegas, Nevada, 22-25 Sept. SPE-14269-MS.

Leibovici, C.F. 1993. A Consistent Procedure for the Estimation of Properties Associated to Lumped Systems. *Fluid Phase Equilib.* **87** (2): 189-197.

Lolley, C.S. and Richardson, W.C. 1997. Compositional Input for Thermal Simulation of Heavy Oils with Application to the San Ardo Field. Presented at International Thermal Operation & Heavy Oil Symposium, Bakersfield, California, 10-12 Dec. SPE-37538-MS

Lomeland, F. and Harstad, O. 1995. Simplifying the Task of Grouping Components in Compositional Reservoir Simulation. *SPE Comp Appl.* **7** (2): 38-43.

McVay, D.A. 1994. Generalization of PVT Properties for Modified Black-Oil Simulation of Volatile and Gas Condensate Reservoirs. PhD dissertation, Texas A&M University, Texas.

Merrill, R.C. and Newley, T.M.J. 1993. A Systematic Investigation into the most Suitable Data for Development of Equation of State for Petroleum Reservoir Fluids. *Fluid Phase Equilib.* **82**: 101-110.

Mohanty, K.K., Masino, W.H., Ma, T.D. et al. 1995. Role of Three-Hydrocarbon-Phase Flow in a Gas-Displacement Process. *SPE Res Eng* **10** (3): 214-221.

Montel, F. and Gouel, P.L. 1984. A New Lumping Scheme of Analytical Data for Compositional Studies. Presented at the SPE Annual Technical Conference and Exhibition, Houston, Texas, 16-19 Sept. Paper SPE 13119.

Moore, D.C. 1989. Simulation of Gas-Condensate Reservoir Performance Using Schmidt-Wenzel Equation of State*.* MSc thesis, Montana College of Mineral Science and Technology, Montana..

Nagy, B. and Colombo, U. 1967. Fundamental Aspects of Petroleum Geochemistry, Elsevier, Amsterdam.

Okuno, R., Johns, R.T., and Sepehrnoori, K. 2011. Mechanisms for High Displacement Efficiency of Low-Temperature CO_2 Floods. *SPE J.* 16 (4): 751-767.

Pedersen, K.S. and Christensen, P. L. 2007. Phase Behavior of Petroleum Reservoir Fluids. CRC Press, Taylor & Francis Group, Boca Raton, FL, USA.

Pedersen, K.S., Thomassen, P., and Fredenslund, Aa. 1983. SRK- EOS Calculation for Crude Oil. *Fluid Phase Equilib.* **14:** 209–218.

Pedersen, K.S., Thomassen, P., and Fredenslund, Aa. 1984. Thermodynamics of Petroleum Mixture Containing Heavy Hydrocarbons. 1. Phase Envelope Calculation by Use of the Soave-Redlich-Kwong Equation of State. *Ind. Eng. Chem. Proc. Des. Dev.* **23** (1): 163–170.

Pedersen, K.S., Blilie, A.L., and Meisingset, K.K. 1992. Calculations On Petroleum Reservoir Fluids Using Measured And Estimated Compositional Data for the Plus Fraction. *Ind. Eng. Chem. Res.* **31** (5): 1378-1384.

Pedersen, K.S., Milter, J., and Sørensen, H. 2004. Cubic Equations of State Applied to HT/HP and Highly Aromatic Fluids. *SPE J.* **9** (2): 186-192.

Pedersen, K.S., Thomassen, P., and Fredenslund, Aa. 1989. Characterization of Gas Condensate Mixtures. Advances in Thermodynamics, Taylor & Francis, New York.

Pedersen, K.S., Thomassen, P., and Fredenslund, Aa. 1988. Characterization of Gas Condensates. Presented at AIChE Spring National Meeting, New Orleans, Louisiana, 6-10 March.

Peneloux, A., Jain, C., and Behar, E. 1979. Application Of The Developed Redlich-Kwong Equation Of State To Predict The Thermodynamic Properties Of Condensate Gases. Presented at the Annual Fall Technical Conference and Exhibition of the Society of Petroleum Engineers of AIME, Las Vegas, Nevada, 23-26 Sept. SPE-8287-MS.

Peneloux, A., Rauzy, E., and Fréze, R. 1982. A Consistent Correction for Redlich-Kwong-Soave Volume. *Fluid Phase Equilib.* **8** (1): 7-23.

Peng, D.-Y. and Robinson, D.B. 1976. A New Two-Constant Equation of State. *Ind. Eng. Chem. Fund.* **15** (1): 59-64.

Peng, D.-Y. and Robinson, D.B. 1978. The Characterization of the Heptanes and Heavier Fractions for the GPA Peng-Robinson Programs. *GPA Research Report* RR-28.

PennPVT Toolkit, Gas Flooding Joint Industrial Project, Director: Dr. Russell T. Johns, EMS Energy Institute, The Pennsylvania State University, University Park, PA.

Pitzer, K.S. 1955. The Volumetric and Thermodynamic Properties of Fluids. I. Theoretical Basis and Viral Coefficients. *J. Am. Chem. Soc.* **77** (13): 3427-3433.

Pitzer, K.S., Lippmann, D.Z., Curl Jr, R.F. et al. 1955. The Volumetric and Thermodynamic Properties of Fluids. II. Compressibility Factor, Vapor Pressure, and Entropy of Vaporization. *J. Am. Chem. Soc.* **77** (13): 3433-3440.

Polishuk, I., Wisniak, J., and Segura, H. 2004. Estimation of Liquid-Liquid-Vapor Equilibria in Binary Mixtures of n-Alkanes. *Ind. Eng. Chem. Res.* **43** (18): 5957-5964.

PVTsim 20.0. 2011. Calsep A/S, Lyngby, Denmark.

Quiñones -Cisneros, S.E., Zéberg-Mikkelsen, C.K., and Stenby, E.H. 2003. Friction Theory Prediction of Crude Oil Viscosity at Reservoir Conditions Based on Dead Oil Properties. *Fluid Phase Equilib*. **212** (1-2): 233–243.

Quiñones-Cisneros, S.E., Andersen, S.I., and Creek, J. 2005. Density and Viscosity Modeling and Characterization of Heavy Oils. *Energy Fuels* **19** (4): 1314-1318.

Quiñones-Cisneros, S.E., Dalberg, A., and Stenby, E.H. 2004b. PVT Characterization and Viscosity Modeling and Prediction of Crude Oils. *Pet. Sci. Technol.*, **22** (9-10): 1309–1325.

Quiñones-Cisneros, S.E., Zéberg-Mikkelsen, C.K., Baylaucq, A. et al. 2004a. Viscosity Modeling and Prediction of Reservoir Fluids: From Natural Gas to Heavy Oils. *Int. J. Therm.* **25** (5): 1353-1366.

Sharma, G.D. 1990. Development of Effective Gas Solvents Including Carbon Dioxide for the Improved Recovery of West Sak Oil, Report No. DOE/FE/61114-2, University of Alaska Fairbanks, Alaska.

Søreide, I. 1989. Improved Phase Behavior Predictions of Petroleum Reservoir Fluids from a Cubic Equation of State, Ph.D. dissertation, Norwegian University of Science and Technology, Trondheim, Norway, 1989.

Stamataki, S.K. and Magoulas, K.G. 2001. Characterization of Heavy Undefined Fractions. Presented at SPE International Symposium on Oilfield Chemistry, Houston, Texas, 13-16 Feb. SPE-64996-MS.

Van Konynenburg, P.H. and Scott, R.L. 1980. Critical Lines and Phase Equilibria in Binary Van Der Waals Mixtures. *Philos. Trans. R. Soc. Lond.* **298** (1442): 495-540.

Wang, P. and Pope, G.A. 2001. Proper Use of Equations of State for Compositional Reservoir Simulation. *J. Petrol. Tech*. **53** (7): 74-81.

Whitson, C.H. 1983. Characterizing Hydrocarbon Plus Fractions. *SPE J.* **23** (4): 683-694.

Whitson, C.H. and Brulè, M.R. 2000. Phase Behaviour. SPE Henry L. Doherty Series, Vol. 20, SPE, Richardson, Texas.

Whitson, C.H. and Torp, S.B. 1983. Evaluating Constant Volume Depletion Data. *J Petrol Tech* **35** (3): 610-620.

Yang, T., Chan, W.-D., and Guo, T.M. 1997. Phase Behavior of a Near-Critical Reservoir Fluid Mixture. *Fluid Phase Equilib.* **128** (1-2): 183-197.

Yarborough, L. 1979. Application of the Generalized Equation of State to Petroleum Reservoir Fluids, Equation of State in Engineering and Research, in: K.C. Choa, R.L. Robinson Jr. (Eds.), Advances in Chemistry Series, Am. Chem. Soc. 182 (1979) 386–439.

Yazdani, A. and Maini, B.B. 2010. Measurements and Modeling of Phase Behaviour and Viscosity of a Heavy Oil/Butane System. *J Can Pet Technol* **49** (2): 9-14.

Zuo, J.Y. and Zhang, D. 2000. Plus Fraction Characterization and PVT Data Regression for Reservoir Fluids near Critical Conditions. Presented at SPE Asia Pacific Oil and Gas Conference and Exhibition, Brisbane, Australia, 16-18 Oct. SPE 64520-MS

			PR EOS with volume shift				PR EOS without volume shift		
Components	Mole Fractions	MW (gm/mol)	T_C (K)	P_C (bars)	ω	CPEN (cc/mol)	T_C (K)	P_C (bars)	ω
L	0.4219	16.10	190.86	46.07	0.0089	-5.19	190.86	46.07	0.0089
I	0.0176	31.66	315.59	47.83	0.1065	-5.85	315.59	47.83	0.1065
H	0.5605	291.30	848.33	24.18	0.4373	-110.14	1022.44	19.48	0.5108

Table 4-1. Ternary fluid using the conventional characterization method with/without volume shift in regression.

Temperature (K)　　　　　330.40
Saturation Pressure (bars)　196.48
$L = N_2 + CO_2 + C_1$, $I = C_2 + C_3$, $H = C_{4+}$

Table 4-2. Converged f_T, f_P, f_m, p, and γ values for reservoir oils characterized using the PnA method. Slim-tube MMPs are reported for these oils in the literature.

Oil No.	References	MW (gm/mol)	°API	T_{RES} (K)	k*	f_T	f_P	f_m	p	γ
1	Jaubert et al. 2002, F1	135.24	35.22	374.85	5	1.091	1.101	0.399	4.5	1.236
2	Jaubert et al. 2002, F2	136.25	39.89	372.05	6	1.574	1.143	0.389	4.7	1.481
3	Jaubert et al. 2002, F3	82.41	39.31	387.35	11	1.239	1.026	0.500	6.3	0.977
4	Jaubert et al. 2002, F4	63.17	40.34	388.20	7	0.959	0.959	0.545	3.0	0.770
5	Jaubert et al. 2002, F5	125.82	32.04	394.25	12	1.347	1.124	0.412	4.5	1.318
6	Jaubert et al. 2002, F6	96.25	37.73	373.15	5	1.072	1.060	0.488	4.2	1.067
7	Jaubert et al. 2002, F7	96.19	41.06	393.15	12	1.357	1.060	0.443	4.9	1.383
8	Jaubert et al. 2002,F11	82.55	38.71	373.75	11	1.172	1.066	0.501	3.8	0.921
9	Jaubert et al. 2002,F13	150.2	35.64	377.55	8	1.499	1.038	0.319	4.4	0.996
10	Al-Ajmi et al. 2011, F1	161.42	31.85	350.40	16	1.538	1.196	0.347	4.6	1.341
11	Al-Ajmi et al. 2011, F2	109.37	40.03	353.70	17	1.418	1.086	0.392	3.9	1.304

[‡]As reported. All other API gravities are calculated from density at 288.15 K and 1.01325 bars.
*k is number of density data.

Table 4-3. Slim-tube and calculated MMPs for eight oils from Table 4-2.

Oil No. (From Table 4-2)	°API	Slim-Tube MMP, Bars	Variable Perturbation PnA Method, MMP (Bars)	Uniform Perturbation PnA Method (γ = 0), MMP (Bars)
1	35.22	220	207.86	262.00
2	39.89	220	258.79	339.00
3	39.31	376	366.84	446.52
4	40.34	379	350.61	437.56
5	32.04	366	341.00	496.12
6	37.73	309	296.16	371.33
7	41.06	296	317.00	357.50
8	38.71	335	343.00	435.03
AAD%			6.70	26.70

Table 4-4. Converged f_T, f_P, f_m, p, and γ values for reservoir oils characterized using the PnA method. For these oils, available data are limited to overall compositions, saturation pressures, and liquid densities.

Oil No.	References	MW (gm/mol)	°API	T_{RES} (K)	k[#]	f_T	f_P	f_m	p	γ
1	Quiñones -Cisneros et al. (2005), Oil-8	443.08	9.50	322.05	13	2.064	1.728	0.361	8.0	0.091
2	Quiñones -Cisneros et al. (2005), Oil-7	431.59	11.63	322.05	12	1.683	1.647	0.370	8.0	0.041
3	Quiñones -Cisneros et al. (2004a), Oil-6	377.88	13.38	322.05	13	2.871	1.819	0.245	7.5	0.063
4	Quiñones -Cisneros et al. (2004a), Oil-5	422.94	11.98	322.05	13	1.787	1.659	0.381	7.5	0.048
5	Quiñones -Cisneros et al. (2004a), Oil-1	170.59	20.81	330.40	16	2.879	1.760	0.403	6.0	0.084
6	Quiñones -Cisneros et al. (2004b), Oil-8	182.05	24.25	333.15	16	2.771	1.893	0.429	9.0	0.227
7	Quiñones -Cisneros et al. (2004b), Oil-7	159.99	29.24	330.40	16	2.288	1.731	0.439	8.0	0.088
8	Quiñones -Cisneros et al. (2004b), Oil-6	118.18	35.61	346.15	5	1.802	1.514	0.414	7.0	1.092
9	Quiñones -Cisneros et al. (2004b), Oil-5	130.55	28.30	337.85	3	2.781	1.786	0.444	6.0	0.200
10	Quiñones -Cisneros et al. (2004b), Oil-4	114.57	33.35	337.85	6	2.248	1.600	0.468	5.5	0.443
11	Quiñones -Cisneros et al. (2004b), Oil-3	87.80	40.46	337.25	5	1.744	1.256	0.470	4.0	0.988
12	Quiñones -Cisneros et al. (2004b), Oil-2	89.83	47.63	366.45	11	1.419	1.047	0.446	4.0	0.809
13	Quiñones -Cisneros et al. (2004b), Oil-1	86.57	60.18	427.60	13	1.128	1.000	0.585	2.5	0.340
14	Oil*	296.90	22.60[‡]	357.50	13	1.936	1.433	0.284	5.7	0.535
15	Coats and Smart 1986, Oil-1	123.79	34.04	355.37	8	2.249	1.646	0.394	6.6	1.011
16	Coats and Smart 1986, Oil-6	83.31	40.90[‡]	385.37	20	1.325	1.033	0.440	4.1	1.390
17	Coats and Smart 1986, Oil-7	113.60	39.70[‡]	328.15	20	1.334	0.997	0.390	3.7	1.459
18	Quiñones -Cisneros et al. (2003), Oil-5	240.24	20.19	345.93	15	2.615	1.815	0.343	4.0	0.110
19	Cullick et al. 1989, Light Oil	105.28	43.68	377.59	8	1.075	0.978	0.436	6.1	1.309
20	Pedersen et al. 1992, Fluid-1	124.57	35.73	344.75	8	2.160	1.532	0.462	5.8	0.402
21	Coats and Smart 1986, Oil-4	96.22	41.30[‡]	316.48	10	1.546	1.152	0.423	4.6	1.498
22	Quiñones -Cisneros et al. (2005),L-Oil-2	80.90	62.40	418.15	22	1.402	1.033	0.446	2.5	1.312
23	Sharma 2004, West Sak Oil	228.88	18.68	299.81	10	1.635	1.605	0.566	5.7	0.048

* This is an actual oil, but the source is not mentioned for confidentiality.
‡ As reported. All other API gravities are calculated from density at 288.15 K and 1.01325 bars.
# k is number of density data.

Table 4-5. Converged f_T, f_P, f_m, p, and γ values for volatile oils characterized using the PnA method. PVT data are available for these oils, such as CVD and CCE data.

Oil No.	References	MW (gm/mol)	°API	T_{RES} (K)	f_T	f_P	f_m	p	γ	Data Limits Value (Type[#])	Dev.[¥]
1	Al-Meshari 2004, Fluid-12	46.07	50.3	354.82	1.018	1.018	0.562	2.3	0.620	38.20 (1)	3.19
2	Al-Meshari 2004, Fluid-13	56.06	36.7	364.82	1.972	1.344	0.437	2.3	0.503	3.93 (3)	0.02
3	Al-Meshari 2004, Fluid-14	54.57	40.7	360.93	1.412	1.188	0.486	2.4	0.555	1.00 (3)	0.01
4	Al-Meshari 2004, Fluid-15	51.11	57.5	353.15	1.106	0.973	0.662	2.9	0.829	2.98 (3)	0.02
5	Al-Meshari 2004, Fluid-16	59.63	55.6	425.93	0.957	0.957	0.525	2.5	0.600	35.30 (1)	2.12
6	Al-Meshari 2004, Fluid-17	67.32	44.5	414.82	1.179	0.998	0.418	2.5	0.806	6.84 (3)	0.03
7	Al-Meshari 2004, Fluid-18	59.90	54.4	423.15	0.980	0.991	0.628	3.2	0.569	7.57 (3)	0.03
8	Al-Meshari 2004, Fluid-19	62.65	59.5	377.59	1.092	0.977	0.458	4.3	1.315	4.06 (3)	0.01
9	Oil*	86.68	56.6	376.75	1.568	1.048	0.487	4.0	1.144	2.46 (3)	0.01
10	McVay 1994, Oil A	50.93	44.5[‡]	408.70	0.956	0.956	0.643	2.5	0.670	33.30 (1)	6.38
11	McVay 1994, Oil B	57.50	56.7	393.70	0.956	0.956	0.596	3.1	0.760	49.50 (1)	3.13
12	Yang et al. 1997.‡	37.94	57.5	371.60	1.043	1.043	0.648	2.0	0.280	13.69 (2)	2.93

[‡] As reported. All other API gravities are calculated from density at 288.15 K and 1.01325 bars.
[#] (1) is CVD liquid saturation (%), (2) is CCE liquid saturation (%), (3) is CCE relative volume (volume/volume)
[¥] Deviation = Sum of absolute of (experimental value –predicted value)/number of data point
‡ Oil no. 12 is near critical.
*This is an actual oil, but the source is not mentioned for confidentiality.

Table 4-6. Converged f_T, f_P, f_m, p, and γ values for gas condensates characterized using the PnA method. PVT data are available for these oils, such as CVD and CCE data.

Fluid No.	References	MW (gm/mol)	°API	T_{RES} (K)	f_T & f_P	f_m	p	γ	Maximum Data Value (Type[#])	Dev.[¥]
1	Al-Meshari 2004, Fluid-3	31.53	58.3	424.82	0.972	0.485	2.0	0.760	11.70 (1)	1.15
2	Al-Meshari 2004, Fluid-4	31.44	59.9	403.15	0.970	0.513	2.0	0.680	13.00 (1)	2.12
3	Al-Meshari 2004, Fluid-5	32.41	60.4	382.59	0.974	0.530	2.1	0.730	23.30 (2)	5.54
4	Al-Meshari 2004, Fluid-7	36.62	59.6	397.59	0.975	0.756	2.6	0.720	25.00 (1)	5.38
5	Al-Meshari 2004, Fluid-8	40.77	62.9	424.82	0.970	0.710	2.2	0.410	30.40 (1)	1.63
6‡	Al-Meshari 2004, Fluid-10	39.23	64.7	422.59	0.971	0.545	3.3	0.670	33.60 (1)	1.15
7‡	Al-Meshari 2004, Fluid-11	41.71	62.3	424.82	0.970	0.516	3.0	0.820	32.20 (1)	1.91
8‡	Coats and Smart 1986, Gas-5	30.29	61.8	403.70	0.971	0.552	2.0	0.660	4.17 (3)	0.01
9	Guo and Du 1989, Sample-7	25.53	71.2	406.45	0.971	0.527	2.0	0.780	5.82 (1)	0.65
10	Imo-Jack 2010	25.76	54.0	382.59	0.972	0.725	2.2	0.520	9.25 (1)	1.55
11‡	Coats 1985	44.40	66.4	435.93	0.965	0.629	4.0	0.790	2.61 (3)	0.01
12‡	McVay 1994, Gas B	40.58	58.5	387.59	0.974	0.444	2.0	0.660	40.90 (1)	0.78
13	Danesh 1998	27.29	55.3	394.00	0.973	0.430	2.0	1.060	11.32 (1)	1.82
14	Pedersen and Christensen 2007	29.14	58.5	428.15	0.973	0.540	2.0	0.800	11.89 (2)	2.24
15	Hosein et al. 2013, PL-1	23.64	58.9	358.78	0.972	0.528	2.0	0.760	8.15 (1)	0.72
16	Hosein et al. 2013, PL-2	22.10	52.8	378.15	0.974	0.513	2.0	1.280	5.08 (1)	0.42
17	Hosein et al. 2013, PL-3	21.55	64.9	357.59	0.972	0.622	2.0	0.520	4.00 (1)	1.56
18	Hosein et al. 2013, PL-4	20.62	57.3	364.22	0.971	0.566	2.0	1.050	3.73 (1)	0.37
19	Hosein et al. 2013, PL-5	20.30	64.3	355.37	0.973	0.640	2.0	0.610	3.79 (1)	0.55
20	Hosein et al. 2013, PL-6	19.75	55.1	367.59	0.972	0.607	2.0	1.350	1.89 (1)	0.23
21	Moore 1989, CS-1	32.61	71.1	366.48	0.972	0.690	2.5	0.350	19.90 (1)	5.21
22	Moore 1989, CS-2	35.04	59.7	410.93	0.970	0.659	2.0	0.490	21.60 (1)	2.84
23	Moore 1989, CS-3	24.45	61.4	365.37	0.971	0.721	2.0	0.930	2.17 (1)	0.48
24	Whitson and Torp 1983, NS-1	35.04	44.0[‡]	410.43	0.971	0.659	2.0	0.490	21.60 (1)	2.83
25	Whitson and Brulè 2000,GOCW-7	33.62	60.5	358.70	0.973	0.575	2.5	1.050	23.90 (1)	2.50
26	Drohm et al. 1988, Example-1	54.92	57.1	410.90	0.890	0.572	2.9	0.960	69.81 (1)	8.79
27	Drohm et al. 1988, Example-2	32.65	59.5	436.70	0.975	0.684	2.0	0.530	15.63 (1)	0.96
28	Drohm et al. 1988, Example-3	26.26	58.4	393.20	0.973	0.604	2.0	1.000	4.75 (1)	0.63
29	Drohm et al. 1988, Example-4	28.34	59.0	377.60	0.971	0.586	2.1	0.830	11.84 (1)	0.73
30	Drohm et al. 1988, Example-5	21.27	56.4	377.60	0.970	0.716	2.0	1.340	1.69 (1)	0.43
31	JAPEX	29.81	58.9	402.59	0.972	0.641	2.0	0.570	6.67 (3)	0.06

[‡] As reported. All other API gravities are calculated from density at 288.15 K and 1.01325 bars.
[#] (1) is CVD liquid saturation (%), (2) is CCE liquid saturation (%), (3) is CCE relative volume (volume/volume)
[¥] Deviation = Sum of absolute of (experimental value –predicted value)/number of data point
‡ Gas condensates 6, 7, 8, 11, and 12 are near critical
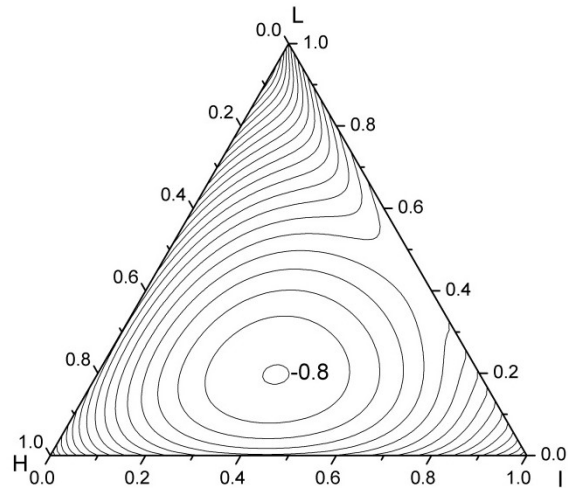
Figure 4-1. Dimensionless molar Gibbs free energy change on mixing for the ternary fluid given in Table 4-1 at 330.4 K and 196.48 bars.
Contour lines are drawn with the interval of 0.05 between -0.85 to 2.0. The PR EOS is used without volume shift.
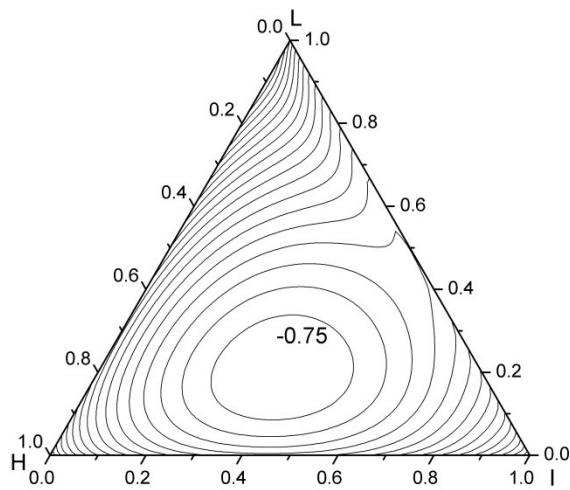
Figure 4-2. Dimensionless molar Gibbs free energy change on mixing for the ternary fluid given in Table 4-1 at 330.4 K and 196.48 bars.
Contour lines are drawn with the interval of 0.05 between -0.85 to 2.0. The PR EOS is used. Volume shift parameters are used in regression.

124
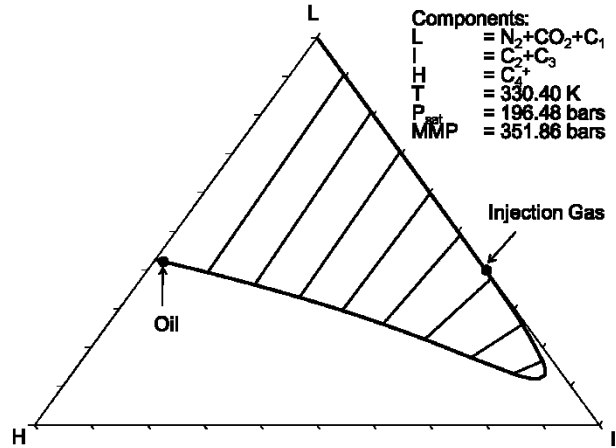
Figure 4-3. Phase envelope for the ternary fluid given in Table 4-1.
The PR EOS is used without volume shift. MMP calculated for the injection gas is 351.86 bars at 330.40 K.
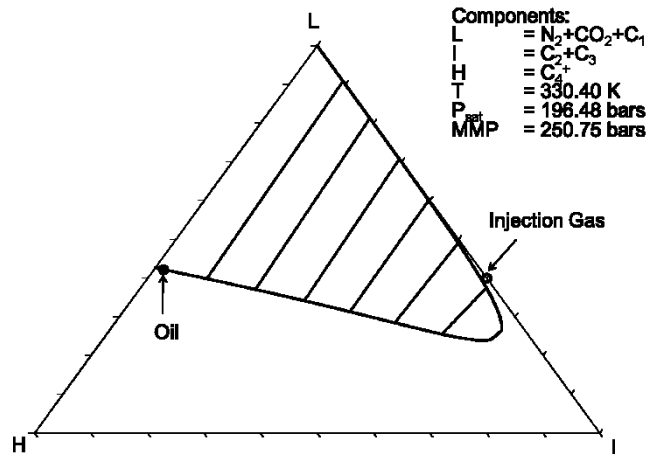
Figure 4-4. Phase envelope for the ternary fluid given in Table 4-1.
The PR EOS is used. Volume shift parameters are used in regression. Use of volume shift results in a two-phase envelope that is significantly smaller than that in Figure 4-3. MMP calculated for the injection gas is 250.75 bars 330.40 K.

$$f_{dis} = \frac{2^{-\frac{p}{2}} e^{-\frac{S}{2}} S^{\left(\frac{p}{2}-1\right)}}{\Gamma\left(\frac{p}{2}\right)}$$
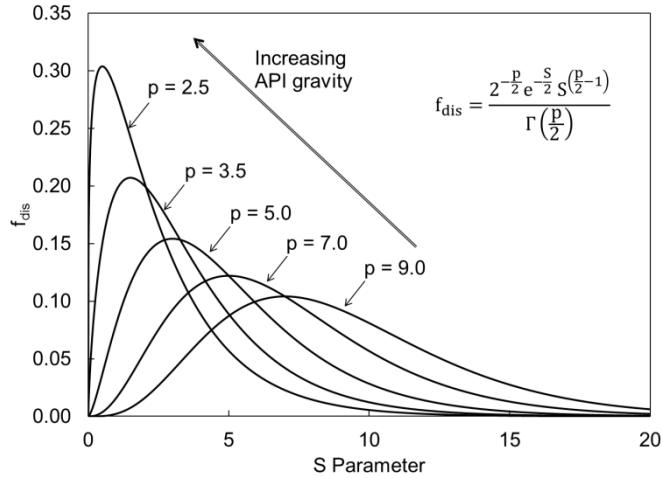
Figure 4-5. Chi-squared distributions for different p values in Equation 4-5.
The p parameter controls the degree of skew and the size of effective composition space. A lighter fluid tends to have a smaller p value. For light fluids, the effective CN (or MW) range is small compared to heavy oils.
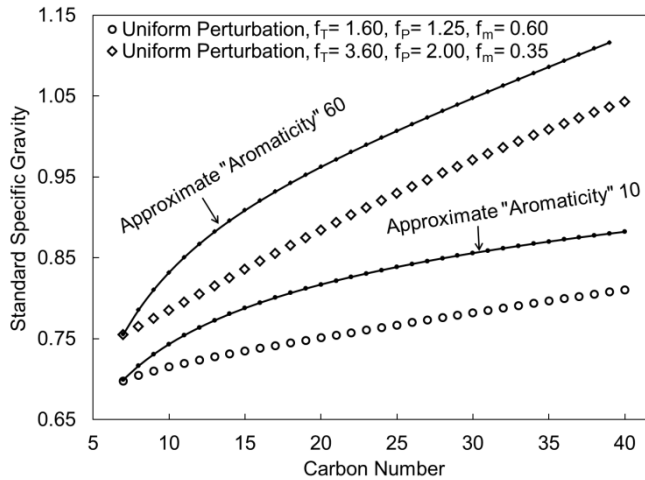
Figure 4-6. Standard specific gravity (SG) calculated for aromaticity levels 10 and 60 using uniform perturbation from n-alkanes.
The perturbation was made by matching the standard SG for C_7 at the two aromaticity levels given in Yarborough (1979). Critical parameters are calculated using the correlations of Kumar and Okuno (2012a). The plots show that the uniform perturbation gives deviation from Yarborough's trend curves for higher CN. However, the deviation levels off at a certain CN.

126
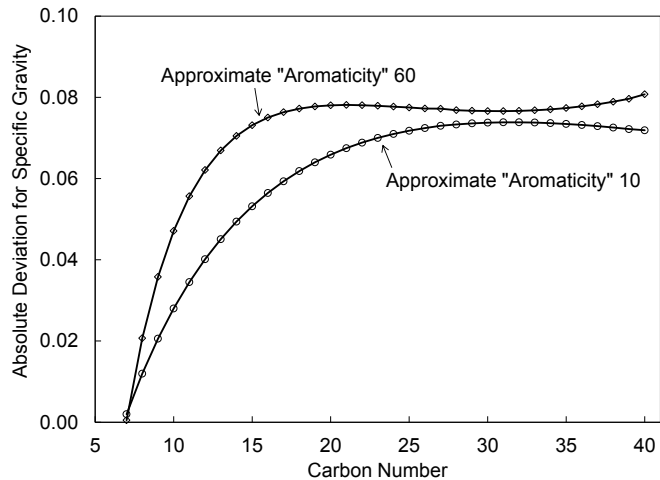
Figure 4-7. Absolute deviation for standard SG calculated for two aromaticity levels 10 and 60 using uniform perturbation from n-alkanes.
Absolute deviation increases with increasing carbon number and becomes nearly constant for high CNs.
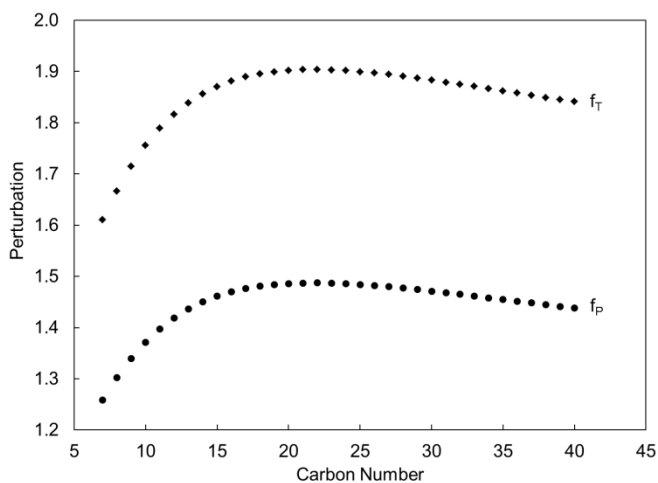
Figure 4-8. Variable perturbation from n-alkanes to match the standard SG curves from Yarborough (1979).
Aromaticity of 10 is considered. Uniform perturbation is appropriate for the higher CN range, while sharply increasing perturbation is required for the lower CN range.

127
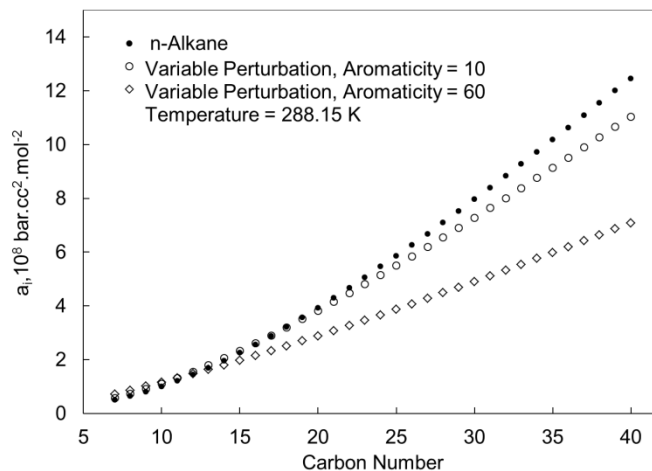
Figure 4-9. The attraction (a) parameter for three levels of aromaticity 0, 10, and 60.
The original correlations of Kumar and Okuno (2012b) are used for n-alkanes (i.e., zero aromaticity).
The f_T, f_P, and f_m values fitted to Yarborough's trend curves are used for the aromaticity levels 10 and 60. Temperature is 288.15 K.
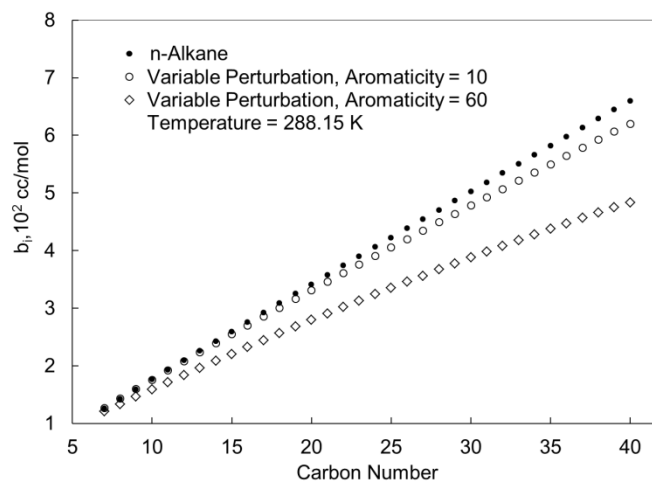
Figure 4-10. The covolume (b) parameter for three levels of aromaticity 0, 10, and 60.
The original correlations of Kumar and Okuno (2012b) are used for n-alkanes (i.e., zero aromaticity).
The f_T, f_P, and f_m values fitted to Yarborough's trend curves are used for the aromaticity levels 10 and 60. Temperature is 288.15 K.
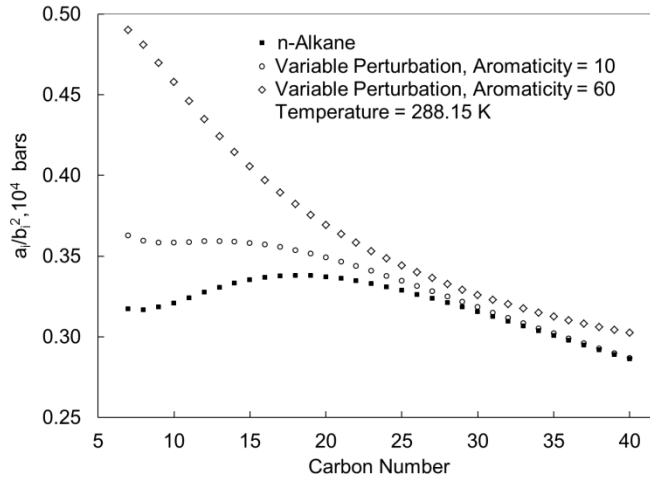
Figure 4-11. The ψ parameter (ψ = a/b^2) for three levels of aromaticity based on the values for a and b parameters in Figures 4-9 and 4-10.
Temperature is 288.15 K. The ψ parameter for each component is calculated using Equation 4-13.
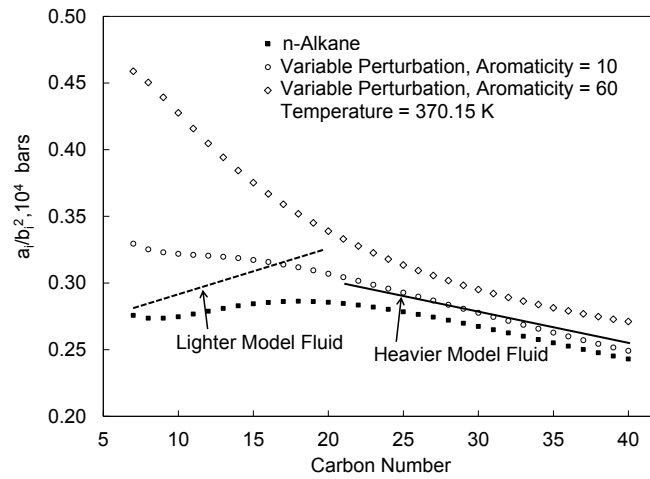
Figure 4-12. The ψ parameter (ψ = a/b^2) for three levels of aromaticity at 370.15 K.
All critical parameters and acentric factors are the same as in Figures 4-9 and 4-10. The ψ parameter changes its sensitive to aromaticity around the CN of 20. Trend curves are given for the lighter and heavier model fluids. For the model trends, the physical trend is also considered that heavier fractions are relatively more naphthenic and aromatic than lighter fractions.

129
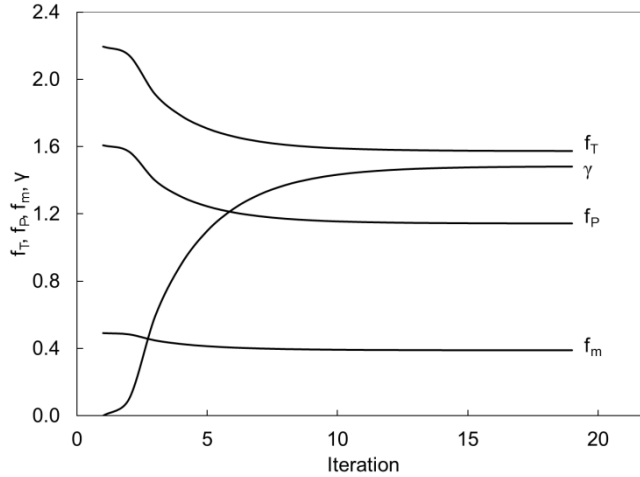
Figure 4-13. Trends of the f_T, f_P, f_m, and γ parameters during iteration for oil 2 given in Table 4-2. As γ increases from the starting value of zero, f_T, f_P, and f_m decrease. Convergence is achieved when the rate of increase in γ or the rate of decrease in f_T, f_P, and f_m becomes negligible.
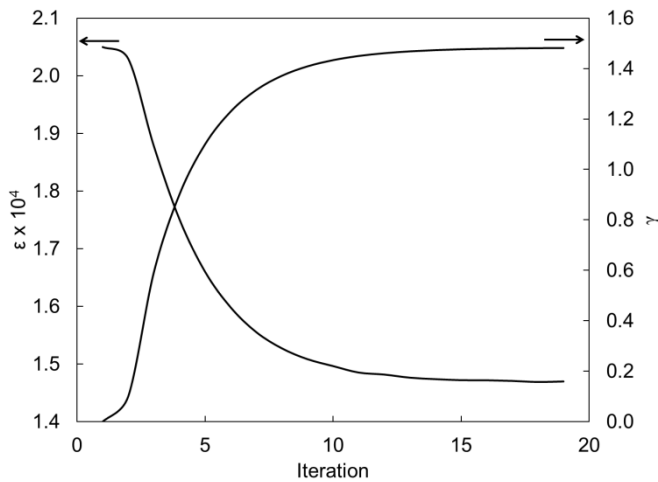
Figure 4-14. Trends of the ε function and the γ parameter during iteration for oil 2 given in Table 4-2. The ε function is defined in Equation 4-12. In our earlier work (Kumar and Okuno 2012a), the ε function was the stopping criterion in regression. Here, the ε function is not the stopping criterion in regression. The ε function decreases with increasing γ value, and is sufficiently small on convergence
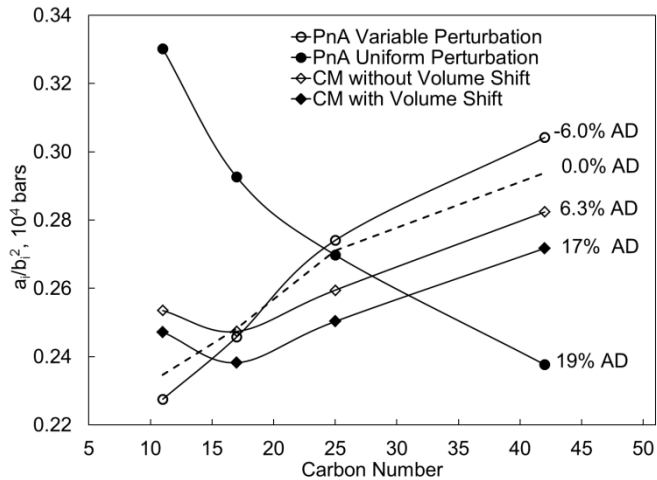
Figure 4-15. The ψ parameter (ψ = a/b^2) for oil 1 given in Table 4-2.
Four different schemes are used for characterization; PnA with uniform perturbation, PnA with variable perturbation, $CM_{w/o}V$, and CM_wV. The dashed curve shows the ψ trend when the PnA method uses γ of 1.08 to match the slim-tube MMP of 220 bars.
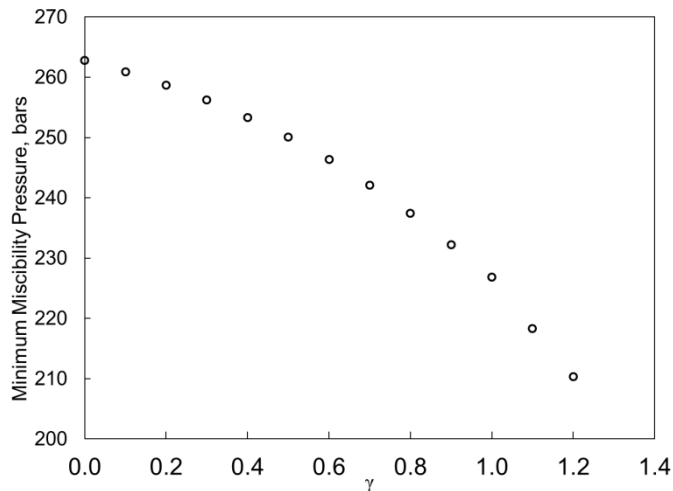
Figure 4-16. Minimum miscibility pressures calculated for different γ values for oil 1 (Table 4-2) at 374.85 K.
The injection gas has molar composition of 0.48% N_2, 4.97% CO_2, 58.22% C_1, 17.14% C_2, 12.10% C_3, 4.97% C_4, 1.66% C_5, and 0.53% C_6. A monotonic change in the calculated MMP is observed with respect to γ. The slim-tube MMP of 220 bars can be predicted with γ of 1.08.
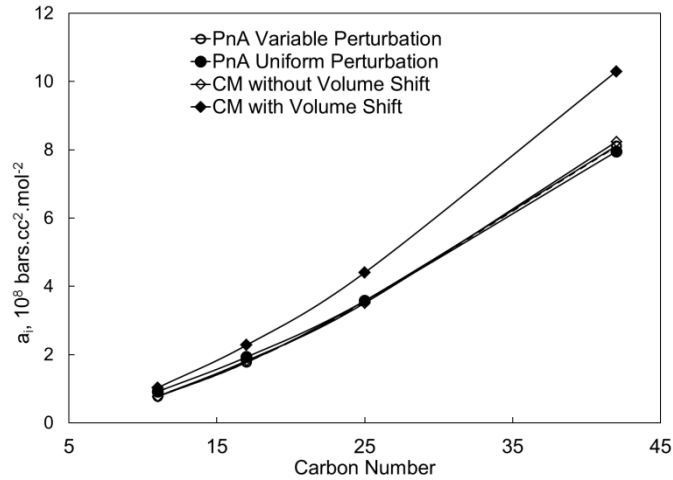
Figure 4-17. The trend of the a parameter for the four pseudocomponents for each of four cases considered in Figure 4-15.
The dashed curve shows the trend for the a parameter when the PnA method uses γ of 1.08 to match the slim-tube MMP of 220 bars.
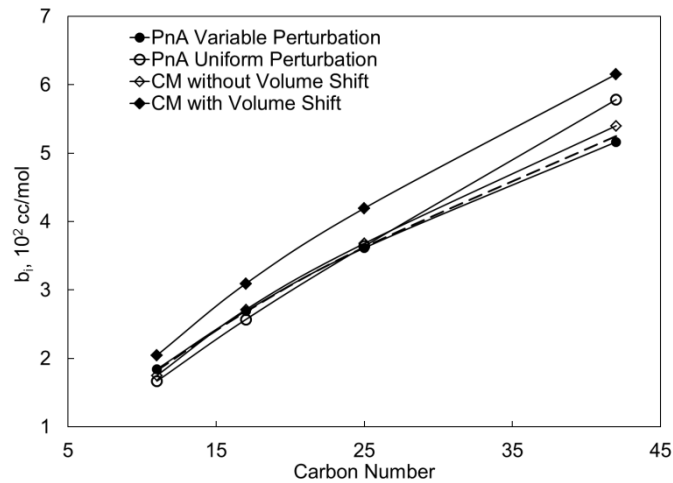
Figure 4-18. The trend of the b parameter for the four pseudocomponents for each of four cases considered in Figure 4-15.
The dashed curve shows the trend for the b parameter when the PnA method uses γ of 1.08 to match the slim-tube MMP of 220 bars.
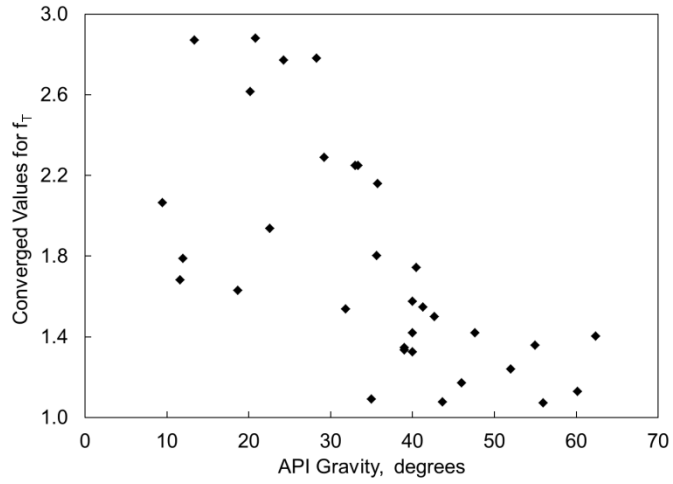
Figure 4-19. Trend of the converged f_T values with respect to the API gravity. Heavier fluids tend to require more perturbation from n-alkanes.
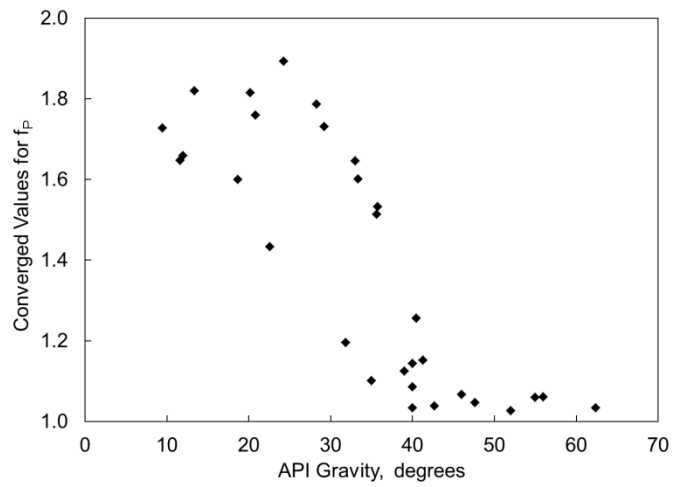
Figure 4-20. Trend of the converged f_P values with respect to the API gravity. Heavier fluids tend to require more perturbation from n-alkanes.
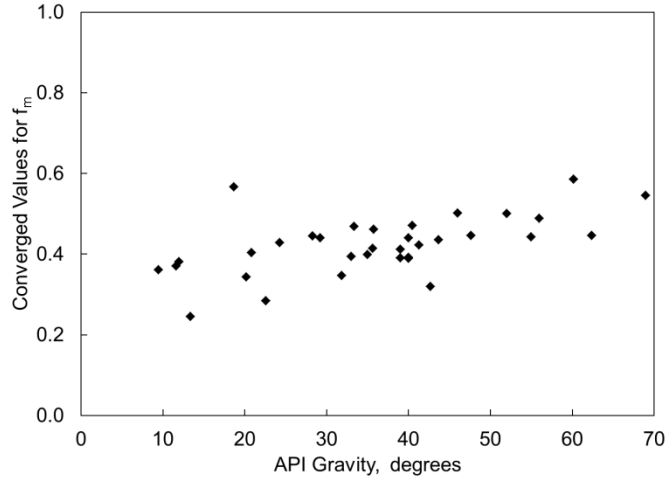
Figure 4-21. Trend of the converged f_m values with respect to the API gravity.
Heavier fluids tend to require more perturbation from n-alkanes.
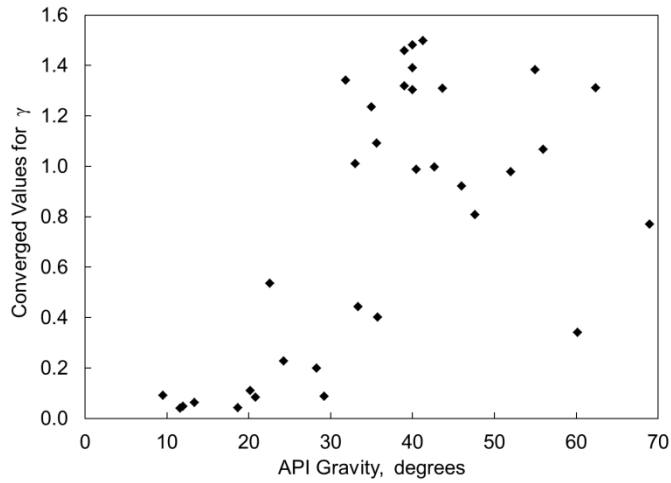
Figure 4-22. Trend of γ parameter with fluid API gravity.
The γ parameter becomes greater for lighter fluids. For heavy oils, variable perturbation from n-alkanes is less significant; the importance of the ψ and γ parameters diminishes as the API gravity becomes lower. For extra heavy oils, the PnA method reduces to the previous PnA method developed in Kumar and Okuno (2012a).
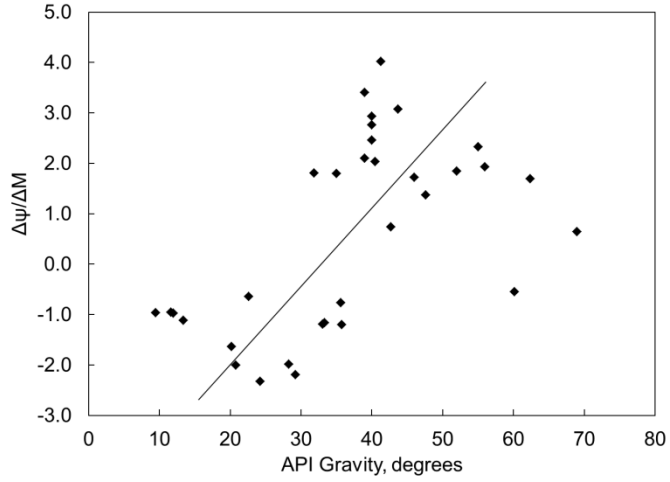
Figure 4-23. Average gradient of ψ (Δψ/ΔM) for different fluids.
This average gradient is calculated using ψ's and MWs for the lightest and heaviest pseudocomponents.
The gradient is small for heavy fluids, and gradually increases as the API gravity increases.
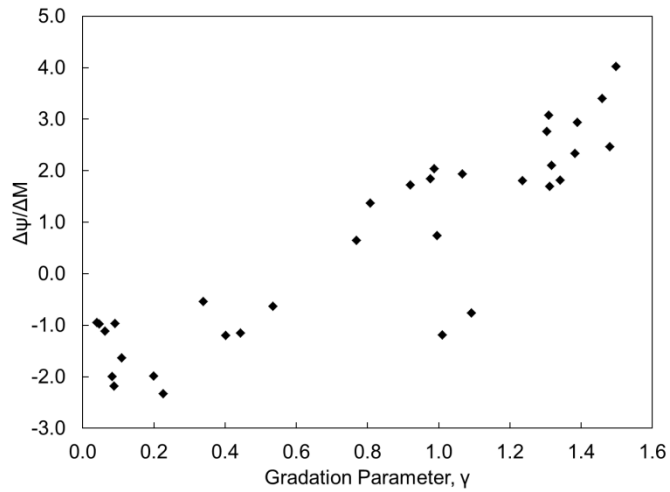
Figure 4-24. Average gradient of ψ (Δψ/ΔM) with respect to γ.
As γ increases, the average gradient also increases.
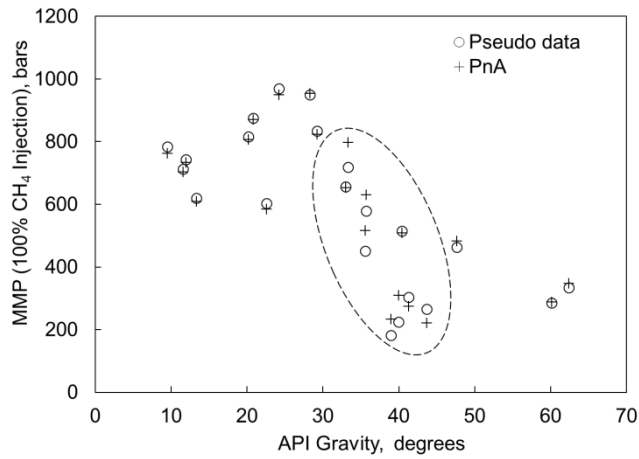
Figure 4-25. Comparisons of C_1-MMPs for 22 oils in Table 4-4 using the PnA method and those from pseudo data.
Good agreement is observed except for the API gravity range between 30 and 40. This is attributed to the discontinuity in the $CM_{w/o}V$ characterization used to generate pseudo data. PVTsim used in the $CM_{w/o}V$ gives two different characterization options, normal and heavy characterizations, based on an oil gravity criterion of 30°API.
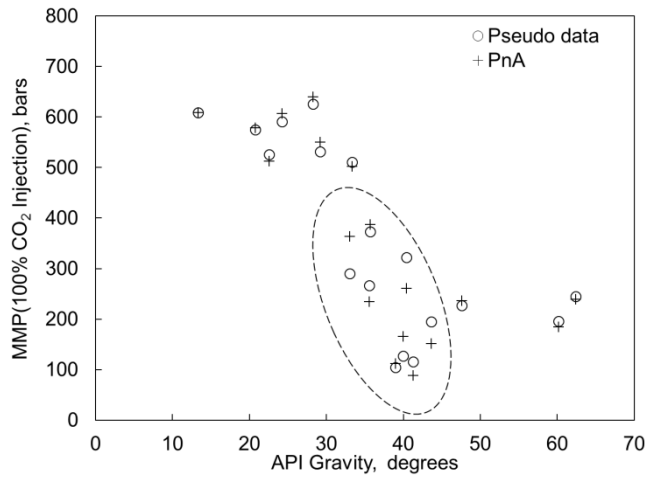
Figure 4-26. Comparisons of CO_2-MMPs for 18 oils in Table 4-4 using the PnA method and those from pseudo data.
Good agreement is observed except for the API gravity range between 30 and 40. This is attributed to the discontinuity in the $CM_{w/o}V$ characterization used to generate pseudo data. PVTsim used in the $CM_{w/o}V$ gives two different characterization options, normal and heavy characterizations, based on an oil gravity criterion of 30°API.

136
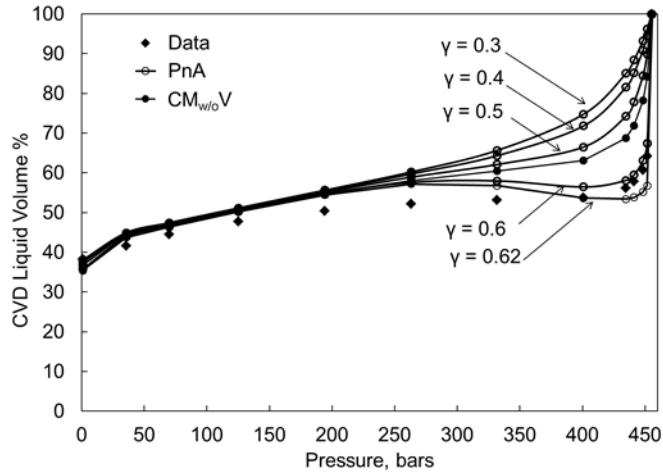
Figure 4-27. CVD liquid saturation for volatile oil 1 given in Table 4-5.
The reservoir temperature is 354.82 K. The oil has 12.92% C_{7+} mole fraction. The molecular weight of C_{7+} is 205 gm/mol, and the overall molecular weight is 46.07 gm/mol. Predictions are also presented using the PnA method with different γ values and $CM_{w/o}V$ methods. The γ parameter converges to 0.62 using the algorithm given in section 4.3.4.
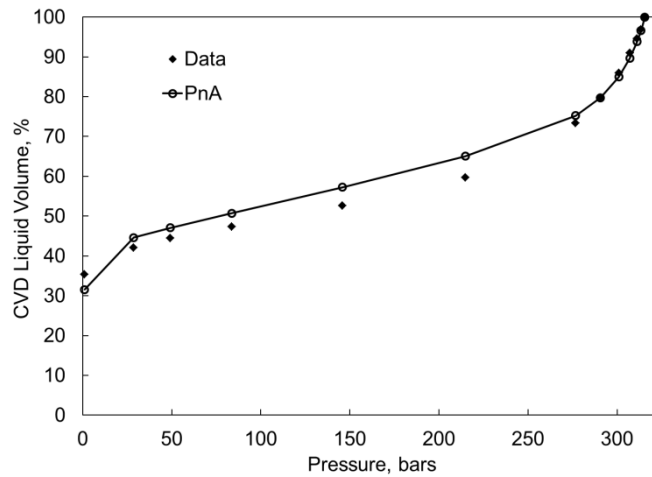
Figure 4-28. CVD liquid saturation for volatile oil 5 given in Table 4-5.
The reservoir temperature is 425.93 K. The oil has 17.2% C_{7+} mole fraction. The molecular weight of C_{7+} is 218 gm/mol, and the overall molecular weight is 59.63 gm/mol. Predicted values are also presented using the PnA methods.

137
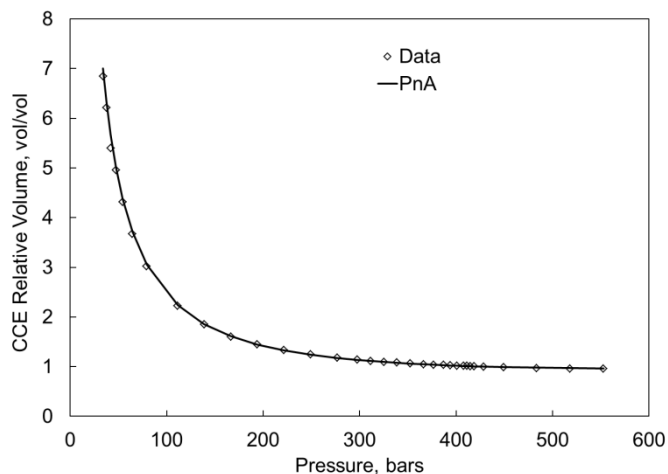
Figure 4-29. CCE relative volume curve for volatile oil 6 given in Table 4-5.
The reservoir temperature is 414.82 K. The oil has 19.0% C_{7+} mole fraction. The molecular weight of C_{7+} is 250 gm/mol, and the overall molecular weight is 67.32 gm/mol. Predicted values are also presented using the PnA methods.
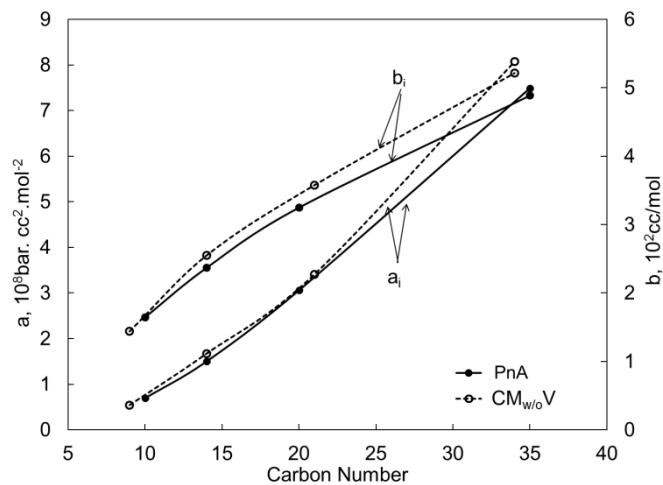
Figure 4-30. Comparison of the a_i and b_i parameters for pseudocomponents for volatile oil 1 given in Table 4-5.
Characterizations were made using the PnA and $CM_{w/o}V$ methods.
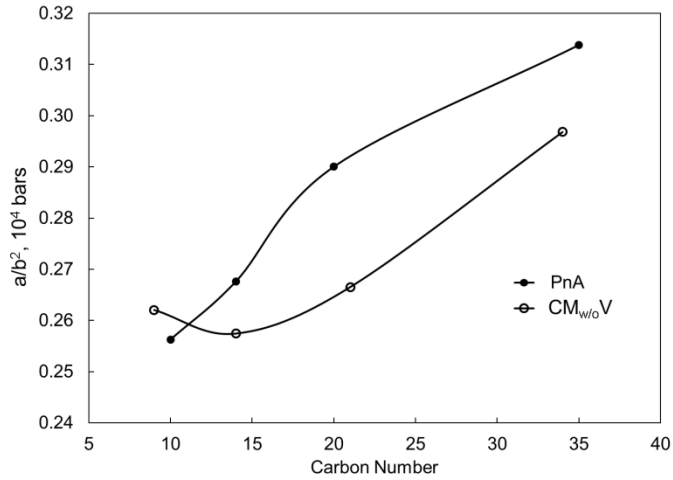
Figure 4-31. Comparison of ψ trends for pseudocomponents for volatile oil 1 given in Table 4-5. Characterizations were made using the PnA and $CM_{w/o}V$ methods. The ψ trend for the PnA method exhibits a combined trend of the two model fluids in Figure 4-12. The $CM_{w/o}V$ method results in the ψ trend that exhibits a minimum for the second lightest pseudocomponent.
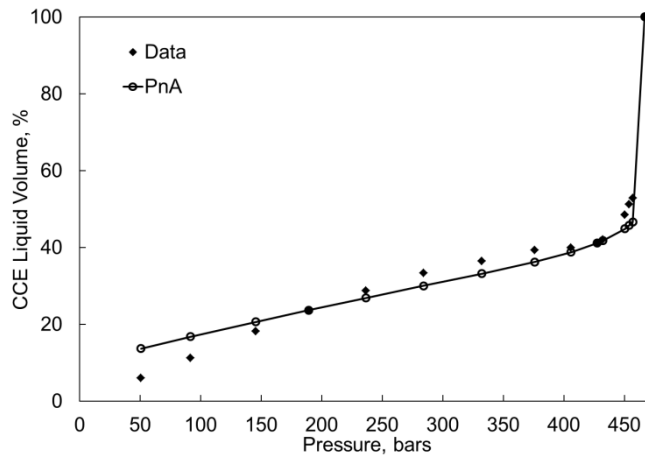
Figure 4-32. CCE liquid saturation for near-critical volatile oil 12 given in Table 4-5. Predicted values are also presented using the PnA method. The reservoir temperature is 371.6 K, and the critical temperature is 388.1 K. The oil has 9.86% C_{7+} mole fraction. The molecular weight of the C_{7+} fraction is 192.8 gm/mol, and the overall molecular weight is 37.94 gm/mol.
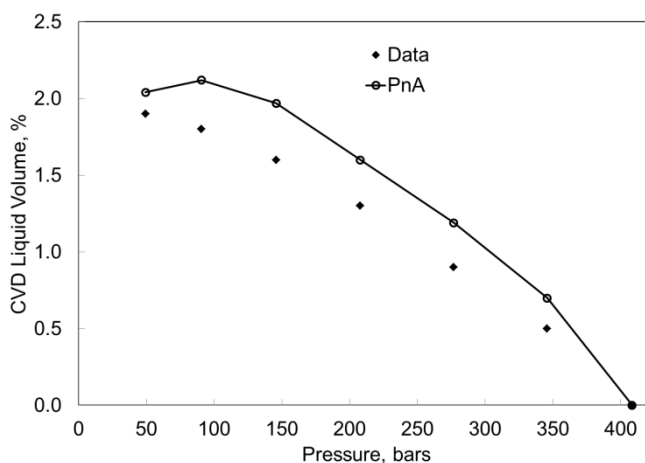
Figure 4-33. CVD liquid saturation for gas condensate 20 given in Table 4-6 at 367.6 K. The gas condensate has 1.62% C_{7+} mole fraction. The molecular weight of the C_{7+} fraction is 143 gm/mol, and the overall molecular weight is 19.75 gm/mol.
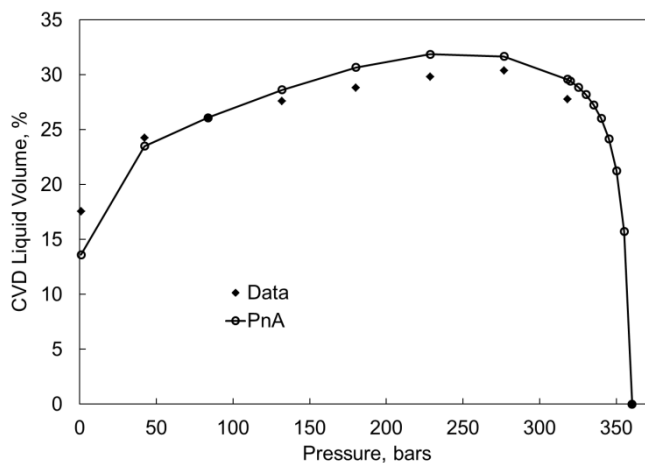
Figure 4-34. CVD liquid saturation for gas condensate 5 given in Table 4-6 at 424.82 K. The gas condensate has 10.87% C_{7+} mole fraction. The molecular weight of the C_{7+} fraction is 173.0 gm/mol, and the overall molecular weight is 40.77 gm/mol.
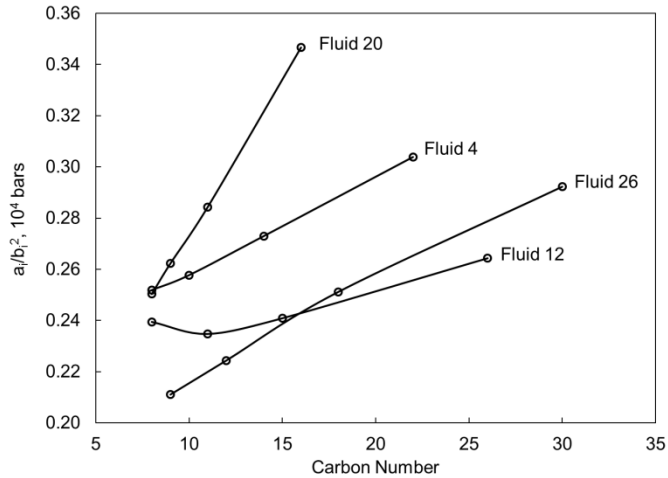
Figure 4-35. Trends of ψ for gas condensates 4, 12, 20, and 26 given in Table 4-6.
For gas condensates, the CN range of pseudocomponents is narrow. Therefore, ψ trends are increasing as shown in Figure 4-12. In general, the slope of ψ becomes smaller as the CN range of pseudocomponents becomes wider.
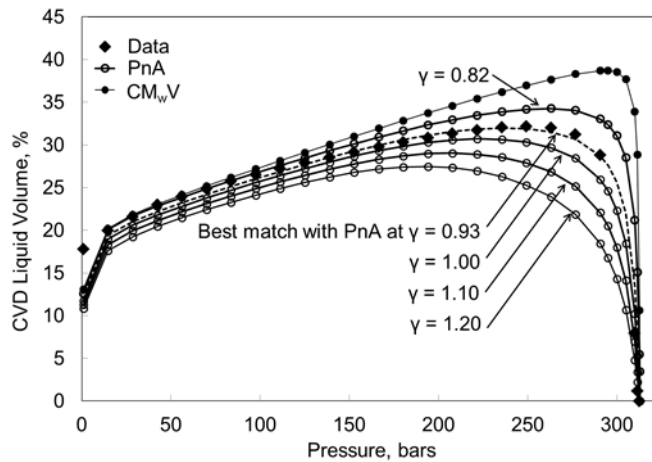
Figure 4-36. CVD liquid saturation for near-critical gas condensate 7 given in Table 4-6 at 424.82 K. The gas condensate has 12.39% C_{7+} mole fraction. The molecular weight of the C_{7+} fraction is 158.23 gm/mol, and the overall molecular weight is 41.71 gm/mol. Predictions are presented using the CM_wV method and the PnA method with different γ values; 0.82, 0.93, 1.00, 1.10, and 1.20. The γ parameter converges to 0.82 using the algorithm given in section 4.3.4.
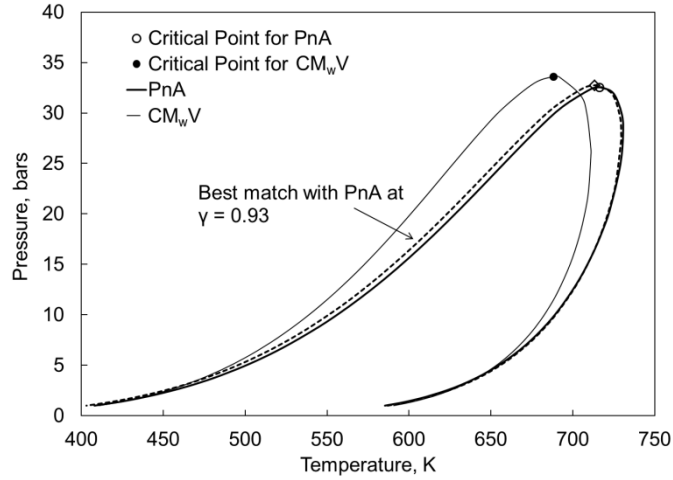
Figure 4-37. P-T phase envelope for the C_7^+ fraction using the three fluid models shown in Figure 4-36. The three models have similar phase behavior for the C_{7+} fraction. Liquid saturation given in Figure 4-36 is sensitive to the C_{7+} phase behavior.
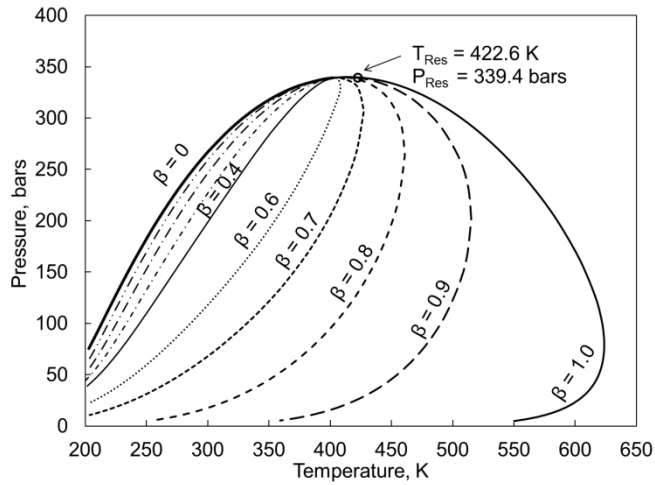
Figure 4-38. Quality lines for near-critical gas condensate 6 given in Table 4-6.
Vapor molar phase fractions (β) are shown beside the curves. The calculated critical temperature and critical pressure are 402.0 K and 339.2 bars, respectively. The reservoir temperature (T_{Res}) and pressure (P_{Res}) are is 422.6 K and 339.4 bars, respectively.
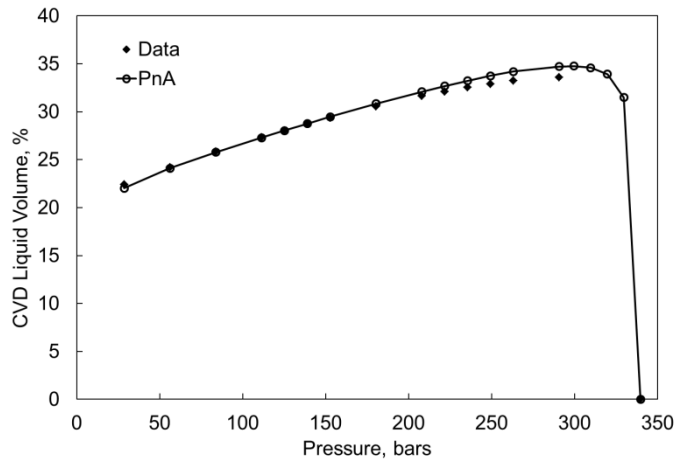
Figure 4-39. CVD liquid saturation for near-critical gas condensate 6 given in Table 4-6 at 422.6 K. The gas condensate has 12.27% C_7^+ mole fraction. The molecular weight of the C_7^+ fraction is 154.93 gm/mol, and the overall molecular weight is 39.23 gm/mol.
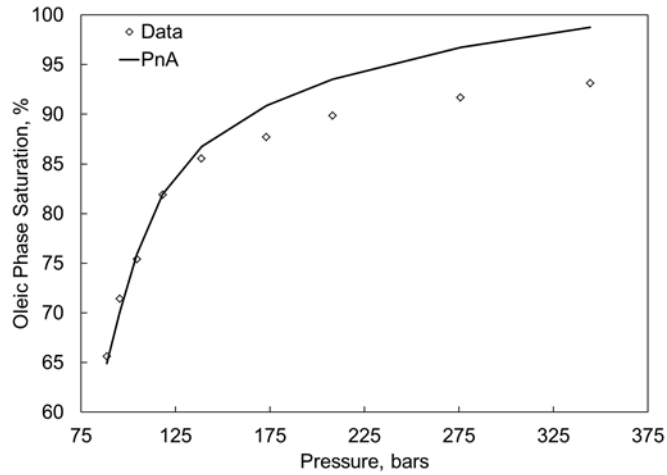
Figure 4-40. Oleic phase saturation data and predictions using the PnA method for heavy oil 23 given in Table 4-4 (Sharma 1990) at 299.81 K.
This is a mixture of 40% oil and 60% CO_2.
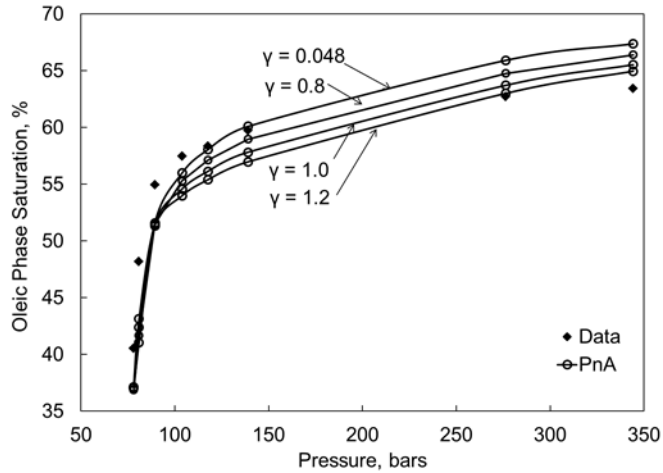
Figure 4-41. Oleic phase saturation data and predictions using the PnA method for heavy oil 23 given in Table 4-4 (Sharma 1990) at 299.81 K.
This is a mixture of 20% oil and 80% CO2. The converged γ value is 0.048 using the algorithm given in section 4.3.4
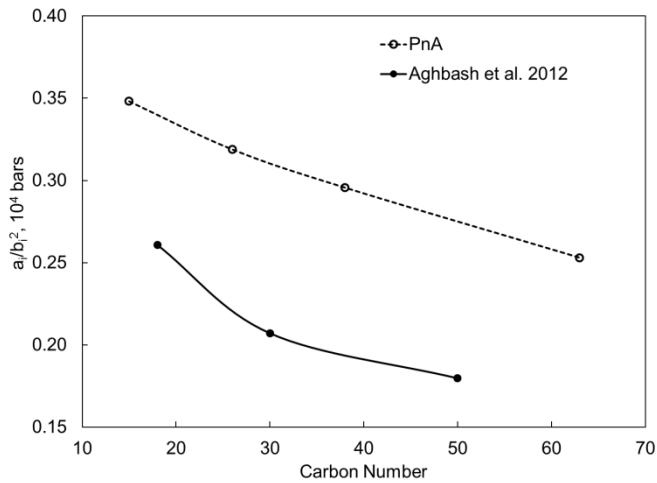
Figure 4-42. The ψ parameter ($ψ = a_i/b_i^2$) for pseudocomponents for heavy oil 23 given in Table 4-4. Two characterizations compared are from Aghbash and Ahmadi (2012) and the PnA method. The ψ parameter monotonically decreases with CN for the two cases, which is in line with our discussion for heavy oils in Figure 4-12.

144
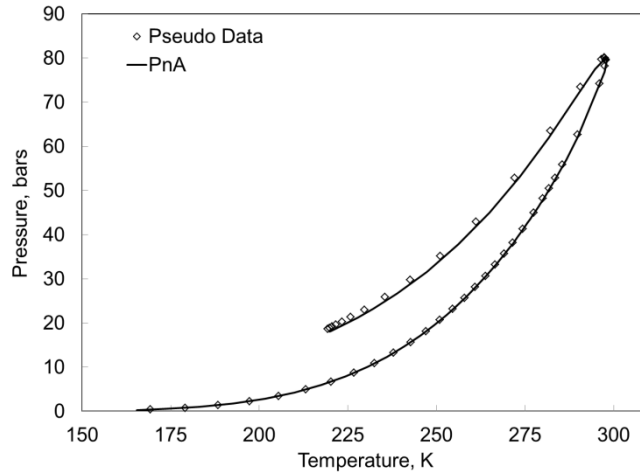
Figure 4-43. Three-phase region from the PnA method is compared with pseudo data for a mixture of 20% oil 23 (Table 4-4) and 80% CO_2.

Pseudo data has been created using 30 components (with 22 pseudocomponents) based on the conventional characterization using the PR EOS without volume shift.
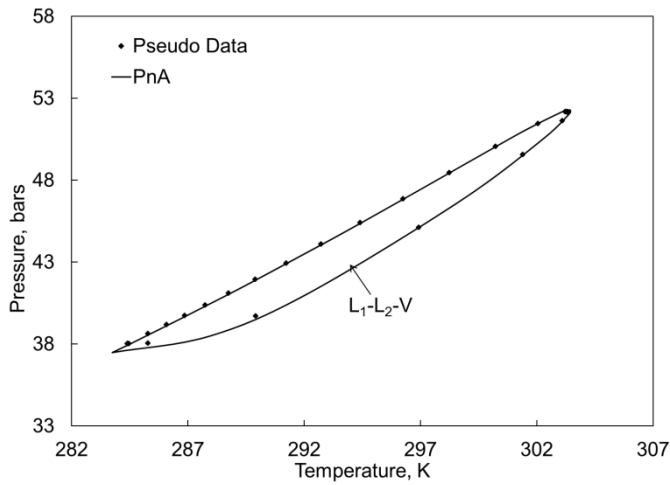
Figure 4- 44. Three-phase region from the PnA method is compared with pseudo data for a mixture of 10% oil 5 (Table 4-4) and 90% C_2.

Pseudo data has been created using 30 components (with 22 pseudocomponents) based on the conventional characterization using the PR EOS without volume shift.

145
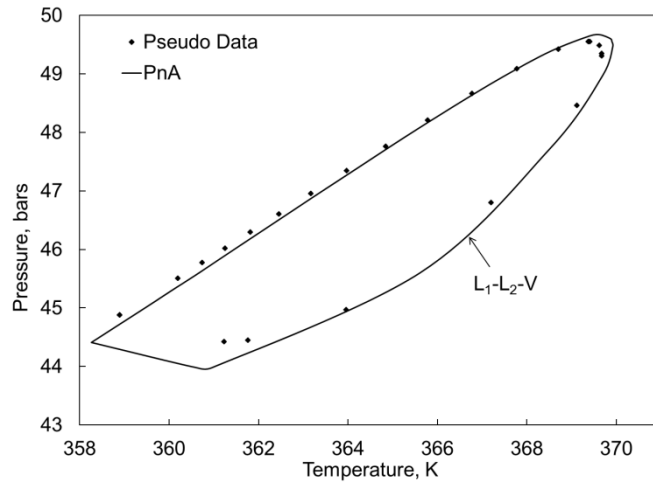
Figure 4-45. Three-phase region from the PnA method is compared with pseudo data for a mixture of 10% oil 5 (Table 4-4) and 90% C_3.

Pseudo data has been created using 30 components (with 22 pseudocomponents) based on the conventional characterization using the PR EOS without volume shift.

Chapter 5: Direct Perturbation of the Peng-Robinson Attraction and Covolume Parameters for Reservoir Fluid Characterization

A version of this has been published in Chemical Engineering Science, Year (2014), Volume: 127, Pages: 293-309.

5.1. Introduction

The interaction of fluid flow with phase behavior can be significant in many petroleum reservoir processes, such as hydrocarbon-gas, CO_2, and steam injection. Reliable design of these reservoir processes requires compositional simulation, where the fluid system is characterized using a cubic equation of states (EOS). Widely used EOSs in the petroleum industry include the Peng-Robinson (PR) EOS (1976, 1978) and the Soave-Redlich-Kwong (SRK) EOS (1972). These EOSs along with the van der Waals (vdW) mixing rules, when properly used, give reasonable accuracy and high computational efficiency (Ikeda and Schaefer 2011).

Reservoir fluids contain a large number of compounds, most of which are non-identifiable. They are reported as single carbon number (SCN) fractions and a lumped fraction (a plus fraction; e.g., the heptane-plus fraction or C_{7+}) in a compositional analysis. The uncertainties associated with non-identifiable compounds are more significant for heavier reservoir fluids because their fractions are higher. Even for a well-defined series of n-alkanes, for example, critical points are uncertain for carbon numbers (CNs) higher than 36 (Niktin et al. 1997). Also, different types of hydrocarbons are present within each SCN fraction, such as paraffins (P), naphthenes (N) and aromatics (A). Their concentrations and critical properties are unknown.

A conventional procedure for reservoir fluid characterization using an EOS is to adjust various EOS-related parameters to match the experimental data available, such as bubble- and dew-points and densities. The adjustment parameters often used include critical temperature (T_C), critical pressure (P_C), acentric factor (ω), volume-shift parameters, and binary interaction parameters (BIPs). The constant terms for the attraction (a) and covolume (b) parameters, Ω_a and Ω_b, are also sometimes used as adjustment parameters. Since the relationship between these EOS-related parameters and phase behavior predictions is rather implicit and non-linear, matching the experimental data available does not always yields a reliable fluid model that is accurate at thermodynamic conditions away from experimental conditions. This is true especially when many EOS-related parameters are simultaneously regressed to the available experimental data. Thus, the correlative accuracy of a fluid model does not necessarily mean the predictive capability.

How phase behavior predictions can be controlled through a cubic EOS is not fully understood in the literature. Phase behavior predictions using a cubic EOS depend on the attraction (a) and covolume (b) parameters. When BIPs are used for a mixture, they affect the phase behavior predictions through the mixing rules used. It is obvious that phase behavior predictions can be controlled more directly by the attraction and covolume parameters than by T_C, P_C, and ω. Current practice of reservoir fluid characterization mentioned above does not effectively utilize the original simplicity of cubic EOSs.

For single-component fluids, various researchers conducted direct adjustment of the attraction and covolume parameters. Thodos (1955a) estimated the attraction and covolume parameters of the vdW EOS for n-alkanes using a group contribution method. The approach was later applied to unsaturated aliphatic, naphthenes, and aromatics (Thodos 1955b, 1956, 1957). Deriving T_C and P_C from the

148

attraction and covolume parameters is straightforward in this case since the vdW attraction parameter does not depend on temperature. Tsonopoulos and Wilson (1983), Heidman et al. (1985), Enick et al. (1987), and Economou et al. (1997) directly adjusted the attraction and covolume parameters of an EOS to match the vapor pressure and liquid density data for water. They used the Zudkevitch and Joffe modification of the Redlich-Kwong EOS (Zudkevitch and Joffe 1970). Optimization of components' parameters to match vapor pressure and liquid density data has been also performed with other types of EOSs (Voutsas et al. 2006, Aparicio-Martínez and Hall 2006).

Ahmed and Meehan (2010) developed correlations for the attraction and covolume parameters of the PR EOS for the C_{7+} fraction as a single component. They generated 49 hypothetical plus-fractions based on the correlations of Riazi and Daubert (1986) for molecular weight (MW), boiling point (T_b), and specific gravity (γ). For each fraction, 100 densities were specified in pressure-temperature space. The attraction and covolume parameters adjusted to match the densities were correlated with MW, T_b, and γ. Their correlations were recommended for density prediction of crude oil and gas condensate. Their EOS models exhibited significant improvement in phase behavior predictions for gas condensates and oils without volume shift. They concluded that splitting of a plus fraction was not required. Although saturation pressures were matched by adjusting BIPs, their approach was not tested in term of the predictive capability of compositional phase behavior, such as minimum miscibility pressures, swelling test, and gas solubilities.

Characterization of a plus fraction using multiple pseudocomponents becomes important when an EOS model is used not only to predict phase densities, but also to simulate vaporization and condensation of intermediate components in various enhanced oil recovery processes. To the best of our knowledge, however, no method has been presented in the literature that directly adjusts the attraction and covolume parameters of a cubic EOS to characterize volumetric and compositional phase behavior of petroleum reservoir fluids.

The attraction and covolume parameters have been indirectly adjusted through T_C, P_C, and ω in prior characterization methods. This is likely because the attraction and covolume parameters are not measurable and EOS-specific. However, this is also true for T_C, P_C, and ω for non-identifiable compounds in fluid characterization using an EOS. Each of SCNs and plus fractions contains a number of different compounds, such as the paraffinic, naphthenic, and aromatic compounds, with unknown concentrations. Furthermore, these fractions are grouped into a few pseudocomponents so that EOS computations are efficient in reservoir flow simulation. Therefore, apparent properties (e.g., T_C, P_C, and ω) of pseudocomponents are only estimated, and even extrapolated for high-CN fractions. It is difficult to justify the reliability of the estimated critical properties in the absence of measured values. Also, the parameter values estimated for pseudocomponents are usually adjusted to correlate experimental data based on the EOS used. Thus, the properties of these components eventually become EOS-specific.

A characterization method was recently presented in our previous publications (Kumar and Okuno 2013) based on the concept of perturbation from n-alkanes (PnA). Instead of attempting to estimate

apparent critical properties of pseudocomponents, the PnA method first assigned the pseudocomponents the optimized T_C, P_C, and ω values with which the PR EOS gives accurate predictions of vapor pressures and liquid densities for n-alkanes. Then, they were perturbed from the n-alkane values in well-defined directions until the saturation pressure and liquid density data at the reservoir temperature were matched. The perturbation was conducted in the increasing direction for T_C and P_C, and in the decreasing direction for ω to make the pseudocomponents gradually more aromatic. The perturbation also controlled the qualitative trend of the ψ parameter ($\psi = a/b^2$) with respect to CN. This ensured that the attraction (a) and covolume (b) parameters for each pseudocomponent had proper interrelationship depending on the CN range of pseudocomponents. Extensive testing of the PnA method by use of 77 different reservoir fluids showed that various types of phase behavior were accurately predicted once the saturation pressures and liquid densities were matched.

The PnA method did not require volume shift to match densities for the fluids studied. This is desirable for the following reasons; i) when used as adjustment parameters, volume shift affects phase behavior predictions at the thermodynamic conditions that the available PVT data do not cover (Kumar and Okuno 2013, 2014), and ii) volume shift parameters cannot be canceled out from the fugacity equations, if the effect of capillary pressures is significant on the equations. The second reason is becoming important considering the increasing interests in hydrocarbon recovery from tight/shale reservoirs, where pore geometries affect phase behavior (Schulte 1980; Whitson and Belery 1994; Nojabaei et al. 2013).

In this research, the PnA method is simplified by directly perturbing the attraction and covolume parameters, instead of T_C, P_C, and ω, for reservoir fluid characterization by use of the PR EOS. The development of the direct PnA method begins by establishing the attraction and covolume parameters for n-alkanes up to n-C_{100}. The effects of aromaticity on the a, b, and ψ parameters are then discussed. A new algorithm developed for reservoir fluid characterization controls phase behavior predictions through direct perturbation of the b and ψ parameters. The algorithm is applied to 84 different reservoir fluids, for which phase behavior data are available in the literature. Results show the reliability, robustness, and simplicity of the direct PnA method.

5.2. Attraction and Covolume Parameters for Hydrocarbons

T_C, P_C, and ω for n-alkanes from n-C_7 through n-C_{100} were optimized in terms of liquid densities and vapor pressures by use of the PR EOS (Kumar and Okuno 2012). As presented in the Supporting Information (Section 5-S1), it has been confirmed that the PR attraction and covolume parameters for n-alkanes based on Kumar and Okuno (2012) are suitable for the direct perturbation in this research.

In the previous PnA method (Kumar and Okuno 2013), the perturbations of T_C, P_C, and m were conducted from the n-alkane values towards a higher level of aromaticity to match the saturation pressure and liquid densities at a given reservoir temperature. This is essentially to perturb the attraction and covolume parameters from n-alkane values in the direction of increasing level of aromaticity, but only indirectly. The effect of aromaticity on the parameters and proper interrelationship between the

150

attraction and covolume parameters (Kumar and Okuno 2013) are briefly explained in the Supporting Information (Section 5-S2). The term "aromaticity" was defined by Yarborough (1979) as the percentage of total carbon atoms in a molecule, which are within the benzene ring. Yarborough (1979) presented trend curves for specific gravity at 288.15 K and 1.01325 bars as a function of CN and aromaticity. In his presentation, CN ranged from 7 to 40, and aromaticity from 0 to 80, as reproduced in the Supporting Information (Section 5-S2, Figure 5-S12).

In Kumar and Okuno (2013), these trend curves were successfully used to explain how perturbation of critical parameters (equivalently, the attraction and covolume parameters) should be done for the different CNs. Details were presented in Kumar and Okuno (2013) and summarized in the Supporting Information (Section 5-S2). In the current paper, the same knowledge is used to guide the direct perturbation of the attraction and covolume parameters.

The attraction parameter increases with CN for a fixed aromaticity level (Figure 5-S13). The effect of aromaticity on the attraction parameter is not systematic; i.e., the attraction parameter increases with aromaticity for light hydrocarbons, and the trend is the other way around for heavier hydrocarbons. The trend of the covolume parameter is more systematic (Figure 5-S14). The covolume parameter for n-alkane is higher than that for aromatic hydrocarbons for a given CN. Also, n-alkanes exhibit the largest gradient of the covolume parameter with respect to CN. Note that aromaticity should be interpreted as qualitative deviation from n-alkanes within this research.

One of the most important parameters in the PnA method is ψ (**Equation 5-1**).

$$\psi = \frac{a}{b^2} = \frac{\Omega_a}{\Omega_b^2} P_C (1 + m[1 - (T/T_C)^{0.5}])^2 \tag{5-1}$$

on the basis of the PR EOS. The ψ parameter is sensitive to the level of aromaticity for light and intermediate hydrocarbons (Figure 5-S15). The ψ parameter monotonically decreases with CN for high aromaticity levels, but exhibits a maximum for low aromaticity levels, including n-alkanes. The ψ parameter for a fixed CN increases with increasing level of aromaticity, and changes its sensitivity to aromaticity around CN 20. The ψ parameter is useful in controlling variable perturbation at different CNs.

5.3.   Direct Perturbation of the Attraction and Covolume Parameters

The development of the direct PnA method was motivated by the question as to how many parameters are required to represent phase behavior of reservoir fluids on the basis of the PR EOS with the vdW mixing rules. A detailed investigation of phase behavior predictions from the PR EOS has indicated that the volumetric and compositional phase behaviors are largely determined by the covolume and ψ parameters, respectively. Also, these parameters for the pseudocomponents of a given fluid can be controlled systematically by a few adjustment parameters. The objective of this section is to present a fluid-characterization algorithm that reflects our findings regarding systematic control over phase behavior predictions through the PR EOS.

In the subsequent subsections, a new set of equations is first presented for perturbation of the covolume and ψ parameters in MW space. Then, a new algorithm is presented that uses the equations to match experimental data in reservoir fluid characterization.

5.3.1. Equations for Direct Perturbation

Figure 5-S14 in the Supporting Information shows the covolume parameters calculated on the basis of Equations 5-S8 and 5-S9. The covolume values for n-alkanes can be correlated with MW as shown in **Equation 5-2**:

$$b = -14.6992113939827 + 1.36977232166027(MW) - 9.12089276536298 \times 10^{-5}(MW)^2 \quad (5\text{-}2)$$

As shown in Figure 5-S14, the covolume parameter for a given pseudocomponent tends to decrease as it becomes more aromatic. Also, the effect of aromaticity on the covolume parameter tends to be more significant for a heavier component. The following equation can accommodate these desired trends with respect to the f_b perturbation parameter (**Equation 5-3**):

$$b_i = -14.6992113939827 + 1.36977232166027(MW_i/m_{bi}) - 9.12089276536298 \times 10^{-5}(MW_i/m_{bi})^2$$
$$(5\text{-}3)$$

where i is the index for pseudocomponents and $m_{bi} = (MW_i/86.0)^{fb}$. The f_b perturbation parameter is zero for n-alkanes, and increases with increasing level of aromaticity in terms of volumetric phase behavior. The m_{bi} parameter increases with MW for a given f_b value. When a pseudocomponent has a MW of 86.0, which corresponds to the MW of n-hexane, the m_{bi} parameter is unity regardless of the f_b value applied uniformly to all pseudocomponents within a given fluid.

Figure 5-S15 shows the qualitative trends of the ψ parameters for two model fluids. The lighter model fluid exhibits an increasing trend, while the heavier model fluid exhibits a decreasing trend with respect to MW. The indirect PnA method of Kumar and Okuno (2013) resulted in non-linear ψ curves with respect to MW. However, an extensive testing of the method has indicated that the ψ parameter can be linear with respect to MW (**Equation 5-4**) without loss of reliability. Thus,

$$\psi_i = g(MW_i - MW_1) + C\psi_{n1}, \quad (5\text{-}4)$$

where MW_1 is the MW of the lightest pseudocomponent (i = 1), and g is the gradient of ψ with respect to MW. $C\psi_{n1}$ represents the ψ parameter for the lightest pseudocomponent as a product of the C multiplier and the ψ parameter for the lightest pseudocomponent as an n-alkane (ψ_{n1}). The value of ψ_{n1} is calculated by use of Equation 5-1 with T_C, P_C, and m from Kumar and Okuno (2012); that is, MW_i and ψ_{n1} are constants for a given fluid once the compositional characterization is conducted. Then, the ψ parameter in MW space can be perturbed through g and C.

Perturbation of the ψ parameters is not as straightforward as that of the covolume parameters through Equation 5-3. This is because the ψ trend depends on the CN range of pseudocomponents, the level of aromaticity, and temperature. Therefore, a perturbation scheme for ψ has been developed

on the basis of a set of the f_b, g, and C parameters that were optimized for 74 different reservoir fluids. Four pseudocomponents were used for their plus fractions as in Kumar and Okuno (2013). The gradient (i.e., g in Equation 5-4) was represented by the summation of f_b and f_ψ. The C multiplier in Equation 5-4 was split into two parts; c that is independent of f_b, and c' that is linear with f_b with zero intercept.

Out of the 74 fluids, 54 fluids were light, where density data were well represented by f_b of zero. Thus, they behave as n-alkanes in terms of volumetric phase behavior. The C parameters optimized for these 54 light fluids correspond to the c part, which is considered to represent the effects of the CN range of pseudocomponents and temperature on the C multiplier. They were correlated with MW_1 and temperature as shown in **Equation 5-5**:

$$c = 0.1088[(T_r)^{1.0405} + (M_r)^{1.2656}] + 0.5825, \tag{5-5}$$

where T_r is the reservoir temperature (T_{RES}) in Kelvin divided by 277.0, and M_r is MW_1 divided by the MW of n-heptane (100.2 gm/mol). The absolute average deviation (AAD) of Equation 5-5 from the c values for the 54 fluids is 4.5%. Equation 5-5 does not need to be very accurate since it will be part of the regression algorithm that has a few adjustable parameters to match experimental data. This is also true for the c' part of the C multiplier to be described below.

For the 20 heavier fluids out of the 74 reservoir fluids, f_b was positive, representing the effect of aromaticity on volumetric behavior predictions. To extract the c' part from the C multipliers optimized for these 20 fluids, the c values calculated by use of Equation 5-5 were subtracted from the optimized C multipliers. Then, the resulting c' part, which is considered to represent the aromaticity effect on the C multiplier, was correlated as shown in **Equation 5-6**.

$$c' = [1.0998(f_b + f_\psi)/P_r + 0.1763]Z_{SAT}f_b. \tag{5-6}$$

Z_{SAT} is the liquid compressibility factor calculated at the experimental saturation pressure (P_{SAT}) at T_{RES}. P_r is the saturation pressure at T_{RES} under the assumption that the pseudocomponents are n-alkanes, divided by P_{SAT}. The calculation of P_r requires the PR EOS with T_C, P_C, and m from Kumar and Okuno (2012) and P_{SAT}. **Figure 5-1** shows the quality of Equation 5-6 in correlating $c'/Z_{SAT}f_b$ with $(f_b + f_\psi)/P_r$. Although the AAD of Equation 5-6 for the 20 fluids is 35%, it is successfully used in the regression processes with f_b and f_ψ as will be shown later.

Equation 5-4 is then rewritten as **Equation 5-7**.

$$\psi_i = g(MW_i - MW_1) + C\psi_{n1} = (f_b + f_\psi)(MW_i - MW_1) + (c + c')\psi_{n1} \tag{5-7}$$

in this research. Obviously, this is only one of many possible ways to use the linear form of the ψ parameter in MW space. Equations 5-3 and 5-7 are simple, but flexible enough for perturbation of the f_b, g, and C parameters in reservoir fluid characterization as presented in the next subsection.

A single value is assigned to each of the perturbation parameters f_b, g, and C for a given fluid. However, the different levels of aromaticity for different components within a fluid have been considered

153

in the development of Equation 5-3 for covolume by using m_{bi}. As shown in the Supporting Information (Section 5-S2), the aromaticity effect on the attraction parameter through ψ is not as systematic as that on covolume. As will be also shown in Section 5.4, this is likely because the trend of pseudocomponents' attraction parameters depends not only on aromaticity, but also on temperature and CNs.

5.3.2. Algorithm

The algorithm presented in this research is kept as simple as possible. The covolume parameters are perturbed by use of Equation 5-3 through f_b. The ψ parameters are perturbed by use of Equation 5-7 through g and C, or through f_b, f_ψ, and c. Note that c is adjustable to some extent because it is not exact as the C multiplier when f_b is zero, as mentioned previously. The data to be matched are the P_{SAT} at T_{RES} and liquid density data at T_{RES} at different pressures. Other available data are saved for testing the predictive capability of the resulting fluid models, such as minimum miscibility pressures (MMPs), and liquid saturation curves from constant volume depletion (CVD) and constant composition expansion (CCE).

The algorithm consists of two nested loops as shown in the flow chart, **Figure 5-A1,** in **Appendix 5-A**. The inner loop is to match the P_{SAT} by adjusting f_ψ in Equation 5-7 for a set of f_b and c given by the outer loop. The initial value for f_ψ is zero, and f_ψ is adjusted by Δf_ψ per iteration (e.g., $\Delta f_\psi = 0.0001$). The sign for Δf_ψ (i.e., $+ \Delta f_\psi$ or $- \Delta f_\psi$) is negative if the saturation pressure is calculated to be higher than the experimental value. Otherwise, it is positive.

The outer loop is to match density data by adjusting either c in Equation 5-7 or f_b in Equations 5-3 and 5-7. Adjustment of c is first attempted to see if the deviation of density predictions is entirely attributed to the c correlation (Equation 5-5); that is, f_b is always zero when c is adjusted. Adjustment of c is made by Δc (e.g., $\Delta c = 0.001$) in each iteration. The sign for Δc (i.e., $+ \Delta c$ or $- \Delta c$) is determined to make the average deviation (AD) of density predictions smaller. Once the sign is determined in the first iteration step, it can be kept for the subsequent iteration steps until the AD changes its sign because the relationship between the density AD and c is monotonic within the range of investigation in this research. **Figure 5-2** shows the monotonic change of the density AD with respect to c for two example cases. The zero deviation can be obtained by either $+ \Delta c$ or $- \Delta c$.

It is not always possible to achieve zero density AD by adjusting c with zero f_b. This is because the covolume parameters should be adjusted for heavy hydrocarbon mixtures, for which the PR EOS tends to underpredict liquid densities (Søreide 1989; Kumar and Okuno 2014). It has been observed that, with the fluids examined, c is between 0.75 and 1.20 when the correction of c with zero f_b can achieve zero density AD. If this does not occur, c is overwritten by the original value based on Equation 5-5, and adjustment of f_b is initiated. The initial value for f_b is zero, and f_b is increased by Δf_b per iteration (e.g., $\Delta f_b = 0.0001$).

The example values given for Δf_b, Δc, and Δf_ψ in previous paragraphs are sufficient to match the P_{SAT} and densities. To reduce the number of iterations, however, these values can be made proportional to the AD during regression.

154

A step-wise description of the algorithm is as follows:

Step 1. Composition characterization

On the basis of the compositional data available, the plus fraction is split into n pseudocomponents using the chi-squared distribution function. Details can be found in Quiñones-Cisneros et al. (2004). The i subscript is the index for pseudocomponents; i = 1, 2, …, n.

Step 2. Calculation of c, P_r, Z_{SAT}, and ψ_{n1}

Equations 5-5, 5-6, and 5-7 require c, P_r, Z_{SAT}, and ψ_{n1} to be calculated. The definitions of these variables were given in subsection 5.3.1.

Step 3. Adjustment of the covolume and ψ parameters for the pseudocomponents

The iteration index is j for f_ψ and k for f_b. j = k = 1.

(1) $f_b = f_\psi = 0.0$

(2) Calculate the covolume parameters ($b_{i,k}$) by use of Equation 5-3.

(3) Calculate the ψ parameters ($\psi_{i,j,k}$) by use of Equations 5-6 and 5-7.

(4) Calculate the attraction parameters ($a_{i,j,k}$) as $a_{i,j,k} = \psi_{i,j,k}\,(b_{i,k})^2$.

(5) Calculate the saturation pressure (P_{SATCAL}) at T_{RES}. Calculate $\varepsilon = |P_{SATCAL} - P_{SAT}|/ P_{SAT}$. If $\varepsilon < \varepsilon_{TOL}$, go to Step 3(6) with j = 1. Otherwise, f_ψ is adjusted. $f_\psi = f_\psi + \Delta f_\psi$ if $P_{SATCAL} - P_{SAT} < 0$. Otherwise, $f_\psi = f_\psi - \Delta f_\psi$. j = j + 1 and go to Step 3(3). ε_{TOL} is 0.0001 in this research.

(6) Calculate densities at T_{RES} and the experimental pressures. Calculate the AAD (δ) of the densities calculated. If $\delta < \delta_{TOL}$, stop. Otherwise, adjust either c or f_b as described earlier in this subsection; go to Step 3(1) with c = c ± Δc, or Step 3(2) with $f_b = f_b + \Delta f_b$, $f_\psi = 0$, and k = k + 1. δ_{TOL} is 0.1% in this research.

The algorithm does not require T_C, P_C, and ω for the pseudocomponents in the fluid model of interest, in contrast to the indirect PnA algorithm (Kumar and Okuno 2013). The new algorithm took approximately 3 seconds to conduct characterization of a fluid, while the previous algorithm for the indirect PnA method took a few minutes. Both algorithms were written in FORTRAN and based on exhaustive search methods, instead of gradient-based methods. The computations were performed on the Intel Core i7-960 processor at 3.20 GHz and 8.0 GB RAM. **Appendix 5-B** describes the approach to derive T_C, P_C, and ω from the attraction and covolume parameters for pseudocomponents. This is useful when one uses commercial software that requires these parameters as input information.

5.3.3. Variation of Phase Behavior during Regression

The direct PnA algorithm systematically controls the attraction and covolume parameters for the pseudocomponents through f_ψ and f_b, or f_ψ and c. This subsection shows how two-phase behavior in P-T space for a given fluid varies with the adjustment parameters during the regression process. **Figure 5-3** shows an example for a fluid of 42°API. Curve 1 represents the phase envelope at the initialization of the algorithm, where f_ψ and f_b are zero. Curve 2 is the phase envelope when P_{SAT} is matched by adjusting f_ψ (i.e., densities have not been matched yet). Curve 3 shows the final phase envelope when

P_{SAT} and densities are matched, as indicated by the value of δ. Curves 1, 2, and 3 are also compared with the solid curve that represents the phase envelope when the pseudocomponents are assumed to be n-alkanes with T_C, P_C, and ω from Kumar and Okuno (2012). As the regression proceeds, the critical point becomes higher, and the phase envelope accordingly becomes greater in P-T space.

Figure 5-4 shows a similar example for a light fluid, where densities are matched by adjusting c with $f_b = 0.0$. Unlike in the previous example, the variation of the critical point is irregular as the regression proceeds from curve 1 to 3. This may be because this particular fluid behaves as an n-alkane mixture in terms of volumetric phase behavior, and the effect of aromaticity on two-phase behavior is not as obvious as the previous example fluid. Nevertheless, curve 3 entirely contains the n-alkane envelope, as in the previous example. This is the common observation made in all fluids examined so far.

5.4. Case Studies

In this section, the direct PnA method is applied to 84 different reservoir fluids, for which experimental data are available in the literature. They are 47 gas condensates, 33 conventional oils, and 4 heavy oils. As mentioned previously, the direct PnA algorithm is to match the P_{SAT} at T_{RES} and liquid densities at T_{RES} and different pressures using f_ψ and f_b, or f_ψ and c. Matching of densities tends to be conducted by c for light fluids, and by f_b for heavier fluids. f_ψ mainly controls compositional phase behavior, which consequently affects volumetric phase behavior. Available data other than those used in the regression process are used to test the predictive capability of the resulting fluid models. For example, CVD liquid saturation data are available for 34 gas condensates and 7 conventional oils. The other 18 conventional oils have MMP data, one of which is a corrosive volatile oil containing 19% CO_2. For the heavy oils used, swelling test and phase envelope data are available.

For characterization of light fluids with f_ψ and c, density data for the liquid phase that is equilibrium with the gaseous phase have been found to be more important than single-phase density data. This is plausible because the equilibrium liquid phase is richer in heavy components and more aromatic than the equilibrium gaseous phase and liquid phases in a single-phase region. Capturing the deviation from n-alkanes in the PnA method is more effective with density data of the denser phase. Therefore, simulated liquid density data have been created in two-phase regions for the gas condensates and a few volatile oils on the basis of the fluid models with optimized g and C (see Section 5.3.1). These optimized models accurately reproduce measured single-phase density data with an AAD of less than 1%; that is, the consistency has been retained between the measured and simulated density data for each of these light fluids.

The number of components is 12 throughout this research, four of which are pseudocomponents for C_{7+}. The others are N_2, CO_2, C_1, C_2, C_3, C_4, C_5, and C_6, where grouping of n- and i-alkanes is based on the conventional mass-based mixing rule (Pedersen and Christensen 2007). Unless otherwise stated, the BIPs are kept constant as described in Kumar and Okuno (2014); 0.0 for N_2-CO_2, 0.1 for N_2-C_i, where $1 \leq i \leq 6$, 0.13 for N_2-pseudocomponents, 0.1 for CO_2-hydrocarbons, and 0.0 for all hydrocarbon-hydrocarbon pairs.

The converged values for f_ψ and f_b are listed for all tested fluids in separate tables as will be discussed later. f_b is representative of the aromaticity level; it is zero for n-alkanes and increases with increasing aromaticity level. **Figure 5-5** presents the overall trend that the converged f_b tends to increase with increasing specific gravity of the fluid characterized. However, such a clear trend is not observed for f_ψ. This is because it controls g and C through Equations 5-6 and 5-7, which are dependent on temperature, aromaticity, and the MW range.

5.4.1. MMP Calculation

The direct PnA method has been applied to characterize the 18 oils given in **Table 5-1.** MMP data are available for these oils in the literature. For fluids 14, 16, and 17 in Table 5-1, MMPs with multiple injection gases were measured. This subsection compares MMPs calculated by the fluid models from the direct PnA method with the corresponding MMP data. This serves as a severe test of the predictive capability of the direct PnA method since an MMP is affected by phase behavior in a wide region of composition space between the oil and injection gas compositions (Egwuenu and Johns 2008). The PnA method uses the P_{SAT} and liquid densities at T_{RES} only at the composition of the fluid characterized. Thus, MMPs calculated in this subsection are predictions from the fluid models developed based on the limited data at a point in composition space.

The gravities of the 18 oils range from 31°API to 61°API. Table 5-1 shows the converged values for f_ψ and f_b. The slope of the ψ parameters with respect to MW is g = f_ψ + f_b as given in Equation 5-7. Table 5-1 presents positive slopes except for Fluid 9. The negative slope of Fluid 9 is expected since only one of the pseudocomponents is in the CN range less than 20 (see Figure 5-S15, and Kumar and Okuno 2013).

MMP calculations were performed by use of the PVTsim version 19.2 (PVTsim 2010) and PennPVT (Ahmadi and Johns 2011) software. The calculations with PVTsim based on the method of characteristics were unsuccessful for Fluids 10, 11, 16, and 18. The mixing-cell method within PennPVT was used for these fluids and Fluid 17. AADs of the calculated MMPs are listed in Table 5-1. **Table 5-2** presents ADs for all injection gases for Fluid 17. For the cases given in Tables 5-1 and 5-2, the calculations resulted in an overall AAD of 6.4%, which is reasonable considering uncertainties such as the effect of dispersion on the experimentally determined MMPs. Adjustment of BIPs can improve the calculated MMPs especially when non-hydrocarbon components are present at high concentrations. This will be discussed in Section 5.5.

5.4.2. Gas Condensates

Table 5-3 presents the 47 gas condensates tested, for which MWs range from 19.75 g/mol to 54.92 g/mol. Gas condensates 6, 7, 8, 11, 12, 36, and 38 are near critical at their reservoir conditions. The regression was conducted by f_ψ and c with zero f_b for all the gas condensates. The values listed as Δc are the adjustments in c required to match density data. The pseudocomponents of these gas condensates are in a relatively low CN range between 7 and 30. Therefore, positive slopes of ψ with

respect to MW are observed for 42 gas condensates in Table 5-3. Note that $g = f_\psi + f_b = f_\psi$ since f_b is zero for these fluids.

Data types available for the gas condensates are indicated as 1 for CVD liquid saturations, 2 for CCE liquid saturations, and 3 for CCE relative volumes. The maximum value in these experimental data is listed for each of the gas condensates. For example, **Figure 5-6** shows CVD liquid saturations measured for gas condensate 12 at 387.59 K. It is zero at the dew point of 333.0 bars. The maximum value, 40.90, at 283.7 bars is the value listed for this gas condensate in the second right-most column of Table 5-3. Figure 5-6 shows that the predictions from the resulting fluid model are in good agreement with the data. The AAD is calculated to be 0.94 for this case, which is listed in the right-most column of Table 5-3. Figure 5-6 also presents the CVD liquid volume predictions with the conventional characterization method based on Pedersen and Christensen (2007), in which volume shift is used to correct density predictions. This conventional method with volume shifting is referred to as CM_wV, which were described in detail in Kumar and Okuno (2014). The AAD for CM_wV with 12 components is 1.9% for Figure 5-6.

Figure 5-7 depicts the CCE liquid saturations measured for gas condensate 3 at 382.59 K. The data indicate that the CCE liquid volume first increases gradually, and then decreases with decreasing pressure. The predictions from the EOS fluid model are reasonably accurate, although the deviation at 289.57 bars is relatively large. The AAD is 1.71% with the direct PnA method and 3.7% with CM_wV.

Accurate predictions of volume ratios in CVD and CCE require accurate predictions of both compositional and volumetric phase behavior. The AADs summarized in Table 5-3 indicate that the fluid models developed by the direct PnA method are reasonable in predicting gas condensates.

5.4.3. Volatile Oils

The direct PnA method has been used to characterize the 15 volatile oils given in **Table 5-4.** Oils 10, 12, and 14 are near critical at their reservoir conditions. As mentioned previously in this section, simulated density data for the equilibrium liquid phase were used in the regression for oils 1, 5, 10, 11, 13, 14, and 15. The regression resulted in positive slopes of ψ with respect to MW for all cases except for oil 12 as indicated in Table 5-4.

Three types of data available for these oils are given in the second right-most column as 1 for CVD liquid saturations, 2 for CCE liquid saturation, and 3 for CCE relative volumes. This column also shows the measured value at the lowest measured pressure for each fluid. The fluid models developed based on the direct PnA method are able to accurately predict the measured phase behavior. The right-most column of Table 5-4 indicates the AAD for each fluid. The predicted CCE relative volumes are nearly perfect. The AADs for CVD liquid saturations are relatively large. However, their overall AD is only 1.4%. As a sample result, **Figure 5-8** gives the comparison between the measured and predicted CVD liquid saturations for near-critical volatile oil 14 at 424.25 K. The value, 42.20, at the lowest measured pressure is listed in the second right-most column for this oil in Table 5-4. The critical point was measured at 426 K and 388 bars, but it is calculated to be 433.00 K and 389.95 bars by the fluid model

based on the PnA method. Although the calculated T_C is 7 K higher than the measured T_C, the CVD liquid saturations are accurately predicted. Figure 5-8 also shows the predictions from CM_wV. The critical point calculated with CM_wV is 437.43 K and 393.18 bars. The two methods are reasonably accurate for this case.

5.4.4. Heavy Oils

Four different heavy oils have been characterized by use of the direct PnA method. As shown in **Table 5-5,** their API gravities are 19°, 28°, 11°, and 11° for heavy oils 1 to 4, respectively. Heavy oil 2 was classified as a heavy oil on the basis of the definition of Pedersen and Christensen (2007). The heaviest oil considered in this paper is heavy oil 4 with a MW of 482, and the p value in Equation 5-S11 is as high as 9.0 for this oil. Table 5-5 shows that the slope of ψ with respect to MW is negative for this heavy oil.

For heavy oil 1, swelling test data are available for two mixtures at 299.81 K; 60% CO_2 and 40% oil, and 80% CO_2 and 20% oil. **Figure 5-9** presents predictions of the oleic phase saturation in comparison with the corresponding data for the latter mixture. The AAD for this mixture is 5.2% with the direct PnA method and 6.15% with CM_wV. For pressures higher than 100 bars, the AAD is 2.71% with the direct PnA method and 6.71% with CM_wV. For the former mixture, the AAD with the direct PnA method is 2.2%. CM_wV erroneously predicts a single liquid phase at the highest and second highest pressures. For the lower pressures, the AAD with CM_wV is 5.89%.

For heavy oil 2, saturation pressures measured in swelling tests with CO_2 and a light gas mixture are considered. **Figure 5-10** compares the predictions with the data presented in Kredjbjerg and Pedersen (2006). The AAD is 3.9% for the CO_2 case and 2.8% for the gas mixture case with the direct PnA method. With CM_wV, it is 5.7% for the two injection gases. For heavy oil 3, gas-oil-ratio (GOR) data are available at the reservoir temperature 305.45 K. **Figure 5-11** shows that the fluid model based on the direct PnA method can accurately predict the GOR for this case. The deviation is relatively high only near the saturation pressure. The AAD is calculated to be 2.9%. The predictions with CM_wV are close to those from the direct PnA method in this case.

For heavy oil 4, the regression in the direct PnA method used the P_{SAT} of 56.64 bars at 347.67 K for the live oil reported (Feed #5 in Li et al. 2013a). Density data for this live oil were unavailable, and, therefore, generated on the basis of the EOS model given by Li et al. (2013a). **Figure 5-12** presents saturation pressures measured at different temperatures for two mixtures (Feeds #4 and #5 in Li et al. 2013a). Feed #4 is 38.6% CO_2, 36.2% C_3, and 25.2% heavy oil 4 on the molar basis. Feed #5 is 31.7% CO_2, 34.3% n-C_4, and 34.0% heavy oil 4. The fluid model developed by the direct PnA method is reasonably accurate in predicting the saturation pressures in spite of the uncertainties due to the simulated density data that were not validated against any data. The AAD of the saturation pressure predictions is 13.7% for Feed #4 and 6.0% for Feed #5. If the BIPs for CO_2 with the pseudocomponents are altered from 0.10 to 0.15, the AAD is reduced to 7.6% for Feed #4 and to 0.4% for Feed #5.

Li et al. (2013b) presented P-T conditions for three-phase behavior for the mixture of 83.2% CO_2, 11.8% n-C_4, and 5.0% heavy oil 4 on the molar basis (Feed #15 in Li et al. 2013b). **Figure 5-13**

159

compares the predicted phase boundaries with the data points given in Li et al. (2013b). Although the lower pressure boundary is overestimated, the higher pressure boundary is predicted quite accurately with no further adjustment of the fluid model from the direct PnA algorithm.

5.5. Discussion

The direct PnA method is simpler than the previous PnA method (Kumar and Okuno 2013), but exhibits equivalent or improved predictive capability. For example, the previous PnA method resulted in an AAD of 6.7% in MMP calculation for 8 fluids tested in Kumar and Okuno (2013), which is higher than the AAD of 6.4% obtained for MMPs of the cases given in Tables 5-1 and 5-2 (see Section 5.4.1). The AAD for CVD liquid saturation for 34 gas condensates (data type 1 in Table 5-3) was 1.06% using the direct PnA method, but it was 1.8% for 27 gas condensates tested in Kumar and Okuno (2013). The AAD for CVD liquid saturation for volatile oils calculated with the direct PnA method was 2.7% (data type 1 in Table 5-4), but it was 3.7% for 4 fluids tested in Kumar and Okuno (2013). The oleic phase saturations calculated for the swelling test for the West Sak heavy oil showed the AAD of 3.6% with the direct PnA method (see Table 5-5) and 4.1% with the previous PnA method (Kumar and Okuno 2013). In the preceding section, the improved predictions with the direct PnA method were also shown in comparison with CM_wV (Figures 5-6 to 5-11).

In this section, a few fundamental aspects of the direct PnA method are discussed. Section 5.5.1 discusses systematic control of phase behavior predictions through Equation 5-7. Section 5.5.2 presents the advantage of the optimized critical parameters (Equations 5-S8, 5-S9, and 5-S10) over estimated physical critical parameters for n-alkanes in reservoir fluid characterization. Section 5.5.3 discusses adjustment of BIPs with the direct PnA method.

5.5.1. Systematic Control of Phase Behavior Predictions

The unique feature of the direct PnA method is that it systematically controls phase behavior predictions through three key parameters. As discussed in section 5.3, f_b is able to monotonically change volumetric phase behavior predictions from the PR EOS through Equation 5-3. The ψ parameter as a linear function of MW is adjusted by g and C in Equation 5-7, which controls compositional phase behavior predictions. These three key parameters, f_b, g, and C, are not component-specific, and applied to all pseudocomponents for the fluid of interest. This is the fundamental reason for the systematic control of phase behavior predictions in the direct PnA method.

In the algorithm presented in the current paper, a mechanism was developed for adjustment of g and C through f_ψ for a given f_b, or for a given c in characterization of light fluids for which f_b is zero. However, it is also possible to control compositional phase behavior predictions by adjusting C, which uniquely gives a corresponding value for g through the constraint $\varepsilon < \varepsilon_{TOL}$; matching of P_{SAT} for the fluid of interest. This is useful to match other phase behavior data, such as CVD liquid saturations and MMPs.

Figure 5-14 presents CVD liquid saturations predicted with different values for C for gas condensate 6 in Table 5-3. Note that C is equal to c for this fluid because f_b is zero. A monotonic variation of the CVD liquid saturation curve with the C parameter is evident in the figure. An optimum value for C, which is 0.91 in this case, is easy to find because of the monotonic, systematic change of the CVD liquid saturation curve.

Figure 5-15 shows MMPs calculated with different C values for oil 1 in Table 5-1. The calculated MMP decreases monotonically with decreasing C. It is not difficult to find the value for C with which the measured MMP is matched.

5.5.2. Phase Behavior Predictions in Composition Space with Optimized Critical Parameters

In the PnA methods of Kumar and Okuno (2013) and in this research, the initializations of the attraction and covolume parameters are based on the T_C, P_C, and m parameters optimized for n-alkanes by use of the PR EOS (Equations 5-S8, 5-S9, and 5-S10). The differences from physical critical parameters estimated by Constantinou and Gani (1994) were discussed in the Supporting Information (Section 5-S1). In general, the optimized critical parameters tend to be higher than estimated physical values for n-alkanes; e.g., the sets of critical parameters from Constantinou and Gani (1994) and Gao et al. (2001). The higher critical parameters result in extended two-phase lines in P-T space for pure components. To show the effect of the higher critical parameters on phase behavior predictions in composition space, Kumar and Okuno (2012) compared bubble- and dew-point predictions for n-alkane binaries by using two sets of critical parameters; i.e., the optimized parameters from Kumar and Okuno (2012) and the estimated physical parameters from Gao et al. (2001). BIPs were set to zero for systematic comparisons. Predictions of bubble- and dew-points for nine n-alkane binaries were closer to experimentally measured data points when the optimized parameters were used. It was also shown that critical points of three n-alkane binaries (n-C_6 with n-C_{16}, n-C_{24}, and n-C_{36}) were more accurately predicted by use of the optimized parameter set.

This subsection gives further comparisons of phase behavior predictions for more than two components by using the optimized parameters of Kumar and Okuno (2012) and the physical parameter estimated by Constantinou and Gani (1994). For both cases, BIPs for hydrocarbon pairs are set to zero for systematic comparisons. **Figure 5-16** presents the two-phase envelopes predicted with the two sets of critical parameters for an n-alkane mixture consisting of 44.0% C_1, 45.8% n-C_{10}, 6.8% n-C_{18}, and 3.4% n-C_{30}. The bubble-point data were taken from Daridon et al. (1996). The two-phase envelope is predicted to be greater in P-T space when the optimized parameters are used. This is in line with the comparisons made for n-alkane binaries in Kumar and Okuno (2012). The PR EOS with the optimized critical parameters gives more accurate predictions in composition space than with the estimated physical critical parameters.

Figure 5-17 shows saturation pressure predictions in a swelling test for a 25-component oil with a gas at 373.15 K presented in Danesh et al. (1991). The oil consists of 90.68% n-alkanes from C_1 through

n-C_{20}, 0.72% toluene, 1.79% xylene, 2.20% cyclo-hexane, 2.25% methyl-cyclo-pentane, and 2.36% methyl-cyclo-hexane. The injection gas consists of 69.82% C_1, 13.09% C_2, 11.10% C_3, and 5.99% n-C_4. The AAD of the saturation pressure predictions is 11% when the physical parameter set is used, whereas it is 4% with the optimized parameter set.

Figure 5-18 depicts the two-phase envelopes predicted in composition space for a ternary system of CO_2, C_3, and n-C_{20} at 338.65 K and 69.92 bars. Experimental data were taken from Al-Marri (2006). As recommended by Peng and Robinson (1978), 0.10 is used for the BIPs of CO_2 with the n-alkanes. The optimized parameter set results in more accurate predictions of two-phase equilibrium for the n-alkane mixtures containing CO_2. When the CO_2 BIPs are set to 0.0, the two-phase region is predicted to be smaller in composition space.

The results presented in this subsection show that the PR EOS gives reasonably accurate predictions for n-alkane mixtures even with zero BIPs when the optimized set of critical parameters is used. When non-zero BIPs are required for CO_2-n-alkane mixtures, required deviations from zero are smaller with the optimized critical parameters than with estimated physical critical parameters. However, these results are limited by the availability of experimental data. Note that the optimized critical parameters were developed for use in reservoir fluid characterization, as described in this paper and Kumar and Okuno (2012, 2013). If they were used for pure n-alkanes with the PR EOS, the altered critical points would give extended vapor-pressure curves for heavy n-alkanes, as shown in Figure 5-S1.

5.5.3. Adjustment of BIPs

The extensive testing of the PnA methods of Kumar and Okuno (2013) and in this research has indicated that the PR EOS gives satisfactory predictions of reservoir fluid phase behavior with zero BIPs for all hydrocarbon pairs. Recommended values have been used for non-hydrocarbon components, such as N_2 and CO_2, as constants (Peng and Robinson 1978). However, these default BIPs may be adjusted especially for non-hydrocarbon components with pseudocomponents.

Figure 5-19 shows saturation pressures measured in the swelling test of Fluid 18 (Table 5-1) with CO_2 at 394 K (Negahban et al. 2010). The experimental MMP for this oil with CO_2 is 178 ± 2 bars at 394 K. The fluid model developed based on the direct PnA method gives an MMP of 188 bars with the default BIPs of CO_2 with pseudocomponents as 0.10. Although it correctly predicts the transition from bubble- to dew-point at CO_2 concentration of 0.69, this fluid model gives progressively higher saturation pressures than the experimental values with increasing CO_2 concentration. When the BIPs of CO_2 with pseudocomponents are reduced from 0.10 to 0.05, the model is much improved in saturation pressure predictions as shown in Figure 5-19. The MMP predicted is 174 bars, which is still close to the experimental result.

5.6.   Conclusions

A new method was developed for reservoir fluid characterization that directly perturbs the attraction and covolume parameters of pseudocomponents from n-alkanes' values (direct perturbation from n-alkanes, or direct PnA). The direct PnA method was successfully applied to 84 different reservoir fluids, such as gas condensates, volatile oils, black oils, and heavy oils. The regression algorithm used only the P_{SAT} at T_{RES} and liquid densities at T_{RES} at different pressures for each fluid. Other available data, such as MMPs, liquid saturations in CVD and CCE, and gas solubilities, were used to test the predictive capability of the fluid models developed by the direct PnA method. The PR EOS with the vdW mixing rules was used throughout this research. Conclusions are as follows:

o   The reservoir fluids tested were reliably characterized by systematic adjustment of the attraction and covolume parameters of pseudocomponents. The covolume parameters were perturbed from n-alkane values by f_b in Equation 5-3. The f_b parameter monotonically changes volumetric phase behavior predictions. As in our previous research, the ψ (= a/b^2) parameter was used to ensure proper interrelationship between the attraction (a) and covolume (b) parameters. A new approach to adjustment of the ψ parameters was developed with a linear ψ function of MW. The g and C parameters in Equation 5-7 control compositional phase behavior predictions in a regular manner in the regression algorithm presented.

o   The three key parameters, f_b, g, and C, are not component-specific, and applied to all pseudocomponents for the fluid of interest. This enables to control phase behavior predictions in a systematic, monotonic manner in the direct PnA method. The direct PnA method does not require estimation or extrapolation for apparent critical parameters of heavy fractions, which are mixtures of non-identifiable compounds.

o   The direct PnA method substantially simplifies the characterization of reservoir fluids by use of the PR EOS. The simplification was possible because of the inherent accuracy and simplicity of the PR EOS and the adjustment parameters found in this research. The regression process of the PnA method requires only a few seconds per fluid using a personal computer.

o   One of the important data types required for the direct PnA method is liquid densities that capture the level of aromaticity in the fluid system of interest. Results indicated that densities of equilibrium liquid phases in a multiphase region are more effective than densities in a single-phase region for capturing the level of aromaticity in the PnA method.

o   No change is required for the functional form of the EOS and mixing rules. The method can be readily implemented in existing software based on the PR EOS with the vdW mixing rules.

5.7. Nomenclature

Roman Symbols

a	= Attraction parameter defined in Equation 5-S2
a_c	= Attraction parameter at a critical temperature defined in Equation 5-S3
α	= Temperature dependent parameter defined in Equation 5-S4.
A	= Aromatics
b	= Covolume parameter defined in Equation 5-S5
c	= Parameter defined in Equation 5-5
c'	= Parameter defined in Equation 5-6
C	= c + c'
$f_ψ$	= Perturbation factor for the ψ parameters
f_b	= Perturbation factor for the covolume parameters
f_m	= Perturbation factor for the m parameters in Equation 5-S10
f_P	= Perturbation factor for P_C in Equation 5-S9
f_T	= Perturbation factor for T_C in Equation 5-S8
m_{bi}	= Parameter defined with Equation 5-3
g	= Slope of the ψ parameter in MW space
m	= Parameter defined in Equations 5-S6 and 5-S7
M_r	= Molecular weight of the lightest pseudocomponent divided by 100.20
n	= Number of pseudocomponents
N	= Napthenes
e_i	= Objective function for the ith pseudocomponent defined in Equation 5-B4
p	= Pressure, bar
P	= Paraffins
P_C	= Critical pressure, bar
P_r	= Ratio of the saturation pressure calculated as n-alkanes to P_{SAT}
P_{SAT}	= Experimental saturation pressure at reservoir temperature
P_{SATCAL}	= Calculated saturation pressure
P_{vap}	= Vapor pressure
R	= Universal gas constant
S	= Parameter in the chi-squared distribution function given in Equation 5-S11
T	= Temperature, K
T_b	= Boiling point temperature, K
T_C	= Critical temperature, K
T_r	= T in Kelvin divided by 277.0
T_{RES}	= Reservoir temperature
v	= Molar volume, gm/mol (Equation 5-S1)

V_C = Critical volume, gm/mol

Y_a = Aromaticity as defined by Yarborough (1979)

Z_{SAT} = Liquid compressibility factor at the saturation pressure at T_{RES}

Greek symbols

ε = Absolute average deviation for saturation pressure calculations

δ = Deviation for density calculations

γ = Standard specific gravity

Γ = Gamma function

ρ_L^S = Saturated liquid density

ρ_{SAT} = Density at saturation pressure

Ω_a = Constant term (= 0.45723552892138219) in the attraction parameter of the PR EOS

Ω_b = Constant term (= 0.0777960739038884574) in the covolume parameter of the PR EOS

ψ = Parameter given by Equation 5-1

ψ_{n1} = Normal-alkane equivalent ψ for the lightest pseudocomponent

ω = Acentric factor

Abbreviations

^{o}API = API (American Petroleum Institute) gravity (= 141.5/γ -131.5)

AAD = Average absolute deviation

AD = Average deviation

BIP = Binary interaction parameter

CM_wV = Conventional fluid characterization method with volume shifting (Pedersen and

Christensen   2007)

CN = Carbon number

CVD = Constant volume depletion

CCE = Constant composition expansion

CP = Critical point

EOS = Equation of state

GOR = Gas oil ratio

LL = Liquid-liquid

LLV = Liquid-liquid-vapor

LV = Liquid-vapor

MMP = Minimum miscibility pressure, bar

MW = Molecular weight, g/mol

MW_{avg} = Average molecular weight

PC = Pseudocomponent

PnA   = Perturbation from n-alkanes

PR   = Peng-Robinson

P-T   = Pressure –temperature

SCN   = Single carbon number fraction

SRK   = Soave-Redlich-Kwong

Tol.   = Tolerance

vdW   = van der Waals

Subscripts

i   = Index for pseudocomponents

j   = Index for the iteration loop for matching the saturation pressure by adjusting f_ψ

k   = Index for the iteration loop for mating densities by adjusting f_b

5.8.   References

Ahmed, T. and Meehan, D. N., 2010. A Practical Approach for Calculating EOS Coefficients. Presented at SPE Russian Oil & Gas Technical Conference and Exhibition held in Moscow, Russia, 26-28 Oct. SPE-132455-MS

Ahmadi, K. and Johns, R.T. 2011. Multiple Mixing-Cell Model for MMP Determination. *SPE J.* **16** (4): 733-742.

Al-Ajmi, M.F., Tybjerg, P., Rasmussen, C.P. et al. 2011. EoS Modeling for Two Major Kuwaiti Oil Reservoirs. Presented at the SPE Middle East Oil and Gas Show and Conference, Manama, Bahrain, 25-28 Sept. SPE-141241-MS.

Al-Marri, S.S. 2006. PVT, Phase Behavior and Viscosity Measurements and Modeling of the Ternary and Binary Systems of Carbon Dioxide +Heavy Hydrocarbon (n-Eicosane) + Light Gas (Ethane or Propane). PhD. Dissertation, University of Southern California, USA.

Al-Meshari, A. 2004. New Strategic Method to Tune Equation of State to Match Experimental Data for Compositional Simulation. PhD dissertation. Texas A&M University, Texas. USA.

Al-Subai, K.O., 2001. Compositional Gradient Calculations for a Saudi Arabian Gas Condensate Reservoir. M.Sc. Thesis. King Fahd University of Petroleum & Minerals, Saudi Arabia.

Ambrose, D., 1978. Correlation and Estimation of Vapour-Liquid Critical Properties. I: Critical Temperatures of Organic Compounds. NPL Technical Report. Chem. 92, (Nat. Physical Lab., Teddington, UK, 1978).

Ambrose, D. and Tsonopoulos, C. 1995. Vapor-Liquid Critical Properties of Elements and Compounds. 2. Normal Alkanes. *J. Chem. Eng. Data* **40** (3): 531-546.

Anselme, M.J., Gude, M., and Teja, A.S., 1990. The Critical Temperatures and Densities of the n-Alkanes from Pentane to Octadecane. *Fluid Phase Equilib.* **57** (3): 317-326.

Aparicio-Martínez, S. and Hall, K.R., 2006. Phase Equilibria in Water Containing Binary Systems from Molecular Based Equation of State. *Fluid Phase Equilib.* **254** (1-2): 112-125.

PVTsim, 19.2, 2010. Calsep International Consultants, Copenhagen, Denmark.

Clark, P., Toulekima, S., Sarma, H., 2008. A Miscibility Scoping Study for Gas Injection into a High-Temperature Volatile Oil Reservoir in the Cooper Basin, Australia. Presented at the SPE Asia Pacific Oil and Gas Conference and Exhibition, Perth, Australia. 20-22 Oct.

Coats, K.H. 1985. Simulation of Gas Condensate Reservoir Performance. *J Petrol Tech* **37** (10): 1870-1886.

Coats, K.H. and Smart, G.T. 1986. Application of a Regression Based EOS PVT Program to Laboratory Data. *SPE Res Eng* **1** (3): 277-299.

Constantinou, L. and Gani, R., 1994. New Group Contribution Method for the Estimating Properties of Pure Compounds. *AIChE J.* **40** (10): 1697-1710.

Constantinou, L., Gani, R., and O'Connell, J.P. 1995. Estimation of the Acentric Factor and the Liquid Molar Volume at 298 K Using a New Group Contribution Method. *Fluid Phase Equilib.* **103** (1): 11-22.

Danesh, A., Xu, D.-H., and Todd, A.C. 1991. Comparative Study of Cubic Equation of State for Predictive Phase Behavior and Volumetric Properties of Injection Gas-Reservoir Oil Systems. *Fluid Phase Equilib.* **63** (3): 259-278.

Danesh, A. 1998. PVT and Phase Behavior of Petroleum Reservoir Fluids, Elsevier Science & Technology Books, 1998.

Daridon, J.L., Xans, P., and Montel, F. 1996. Phase Boundary Measurement on a Methane + Decane + Multiparaffins System. *Fluid Phase Equilib.* **117** (1-2): 241-248.

Drohm, J.K., Trengove, R.D., and Goldthrope, W.H. 1988. On the Quality of Data from Standard Gas-Condensate PVT Experiments. Presented at the SPE Gas Technology Symposium, Dallas, Texas, 13-15 June. SPE-17768-MS

Dutour, S., Lagourette, B., and Daridon, J. L., 2001. High-Pressure Speed of Sound, Density and Compressibility of Heavy Normal Paraffins: $C_{28}H_{58}$ and $C_{36}H_{74}$. *J. Chem. Therm.* **33** (7): 765-774.

Economou, I.G., Heidman, J.L., Tsonopoulos, C. et al. 1997. Mutual Solubilities of Hydrocarbons and Water : III. 1-Hexene, 1-Octene, C_{10}-C_{12} Hydrocarbons. *AIChE J.* **43** (2): 535-546.

Egwuenu, A.M., Johns, R.T., and Li, Y. 2008. Improved Fluid Characterization for Miscible Gas Floods. *SPE Res Eval Eng* **11** (4): 655-665.

Ekundayo, J. M. 2012. Configuration of Slim Tube Apparatus for Consistent Determination of Minimum Miscibility Pressure (MMP) Data, M.Sc. Thesis. The Petroleum Institute, Abu Dhabi, UAE.

Enick, R.M., Holder, G.D., and Mohamed, R. 1987. Four-Phase Flash Equilibrium Calculations Using the Peng-Robinson Equation of State and a Mixing Rule for Asymmetric Systems. *SPE Res. Eng.* **2** (4): 687-694.

Fawumi, O.K., 1999. Effect of Liquid Drop-out on the Productivity of a Rich Gas Condensate Reservoir. M.Sc. Thesis. King Fahd University of Petroleum & Minerals, Saudi Arabia.

Flory, P.J., Orwell, R.A., and Vrij, A. 1964. Statistical Thermodynamics of Chain Molecule Liquids. I. An Equation of State for Normal Paraffin Hydrocarbons. *J. Am. Chem. Soc*. **86** (17): 3507-3514.

Gao, W., Robinson Jr., R.L., and Gasem, K.A.M. 2001. Improved Correlations for Heavy n-Paraffin Physical Properties. *Fluid Phase Equilib.* **179** (1-2): 207-216.

Graue, D.J. and Zana, E. T., 1981. Study of a Possible CO_2 Flood in Rangely Field. *J Pet Technol* **33** (7): 1312-1318.

Guo, T.M. and Du, L. 1989. A New Three-Parameter Cubic Equation of States for Reservoir Fluids: Part 3- Application to Gas Condensates. SPE e-library, Paper SPE-19374-MS.

Heidman, J.L., Tsonopoulos, C., Bardy, C.J. et al. 1985. High-Temperature Mutual Solubilities of Hydrocarbons and Water. *AIChE J.* **31** (3): 376-384.

Høier, L., 1997. Miscibility Variation in Compositional Grading. PhD. dissertation. Norwegian University of Science and Technology, Norway.

Hosein, R., Jagai, T., and Dawe, R.A. 2013. A Method for Predicting the Phase behavior of Trinidad Gas Condensates. *The West Indian Journal of Engineering* **35** (2): 22-30.

Ikeda, M. and Schaefer, L. 2011. Examining the Effect of Binary Interaction Parameters on VLE Modelling Using Cubic Equations of State. *Fluid Phase Equilib.* **305** (2): 233-237.

Imo-Jack, O. 2010. PVT Characterization of a Gas Condensate Reservoir and Investigation of Factors Affecting Deliverability. Presented at the Annual SPE International Conference and Exhibition, Tinapa-Calabar, Nigeria, 31 July-7 Aug. SPE-140629-MS.

Jacoby, R.H., Koeller, R.C., and Berry, V.J. 1959. Effect of Composition and Temperature on Phase Behavior and Depletion Performance of Rich Gas-Condensate Systems. *J Pet Technol* **11** (7): 58-63.

Jacoby, R.H. and Yarborough, L. 1967. Reservoir Fluids and Their Uses. Applied Thermodynamics Symposium. 59, 49-62.

Jaubert, J-N., Avaullee, L., and Souvay, J.F. 2002. A Crude Oil Data Bank Containing more than 5000 PVT and Gas Injection Data. *J Pet Sci Technol* **34** (1): 65-107.

Joback, K.G. and Reid, R.C. 1987. Estimation of Pure-Component Properties from Group Contributions. *Chem. Eng. Commun.* 57 (1-6): 233-243.

Kesler, M.G. and Lee, B.I. 1976. Improve Prediction of Enthalpy of Fractions, Hydrocarbon Processing. *Hydrocarb Process* **55** (3): 153-158.

Kilgren, K.H. 1966. Phase Behavior of a High-Pressure Condensate Reservoir Fluid. *J Pet Technol* **18** (8): 1001-1005.

Kontogeorgis, G.M. and Tassios, D.P. 1997. Critical Constants and Acentric Factors for Long-Chain and Short-Chain Alkanes Suitable for Corresponding State Applications. A Critical Review. *Chem. Eng. J.* **66** (1), 35-49.

Krejbjerg, K. and Pedersen, K.S. 2006. Controlling VLLE Equilibrium with a Cubic EoS in Heavy Oil Modeling. Presented at 57th Annual Technical Meeting of the Petroleum Society (Canadian International Petroleum Conference), Calgary. 13-15 June. PETSOC-2006-052.

Kumar, A. and Okuno, R. 2012. Critical Parameters Optimized for Accurate Phase Behavior Modeling for Heavy n-Alkanes up to C_{100} using the Peng-Robinson Equation of State. *Fluid Phase Equilib.* **335**: 46-59.

Kumar, A. and Okuno, R., 2013. Characterization of Reservoir Fluids Using an EOS based on Perturbation from n-Alkanes. *Fluid Phase Equilib.* **358**: 250-271.

Kumar, A. and Okuno, R., 2014. Reservoir Oil Characterization for Compositional Simulation of Solvent Injection Process. *Ind. Eng. Chem. Res.* **53** (1): 440-455.

Lee, B.I. and Kesler, M.G. 1975. A Generalized Thermodynamic Correlation Based on Three-Parameter Corresponding States. *AIChE J.* **21** (3): 510-527.

Li, H., Zheng, S., and Yang. D. 2013a. Enhanced Swelling Effect and Viscosity Reduction of Solvent(s)/CO2/Heavy-Oil Systems. *SPE J.* **18** (4): 695-707.

Li, X., Li, H., and Yang, D. 2013b. Determination of Multiphase Boundaries and Swelling Factors of Solvent(s)−CO₂−Heavy Oil Systems at High Pressures and Elevated Temperatures. *Energy Fuels* **27** (3): 1293-1306.

Lindeloff, N., Mogensen, K., Pedersen, K. S. et al. 2013. Investigation of Miscibility Behavior of CO₂ Rich Hydrocarbon Systems- With Application for Gas Injection EOR. Presented at the SPE Annual Technical Conference and Exhibition, New Orleans, Louisiana, USA, 30 Spet.-2 Oct. SPE-166270-MS

Magoulas, K. and Tassios, D. 1990. Thermophysical Properties of n-Alkanes from C₁ to C₂₀ and Their Prediction for Higher Ones. *Fluid Phase Equilib.* **56**: 119-140.

McVay, D.A. 1994. Generalization of PVT Properties for Modified Black-Oil Simulation of Volatile and Gas Condensate Reservoirs. PhD dissertation. Texas A&M University, Texas, USA.

Moore, D.C., 1989. Simulation of Gas-Condensate Reservoir Performance Using Schmidt-Wenzel Equation of State. MSc Thesis. Montana College of Mineral Science and Technology, Montana, USA.

Negahban, S., Pedersen, K.S., Baisoni, M.A. et al. 2010. An EoS Model for a Middle East Reservoir Fluid with an Extensive EOR PVT Data Material. Presented at Abu Dhabi International Petroleum Exhibition & Conference, Abu Dhabi, UAE, 1-4 Nov. SPE-136530-MS

Nikitin, E.D., Pavlov, P.A., and Popov, A.P. 1997. Vapour-Liquid Critical Temperature and Pressure of Normal Alkanes with from 19 to 36 Carbon Atoms, Napthalene and m-Terphenyl Determined by the Pulse-Heating Technique. *Fluid Phase Equilib.* **141** (1-2): 155-164.

Nojabaei, B., Johns, R.T., and Chu, L., 2013. Effect of Capillary Pressure on Phase Behavior in Tight Rocks and Shales. *SPE Res Eval Eng* **16** (3): 281-289.

Pedersen, K.S. and Christensen, P.L. 2007. Phase Behavior of Petroleum Reservoir Fluids. CRC Press, Taylor & Francis Group, Boca Raton, FL, USA.

Pedersen, K.S., Thomassen, P., and Fredenslund, Aa. 1989. Characterization of Gas Condensate Mixtures. Advances in Thermodynamics, Taylor & Francis, New York.

Pedersen, K.S., Milter, J., and Sørensen, H. 2004. Cubic Equations of State Applied to HT/HP and Highly Aromatic Fluids. *SPE J.* **9** (2): 186-192.

Peng, D.-Y. and Robinson, D.B. 1976. A New Two-Constant Equation of State. *Ind. Eng. Chem. Fund.* **15** (1): 59-64.

Peng, D.-Y. and Robinson, D.B. 1978. The Characterization of the Heptanes and Heavier Fractions for the GPA Peng-Robinson Programs. *GPA Research Report* RR-28.

PVTsim, 19.2, 2010. CALSEP International Consultants, Copenhagen, Denmark.

Quiñones-Cisneros, S.E., Zéberg-Mikkelsen, C.K., Baylaucq, A. et al. 2004. Viscosity Modeling and Prediction of Reservoir Fluids: From Natural Gas to Heavy Oils. *Int. J. Therm.* **25** (5): 1353-1366.

Renner, T.A., Metcalfe, R.S., Yellig, W. F. et al. 1989. Displacement of Rich Gas Condensate by Nitrogen: Laboratory Corefloods and Numerical Simulations. *SPE Res Eng* **4** (1): 52-58.

Reudelhuber, F.O. and Hinds, R.F. 1956. A Compositional Material Balance Method for Prediction of Recovery from Volatile Oil Depletion Drive Reservoirs. *Pet. Trans. AIME.* **210**: 19-26.

Riazi, M.R. and AlQaheem, Y.S. 2010. Predicting Vapor Pressure of Heavy Hydrocarbons from Molar Refraction and Its Applications to Petroleum Mixture. *Ind Eng Chem Res* **49** (15): 7104 -7112.

Riazi, M.R. and Al-Sahhaf, T.A. 1996. Physical Properties of Heavy Petroleum Fractions and Crude Oils. *Fluid Phase Equilib*. **117** (1-2): 217-224.

Riazi, M.R. and Daubert, T.E. 1987. Characterization Parameters for Petroleum Fractions. *Ind. Eng. Chem. Res.* **26** (4): 755-759.

Rowley, R.L., Wilding, W.V., Oscarson, J.L. et al. 2006. DIPPR Data Compilation of Pure Chemical Properties Design Institute for Physical Properties. Provo, UT: Brigham Young University.

Schulte, A.M. 1980. Compositional Variation within a Hydrocarbon Column due to Gravity. Presented at the SPE Annual Technical Conference and Exhibition, Dallas. 21-24 Sept. SPE-9235-MS

Sharma, G.D. 1990. Development of Effective Gas Solvents Including Carbon Dioxide for the Improved Recovery of West Sak Oil, Report No. DOE/FE/61114-2. University of Alaska Fairbanks, Alaska, USA.

Soave, G. 1972. Equilibrium Constants from a Modified Redlich-Kwong Equation of State. *Chem. Eng. Sci.* **27**:1197-1203.

Spivak, A. 1971. Mathematical Simulation of Condensate-Gas Reservoirs. PhD. dissertation, University of Texas at Austin, Texas, USA.

Søreide, I., 1989. Improved Phase Behavior Predictions of Petroleum Reservoir Fluids from a Cubic Equation of State. Ph.D. dissertation, the Norwegian Institute of Technology, Norway.

Subero, C.L., 2009. Numerical Modeling of Nitrogen Injection into Gas Condensate Reservoir. M.Sc. Thesis. West Virginia University, Morgantown, West Virginia, USA.

Teja, A.S., Lee, R.J., Rosenthal, D.J. et al. 1990. Correlation of the Critical Properties of Alkanes and Alkanols. *Fluid Phase Equilib.* **56**: 153-159.

Thodos, G., 1955a. Critical Constants of Saturated Aliphatic Hydrocarbons. *AIChE J.* **1** (2): 168–173.

Thodos, G., 1955b. Critical Constants of Unsaturated Aliphatic Hydrocarbons. *AIChE J.* **1** (2), 165–168.

Thodos, G., 1956. Critical Constants of Naphthenic Hydrocarbons, *AIChE J.* **2** (4): 508–513.

Thodos, G., 1957. Critical Constants of Aromatic Hydrocarbons, *AIChE J.* **3** (3): 428–431.

Ting, P.D., Joyce, P.C., Jog, P.K. et al. 2003. Phase Equilibrium Modeling of Mixtures of Long-Chain and Short-Chain Alkanes Using Peng–Robinson and SAFT. *Fluid Phase Equilib.* **206** (1-2), 267-286.

Tsonopoulos, C. and Tan, Z. 1993. The Critical Constants of Normal Alkanes from Methane to Polyethylene II. Application of the Flory Theory. *Fluid Phase Equilib*. **83**: 127-138.

Tsonopoulos, C. and Wilson, G.M. 1983. High-Temperature Mutual Solubilities of Hydrocarbons and Water. *AIChE J.* **29** (6): 990-999.

Vogel, J.L. and Yarborough, L. 1980. The Effect of Nitrogen on the Phase Behavior and Physical Properties of Reservoir Fluids. Presented at First Joint SPE/DOE Symposium on Enhanced Oil Recovery, 20-23 April. Tulsa, Oklahoma. SPE-8815-MS.

Voutsas, E.C., Pappa, G.D., Magoulas, K. et al. 2006. Vapor Liquid Equilibrium Modeling of Alkane Systems with Equations of State: "Simplicity versus Complexity. *Fluid Phase Equilib.* **240** (2): 127-139.

Whitaker, C.A. and Kim, J.S., 1993. Application of Extended Equation of State Work to Optimize the Pegasus Devonian Field Unit No. 3 Gas Cycling Operation. Presented at SPE Annual Technical Conference and Exhibition, Houston, Texas. 3-6 Oct. SPE-26656-MS.

Whitson, C.H. and Brulè, M.R. 2000. Phase Behaviour. SPE Henry L. Doherty Series, Vol. 20, SPE, Richardson, Texas

Whitson, C.H. and Torp, S.B. 1983. Evaluating Constant Volume Depletion Data. *J Petrol Tech* 35 (3): 610-620.

Whitson, C.H. and Belery, P., 1994. Compositional Gradients in Petroleum Reservoirs. Paper presented at the University of Tulsa Centennial Petroleum Engineering Symposium, Tulsa, OK, 29-31 Aug. SPE-28000-MS.

Wijaya, Z. 2006. CO_2 Injection in an Oil Reservoir with Gas Cap (Compositional Simulation Case at Heidrum Field Norway). M.Sc. Thesis. Norwegian University of Science and Technology, Norway.

Yang, T., Chan, W.-D. and Guo, T.M. 1997. Phase Behavior of a Near-Critical Fluid Mixture. *Fluid Phase Equilib.* **128** (1-2): 183-197.

Yarborough, L. 1979. Application of a Generalized Equation of State to Petroleum Reservoir Fluids. Advances in Chemistry, 182, 385-439.

Yaws, C. L., 2010. Yaws' Thermo Physical Properties of Chemicals and Hydrocarbons (Electronic Edition), Knovel.

Zudkevitch, D. and Joffe, J., 1970. Correlation and Prediction of Vapor-Liquid Equation with the Redlich-Kwong Equation of State. *AIChE J.* **16** (1): 112-119.
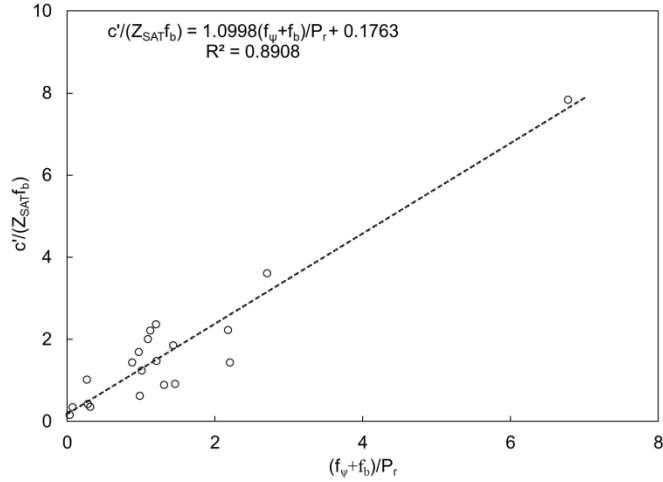
Figure 5-1. Correlation of $c'/Z_{SAT}f_b$ with $(f_b + f_\psi)/P_r$ using a linear function.
For each of the 20 data points, c' is obtained by subtracting the c value calculated from Equation 5-5 from the optimized C multiplier. The 20 fluids considered are not light, and their f_b values are positive.
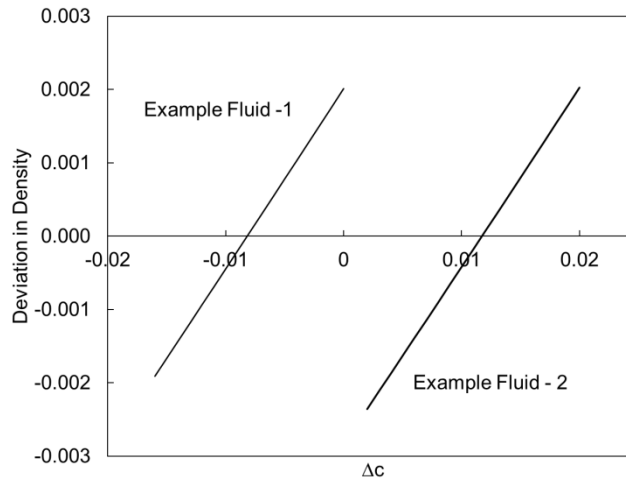
Figure 5-2. Average deviations of density predictions from experimental data during the regressions for two different fluids.
Density matching is achieved by adjustment of the c parameter for light fluids. For example fluid 1, the c parameter is decreased from the value calculated using Equation 5-5. For example fluid 2, it is increased from the value calculated using Equation 5-5, in order to obtain the density match.
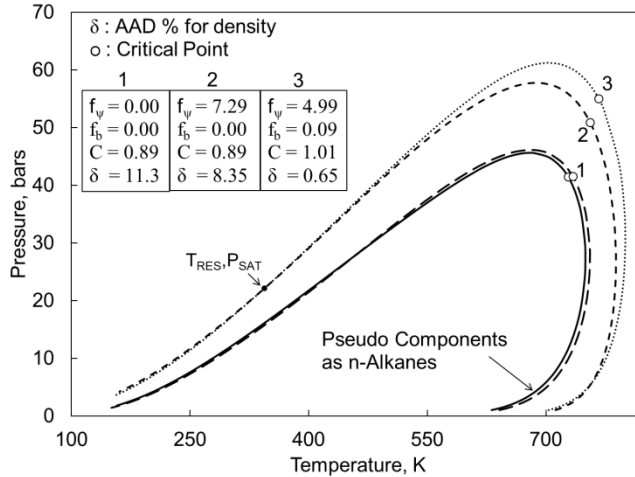
Figure 5-3. Variation of the phase envelope in P-T space during the PnA regression for a fluid of 42 °API. Curve 1 represents the phase envelope at the initialization of the algorithm, where f_ψ and f_b are zero. Curve 2 is the phase envelope when P_{SAT} is matched by adjusting f_ψ (i.e., densities have not been matched yet). Curve 3 shows the final phase envelope when P_{SAT} and densities are matched, as indicated by the value of δ. Curves 1, 2, and 3 are also compared with the solid curve that represents the phase envelope when the pseudocomponents are assumed to be n-alkanes with T_C, P_C, and ω from Kumar and Okuno (2012). As the regression proceeds, the critical point becomes higher, and the phase envelope accordingly becomes greater in P-T space.

Figure 5-4. Variation of the phase envelope in P-T space during the PnA regression for a light fluid. Densities are matched by adjusting c with f_b = 0.0. Curve 1 represents the phase envelope at the initialization of the algorithm, where f_ψ is zero. Curve 2 is the phase envelope when P_{SAT} is matched by adjusting f_ψ (i.e., densities have not been matched yet). Curve 3 shows the final phase envelope when P_{SAT} and densities are matched, as indicated by the value of δ. Curves 1, 2, and 3 are also compared with the solid curve that represents the phase envelope when the pseudocomponents are assumed to be n-alkanes with T_C, P_C, and ω from Kumar and Okuno (2012). Curve 3 entirely contains the n-alkane envelope, as in the previous example given in Figure 5-3.

174
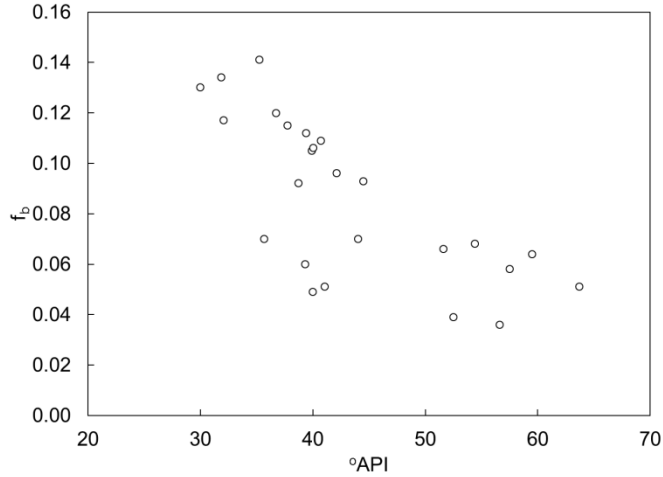
Figure 5-5. The converged f_b value tends to increase with increasing specific gravity of the fluid. The regression parameter f_b is representative of the aromaticity level; it is zero for n-alkanes and increases with increasing aromaticity level.
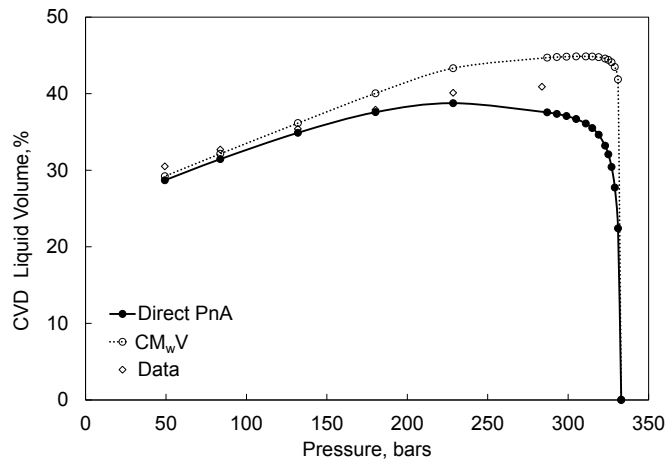
Figure 5-6. CVD liquid saturations measured for gas condensate 12 given in Table 5-3 (McVay 1994) at 387.59 K.
The gas condensate has 11.72 mol% C_{7+}. The MW of the C_{7+} fraction is 169 g/mol, and the overall MW is 40.58 g/mol.
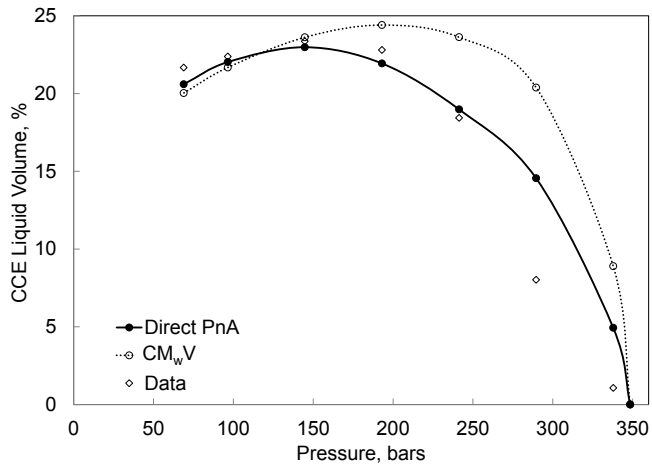
Figure 5-7. CCE liquid saturations measured for gas condensate 3 given in Table 5-3 (Al-Meshari 2004) at 382.59 K.
The gas condensate has 1.81 mol% C_{7+}. The MW of the C_{7+} fraction is 152.80 g/mol, and the overall MW is 32.41 g/mol.
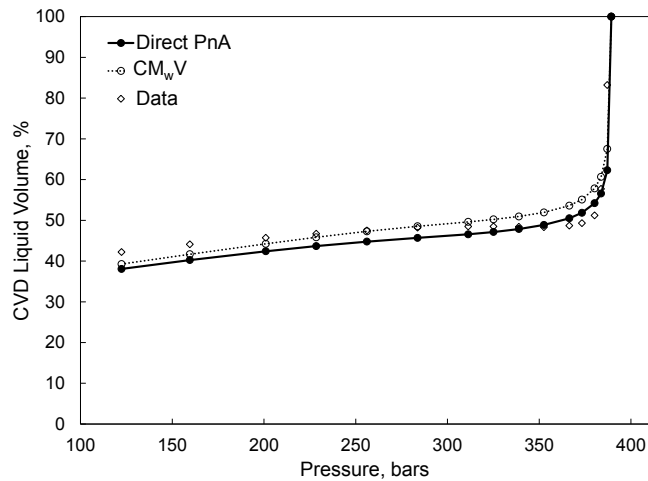
Figure 5-8. Comparison between the measured and predicted CVD liquid saturations for near-critical volatile oil 14 in Table 5-4 at 424.25 K (Pedersen et al. 1988).
The critical point was measured at 426 K and 388 bars, but it is calculated to be 433.00 K and 389.95 bars by the fluid model based on the direct PnA method. Although the calculated T_C is 7 K higher than the measured T_C, the CVD liquid saturations are accurately predicted.
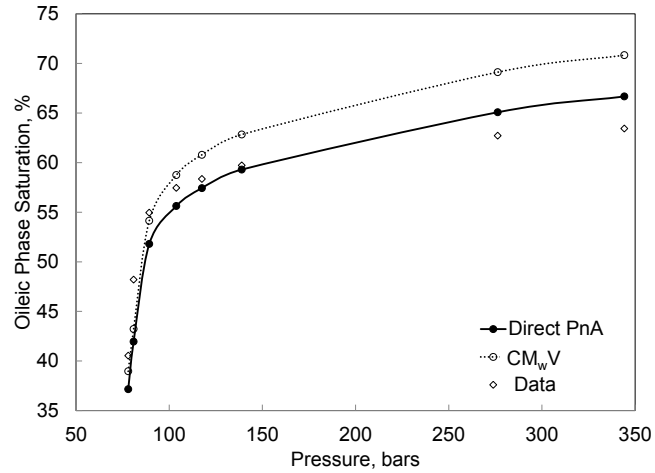
Figure 5-9. Oleic phase saturation data and predictions for heavy oil 1 (Sharma 1990) given in Table 5-5 at 299.81 K.
This is a mixture of 20% oil and 80% CO_2. The AAD for these oleic phase saturation calculations is 5.2% with the direct PnA method.
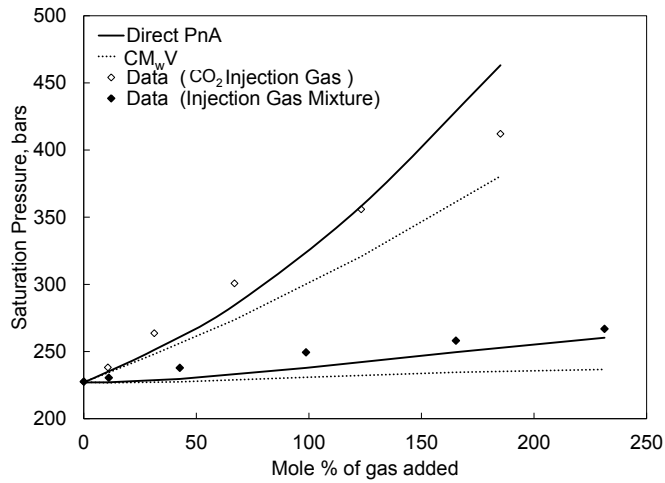
Figure 5-10. Data and predictions for saturation pressures in the swelling tests of heavy oil 2 with two injection gases; CO_2 and a light gas mixture (Kredjbjerg and Pedersen 2006).
The AAD is 3.9% for the CO_2 case and 2.8% for the gas mixture case with the direct PnA method.
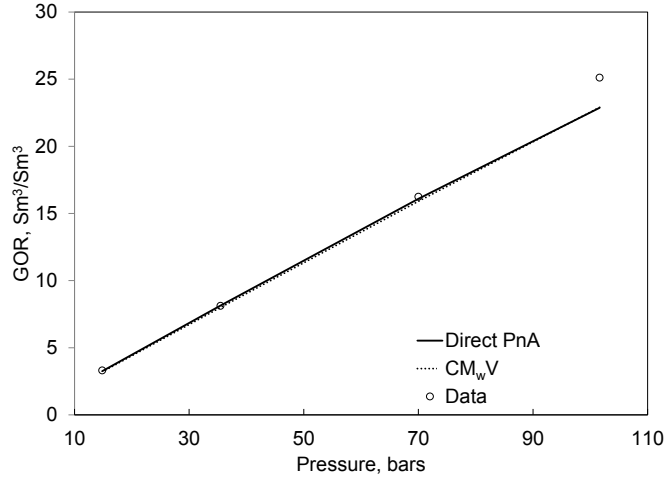
Figure 5-11. Data and predictions for the gas-oil-ratios (GOR) for heavy oil 3 (Pedersen et al. 2004) at the reservoir temperature of 305.45 K.
The AAD of the GOR predictions is 2.9% with the direct PnA method.
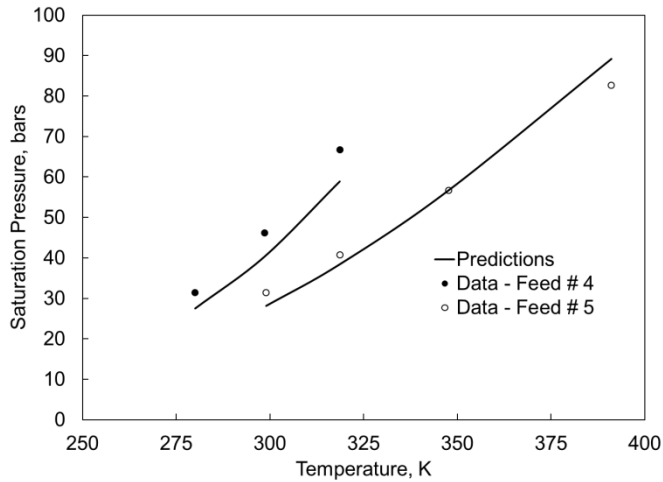
Figure 5-12. Saturation pressures measured and predicted for two mixtures with the Lloydminster heavy oil (heavy oil 4 in Table 5-5), Feeds #4 and #5 in Li et al. (2013a).
The AAD of the saturation pressure predictions is 13.7% for Feed #4 and 6.0% for Feed #5. If the BIPs for CO_2 with the pseudocomponents are altered from 0.10 to 0.15, the AAD is reduced to 7.6% for Feed #4 and to 0.4% for Feed #5.
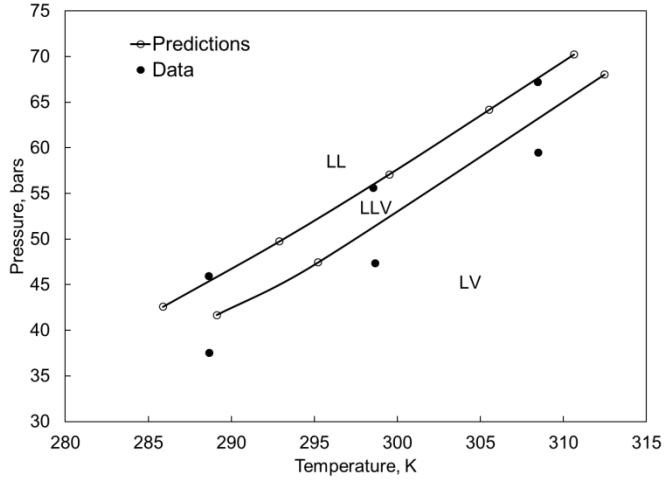
Figure 5-13. The three-phase boundaries measured and predicted for a mixture of heavy oil 4 (Table 5-5) with CO_2 and $n-C_4$ (Feed #15 of Li et al. 2013b).
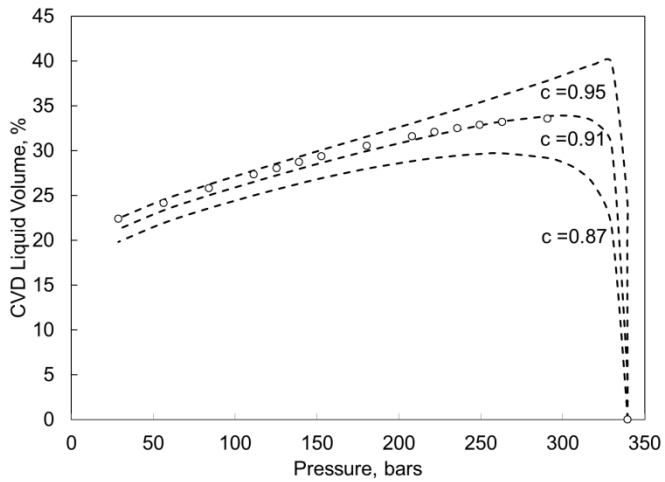
Figure 5-14. CVD liquid saturations predicted with different values for C for gas condensate 6 in Table 5-3.

C is equal to c for this fluid because f_b is zero. An optimum value for C, which is 0.91 in this case, is easy to find because of the monotonic, systematic change of the CVD liquid saturation curve.
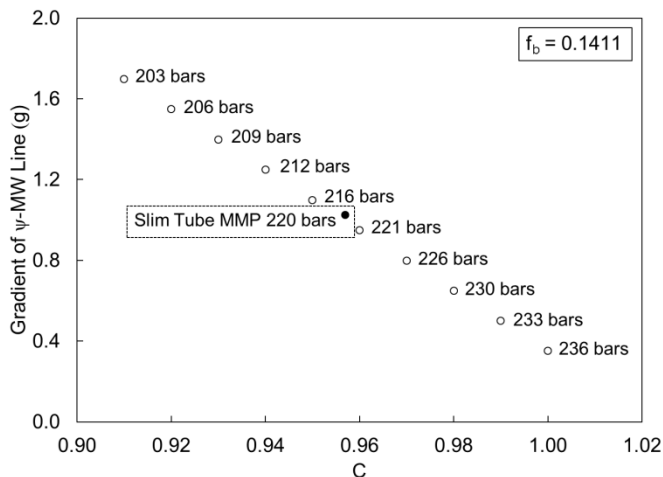
Figure 5-15. MMPs calculated with different C values for oil 1 given in Table 5-1.
The calculated MMP decreases monotonically with decreasing C. It is not difficult to find the value for C with which the measured MMP is matched.
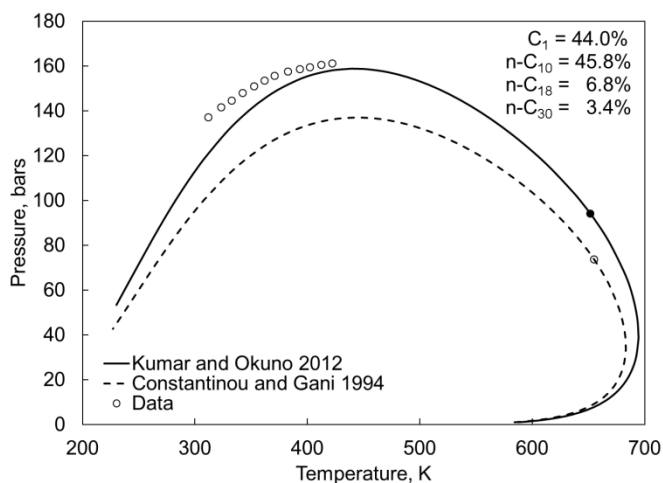
Figure 5-16. Two-phase envelopes predicted with the two sets of critical parameters for an n-alkane mixture.
The mixture contains 44.0% C_1, 45.8% $n\text{-}C_{10}$, 6.8% $n\text{-}C_{18}$, and 3.4% $n\text{-}C_{30}$. The optimized critical parameters of Kumar and Okuno (2012) and the estimated physical critical parameters of Constantinou and Gani (1994) are used with the PR EOS. The BIPs are zero for both cases. The bubble-point data were taken from Daridon et al. (1996). Use of the optimized critical parameters results in a more accurate P-T envelope.
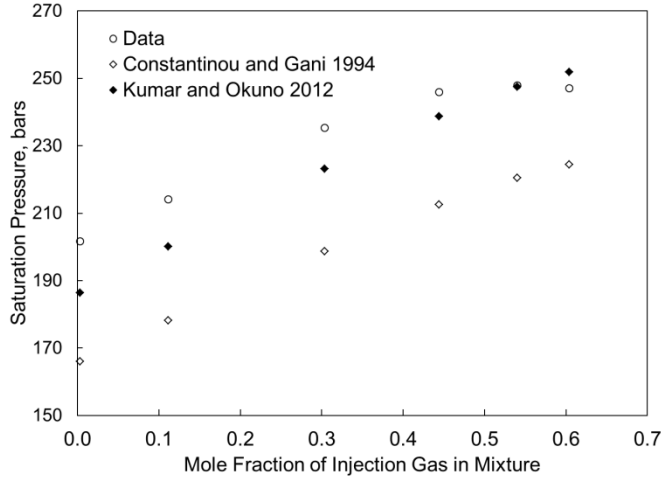
Figure 5-17. Saturation pressures measured and predicted for a 25-component oil with a gas at 373.15 K presented in Danesh et al. (1991).

The AAD of the saturation pressure predictions is 11% when the physical parameter set (Constantinou and Gani 1994) is used, whereas it is 4% with the optimized parameter set (Kumar and Okuno 2012). The BIPs are zero for both sets of predictions.
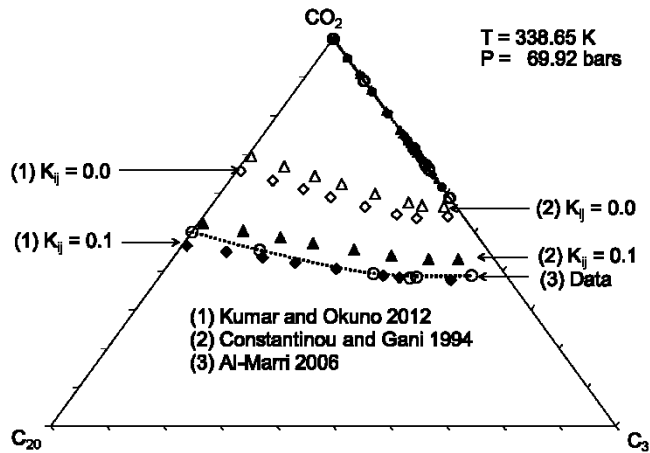
Figure 5-18. Comparison of two-phase envelopes for ternary mixture predicted with two PR EOS with two different set of critical parameters.

Two-phase envelopes predicted for a ternary system of CO_2, C_3, and n-C_{20} at 338.65 K and 69.92 bars using the PR EOS with the critical parameters from Kumar and Okuno (2012a) and Constantinou and Gani (1994). The BIPs considered for CO_2 with the other two components are 0.0 and 0.1. Peng and Robinson (1978) recommended 0.1 for these BIPs. The optimized parameter set results in more accurate predictions of two-phase equilibrium for the n-alkane mixtures containing CO_2. The data were taken from Al-Marri (2006).

181
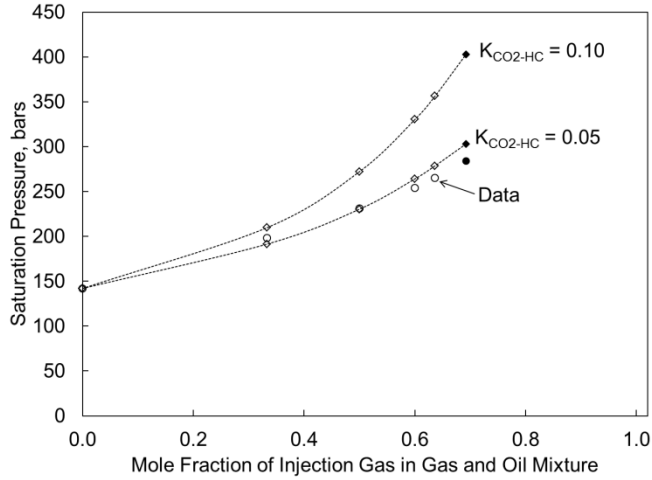
Figure 5-19. Saturation pressures measured in the swelling test of Fluid 18 (Table 5-1) with CO_2 at 394 K (Negahban et al. 2010).

The experimental MMP for this oil with CO_2 is 178 ± 2 bars at 394 K. The fluid model developed based on the direct PnA method gives an MMP of 188 bars with the default BIPs of CO_2 with pseudo components as 0.10. Although it correctly predicts the transition from bubble- to dew-point at CO_2 concentration of 0.69, this fluid model gives progressively higher saturation pressures than the experimental values with increasing CO_2 concentration. When the BIPs of CO_2 with pseudocomponents are reduced from 0.10 to 0.05, the model is much improved in saturation pressure predictions. The MMP predicted is 174 bars, which is still close to the experimental result. The blank and filled markers represent bubble- and dew-points, respectively.

Table 5-1. Converged f_ψ, f_b, and p values for reservoir oils characterized using the direct PnA method. Slim-tube MMPs are reported for these oils in the literature.

Oil No.	References	MW (gm/mol)	°API	T_{RES} (K)	k	f_ψ	f_b	p	% AD MMP Prediction
1	Jaubert et al. (2002), F1	135.2	35.22[‡]	374.85	5	0.4223	0.1411	4.5	5.60
2	Jaubert et al. (2002), F2	136.2	39.89	372.05	6	1.0947	0.1051	4.7	14.28
3	Jaubert et al. (2002), F3	82.41	39.31[‡]	387.35	11	0.8280	0.0690	6.3	1.27
4	Jaubert et al. (2002), F4	63.17	40.34[‡]	388.20	7	0.1683	0.074[x]	3.0	0.09
5	Jaubert et al. (2002), F5	125.8	32.04[‡]	394.25	12	0.8105	0.1171	4.5	0.55
6	Jaubert et al. (2002), F6	96.25	37.73[‡]	383.15	5	0.6294	0.1151	4.2	5.76
7	Jaubert et al. (2002), F7	96.19	41.06[‡]	393.15	12	1.6151	0.0520	4.9	1.29
8	Jaubert et al. (2002), F11	82.55	38.71[‡]	373.75	11	0.6737	0.0921	3.8	8.96
9	Jaubert et al. (2002), F13	150.2	35.64[‡]	377.55	8	-0.2542	0.0701	4.4	2.65
10	Al-Ajmi et al. (2011), F1	161.4	31.85	350.40	16	0.6427	0.1341	4.6	12.45
11	Al-Ajmi et al. (2011), F2	109.3	40.03	353.70	17	0.7924	0.1061	3.9	14.56
12	Ekundayo (2012)	86.57	51.60	402.59	7	1.1011	0.0671	4.6	3.03
13	Wijaya (2006)	113.9	44.00	302.59	17	1.3260	0.0701	4.5	9.94
14	Høier (1997), System 1[¥]	97.0	39.40	368.15	6	0.6933	0.1121	4.4	8.01
	Høier (1997), System 2[¥]	97.0	39.40	368.15	6			4.4	4.54
	Høier (1997), System 3[¥]	97.0	39.40	368.15	6			4.4	4.81
	Høier (1997), System 4[¥]	97.0	39.40	368.15	6			4.4	5.37
15	Lindeloff et al. (2013),Oil A	148.2	30.00[‡]	329.26	10	1.0253	0.1301	4.6	12.25
16	Graue and Zana (1981)[#]	177.0	42.10	344.26	1	4.8227	0.0971	7.7	5.15
	Graue and Zana (1981)[#]	177.0	42.10	344.26	1			7.7	9.16
17	Clark et al. (2008)	53.87	47.00	413.70	12	0.7289	0.1591	3.0	6. 80*
18	Negahban et al. 2010	101.9	40.00	394.00	16	1.1901	0.0491	4.8	5.62

x Δc value (f_b is zero).
‡ As reported. All other API gravities are calculated from the density at 288.15 K and 1.01325 bars.
¥ Oil composition and saturation data used were taken from Whitson and Belery (1994). Systems 1-4 indicate four different injection gases.
%ADs of 5.15 and 9.16 are for injection gases 1 and 2 respectively.
* AAD for 26 different injection gases is 6.8 %. Deviations for these injection gases are shown in Table 5-2.

Table 5-2. Deviations for MMP predictions for volatile oil 17 (Clark et al. 2008) based on the direct PnA method of volatile oil.

Injection gas (Mole %)*	Dev. %	Injection gas (Mole %)*	Dev. %	Injection gas (Mole %)*	Dev. %	Injection gas (Mole %)*	Dev. %
CO_2 (100)	5.26	CO_2 (95) + C_2 (5)	4.85	CO_2 (95) + C_5 (5)	-7.83	CO_2 (95) + N_2 (5)	0.18
CO_2 (95) + C_1 (5)	6.47	CO_2 (90) + C_2 (10)	4.53	CO_2 (90) + C_5 (10)	-17.34	CO_2 (90) + N_2 (10)	-3.44
CO_2 (90) + C_1 (10)	6.47	CO_2 (85) + C_2 (15)	5.35	CO_2 (85) + C_5 (15)	-20.67	CO_2 (85) + N_2 (15)	0.48
CO_2 (85) + C_1 (15)	6.94	CO_2 (80) + C_2 (20)	5.70	CO_2 (80) + C_5 (20)	-1.56	CO_2 (80) + N_2 (20)	3.57
CO_2 (80) + C_1 (20)	6.87	CO_2 (75) + C_2 (25)	7.62	CO_2 (75) + C_5 (25)	5.67	CO_2 (75) + N_2 (25)	7.59
CO_2 (75) + C_1 (25)	6.86	CO_2 (70) + C_2 (30)	9.55	CO_2 (70) + C_5 (30)	6.30	CO_2 (70) + N_2 (30)	10.78
CO_2 (70) + C_1 (30)	5.00					N_2 (100)	13.75

* Numbers inside bracket shows mole % of the component in injection gas.

Table 5-3. Converged f_ψ, Δc, and p values for gas condensates characterized using the direct PnA method. CVD or CCE data are available for these oils. f_b is zero for these gas condensates.

Fluid No.	References	MW (gm/mol)	°API	T_{RES} (K)	f_ψ	Δc	p	Maximum Data Value (Type[#])	Dev.[¥]
1	Al-Meshari (2004), Fluid-3	31.53	58.3	424.82	0.9774	+0.012	2.0	11.70 (1)	1.42
2	Al-Meshari (2004), Fluid-4	31.44	59.9	403.15	1.4443	-0.016	2.0	13.00 (1)	1.17
3	Al-Meshari (2004), Fluid-5	32.41	60.4	382.59	0.7700	+0.065	2.1	23.36 (2)	1.71
4	Al-Meshari (2004), Fluid-7	36.62	59.6	397.59	2.9688	-0.009	2.6	25.00 (1)	1.51
5	Al-Meshari (2004), Fluid-8	40.77	62.9	424.82	-0.0099	+0.043	2.2	30.40 (1)	0.95
6‡	Al-Meshari (2004), Fluid-10	39.23	64.7	422.59	-0.2355	+0.043	3.3	33.60 (1)	0.42
7‡	Al-Meshari (2004), Fluid-11	41.71	62.3	424.82	0.6702	+0.018	3.0	32.20 (1)	1.47
8‡	Coats and Smart (1986), Gas-5	30.29	61.8	403.70	1.4817	-0.005	2.0	10.40 (2)	0.12
9	Guo and Du (1989), Sample-7	25.53	71.2	406.45	2.1065	-0.033	2.0	5.82 (1)	0.09
10	Imo-Jack (2010)	25.76	54.0	382.59	-4.8869	+0.265	2.2	9.25 (1)	0.85
11‡	Coats (1985), Recombined	44.40	66.4	435.93	2.0540	+0.020	4.0	32.00 (2)	2.78
12‡	McVay (1994), Gas B	40.58	58.5	387.59	0.4190	+0.002	2.0	40.90 (1)	0.94
13	Danesh (1998)	27.29	55.3	394.00	1.4306	+0.037	2.0	11.32 (1)	0.27
14	Pedersen and Christensen (2007)	29.14	58.5	428.15	0.0168	+0.120	2.0	11.89 (2)	2.46
15	Hosein et al. (2013), PL-1	23.64	58.9	358.78	2.2649	-0.013	2.0	8.15 (1)	0.48
16	Hosein et al. (2013), PL-2	22.10	52.8	378.15	5.3774	-0.012	2.0	5.08 (1)	0.48
17	Hosein et al. (2013), PL-3	21.55	64.9	357.59	3.6390	-0.097	2.0	4.00 (1)	0.18
18	Hosein et al. (2013), PL-4	20.62	57.3	364.22	4.4763	-0.006	2.0	3.73 (1)	0.32
19	Hosein et al. (2013), PL-5	20.30	64.3	355.37	2.7869	-0.014	2.0	3.79 (1)	0.14
20	Hosein et al. (2013), PL-6	19.75	55.1	367.59	7.9725	-0.016	2.0	1.89 (1)	0.15
21	Moore (1989), CS-1	32.61	71.1	366.48	2.2538	-0.030	2.5	19.90 (1)	0.37
22	Moore (1989), CS-2	35.04	59.7	410.93	1.0086	-0.032	2.0	21.60 (1)	0.35
23	Moore (1989), CS-3	24.45	61.4	365.37	7.2733	-0.015	2.0	2.17 (1)	0.25
24	Whitson and Torp (1983), NS-1	35.04	44.0‡	410.43	0.9200	-0.023	2.0	21.60 (1)	0.48
25	Whitson and Brulé (2000), GOCW-7	33.62	60.5	358.70	4.8755	-0.008	2.5	23.90 (1)	1.96
26	Drohm et al. (1988), Example-1	54.92	57.1	410.90	1.8164	-0.050	2.9	69.81 (1)	11.34
27	Drohm et al. (1988), Example-2	32.65	59.5	436.70	0.9472	-0.000	2.0	15.63 (1)	0.95
28	Drohm et al. (1988), Example-3	26.26	58.4	393.20	5.1549	-0.022	2.0	4.75 (1)	0.50
29	Drohm et al. (1988), Example-4	28.34	59.0	377.60	3.1677	+0.018	2.1	11.84 (1)	0.49
30	Drohm et al. (1988), Example-5	21.27	56.4	377.60	-0.0195	+0.284	2.0	1.69 (1)	0.09
31	JAPEX	29.81	58.9	402.59	0.9672	+0.000	2.0	6.67 (3)	0.05
32	Pedersen et al. (1988)	26.98	61.82	392.10	4.8159	+0.020	2.1	5.72 (1)	0.62
33	Vogel and Yarborough (1980), Gas-1	36.03	49.6	381.00	0.3244	-0.003	2.2	25.85 (2)	1.49
34	Vogel and Yarborough (1980), Gas-2	30.75	64.6	381.00	1.9861	-0.068	2.1	9.79 (2)	0.69
35	Vogel and Yarborough (1980), Gas-3	23.73	63.2	333.00	-4.0671	+0.280	2.1	3.40 (2)	0.41
36‡	Whitaker and Kim (1993)	39.34	59.7	366.48	0.2427	+0.061	2.2	47.40 (2)	3.07
37	Kilgren (1966)	36.52	59.5	399.82	0.1825	-0.019	2.1	39.99 (2)	3.83
38‡	Subero (2009)	40.03	50.5	377.04	1.3835	-0.024	2.1	38.90 (1)	1.03
39	Fawumi (1999)	34.04	57.9	422.59	0.0383	+0.026	2.1	17.16 (1)	1.23
40	Al-Subai (2001), Well-A	32.64	57.4	420.93	0.5792	-0.007	2.6	14.34 (1)	1.60
41	Al-Subai (2001), Well-B	42.44	54.2	424.82	0.2787	-0.012	2.6	32.02 (1)	1.30
42	Al-Subai (2001), Well-D	34.50	63.6	424.82	0.0016	+0.025	2.1	17.17 (1)	1.53
43	Al-Subai (2001), Well-E	23.03	61.4	412.59	5.1525	+0.008	2.1	2.18 (1)	0.35
44	Jacoby et al. (1959)	32.76	63.7	404.82	0.8206	-0.015	2.1	16.10 (2)	1.62
45	Renner et al. (1989)	35.69	63.6	374.82	0.9377	+0.001	2.1	25.02 (2)	1.20
46‡	Coats (1985), Bottom hole	44.40	67.9	435.93	0.5331	+0.032	4.0	33.49 (2)	1.72
47	Spivak (1941)	27.13	65.6	352.59	0.9568	+0.045	2.1	12.68 (1)	0.98

‡ As reported. All other API gravities are calculated from the density at 288.15 K and 1.01325 bars.
# (1) is CVD liquid saturations (%), (2) is CCE liquid saturations (%), and (3) is CCE relative volumes.
¥ Deviation is the summation of |experimental value –predicted value| divided by the number of data point.
‡ Near critical gas condensates.

Table 5-4. Converged f_ψ, f_b, and p values for volatile oils characterized using the direct PnA method. CVD or CCE data are available for these oils.

Oil No.	References	MW (gm/mol)	°API	Res. Temp. (K)	f_ψ	f_b	p	Data Limits Value (Type[#])	Dev.[¥]
1	Al-Meshari (2004), Fluid-12	46.07	50.3	354.82	0.8544	+0.033[x]	2.3	38.20 (1)	2.80
2	Al-Meshari (2004), Fluid-13	56.06	36.7	364.82	0.2188	0.1091	2.3	3.93 (3)	0.02
3	Al-Meshari (2004), Fluid-14	54.57	40.7	360.93	0.3069	0.1081	2.4	1.00 (3)	0.01
4	Al-Meshari (2004), Fluid-15	51.11	57.5	353.15	1.5275	0.0581	2.9	2.98 (3)	0.01
5	Al-Meshari (2004), Fluid-16	59.63	55.6	425.93	0.0591	-0.006[x]	2.5	35.30 (1)	2.29
6	Al-Meshari (2004), Fluid-17	67.32	44.5	414.82	0.2061	0.0920	2.5	6.84 (3)	0.04
7	Al-Meshari (2004), Fluid-18	59.90	54.4	423.15	0.2876	0.0591	3.2	7.57 (3)	0.04
8	Al-Meshari (2004), Fluid-19	62.65	59.5	377.59	1.2666	0.0540	4.3	4.08 (3)	0.00
9	Oil*	86.68	56.6	376.75	1.7416	0.0360	4.0	2.46 (3)	0.01
10[‡]	McVay (1994), Oil A	50.93	44.5	408.70	1.1997	+0.000[x]	2.5	33.30 (1)	4.38
11	McVay (1994), Oil B	57.50	56.7	393.70	1.0877	+0.000[x]	3.1	49.50 (1)	2.60
12[‡]	Yang et al. (1997)‡	37.94	57.5	371.60	-0.6776	+0.085[x]	2.0	6.06 (2)	2.12
13	Jacoby and Yarborough (1967)	54.32	63.7	346.48	1.1580	0.0540	2.8	24.29 (1)	1.60
14[‡]	Pedersen et al. (1988)	47.84	52.5	424.25	0.2597	-0.013[x]	2.3	42.20 (1)	3.87
15	Reudelhuber and Hinds (1957)	42.55	49.1	374.82	0.6933	-0.024[x]	2.3	34.50 (1)	1.60

[x] Δc value (f_b is zero).
[‡] As reported. All other API gravities are calculated from density at 288.15 K and 1.01325 bars.
[#] (1) is CVD liquid saturation (%), (2) is CCE liquid saturation (%), and (3) is CCE relative volume.
[¥] Deviation is the summation of |experimental value –predicted value| divided by the number of data point.
[‡] Near critical volatile oil.
[*] Data source is not mentioned for confidentiality.

Table 5-5. Converged f_ψ, f_b, and p values for heavy oils characterized using the direct PnA method. PVT data available for these oils include swelling tests, gas solubility, and phase envelopes.

Oil No.	References	MW (gm/mol)	°API	T_{RES} (K)	k[#]	f_ψ	f_b	p	AAD %	Type of Data
1	Sharma (1990), West Sak Oil	228.88	18.68	299.81	10	0.0568	0.1491	5.7	3.62	Swelling Test
2	Krejbjerg and Pedersen (2006),Fluid-1	125.72	28.00[‡]	347.15	13	0.2762	0.2341	5.5	3.40	Swelling Test
3	Pedersen et al. (2004), Fluid-22	311.06	10.87	305.45	11	-0.0607	0.1592	5.5	3.13	GOR
4	Li et al. (2013a), Lloydminster Oil	482.00	10.80	294.15	1	-0.3409	0.1320	9.0	9.30	Swelling Test

[‡] As reported. All other API gravities are calculated from density at 288.15 K and 1.01325 bars.
[#] k is number of density data

Chapter 6: Systematic Characterization of Bitumen-Solvent Interactions in Steam-Solvent Coinjection Simulation

A version of this has been submitted to Fuel for publication. The manuscript is under review.

6.1. Introduction

Steam-assisted gravity drainage (SAGD) is a widely-used method for in-situ bitumen recovery (Butler 1991, Lake et al. 2014). The most important mechanism in SAGD is the reduction of oleic-phase viscosity owing to the heat that the injected steam releases when condensing into hot water near the steam-chamber edge. The main drawback of SAGD is the substantial usage of steam, which may also cause various environmental concerns.

Coinjection of solvent with steam, such as expanding-solvent-steam assisted gravity drainage (ES-SAGD), has been proposed and pilot-tested to improve the efficiency of SAGD (Nasr et al. 2003, Gupta and Gittins 2006). In ES-SAGD, a small amount of hydrocarbon solvent is coinjected with steam. It aims to reduce oleic-phase viscosity by diluting bitumen with condensed solvent, in addition to the thermal mechanism, along the chamber edge.

Unlike SAGD, ES-SAGD involves multiphase behavior of solvent/bitumen mixtures at a wide range of temperature and its interaction with non-isothermal flow under heterogeneities. The efficiency of ES-SAGD is substantially dependent on pressure, temperature, and composition near the chamber edge, in which condensation of steam and solvent and the mixing of solvent with bitumen take place through gravity drainage (Keshavarz et al. 2014).

Due to the complexity, design of ES-SAGD requires numerical simulation that accommodates the compositional effect on non-isothermal reservoir flow. Numerical simulation studies have been presented in the literature to understand various aspects of this complex process (Nasr and Ayodele 2006, Nasr et al. 2003, Jha et al. 2013, Keshavarz et al. 2015). However, the effect of fluid characterization on ES-SAGD simulation has not been investigated in detail, although such simulations are directly affected by how the fluid is characterized.

Fluid characterization for ES-SAGD is challenging because it requires a reliable method for modeling phase properties that does not give physically absurd values at a wide range of composition and temperature for the operating range of pressure. For example, the temperature range in ES-SAGD can be from 300 K to 500 K. The oleic-phase composition can vary widely from nearly 100% solvent to 100% bitumen in the vicinity of the chamber edge.

Even with such a reliable method, however, it is still important to ensure that the simulation results are not sensitive to the phase-behavior model used. This is because fluid characterization for ES-SAGD is performed under inherent uncertainties in terms of experimental data. It would not be easy to measure phase properties at the thermodynamic conditions that occur during ES-SAGD, even if such conditions could be precisely predicted. Different fluid models created under such uncertainties may give a similar level of correlative accuracy for the limited experimental data available; however, they do not necessarily give similar results in numerical reservoir simulation, in which phase behavior should be predicted at a variety of thermodynamic conditions. Currently, there is no method for assessing the sensitivity of simulation results to the phase-behavior model without performing actual flow simulations.

There are two main objectives in this research. The first is to show reliable characterization of bitumen by using the method that was developed by the authors (Section 6.2). The second is to develop a novel method for analytically assessing the sensitivity of ES-SAGD simulation to the phase behavior model used (Section 6.3). The analytical method is validated in the simulation case study (Section 6.4).

6.2. Bitumen characterization based on Perturbation from n-Alkanes

This section presents characterization of six different bitumen samples using the Peng-Robinson equation of state (PR EOS) (1976, 78) along with the van der Waals mixing rules on the basis of perturbation from n-alkanes (PnA). The PnA method of reservoir fluid characterization was successfully applied to a number of reservoir fluids (Kumar and Okuno 2015), but not yet to any bitumen. The main difference between the PnA method and the conventional method of bitumen characterization lies in how pseudo components' properties are adjusted during the regression of an EOS model to phase-behavior data. Before presenting the PnA method for bitumen characterization in Section 6.2.1, the conventional method is briefly explained below.

Several researchers presented EOS models to represent bitumens and their gas solubilities (James and Malhotra 1988, Malhotra and Svrcek 1988, Malhotra et al. 1989, Kariznovi et al. 2010). The three main steps of bitumen characterization in their papers are (1) representation of bitumen by a user-defined number of pseudo components, (2) estimation of pseudo components' parameters, such as critical temperature (T_C), critical pressure (P_C), acentric factor (ω), and critical volume (V_C), using various correlations, and (3) regression of the parameters to match experimental data.

Step 1 of the conventional method uses atmospheric and vacuum distillation data. Bitumens are represented by SARA (saturate, aromatic, resin, and asphaltene) fractions or by pseudo components obtained from a certain probability distribution function, such as the gamma distribution function (Whitson 1983). Step 2 of the conventional method is often based on the correlations with normal boiling point (T_b) and specific gravity (γ). Binary interaction parameters (BIPs) are also estimated as functions of one or more parameters, such as T_C, P_C, V_C, and ω. Step 3 of the conventional method is to reduce the deviation of EOS predictions from experimental phase behavior data because the general correlations used in step 2 tend to be in substantial error when extrapolated to high carbon numbers (CNs) relevant to bitumen components. Therefore, many parameters, such as T_C, P_C, V_C, ω, BIP, and volume shift, for pseudo components are adjusted to match various data, such as gas solubilities and densities.

The conventional method described above is concerned mainly with the correlative accuracy for the experimental data available. Due likely to a high level of uncertainties in bitumen data, the number of pseudo components required for the conventional method to match experimental data ranges up to 6 (Fu et al. 1985, Lu et al. 1986, Mehrotra and Svrcek 1988a, Mehrotra et al. 1989, Kariznovi et al. 2010). With the conventional method, use of one pseudo component was unsuccessful for matching bitumen data (Mehrotra and Svrcek 1988a, Mehrotra et al. 1989). No approach to predicting the number of pseudocomponents representing bitumen for reliable recovery simulation has been developed. The

general approach to representing the plus fraction by multiple pseudocomponents is based on the understanding that lumping of components results in loss of information and flexibility (Leibovici 1993). It is unknown in the literature whether characterization of bitumen/solvent mixtures, although challenging, requires as many as 6 pseudo components for thermal flow simulation. Use of more components certainly offers the flexibility in matching experimental data; however, the correlative accuracy obtained with a large number of pseudo components does not necessarily yield accurate predictions of phase behavior during thermal flow simulation due to a wide range of thermodynamic conditions encountered. As will be shown later in this paper, a proper number of pseudo components in bitumen characterization cannot be determined without consideration of compositional effects in the oil recovery process of interest, which is ES-SAGD in this paper.

6.2.1. Algorithm for Bitumen Characterization

The PnA method begins with a PR-EOS model calibrated for n-alkanes; hence, pseudo components are initially assumed to be n-alkanes. Then, the a and b parameters for pseudo components are adjusted in the direction of increasing aromaticity from n-alkanes (i.e., zero aromaticity) until a saturation pressure and densities at a given temperature are matched for the fluid of interest. Volumetric and compositional phase behavior are corrected largely by adjusting the b parameter to match densities and by adjusting the ψ parameter to match a saturation pressure, respectively. The ψ parameter is expressed as **Equation 6-1**.

$$\psi = a/b^2, \text{ or } \frac{\Omega_a}{\Omega_b^2}P_C(1 + m[1 - (T/T_C)^{0.5}])^2 \tag{6-1}$$

on the basis of the PR EOS. Details of the original PnA method can be found in (Kumar and Okuno 2015).

The two types of experimental data, density and saturation pressure, are important in the PnA method since the b and ψ parameters are adjusted specifically for volumetric and compositional predictions, respectively. In this research, such experimental data are taken from a bitumen/gas mixture, because a bitumen sample often exhibits no obvious saturation pressure even at 450 K, which is near the highest operating temperature of the conventional phase-behavior experimental setup. More specifically to this paper, we use the saturation pressure and density data for the bitumen saturated with methane around 373.15 K (100°C), although the selection of gas and temperature is arbitrary in principle. The BIPs of methane with bitumen components are set to zero in this paper, although other default values are also possible.

As presented in Kumar and Okuno (2015), the adjustment of the b parameter for matching density data is performed using **Equation 6-2**.

$$b_i = -14.6992113939827 + 1.36977232166027\left(\frac{MW_i}{m_{bi}}\right) - 9.12089276536298 \times 10^{-5}\left(\frac{MW_i}{m_{bi}}\right)^2 \tag{6-2}$$

where i is the index for pseudo components, $m_{bi} = (MW_i/86.0)^{fb}$, and MW_i is the molecular weight of component i. The f_b perturbation parameter is zero for n-alkanes, and increases with increasing level of aromaticity in terms of volumetric phase behavior. The m_{bi} parameter increases with MW for a given f_b value.

The a parameter is adjusted through the ψ parameter for a given b parameter (i.e., $a = ψb^2$). Unlike in the original PnA method (Kumar and Okuno 2015), however, the adjustment of ψ can be conducted using a simplified equation:

$$\psi_i = -0.9415MW_i + 2495.8f_\psi. \tag{6-3}$$

Coefficients in **Equation 6.3** corresponds to temperature of 373.15 K. Equation 6.3 represents the n-alkane case when the f_ψ perturbation parameter is the initial value of 1.0. The simplification is possible because a large fraction of bitumen components are heavier than CN 20, in which ψ linearly decreases with MW as shown in (Kumar and Okuno 2015). The ψ function can be systematically increased by increasing the f_ψ perturbation parameter, which increases the y-intercept of the function. When only one pseudo component is used, the ψ parameter is adjusted by changing the f_ψ perturbation parameter in **Equation 6-4**.

$$\psi = \Psi_n f_\psi = (-0.9415MW + 2495.8)f_\psi \tag{6-4}$$

where $ψ_n$ is the ψ parameter calculated for an n-alkane with MW.

Unlike the conventional method, the PnA method systematically changes the vapor pressure curves of all pseudo components through direct adjustment of the two parameters. **Figure 6.1** shows the change in phase envelope for an example mixture of bitumen and methane, in which bitumen is represented by a single pseudo component. The solid curve in this figure is the initial phase envelope for which the bitumen is assumed to be an n-alkane (i.e., $f_b = 0.0$ and $f_\psi = 1.0$). The other curves correspond to positive level of aromaticity of the bitumen (i.e., $f_b > 0.0$ and $f_\psi > 1.0$). The step-wise description of the algorithm is given below.

Step 1. Compositional characterization

This step is required only when bitumen is to be represented by multiple pseudo components. The chi-squared distribution function (Quiñones-Cisneros et al. 2004) is applied to split bitumen into pseudo components. Quiñones-Cisneros et al. (2004) observed in their study that degree of freedom of 10 was sufficient for heavy oils used. In this work, a degree of freedom of 12 is assumed for bitumen. The C_{7+} molecular weight is taken from the molar mass reported for the bitumen sample of interest. The bitumen is split into a desired number (n) of pseudo components with equal mass fractions. In this paper, four pseudo components (i.e. n = 4) are used for multicomponent representation of bitumen. Set $f_b = 0.0$, and $f_\psi = 1.0$.

Step 2. Initialization of the a and b parameters for each pseudo component

Equation 6.2 is used for covolumes, b_i, for i = 1, …n. Equation 6.3 is used for ψ_i (i = 1,.n) if n > 1. Otherwise, Equation 6.4 is used. Then, the attraction parameter is calculated by $a_i = \psi_i b_i^2$ for each pseudo component.

Step 3. Perturbation of f_ψ to match the saturation pressure

Calculate $\delta = (P_S - P_{S\_EOS})/P_S$, where P_S is the saturation pressure measured for a bitumen/methane mixture at 373.15 K as discussed previously. P_{S_EOS} is the calculated saturation pressure, and δ is the average absolute relative deviation (AARD) in saturation pressure. If $\delta < \delta_{TOL}$ (e.g., 10^{-4}), go to Step 4. Otherwise, increase f_ψ (i.e. $f_\psi = f_\psi + \Delta f_\psi$; $\Delta f_\psi = 10^{-4}$) and go to Step 2.

Step 4. Perturbation of f_b to match the saturated liquid density

Calculate the AARD in density, ε, as $(D_N - D_{N\_EOS})/D_N$, where D_N is the density at the saturation point used in step 3, and D_{N_EOS} is the calculated density. If $\varepsilon < \varepsilon_{TOL}$ (e.g., 10^{-3}), stop. Otherwise, increase f_b (i.e., $f_b = f_b + \Delta f_b$; $\Delta f_b = 10^{-4}$), reset f_ψ to 1.0, and go to Step 2.

Step 5. Conversion of the final set of the a and b parameters to T_C, P_C, and ω

This step uses the procedure of Kumar and Okuno (2015), in which a physically reasonable set of T_C, P_C, and ω is back calculated from the final set of the a and b parameters from the PnA method. This calculation also gives T_b and γ for each pseudo component as it uses the Lee-Kesler (1975) and Kesler-Lee (1976) correlations. The correlation of Riazi and Daubert (1987) can be used along with the T_b and γ to calculate V_C for each pseudo component.

6.2.2. Case Studies for Bitumen Characterization.

The algorithm presented in the previous subsection is used to characterize six bitumens: Athabasca (Svrcek and Mehrotra 1982, Mehrotra and Svrcek 1985a), Cold Lake (Mehrotra and Svrcek 1988b), Peace River (Mehrotra and Svrcek 1985b), Wabasca (Mehrotra and Svrcek 1985c), JACOS (Kariznovi 2013, Nourozieh 2013) and Surmont (Kariznovi 2013, Nourozieh 2013). For each bitumen, data are available for methane/bitumen mixtures so that the algorithm can use the density at the methane-saturation pressure near 373.15 K (100°C) in Steps 3 and 4. As mentioned previously, the BIPs for methane with pseudo components are set to zero for all cases in this paper.

The systematic change in pseudo components' properties during the regression allows to conduct a comparative study of bitumen characterization in terms of the number of pseudo components used. Hence, each bitumen is characterized by using four pseudo components (the 4-PC case) and one pseudo component (the 1-PC case). **Table 6.1** shows the data used for the characterization and the converged values for f_b and f_ψ for each bitumen. The densities of methane-saturated bitumens, D_N, at P_S are similar to each other; therefore, no correlation is obvious for D_N and f_b. However, it is relatively clear that f_ψ increases with P_S, which comes from the systematic change in phase envelope in the PnA method; that is, the two-phase envelope for a bitumen/methane mixture gradually expands in pressure-temperature space as the perturbation proceeds (see Figure 6.1).

For each bitumen, additional data available for methane solubilities are used to test the predictive accuracy of the resulting EOS model. Table 6.1 summarized the AARDs for these additional data. The AARD in methane solubility predicted for 99 temperature-pressure points for six bitumens is 10.75% with the 4-PC case and 10.44% with the 1-PC case. The difference is insignificant between the 4-PC and 1-PC cases likely because the relative volatility of methane to each pseudo component is not much different due to the substantial asymmetricity between methane and bitumen.

As reported by Mehrotra and Svrcek (1988a), some data are unreliable. For example, Table 6.1 shows that the PnA method yields the AARD of 9.24% in the 4-PC case and 11.05% in the 1-PC case for methane solubilities for Athabasca bitumen. However, if the four unreliable data are excluded from the evaluation, the AARD reduces to 5.77% in the 4-PC case and 5.86% in the 1-PC case. Mehrotra and Svrcek (1988a) showed their characterizations of the same bitumen excluding the four unreliable data. The characterization of Mehrotra and Svrcek (1988a) resulted in the AARD of 4.9% using five pseudo components. Kariznovi et al. (2010) reported the AARD of 7.95% using 6 pseudo components EOS model.

A bitumen sample usually does not contain gas components, such as N_2, CO_2, and hydrocarbon gases. This is why the density at a saturation pressure for a gas/bitumen mixture is required for the PnA method to capture the compositional and volumetric phase behavior of bitumen through the a and b parameters. Although the density at a methane-saturation pressure was matched with zero BIPs for methane with bitumen components in this section, matching solubilities of a gas in a bitumen generally requires adjustment of their BIPs because the gas is not a part of the characterized bitumen. Such adjustment of BIPs is presented here for matching gas solubilities: N_2, CO_2, and C_2 for Athabasca (Svrcek and Mehrotra 1982, Mehrotra and Svrcek 1985a), Cold Lake (Mehrotra and Svrcek 1988b), Peace River (Mehrotra and Svrcek 1985b), Wabasca (Mehrotra and Svrcek 1985c), C_2 for JACOS bitumens, and C_2, C_3, and C_4 for Surmont bitumen (note that results for methane solubilities were presented in Table 6.1).

Table 6.2 shows the optimized BIPs and AARDs for the solubility data for these gases. As in Table 6.1, results for the 4-PC and 1-PC cases are shown in this table. The AARDs in the two cases are similar to each other; that is, bitumen characterization by the PnA method is insensitive to the number of pseudo components used for the cases tested. For comparison purposes, the last column of Table 2 presents the AARDs reported by Kariznovi et al. (2010) using the PR EOS with six pseudo components. The comparison shows that use of one pseudo component may be sufficient, at least, for correlating experimental data using the PR EOS. However, a proper number of pseudo components should be evaluated in the context of flow in a specific reservoir process, which is ES-SAGD in this research. This will be discussed in detail in the next section.

The AARD for ethane solubilities at 107 pressure-temperature points is 7.38% in the 4-PC case and 7.25% for the 1-PC case. Mehrotra and Svrcek (1989) reported that at least three data points for Wabasca bitumen were unreliable. When these unreliable points are excluded, the AARDs for the

ethane solubility in Wabasca bitumen are 4.06% and 3.96% for 1-PC and 4-PC respectively with the PnA method, 4.1% by Mehrotra and Svrcek (1989) using 3 pseudo components. Kariznovi et al. (2010) reported AARD of 6.56% using 6 pseudo components. **Figure 6.2** compares the ethane solubilities calculated based on the PnA method and the corresponding data for Cold Lake (Figure 2a) and Athabasca (Figure 2b). This figure indicates that the bitumen model has been better calibrated at higher temperatures likely because the methane saturation pressure, P_S, used is near 373 K.

The AARD for CO_2 solubilities at 91 pressure-temperature points is 6.05% in the 4-PC case and 6.06% in the 1-PC case. For Athabasca, the AARD is 5.6% with PnA method for 1-PC and 4-PC, 7.3% with the characterization by Mehrotra and Svrcek (1988a) with five pseudo components, and 9.34% by Kariznovi et al. (2010) with six pseudo components. For Wabasca, the AARD is 6.9% with PnA method for 1-PC and 4-PC, 4.1% by Mehrotra and Svrcek (1989), and 8.88% by Kariznovi et al. (2010). Experimental data for the Cold Lake bitumen shows that the CO_2 solubility levels off at an increased pressure along some isotherms, and that some solubility isotherms cross each other. **Figure 6.3** compares the CO_2 solubilities calculated based on the PnA method with the corresponding data for the Cold Lake bitumen. The above-mentioned characteristics are observed for the data and predictions for 288 K and 299 K.

The gas-solubility data for JACOS (Kariznovi 2013, Nourozieh 2013) and Surmont (Kariznovi 2013, Nourozieh 2013) bitumens contain the liquid-liquid (L-L) equilibrium in addition to the liquid-vapor (L-V) equilibrium. It was observed in this research that a positive BIP was required to match L-L data using the PnA method, but the use of a positive BIP did not affect the L-V predictions significantly. For example, the optimized BIP between propane and the single bitumen component is 0.066 for Surmont bitumen as given in Table 6.2. The L-L data could not be matched with zero BIP for propane and the bitumen component.

It is important to analyze the sensitivity of bitumen characterization to the MW used in Step 1, considering the inherent uncertainty in the quality of bitumen samples. JACOS bitumen is re-characterized using the 1-PC PnA method assuming different MWs from perturbation of the MW between -15% and +15%. Then, predictions are made for methane and ethane solubilities. The BIP for methane with the bitumen is zero, and that for ethane with the bitumen is 0.01. **Figure 6.4** shows the variation of AARDs with respect to MW deviation. The variation in AARD is quite small; e.g., it is less than 1.2% and 2.25% between -15% and +15% deviation in MW for the methane and ethane solubilities respectively. Higher AARD in case of ethane may be because of used BIP of 0.01 for all cases of MW variation. The results indicate that the PnA method of bitumen characterization is not much affected by the uncertainty of bitumen MW. However, it is important to use reliable data for the density at a saturation pressure for a gas-saturated bitumen because it directly affects the a and b parameters in the PnA method.

6.3.   Sensitivity Analysis of Oleic-Phase Viscosity at the Chamber Edge

Results in the previous section indicate that the usage of one pseudo component (the 1-PC case) yields a similar level of accuracy to that of four pseudo components (the 4-PC case) in terms of gas solubility calculations. However, they may still exhibit substantial differences when used in flow simulation of steam-solvent coinjection for bitumen recovery. This is because bitumen recovery in such processes is dependent mainly on the L-phase viscosity near the steam-chamber edge. Currently, however, the effect of bitumen characterization on bitumen recovery simulation can be evaluated only by running multiple flow simulations with different sets of fluid models, which is time-consuming. This section presents a new analytical method to evaluate the sensitivity of coinjection simulation results to bitumen characterization, without running actual flow simulations.

The main idea is to see if there is a substantial difference between the lightest and heaviest pseudo components of a multi-component model in terms of viscosity when they are treated as a single-component bitumen and mixed with solvent at the chamber-edge conditions. If the difference is small, the pseudo components (bracketed by the lightest and heaviest) likely behave similarly in thermal flow simulation, and may be modeled as a grouped single component.   Otherwise, use of multiple components is recommended for proper representation of bitumen for steam-solvent coinjection simulation.

6.3.1. Temperature, Oil-Phase Composition, and Viscosity at the Chamber Edge

The first step is to estimate the temperature and oil-phase composition at the steam-chamber edge, which significantly affect oil recovery in coinjection. A chamber edge is defined where the phase transition occurs between the oil-water (L-W) and vapor-oil-water (V-L-W) phase equilibria; hence, it is where the V phase (dis)appears. A brief description of the L-phase composition at a chamber edge is given below. More details of similar calculations can be found in Keshavarz et al. (2013).

The thermodynamic formulation is based on the following assumptions as conventionally done in this area of research: (a) ternary mixtures of water, a solvent component, and a bitumen component; (b) complete immiscibility between the W and L phases; (c) Raoult's law for partitioning of the water component between the W and V phases; and (d) hydrocarbon K values based on the PR EOS. The water, oil, and solvent components are labeled with indices i = w, o, and s, respectively. The W, L, and V phases are expressed using indices j = W, L, and V, respectively. x_{ij} is the mole fraction of component i in phase j. Then, phase equilibrium for such a ternary three-phase system at a given temperature (T) and pressure (P) is given by **Equations 6-5** to **6-9**.

$$P_w^{vap} = x_{wV}P \tag{6-5}$$

$$x_{oV} = K_o x_{oL} \tag{6-6}$$

$$x_{sV} = K_s x_{sL} \tag{6-7}$$

$$x_{oL} + x_{sL} = 1.0 \tag{6-8}$$

$$x_{wV} + x_{oV} + x_{sV} = 1.0 \tag{6-9}$$

where P_w^{vap} is the vapor pressure of water at T, and K_i is the K value for component i. Equation 6-5 is for the V-W equilibrium, and Equations 6 and 7 are for the V-L equilibrium. Equations 8 and 9 are summation constraints. Note that the W phase consists of only water, and the L phase contains no water, due to assumption (b).

Using the multiphase Rachford-Rice procedure (Okuno et al. 2010) as used in Keshavarz et al. (2015), it is easy to solve for the L-phase composition (x_{iL}; i = {o, s}) at a given P and T because the compositions of three equilibrium phases are uniquely determined for a ternary system at a given P and T. The L-phase composition so obtained corresponds to the one at the chamber-edge temperature (T_e) at a given P; that is, the specified T is taken as T_e. This procedure gives the relationship between the L-phase composition and temperature at the chamber edge for a given operating pressure for a specified solvent-bitumen system.

Once the relationship between T_e and the L-phase composition at P is set, the second step is to calculate the L-phase viscosity through a certain model. The following viscosity model has been implemented in the STARS (2012) reservoir simulator:

$$\ln\mu_{mix} = \sum_{i=1}^{N_C} x_i \ln\mu_i,$$

$$(6\text{-}10)$$

which is used in this section in order to keep the consistency with the simulation case study given in Section 6-4. In **Equation 6-10**, x_i and μ_i are the mole fraction and the effective viscosity of component i, respectively. N_C is the number of components in the phase for which the viscosity, μ_{mix}, is calculated (N_C = 2 in this section because only the o and s components are present in the L phase). Note that an effective viscosity is in general different from the viscosity of that component because it is determined by matching experimental viscosity data for mixtures using Equation 6-10.

Experimental data are used for μ_o for the 1-PC bitumen. For the 4-PC case, μ_o for each pseudo component is determined by fitting Equation 6-10 to that of the 1-PC bitumen using the known overall composition. An effective viscosity for a gas or solvent (e.g., methane and solvent components used in steam-solvent coinjection) is determined by fitting Equation 6-10 to experimental viscosity data for a given composition. Viscosity data is available only for mixture of methane with JACOS bitumen. As evident from Table 6-1, JACOS and Surmont bitumens' molecular weights, methane solubilities, and characterization parameters (f_b and f_ψ) are not significantly different. Hence, viscosity data for propane's mixture with Surmont bitumen (Nourozieh 2013) is used for JACOS. Effective viscosity for methane and for propane is estimated at isobaric (35 bars) temperature points using Equation 6-10 and their respective mixture viscosity data. When experimental data are not available for the bitumen/gas system of interest, correlations shown in **Equation 6-11** (e.g., the corresponding state viscosity model (Lindeloff et al. 2004)) can be used to obtain a reasonable estimation of an effective viscosity for the gas/solvent, as in the next subsection.

$$\mu_{s,eff} = \left[\frac{T_{c,mix}}{T_{c,ref}}\right]^{\left(-\frac{1}{6}\right)} \left[\frac{P_{c,mix}}{P_{c,ref}}\right]^{\left(\frac{2}{3}\right)} \left[\frac{M_{mix}}{M_{ref}}\right]^{(0.5)} \left(\frac{\mu_{s,pure}}{\mu_{C3,pure}}\right)^{0.5} \mu_{C3,eff}$$

$$(6\text{-}11)$$

Like corresponding state viscosity model (Lindeloff et al. 2004), Equation 6-11 establishes the relationship between two sets of information; one set is $\{T_{c,ref}, P_{c,ref}, M_{ref}, \mu_{C3,pure}, \mu_{C3,eff}\}$, and other set is $\{T_{c,mix}, P_{c,mix}, M_{mix}, \mu_{S,pure}, \mu_{S,eff}\}$. In Equation 6-11, subscripts ref and mix show reference and mixture states. Reference state indicates to propane (C_3) and its mixture with bitumen. The terms $T_{c,ref}$, $P_{c,ref}$, M_{ref} refers to pseudo critical temperature, pseudo critical pressure, molecular weight of mixture of bitumen and propane; and $T_{c,mix}$, $P_{c,mix}$, M_{mix} refers to pseudo critical temperature, pseudo critical pressure, molecular weight of mixtures of bitumen and solvent (other than propane). The terms $\mu_{C3,pure}$ and $\mu_{C3,eff}$ are pure C_3 viscosity and effective C_3 viscosity (in bitumen and C_3 mixture), respectively, at pressure P and temperature T; $\mu_{s,pure}$ and $\mu_{S,eff}$ are pure solvent (other than propane) viscosity and effective solvent viscosity (in bitumen and solvent mixture), respectively, at pressure P and temperature T. Liquid phase viscosity for pure solvents, such as n-C_6, n-C_7, n-C_8, and n-C_{10}, are available from the literature (Dymond and Øye 1994); for other solvents, liquid phase viscosity is found by extrapolation and interpolation.

In the third, last step, two curves for μ_{mix} at T_e for an operating P with a specific solvent coinjected with steam are plotted along the mixing line between 100% solvent and 100% bitumen; one with the lightest pseudo component, and the other with the heaviest pseudo component, in a multi-component representation of bitumen. Note that T_e varies with the L-phase composition, through the temperature dependency of K values. That is, the resulting μ_{mix} function has taken into account the effect the varying temperature on μ_{mix}. If a large difference is observed for the two curves along the mixing line between the solvent and bitumen, use of multiple pseudo components is recommended for proper representation of bitumen in the steam-solvent coinjection of interest. Otherwise, a single-component bitumen model is likely sufficient. For further explanation, an example calculation will be shown using JACOS Bitumen in the next subsection.

6.3.2. Application to JACOS Bitumen

The analytical method given in section 6.3.1 is applied to JACOS bitumen. The sensitivity of the L-phase viscosity at T_e at a typical operating pressure (35 bars) to the number of components used in bitumen characterization is studied for different single-component solvents, n-alkanes from C_3 to C_{10}. The 4-PC and 1-PC representations are compared.

JACOS Bitumen was characterized in Section 6.2. However, it is re-characterized here using unequal mass fractions, in place of the equal mass used previously. This is to have a wider variety of pseudo components in terms of volatility, which is expected to amplify the difference in terms of μ_{mix} among pseudo components in the analytical method. **Table 6.3** presents the resulting 4-PC model along with the original 4-PC and 1-PC models from Section 6.2. The mass fraction is 0.85 for the heaviest and 0.05 for the lightest pseudo component.

Figure 6.5 compares the temperature-composition (T-x) diagrams for binary mixtures of C_3 with different pseudo components. Figure 6.5a uses 4 pseudo components on the equal mass basis (from Section 6.2) and the 1-PC model. Figure 6.5b uses 4 pseudo components on the unequal mass basis

and the 1-PC model. As expected, the latter shows a larger difference between the lightest (4-PC-L) and heaviest (4-PC-H) pseudo components in terms of two-phase envelope with C_3.

BIPs of solvents with pseudo components are based on the correlation developed using experimental data as follows:

$$k_{sb} = 0.0349 \ln\left(\frac{V_{c,s}}{V_{c,b}}\right) + 0.1329 \tag{12}$$

where k_{sb} is the BIP between the solvent and bitumen components. $V_{c,s}$ and $V_{c,b}$ are the critical volumes of the solvent and bitumen components, respectively. They can be obtained from Step 5 of the PnA algorithm (see Section 6.2.1). As discussed earlier, JACOS and Surmont bitumen do not appear to be significantly different, hence, **Equation 6-12** has been developed using optimized BIPs for propane and butane solubility in Surmont bitumen.

Then, K values are obtained for water and hydrocarbon components at 35 bars, as described in the previous section. Raoult's law is used for partitioning of water between the V and W phases. The PR EOS model is used for L-V equilibrium for binary systems, each of which consists of a solvent component and a pseudo component (the lightest or the heaviest pseudo component). The K values are then used to obtain the relationship between T_e and the L-phase composition. Since the L phase does not contain the water component, T_e is given as a function of x_{sL} for each of the lightest and heaviest pseudo components.

On the basis of experimental data, the effective viscosities for methane and propane have been obtained at 35 bars at different temperatures. Effective viscosities for other solvent components are estimated by using a corresponding state method, which is similar to Lindeloff et al. (2004). **Figure 6.6** shows the effective viscosities with varying temperature at 35 bars obtained for different solvents. The number next to each curve is the solvent CN.

Finally, Equation 6.10 is used with the effective viscosities and the relationship between T_e and x_{sL} at 35 bars for the lightest and heaviest pseudo components for each solvent. This gives the L-phase viscosity at the chamber-edge conditions (μ_{edge}) as a function of x_{sL} for each solvent/pseudo-component pair. **Figure 6.7a, b, and c** respectively present the results for C_3, C_4, and C_6. In each figure, μ_{edge} for the 1-PC model is also given as a reference. The difference between the μ_{edge} curves for the lightest and heaviest pseudo components is the largest for the C_3 coinjection case, and diminishes as the solvent becomes heavier. In Figures 6.7a, b, and c, μ_{edge} at lower and higher ends of x_{sL} are mainly determined by viscosity of bitumen components (i.e. 1-PC, 4-PC-L, 4-PC-H) and solvents respectively.   It is important to analyze the trends in mid-range of x_{sL}.

Difference in μ_{edge} trends in mid-range of x_{sL} is mainly because of two factors: (1) difference in chamber edge temperatures (T_e), and (2) varying viscosity gradient ($\Delta\mu/\Delta T$) with temperature. Volatility decreases with increase in carbon number of solvents. For a given bitumen component, T_e increases with increasing carbon number of solvent. Gradient of viscosity ($\Delta\mu/\Delta T$) is significantly higher in lower temperature range than that at higher temperatures; for example, viscosity data for JACOS bitumen

show gradients **(Figure 6-8**) of -115 cP/K at 345 K and -0.45 cP/K at 445 K at 35 bars. The impact of varying gradient of viscosity on μ_{edge} becomes less significant with increasing T_e or carbon number of solvent.

Let us consider the liquid phase with 0.5 mole fraction of propane which exists at T_e of 391 K for 1-PC, 401 K for 4-PC-L, and 390 K for 4-PC-H; viscosities at these temperatures for propane are 0.97 cP, 0.94 cP, and 0.97 cP, and for 1-PC, 4-PC-L, and 4-PC-H are 96.3 cP, 61.0 cP, and 100.6 cP respectively. Corresponding temperatures (T_e) for butane as solvent are 440 K, 451 K, and 438 K, and viscosities at these temperatures for butane are 1.16 cP, 1.12 cP, and 1.17 cP, and for 1-PC, 4-PC-L, and 4-PC-H are 19.84 cP, 15.14 cP, and 21.13 cP respectively. The T_e and viscosity for 1-PC and 4-PC-H cases are not significantly different; hence, the trends of μ_{edge} with x_{sL} for these are not significantly different. The difference in trends for 4-PC-L and 4-PC-H is caused by difference in viscosities; for 11 K difference in their temperatures (T_e), the difference in viscosities is 39.6 cP for propane solvent in temperature range of 390-401 K, whereas for 13 K difference in temperature (T_e), the difference in viscosities for 4-PC-L and 4-PC-H is 5.99 cP for butane solvent in temperature range of 438-451 K. Due to decreasing volatility with increasing carbon number of solvent, T_es increases and impact of varying viscosity gradient becomes less significant. Hence, highest contrast in trends of μ_{edge} with x_{sL} for 4-PC-L and 4-PC-H is observed in case of propane, and this contrast increasingly diminishes with increasing carbon number of solvent.

6.4.   Simulation Case Study

This section shows the simulation case study for steam-solvent coinjection for JACOS bitumen based on the reservoir model used in Keshavarz et al. (2014). The simulation is performed using the STARS (2012) simulator with the phase behavior models from the 4-PC and 1-PC cases (see Table 6.3). Results from Section 6.3 indicate that the simulation of C_3-steam coinjection for JACOS bitumen may be sensitive to the number of pseudo components used for bitumen characterization; that is, use of the 4-PC model may result in different simulation results than that of the 1-PC model. This is validated in this section.

The reservoir and fluid properties are summarized in **Table 6.4.** This is a vertical-cross-sectional 2-D reservoir with 70 (horizontal) × 20 (vertical) grid blocks. The uniform grid-block size is 1.0 × 37.5 × 1 m. Grids are numbered from left to right in the horizontal direction, and from top to bottom in the vertical direction. The injector is located at the grid bock (1, 14), and the producer is at (1, 18); i.e., only a half of a steam chamber is simulated.

The gas-to-oil ratio is assumed to be 4 Sm^3/Sm^3, for which the reservoir oil consists of 91 mol% JACOS bitumen and 9 mol% methane. The solvents tested are n-alkanes between C_3 and C_{10}. The coinjection pressure is 35 bars, at which the saturation temperature of water is 515.86 K. The K values for water, solvents, and pseudo component(s) of bitumen are generated using the Winprop software (CMG 2012) for 80 mol% reservoir-oil and 20 mol% solvent. The injectant consists of 2 mol% single-component solvent and 98 mol% water.

The viscosity model used was given in Section 6.3. The density data are available for mixtures of bitumen with methane and propane. Densities for mixtures of bitumen and other solvents can be calculated by using the EOS models (Table 6.3). However, the STARS simulator uses

$$\frac{1}{\rho_L} = \sum_{i=1}^{N_C} \frac{x_{iL}}{\rho_{iL}}$$ (13)

to calculate the L-phase density. Therefore, the L-phase density values from experimental data and EOS models are used to calculate the effective densities of components in the L phase using **Equation 6.13.** In this equation, ρ_L is the molar density of the L phase, x_{iL} is the mole fraction of component i in the L phase, and ρ_{iL} is the effective molar density of component i in the L phase. The starting value for ρ_{iL} is obtained from the a and b parameters for component i with the PR EOS at the pressure and temperature. Then, ρ_{iL} are regressed to match ρ_L with Equation 6-13. Other parameters, such as liquid compressibility, coefficients of thermal expansion, enthalpy, are generated using the Winprop software (CMG 2012) with the EOS models.

Production starts after six months of preheating for achieving the thermal communication between the injector and the producer. **Figure 6-9** presents the bitumen production histories for four cases of coinjection: C_3, C_4, C_5, and C_6. For each solvent coinjection case, two curves are given for the 4-PC and 1-PC bitumen models. The recovery histories for heavier solvent cases are too close to the C_6 coinjection case, and not shown in Figure 6-9. In general, bitumen production is more rapid in coinjection of heavier solvent because of higher T_e and dilution of bitumen. Although an optimum solvent should be selected based on economic evaluations of the entire process, Figure 6-9 indicates the effect of solvent on bitumen production may diminish at CN 5 in these simple simulations.

Figure 6-9 shows that the difference between the 4-PC and 1-PC cases is pronounced for the C_3-steam coinjection case. This is because different pseudo components behave differently in the coinjection simulation in terms of the L-phase viscosity, which is the primary factor affecting bitumen production. The difference in phase behavior can be quantified by looking at the difference between the lightest and heaviest pseudo components (4-PC-L and 4-PC-H). The results given in Figure 6-9 is in line with the observation from the previous section that the μ_{edge} curves for the 4-PC-L and 4-PC-H exhibit more deviation for the C_3 coinjection case than for coinjection of heavier solvents. This simulation case validates the simple procedure developed for assessing the sensitivity of coinjection simulation to the number of bitumen components.

Figure 6-10 shows μ_{edge} observed along the chamber edge in the C_3, C_4, and C_6 coinjection cases using the 4-PC and 1-PC models after 580 days of production. The horizontal axis in the figure is the number of grid block from the reservoir top. Note that the plots for the 4-PC cases come from the mixing of all components, including the coinjected solvent and 4 pseudo components. The simulated μ_{edge} shows the largest difference between the 4-PC and 1-PC cases for the C_3 coinjection case. The difference diminishes as the coinjected solvent becomes heavier. The absolute average deviation

(AAD) for μ_{edge} between the 4-PC and 1-PC cases is 1.64 cp for C_3 coinjection, 0.31 cp for C_4 coinjection, and 0.21 cp for C_6 coinjection.

6.5. Conclusions

In this paper, a new analytical method was presented for assessing the sensitivity of ES-SAGD simulation to the number of components used for bitumen characterization. The method was compared with the flow simulation based on experimental phase behavior data and reliable bitumen characterization. The PnA method of fluid characterization was applied for the first time to bitumen characterization. Conclusions are as follows:

- o The analytical method for assessing the effect of bitumen characterization on ES-SAGD simulation results was successfully validated in the simulation case study. Use of multiple pseudo components is recommended if the lightest and heaviest pseudo components from a multi-component representation of bitumen behave differently in terms of the L-phase viscosity at the chamber-edge conditions. The analytical method can detect the sensitivity of ES-SAGD simulation to bitumen characterization without performing multiple flow simulations using different sets of fluid models.

- o The PnA method was successfully applied to characterization of six different bitumens. With the PnA method, no obvious difference was observed between the one-component and four-component representations of bitumen in terms of the correlative accuracy for gas solubilities and densities using the PR EOS.

- o A proper number of pseudo components for bitumen characterization for ES-SAGD simulation cannot be determined without considering the effect of phase behavior on the L-phase viscosity at the chamber-edge conditions. Results show that the one-component representation of bitumen may be sufficient for correlating gas solubilities and densities, but may not for reliable ES-SAGD simulation. This is because ES-SAGD simulation is substantially affected by the L-phase viscosity near the chamber edge, in which the gravity drainage of oil takes place.

- o Matching L-L equilibrium data required positive BIPs between solvent and bitumen. The L-V equilibrium for bitumen and solvent was not sensitive to the BIPs used. Therefore, use of positive BIPs improved the accuracy of L-L representation without significantly affecting the accuracy of L-V representation.

- o Bitumen characterization with the PnA method was not much affected by the uncertainty of bitumen MW. However, it is important for the PnA method to use accurate phase behavior data for saturation pressure and densities for gas-saturated bitumen.

- o Bitumen can be characterized as single pseudo component with the PnA method, with predictive capability similar to multiple pseudocomponents conventional characterization. Unlike conventional characterization which requires multiple data sets, the PnA method requires only molecular weight, one saturation pressure, and one density data for reliable characterization of bitumen.

200

6.6. Nomenclature

AARD   : Average absolute relative deviation $= \frac{1}{M} \sum_{j=1}^{M} \left| \frac{prediction - data}{Data} \right|_j$

AAD   : Average absolute deviation $= \frac{1}{M} \sum_{j=1}^{M} |prediction - data|_j$

BIP   : Binary Interaction Parameter

CN   : Carbon number

ES-SAGD   : Expanded Solvent-Steam Assisted Gravity Drainage

L-L   : Liquid (L)-liquid (L) phase equilibrium

L-V   : Liquid (L)-vapor (V) phase equilibrium

NC   : Number of components

PC   : Pseudo components

PR EOS   : Peng and Robinson (1976, 78) equation of state

SAGD   : Steam Assisted Gravity Drainage

T-x   : Temperature-composition

Greek Symbols:

δ : Deviation of calculated saturation pressure from experimental value

δ_{TOL} : Tolerance set for deviation (δ)

ϵ : AARD for density prediction

ϵ_{TOL} : Tolerance for density prediction for density data match.

μ : Viscosity

μ_{edge} : Viscosity of oleic phase in equilibrium with other two HC phases at chamber edge.

ρ_L : Molar density of liquid phase (Equation 12)

ρ_{iL} : Effective molar density of ith component in liquid phase (Equation 12)

γ : Specific gravity

ψ : Parameter defined in Equation 1.

x_{SL} : Solvent mole-fraction in oleic phase in equilibrium with other two HC phases.

ω : Acentric factor

Roman Symbols:

a   : Attraction parameter in Equation of State

b   : Covolume parameter in Equation of State

f_b : Regression perturbation parameter for covolume parameter in PR EOS

f_ψ : Regression perturbation parameter for ψ as shown in Equations 3 and 4.

D_N : Experimental density data

D_{N_EOS} : Predicted density with PR EOS

K_{Sb}	: Binary interaction parameter for solvent and bitumen pair (Equation 11).
MW	: Molecular Weight
n	: Number of pseudocomponents
m	: Parameter in PR EOS as function of acentric factor
m_b	: Parameter defined in Equation 2.
P_C	: Critical pressure
PC	: Pseudo components
P_S	: Experimental saturation pressure
P_{S_EOS}	: Calculated saturation pressure with the PR EOS
T_b	: Boiling point
T_C	: Critical temperature
T_e	: Chamber edge three-phase temperature
$V_{C,b}$	: Critical volume of bitumen
$V_{C,s}$	: Critical volume of solvent

Subscripts:

i	: Index for pseudocomponent
mix	: Mixture property
s	: Solvent
L	: Liquid hydrocarbon phase with solvent and bitumen components
w	: Water
W	: Liquid water phase
V	: Vapor phase

Superscript:

| Vap | : Vapor pressure |

6.7. References:

Butler, R.M. 1997. *Thermal Recovery of Oil and Bitumen.* Calgary, Alberta: Black book series, GravDrain Inc.

Computer Modelling Group (CMG) Ltd. Version 2012. Calgary, Alberta, Canada, 2012.

Dymond, J.H. and Øye, H.A. 1994. Viscosity of Selected Liquid n-Alkanes. *J Phys Chem Ref Data* **23** (1):41-53.

Fu, C.-T., Puttagunta, V.R., and Vilcsak, G. 1985. Vapour-Liquid Equilibrium Properties for Pseudo-Binary Mixtures of CO_2-Athabasca and N_2-Athabasca Bitumen. *AOSTRA J. Research*, **2** (2): 73-81.

Gupta, S. and Gittins, S.D. 2006. Christina Lake Solvent Aided Process Pilot. *Journal of Canadian Petroleum Technology* **45** (9): 15-18.

James, N.E. and Mehrotra, A.K. 1988. V-L-S Multiphase Equilibrium in Bitumen-Diluent Systems. *Can J Chem Eng* **66** (5): 870-878.

Jha R.K., Kumar, M., Benson, I. et al. 2013. New Insights into Steam/Solvent-Coinjection-Process Mechanism. *SPE J.* **18** (5): 867-877.

Kariznovi, M. 2013. Phase Behaviour Study and Physical Properties Measurement for Athabasca Bitumen / Solvent Systems Applicable for Thermal and Hybrid Solvent Recovery Processes. Ph.D. Thesis. University of Calgary, Alberta, Canada.

Kariznovi, M., Nourozieh, H., and Abedi, J. 2010. Bitumen Characterization and Pseudo Components Determination for Equation of State Modeling. *Energy Fuels* **24** (1):624-633.

Keser, M.G. and Lee, B.I. 1976. Improved Prediction of Enthalpy of Fractions, *Hydrocarb Process*. **55**, 153-158.

Keshavarz, M., Okuno, R., and Babadagli, T. 2014. Optimal Application Conditions for Steam/Solvent Coinjection. *SPE Res Eng Eval* **18** (1):20-28.

Keshavarz, M., Okuno, R., and Babadagli, T. 2015. A Semi-Analytical Solution to Optimize Single-Component Solvent Coinjection with Steam during SAGD. *Fuel* **144**: 400-414.

Kumar, A. and Okuno, R. 2015. Direct Perturbation of the Peng-Robinson Attraction and Covolume Parameters for Reservoir Fluid Characterization. *Chem Eng Sci* **127**: 293-309.

Lake, L.W., Johns, R., Rossen, B., and Pope, G. 2014. Fundamentals of Enhanced Oil Recovery. Society of Petroleum Engineers, Richardson, Texas, USA.

Lee, B.I. and Kesler, M. G. 1975. A Generalized Thermodynamic Correlation Based on Three-Parameter Corresponding States. *AIChE J.* 21, 510-527.

Leibovici, C.F. 1993. A Consistent Procedure for the Estimation of Properties Associated to Lumped Systems. *Fluid Phase Equilib.* **87** (2): 189-197.

Lindeloff, N., Pedersen, K.S., Ronningsen, H.P. et al. 2004. The Corresponding States Viscosity Model Applied to Heavy Oil Systems. *J Can Petro Technol* **43** (9):47-53.

Lu, B.C.-Y, Chung, W.K., Adachi, Y. et al. 1986. Correlation and Prediction of Solubilities of Gases in Athabasca Bitumen. *AOSTRA J. Research*, **2** (3): 139-146.

Mehrotra, A.K. and Svrcek, W.Y. 1985a. Viscosity, Density and Gas Solubility Data for Oil Sand Bitumens. Part I: Athabasca Bitumen Saturated with CO and C_2H_6. *AOSTRA J. Res* **1** (4): 263-268.

Mehrotra, A.K. and Svrcek, W.Y. 1985b. Viscosity, Density and Gas Solubility Data for Oil Sand Bitumens. Part II: Peace River Bitumen Saturated with N_2, CO, CH_4, CO_2 and C_2H_6. *AOSTRA J. Res* **1** (4):269-279.

Mehrotra, A.K. and Svrcek, W.Y. 1985c. Viscosity, Density and Gas Solubility Data for Oil Sand Bitumens. Part III: Wabasca Bitumen Saturated with N_2, CO, CH_4, CO, and C_2H_6. *AOSTRA J. Res* **2** (2):83-93.

Mehrotra, A.K. and Svrcek, W.Y. 1988b. Properties of Cold Lake Bitumen Saturated with Pure Gases and Gas Mixtures. *Can J Chem Eng* 66 (4):656-665.

Mehrotra, A.K., Patience, G.S., and Svrcek, W.Y. 1989. Calculation of Gas Solubility in Wabasca Bitumen. *J Can Pet Technol* **28** (3):81-83.

Merotra, A.K. and Svrcek, W.Y. 1988a. Characterization of Athabasca Bitumen for Gas Solubility Calculations. *J Can Pet Technol* **27** (6):107-110.

Nasr, T.N. and Ayodele, O.R. 2006. New Hybrid Steam-Solvent Processes for the Recovery of Heavy Oil and Bitumen. Presented at Abu Dhabi International Petroleum Exhibition and Conference, Abu Dhabi, U.A.E., 5-8 Nov. SPE-101717-MS.

Nasr, T.N., Beaulieu, G., Golbeck, H, et al. 2003. Novel Expanding Solvent-SAGD Process "ES-SAGD". *J Can Pet Technol* **42** (1):13-16.

Nourozieh, H. 2013. Phase Partitioning and Thermo-physical Properties of Athabasca Bitumen / Solvent Mixtures. Ph.D. Thesis. University of Calgary, Alberta, Canada.

Okuno, R., Johns, R.T., and Sepehrnoori, K. 2010. A New Algorithm for Rachford-Rice for Multiphase Compositional Simulation. *SPE Journal* **15** (2): 313-325.

Peg, D.-Y. and Robinson, D.B. 1976. A New Two-Constant Equation of State. *Ind. Eng. Chem. Fund.* **15** (1): 59-64.

Peng, D.-Y. and Robinson, D.B. 1978. The Characterization of the Heptanes and Heavier Fractions for the GPA Peng-Robinson Programs. *GPA Research Report* RR-28.

Quiñones-Cisneros, S.E., Zéberg-Mikkelsen, C.K., Baylaucq, A. et al. 2004. Viscosity Modeling and Prediction of Reservoir Fluids: From Natural Gas to Heavy Oils. *Int. J. Therm.* **25** (5): 1353-1366.

Riai, M.R. and Daubert, T.E. 1987. Molecular Weight of Heavy Fractions from Viscosity. *Oil Gas J* **58** (2):110-113.

Svrcek, W.Y. and Mehrotra, A.K. 1982. Gas Solubility, Viscosity and Density Measurements for Athabasca Bitumen. *J Can Pet Technol* **21** (4):31-38.

Whitson, C.H. 1983. Characterizing Hydrocarbon Plus Fractions. *SPE J.* **23** (4): 683-694

Yazdani, A., Alvestad, J., Kjonsvik, D., et al. 2011. A Parametric Simulation Study for Solvent Co-injection Process in Bitumen Deposits. Presented at the Canadian Unconventional Resources Conference, Calgary, Alberta, Canada, 15-17 November. SPE-148804-MS.

Table 6-1. Data used in characterization, and regressed fb and fψ values for bitumens characterized. AARDs shown are for prediction of methane solubility at pressure and temperature points other than that used in characterization.

Bitumen	Data used in characterization				1-PC (PnA Characterization)			4-PC (PnA Characterization)			Conventional Characterization
	MW. (g/mol)	X_{CH4} (%)[*]	P_S (bars)	D_N at P_S (gram/CC)	f_b	f_ψ	AARD (%)	f_b	f_ψ	AARD (%)	AARD (Kariznovi et al. 2010) (%)
Athabasca	594.6	26.17	94.40	0.9510	0.1420	1.2494	11.05	0.1353	1.2196	9.24	7.95
Cold Lake	533.0	18.95	51.60	0.9384	0.1517	1.0046	5.72	0.1447	1.0329	7.22	3.74
Peace River	527.5	25.19	76.50	0.9660	0.1718	1.0637	11.08	0.1643	1.0797	11.75	10.14
Wabasca	446.6	28.33	93.50	0.9310	0.1688	1.0857	8.35	0.1651	1.1056	11.23	7.51
JACOS	530.0	27.00	81.00	0.9440	0.1573	1.0378	15.78	0.1502	1.0588	16.76	
Surmont	540.0	27.00	80.00	0.9410	0.1585	1.0228	7.58	0.1513	1.0473	7.33	

[*] Mole fraction of methane in methane saturated bitumen at 373.15 K and P_S shown. Temperature in case of Athabasca is 372.95 K.

Table 6-2. Summary of case studies results.
The AARDs for solubility data match for optimized BIPs are presented and compared with conventional characterization methods.

Bitumen	Gas	1-PC (PnA Characterization)		4-PC (PnA Characterization)		Conventional Characterization
		Optimized BIP	AARD (%)	Optimized BIP	AARD (%)	AARD (Kariznovi et al. 2010) (%)
Athabasca (Svrcek and Mehrotra 1982, Mehrotra and Svrcek 1985a)						
	N_2	0.078	11.51	0.079	11.50	10.57
	CO_2	0.088	5.60	0.088	5.60	9.34
	C_2H_6	0.012	4.78	0.013	4.82	5.52
Cold Lake (Mehrotra and Svrcek 1988b)						
	N_2	0.175	6.00	0.175	5.94	5.62
	CO_2	0.096	4.34	0.096	4.30	8.89
	C_2H_6	0.031	7.50	0.032	7.35	7.64
Peace River (Mehrotra and Svrcek 1985b)						
	N_2	0.068	11.78	0.068	11.79	14.40
	CO_2	0.098	7.89	0.098	7.89	8.77
	C_2H_6	0.050	8.68	0.050	8.62	9.47
Wabasca (Mehrotra and Svrcek 1985c)						
	N_2	0.230	16.03	0.000	16.93	19.91
	CO_2	0.094	6.91	0.084	6.90	8.88
	C_2H_6	0.028	6.65	0.028	6.55	6.56
JACOS (Nourozieh 2013)						
	C_2H_6	0.010	9.83	0.010	9.84	
Surmont (Kariznovi 2013, Nourozieh 2013)						
	C_2H_6	0.000	6.94	0.000	7.31	
	C_3H_8	0.066	6.83	0.063	6.52	
	C_4H_{10}	0.076	8.74	0.076	7.77	

Table 6-3: Molecular weights, T_C, P_C, and ω for pseudo components from the proposed characterization for JACOS bitumen

Bitumen as single pseudo component				
Pseudo Component	MW	T_C (K)	P_C (bars)	ω
1-PC	530.00	847.17	10.64	1.0406

Bitumen split into four pseudo components with equal mass fractions					
Pseudo Components	Mole Fraction	MW	T_C (K)	P_C (bars)	ω
4-PC-1	0.4001	331.77	775.08	14.36	0.81599
4-PC-2	0.2616	507.44	859.24	11.05	1.03422
4-PC-3	0.1995	665.41	905.82	9.27	1.16443
4-PC-4	0.1388	956.63	946.51	7.16	1.32306

Bitumen split into four pseudo components with different mass fractions					
Pseudo Components	Mole Fraction	MW	T_C (K)	P_C (bars)	ω
4-PC-1	0.1189	222.88	686.53	18.07	0.59623
4-PC-2	0.0868	305.20	751.60	15.01	0.76675
4-PC-3	0.0751	353.73	781.52	13.73	0.84498
4-PC-4	0.7192	626.41	887.27	9.58	1.13115

Table 6-4. Reservoir and fluid properties used in recovery simulation of JACOS bitumen.

Properties	Values
Porosity	33%
Horizontal permeability	4000 md
Vertical permeability	3000 md
Initial reservoir pressure at depth of 500 m	1500 kPa
Initial reservoir temperature	13°C
Initial oil saturation	0.75
Initial water saturation	0.25
Three-phase relative permeability model (CMG 2012)	Stone's model II
Formation compressibility	1.8E-5 1/kPa
Rock heat capacity (Butler 1997)	2600 kJ/m^3 °C
Rock thermal conductivity (Butler 1997)	660 kJ/m day °C
Over/underburden heat capacity (Butler 1997)	2600 kJ/m^3 °C
Over/underburden thermal conductivity (Butler 1997)	660 kJ/m day °C
Bitumen thermal conductivity (Butler 1997)	11.5 kJ/m day °C
Gas thermal conductivity (Yazdani et al. 2011)	2.89 kJ/m day °C
Water thermal conductivity	1500 kJ/m day °C
Bitumen molecular weight	530 kg/kg-mole
Bitumen specific gravity	1.077
Injector bottom-hole pressure (maximum)	3500 kPa
Producer bottom-hole pressure (minimum)	1500 kPa
Producer steam flow rate (maximum)	1 m^3/Day
Steam quality	0.9
Temperature of injected steam	242.71°C
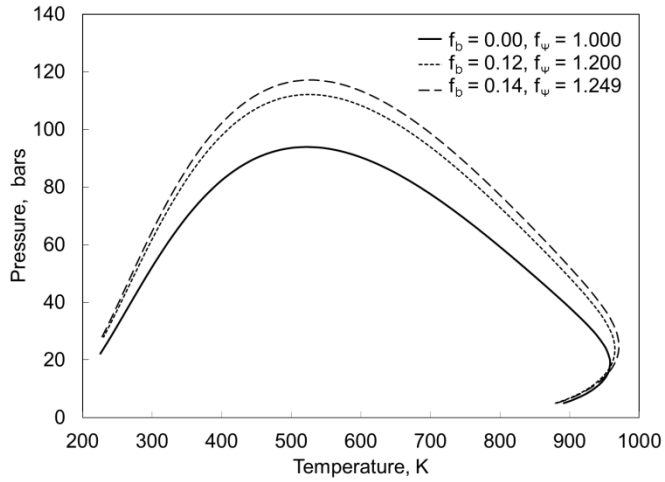
Figure 6-1. Systematic development of phase envelope for a sample mixture of bitumen and methane during regression algorithm.
The phase envelope expands with increasing f_b and f_Ψ values.
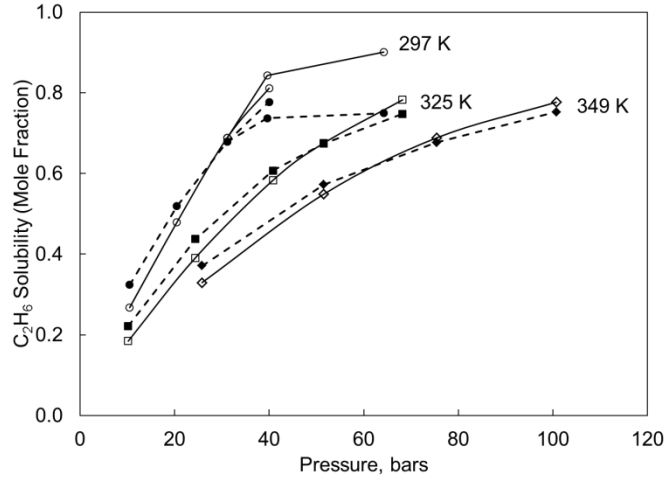
(a)
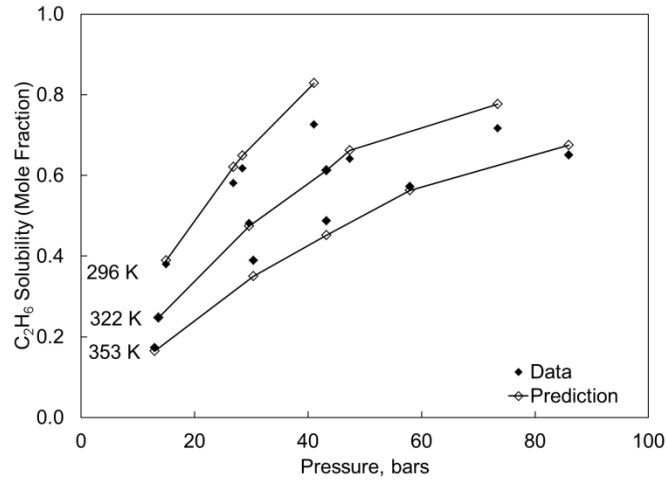
(b)

Figure 6-2. Comparison of the data and predictions for ethane solubilities for (a) Cold Lake and (b) Athabasca bitumens. For Cold Lake bitumen, solid curves show the predictions and dashed curves show the data.
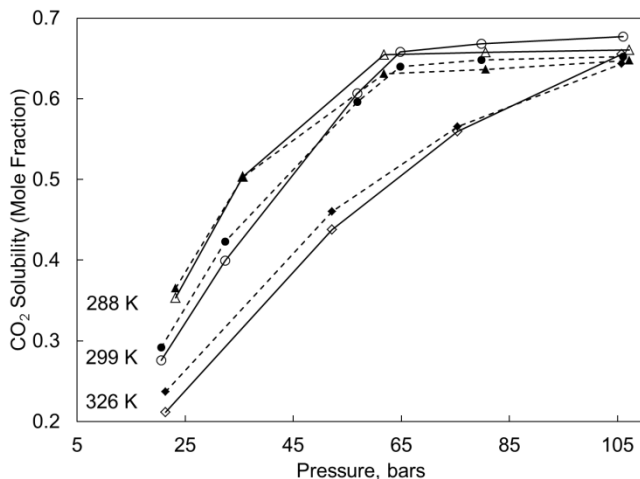
Figure 6-3. Comparison of matched solubility with data for CO_2 in Cold Lake bitumen.
The solid lines present the predictions and dotted lines are for data. Solubilities at two temperatures 288 and 299 K are nearly constant at pressure greater than 65 bars. It is also observed that the solubility at 288 K is lower than that at 299 K for pressure greater than 65 bars.
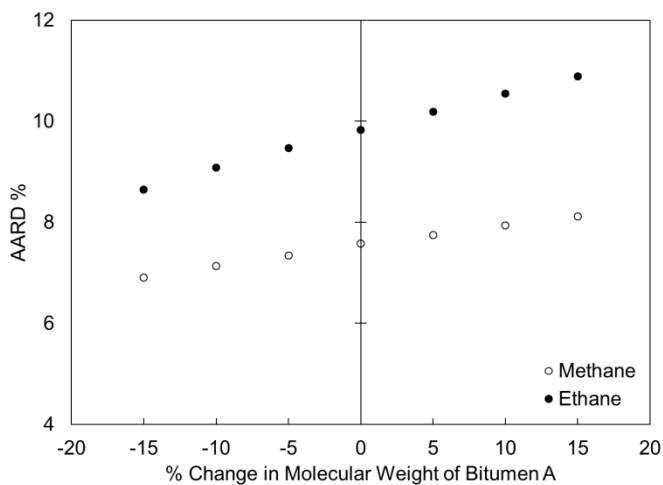
Figure 6-4. AARDs for methane and ethane solubilities in JACOS bitumen with different MWs used in the PnA algorithm.
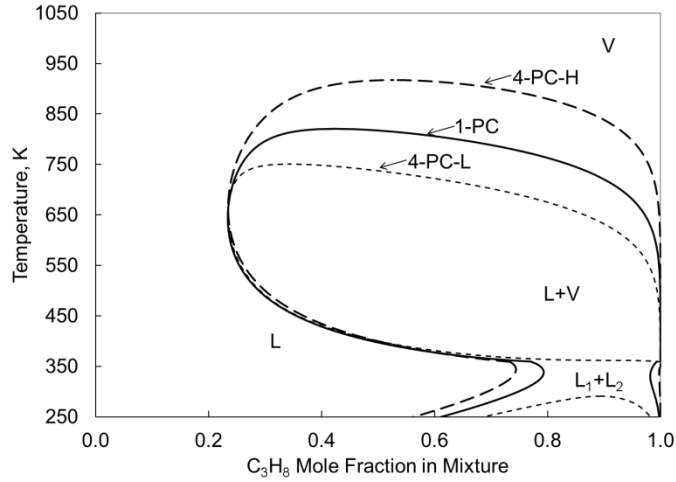
(a)
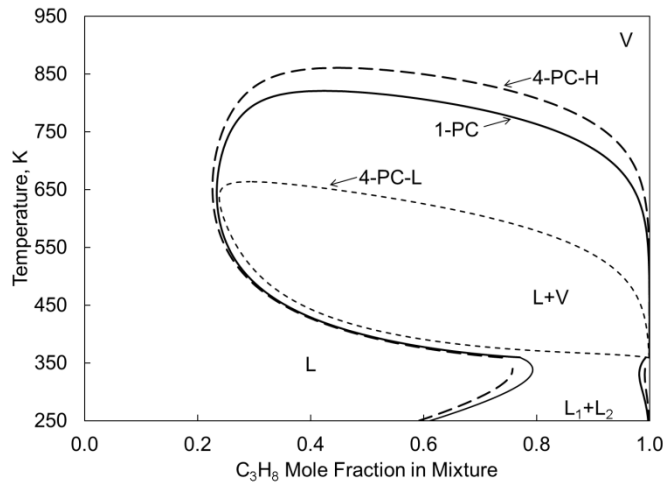
(b)

Figure 6-5. Comparison of T-x diagrams at 35.0 bars for bitumen and propane mixture for two different compositional characterizations of JACOS bitumen.

Figure (a) uses same mass fractions (0.25) for all pseudocomponents, and figure (b) uses different mass fractions (0.05 for 4-PC-L and 0.85 for 4-PC-H). The envelope shown by solid curve is for 1-PC, and dotted curves are for the 4-PC-L and 4-PC-H. The T-x diagram is generated for binary mixture of propane and pseudocomponent (1-PC, 4-PC-L, and 4-PC-H) of bitumen. The T-x diagram for 4-PC-1 is more separated from T-x diagram for others (1-PC and 4-PC-4) in figure (b) than that in figure (a).

210
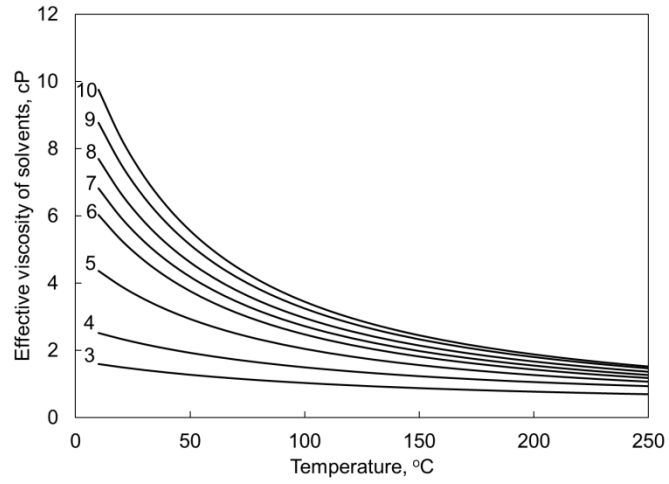
Figure 6-6. Effective viscosity of solvents calculated at pressure 35.0 bars for solvent and JACOS bitumen mixture.
Numbers on curves show the carbon number of normal alkane solvents.
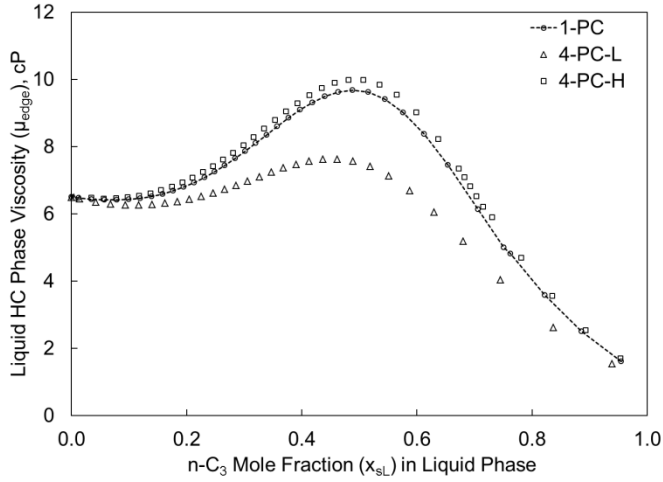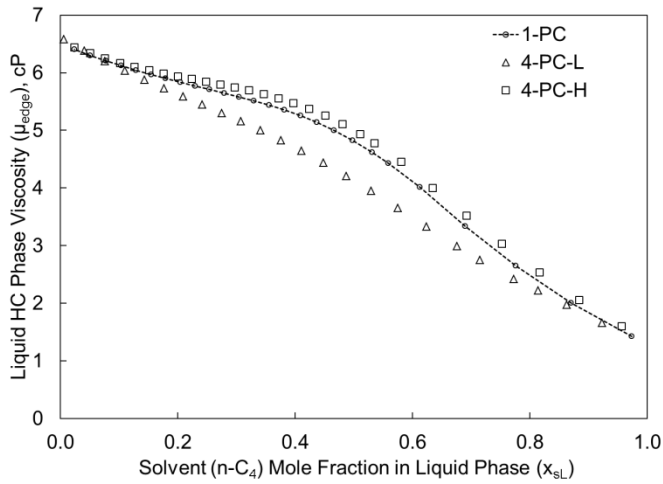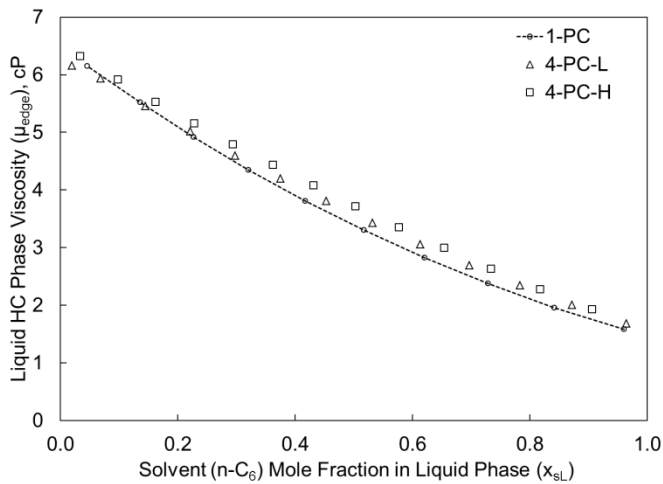
Figure 6-7. Estimated trends for the L-phase viscosity at the chamber-edge conditions (μ_{edge}) with respect to the solvent mole fraction in the L-phase (x_{sL}).

Figures (a), (b), and (c) are for propane-steam coinjection, butane-steam coinjection, and hexane-steam coinjection respectively.
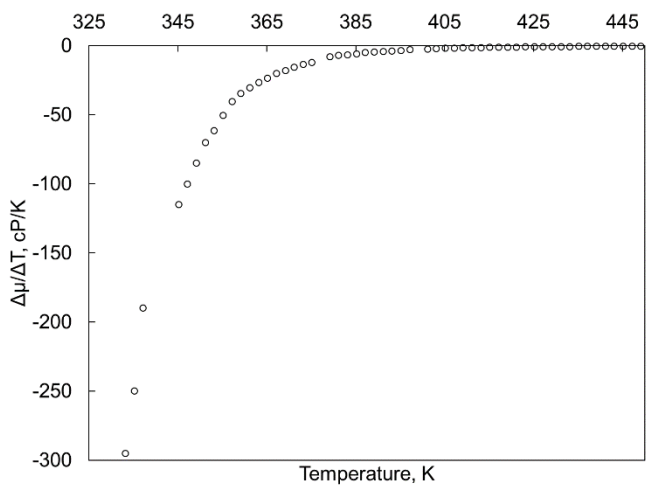
Figure 6-8. Trend of viscosity gradient ($\Delta\mu/\Delta T$) with temperature for JACOS bitumen.
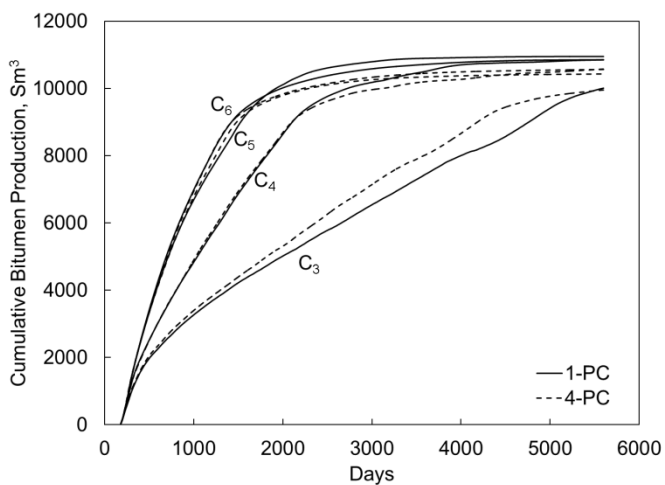
Figure 6-9. Simulated bitumen recovery with steam-solvent coinjection method for different solvent cases (n-C_3, n-C_4, n-C_5, and n-C_6).
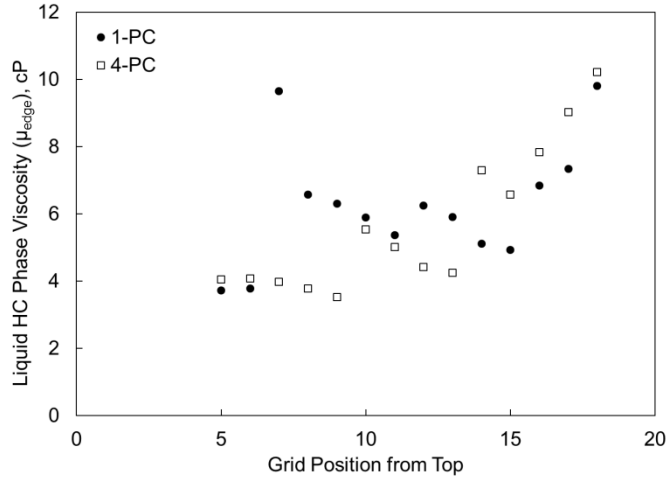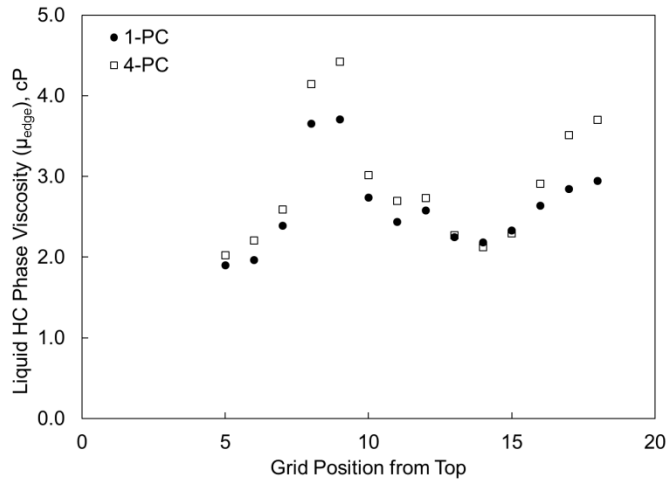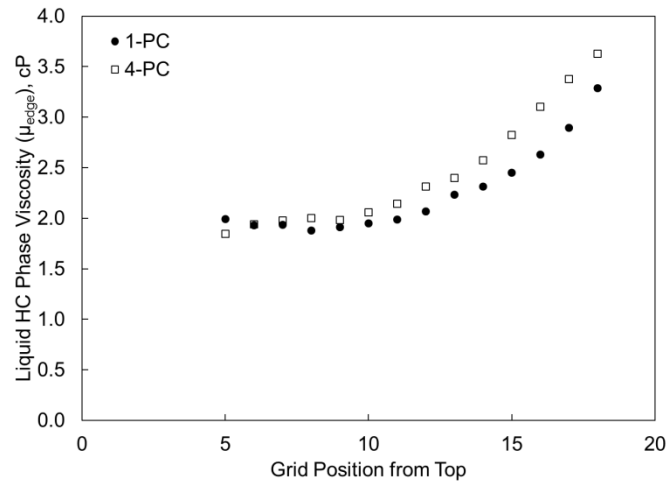
Figure 6-10. L-phase viscosity along the chamber edge from the simulation results: (a) propane-steam coinjection, (b) butane-steam coinjection, and (c) hexane-steam coinjection.
The number on the horizontal axis shows the grid's location from the reservoir top.

Chapter 7: A New Algorithm for Multiphase Fluid Characterization for Solvent Injection

A version of this has been submitted to SPE J for publication. The manuscript is under review.

7.1. Introduction

Solvent injection has been successfully implemented for enhanced oil recovery; e.g., in the Western United States (Mizenko 1992; Stein et al. 1992; Tanner et al. 1992; Fulco, G. J. 1999; McGuire et al. 2001), Canada (Malik and Islam 2000), and the North Sea (Varotsis et el. 1986). Field pilot tests were also reported for coinjection of solvent with steam for bitumen recovery in Canada (Gupta et al. 2005; Gupta and Gittins 2006; Dickson et al. 2011).

Solvent injection can involve complex phase behavior, which consists of three hydrocarbon phases, the oleic (L_1), gaseous (V), and solvent-rich liquid (L_2) phases. Such phase behavior has been reported for various mixtures in the literature. For binary mixtures, CO_2, methane, ethane, and propane were studied as the solvent component mixed with a heavier n-alkane component (Rodrigues and Kohn 1967; Kulkarni et al. 1974; Hottovy et al. 1981a; Enick et al. 1985; Fall and Luks 1985; Fall et al. 1985; Estrera and Luks 1987; Peters et al. 1987a, 1987b; Peters et al. 1989; Van der Steen et al. 1989; Secuianu et al. 2007). Ternary mixtures were studied by Horn and Kobayashi (1967), Hottovy et al. (1981b), Hottovy et al. (1982), Llave et al. (1986), Jangkamolkulchal and Luks (1989), and Gregorowicz et al. (1993a, 1993b). Mixtures of solvents with reservoir oils were also studied by various researchers (Shelton and Yarborough 1977; Henry and Metcalfe 1983; Turek et al. 1988; Roper 1989; Sharma et al. 1989; Okuyiga 1992; Creek and Sheffield 1993; DeRuiter et al. 1994; Mohanty et al. 1995; Godbole et al. 1995).

Three-hydrocarbon-phase behavior was characterized by use of a cubic equation of state (EOS) for specific solvent-injection cases (Nghiem and Li 1986; Sharma et al. 1989; Negahban and Kremesec 1989; Okuyiga 1992; Khan et al. 1992; Creek and Sheffield 1993; Reid 1994; Mohanty et al. 1995; Godbole et al. 1995; Guler et al. 2001; Aghbash and Ahmadi 2012). The EOSs used by them include the Peng-Robinson (PR) EOS (Peng and Robinson 1976, 1978) and the Soave-Redlich-Kwong EOS (Soave 1972). Their results indicate that these EOSs are capable of correlating three-hydrocarbon-phase behavior quantitatively. However, their characterization procedures were specific to the fluids studied. No systematic knowledge has been presented of how three-hydrocarbon-phase behavior can be reliably characterized for solvent injection (Okuno and Xu 2014)

This paper presents a new algorithm for characterization of multiphase behavior with the PR EOS. The term "multiphase behavior" in this paper refers to volumetric and compositional behavior of equilibrium phases consisting of at most three hydrocarbon phases. Hence, the algorithm accommodates the traditional vapor-liquid phase behavior as a subset of the research scope. The next section describes the algorithm developed. Then, case studies are presented for 90 reservoir fluids, for which experimental data are available in the literature.

7.2. Multiphase Fluid Characterization

Fluid characterization consists of three major steps: (i) compositional characterization of the plus fraction; (ii) initial estimates for components' properties, such as critical temperature (T_C), critical

pressure (P_C), and acentric factor (ω); and (iii) regression to the PVT data available. The current research uses the method of Quiñones-Cisneros et al. (2004) for step i.

Steps ii and iii broadly follow the methodology of Kumar and Okuno (2013), which is referred to as perturbation from n-alkanes (PnA). In the PnA method, step ii assumes that pseudocomponents are n-alkanes; that is, they are assigned T_C, P_C, and ω of equivalent n-alkanes in terms of carbon number (CN). This assumption is based on well-defined thermo physical properties of three important hydrocarbon groups i.e. paraffins, napthenes, and aromatics present in pseudocomponents. For same carbon number, paraffins have lowest T_C and P_C, and highest acentric factor among these three groups. **Figure 7-1** presents the comparison of critical parameters and resulting vapor pressure curves for hexadecane (n-C_{16}) and pyrene ($C_{16}H_{10}$). Vapor pressure curve for pyrene is below the vapor pressure curve for n-C_{16} and extended to higher T_C and P_C in P-T space. As a result, among the P-T envelopes for mixtures of same carbon number paraffin, napthene, and aromatic component with a given light component, paraffin's P-T envelope is innermost. This is shown in **Figure 7-2,** which presents the P-T envelopes for 99.99% binary mixture of methane with nonane (n-C_9), propyl cyclo hexane (C_9H_{18}), and 2-propyl benzene (C_9H_{12}). The P-T envelope for n-C_9 is inside the P-T envelopes for C_9H_{18} and C_9H_{12}. The analysis presented here supports assumption that lower limits for T_C and P_C for pseudocomponents are determined by its n-alkane equivalent values in fluid characterization. Then, step iii systematically adjusts the properties of all pseudocomponents in the direction of increasing aromaticity from n-alkanes (i.e., zero aromaticity). In the initial stage of this research, the validity of this methodology for three phases was confirmed with the data for ternary mixtures of methane, ethane, and tetradecylbenzene ($C_{20}H_{34}$) given in Jangkamolkulchal and Luks (1989).

In step ii of Kumar and Okuno (2013, 2015), the n-alkane properties were taken from Kumar and Okuno (2012), in which T_C, P_C, and ω of n-alkanes were optimized for the PR EOS to accurately predict vapor pressure and liquid density. Hence, the PR EOS was initially calibrated with vapor pressure and liquid density of n-alkanes prior to characterizing reservoir fluid. For the current research, however, step ii requires that the PR EOS be calibrated with binary three-phase behavior. To this end, binary interaction parameters (BIPs) have been optimized for the PR EOS to represent binary three-phase data taken from the literature, such as those for CO_2, methane, ethane, and propane with heavier n-alkanes. The three-phase data mainly included upper critical end point (UCEP) for binary mixtures. At UCEP, solvent rich liquid phase becomes critical with the vapor phase in presence of oil rich liquid phase. The UCEP for binary mixtures of CO_2, methane, ethane, and propane with heavier n-alkanes were matched adjusting only BIP; physical critical parameters for components not changed. **Appendix A** presents the details of optimization process and development of correlations for BIPs**. Appendix B** presents the predictive capability of optimized BIPs for three-phase prediction for binary mixtures of CO_2, methane, ethane, and propane with heavier n-alkanes.

It was observed that UCEP match for pairs like ethane and n-C_{18} could not be achieved by BIP adjustment when physical critical parameters for n-C_{18} was replaced with its optimized critical

217

parameters (Kumar and Okuno 2012). **Figure 7-3** shows the predicted temperatures at UCEP at different BIPs for ethane and n-C_{18} pair**.** The UCEP for this binary mixture is 312.45 K and 55.31 bars (Peters et al. 1986). The best match that could be achieved with BIP adjustment was 307.03 K and 50.21 bars at BIP of 0.01. **Figure 7-4** shows the trend of reduced Gibbs free energy for ethane and n-C_{18} mixture at UCEP temperature and pressure. The dotted curve is prediction with physical critical parameters for n-C_{18} and optimized BIP (that matched UCEP); this curve is taken as reference. Solid curves are for optimized critical parameters (Kumar and Okuno 2012) for n-C_{18} and different BIPs (shown on the curves). Optimized critical parameters could not match the desired trend of reduced Gibbs free energy for UCEP match i.e. the trend of reference curve. Hence, the BIP was optimized by using physical critical parameters from Gao et al. (2001) correlations (**Equation 7-1** and **7-2).**

$$T_{CP} = \left[6573.87 - 4680.77\exp\left(-0.1831(CN^{0.6667} - 2.08)\right)\right]^{\frac{1}{1.276}} \tag{7-1}$$

$$P_{CP} = 42.44\exp\left[-0.3757(CN^{0.5684} - 1.8672)\right], \tag{7-2}$$

for n-alkanes (or paraffins) heavier than hexane. Gao et al. (2001) also presented a correlation for ω for n-alkanes (**Equation 7-3),**

$$\omega_P = \left[3.212102 - 2.937628\exp\left(-0.04699(CN^{0.6667} - 2.08)\right)\right]^{\frac{1}{0.6851}} \tag{7-3}$$

As discussed in Appendix A, however, the correlation presented in **Equation 7-4** has been found to perform better for the BIP optimization in this research. The deviation of Equation 7-4 from Equation 7-3 is minor as presented in Appendix A (see **Figure 7-A3**).

$$\dot{\omega}_P = 0.217066 + 5.27405CN^{-\left(\frac{14.8147}{CN}\right)}. \tag{7-4}$$

Equations 7-1 and 7-2 are used for the initialization of pseudocomponents in step ii. The initial values for ω are all zero for pseudocomponents.

A comparative study is done on the predictive capability of two sets of EOS parameters (1) optimized BIP and physical critical parameters (Gao et al. 2001), (2) zero BIP and optimized critical parameters (Kumar and Okuno 2012). Predicted pressure-composition (P-x) diagrams for binary and quaternary mixture of n-alkanes from these two sets of EOS parameters are compared with experimental data. **Figures 7-5 and 7-6** present comparison for P-x diagrams for ethane with n-C_{16} at 363.15 K and with n-C_{24} at 340 K respectively. **Figure 7-7** presents similar comparison for hexane mixture with n-C_{36} at 621.8 K, however, due to unavailability of any optimized BIP for n-C_6-n-C_{36} pair, BIP is kept zero for first set of EOS parameter also. **Figure 7-8** presents comparison of predicted P-T phase envelopes for quaternary mixture of n-alkanes with data. Though first set of EOS parameter satisfactorily matched the P-x diagrams in Figure 7-5 and 7-6, its predictions in Figure 7-7 and 7-8 deviated from data significantly. Attempts were made to improve these predictions by adjusting BIPs. However, such attempts did not show significant improvement. It is observed that BIPs (with physical critical parameters) have limited potential to improve two-phase behavior by their adjustment, whereas

optimized critical parameters (with zero BIPs) have shown consistently better two-phase predictions. This indicates that critical parameter adjustment is important for two-phase behavior; however, three-phase behavior is sensitive to BIPs. In this research, use of optimized BIPs whereas ensures reliable three-phase behavior, critical parameter adjustment ensures reliable two-phase behavior. However, such observations are limited to two-parameter EOS like PR EOS.

In step iii, the properties for all pseudocomponents are systematically perturbed from the initial values until the saturation pressure at the reservoir temperature is matched. They are perturbed monotonically in the increasing direction. The monotonic, systematic increases of T_C, P_C, and ω require certain trends with respect to CN. For this purpose, higher values have been empirically determined for T_C, P_C, and ω for a non-zero aromaticity as presented in **Equations 7-5**, **7-6**, and **7-7.**

$$T_{CH} = 5339.14 - 4850.41\exp^{(-0.001650727669CN^{1.4223})} \tag{7-5}$$

$$P_{CH} = 48.0823 - 21.7852\exp^{(-11.372937CN^{-1.326532})} \tag{7-6}$$

$$\omega_H = 0.026547(0.985567^{CN})(CN^{1.295419}). \tag{7-7}$$

These correlations are determined on the basis of phase behavior data for a wide range of fluid types, such as gas condensate, volatile oil, and heavy oil, in order to cover a wide CN range. The data used include constant volume depletion (CVD), slim-tube minimum miscibility pressure (MMP), and swelling test. Equations 7-5 to 7-7 are empirical within this research, although they have been confirmed quantitatively reasonable by comparing with measured T_C, P_C, and ω for aromatics given in Yaws (2010) and Nikitin and Popov (2015) as shown in **Figure 7-9 and 7-10**.

BIPs are not adjusted in step iii. As given in Appendix A, correlations presented in **Equations 7-8** to **7-11** have been developed for BIPs for CO_2, methane, ethane, and propane:

$$K_{CO_2} = (-24.7255 + 0.1412CN^{2.7213})/(663.288 + CN^{2.7213}) \tag{7-8}$$

$$K_{methane} = 0.0428 + 0.0009CN \tag{7-9}$$

$$K_{ethane} = 0.0405 + 0.00011CN \tag{7-10}$$

$$K_{propane} = 0.07419 - 0.04326\exp^{(-0.00013754CN^{2.518052})}, \tag{7-11}$$

for CN > 6. Extrapolation of the BIPs for methane, ethane, and propane has yielded the following correlations (**Equations 7-12** and **7-13**) for butane and pentane:

$$K_{butane} = 0.11\left(0.000133426^{\frac{1.0}{CN}}\right)CN^{-0.0324628} \tag{7-12}$$

$$K_{pentane} = 0.13\exp^{(-\frac{15.5385}{CN})}. \tag{7-13}$$

The developed algorithm is presented below.

Step 1. Compositional characterization

> The plus fraction for the fluid of interest is split into the user-specified number (n) of pseudocomponents with a chi-squared distribution (Quiñones-Cisneros et al. 2004).

Step 2. Deviation in saturation pressure

The initial deviation in saturation pressure is calculated as the ratio of the measured saturation pressure (P_S) to the calculated saturation pressure (P_{S_EOS}) by use of the PR EOS with equations 7-1, 7-2, and 7-4. The ratio is denoted as β.

Step 3. Incremental values for T_C, P_C, and ω

Incremental values for T_C, P_C, and ω during the regression are determined using **Equations 7-14, 7-15,** and **7-16** respectively.

$$\Delta T_{C,i} = [T_{CH,i} - T_{CP,i}]/(\beta N) \tag{7-14}$$

$$\Delta P_{C,i} = [P_{CH,i} - P_{CP,i}]/N \tag{7-15}$$

$$\Delta \omega_i = \omega_{H,i}/N, \tag{7-16}$$

for i = 1, 2, …, n, where N is an integer to be specified by the user (e.g., $N = 10^4$ as used in this research). Set the iteration-step index k to be one.

Step 4. Update of T_C, P_C, and ω using **Equations 7-17**, **7-18**, and **7-19** respectively.

$$T_{C,i} = T_{CP,i} + k\Delta T_{C,i} \tag{7-17}$$

$$P_{C,i} = P_{CP,i} + k\Delta P_{C,i} \tag{7-18}$$

$$\omega_i = k\Delta\omega_i \tag{7-19}$$

Step 5. Convergence test

Calculate $\delta = (P_S - P_{S\_EOS})/P_S$. Go to step 6 if $|\delta| < \delta_{TOL}$ (e.g., $\delta_{TOL} = 10^{-4}$). Otherwise, go to step 4 after increasing k by one; k = k + 1.

Step 6. Volume shift

Volume shift parameters are adjusted to match liquid density data, as required.

Critical parameters and acentric factors are perturbed as monotonic functions of the iteration-step index, k. It has been consistently observed in this research that the calculated P_S increases with increasing k during the iteration. **Figure 7-11a** depicts that vapor pressure curves for all pseudocomponents change systematically and monotonically as the iteration proceeds for an example case of light oil. **Figure 7-11b** shows the two-phase envelopes corresponding to the three sets of vapor pressure curves given in Figure 7-11a. **Figure 7-11c** shows the monotonic change in saturation pressure with iteration parameter (k).

Volume shift is performed to match liquid density data only after the model is set in terms of compositional phase behavior. This is because a change in compositional behavior prediction affects volumetric predictions, as discussed in detail in Kumar and Okuno (2013). For fluid characterization with a PnA-based approach, density data for a liquid phase that is equilibrium with the V phase are more important than those from a single-phase fluid or equilibrium V phase (Kumar and Okuno 2015). This was confirmed also in this research. Hence, it is recommended that step 6 use density data from an equilibrium liquid phase.

7.3. Case Studies

The algorithm is applied to 90 reservoir fluids in this section, which are gas condensates, volatile oils, heavy oils, and bitumens. The fluids tested are characterized as 12 components, which consist of N_2, CO_2, C_1, C_2, C_3, C_4, C_5, C_6, and four pseudocomponents, by use of the PR EOS with the van der Waals mixing rules. The regression algorithm uses only P_S and saturated liquid density data, as shown in the previous section. The EOS models for the 90 fluids developed with new algorithm are listed in **Appendix 7-C**. For each fluid, two separate tables are presented, one contains composition, molecular weight, T_C, P_C, ω, volume shift parameters for components, and other table contains the BIP matrix.

T_C, P_C, and ω for well-defined pure components are taken from Yaws (2010), and they are not adjusted. **Table 7-1** gives the BIPs used in this section. Note that BIPs are not adjusted in the regression algorithm developed. However, it is possible to adjust them individually when specific data are to be matched. T_C, P_C, and ω for pseudocomponents are adjusted to match P_S. Volume shift parameters are adjusted to match saturated liquid density data at the final step of the algorithm. Then, the quality of prediction from the resulting EOS model is demonstrated with other types of data, such as three hydrocarbon phases, CVD, constant mass expansion (CME), and MMP for V-L.

7.3.1. L-V Phase Behavior

This subsection shows results for two-phase predictions. **Table 7-2** lists 55 light fluids for which CVD and CME data are available in the literature. In the table, fluids 1 to 48 are gas condensates and the others are volatile oils. The fifth, sixth and seventh columns show the value of β, the number of iterations (i.e., k in the previous section) and the degree of freedom in the chi-squired distribution, respectively. The eighth column indicates CVD data as data type 1 and CME as data type 2. This column also indicates the limiting value from measured data. The right-most column gives the average absolute deviation (AAD) for the data type indicated for each fluid.

Before performing step 6, the AAD for saturated liquid densities for all the fluids in Table 7-2 was less than 2%, indicating the accuracy of the PR EOS for light fluids. They were eventually matched in step 6.

The results given in Table 7-2 show that the new algorithm is capable of predicting CVD and CME liquid saturations well. The deviation tends to be high for near-critical fluids (No. 6, 7, 8, 12, 13, 14, 36, 38, 48, 51, and 54). This is because liquid saturation is sensitive to pressure near saturation pressure for those fluids. The AADs for 42 CVD and 13 CME liquid saturation predictions are 1.5 and 2.5% respectively. **Figure 7-12** shows the CME liquid saturation for Fluid 36, which gives the highest AAD in Table 7-2. Fluid 54 is also a near-critical fluid. However, **Figure 7-13** shows satisfactory predictions of CVD liquid saturations for this near-critical fluid. Pedersen and Christensen (2007) presents an SRK EOS model (Pedersen and Christensen 2007) with 6 pseudocomponents model that was developed to match the CVD and saturation pressure data. A comparison of predicted P-x diagram at 424.25 K with this EOS model (injection gas: 0.005 N_2, 0.050 CO_2, 0.582 CH_4, 0.171 C_2H_6, 0.120 C_3H_8, 0.050 C_4H_{10}, 0.017 C_5H_{12}, and 0.005 C_6H_{14}) shows good match with that predicted with the new algorithm. The MMPs

predicted at 424.25 K are 251.32 bars and 245.71 bars respectively for the new algorithm and SRK EOS model. This comparison further validates the reliability of new algorithm for phase behavior predictions at P-T-x conditions different from data used in characterization.

Table 7-3 shows reservoir oils for which MMP data from slim-tube tests are available in the literature. MMP prediction serves as a severe test for fluid characterization since it requires accurate prediction of compositional phase behavior away from the original oil composition in multicomponent composition space. Thermodynamic MMPs are calculated with the method of characteristics within PVTsim (Calsep 2012), and compared with data. The calculated MMPs likely correspond to the V-L miscibility, considering their reservoir temperatures and that PVTsim did not indicate any difficulty associated with three phases in the calculations. The average absolute relative deviation (AARD) for all 26 MMP predictions is 4.57%. Some level of deviation of thermodynamic MMP from slim-tube MMP is inevitable due to the presence of dispersion in real displacement of oil by gas. However, the present algorithm shows improved MMP predictions, as the AARDs with earlier characterizations were 6.7% (Kumar and Okuno 2013) and 6.4% (Kumar and Okuno 2015).

The algorithm was also tested in terms of other types of phase behavior. Table 7-4 lists heavy oils for which swelling test data, GOR, and V-L boundary in P-T space are available in the literature. Oil 1 in Table 7-4 is West Sak oil (Sharma 1990), for which the AARD in GOR prediction is 7%.

Swelling test data are available for Oil 2 with a gas mixture of 14% CO_2, 17% methane, 60% ethane, 4% propane, 3% butane, and 2% pentane (Krejbjerg and Pedersen 2006). The saturation pressures for different gas-oil mixing ratios were predicted satisfactorily as shown in Figure 7-14. The AARD for the predictions is 3.4%. Pedersen et al. (2004) showed GOR data for Oil 3, for which the PR-EOS model with the current characterization algorithm gives an AARD of 4.42%. As shown in Figure 7-15, the GOR predictions are in good agreement with the data.

PVT data for Lloydminster heavy oil were presented in Li et al. (2013a) (oil 4 in Table 7-4). The dead oil composition was characterized with four pseudocomponents on the basis of the chi-squired distribution with a degree of freedom of 9. The saturation pressure of 56.64 bars at 347.67 K for feed #5 (31.7% CO_2, 34.3% butane, and 0.34% heavy oil) was used for characterization with the new algorithm. The characterized oil was then used to predict the saturation pressure for feed #4 (38.6% CO_2, 36.2% propane, and 25.2% heavy oil). Figure 7-16 shows that the predictions are close to the reported data, yielding an AARD of 5.60% for the seven data points.

7.3.2. L-L-V Phase Behavior

In this subsection, the new algorithm is tested by comparing three-phase behavior predictions with experimental data. Note that the algorithm matches only P_S at the oil composition as far as compositional phase behavior is concerned; that is, no parameter is adjusted for matching three-phase data for oil/solvent mixtures to be presented here.

Apart from the three-phase predictions for fluids with PR EOS model developed with the new algorithm and optimized BIP, this subsection, also present predictions when fluids are characterized

with the new algorithm but with zero hydrocarbon-hydrocarbon BIPs. In this case, all hydrocarbon-hydrocarbon BIPs are set to zero, and the BIP of CO_2 with pseudocomponents are set to 0.1 (Peng and Robinson 1978). No other change in the BIP matrix shown in Table 7-1 is made. Predictions with zero BIP case in the figures are shown as "Prediction with zero BIP". The objective of this additional demonstration is to show the importance of non-zero optimized BIPs for reliable three-phase predictions.

Three-phase data are available for oils 1, 4, 5, and 6 from Table 7-4. Three phases were reported for the mixture of 20% oil 1 and 80% CO_2 at 299.81 K. **Figure 7-17** compares predicted saturations for the L_1 (Figure 7-17a) and L_2 (Figure 7-7b) phases with experimental data. The AARD for the L_1-phase saturations is 5.61%. With the new algorithm, the PR EOS correctly predicts the presence of three phases for this mixture; i.e., they were experimentally observed between 77.20 and 83.75 bars, and predicted between 76.46 and 82.47 bars. Similar prediction with zero hydrocarbon-hydrocarbon BIPs shows the presence of three-phases in comparatively small pressure range (79.21- 83.0 bars). Figure 7-17b also shows the three-phase prediction from Aghbash and Ahmadi (2012) EOS model. Ranges of pressure for three-phase predicted from new algorithm and Aghbash and Ahmadi are nearly same. A comparison of P-x diagrams at 370 K with equimolar mixture of methane, ethane, propane, and butane as injection gas predicted with EOS models from new algorithm and that from Aghbash and Ahmadi (2012) is presented in **Figure 7-18.** The two models show significantly different predictions for P-x diagrams. The possible reason for this difference is non-zero BIPs used for pseudocomponent-pseudocomponent pairs by Aghabsh and Ahmadi; these BIPs are zero for the new algorithm. The MMPs with this injection gas at 370 K are 72.77 bars, and 68.66 bars respectively for the new algorithm and Aghbash and Ahmadi. Although, MMP predictions which depend on the composition paths, are nearly same, significantly different P-x diagrams indicate to careful use of non-zero BIPs for pseudocomponent – pseudocomponent pairs.

Figure 7-19 shows the comparison of predicted P-T diagram with SRK EOS from Krejbjerg and Pedersen (2006) with the prediction from new algorithm for oil 2 in Table 7-4. Both the predictions match significantly except for high temperature two-phase envelope. **Figure 7-20** shows phase boundaries between two and three phases in P-T space for feeds 14 (Figure 7-20a) and 15 (Figure 7-20b) with oil 4 in Table 7-4. Feed 14 is 23.6% propane, 67.2% CO_2, and 9.2% oil, and feed 15 is 11.8% butane, 83.2% CO_2, and 5.0% oil. The results show that the PR-EOS models with the new characterization algorithm give satisfactory predictions for these complex mixtures. This also validates the reliability of the BIP correlation (equation 7-12) for butane, which was developed by extrapolation of BIP values for methane, ethane, and propane. However, the predictions with zero hydrocarbon-hydrocarbon BIPs show narrow three-phase area close to LL-LLV boundary.

Oil 5 given in Table 7-4 is Athabasca bitumen, for which Badamchi-Zadeh et al. (2009) presented three-phase data. The dead-oil composition was characterized with four pseudocomponents on the basis of the chi-squired distribution with a degree of freedom of 12. The algorithm was applied with the saturation pressure, 10.82 bars, reported for a mixture of 59.3% bitumen with 40.7% propane at 333.15

K. The resulting fluid model was then used to predict three-phase behavior for the mixture of 51.0% CO_2, 34.7% propane, and 14.3% bitumen. **Figure 7-21** shows satisfactory predictions of phase boundaries in spite of the large amount of CO_2 present in the predicted mixture. Prediction from zero hydrocarbon-hydrocarbon BIPs shows the presence of larger three-phase region.

Oil 6 given in 7-4 is Peace River bitumen. The molecular weight (MW) used in the characterization is 527.5 g/mol according to Mehrotra and Svrcek (1985). This bitumen was characterized using the saturation pressure, 50.50 bars, reported by Mehrotra and Svrcek (1985) for a mixture of 21.83% methane and 78.17% bitumen at 326.65 K. The resulting fluid model was then used to predict three phases in P-T space for another mixture, 89.94% pentane and 10.06% bitumen. The predicted three-phase behavior was compared with three-phase behavior for this mixture composition simulated by Agrawal (2012). **Figure 7-22** presents that the predicted three-phase region is narrower than in Agrawal (2012) in P-T space. The difference is inevitable due to the lack of comprehensive data; i.e., the bitumen MW in the characterization by Agrawal (2012) was 580 g/mol. Nevertheless, the successful prediction of three phases indicates the validity of the BIP correlation (equation 7-13) for pentane, which was developed by extrapolation of BIP values for methane, ethane, and propane. Prediction with zero hydrocarbon– hydrocarbon BIPs case did not show presence of three-phase region.

Table 7-5 lists reservoir oils for which three phases with CO_2 were reported in the literature. Results show that the new algorithm gives reasonable predictions for these fluids. As an example, **Figure 7-23** presents phase boundaries in P-x space for oil C2 with CO_2 at 313.71 K, for which the data were taken from Turek et al. (1988). Although the EOS gives higher immiscibility than the data in this diagram, their agreement is remarkable considering that only P_S and liquid density data at the oil composition were used in the characterization. Also, the regression was conducted only for T_C, P_C, and ω of pseudocomponents. That is, the effect of oil aromaticity on the interaction between oil and CO_2 was not explicitly considered in the algorithm. The prediction from zero hydrocarbon-hydrocarbon BIPs for this reservoir oil did not show presence of three-phase. All the fluids in Table 7-5 were characterized with the new algorithm and zero hydrocarbon-hydrocarbon BIPs. Out of 9 oils, the presence of three-phase was shown for only three oils (oil nos. 6, 8, and 9). **Figure 7-24** presents one such example for Oil G (Table 7-5) where zero hydrocarbon-hydrocarbon BIPs could predict the three phase successfully. However, predicted three phase area is detached from the single-phase boundary.

The predictions from EOS models developed using new algorithm with zero hydrocarbon-hydrocarbon BIPs either failed to show the presence of three phases or predicted three phases were significantly deviated from the data in P-T-x space. This shows that non-zero hydrocarbon-hydrocarbon BIPs are required to model the interaction among PR EOS attraction parameters for components for multiphase behavior. Optimized BIPs, on the other hand, reliably predicted the presence of three-phases for all fluids with satisfactory accuracy.

Figures 7-25 to 7-28 show the comparison of prediction of P-x diagrams from PR EOS models developed by Khan (1992) for mixture of CO_2 and oil 5, 6, 7, and 8 with the predictions from new

algorithm. Khan (1992) adjusted the BIPs to match the three-phase region on the P-x diagrams. Turek et al. (1988) observed that three-phase boundaries are difficult to determine, and reported boundaries may be reliable within ±1.7 bars. The new algorithm predicts the three-phase region correctly only by matching saturation pressure in all cases. This indicates to reliability of the regression algorithm and the optimized BIPs.

The analysis of multiphase behavior predictions in this research has indicated that the simple algorithm is reliable even with the limited PVT data used (P_S and liquid density). However, further adjustment of parameters may be required if additional phase behavior data are to be matched. Obvious candidates are BIPs for solvents with pseudocomponents. In particular, CO_2 BIPs may be adjusted to accommodate the effects of oil aromaticity and reservoir temperature on compositional phase behavior for CO_2 flooding. In addition, the parameters, N and β, in the algorithm can be flexible; e.g., N can be different for T_C, P_C, and ω.

7.4. Conclusions

A new algorithm was presented for characterization of multiphase behavior for solvent injection simulation. The PR EOS was used with the van der Waals mixing rules. The developed algorithm requires only the saturation pressure and liquid density for a given composition and reservoir temperature, in its simplest form. Case studies were conducted for 90 reservoir fluids and their mixtures with solvents for up to three hydrocarbon phases. Conclusions are as follows:

o   The algorithm with the BIPs developed in this research enables the PR EOS to give reliable predictions of multiphase behavior for reservoir fluids. The PnA method was found to be applicable for multiphase characterization; that is, the effect of aromaticity on phase behavior can be modeled through T_C, P_C, and ω of pseudocomponents as monotonic functions of a single parameter in the regression algorithm developed.

o   Results show that positive BIPs are required for the PR EOS to properly represent three-hydrocarbon-phase behavior of reservoir fluids. The fundamental reason comes from the necessity for accurate predictions of binary three-phase curves. This is in contrast to the usage of zero BIPs for hydrocarbon pairs that has been recommended for simpler two-phase characterization in the literature.

7.5. Nomenclature

AARD : Average absolute relative deviation $= \frac{1}{M}\sum_{j=1}^{M}\left|\frac{\text{prediction}-\text{data}}{\text{Data}}\right|_j$

AAD : Average absolute deviation $= \frac{1}{M}\sum_{j=1}^{M}|\text{prediction}-\text{data}|_j$

BIP : Binary interaction parameter

CEP : Critical endpoint

CME : Constant mass expansion

CN : Caron number

CVD : Constant volume depletion

EOS : Equation of state

LCEP : Lower critical end point

L-V : Liquid (L)-vapor (V) phase equilibrium

MMP : Minimum miscibility pressure

PR EOS : Peng and Robinson (1976, 1978) equation of state

PT : Pressure-temperature

p : Degree of freedom in the chi-squared distribution

ST : Swelling test

UCEP : Upper critical endpoint

Greek Symbols:

β : P_S/P_{S_EOS}; P_{S_EOS} is calculated assuming pseudocomponents as n-alkanes.

δ : Deviation of calculated saturation pressure from experimental value

δ_{TOL} : Tolerance set for deviation (δ)

ω : Acentric factor

$\acute{\omega}_P$: Acentric factor calculated from Eq. 7-4

ω_P : Acentric factor calculated from Eq. 7-3

ω_H : Acentric factor calculated from Eq. 7-7

Roman Symbols:

A : Aromatics

k : Number of iterations in the algorithm

K : Binary interaction parameters (Eqs. 7-8 to 7-13)

L_1-L_2-V : Three hydrocarbon phases (L_1: oleic, L_2: solvent-rich liquid, and V: Gaseous)

L-V : Liquid (L)-vapor (V) phase equilibrium

n : Number of pseudocomponents

P_C : Critical pressure

P_{CP} : Critical pressure calculated from Eq. 7-2

P_{CH} : Critical pressure calculated from Eq. 7-6

P_S	: Experimental saturation pressure
P_{S_EOS}	: Calculated saturation pressure with the PR EOS
T_C	: Critical temperature
T_{CP}	: Critical temperature calculated from Eq.7-1
T_{CH}	: Critical temperature calculated from Eq. 7-5

Subscript:

i	: Index for pseudocomponent

7.6. References

Aghbash, V.N. and Ahmadi, M. 2012. Evaluation of CO_2-EOR and Sequestration in Alaska West Sak Reservoir Using Four-Phase Simulation Model. Presented at the SPE Western Regional Meeting, Bakers-field, California, 21-23 March. SPE-153920-MS.

Agrawal, P. 2012. Measurement and Modeling of the Phase Behavior of Solvent Diluted Bitumens. MS Thesis. University of Calgary, Alberta, Canada.

Akpabio, J.U., Udofia, E.E., and Ogbu, M. 2014. PVT Fluid Characterization and Consistency Check for Retrograde Condensate Reservoir Modeling. Presented at SPE Nigeria Annual International Conference and Exhibition, Lagos, Nigeria, 5-7 August. SPE-172359-MS.

Al-Meshari, A. 2004. New Strategic Method to Tune Equation of State to Match Experimental Data for Compositional Simulation. PhD Thesis. Texas A&M University, Texas. USA.

Al-Subai, K.O. 2001. Compositional Gradient Calculations for a Saudi Arabian Gas Condensate Reservoir. MS Thesis. King Fahd University of Petroleum & Minerals, Saudi Arabia.

Badamchi-Zadeh, A., Yarranton, H. W., Svrcek, W. Y. et al. 2009. Phase Behavior and Physical Property Measurements for VAPEX Solvents: Part I. Propane and Athabasca Bitumen. *J Can Pet Technol* **48** (1): 54-61.

Chang, H.L., Hurt, L.J., and Kobayashi, R. 1966. Vapour-Liquid Equilibria of Light Hydrocarbons at Low Temperatures and High Pressures: The Methane-n-Heptane System. *AIChE J.* **12** (6): 1212-1216.

Calsep. 2012. PVTsim Version 19.2.0. Lyngby, Denmark: Calsep International Consultants,

Choi, E. and Yeo, S. 1998. Critical Properties for Carbon Dioxide + n-Alkane Mixtures Using a Variable-Volume View Cell. *J. Chem. Eng. Data.* **43** (5): 714-716.

Cismondi, M., Nuñez, D.N., Zabaloy, M.S. et al. 2006. GPEC: A Program for Global Phase Equilibrium Calculations in Binary Systems. Presented at EQUIFASE VII Iberoamerican Conference on Phase Equilibria and Fluid Properties for Process Design, Morelia, Mexico, 21-25 Oct.

Coats, K. H. 1985. Simulation of Gas Condensate Reservoir Performance. *J Pet Technol* **37** (10): 1870-1886. SPE-10512-PA.

Coats, K.H. and Smart, G. T. 1986. Application of a Regression Based EOS PVT Program to Laboratory Data. *SPE Res Eng* **1** (3): 277-299. SPE-11197-PA.

Creek, J.L. and Sheffield, J.M. 1993. Phase Behavior, Fluid Properties, and Displacement Characteristics of Permian Basin Reservoir Fluid/ CO_2 Systems. *SPE Res Eval & Eng* **8** (1): 34-42. SPE-20188-PA.

Danesh, A. 1998. PVT and Phase Behavior of Petroleum Reservoir Fluids. Elsevier Science B.V., Amsterdam, The Netherlands.

Daridon, J. L., Xans, P., and Montel, F. 1996. Phase Boundary Measurement on a Methane + Decane + Multiparaffins System. *Fluid Phase Equilib.* **117** (1-2), 241-248.

DeRuiter, R.A., Nash, L.J., and Singletary, M.S. 1994. Solubility and Displacement Behavior of a Viscous Crude with CO_2 and Hydrocarbon Gases. *SPE Res Eval & Eng* **9** (2): 101-106. SPE-20523-PA.

Dickson, J.L., Clingman, S., Dittaro, L.M. et al. 2011. Design Approach and Early Field Performance for a Solvent-Assisted SAGD Pilot at Cold Lake, Canada. Presented at the SPE Heavy Oil Conference and Exhibition, Kuwait City, Kuwait, 12-14 December. SPE-150639-MS.

Drohm, J.K., Trengove, R.D., and Goldthrope, W.H. 1988. On the Quality of Data from Standard Gas-Condensate PVT Experiments. Presented at the SPE Gas Technology Symposium, Dallas, Texas, 13-15 June. SPE-17768-MS.

Ekundayo, J.M. 2012. Configuration of Slim Tube Apparatus for Consistent Determination of Minimum Miscibility Pressure (MMP) Data, MS Thesis. The Petroleum Institute, Abu Dhabi, UAE.

Enick, R., Holder, G.D., and Morsi, B.I. 1985. Critical and Three Phase Behavior in the Carbon Dioxide/Tridecane System. *Fluid Phase Equilib.* **22** (2): 209-224.

Estrera, S.S. and Luks, K.D. 1987. Liquid-Liquid-Vapor Equilibrium Behavior of Certain Ethane + n-Paraffin Mix. *J. Chem. Eng. Data.* **32** (2): 201-204.

Fall, D.J. and Luks, K.D. 1985. Liquid-Liquid-Vapor Phase Equilibria of the Binary System Carbon Dioxide + n-Tridecane. *J. Chem. Eng. Data.* **30** (3): 276-279.

Fall, D.J., Fall, J.L., and Luks, K.D. 1985. Liquid-Liquid-Vapor Immiscibility Limits in Carbon Dioxide + n-Paraffin Mixtures. *J. Chem. Eng. Data.* **30** (1): 82-88.

Fawumi, O.K. 1999. Effect of Liquid Drop-out on the Productivity of a Rich Gas Condensate Reservoir. MS Thesis. King Fahd University of Petroleum & Minerals, Saudi Arabia.

Firoozabadi, A. and Khalid, A. 1986. Analysis and Correlation of Nitrogen and Lean-Gas Miscibility Pressure. *SPE Res Eng* **1** (6): 575-582. SPE-13669-PA.

Firoozabadi, A., Hekim, Y., and Katz, D. L. 1978, Reservoir Depletion Calculations for Gas Condensates Using Extended Analyses in the Peng-Robinson Equation of State. *Can. J. Chem. Eng.*, **56** (5): 610–615.

Fulco, G.J. 1999. Case History of Miscible Gas Flooding in the Powder River Basin North Buck Draw Unit. Presented at the SPE Rocky Mountain Regional Meeting, Gillette, Wyoming, 15-18 April. SPE-55634-MS.

Gajda, M. 2014. Comparison of Black Oil Tables and EOS Fluid Characterization in Reservoir Simulation. MS Thesis. University of Miskolc, Hungary.

Gao, W., Robinson Jr., R.L., and Gasem, K.A.M. 2001. Improved Correlations for Heavy n-Paraffin Physical Properties. *Fluid Phase Equilib*. **179** (1-2): 207-216.

Godbole, S.P., Thele, K.J., and Reinbold, E.W. 1995. EOS Modeling and Experimental Observations of Three-Hydrocarbon-Phase Equilibria. *SPE Res. Eng.* **10** (2): 101-108. SPE-24936-PA.

Graue, D.J. and Zana, E.T. 1981. Study of a Possible CO_2 Flood in Rangely Field. *J Pet Technol* **33** (7): 1312-1318. SPE-7060-PA.

Gregorowicz, J., De Loos, T.W., and De Swaan Arons, J. 1993a. Liquid-Liquid-Vapour Phase Equilibria in the System Ethane + Propane + Eicosane: Retrograde Behaviour of the Heavy Liquid Phase, *Fluid Phase Equilib.* **84**: 225-250.

Gregorowicz, J., Smits, P.J., de Loos, T.W. et al. 1993b. Liquid-Liquid-Vapour Phase Equilibria in the System Methane + Ethane + Eicosane: Retrograde Behaviour of the Heavy Liquid Phase. *Fluid Phase Equilib.* **85**, 225-238.

Guler, B., Wang, P., Delshad, M. et al. 2001. Three- and Four- Phase Flow Compositional Simulations of CO_2/NGL EOR. Presented at the SPE Annual Technical Conference and Exhibition, New Orleans, Louisiana, 30 September-3 October. SPE-71485-MS.

Guo, T.M. and Du, L. 1989. A New Three-Parameter Cubic Equation of State for Reservoir Fluids. Parts-III, Application to Gas Condensates, SPE 19374-MS.

Gupta, S.C. and Gittins, S.D. 2006. Christina Lake Solvent Aided Process Pilot. *J Can Pet Technol* **45** (9): 15-18. PETSOC-06-09-TN.

Gupta, S.C., Gittins, S., and Picherack, P. 2005. Field Implementation of Solvent Aided Process. *J Can Pet Technol* **44** (11): 8-13. PETSOC-05-11-TN1.

Heidemann, R.A. and Khalil, A.M. 1980. The Calculation of Critical Points. *AIChE J.*, **26** (5): 769–779.

Henry, R.L. and Metcalfe, R.S. 1983. Multiple-Phase Generation During Carbon Dioxide Flooding. *SPE J.* **23** (4): 595-601. SPE-8812-PA.

Høier, L. 1997. Miscibility Variation in Compositional Grading. PhD. Thesis. Norwegian University of Science and Technology, Norway.

Horn, L.D.V. and Kobayashi.R. 1967. Vapor-Liquid Equilibria of Light Hydrocarbons at Low Temperatures and Elevated Pressures in Hydrocarbon Solvents. Methane-Propane-n-Heptane, Methane-Ethane-n-Heptane, and Methane-Propane-Toluene Systems. *J. Chem. Eng. Data*. **12** (3):294-303.

Hosein, R., Jagai, T., and Dawe, R.A. 2013. A Method for Predicting the Phase Behaviour of Trinidad Gas Condensates. *WIJE*. **35**:22-30.

Hottovy, J.D., Kohn, J.P., and Luks, K.D. 1981b. Partial Miscibility Behavior of the Methane-Ethane-n-Octane System. *J. Chem. Eng. Data.* **26** (2): 135-137.

Hottovy, J.D., Kohn, J.P., and Luks, K.D. 1982. Partial Miscibility Behavior of the Ternary Systems Methane-Propane-n-Octane, Methane-n-Butane-n-Octane, and Methane-Carbon Dioxide-n-Octane. *J. Chem. Eng. Data.* **27** (3): 298-302.

Hottovy, J.D., Luks, K.D., and Kohn, J.P. 1981a. Three-phase liquid-liquid-vapor equilibriums behavior of certain binary carbon dioxide-n-paraffin systems. *J. Chem. Eng. Data* **26** (3): 256-258.

Jacoby, R.H. and Yarborough, L. 1967. PVT Measurements on Petroleum Reservoir Fluids and Their Uses. *Ind. Eng. Chem.* **59** (10): 48-62.

Jacoby, R.H., Koeller, R.C., and Berry, V.J. Jr. 1959. Effect of Composition and Temperature on Phase Behavior and Depletion Performance of Rich Gas-Condensate Systems. *J Pet Technol.* **11** (7): 58-63. SPE-1093-G.

Jangkamolkulchai, A. and Luks, K.D. 1989. Partial Miscibility Behavior of the Methane + Ethane + n-Docosane and the Methane + Ethane + n-Tetradecylbenzene Ternary Mixtures. *J. Chem. Eng. Data*. **34** (1): 92-99.

Jaubert, J-N., Avaullee, L., and Souvay, J-F. 2002. A Crude Oil Data Bank Containing More Than 5000 PVT and Gas Injection Data. *J. Pet. Sci. Technol.* **34** (1-4): 65-107.

Kato, K., Nagahama, K., and Hirata, M. 1981. Generalized Interaction Parameters for the Peng—Robinson Equation of State: Carbon Dioxide—n-Paraffin Binary Systems, *Fluid Phase Equilib.* **7** (3–4): 219-231.

Kenyon, D.E. and Behie, G.A. 1987. Third SPE Comparative Solution Project: Gas Cycling of Retrograde Condensate Reservoirs. *J Pet Technol* **39** (8): 981-997. SPE-12278-PA.

Khan, S.A., Pope, G.A., and Sepehrnoori, K. 1992. Fluid Characterization of Three-Phase CO_2/Oil Mixtures. Presented at the SPE/DOE Enhanced Oil Recovery Symposium, Tulsa, Oklahoma, 22-24 April. SPE-24130-MS.

Kilgren, K.H. 1966. Phase Behavior of a High-Pressure Condensate Reservoir Fluid. *J Pet Technol* **18** (8): 1001-1005. SPE-1277-PA.

Koch, H.A. and Hutchinson, C.A. 1958. Miscible Displacements of Reservoir Oil Using Flue Gas. *Pet. Trans. AIME*, **213**: 7-10.

Kordas, A., Tsoutsouras, K., Stamataki, S. et al. 1994. A generalized correlation for the interaction coefficients of CO_2—hydrocarbon binary mixtures, *Fluid Phase Equilib*. **93**: 141-166.

Krejbjerg, K. and Pedersen, K. S. 2006. Controlling VLLE Equilibrium with a Cubic EoS in Heavy Oil Modeling. Presented at Canadian International Petroleum Conference, Calgary, Alberta, 13-15 June. PETSOC-2006-052.

Kukarni, A.A., Zarah, B.Y., Luks, K.D. et al. 1974. Phase-Equilbriums Behavior of System Carbon Dioxide-n-Decane at Low Temperatures. *J. Chem. Eng. Data* **19** (1), 92-94.

Kumar, A. and Okuno, R. 2012. Critical Parameters Optimized for Accurate Phase Behavior Modeling for Heavy n-Alkanes up to C_{100} using the Peng–Robinson Equation of State, *Fluid Phase Equilib.* **335**: 46-59.

Kumar, A. and Okuno, R. 2013. Characterization of Reservoir Fluids using an EOS based on Perturbation from n-Alkanes. *Fluid Phase Equilib*, **358**, 250-271.

Kumar. A. and Okuno, R. 2015. Direct Perturbation of the Peng–Robinson Attraction and Covolume Parameters for Reservoir Fluid Characterization. *Chem. Eng. Sc.* **127**: 293-309.

Lee, J.I. and Reitzel, G.A. 1982. High Pressure, Dry Gas Miscible Flood Brazeau River Nisku Oil Pools. *J Pet Technol* **34** (11): 2503-2509. SPE-10243-PA.

Li, H., Zheng, S., and Yang. D. 2013a. Enhanced Swelling Effect and Viscosity Reduction of Solvent(s)/CO_2/Heavy-Oil Systems. *SPE J.* **18** (4): 695-707. SPE-150168-PA.

Li, X., Li, H., and Yang, D. 2013b. Determination of Multiphase Boundaries and Swelling Factors of Solvent(s)−CO_2−Heavy Oil Systems at High Pressures and Elevated Temperatures. *Energy Fuels*. **27** (3): 1293-1306.

Lin, H. 1984. Peng-Robinson Equation of State for Vapor-Liquid Equilibrium Calculations for Carbon dioxide + Hydrocarbon Mixtures. *Fluid Phase Equilib*., **16** (2): 151-169.

Lin, Y.-N., Chen, R. J.J., Chappelear, P.S. et al. 1977. Vapor-Liquid Equilibrium of the Methane-n-Hexane System at Low Temperature. *J. Chem. Eng. Data.* **22** (4): 402-408.

Llave, F.M., Luks, K.D., and Kohn, J.P. 1987. Three-Phase Liquid-Liquid-Vapor Equilibria in the Nitrogen-Methane-Ethane and Nitrogen-Methane-Propane Systems. *J. Chem. Eng. Data.* **32** (1): 14-17.

Malik, Q.M. and Islam, M.R. 2000. CO_2 Injection in the Weyburn Field of Canada: Optimization of Enhanced Oil Recovery and Greenhouse Gas Storage with Horizontal Wells. Presented at the SPE/DOE Improved Oil Recovery Symposium, Tulsa, Oklahoma, 3-5 April. SPE-59327-MS.

McGuire, P.L., Spence, A.P., and Redman, R.S. 2001. Performance Evaluation of a Mature Miscible Gasflood at Prudhoe Bay. *SPE Res Eval & Eng* **4** (4): 318-326. SPE-72466-PA.

McVay, D.A. 1994. Generalization of PVT Properties for Modified Black-Oil Simulation of Volatile and Gas Condensate Reservoirs. PhD Thesis. Texas A&M University, Texas, USA.

Mehrotra, A.K. and Svrcek, W.Y. 1985. Viscosity, Density and Gas Solubility Data for Oil Sand Bitumens; Part II, Peace River Bitumen Saturated with N_2, CO, CH_4, CO_2, and C_2H_6. *AOSTRA Journal of Research* **1** (4): 269-279.

Metcalfe, R.S. and Raby, W.J. 1986. Phase Equilibria for a Rich Gas Condensate-Nitrogen System. *Fluid Phase Equilib*. **29**: 563-573.

Mizenko, G.J. 1992. North Cross (Devonian) Unit CO_2 Flood: Status Report. Presented at the SPE/DOE Enhanced Oil Recovery Symposium, Tulsa, Oklahoma, 22-24 April. SPE-24210-MS.

Mohanty, K.K., Masino, W.H. Jr., Ma, T.D. et al. 1995. Role of Three-Hydrocarbon-Phase Flow in a Gas-Displacement Process. *SPE Res Eng* **10** (3): 214-221. SPE-24115-PA.

Moore, D.C., 1989. Simulation of Gas-Condensate Reservoir Performance Using Schmidt-Wenzel Equation of State. MS Thesis. Montana College of Mineral Science and Technology, Montana, USA.

Mushrif, S.H. 2004. Determining Equation of State Binary Interaction Parameters Using K- and L-Points. MS Thesis, the University of Saskatchewan, Saskatoon, Canada (October 2004).

Negahban, S. and V. J. Kremesec Jr. 1989. Development and Validation of Equation-of-State Fluid Descriptions for CO_2-Reservoir Oil Systems. SPE 19637. Presented at the 64th Annual Technical Conference and Exhibition, San Antonio, 8-11 March. SPE 19637-PA.

Negahban, S., Pedersen, K.S., Baisoni, M.A. et al. 2010. An EoS Model for a Middle East Reservoir Fluid with an Extensive EOR PVT Data Material, Presented at Abu Dhabi International Petroleum Exhibition & Conference, 1-4 Nov. Abu Dhabi, UAE. SPE-136530-MS.

Nghiem, L. X. and Li, Y.K. 1986. Effect of Phase Behavior on CO_2 Displacement Efficiency at Low Temperatures: Model Studies with an Equation of State. *SPE Res Eng* **1** (4): 414-422. SPE-13116-PA

Nikitin, E.D. and Popov, A.P. 2015. Critical point measurement of some polycyclic aromatic hydrocarbons. *J. Chem. Thermodyn.* **80** :124-127.

Okuno, R. and Xu, Z. 2014. Mass Transfer on Multiphase Transitions in Low-Temperature Carbon-Dioxide Floods. *SPE J.* **19** (6):1005-1023. SPE-166345-PA.

Okuno, R. and Xu, Z. 2014. Efficient Displacement of Heavy Oil by Use of Three Hydrocarbon Phases. *SPE J.* **19** (5): 956-973. SPE-165470-PA.

Okuyiga, M.O. 1992. Equation of State Characterization and Miscibility Development in a Multiple Phase Hydrocarbon System. Presented at the SPE Annual Technical Conference and Exhibition, Washington, DC, 4-7 October. SPE-24937-MS.

Pedersen, K. S. and Christensen, P. L. 2007. Phase Behavior of Petroleum Reservoir Fluids. CRC Press, Taylor & Francis Group, Boca Raton, FL, USA.

Pedersen, K. S., Milter, J., and Sørensen, H. 2004. Cubic Equations of State Applied to HT/HP and Highly Aromatic Fluids. *SPE J.* **9** (2): 186-192. SPE-88364-PA.

Pedersen, K.S., Thomassen, P.,   and Fredenslund, Aa. 1989. Characterization of Gas Condensate Mixtures. *Advances in Thermodynamics*, Taylor and Francis, New York, 1, 137-152.

Peng, D.-Y. and Robinson, D.B. 1976. A New Two-Constant Equation of State. *Ind. Eng. Chem. Fund.* **15** (1): 59-64.

Peng, D.-Y. and Robinson, D.B. 1978. The Characterization of the Heptanes and Heavier Fractions for the GPA Peng-Robinson Programs. *GPA Research Report RR-28.*

Peters, C.J. 1994. Multiphase Equilibria in Near-Critical Solvents. In Supercritical Fluids, ed. E. Kiran and J.M.H. Levelt Sengers, 117-145. Dordrecht, The Netherlands: Springer Netherlands.

Peters, C.J., De Roo, J.L., and De Swaan Arons, J. 1987b. Three-Phase Equilibria in (Ethane + Pentacosane). *J. Chem. Thermodyn*. **19** (3): 265-272.

Peters, C.J., de Roo, J.L., and De Swaan Arons, J. 1992. Measurements and Calculations of Phase Equilibria in Binary Mixtures of Propane + Tetratriacontane. *Fluid Phase Equilib*. **72**: 251-266.

Peters, C.J., de Roo, J.L., and De Swaan Arons, J. 1993. Phase Equilibria in Binary Mixtures of Propane and Hexacontane. *Fluid Phase Equilib.* **85:** 301-312.

Peters, C.J., Lichtenthaler, R.N., and De Swaan Arons, J. 1986. Three Phase Equilibria in Binary Mixtures of Ethane and Higher n-Alkanes. *Fluid Phase Equilib.* **29:** 495-504.

Peters, C.J., Van der Kooi, H.J., and De Swaan Arons, J. 1987a. Measurements and Calculations of Phase Equilibria for (Ethane + Tetracosane) and (p, V_m^*, T) of Liquid Tetracosane. *J. Chem. Thermodyn.* **19** (4): 395-405.

Peters, C.J., Van Der Kooi, H.J., De Roo, J.L. et al. 1989. The Search for Tricriticality in Binary Mixtures of Near-Critical Propane and Normal Paraffins. *Fluid Phase Equilib.* **51:** 339-351.

Quiñones-Cisneros, S.E., Zéberg-Mikkelsen, C.K., Baylaucq, A. et al. 2004. Viscosity Modeling and Prediction of Reservoir Fluids: From Natural Gas to Heavy Oils. *Int. J. Therm.* **25** (5): 1353-1366.

Reamer, H.H. and Sage, B.H. 1963. Phase Equilibria in Hydrocarbon Systems. Volumetric and Phase Behavior of the n-Decane-CO_2 System. *J. Chem. Eng. Data*. **8** (4): 508-513.

Reid, T. 1994. Study of Hydrocarbon Miscible Solvent Slug Injection Process for Improved Recovery of Heavy Oil From Schrader Bluff Pool, Milne Point Unit, Alaska. Annual Report for DE-FG22-93BC14864 for the US Department of Energy. University of Alaska Fairbanks, Alaska.

Renner, T.A., Metcalfe, R.S., and Yellig, W.F.Jr. et al. 1989. Displacement of Rich Gas Condensate by Nitrogen: Laboratory Corefloods and Numerical Simulations. *SPE Res Eng* **4** (1): 52-58. SPE-16714-PA.

Reudelhuber, F.O. and Hinds, R.F. 1957. A Compositional Material Balance Method for Prediction of Recovery from Volatile Oil Depletion Drive Reservoirs. *Pet. Trans. AIME*. **210**: 19-26.

Rodrigues, A.B. and Kohn, J.P. 1967. Three Phase Equilibria in the Binary Systems Ethane-n-Docosane and Ethane-n-Octacosane. *J. Chem. Eng. Data*. **12** (2): 191-193.

Roper, M. 1989. An Experimental Study of CO_2/West-Sak-Crude-Oil Phase Behavior. MS thesis, University of Alaska Fairbanks, Fairbanks, Alaska.

Secuianu, C., Feroiu, V., and Geana, D. 2007. Investigation of Phase Equilibria in the Ternary System Carbon Dioxide + 1-Heptanol + n-Pentadecane. *Fluid Phase Equilib*. **261** (1-2): 337-342.

Sharma, A.K., Patil, S.L., Kamath, V.A. et al. 1989. Miscible Displacement of Heavy West Sak Crude by Solvents in Slim Tube. Presented at the SPE California Regional Meeting, Bakersfield, California, 5-7 April. SPE-18761-MS.

Sharma, G.D. 1990. Development of Effective Gas Solvents Including Carbon Dioxide for the Improved Recovery of West Sak Oil. Report No. DOE/FE/61114-2. University of Alaska Fairbanks, Alaska, USA.

Shelton, J.L. and Yarborough, L. 1977. Multiple Phase Behavior in Porous Media During CO_2 or Rich-Gas Flooding. *J Pet Technol* **29** (9): 1171-1178. SPE-5827-PA.

Soave, G. 1972. Equilibrium Constants from a Modified Redlich-Kwong Equation of State. *Chem. Eng. Sci.* **27** (6): 1197-1203.

Spivak, A. 1971. Mathematical Simulation of Condensate-Gas Reservoirs. PhD. Thesis, University of Texas at Austin, Texas, USA.

Stein, M.H., Frey, D.D., Walker, R.D. et al. 1992. Slaughter Estate Unit CO_2 Flood: Comparison between Pilot and Field-Scale Performance. *J Pet Technol* **44** (9): 1026-1032. SPE-19375-PA.

Subero, C.L. 2009. Numerical Modeling of Nitrogen Injection into Gas Condensate Reservoir. MS Thesis. West Virginia University, Morgantown, West Virginia, USA.

Tanner, C.S., Baxley, P.T., Crump III, J.G. et al. 1992. Production Performance of the Wasson Denver Unit CO_2 Flood. Presented at the SPE/DOE Enhanced Oil Recovery Symposium, Tulsa, Oklahoma, 22-24 April. SPE-24156-MS.

Turek, E.A., Metcalfe, R.S., and Fishback, R.E. 1988. Phase Behavior of Several CO_2/ West Texas-Reservoir-Oil Systems. *SPE Res Eng* **3** (2): 505-516. SPE-13117-PA.

Uzunov, D.I. 1993. Introduction to the Theory of Critical Phenomena. Singapore, World Scientific Publishing.

Van der Steen, J., De Loos, T.W., and de Swaan, A.J. 1989. The Volumetric Analysis and Prediction of Liquid-Liquid-Vapor Equilibria in Certain Carbon Dioxide + n-Alkane Systems. *Fluid Phase Equilib*. **51:** 353-367.

Varotsis, N., Stewart, G., Todd, A.C. et al. 1986. Phase Behavior of Systems Comprising North Sea Reservoir Fluids and Injection Gases. *J Pet Technol* **38** (11): 1221-1233. SPE-12647-PA.

Vogel, J.L. and Yarborough, L. 1980. The Effect of Nitrogen on the Phase Behavior and Physical Properties of Reservoir Fluids. Presented at First Joint SPE/DOE Symposium on Enhanced Oil Recovery, Tulsa, Oklahoma, 20-23 April. SPE-8815-MS.

Whitaker, C.A. and Kim, J.S. 1993. Application of Extended Equation of State Work to Optimize the Pegasus Devonian Field Unit No. 3 Gas Cycling Operation. Presented at SPE Annual Technical Conference and Exhibition, Houston, Texas, 3-6 October. SPE-8815-MS.

Whitson, C.H. and Torp, S.B. 1983. Evaluating Constant-Volume Depletion Data. *J Pet Technol* **35** (3): 610-620. SPE-10067-PA.

Whitson, C.H. and Belery, P. 1994. Compositional Gradients in Petroleum Reservoirs. Presented at University of Tulsa Centennial Petroleum Engineering Symposium, Tulsa, Oklahoma, 29-31 August. SPE-28000-MS.

Whitson, C.H. and Brulè, M.R. 2000. Phase Behaviour. SPE Henry L. Doherty Series, Vol. 20, SPE, Richardson, Texas.

Winzinger, R., Brink, J.L., Patel, K.S. et al. 1991. Design of a Major CO2 Flood, North Ward Estes Field, Ward County, Texas. *SPE Res Eng* 6 (1): 11-16.

Yaws, C. L. 2010. Thermo Physical Properties of Chemicals and Hydrocarbons (Electronic Edition), Knovel, 2010.

	N$_2$	CO$_2$	CH$_4$	C$_2$	C$_3$	C$_4$	C$_5$	C$_6$	PC-1	PC-2	PC-3	PC-4
Table 7-1. Binary interaction parameters used with the new algorithm. Numbers inside brackets indicate the corresponding equations in this paper.												
N$_2$	0.0000											
CO$_2$	0.0000	0.0000										
CH$_4$	0.1000	0.1000	0.0000									
C$_2$	0.1000	0.1450	0.0420	0.0000								
C$_3$	0.1000	Kato et al.[#]	0.0420	0.0400	0.0000							
C$_4$	0.1000	Kato et al.[#]	0.0420	0.0400	0.0300	0.0000						
C$_5$	0.1000	Kato et al.[#]	0.0420	0.0400	0.0300	0.0116	0.0000					
C$_6$	0.1000	Kato et al.[#]	0.0420	0.0400	0.0300	0.0155	0.0058	0.0000				
PC-1	0.1300	(7-8)	(7-9)	(7-10)	(7-11)	(7-12)	(7-13)	0.0000	0.0000			
PC-2	0.1300	(7-8)	(7-9)	(7-10)	(7-11)	(7-12)	(7-13)	0.0000	0.0000	0.0000		
PC-4	0.1300	(7-8)	(7-9)	(7-10)	(7-11)	(7-12)	(7-13)	0.0000	0.0000	0.0000	0.0000	
PC-4	0.1300	(7-8)	(7-9)	(7-10)	(7-11)	(7-12)	(7-13)	0.0000	0.0000	0.0000	0.0000	0.0000
[#] Equations 11, 12, 13, and 14 of Kato et al. (1981)												

Table 7-2. Characterization results for gas condensates and volatile oils with the new algorithm. CVD or CCE data are available for these fluids. Parameters β and k are defined in the algorithm section. Parameter p indicates the degree of freedom in the chi-squired distribution.

Fluid No.	References	MW (gm/mol)	Res. Temp. (K)	β	k	p	Limiting Data Value (Type[#])	AAD[¥]
1	Al-Meshari (2004), Fluid-3	31.53	424.82	1.376	4730	2.0	11.70 (1)	0.58
2	Al-Meshari (2004), Fluid-4	31.44	403.15	1.323	4687	2.0	13.00 (1)	1.25
3	Al-Meshari (2004), Fluid-5	32.41	382.59	1.271	4764	2.1	23.36 (2)	2.38
4	Al-Meshari (2004), Fluid-7	36.62	397.59	1.493	5420	2.6	25.00 (1)	2.49
5	Al-Meshari (2004), Fluid-8	40.77	424.82	1.309	4204	2.2	30.40 (1)	4.73
6‡	Al-Meshari (2004), Fluid-10	39.23	422.59	1.135	3879	3.3	33.60 (1)	0.63
7‡	Al-Meshari (2004), Fluid-11	41.71	424.82	1.211	4348	3.0	32.20 (1)	2.94
8‡	Coats and Smart (1986), Gas-5	30.29	403.70	1.241	4593	2.0	10.40 (2)	0.59
9	Coats and Smart (1986), Gas-2	44.92	360.92	2.334	4399	4.0	53.06(1)	1.40
10	Guo and Du (1989), Sample-7	25.53	406.45	1.310	4800	2.0	5.82 (1)	0.34
11	Metcalfe and Raby (1986)	35.70	374.82	1.230	4075	2.2	23.89 (1)	2.96
12‡	Coats (1985), Recombined	44.40	435.93	1.042	4340	4.0	32.00 (2)	2.34
13‡	Coats (1985), Bottom hole	44.40	435.93	1.085	4155	4.0	33.49 (2)	4.20
14‡	McVay (1994), Gas B	40.58	387.59	1.184	3785	2.0	40.90 (1)	1.18
15	Danesh (1998)	27.29	394.00	1.443	4864	2.0	11.32 (1)	1.91
16	Pedersen and Christensen (2007)	29.14	428.15	1.453	5566	2.0	11.89 (2)	2.46
17	Hosein et al. (2013), PL-1	23.64	358.78	1.270	4591	2.0	8.15 (1)	1.12
18	Hosein et al. (2013), PL-2	22.10	378.15	1.744	6575	2.0	5.08 (1)	0.49
19	Hosein et al. (2013), PL-3	21.55	357.59	1.120	4429	2.0	4.00 (1)	0.31
20	Hosein et al. (2013), PL-4	20.62	364.22	1.490	5949	2.0	3.73 (1)	0.28
21	Hosein et al. (2013), PL-5	20.30	355.37	1.158	4806	2.0	3.79 (1)	0.30
22	Hosein et al. (2013), PL-6	19.75	367.59	1.769	7597	2.0	1.89 (1)	0.07
23	Kenyon and Behie (1987)	32.61	366.48	1.025	3956	2.5	19.90 (1)	2.61
24	Moore (1989)	24.45	365.37	1.476	7412	2.0	2.17 (1)	0.24
25	Whitson and Torp (1983), NS-1	35.04	410.43	1.390	4208	2.0	21.60 (1)	0.88
26	Whitson and Brulé (2000), GOCW-7	33.62	358.70	1.304	5690	2.5	23.90 (1)	2.82
27	Drohm et al. (1988), Example-2	32.65	436.70	1.475	4643	2.0	15.63 (1)	2.61
28	Drohm et al. (1988), Example-3	26.26	393.20	1.558	6856	2.0	4.75 (1)	0.70
29	Drohm et al. (1988), Example-4	28.34	377.60	1.443	5962	2.1	11.84 (1)	1.38
30	Drohm et al. (1988), Example-5	21.27	377.60	1.868	8865	2.0	1.69 (1)	0.10
31	Akpabio et al. (2014)	26.35	377.04	1.550	5825	2.0	10.53(1)	0.45
32	Pedersen et al. (1989)[*]	26.98	392.10	1.694	7048	2.1	5.72 (1)	0.78
33	Vogel and Yarborough (1980), Gas-1[*]	36.03	381.00	1.105	3746	2.2	25.85 (2)	1.53
34	Vogel and Yarborough (1980), Gas-2[*]	30.75	381.00	1.194	4229	2.1	9.79 (2)	1.64
35	Vogel and Yarborough (1980), Gas-3[*]	23.73	333.00	1.197	6351	2.1	3.40 (2)	0.60
36‡	Whitaker and Kim (1993)	39.34	366.48	1.218	3982	2.2	47.40 (2)	7.94
37	Kilgren (1966)[*]	36.52	399.82	1.689	3321	2.1	39.99 (2)	5.53
38‡	Subero (2009)[*]	40.03	377.04	1.053	4345	2.1	38.90 (1)	2.63
39	Fawumi (1999)	34.04	422.59	1.226	4205	2.1	17.16 (1)	1.97
40	Al-Subai (2001), Well-A	32.64	420.93	1.254	4296	2.6	14.34 (1)	1.66
41	Al-Subai (2001), Well-B	42.44	424.82	1.156	3759	2.6	32.02 (1)	2.91
42	Al-Subai (2001), Well-D	34.50	424.82	1.232	4225	2.1	17.17 (1)	2.31
43	Al-Subai (2001), Well-E	23.03	412.59	1.910	7907	2.1	2.18 (1)	0.28
44	Jacoby et al. (1959)	32.76	404.82	1.227	4110	2.1	16.10 (2)	0.46
45	Renner et al. (1989)	35.69	374.82	1.227	4058	2.1	25.02 (2)	0.38
46	Spivak (1971)	27.13	352.59	1.063	4408	2.1	12.68 (1)	1.32
47	Firoozabadi et al. 1978	23.83	355.65	1.143	4940	2.0	4.70(1)	0.54
48‡	Gajda 2014	42.94	364.15	1.530	4476	2.0	49.50(1)	2.20
49	Al-Meshari (2004), Fluid-12	46.07	354.82	1.519	4039	2.3	38.20 (1)	1.80
50	Al-Meshari (2004), Fluid-16	59.63	425.93	1.342	3507	2.5	35.30 (1)	1.28
51‡	McVay (1994), Oil A	50.93	408.70	1.357	4335	2.5	33.30 (1)	2.36
52	McVay (1994), Oil B	57.50	393.70	1.332	4027	3.1	49.50 (1)	0.91
53	Jacoby and Yarborough (1967)	54.32	346.48	1.343	4201	2.8	24.29 (2)	1.94
54‡	Pedersen et al. (1989)	47.84	424.25	1.357	3719	2.3	42.20 (1)	4.57
55	Reudelhuber and Hinds (1957)	42.55	374.82	1.152	3548	2.3	34.50 (1)	1.57

\# (1) is CVD liquid saturations (%), (2) is CCE liquid saturations (%).
¥ Deviation (AAD) is the summation of |experimental value – predicted value| divided by the number of data points.
‡ Near critical gas condensates.
* Density data for gas condensates no. 32-35, 37, and 38 are not available. Density matching for these fluids has not been done.

Table 7-3. Characterization results for oils for which slim-tube MMP data are available.
Parameters β and k are defined in the algorithm section.
Parameter p indicates the degree of freedom in the chi-squired distribution.

Oil No.	References	MW (gm/mol)	Res. Temp. (K)	β	k	p	% AARD MMP Prediction
1	Jaubert et al. (2002), F1	135.24	374.85	1.329	3413	4.5	2.76
2	Jaubert et al. (2002), F2	136.25	372.05	1.528	4126	4.7	13.19
3	Jaubert et al. (2002), F3	82.41	387.35	1.438	4050	6.3	0.91
4	Jaubert et al. (2002), F4	63.17	388.20	1.387	3883	3.0	3.17
5	Jaubert et al. (2002), F5	125.82	394.25	1.523	4073	4.5	2.29
6	Jaubert et al. (2002), F6	96.25	383.15	1.324	3731	4.2	3.27
7	Jaubert et al. (2002), F7	96.19	393.15	1.318	4191	4.9	3.17
8	Jaubert et al. (2002), F11	82.55	373.75	1.401	3947	3.8	6.47
9	Ekundayo (2012)	86.57	402.59	1.334	4152	4.6	0.94
10	Høier (1997)[*]						
	Injection Gas (System-1)[¥]	97.0	368.15	1.551	4165	4.4	12.35
	Injection Gas (System-2)[¥]	97.0	368.15	1.551	4165	4.4	6.03
	Injection Gas (System-3)[¥]	97.0	368.15	1.551	4165	4.4	6.70
	Injection Gas (System-4)[¥]	97.0	368.15	1.551	4165	4.4	8.53
11	Graue and Zana (1981)[#]	177.0	344.26	1.493	4874	7.7	7.38
	Graue and Zana (1981)[#]	177.0	344.26	1.493	4874	7.7	14.14
12	Negahban et al. 2010	101.90	394.00	1.279	3822	4.8	1.96
13	Firoozabadi and Aziz 1986, XA	51.58	444.26	1.288	3795	3.1	0.46
14	Firoozabadi and Aziz 1986, XB	67.33	366.48	1.516	4236	3.4	1.45
15	Firoozabadi and Aziz 1986, XC	86.25	380.37	1.764	4087	3.2	0.54
16	Firoozabadi and Aziz 1986, XD	89.07	423.71	1.647	3969	3.3	3.18
17	Lee and Reitzel 1982, A	78.35	376.15	1.320	4247	4.5	2.27
18	Lee and Reitzel 1982, D	79.85	375.15	1.280	3829	4.1	8.64
19	Lee and Reitzel 1982, E	54.33	379.15	1.358	4193	3.2	3.40
20	Koch and Hutchinson 1958, A						
	Injection Gas-1	64.97	333.15	1.582	4604	3.1	7.02
	Injection Gas-2	64.97	333.15	1.582	4604	3.1	1.73
	Injection Gas-3	64.97	333.15	1.582	4604	3.1	2.75
	Injection Gas-4	64.97	333.15	1.582	4604	3.1	3.53

[¥]Oil composition (System VOA) and saturation data used were taken from Whitson and Belery (1994). Systems 1-4 indicate four different injection gases. The MMPs reported were simulated.
[#]Two different injection gases have been used. Details are available in the reference.

Table 7-4. Characterization results for heavy oils and bitumens with the new algorithm.
PVT data for these oils include swelling tests, gas solubility, and phase envelopes.
Parameters β and k are defined in the algorithm section. Parameter p indicates the degree of freedom in the chi-squired distribution.

Oil No.	References	MW (gm/mol)	Temp. (K)	β	k	p	AARD %	Type of Data[*]
1[¥]	Sharma (1990), West Sak Oil	228.88	299.81	1.783	3350	5.7	3.45[#]	ST
2	Krejbjerg and Pedersen (2006),Fluid-1	125.72	347.15	1.705	4272	5.5	3.40	ST
3	Pedersen et al. (2004), Fluid-22	311.06	305.45	2.291	3587	5.5	4.42	GOR
4[¥]	Li et al. (2013a), Lloydminster Oil	482.00	347.67	1.352	3166	9.0	5.60	PT
5[¥]	Badamchi-Zadeh et al. (2009) Athabasca Bitumen	552.00	333.15	1.060	2870	12.0		PT
6[¥]	Mehrotra and Svrcek (1985),Peace River Bitumen	527.50	326.65	1.541	2625	12.0		PT

* ST and GOR stand for Swelling Test and Gas Oil Ratio, respectively. PT stands for 2- and 3-phase Pressure-Temperature data.
# Includes oleic phase saturation prediction for 60% and 80% CO_2 mixtures. For 60% CO_2 mixture only, it is 1.53%.
¥ For Oils 1, 4, 5, and 6, three-phase P-T envelopes are shown in separate figures.

Table 7-5. Characterization results for oils for which three phases with CO_2 were reported in the literature.

Parameters β and k are defined in the algorithm section. Parameter p indicates the degree of freedom in the chi-squired distribution.

Oil No.	References	MW (gm/mol)	Temp. (K)	β	k	p
1	Turek et al. (1988), Oil B1	149.62	314.26	1.550	4921	6.0
2	Turek et al. (1988), Oil B2	151.22	314.26	1.184	3302	6.1
3	Turek et al. (1988), Oil C2	140.30	313.71	1.454	4477	6.1
4	Turek et al. (1988), Oil D	182.42	313.71	1.551	4577	6.9
5	Khan et al. (1992), Oil BSB	148.88	313.70	1.458	4826	5.6
6	Winzinger et al. (1991), Oil NWE	138.45	301.48	1.325	4037	5.8
7	Khan et al. (1992), Oil JEMA	156.72	316.48	1.113	3092	5.2
8	Shelton and Yarborough (1977), Oil-B	161.47	307.60	1.470	4536	7.5
9	Creek and Sheffield (1993), Oil-G	113.13	307.59	1.311	4290	5.8
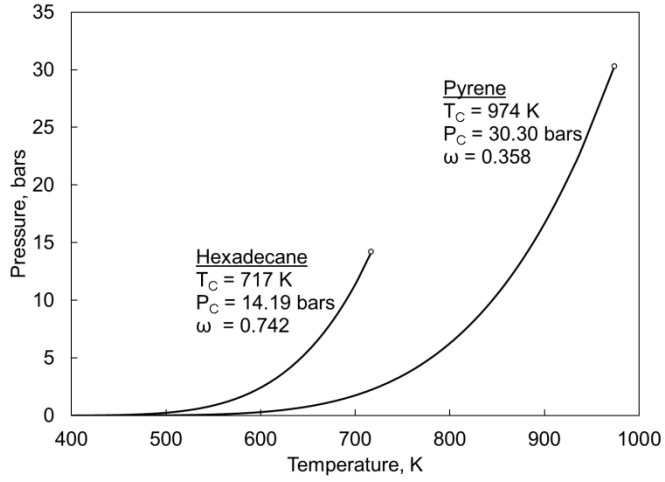
Figure 7-1. Comparison of critical parameters and vapor pressure curves for hexadecane (Yaws 2010) and pyrene (Nikitin and Popov 2015).
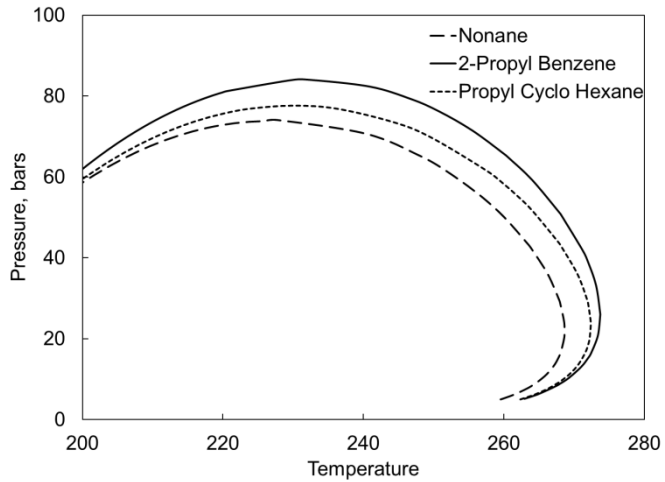
Figure 7-2. Comparison of two-phase envelopes for 99.99% binary mixture of methane with nonane (n-C_9), propyl cyclo hexane (C_9H_{18}), and 2-propyl benzene (C_9H_{12}).
Phase envelope for n-C_9 is innermost.
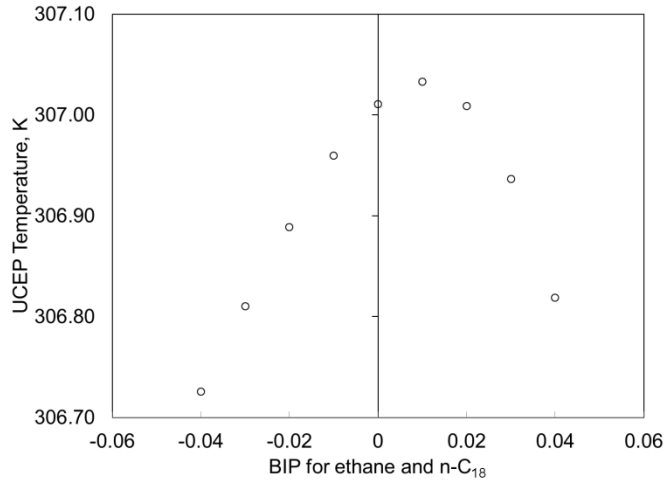
Figure 7-3. Predicted UCEP for ethane and n-C$_{18}$ mixture at different BIP values. For nC$_{18}$ optimized critical parameters (Kumar and Okuno 2012) are used.
The UCEP of this mixture is (312.45 K, 55.31 bars).
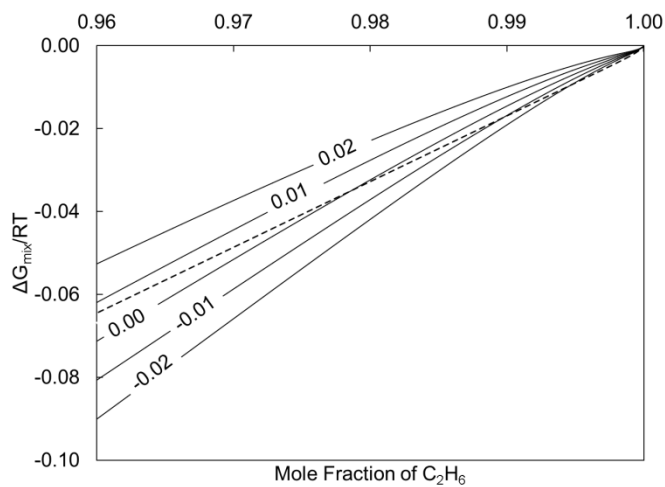
Figure 7-4. Trend of reduced Gibbs free energy of mixing at UCEP of ethane and n-C18 mixture at (312.45 K, 55.31 bars).
The dotted curve is predicted with physical critical parameters from Gao et al. (2001) for n-C$_{18}$, and optimized BIP (that matched UCEP). Solid curves are for optimized critical parameters (Kumar and Okuno 2012) for n-C$_{18}$ and different BIPs (shown on the curves). Optimized critical parameters could not match the desired trend of reduced Gibbs free energy to UCEP match.
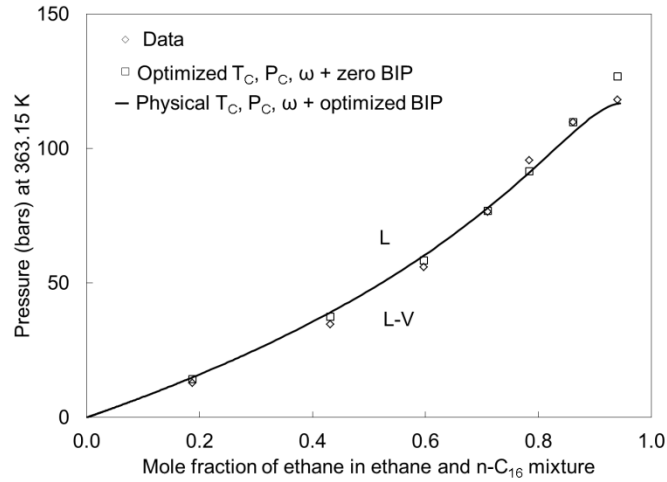
Figure 7-5. Comparison of P-x diagram for ethane and n-C$_{16}$ mixture at 363.15 K with experimental data (Peters et al. 1988).
Predictions are made from (1) optimized critical parameters (Kumar and Okuno 2012) and zero BIP and, (2) physical critical parameters (Gao et al. 2001) and optimized BIP (Kumar and Okuno 2015).
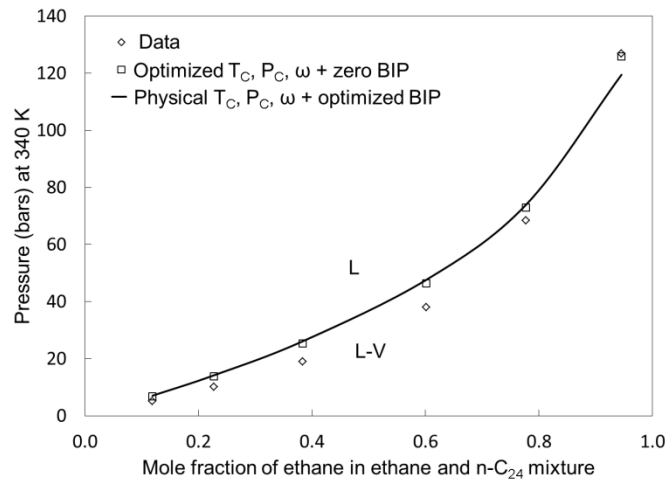
Figure 7-6. Comparison of P-x diagram for ethane and n-C$_{24}$ mixture at 340 K with experimental data (Peters et al. 1988).
Predictions are made from (1) optimized critical parameters (Kumar and Okuno 2012) and zero BIP and, (2) physical critical parameters (Gao et al. 2001) and optimized BIP (Kumar and Okuno 2015).
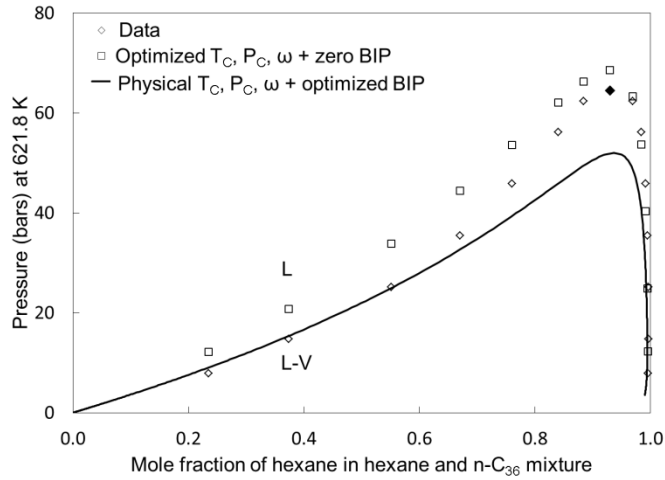
Figure 7-7. Comparison of P-x diagram for hexane and n-C$_{36}$ mixture at 621.8 K with experimental data (Joyce and Gordon 2000).
Predictions are made from (1) optimized critical parameters (Kumar and Okuno 2012) and zero BIP and, (2) physical critical parameters (Gao et al. 2001) and zero BIP.
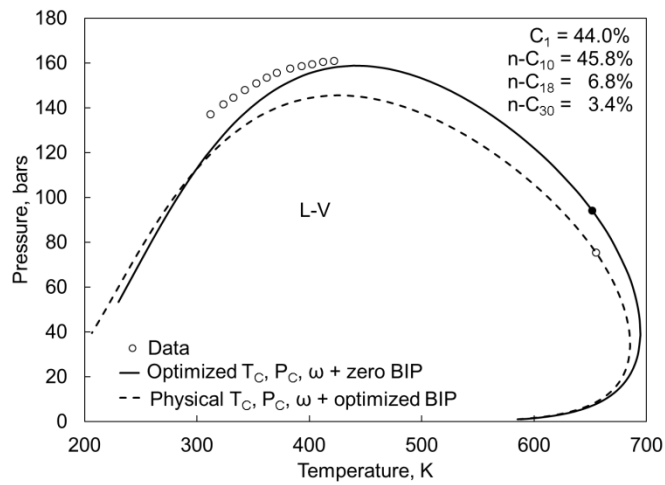
Figure 7-8. Comparison of P-T diagrams for quaternary mixture of methane, n-C$_{10}$, n-C$_{18}$, and n-C$_{30}$ with experimental data (Daridon et al. 1996).
Predictions are made from (1) optimized critical parameters (Kumar and Okuno 2012) and zero BIP and, (2) physical critical parameters (Gao et al. 2001) and optimized BIP (Kumar and Okuno 2015).

243
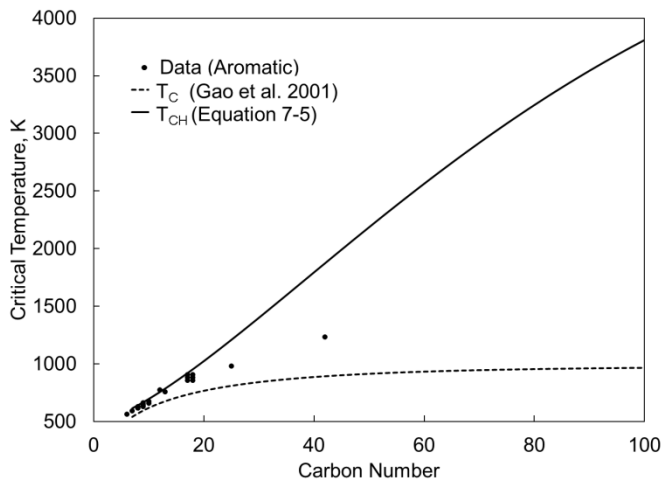
Figure 7-9. Comparison of empirically determined higher boundary correlation for critical temperature in Equation 7-5 with data (Yaws 2010, Nikitin and Popov 2015).
N-alkane equivalent values from Gao et al. (2001) for pseudocomponents form the lower boundary.
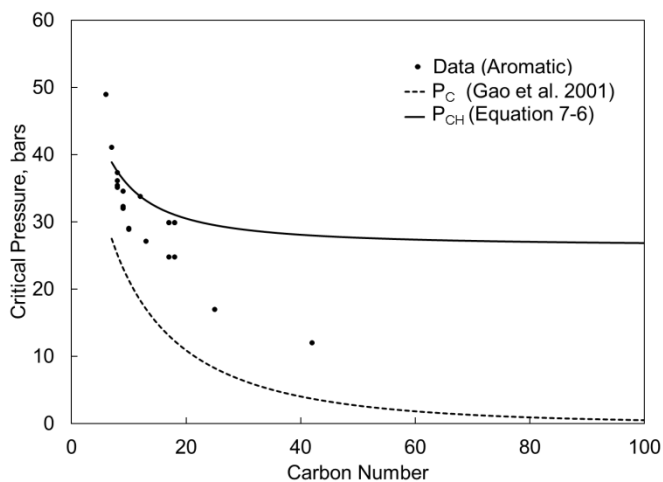
Figure 7-10. Comparison of empirically determined higher boundary correlation for critical pressure in Equation 7-6 with data (Yaws 2010, Nikitin and Popov 2015).
N-alkane equivalent values from Gao et al. (2001) for pseudocomponents form the lower boundary.
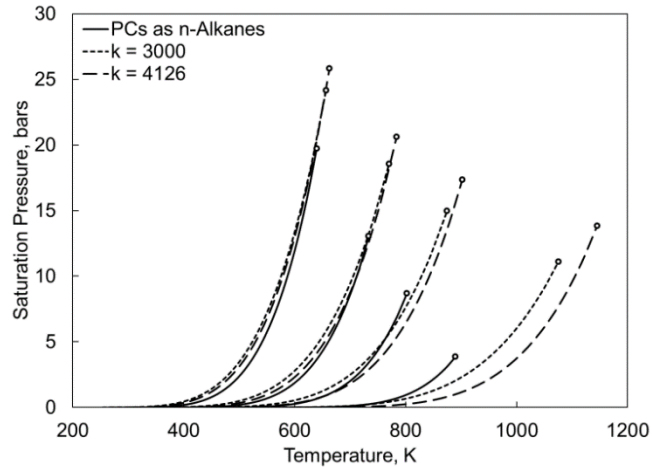
(a)
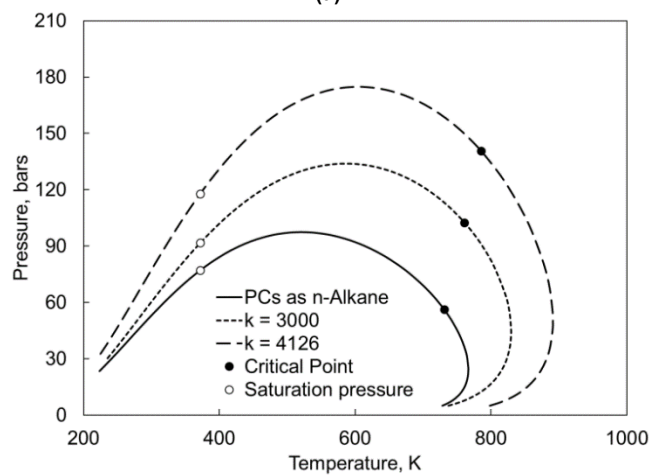
(b)
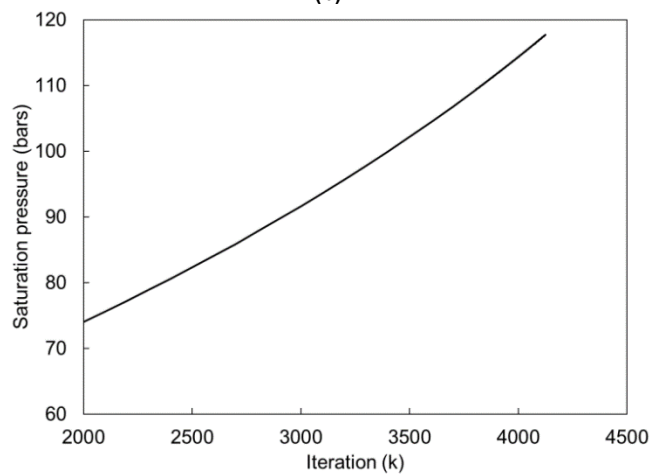
(c)

Figure 7-11. Systematic changes in vapor pressure curves for pseudocomponents and P-T envelope for fluid with changes in k parameter during regression.

Figure 7-11a shows the changes in T_C and P_C of four pseudocomponents and resulting vapor pressure curves. Figure 7-11b shows the change in two-phase envelope for the fluid. There is systematic change in vapor pressure curves for pseudocomponents and two-phase envelope with increasing k parameter.

Figure 7-11c shows change in saturation pressure at 372.05 K with iteration (k).

245
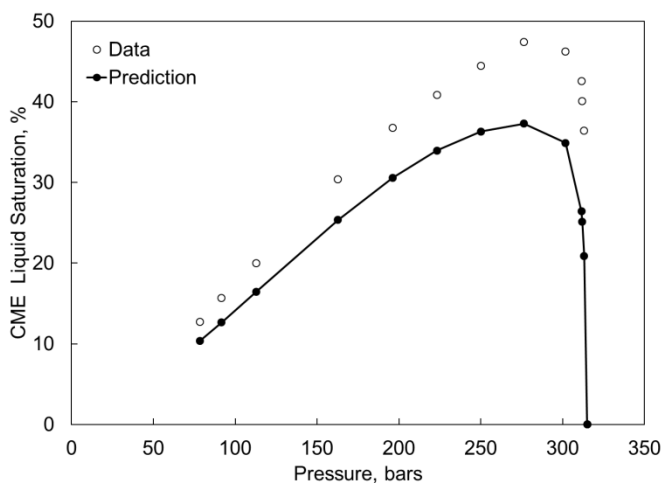
Figure 7-12. CME liquid saturation predicted for near-critical gas condensate, Fluid 36 in Table 7-2, at 366.48 K. The molecular weight is 39.34 gram/mole.
The mole fraction and molecular weight of the heptane plus are 0.1003 and 172.0 gram/mole respectively.
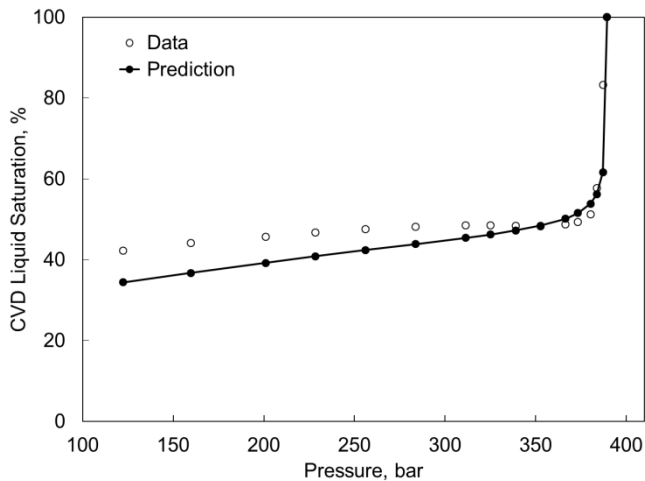
Figure 7-13. CVD liquid saturation predicted for near-critical volatile oil, Fluid 54 in Table 7-2, at 424.25 K. The molecular weight is 47.84 gram/mole.
The mole fraction and molecular weight of the heptane plus are 0.1417 and 194.0 gram/mole respectively. The critical point was measured at 426 K and 388 bars. The critical point predicted with the characterized EOS is at 434.65 K and 391.43 bars.
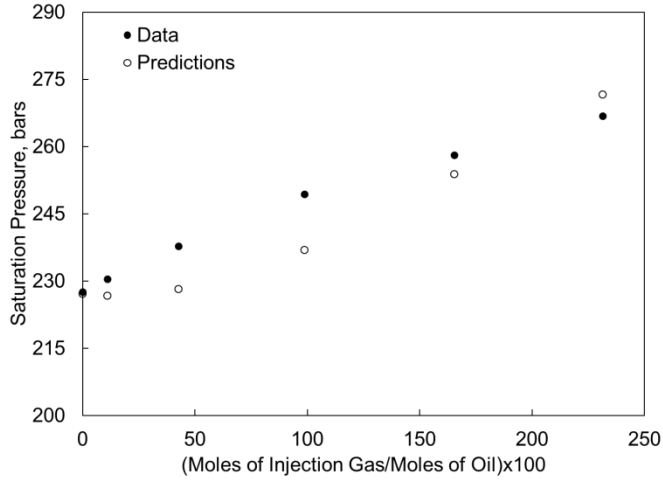
Figure 7-14. Saturation pressures during the swelling test for Oil 2 in Table 7-4 at 347.15 K. The molecular weight and API gravity of the oil are 125.98 gram/mole and 28, respectively.
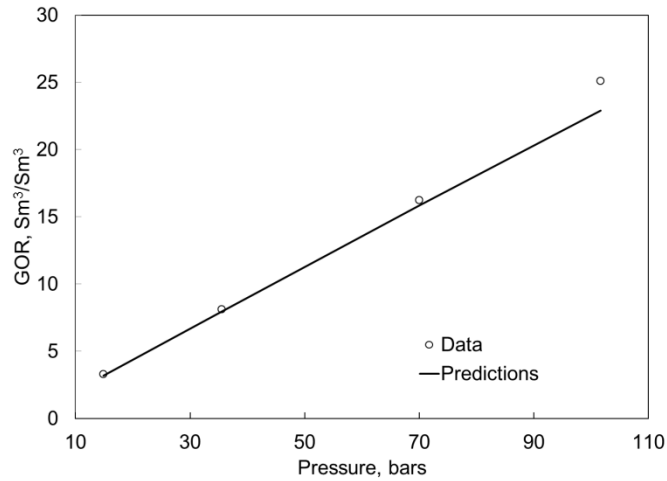
Figure 7-15. Gas-oil ratio (GOR) predictions at 305.45 K for Oil 3 in Table 7-4. The molecular weight of this oil is 311.06 gram/mole. This is highly aromatic oil, according to Pedersen et al. (2004).
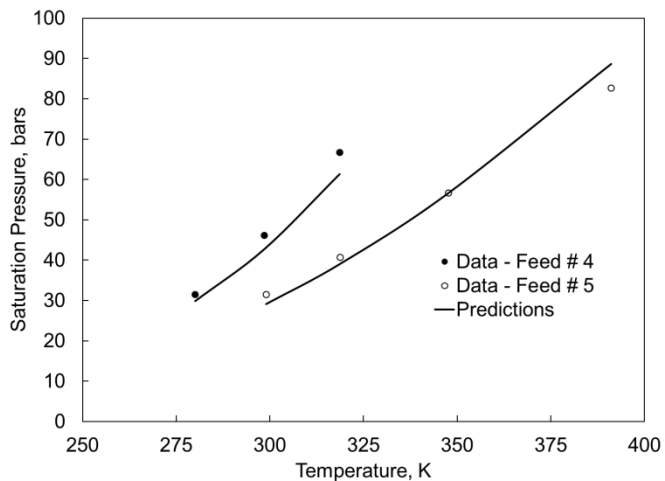
Figure 7-16. Saturation pressures measured and predicted for two mixtures with Lloydminster heavy oil, Oil 4 in Table 4 (Feeds #4 and #5 in Li et al., 2013a).
The AARD of the saturation pressure predictions is 6.8% for Feed #4 and 4.7% for Feed #5.
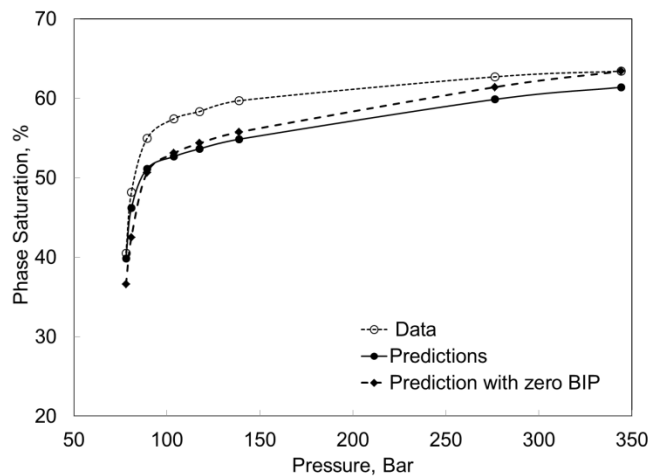
(a)
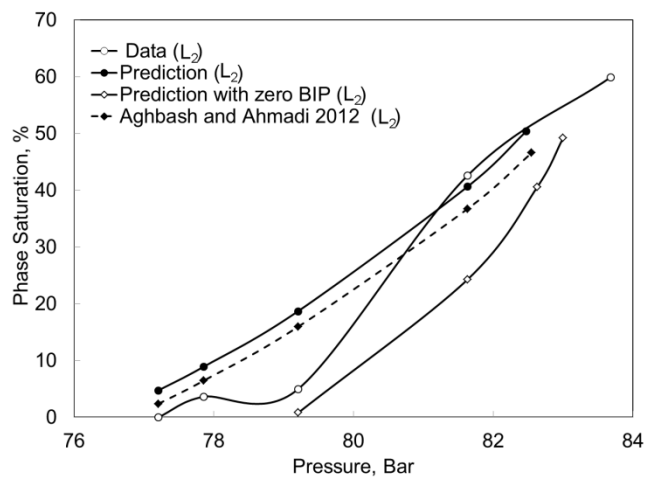
(b)

Figure 7-17. Liquid-phase saturations for West Sak heavy oil (Oil 1 in Table 4) mixed with CO_2 at 299.81 K. (a) Oleic (L_1) phase. (b) Solvent-rich liquid (L_2) phase.
Three phases prediction with zero BIP for hydrocarbon-hydrocarbon is also shown.
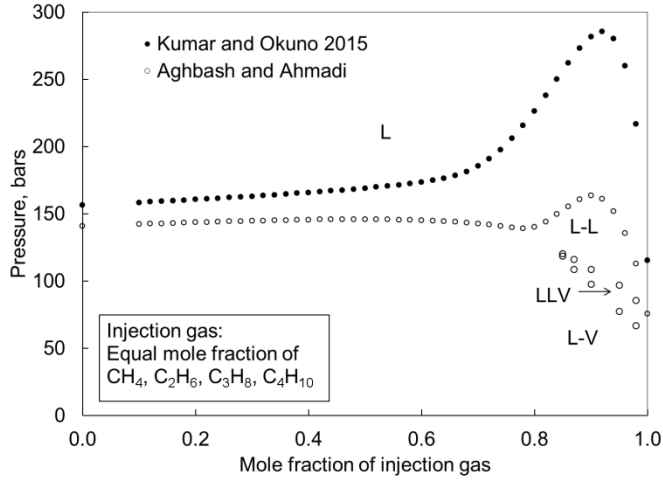
Figure 7-18. Comparison of P-x diagrams for oil 1 in Table 7-5 at 370 K predicted with EOS models from new algorithm and Aghabsh and Ahmadi (2012).
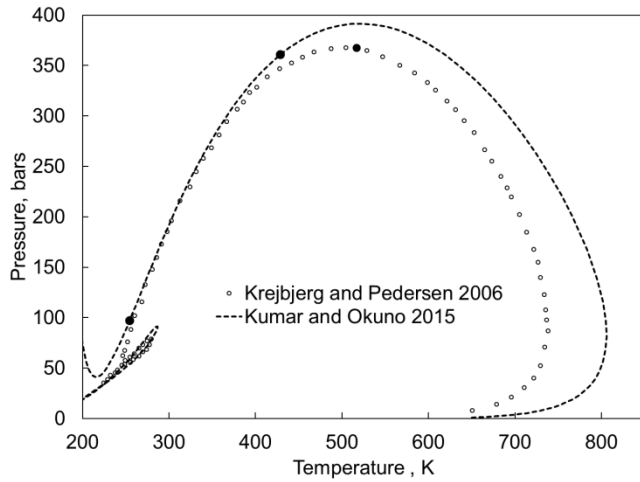
Figure 7-19. Comparison of P-T envelope predicted with SRK EOS by Krejbjerg and Pedersen (2006) with prediction from new algorithm for oil 2 in Table 7-4.
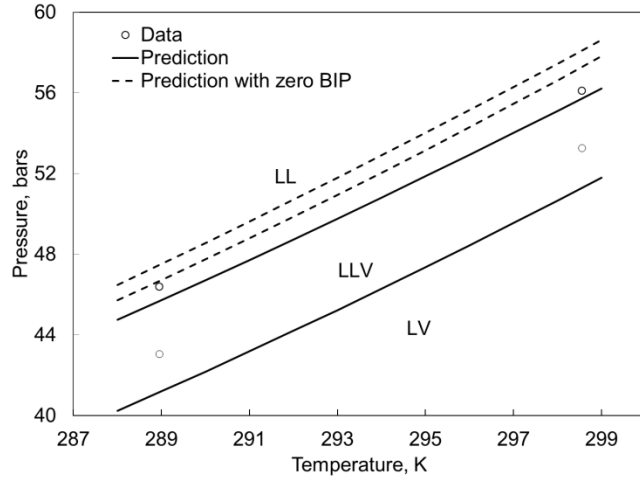
(a)
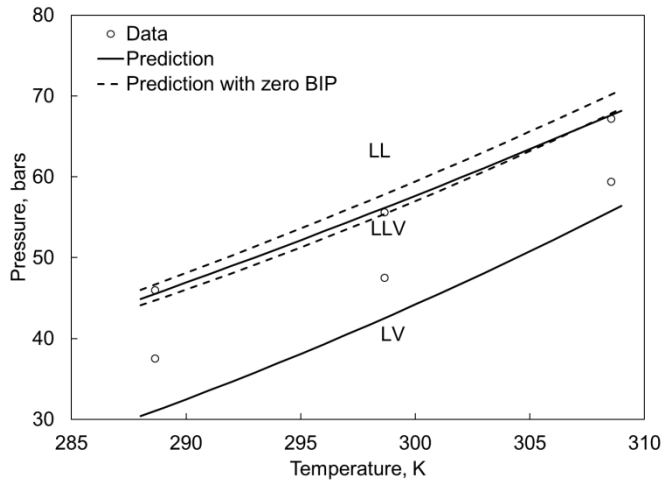
(b)

Figure 7-20. Comparison of three-phase boundaries for the West Sak oil and CO_2 mixture. (a) Feed 14 of Li et al. (2013b), consisting of 23.6% propane, 67.2% CO_2, and 9.2% heavy oil. (b) Feed 15 of Li et al. (2013b), consisting of 11.8% butane, 83.2% CO_2, and 5.0% heavy oil. The heavy oil is from Lloydminster (Table 7-4). Three phases prediction with zero BIP for hydrocarbon-hydrocarbon is also shown.
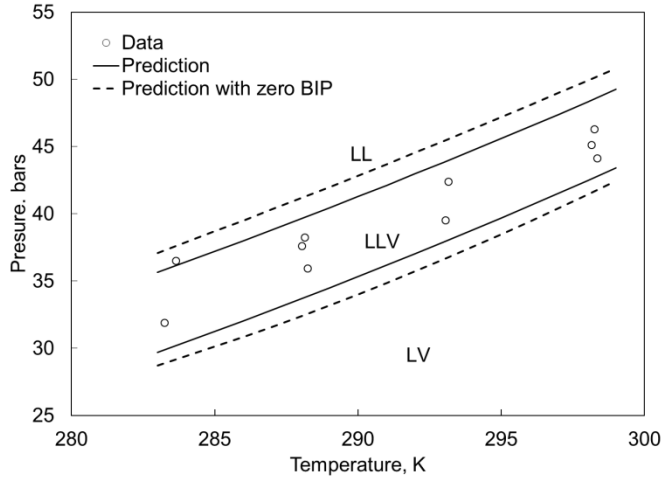
Figure 7-21. Three-phase boundaries measured and predicted for a mixture of Athabasca bitumen: 51.0% CO_2, 34.7% propane, and 14.3% bitumen (Badamchi-Zadeh et al. 2009).
Three phases prediction with zero BIP for hydrocarbon-hydrocarbon is also shown.
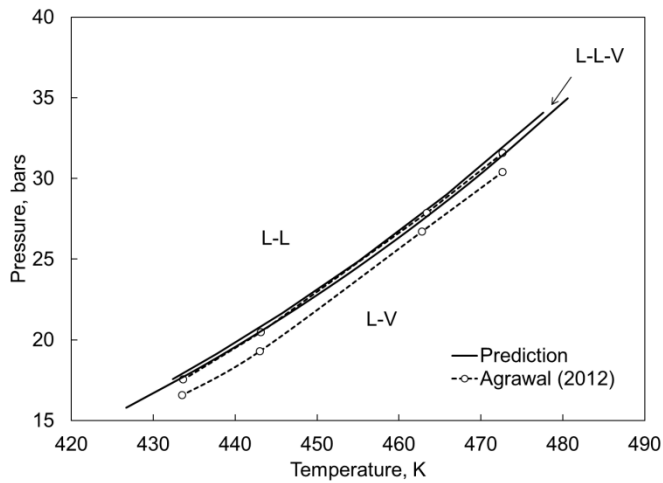
Figure 7-22. Three-phase boundaries measured and predicted for a mixture of Peace River bitumen: 89.90% pentane and 10.10% bitumen.
The bitumen was characterized using the data from Mehrotra and Svrcek (1985).   Three-phase boundaries simulated by Agrawal (2012) are also shown. Prediction with zero BIP for hydrocarbon-hydrocarbon did not show presence of three phases.
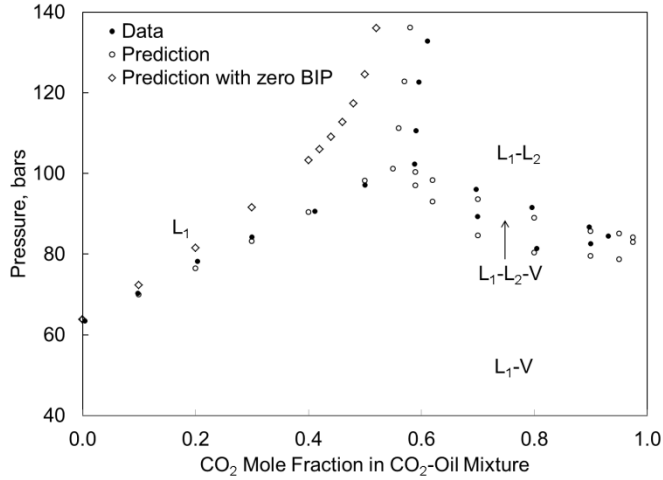
Figure 7-23. Comparison of the predicted P-x diagram with data for Oil C2 (Table 7-5) of Turek et al. (1988) with CO_2 at 313.71 K.
Prediction with zero BIP for hydrocarbon-hydrocarbon did not show presence of three phases.
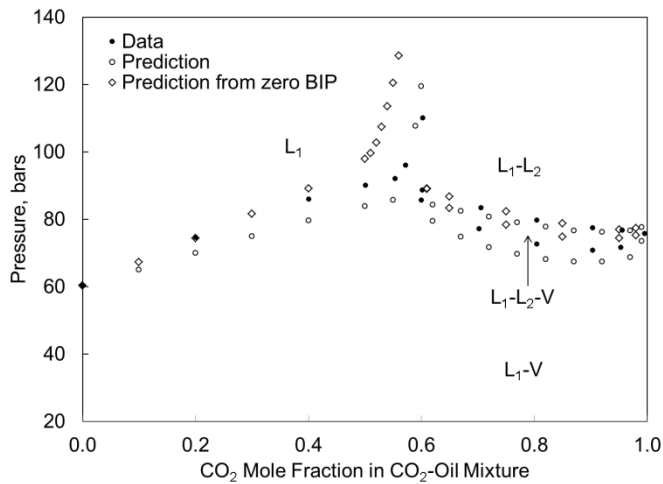
Figure 7-24. Comparison of the predicted P-x diagram for Oil G (Table 5) of Creek and Sheffield (1993) with CO_2 at 307.60 K.
Prediction with zero BIP for hydrocarbon-hydrocarbon shows the presence of three-phase area detached from the single-phase boundary.
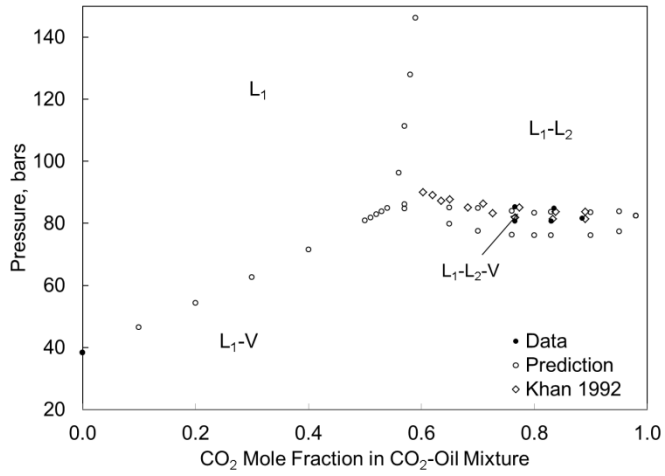
Figure 7-25. Comparison of the predicted P-x diagram at 313.70 K from Khan 1992 EOS model with prediction from new algorithm for oil 5 in Table 7-5.
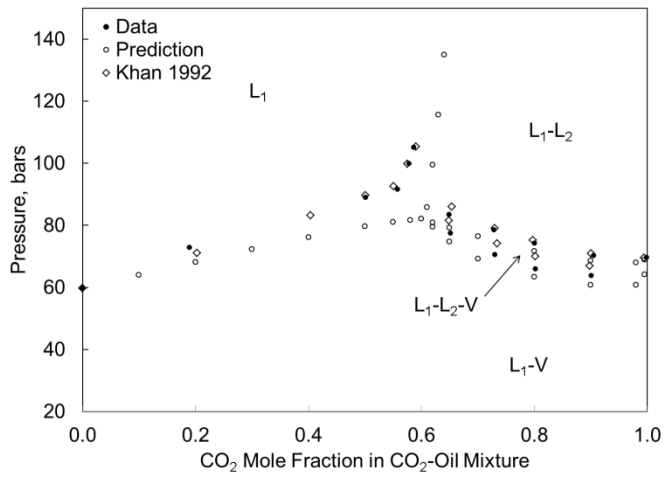
Figure 7-26. Comparison of the predicted P-x diagram at 301.48 K from Khan 1992 EOS model with prediction from new algorithm for oil 6 in Table 7-5.
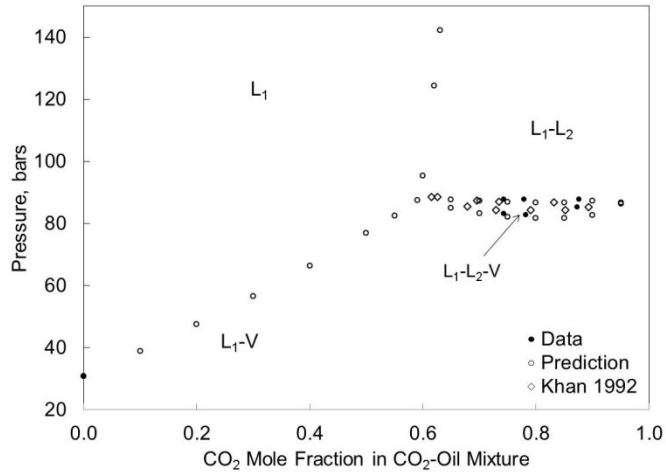
Figure 7-27. Comparison of the predicted P-x diagram at 316.48 K from Khan 1992 EOS model with prediction from new algorithm for oil 7 in Table 7-5.
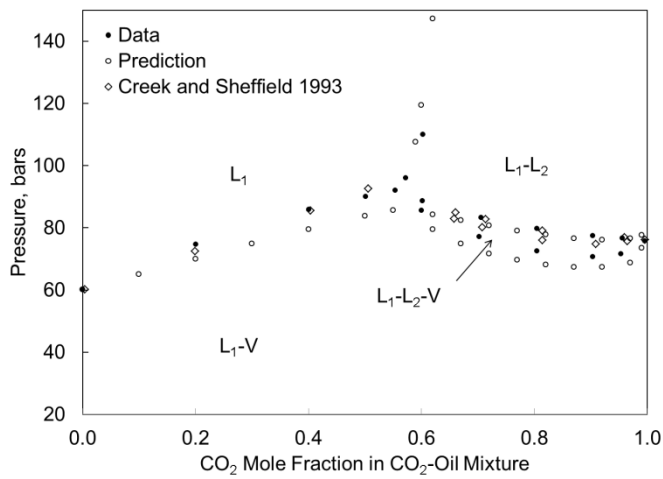
Figure 7-28. Comparison of the predicted P-x diagram at 307.60 K from Creek and Sheffield (1993) EOS model with prediction from new algorithm for oil 9 in Table 7-5.

Chapter 8: Summary, Conclusion and Recommendation

8.1. Summary of Research

Basic objective of this research was to develop a characterization method for multiphase PVT simulation applicable to a hydrocarbon system irrespective of its composition range using systematic approach and reliable BIP. Systematic approach implies well-defined and physically justifiable initial (default) values and search direction for EOS parameters. The approach of perturbation from n-alkane (PnA) has essential features ensuring systematic reservoir fluid characterization; hence, this approach forms the fundamental of the reservoir fluid characterization proposed in this research.

Fundamental of PnA approach is based on well-known systematic behavior of thermo- physical properties of three main hydrocarbon groups of compounds i.e. paraffins, naphthenes, and aromatics. For same carbon number components, paraffins have lowest T_C, and P_C; and highest ω among the three hydrocarbon groups of compounds. Pseudocomponents may be considered as mixture of these three hydrocarbon groups; hence, the lowest T_C, the lowest P_C and the highest ω values for a pseudocomponent correspond to respective values estimated with assumption that pseudocomponent is 100% paraffin. Higher T_C and P_C values and lower ω values for pseudocomponents are then found to match saturation pressure data.

The n-alkane equivalent critical parameter values are estimated in two ways corresponding to two approaches for reservoir fluid density matching i.e. density matching either by critical parameters' adjustment or by volume shift parameters' adjustment. The PnA approaches for reservoir fluid characterization presented in Chapter 3 to 6 adjust attraction and covolume parameters for density match. Normal alkane equivalent critical parameters for pseudocomponents in these approaches are estimated with correlations developed using optimized critical parameters and acentric factors, which match vapor pressure and density data for n-alkanes from n-C_7 to n-C_{100} with PR EOS; development of these correlations is described in Chapter 2. The optimized T_C and P_C are greater than corresponding physical values; optimized acentric factors are smaller than respective physical values. Chapter 7 presents the PnA approach for reservoir fluid characterization, where physical critical parameters from Gao et al. (2001) are used to assign n-alkane equivalent critical parameters for pseudocomponents. In this approach, density matching is done by adjusting temperature independent volume shift parameters like conventional characterization methods.

This research is presented in six different papers with different objectives in line with the research goals presented in the introduction section. Chapter 2 presents correlations to estimate critical parameters for n-alkanes optimized for vapor pressure and density data matching with PR EOS. Development of algorithm for reservoir fluids was at initial stage and limited to verification of perturbation parameter being greater than the minimum value allowed. In Chapter 3, PnA method was developed with three variables and applied to 22 oils. This chapter also compares the phase behavior predictions from characterization with/without using volume shift to match density. Application of PnA approach in Chapter 3 was limited to few oils; hence, the approach needed to be validated by including more fluids. In Chapter 4, the characterization is validated with 77 reservoir fluids comprising of 31 gas condensates,

12 volatile oils and 31 other oils. Application of the approach, particularly to light fluid types, required modification of algorithm developed in the Chapter 3; however, the algorithm in Chapter 3 was special case of algorithm in Chapter 4. This chapter also presented the trend of parameter ψ (= a/b^2) with single carbon number fractions at different aromaticity level, which is distinctive for a given range of carbon number of components present in a reservoir fluid. This trend has been used to verify conformity of attraction and covolume parameters for a characterized reservoir fluid to desired physical trends.

The Chapter 5 presents PnA approach for characterizing 84 reservoir fluids (47 gas condensates, 15 volatile oils, 18 oils, and 4 heavy oils) by direct perturbation of attraction and covolume parameters maintaining characteristic trends defined by ψ parameter as described in Chapter 3 and 4. The regression algorithm, which has two regression parameters, was simpler than that used in Chapter 4 and showed similar or improved phase behavior prediction including prediction for three hydrocarbon phases. Chapter 6 presents application of algorithm presented in Chapter 5 in simple form to 6 bitumens. This algorithm results in similar phase behavior predictions for single pseudocomponent bitumens as compared to multi component conventional characterization. This chapter presents a mechanism for sensitivity of bitumen recovery simulation to characterization methods. Such sensitivity analysis, carried out before running simulation of bitumen recovery with ES-SAGD process, can provide important guidelines for selection of reliable and efficient bitumen characterization method.

Chapter 7 presents a well-developed reservoir fluid characterization using PnA approach for multiphase behavior prediction for 90 reservoir fluids (48 gas condensates, 7 volatile oils, 29 other oils, 4 heavy oils, and 2 bitumens). Similar to the algorithm presented in Chapter 4, algorithm presented in this chapter also directly perturbs T_C, P_C, and ω for pseudocomponents for reservoir fluid characterization. However, the algorithm presented in Chapter 7 differs from that in Chapter 4 in followings ways:

(1) Single parameter is used to adjust T_C, P_C, and ω.
(2) The BIPs are used for components like N_2, CO_2, CH_4, C_2H_6, C_3H_8, C_4H_{10} and C_5H_{12}. The BIPs for CO_2, CH_4, C_2H_6, C_3H_8, C_4H_{10} and C_5H_{12} with heavier n-alkanes are developed using multiphase behavior data for binary and ternary mixtures.
(3) Saturation pressure is matched by T_C, P_C, and ω adjustment and density matching is done using volume shift parameters.

Predictive capability of the algorithm presented in this Chapter 7 is better than that presented in Chapter 4. The average absolute deviation for CVD liquid saturation, CME liquid saturation, and average absolute relative deviation for MMP predictions in Chapter 4 were 2.10%, 3.57% and 6.7 % respectively; corresponding deviations in Chapter 7 are 1.5%, 2.5%, and 4.57% respectively. Chapter 7 included maximum number of fluids for three-phase predictions (9 oils, 2 heavy oils, and 2 bitumens) and for all these cases, three hydrocarbon phases have been predicted satisfactorily.

8.2. Conclusions

This research presents a simple, robust, and reliable fluid characterization for multiphase behavior simulation for hydrocarbon system irrespective of fluid type. Conclusions are the following:

(1) Perturbation from n-alkane approach provides reliable and robust framework for multiphase reservoir fluid characterization because of well-defined initial PR EOS parameters values for pseudocomponents and physically justified search direction for regression parameters.

(2) Irrespective of density matching either by using volume shift parameter or by adjusting critical parameters, the PnA method was found to be applicable for multiphase characterization; that is, the effect of aromaticity on phase behavior can be modeled by adjusting T_C, P_C, and ω of pseudocomponents as monotonic functions of regression parameters.

(3) The regression parameters in the PnA approach, unlike the conventional characterization, are not component specific, which makes the algorithm simple and easy in retaining the physical trend of the PR-EOS parameters with carbon number of pseudocomponents during regression. The regression of adjustable parameters is well defined and physically justified, unlike undefined manual regression approach in the conventional characterization.

(4) The PnA approach used for reservoir fluid characterization is systematic and simple. The phase behavior change during the regression of adjustable parameters is systematic; hence, saturation pressure varies monotonically with the regression parameters in all algorithms developed.

(5) Parameters such as γ (Chapter 4), C (Chapter 5), β (Chapter 7) are presented as correlations; however, these parameters can be used as adjustable variables, if needed, to match other types of PVT data such as CVD liquid saturation, minimum miscibility pressure etc. As shown (Chapter 4 and 5), predictions of other types PVT measurements (apart from saturation pressure) are monotonic functions of these parameters; matching of these PVT measurements may not be possible with conventional approach.

(6) The PnA based fluid characterization algorithms presented in Chapters 2 to 7 were able to achieve the specific objectives set in these chapters. Phase behavior simulation for n-alkanes' mixture is recommended with the optimized T_C, P_C, and ω developed in Chapter 2. The optimized parameters can reliably predict two-phase behavior with zero BIPs. The algorithm presented in Chapter 3 is a specific case of the algorithm presented in Chapter 4, and uses perturbation of T_C, P_C, and ω. The algorithm using direct perturbation of the attraction and covolume parameter is presented in Chapter 5, and its simplified form is applied to bitumens in Chapter 6. The algorithms presented in Chapters 5 and 6 have additional benefit of having fewer regression parameters. All these algorithms use zero BIPs for hydrocarbon-hydrocarbon pairs, zero volume shift parameters and optimized T_C, P_C, and ω. These algorithms are recommended for reliable two-phase behavior simulation. Three-phase behavior simulation from these algorithms may not be reliable because of the following reasons:

o   Algorithms in Chapter 4 and Chapter 6 are based on the PR EOS calibrated for two-phase behavior using optimized T_C, P_C, and ω for n-alkanes.

o   Three-phase behavior is more reliable with physical critical parameters and non-zero hydrocarbon-hydrocarbon BIPs as examined in Chapter 7.

o   The amount of three-phase data used for validation of three-phase behavior in Chapter 4 to Chapter 6 is limited.

The algorithm presented in Chapter 7 is reliable for multiphase behavior simulation. This algorithm uses BIPs that are optimized for multiphase behavior prediction. The algorithm has been validated by using 90 reservoir fluids, including 13 fluids that are used for validation of three-phase behavior simulation. Hence, the characterization approach presented in Chapter 7 is recommended for EOS-model development for multiphase PVT simulation. However, since density matching in this algorithm is same as that for the conventional characterization, it is important that volume shift parameters be properly modeled for reliable density prediction in range of pressure, temperature, and composition that are expected in reservoir oil displacement during gas injection.

(7)   The PnA characterization uses a small amount of data (saturation pressure and density data); however, it does not undermine the importance of including more phase behavior data in fluid characterization. Particularly for gas injection, predictions from the PnA characterization should be validated by using more compositional and volumetric phase behavior data.

(8)   The algorithm presented for multiphase behavior predictions uses unmodified form of PR EOS; hence, application of the characterization method requires no change in commercial software.

8.3. Recommendations for Future Research

Recommendations for future research are as follows:

(1) The impact of three-phase PnA characterization on multiphase flow simulation could not be studied in this research due to the unavailability of detailed data for multiphase oil displacement.

(2) Systematic characterization of critical end points for reservoir fluid and solvent mixture is recommended for future study. Although the condition, under which high displacement efficiency in the presence of three hydrocarbon phases is possible, is known, no systematic approach to achieving that is known.

(3) Heptane plus fractions in the PnA approach are modeled by using the chi-squared distribution function. It is not known how splitting of the plus fraction with a more general form of probability distribution function (i.e. gamma distribution) and a simpler form (i.e. logarithmic distribution) will affect the present characterization. This work can be done, and the present approach may be modified accordingly.

(4) This research did not include the impact of the number of components on phase behavior predictions with the PnA method. A study may be done on the impact of using more pseudo components. This may be helpful for phase behavior prediction for near critical fluids, such as near critical gas condensates or volatile oil.

(5) The correlation for BIP of CO_2 with heavier n-alkanes presented in this research is independent of temperature. However, prior publications show that BIP of CO_2 is sensitive to temperature. A research on this may be conducted using phase behavior data with a wide temperature range.

(6) The SRK EOS is simpler than the PR EOS. The expression of fugacity with the SRK EOS is smaller than that with the PR EOS, which can contribute to computational efficiency. It is possible to develop a fluid characterization method using the PnA approach for the SRK EOS.

(7) Systematic study of aromaticity on fluid characterization has not been carried out. This is because of the unavailability of suitable data for aromatic components. A research of experimental work combined with analytical study to find EOS parameters as function of aromaticity of fluid mixtures containing paraffins, naphthenic and aromatics may be undertaken.

(8) The attraction and covolume parameters developed in Chapter 5 and Chapter 6 may be used for the friction theory based viscosity model developed by Quiñones-Cisneros et al. (2004). The friction theory based viscosity model uses the attraction and covolume parameters. Since the algorithm presented in Chapter 5 yields the attraction and covolume parameters for heavy oils and bitumens for compositional as well as volumetric phase behavior predictions, it is expected that their use in viscosity model will improve the correlative accuracy for viscosity data for heavy oils and bitumens.

(9) Heavy oils have been split into SARA (Saturates, Aromatics, Resin, and Asphaltene). A possibility may be looked into for applying the PnA approach for these fractions for heavy oil characterization.

Appendices

Appendix 2-A: Quality of density and vapor pressure data matching

Table 2-A1. Sources and T-P ranges of data used for optimizing T_C, P_C, ω, and AADs in density predictions. AADs using optimum T_C, P_C, and ω developed in this research are compared to those using the correlations of Gao et al. (2001).

n-Alkane	Reference	No. of Data	T_r Range	P_r Range	This Research	Gao et al.
		Density Data			AAD, Liquid Density	
C_7H_{16}	Doolittle (1964), Schilling et al. 2008	214	0.43-1.06	0.01-180.32	2.0	1.9
C_8H_{18}	Goodwin (1996), Perry and Green (2007)	54	0.52-1.05	0.52-1.05	2.3	3.5
C_9H_{20}	Doolittle (1964), Schilling et al. (2008)	212	0.39-0.98	0.39-0.98	2.2	4.5
$C_{10}H_{22}$	Doolittle (1964), Susnar et al. (1992)	131	0.48-0.98	0.48-0.98	1.5	6.0
$C_{11}H_{24}$	Doolittle (1964), Yaws (2010)	90	0.48-0.91	0.48-0.91	2.9	7.1
$C_{12}H_{26}$	Doolittle (1964), Yaws (2010)	170	0.48-0.79	0.48-0.79	1.5	8.8
$C_{13}H_{28}$	Elizalde-Solis (2007), Yaws (2010)	170	0.46-0.79	0.46-0.79	1.5	10.6
$C_{14}H_{30}$	Khasanshin and Shchemelev (2002), Yaws (2010)	80	0.42-0.79	0.42-0.79	3.1	12.5
$C_{15}H_{32}$	Daridon et al. (2002), Yaws (2010)	162	0.42-0.79	0.42-0.79	3.1	15.3
$C_{16}H_{34}$	Daridon et al. (2002), Yaws (2010)	193	0.43-0.78	0.43-0.78	2.4	14.7
$C_{17}H_{36}$	Doolittle (1964), Yaws (2010)	80	0.44-0.79	0.44-0.79	4.2	17.0
$C_{18}H_{38}$	Dutour et al. (2000), Yaws (2010)	123	0.42-0.88	0.42-0.88	5.0	20.7
$C_{19}H_{40}$	Dutour et al. (2000), Yaws (2010)	119	0.41-0.88	0.41-0.88	5.5	22.0
$C_{20}H_{42}$	Doolittle (1964), Yaws (2010)	70	0.48-0.87	0.48-0.87	4.8	21.4
$C_{21}H_{44}$	Yaws (2010)	20	0.59-0.78	0.59-0.78	1.0	21.1
$C_{22}H_{46}$	Yaws (2010)	20	0.59-0.77	0.59-0.77	1.1	22.7
$C_{23}H_{48}$	Dutour et al. (2001), Yaws (2010)	110	0.41-0.78	0.41-0.78	6.7	28.6
$C_{24}H_{50}$	Dutour et al. (2001), Yaws (2010)	105	0.41-0.77	0.41-0.77	6.6	30.1
$C_{25}H_{52}$	Yaws (2010)	20	0.59-0.77	0.59-0.77	1.3	27.3
$C_{26}H_{54}$	Yaws (2010)	20	0.59-0.77	0.59-0.77	1.6	28.6
$C_{27}H_{56}$	Yaws (2010)	20	0.59-0.77	0.59-0.77	1.7	30.0
$C_{28}H_{58}$	Dutour et al. (2002), Yaws (2010)	101	0.41-0.86	0.41-0.86	6.9	35.8
$C_{29}H_{60}$	Yaws (2010)	20	0.58-0.86	0.58-0.86	2.9	32.9
$C_{30}H_{62}$	Aucejo et al. (1995), Yaws (2010)	70	0.43-0.86	0.43-0.86	5.6	37.3
$C_{31}H_{64}$	Yaws (2010)	20	0.58-0.85	0.58-0.85	0.8	37.7
$C_{32}H_{66}$	Yaws (2010)	19	0.59-0.85	0.59-0.85	4.7	36.9
$C_{33}H_{68}$	Yaws (2010)	19	0.59-0.84	0.59-0.84	0.7	41.9
$C_{34}H_{70}$	Yaws (2010)	19	0.59-0.84	0.59-0.84	1.0	42.3
$C_{35}H_{72}$	Yaws (2010)	19	0.59-0.84	0.59-0.84	0.6	44.5
$C_{36}H_{74}$	Dutour et al. (2002), Yaws (2010)	83	0.40-0.85	0.40-0.85	4.2	46.8
$C_{37}H_{76}$	Yaws (2010)	19	0.57-0.82	0.57-0.82	0.6	47.4
$C_{38}H_{78}$	Yaws (2010)	18	0.60-0.84	0.60-0.84	0.5	48.8
$C_{39}H_{80}$	Yaws (2010)	18	0.59-0.83	0.59-0.83	0.5	50.0
$C_{40}H_{82}$	Doolittle (1964), Yaws (2010)	58	0.45-0.84	0.45-0.84	3.8	50.8
$C_{41}H_{84}$	Yaws (2010)	18	0.59-0.83	0.59-0.83	0.5	52.1
$C_{42}H_{86}$	Yaws (2010)	18	0.59-0.83	0.59-0.83	0.5	53.2
$C_{43}H_{88}$	Yaws (2010)	18	0.59-0.83	0.59-0.83	2.3	53.2
$C_{44}H_{90}$	Yaws (2010)	17	0.60-0.83	0.60-0.83	0.6	55.2
$C_{45}H_{92}$	Yaws (2010)	17	0.60-0.83	0.60-0.83	0.5	56.2
$C_{46}H_{94}$	Yaws (2010)	17	0.60-0.83	0.60-0.83	0.5	57.2
$C_{47}H_{96}$	Yaws (2010)	17	0.61-0.83	0.61-0.83	0.5	58.1
$C_{48}H_{98}$	Yaws (2010)	17	0.60-0.82	0.60-0.82	0.5	59.0
$C_{49}H_{100}$	Yaws (2010)	17	0.60-0.82	0.60-0.82	0.5	59.9
$C_{50}H_{102}$	Yaws (2010)	17	0.60-0.83	0.60-0.83	0.7	60.7
$C_{51}H_{104}$	Yaws (2010)	17	0.60-0.82	0.60-0.82	0.6	61.6
$C_{52}H_{106}$	Yaws (2010)	16	0.61-0.82	0.61-0.82	0.4	62.5
$C_{53}H_{108}$	Yaws (2010)	16	0.61-0.82	0.61-0.82	0.5	63.3
$C_{54}H_{110}$	Yaws (2010)	16	0.61-0.82	0.61-0.82	0.7	64.1
$C_{55}H_{112}$	Yaws (2010)	16	0.61-0.82	0.61-0.82	0.5	64.8
$C_{56}H_{114}$	Yaws (2010)	16	0.61-0.82	0.61-0.82	0.6	65.6
$C_{57}H_{116}$	Yaws (2010)	16	0.63-0.90	0.63-0.90	1.6	68.3
$C_{58}H_{118}$	Yaws (2010)	16	0.61-0.81	0.61-0.81	0.5	67.0
$C_{59}H_{120}$	Yaws (2010)	16	0.61-0.81	0.61-0.81	0.4	67.7
$C_{60}H_{122}$	Yaws (2010)	16	0.62-0.90	0.62-0.90	1.5	70.2
$C_{61}H_{124}$	Yaws (2010)	16	0.62-0.90	0.62-0.90	1.8	70.9
$C_{62}H_{126}$	Yaws (2010)	16	0.62-0.90	0.62-0.90	1.5	71.5

$C_{63}H_{128}$	Yaws (2010)	15	0.64-0.90	0.64-0.90	1.8	72.2
$C_{64}H_{130}$	Yaws (2010)	15	0.64-0.90	0.64-0.90	1.6	72.8
$C_{65}H_{132}$	Yaws (2010)	15	0.64-0.89	0.64-0.89	1.8	73.4
$C_{66}H_{134}$	Yaws (2010)	15	0.64-0.89	0.64-0.89	1.6	73.9
$C_{67}H_{136}$	Yaws (2010)	15	0.64-0.89	0.64-0.89	1.7	74.5
$C_{68}H_{138}$	Yaws (2010)	15	0.64-0.89	0.64-0.89	1.6	75.0
$C_{69}H_{140}$	Yaws (2010)	15	0.64-0.89	0.64-0.89	1.7	75.5
$C_{70}H_{142}$	Yaws (2010)	15	0.64-0.89	0.64-0.89	1.6	76.0
$C_{71}H_{144}$	Yaws (2010)	15	0.64-0.89	0.64-0.89	1.7	76.5
$C_{72}H_{146}$	Yaws (2010)	15	0.63-0.89	0.63-0.89	1.6	77.0
$C_{73}H_{148}$	Yaws (2010)	15	0.63-0.89	0.63-0.89	1.7	77.4
$C_{74}H_{150}$	Yaws (2010)	15	0.63-0.89	0.63-0.89	1.6	77.9
$C_{75}H_{152}$	Yaws (2010)	15	0.63-0.89	0.63-0.89	1.8	78.3
$C_{76}H_{154}$	Yaws (2010)	15	0.63-0.88	0.63-0.88	1.6	78.8
$C_{77}H_{156}$	Yaws (2010)	15	0.63-0.89	0.63-0.89	1.9	79.2
$C_{78}H_{158}$	Yaws (2010)	15	0.63-0.88	0.63-0.88	1.7	79.6
$C_{79}H_{160}$	Yaws (2010)	15	0.63-0.88	0.63-0.88	1.7	80.1
$C_{80}H_{162}$	Yaws (2010)	15	0.63-0.88	0.63-0.88	1.7	80.5
$C_{81}H_{164}$	Yaws (2010)	15	0.61-0.80	0.61-0.80	1.6	79.6
$C_{82}H_{166}$	Yaws (2010)	14	0.62-0.80	0.62-0.80	2	80.0
$C_{83}H_{168}$	Yaws (2010)	14	0.62-0.79	0.62-0.79	1.7	80.4
$C_{84}H_{170}$	Yaws (2010)	14	0.65-0.88	0.65-0.88	2.2	82.1
$C_{85}H_{172}$	Yaws (2010)	14	0.65-0.88	0.65-0.88	1.9	82.4
$C_{86}H_{174}$	Yaws (2010)	14	0.65-0.88	0.65-0.88	1.9	82.8
$C_{87}H_{176}$	Yaws (2010)	14	0.65-0.88	0.65-0.88	2.2	83.1
$C_{88}H_{178}$	Yaws (2010)	14	0.65-0.88	0.65-0.88	2.0	83.4
$C_{89}H_{180}$	Yaws (2010)	14	0.65-0.88	0.65-0.88	2.0	83.8
$C_{90}H_{182}$	Yaws (2010)	14	0.64-0.88	0.64-0.88	2.3	84.1
$C_{91}H_{184}$	Yaws (2010)	14	0.64-0.88	0.64-0.88	2.1	84.4
$C_{92}H_{186}$	Yaws (2010)	14	0.64-0.88	0.64-0.88	2.2	84.7
$C_{93}H_{188}$	Yaws (2010)	14	0.64-0.88	0.64-0.88	2.6	85.0
$C_{94}H_{190}$	Yaws (2010)	14	0.64-0.88	0.64-0.88	2.3	85.3
$C_{95}H_{192}$	Yaws (2010)	14	0.64-0.88	0.64-0.88	2.2	85.6
$C_{96}H_{194}$	Yaws (2010)	14	0.64-0.88	0.64-0.88	2.2	85.8
$C_{97}H_{196}$	Yaws (2010)	14	0.64-0.88	0.64-0.88	2.7	86.1
$C_{98}H_{198}$	Yaws (2010)	14	0.64-0.88	0.64-0.88	2.3	86.4
$C_{99}H_{200}$	Yaws (2010)	14	0.64-0.88	0.64-0.88	2.3	86.6
$C_{100}H_{202}$	Yaws (2010)	14	0.64-0.88	0.64-0.88	2.8	86.9

Table 2-A2. Sources and T-P ranges of data used for optimizing T_C, P_C, ω, and AADs in vapor pressure predictions. AADs using optimum T_C, P_C, and ω developed in this research are compared to those using the correlations of Gao et al. (2001).

n-Alkane	Reference	Vapor Pressure Data		AAD Vapor Pressure	
		No. of Data	T_r Range	This Research	Gao et al. (2001)
C_7H_{16}	Perry and Green (2007), Ewing and Ochoa (2005)	35	0.69-0.95	0.5	0.5
C_8H_{18}	Perry and Green (2007), Gregorowicz et al.(1987)	27	0.53-0.95	0.5	1.7
C_9H_{20}	Perry and Green (2007)	12	0.54-0.91	1.3	2.1
$C_{10}H_{22}$	Perry and Green (2007), Gregorowicz et al.(1987)	28	0.50-0.92	1.1	3.8
$C_{11}H_{24}$	Riazi and AlQaheem (2010)	10	0.60-0.90	2.0	19.3
$C_{12}H_{26}$	Perry and Green (2007)	14	0.53-0.93	4.1	2.0
$C_{13}H_{28}$	Riazi and AlQaheem (2010)	10	0.60-0.90	3.2	16.9
$C_{14}H_{30}$	Morgan and Kobayashi (1994)	20	0.60-0.79	1.6	0.9
$C_{15}H_{32}$	Riazi and AlQaheem (2010)	10	0.59-0.90	5.1	15.0
$C_{16}H_{34}$	Morgan and Kobayashi (1994)	19	0.55-0.80	4.0	0.7
$C_{17}H_{36}$	Riazi and AlQaheem (2010)	10	0.59-0.89	4.5	13.5
$C_{18}H_{38}$	Morgan and Kobayashi (1994)	20	0.60-0.88	3.8	1.1
$C_{19}H_{40}$	Morgan and Kobayashi (1994)	20	0.59-0.88	4.1	1.2
$C_{20}H_{42}$	Morgan and Kobayashi (1994)	20	0.59-0.87	2.8	2.1
$C_{21}H_{44}$	Riazi and AlQaheem (2010)	20	0.59-0.78	1.8	1.3
$C_{22}H_{46}$	Morgan and Kobayashi (1994)	22	0.57-0.88	3.9	5.5
$C_{23}H_{48}$	Riazi and AlQaheem (2010)	20	0.59-0.78	2.3	1.4
$C_{24}H_{50}$	Morgan and Kobayashi (1994)	20	0.59-0.77	2.0	1.4
$C_{25}H_{52}$	Riazi and AlQaheem (2010)	20	0.59-0.77	1.0	1.4
$C_{26}H_{54}$	Riazi and AlQaheem (2010)	20	0.59-0.77	2.7	1.3
$C_{27}H_{56}$	Riazi and AlQaheem (2010)	20	0.59-0.77	0.6	1.3
$C_{28}H_{58}$	Morgan and Kobayashi (1994)	20	0.58-0.86	3.0	1.4
$C_{29}H_{60}$	Riazi and AlQaheem (2010)	20	0.58-0.86	1.4	1.4
$C_{30}H_{62}$	Riazi and AlQaheem (2010)	20	0.58-0.86	1.1	1.5
$C_{31}H_{64}$	Riazi and AlQaheem (2010)	20	0.58-0.85	1.4	1.5
$C_{32}H_{66}$	Riazi and AlQaheem (2010)	19	0.59-0.85	1.8	1.6
$C_{33}H_{68}$	Riazi and AlQaheem (2010)	19	0.59-0.84	0.8	1.9
$C_{34}H_{70}$	Riazi and AlQaheem (2010)	19	0.59-0.84	1.3	2.3
$C_{35}H_{72}$	Riazi and AlQaheem (2010)	19	0.59-0.84	0.9	2.8
$C_{36}H_{74}$	Riazi and AlQaheem (2010)	18	0.60-0.85	2.3	3.3
$C_{37}H_{76}$	Riazi and AlQaheem (2010)	17	0.60-0.82	0.9	3.9
$C_{38}H_{78}$	Riazi and AlQaheem (2010)	18	0.60-0.84	1.0	4.4
$C_{39}H_{80}$	Riazi and AlQaheem (2010)	18	0.59-0.83	1.1	5.0
$C_{40}H_{82}$	Riazi and AlQaheem (2010)	17	0.61-0.84	1.4	11.3
$C_{41}H_{84}$	Riazi and AlQaheem (2010)	17	0.61-0.83	0.9	13.3
$C_{42}H_{86}$	Riazi and AlQaheem (2010)	17	0.61-0.83	1.0	13.8
$C_{43}H_{88}$	Riazi and AlQaheem (2010)	17	0.61-0.83	0.8	14.4
$C_{44}H_{90}$	Riazi and AlQaheem (2010)	17	0.60-0.83	1.4	15.0
$C_{45}H_{92}$	Riazi and AlQaheem (2010)	17	0.60-0.83	1.2	15.6
$C_{46}H_{94}$	Riazi and AlQaheem (2010)	16	0.62-0.83	1.5	15.8
$C_{47}H_{96}$	Riazi and AlQaheem (2010)	16	0.62-0.83	1.6	16.5
$C_{48}H_{98}$	Riazi and AlQaheem (2010)	16	0.61-0.82	1.6	17.3
$C_{49}H_{100}$	Riazi and AlQaheem (2010)	16	0.61-0.82	2.3	18.1
$C_{50}H_{102}$	Riazi and AlQaheem (2010)	16	0.62-0.83	1.0	17.8
$C_{51}H_{104}$	Riazi and AlQaheem (2010)	16	0.61-0.82	3.0	18.9
$C_{52}H_{106}$	Riazi and AlQaheem (2010)	15	0.62-0.82	0.7	19.2
$C_{53}H_{108}$	Riazi and AlQaheem (2010)	15	0.62-0.82	0.7	20.3
$C_{54}H_{110}$	Riazi and AlQaheem (2010)	15	0.62-0.82	0.7	21.3
$C_{55}H_{112}$	Riazi and AlQaheem (2010)	15	0.62-0.82	0.7	22.4
$C_{56}H_{114}$	Riazi and AlQaheem (2010)	15	0.62-0.82	0.7	23.5
$C_{57}H_{116}$	Riazi and AlQaheem (2010)	16	0.63-0.90	1.0	22.2
$C_{58}H_{118}$	Riazi and AlQaheem (2010)	15	0.62-0.81	0.7	25.6
$C_{59}H_{120}$	Riazi and AlQaheem (2010)	15	0.63-0.81	0.5	26.8
$C_{60}H_{122}$	Riazi and AlQaheem (2010)	16	0.62-0.90	1.0	25.2
$C_{61}H_{124}$	Riazi and AlQaheem (2010)	16	0.62-0.90	1.1	26.2
$C_{62}H_{126}$	Riazi and AlQaheem (2010)	16	0.64-0.90	0.9	27.3
$C_{63}H_{128}$	Riazi and AlQaheem (2010)	15	0.64-0.90	1.0	27.0
$C_{64}H_{130}$	Riazi and AlQaheem (2010)	15	0.64-0.90	1.0	28.0
$C_{65}H_{132}$	Riazi and AlQaheem (2010)	15	0.64-0.89	1.0	29.0

$C_{66}H_{134}$	Riazi and AlQaheem (2010)	15	0.64-0.89	0.9	30.0
$C_{67}H_{136}$	Riazi and AlQaheem (2010)	15	0.64-0.89	1.1	31.1
$C_{68}H_{138}$	Riazi and AlQaheem (2010)	15	0.64-0.89	0.8	32.1
$C_{69}H_{140}$	Riazi and AlQaheem (2010)	15	0.64-0.89	1.1	33.2
$C_{70}H_{142}$	Riazi and AlQaheem (2010)	15	0.64-0.89	0.9	34.2
$C_{71}H_{144}$	Riazi and AlQaheem (2010)	15	0.64-0.89	1.0	35.3
$C_{72}H_{146}$	Riazi and AlQaheem (2010)	15	0.63-0.89	0.9	36.3
$C_{73}H_{148}$	Riazi and AlQaheem (2010)	15	0.63-0.89	1.0	37.4
$C_{74}H_{150}$	Riazi and AlQaheem (2010)	15	0.63-0.89	0.9	38.4
$C_{75}H_{152}$	Riazi and AlQaheem (2010)	15	0.63-0.89	1.1	39.5
$C_{76}H_{154}$	Riazi and AlQaheem (2010)	15	0.65-0.88	0.8	40.6
$C_{77}H_{156}$	Riazi and AlQaheem (2010)	14	0.65-0.89	1.3	38.2
$C_{78}H_{158}$	Riazi and AlQaheem (2010)	14	0.65-0.88	0.9	39.3
$C_{79}H_{160}$	Riazi and AlQaheem (2010)	14	0.65-0.88	1.0	40.5
$C_{80}H_{162}$	Riazi and AlQaheem (2010)	14	0.65-0.88	0.9	41.6
$C_{81}H_{164}$	Riazi and AlQaheem (2010)	12	0.65-0.80	0.5	46.3
$C_{82}H_{166}$	Riazi and AlQaheem (2010)	12	0.65-0.80	0.4	47.4
$C_{83}H_{168}$	Riazi and AlQaheem (2010)	12	0.65-0.79	0.4	48.6
$C_{84}H_{170}$	Riazi and AlQaheem (2010)	14	0.65-0.88	1.3	46.0
$C_{85}H_{172}$	Riazi and AlQaheem (2010)	14	0.65-0.88	1.1	47.1
$C_{86}H_{174}$	Riazi and AlQaheem (2010)	14	0.65-0.88	1.2	48.2
$C_{87}H_{176}$	Riazi and AlQaheem (2010)	14	0.65-0.88	1.3	49.3
$C_{88}H_{178}$	Riazi and AlQaheem (2010)	14	0.65-0.88	1.4	50.4
$C_{89}H_{180}$	Riazi and AlQaheem (2010)	14	0.65-0.88	1.8	51.4
$C_{90}H_{182}$	Riazi and AlQaheem (2010)	14	0.64-0.88	1.6	52.5
$C_{91}H_{184}$	Riazi and AlQaheem (2010)	14	0.64-0.88	1.8	53.6
$C_{92}H_{186}$	Riazi and AlQaheem (2010)	14	0.64-0.88	2.2	54.6
$C_{93}H_{188}$	Riazi and AlQaheem (2010)	14	0.64-0.88	2.6	55.6
$C_{94}H_{190}$	Riazi and AlQaheem (2010)	14	0.64-0.88	2.3	56.7
$C_{95}H_{192}$	Riazi and AlQaheem (2010)	14	0.64-0.88	2.5	57.7
$C_{96}H_{194}$	Riazi and AlQaheem (2010)	14	0.64-0.88	2.9	58.7
$C_{97}H_{196}$	Riazi and AlQaheem (2010)	14	0.64-0.88	3.0	59.7
$C_{98}H_{198}$	Riazi and AlQaheem (2010)	13	0.66-0.88	3.3	59.0
$C_{99}H_{200}$	Riazi and AlQaheem (2010)	13	0.66-0.88	3.6	59.9
$C_{100}H_{202}$	Riazi and AlQaheem (2010)	13	0.66-0.88	4.2	60.9

Appendix 2-B: Optimized T_C, P_C, and ω for n-alkanes from n-C_7 to n-C_{100}

Table 2-B. T_C, P_C, m, and ω optimized in this research and T_C, P_C, and ω from the correlations of Gao et al. (2001) for n-alkanes from C_7 to C_{100}.

n-Alkanes	Optimized Values in This Research				Correlations of Gao et al. (2001)		
	T_C /K	P_C/ Bar	m	ω	T_C /K	P_C /Bar	ω
C_7H_{16}	542.48	27.73	0.8687	0.3407	540.40	27.497	0.3474
C_8H_{18}	570.59	25.74	0.9465	0.3986	569.44	25.142	0.3936
C_9H_{20}	595.96	23.97	1.0187	0.4536	595.30	23.097	0.4389
$C_{10}H_{22}$	618.54	22.35	1.0888	0.5043	618.53	21.304	0.4833
$C_{11}H_{24}$	628.90	21.03	1.1436	0.5456	639.55	19.717	0.5269
$C_{12}H_{26}$	657.99	19.81	1.2205	0.6042	658.69	18.302	0.5696
$C_{13}H_{28}$	666.68	18.65	1.2705	0.6426	676.19	17.034	0.6116
$C_{14}H_{30}$	694.01	17.65	1.3197	0.6808	692.28	15.891	0.6529
$C_{15}H_{32}$	698.81	17.01	1.3955	0.7401	707.12	14.856	0.6934
$C_{16}H_{34}$	723.05	16.06	1.4277	0.7657	720.86	13.915	0.7333
$C_{17}H_{36}$	729.58	15.23	1.4737	0.8024	733.61	13.057	0.7725
$C_{18}H_{38}$	751.46	14.86	1.5157	0.8358	745.48	12.271	0.8112
$C_{19}H_{40}$	764.37	14.31	1.5481	0.8618	756.56	11.549	0.8492
$C_{20}H_{42}$	777.28	13.66	1.5936	0.8988	766.91	10.884	0.8866
$C_{21}H_{44}$	787.93	13.09	1.6271	0.9261	776.61	10.271	0.9235
$C_{22}H_{46}$	796.83	12.67	1.6672	0.9589	785.71	9.704	0.9599
$C_{23}H_{48}$	810.48	12.30	1.6956	0.9824	794.27	9.178	0.9957
$C_{24}H_{50}$	821.85	11.95	1.7157	0.9990	802.33	8.690	1.0310
$C_{25}H_{52}$	830.97	11.58	1.7429	1.0216	809.92	8.235	1.0659
$C_{26}H_{54}$	841.21	11.26	1.7738	1.0474	817.09	7.812	1.1002
$C_{27}H_{56}$	849.96	10.96	1.7900	1.0609	823.87	7.417	1.1341
$C_{28}H_{58}$	859.36	10.70	1.8281	1.0930	830.28	7.048	1.1675
$C_{29}H_{60}$	867.48	10.41	1.8433	1.1058	836.35	6.702	1.2005
$C_{30}H_{62}$	876.02	10.27	1.8600	1.1200	842.11	6.378	1.2331
$C_{31}H_{64}$	883.77	9.98	1.8733	1.1313	847.58	6.074	1.2652
$C_{32}H_{66}$	891.11	9.81	1.8948	1.1496	852.77	5.788	1.2970
$C_{33}H_{68}$	899.07	9.67	1.9179	1.1693	857.71	5.519	1.3283
$C_{34}H_{70}$	905.91	9.43	1.9433	1.1911	862.41	5.266	1.3593
$C_{35}H_{72}$	911.58	9.29	1.9665	1.2110	866.88	5.028	1.3898
$C_{36}H_{74}$	918.25	9.16	1.9750	1.2184	871.14	4.803	1.4200
$C_{37}H_{76}$	924.99	8.98	2.0001	1.2400	875.21	4.591	1.4499
$C_{38}H_{78}$	930.93	8.81	2.0173	1.2549	879.08	4.390	1.4794
$C_{39}H_{80}$	936.66	8.64	2.0326	1.2683	882.79	4.200	1.5085
$C_{40}H_{82}$	940.00	8.43	2.0596	1.2918	886.32	4.021	1.5373
$C_{41}H_{84}$	946.66	8.28	2.0681	1.2993	889.71	3.851	1.5657
$C_{42}H_{86}$	951.88	8.16	2.0835	1.3127	892.94	3.690	1.5939
$C_{43}H_{88}$	955.98	8.02	2.1014	1.3285	896.03	3.537	1.6217
$C_{44}H_{90}$	961.81	7.88	2.1121	1.3379	899.00	3.391	1.6492
$C_{45}H_{92}$	965.59	7.69	2.1282	1.3521	901.84	3.254	1.6764
$C_{46}H_{94}$	970.20	7.59	2.1433	1.3655	904.56	3.123	1.7033
$C_{47}H_{96}$	974.00	7.44	2.1602	1.3805	907.16	2.998	1.7299
$C_{48}H_{98}$	978.03	7.30	2.1714	1.3904	909.66	2.879	1.7562
$C_{49}H_{100}$	982.25	7.16	2.1832	1.4009	912.06	2.767	1.7822
$C_{50}H_{102}$	985.00	7.03	2.1947	1.4112	914.37	2.659	1.8080
$C_{51}H_{104}$	990.33	6.93	2.2088	1.4238	916.58	2.557	1.8334
$C_{52}H_{106}$	993.20	6.83	2.2092	1.4242	918.70	2.459	1.8586
$C_{53}H_{108}$	996.97	6.77	2.2185	1.4325	920.75	2.366	1.8836
$C_{54}H_{110}$	1000.64	6.69	2.2267	1.4398	922.71	2.277	1.9082
$C_{55}H_{112}$	1003.20	6.56	2.2404	1.4521	924.60	2.192	1.9327
$C_{56}H_{114}$	1006.68	6.48	2.2475	1.4585	926.42	2.111	1.9568
$C_{57}H_{116}$	1009.06	6.36	2.2610	1.4707	928.16	2.033	1.9808
$C_{58}H_{118}$	1012.36	6.28	2.2669	1.4760	929.85	1.959	2.0044
$C_{59}H_{120}$	1014.56	6.17	2.2800	1.4878	931.47	1.888	2.0279
$C_{60}H_{122}$	1017.69	6.10	2.2853	1.4926	933.03	1.820	2.0511
$C_{61}H_{124}$	1020.75	6.08	2.2938	1.5003	934.53	1.755	2.0741
$C_{62}H_{126}$	1022.71	5.94	2.3037	1.5093	935.98	1.693	2.0968
$C_{63}H_{128}$	1025.62	5.91	2.3112	1.5161	937.38	1.633	2.1193
$C_{64}H_{130}$	1027.42	5.79	2.3216	1.5255	938.73	1.576	2.1416
$C_{65}H_{132}$	1030.20	5.75	2.3275	1.5309	940.02	1.521	2.1637

C$_{66}$H$_{134}$	1032.91	5.65	2.3271	1.5305	941.28	1.469	2.1856
C$_{67}$H$_{136}$	1034.52	5.60	2.3429	1.5449	942.49	1.419	2.2072
C$_{68}$H$_{138}$	1038.14	5.52	2.3333	1.5362	943.66	1.370	2.2287
C$_{69}$H$_{140}$	1038.59	5.46	2.3577	1.5584	944.78	1.324	2.2499
C$_{70}$H$_{142}$	1042.09	5.39	2.3486	1.5501	945.87	1.279	2.2710
C$_{71}$H$_{144}$	1043.48	5.33	2.3622	1.5625	946.92	1.236	2.2918
C$_{72}$H$_{146}$	1045.83	5.26	2.3625	1.5628	947.94	1.195	2.3125
C$_{73}$H$_{148}$	1047.11	5.21	2.3753	1.5745	948.92	1.156	2.3330
C$_{74}$H$_{150}$	1050.40	5.15	2.3652	1.5653	949.87	1.118	2.3532
C$_{75}$H$_{152}$	1050.53	5.10	2.3882	1.5864	950.79	1.081	2.3733
C$_{76}$H$_{154}$	1053.73	5.03	2.3756	1.5748	951.67	1.046	2.3932
C$_{77}$H$_{156}$	1053.77	5.00	2.4006	1.5978	952.53	1.012	2.4129
C$_{78}$H$_{158}$	1056.87	4.94	2.3887	1.5868	953.36	0.980	2.4325
C$_{79}$H$_{160}$	1058.92	4.88	2.3925	1.5903	954.16	0.948	2.4518
C$_{80}$H$_{162}$	1059.86	4.83	2.3983	1.5957	954.94	0.918	2.4710
C$_{81}$H$_{164}$	1061.80	4.78	2.3977	1.5951	955.69	0.889	2.4901
C$_{82}$H$_{166}$	1061.61	4.73	2.4196	1.6153	956.42	0.861	2.5089
C$_{83}$H$_{168}$	1064.53	4.68	2.4069	1.6036	957.12	0.834	2.5276
C$_{84}$H$_{170}$	1065.31	4.66	2.4206	1.6162	957.81	0.808	2.5461
C$_{85}$H$_{172}$	1067.11	4.59	2.4165	1.6124	958.47	0.783	2.5645
C$_{86}$H$_{174}$	1067.80	4.54	2.4247	1.6200	959.11	0.759	2.5826
C$_{87}$H$_{176}$	1069.54	4.52	2.4259	1.6211	959.73	0.736	2.6007
C$_{88}$H$_{178}$	1070.17	4.46	2.4334	1.6280	960.33	0.713	2.6185
C$_{89}$H$_{180}$	1070.78	4.41	2.4455	1.6392	960.91	0.692	2.6363
C$_{90}$H$_{182}$	1072.40	4.39	2.4405	1.6346	961.47	0.671	2.6538
C$_{91}$H$_{184}$	1072.92	4.33	2.4470	1.6406	962.02	0.651	2.6713
C$_{92}$H$_{186}$	1073.45	4.29	2.4596	1.6523	962.55	0.631	2.6885
C$_{93}$H$_{188}$	1073.90	4.27	2.4645	1.6568	963.06	0.612	2.7056
C$_{94}$H$_{190}$	1075.44	4.22	2.4596	1.6523	963.56	0.594	2.7226
C$_{95}$H$_{192}$	1075.84	4.17	2.4664	1.6586	964.05	0.577	2.7395
C$_{96}$H$_{194}$	1076.21	4.13	2.4773	1.6687	964.52	0.560	2.7561
C$_{97}$H$_{196}$	1077.66	4.12	2.4716	1.6634	964.97	0.543	2.7727
C$_{98}$H$_{198}$	1077.99	4.06	2.4775	1.6689	965.41	0.527	2.7891
C$_{99}$H$_{200}$	1078.28	4.02	2.4842	1.6751	965.84	0.512	2.8054
C$_{100}$H$_{202}$	1078.55	4.01	2.4940	1.6842	966.26	0.497	2.8215

Appendix 5-A. Algorithm for Direct Perturbation of Attraction and Covolume Parameters
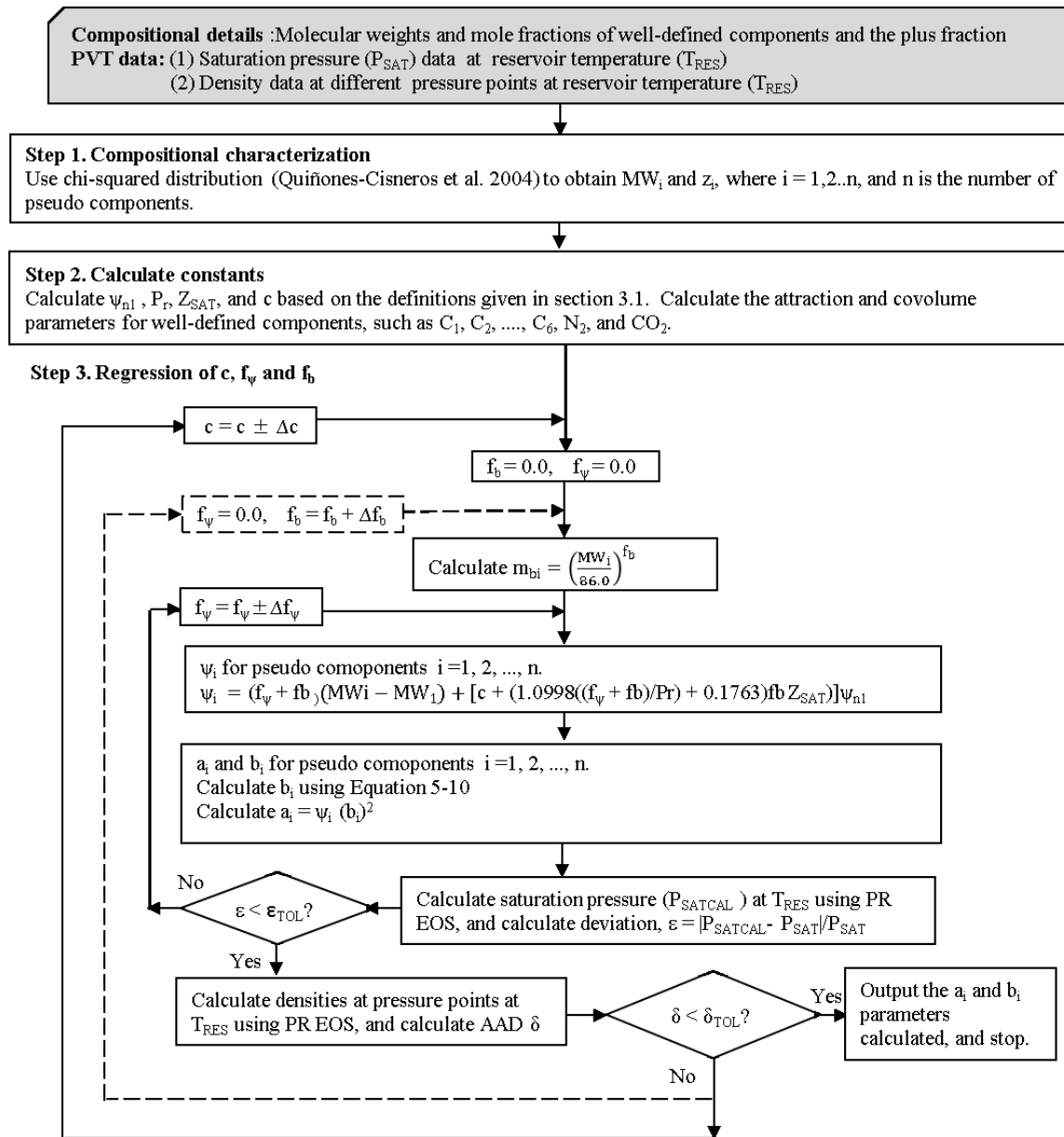
Figure 5-A1. Flow chart for the direct perturbation algorithm presented in Section 3.
The dotted line shows the adjustment of f_b for matching densities. This path is taken when the adjustment of c is unsuccessful in matching densities (See Section 3.2 for details). For the dotted path, the c value calculated in Step 2 is used and kept constant during the regression with f_b and f_ψ.

Appendix 5-B. Estimation of Critical Parameters from Attraction and Covolume Parameters

The attraction and covolume parameters cannot be directly input for the fluid model used in existing commercial software, such as numerical reservoir and PVT simulators. Mathematically, any set of T_C, P_C, and m (or ω) that results in a given set of the attraction and covolume parameters will yield the same phase behavior prediction from the PR EOS fluid model at a given temperature. However, attaining a qualitative and quantitative correctness may be important when such parameters are used for calculation of some other properties, such as parachor values, interfacial tensions, and critical viscosities. A method is presented to back calculate a physically reasonable set of T_C, P_C, and ω that gives a certain set of the attraction and covolume parameters converged by the direct PnA algorithm (Section 3).

The correlations of Kesler-Lee (1976) and Lee-Kesler (1975) are widely used to estimate of T_C, P_C, and ω of petroleum fractions (Whitson and Brulè 2000). They are functions of boiling point (T_b) and specific gravity (γ). Thus, for pseudocomponent i, the method proposed is to find a set of T_{bi} and $γ_i$ that gives the desired values of the attraction (a_i) and covolume (b_i) parameters through the correlations of Kesler-Lee (1976) and Lee-Kesler (1975).

To give reasonable initial values for T_{bi} and $γ_i$, a model is proposed for T_{Ci} by replacing f_T of Equation 5-S8 with m_{bi} used in Equation 5-3. Then, Equation 5-S5 is solved for P_{Ci} for a given T_{Ci} and b_i. After that, m_i can be solved for using Equations 5-S2, 5-S3, and 5-S4 for a given T_{Ci}, P_{Ci}, and a_i. The resulting T_{Ci}, P_{Ci}, and m_i are used with the PR EOS to give initial values for T_{bi} and $γ_i$.

A step-wise description of the method is as follows:

Step 1. Calculate T_{Ci}, P_{Ci}, and m_i by use of the following equations:

$$T_{Ci} = 1154.35 - 844.83(1.0 + 1.7557 \times 10^{-3} m_{bi} MW_i)^{-2.0}$$ (5-B1)

$$P_{Ci} = \Omega_b R T_{Ci} / b_i$$ (5-B2)

$$m_i = \left[\sqrt{\frac{a_i}{\Omega_a (RT_{Ci})^2 / P_{Ci}}} - 1.0 \right] \Big/ \left(1.0 - \sqrt{\frac{T}{T_{Ci}}} \right).$$ (5-B3)

Step 2. Calculate T_{bi} and $γ_i$ using the PR EOS with the T_{Ci}, P_{Ci}, and m_i from step 1.

Step 3. Calculate T_{Ci}, P_{Ci}, and $ω_i$ using the correlations of Kesler-Lee (1976) and Lee-Kesler (1975) with the T_{bi} and $γ_i$ from step 2.

Step 4. Calculate a_i' and b_i' for the PR EOS using Equations 5-S2 and 5-S5 with the T_{Ci}, P_{Ci}, and $ω_i$ from step 3.

Step 5. Calculate the objective function (e_i) for pseudocomponent i as follows:

$$e_i = |a_i - a_i'|/a_i + |b_i - b_i'|/b_i$$ (5-B4)

If e_i is less than a tolerance, repeat the method for other pseudocomponents. Otherwise, update T_{bi} and $γ_i$ to reduce e_i until it becomes less than the tolerance. In the current research, the EXCEL solver was used to perform the iterations. **Table 5-B1** gives the results for four pseudocomponents in a sample calculation.

Table 5-B1. Example of solution for T_C, P_C, and ω from the attraction and covolume parameters using the EXCEL solver. The temperature is 299.81 K.							
Target a_i (bar.cc^2.mol^{-2})	Target b_i (cc.mol^{-1})	γ_i	T_{bi} (K)	T_{Ci}[#] (K)	P_{Ci}[#] (bar)	ω_i[#]	e_i
152780160.65	225.96109	0.82984	517.749	700.347	20.049	0.5680	3.64E-07
415755584.46	371.98724	0.94476	670.127	853.779	14.847	0.8738	2.83E-06
809603339.61	518.89867	1.04283	797.501	982.191	12.244	1.0646	1.79E-06
1893146362.73	796.38678	1.21313	1006.301	1199.746	9.745	1.2633	9.37E-06
[#] T_{Ci}, P_{Ci}, and ω_i are calculated using the correlations of Kesler-Lee (1976), and Lee-Kesler (1975) with the listed γ_i and T_{bi}. The target a_i and b_i values are sample values for the attraction and covolume parameters for pseudocomponent i. Four pseudocomponents are listed.							

Appendix 7-A. Development of Binary Interaction Parameters

BIPs were optimized for CO_2, methane, ethane, and propane with heptane and heavier n-alkanes by use of three-phase data, including critical endpoints (CEPs). A CEP is where two phases merge in the presence of the other immiscible phase (Uzunov 1993). For a three-phase region bounded by two CEPs, two liquid phases are critical in the presence of V phase ($L_1=L_2$-V) at the lower CEP (LCEP). At the upper CEP (UCEP), the V and L_2 phases are critical in the presence of the L_1 phase (L_1-L_2=V). The optimization was concerned primarily with UCEP predictions in this research.

Experimental data are available for UCEPs for the methane binaries with hexane (Lin et al. 1977) and heptane (Chang et al. 1966), for the ethane binaries with n-C_{18}, n-C_{19}, n-C_{20}, n-C_{22}, n-C_{23}, and n-C_{24} (Estrera and Luks 1987; Peters et al. 1986; Peters et al. 1987a), and for the propane binaries with n-C_{32}, n-C_{34}, n-C_{36}, n-C_{38}, n-C_{40}, n-C_{44}, n-C_{46}, n-C_{50}, and n-C_{60} (Peters et al. 1989; Peters et al. 1992; Peters et al. 1993). These data were matched with the PR EOS by use of an in-house FORTRAN code based on the algorithms of Heidemann and Khalil (1980) and Mushrif (2004). Critical parameters and ω for CO_2, methane, ethane, and propane were taken from Yaws (2010). The critical parameters of n-alkanes heavier than hexane were from Equations 7-1 and 7-2 (Gao et al. 2001).

It was observed that matching UCEPs with the PR EOS requires minor deviations from the ω correlation of Gao et al. (2001). To find a smooth ω trend with respect to CN that can be used for matching UCEPs, different pairs of ω and BIP were found for each binary as shown in **Figure 7-A1.** In this figure, the number below a curve indicates the CN of the heavier n-alkane. The curves follow the same trend except for the propane binaries with n-C_{46} and n-C_{60}. The irregularity for these binaries appears to be caused by the fluctuation in the UCEP data measured near the asymptotic limit defined by the critical point of propane, as shown in **Figure 7-A2.** This type of irregularity was also observed in terms of measured UCEP temperature, although not shown here.

Equation 7-4 gives the smooth trend obtained for non-physical acentric factor ($\acute{\omega}$) with respect to CN in this research. Although this equation was found by use of non-physical and physical ω, the non-physical values used were chosen to be as close to the corresponding physical value as possible. The ω shown by the filled circles in Figure 7-A1 have been calculated from Equation 7-4. For n-C_{32}, n-C_{34}, n-C_{36}, n-C_{38}, and n-C_{40}, these are nearly equal to their respective physical values as given in Equation 7-3 (< 0.015 AAD). **Figure 7-A3** shows the comparison between Equations 7-3 and 7-4.

The trend of optimized BIPs for the ethane binaries with n-C_{18}, n-C_{19}, n-C_{20}, n-C_{22}, n-C_{23}, and n-C_{24} is linearly correlated by Equation 7-10. Development of a trend for propane BIPs used three-phase data given in Gregorowicz et al. (1993b), in addition to the UCEP data mentioned previously, in order to add an optimized BIP for propane with n-C_{20}. The data by Gregorowicz et al. (1993b) are 12 P-T envelopes for 12 different mixtures of ethane, propane and n-C_{20}. The BIP of ethane with n-C_{20} was calculated with Equation 7-10. The T_C, P_C, and ω for n-C_{20} were calculated from Equations 7-1, 7-2, and 7-4, respectively. Then, three-phase data were matched by adjusting the propane BIPs with ethane and n-C_{20}. The optimized BIP is 0.017 for ethane-propane and 0.041 for propane-n-C_{20}. Even though three-

phase P-T envelopes have very small temperature windows (2.19 K at most), they were successfully matched. **Figure 7-A4** shows one such matching. The experimental data for UCEP and LCEP are (316.03 K, 54.59 bars) and (315.06 K, 53.33 bars), respectively. The predicted UCEP and LCEP are (315.77 K, 54.40 bars) and (314.73 K, 53.00 bars), respectively. The trend of propane BIPs with respect to CN of the heavier n-alkane is shown in **Figure 7-A5,** which is expressed in Equation 7-11. It is evident that the optimized BIPs for $n-C_{46}$ and $n-C_{60}$ do not follow the trend due to the irregularity as shown in Figure 7-A1.

Development of a trend for methane BIPs required additional three-phase data, due to the scarcity of the UCEP data, such as Hottovy et al. (1981b) for the methane-ethane-$n-C_8$ system, Gregorowicz et al. (1993b) for the methane-ethane-$n-C_{20}$ system, and Jangkamolkulchal and Luks (1989) for the methane-ethane-$n-C_{22}$ system. For the system studied by Hottovy et al. (1981b), three-phase composition data at (202.00 K, 48.40 bars), (204.00 K, 50.80 bars), (206.00 K, 54.20 bars), and (210.00 K, 58.80 bars) were matched. For the system studied by Gregorowicz et al. (1993b), 11 P-T three-phase data were matched. **Figure 7-A6** shows one such P-T three-phase envelope for 6.87% methane, 92.42% ethane, and 0.71% $n-C_{20}$. For the system studied by Jangkamolkulchal and Luks (1989), three-phase composition data at (298.50 K, 46.88 bars), (298.50 K, 56.16 bars), (303.50 K, 47.35 bars), and (303.50 K, 52.43 bars) were matched. Optimized BIPs for methane-ethane, methane-$n-C_8$, methane-$n-C_{20}$, and methane-$n-C_{22}$ are 0.040, 0.048, 0.062, and 0.064, respectively. Equation 7-9 gives a correlation for the methane BIPs with CN of the heavier n-alkane.

Three-phase data for the butane binaries and the pentane binaries are unavailable in the literature. It seems that UCEPs were measured for butane with a few n-alkanes (Peters 1994); however, the data are not available in the public domain. In the absence of relevant data, an extrapolation approach was used to develop BIPs of butane and pentane with heavier n-alkanes. For n-alkanes heavier than hexane, BIPs for methane, ethane, and propane were calculated using Equations 7-9, 7-10, and 7-11, respectively. Then, for each of the heavier n-alkanes, BIPs for methane, ethane, and propane were extrapolated for BIPs for butane and pentane. The resulting correlations are given in Equations 7-12 and 7-13. These correlations were further validated by three-phase predictions, as shown in the case studies section. The correlation for BIP of butane (Equation 7-12) was used to estimate the UCEPs for binary mixture of butane with heavier n-alkane. **Figures 7-A7a and 7-A7b** show the trend of temperature and pressure respectively calculated at UCEP. The two figures also show the critical temperature and pressure of butane. The temperature and pressure at UCEP for butane binaries with heavier n-alkane should not go below the respective temperature and pressure at critical point of butane that is observed between carbon numbers 57 and 76. This deviation may be because of limitations of PR EOS and uncertainties with critical parameters for heavier n-alkane. However, the trend merely shows estimated values and in the absence of experimental data, the amount of error cannot be ascertained.

BIPs for CO_2 with n-alkanes were optimized by Kato et al. (1981), Lin et al. (1984), Kordas et al. (1994); however, they did not use three-phase data or CEP data. In this research, therefore, BIPs of CO_2 with n-alkanes were optimized to match the UCEP data for CO_2-n-alkanes, n-C_{13}, n-C_{14}, n-C_{15}, n-C_{19}, n-C_{20}, and n-C_{21} (Hottovy et al. 1981a; Fall and Luks 1985; Fall et al. 1985). In order to make the trend more reliable, L=V critical-point data for n-C_8, n-C_9, and n-C_{10} (Choi and Yeo 1998; Reamer and Sage 1963) were also used in the BIP optimization. **Figure 7-A8** shows that the optimized BIPs show an increasing trend with increasing CN, but they become nearly constant beyond n-C_{15}. However, higher BIP values were required when matching experimental data for heavy oils for the development of Equations 7-5, 7-6, and 7-7. This observation may be because of the effect of oil aromaticity on phase behavior with CO_2, and was considered for the development of Equation 7-8.

The BIPs developed for the PR EOS in this research are designed for n-alkanes; however, they are used for pseudocomponents in this research. Although these BIPs were successful in predicting three-phase behavior in this research, they can be used as initial guesses if BIP adjustment is needed.
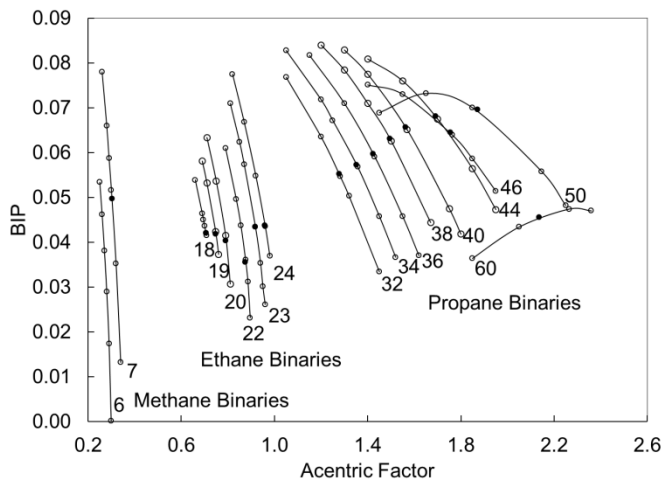
Figure 7-A1. Trend of BIP with respect to ω for the heavier n-alkane for matching the UCEP data for each binary.
The number below a curve indicates the CN of the heavier n-alkane. The filled circles are the points used in developing the methane, ethane, and propane BIP correlations (Equations 7-9, 7-10, and 7-11). The ω for the filled circles are based on Equation 7-4.
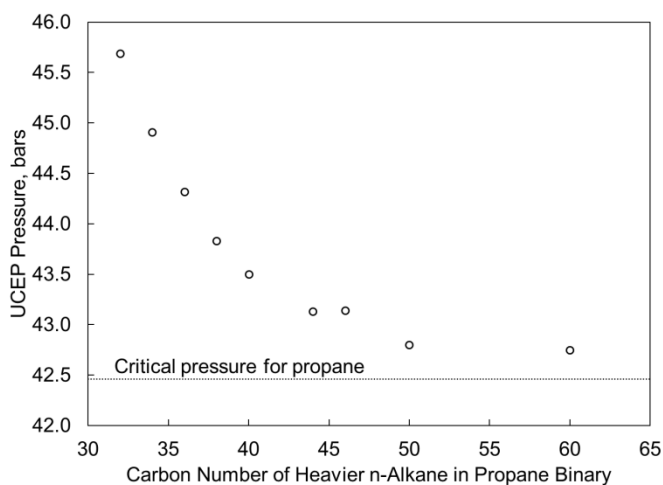
Figure 7-A2. UCEP pressures measured for propane binaries (Peters et al. 1989, 1993).
The horizontal line shows the critical pressure of propane. Fluctuation in measured UCEP pressure is observed as the critical point of propane is approached.
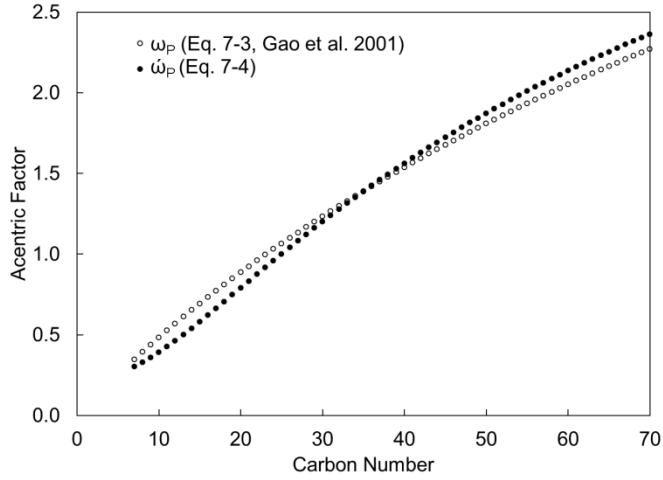
Figure 7-A3. Comparison of physical ω (Equation 7-3) with ώ (Equation 7-4) that can be used to match the UCEP data with the PR EOS.
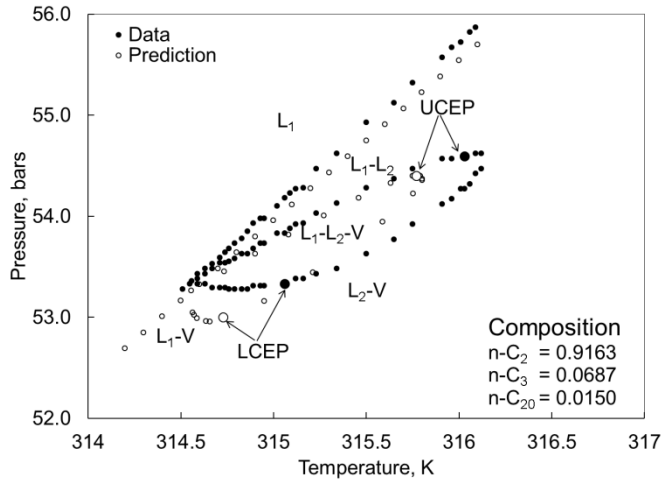
Figure 7-A4. Three-phase envelope for a mixture of ethane, propane, and eicosane (Gregorowicz et al. 1993a).
Predictions are based on the PR EOS with adjustment of propane BIP with eicosane.
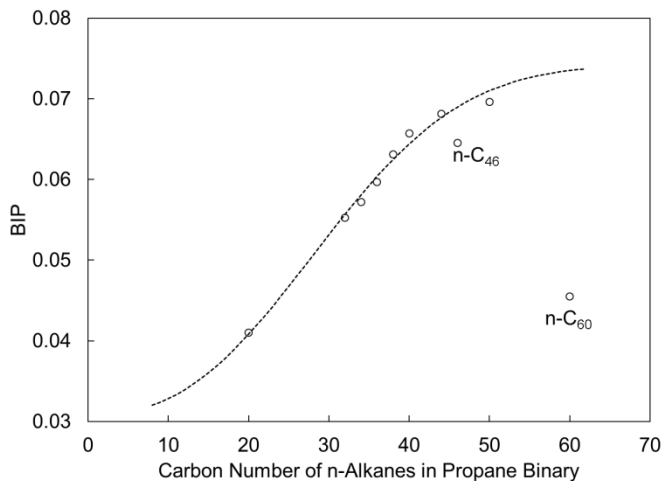
Figure 7-A5. Trend of optimized propane BIPs with respect to CN of the heavier n-alkane. The curve is given by Equation 7-11.
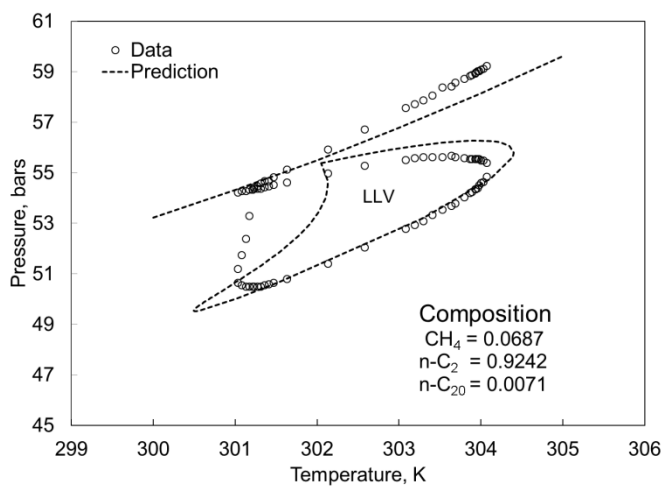
Figure 7-A6. Comparison of predicted three-phase envelope for methane, ethane, and eicosane mixture with data.
Three-phase envelope measured for a mixture of methane, ethane, and eicosane (Gregorowicz et a. 1993b). The predictions are based on the PR EOS with the adjusted methane BIP with eicosane, 0.062.
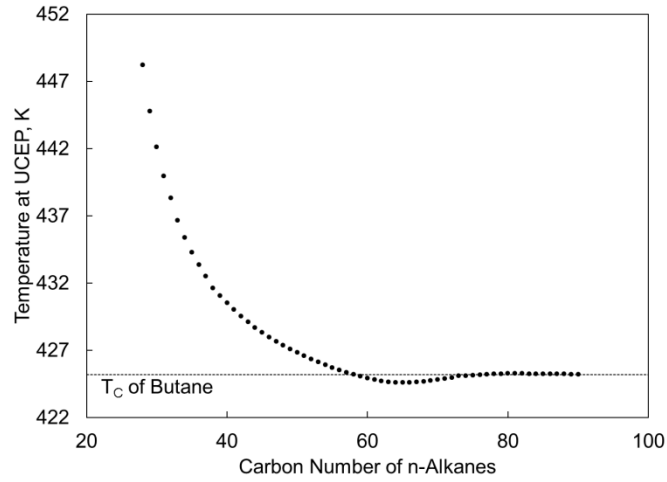
(a)
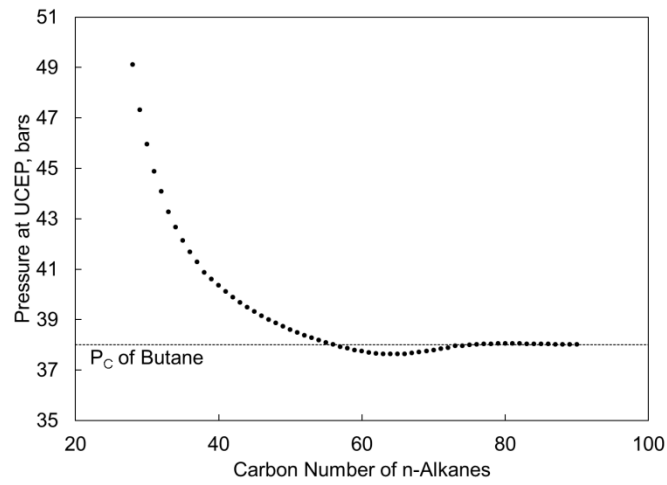
(b)

Figure 7-A7. Predicted temperature and pressure points at UCEP for butane's mixture with heavier n-alkane using BIP correlation Equation 7-12.
Figure (a) shows the trend of temperature at UCEP and figure (b) shows the trend of pressure at UCEP.
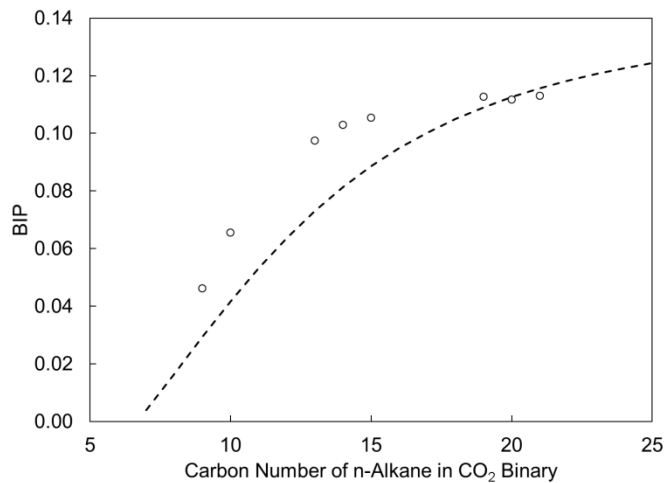
Figure 7-A8. Trend of optimized CO_2 BIPs with respect to CN of the heavier n-alkane. The curve is calculated from Equation 7-8.

Appendix 7-B. Three-Phase Behavior from BIPs Optimized for UCEP Match

This section investigates the predictive capability of BIP optimized for UCEP data match for three-phase behavior for the binary mixture. The UCEP is one of two critical end-points closing the three-phase region in P-T space. Although, LCEP does not exist for all binaries studied in this work, it is desirable to investigate the predictive capability of the optimized BIP for producing a LCEP if it exists. The Global Phase Equilibrium Calculation (GPEC 3.2.0) (Cismondi et al. 2006) is used to produce three-phase behavior for binaries studied.

For methane binaries, only methane and heptane binary mixture is investigated. For this binary, LCEP has not been reported; quadruple point has been reported at 169.71 K and 22.82 bars (Chang et al. 1966). **Figure 7-B1** presents the T-x projection of three-phase predicted in P-T-x space with the optimized BIP (0.0497).

The BIPs, optimized to match the UCEP for ethane binaries, produce the three-phase behavior with presence of LCEP; however, the LCEP matching for some of the binaries is not satisfactory as shown in **Figure 7-B2**. The UCEP matched with BIP optimization (shown as UCEP (UCEP match)) is compared with data. The LCEP predicted (with the BIP optimized for UCEP match) is shown as LCEP (UCEP match) and is compared with data. The AARD for LCEP match for ethane binary with n-C_{18}, n-C_{19}, and n-C_{20} is 0.45%, but with n-C_{20}, and n-C_{22}, the AARD is 8.77%. The LCEPs for ethane binaries were matched by BIP adjustment. **Figure 7-B3** is an example of LCEP match, which shows T-x projection of three-phase in P-T-x space after LCEP match for ethane and n-C_{22} binary. The liquid phase compositions, particularly for L_1 phase (n-C_{22} rich liquid phase), shows good match with the data (Rodrigues and Kohn 1967). **Figure 7-B4** presents the comparison of BIP optimized for LCEP match with BIP from the Equation 7-10, which represents the trend of BIP for UCEP match. It is observed that BIPs required for LCEP match are smaller than that for UCEP match. **Figures 7-B5** presents the comparison of optimized temperature at LCEP (shown as LCEP (LCEP match)) with data. The BIP, optimized for LCEP match, predicts higher UCEP (shown as UCEP (LCEP match)) particularly for ethane binaries with n-C_{22} and n-C_{23}. It may be observed that the Equation 7-10 provides reliable BIPs with satisfactory predictions for three-phase behavior for ethane binaries, as the adjustment required for LCEP match is not too high (< 0.004). In addition, as expected, three-phase is not predicted for ethane binaries with n-alkane with CN < 18.

The BIPs optimized for UCEP match for propane binaries predict the three-phase, but they do not show LCEP. For example, **Figure 7-B6** presents the T-x projection for three-phase in P-T-x space for propane and n-C_{44} binary. The two liquid phases' curves shown by circles at BIP of 0.0677, which match UCEP for n-C_3 and n-C_{44} binary, initially converge with decreasing temperature, and below some temperature, they start diverging, hence LCEP does not exist. At lower BIP, they show tendency to come closer as shown for BIP of 0.03. A closing of the two liquid phases is observed at BIP of 0.02472. From Figure 7-B6, it appears that L_2 (propane rich liquid phase) and vapor phase for BIPs 0.0677 and 0.03 are merging at temperatures 322.30 K and 295.50 K respectively; below these temperatures, these

phases have same composition as that of pure propane. This indicates existence of another UCEP (vapor phase merging with propane rich liquid phase i.e. L_2) at lower temperature; however, existence of such phase behavior for propane binaries may not be realistic.

It is observed that with decrease in BIP to match LCEP for propane binaries, the temperature at UCEP increases. This is in line with observation in case of ethane binaries, which required smaller BIP for LCEP match that increased UCEP. Such adjustments were done for other propane binaries also for LCEP match. However, it is observed that in case of $n-C_{44}$ and $n-C_{46}$, BIP adjustment could not bring the LCEPs close to data. **Figure 7-B7** compares the adjusted BIP for LCEP match with the trend of BIP for UCEP match represented by Equation 7-11. Unlike the case of ethane binary in Figure 7-B4, significant difference in BIPs matching UCEPs and matching LCEPs are observed in case of propane binaries. **Figure 7-B8** compares the optimized temperature at LCEP (shown as LCEP (LCEP match)) with the data. It also compares the UCEP predicted with BIP optimized for LCEP match (shown as UCEP (LCEP match)) with data. It is observed that the temperatures at UCEP are significantly higher than respective data. The three-phase prediction for propane binaries with BIP from Equation 7-11 should stop for n-alkanes with CN< 32; however, it was observed that this takes place for n-alkanes with CN< 29.

Three-phase bounded by UCEP and LCEP exist in case of CO_2 and $n-C_{13}$ binary only. The BIP optimized for UCEP match for this binary predicts the three-phase, but it does not have LCEP like propane binary case described earlier. At BIP of 0.10, the predicted UCEP is (315.26 K and 86.14 bars), whereas data (Fall and Luks 1985) is (314.00 K and 87.20 bars). When BIP is reduced to 0.088, the predicted LCEP is (312.74 K and 80.72 bars), which is close to LCEP data (Fall and Luks 1985) of (310.80 K, 81.10 bar); however, the UCEP now changes to (319.24 K and 91.89 bars). For other CO_2 binaries, three-phase behavior is predicted correctly with no LCEP.

Following observations can be made from the analysis of the three-phase behavior from BIP optimized for UCEP match:

- UCEP and LCEP matching may require different BIPs for a given binary. This observation is significant particularly in case of propane BIPs, which may be possibly because of inaccurate critical parameters for higher n-alkanes, and limitations of PR EOS.

- LCEP match requires smaller BIP compared to that for UCEP match. Hence, while characterizing reservoir fluids with BIPs developed with UCEP match as default BIPs, adjustment of BIPs should lead to smaller values greater than respective BIPs optimized for LCEP match.
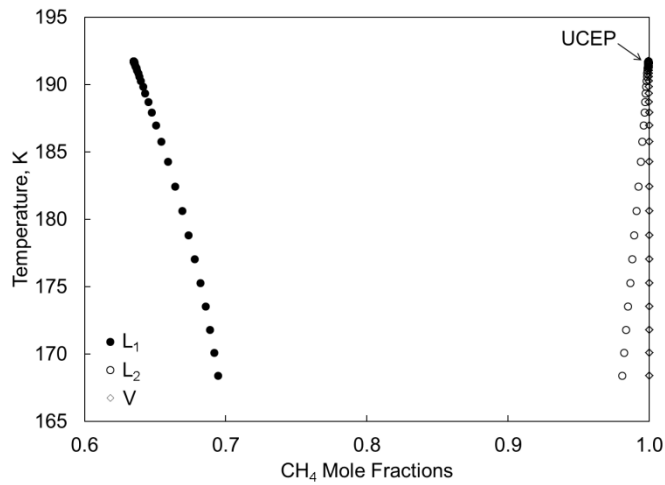
Figure 7-B1. T-x projection of three-phase region in P-T-x space for CH_4 and n-C_7 binary mixture. L_1 phase is n-C_7 rich liquid phase, and L_2 is CH_4 rich liquid phase.
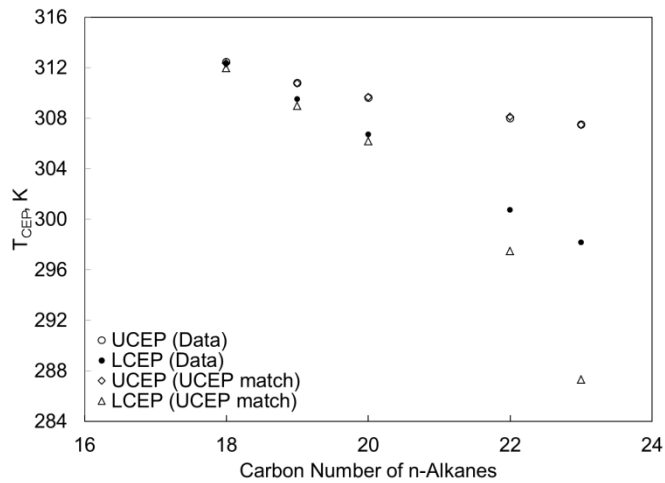
Figure 7-B2. Comparison of the optimized temperature at UCEP (shown as UCEP (UCEP match)) with data for ethane binaries.
Comparison for predicted temperature at LCEP with BIP optimized for UCEP match (shown as LCEP (UCEP match)) with data is also presented.
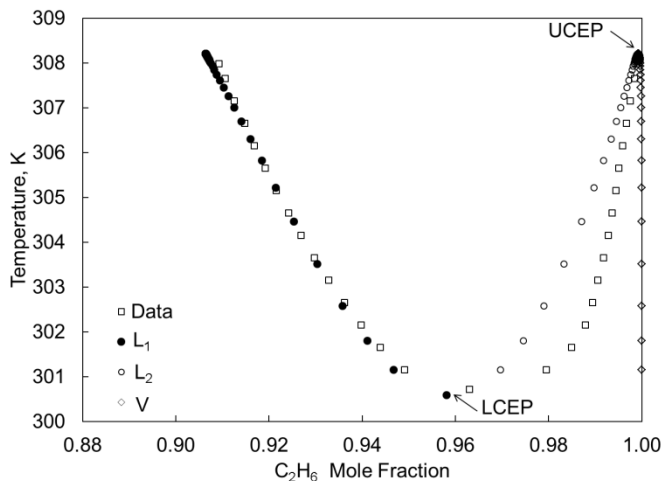
Figure 7-B3. Quality of matching of T-x projection of three-phase region in P-T-x space for C_2H_6 and n-C_{22} binary mixture with data.

L_1 phase is n-C_{22} rich liquid phase, and L_2 is C_2H_6 rich liquid phase. The LCEP has been matched with BIP adjustment. The liquid phase compositions comparison with data (Rodrigues and Kohn 1967) is also shown.
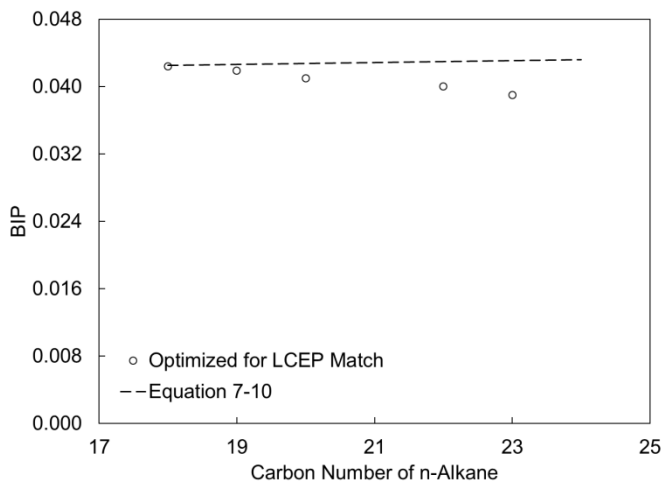
Figure 7-B4. Comparison of the BIP optimized for LCEP match for ethane binaries with trend of BIP (Equation 7-10) for UCEP match.
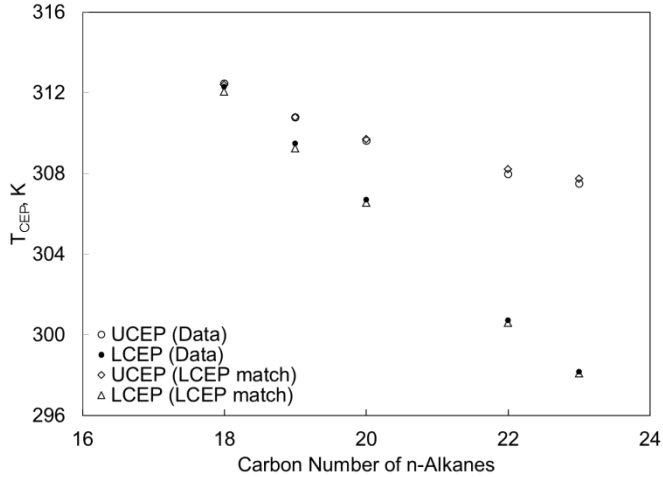
Figure 7-B5. Comparison of the optimized temperature at LCEP (shown as LCEP (LCEP match)) with data for ethane binaries.
Comparison for predicted temperature at UCEP with BIP optimized for LCEP match (shown as UCEP (LCEP match)) with data is also presented.
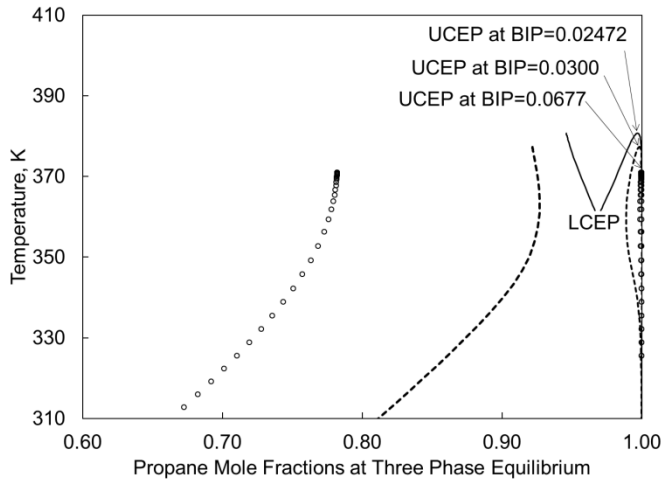
Figure 7-B6. T-x projection for three-phase in P-T-x space for n-C_3 and n-C_{44} binary with different BIPs. BIP of 0.0677 matches UCEP but predicted three-phase has no LCEP. Leftmost curve shown with circle is L_1 phase rich in n-C_{44}, L_2 phase rich in propane is very close to vapor phase, hence could not be shown clearly. L_1 (leftmost) and L_2 (middle) phases for BIP of 0.03 is shown by dotted line; corresponding curves for BIP of 0.02472 are shown by solid lines. Vapor curves for all BIP cases are very close to each other and are shown on rightmost. The LCEP matching requires smaller BIPs, but it increases the UCEP.
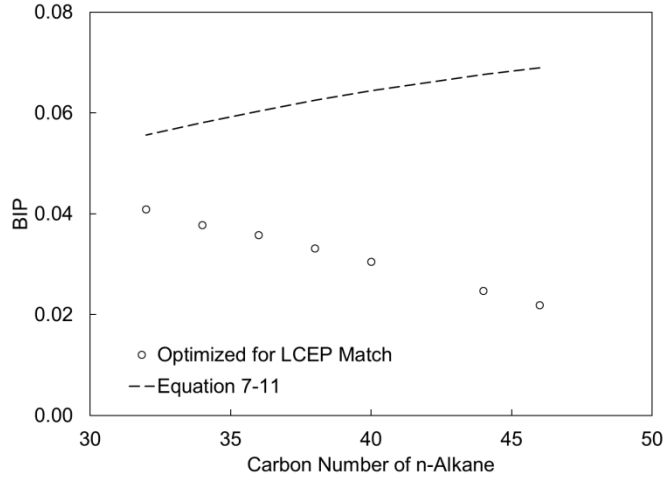
Figure 7-B7. Comparison of the BIPs optimized for LCEP match for propane binaries with the trend of BIP (Equation 7-11) that matched the UCEP.
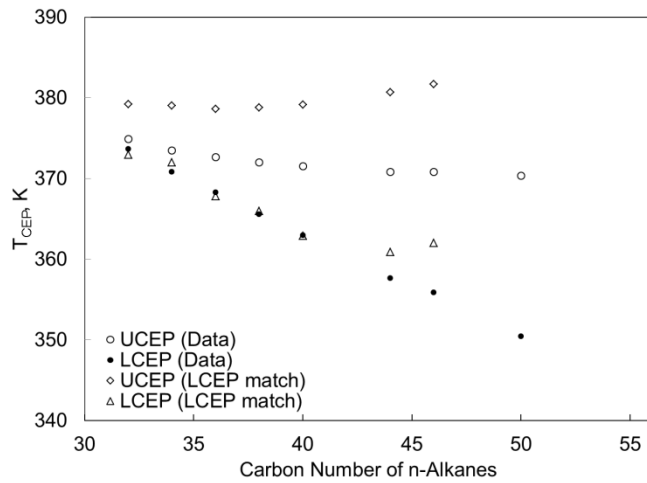
Figure 7-B8. Comparison of the optimized temperature at LCEP (shown as LCEP (LCEP match)) with data for propane binaries is shown.
Comparison for predicted temperature at UCEP with BIP optimized for LCEP match (shown as UCEP (LCEP match)) with data is also presented. It is seen that LCEP matching achieved using smaller BIP increases the UCEP significantly.

Appendix-7C: PR EOS Models for Fluids in Table 7-2 to 7-5.

Table 7C.1a : PR EOS model from PnA characterization for fluid 1 in Table 7.2. Saturation pressure for this fluid is 412.86 bars at 424.82 K.

Components	Z	MW (g/mol)	T_C (K)	P_C (bars)	ω	C_{PEN} (CC/Mol)
N_2	0.0312	28.01	126.20	33.94	0.04000	-4.230
CO_2	0.0323	44.01	304.20	73.76	0.22500	-1.640
CH_4	0.6976	16.04	190.60	46.00	0.00800	-5.200
C_2H_6	0.0903	30.07	305.40	48.84	0.09800	-5.790
C_3H_8	0.0402	44.10	369.80	42.46	0.15200	-6.350
C_4H_{10}	0.0225	58.12	419.04	37.45	0.18690	-6.738
C_5H_{12}	0.0115	72.15	464.80	33.79	0.23850	-5.683
C_6H_{14}	0.0096	86.18	507.40	29.69	0.29600	1.390
PC-1	0.0237	111.55	593.84	30.97	0.16500	3.310
PC-2	0.0186	142.42	645.11	27.93	0.21400	7.770
PC-3	0.0139	189.93	735.69	23.79	0.31220	16.090
PC-4	0.0084	315.17	910.92	18.94	0.52110	39.500

Table 7C.1b : BIPs for PR EOS model from PnA characterization for fluid 1 in Table 7.2

	N_2	CO_2	CH_4	C_2H_6	C_3H_8	C_4H_{10}	C_5H_{12}	C_6H_{14}	PC-1	PC-2	PC-3	PC-4
N_2	0.0000											
CO_2	0.0000	0.0000										
CH_4	0.1000	0.1000	0.0000									
C_2H_6	0.1000	0.1450	0.0420	0.0000								
C_3H_8	0.1000	0.2605	0.0420	0.0400	0.0000							
C_4H_{10}	0.1000	0.2223	0.0420	0.0400	0.0300	0.0000						
C_5H_{12}	0.1000	0.1824	0.0420	0.0400	0.0300	0.0116	0.0000					
C_6H_{14}	0.1000	0.1597	0.0420	0.0400	0.0300	0.0155	0.0058	0.0000				
PC-1	0.1300	0.0166	0.0500	0.0414	0.0320	0.0337	0.0186	0.0000	0.0000			
PC-2	0.1300	0.0417	0.0518	0.0416	0.0328	0.0418	0.0275	0.0000	0.0000	0.0000		
PC-3	0.1300	0.0814	0.0554	0.0420	0.0353	0.0534	0.0428	0.0000	0.0000	0.0000	0.0000	
PC-4	0.1300	0.1206	0.0635	0.0430	0.0443	0.0674	0.0662	0.0000	0.0000	0.0000	0.0000	0.0000

Table 7C.2a : PR EOS model from PnA characterization for fluid 2 in Table 7.2
Saturation pressure (dew point) for this fluid is 424.70 bars at 403.15 K.

Components	Z	MW (g/mol)	T_C (K)	P_C (bars)	ω	C_{PEN} (CC/Mol)
N_2	0.0679	28.01	126.20	33.94	0.04000	-4.230
CO_2	0.0135	44.01	304.20	73.76	0.22500	-1.640
CH_4	0.6869	16.04	190.60	46.00	0.00800	-5.200
C_2H_6	0.0812	30.07	305.40	48.84	0.09800	-5.790
C_3H_8	0.0376	44.10	369.80	42.46	0.15200	-6.350
C_4H_{10}	0.0219	58.12	419.73	37.51	0.18760	-6.710
C_5H_{12}	0.0124	72.15	465.30	33.79	0.23980	-5.630
C_6H_{14}	0.0099	86.18	507.40	29.69	0.29600	1.390
PC-1	0.0253	106.68	594.59	30.92	0.16360	8.780
PC-2	0.0198	136.77	645.93	27.87	0.21220	10.580
PC-3	0.0148	183.09	715.32	24.59	0.28540	13.280
PC-4	0.0089	305.13	895.91	19.22	0.49490	21.270

Table 7C.2b : BIPs for PR EOS model from PnA characterization for fluid 2 in Table 7.2

	N_2	CO_2	CH_4	C_2H_6	C_3H_8	C_4H_{10}	C_5H_{12}	C_6H_{14}	PC-1	PC-2	PC-3	PC-4
N_2	0.0000											
CO_2	0.0000	0.0000										
CH_4	0.1000	0.1000	0.0000									
C_2H_6	0.1000	0.1450	0.0420	0.0000								
C_3H_8	0.1000	0.2252	0.0420	0.0400	0.0000							
C_4H_{10}	0.1000	0.1942	0.0420	0.0400	0.0300	0.0000						
C_5H_{12}	0.1000	0.1620	0.0420	0.0400	0.0300	0.0116	0.0000					
C_6H_{14}	0.1000	0.1439	0.0420	0.0400	0.0300	0.0155	0.0058	0.0000				
PC-1	0.1300	0.0166	0.0500	0.0414	0.0320	0.0337	0.0186	0.0000	0.0000			
PC-2	0.1300	0.0417	0.0518	0.0416	0.0328	0.0418	0.0275	0.0000	0.0000	0.0000		
PC-3	0.1300	0.0731	0.0545	0.0419	0.0346	0.0510	0.0393	0.0000	0.0000	0.0000	0.0000	
PC-4	0.1300	0.1183	0.0626	0.0429	0.0431	0.0663	0.0642	0.0000	0.0000	0.0000	0.0000	0.0000

Table 7C.3a : PR EOS model from PnA characterization for fluid 3 in Table 7.2						
Saturation pressure (dew point) for this fluid is 348.46 bars at 382.59 K.						
Components	Z	MW (g/mol)	T_C (K)	P_C (bars)	ω	C_{PEN} (CC/Mol)
N_2	0.0020	28.01	126.20	33.94	0.04000	-4.230
CO_2	0.0077	44.01	304.20	73.76	0.22500	-1.640
CH_4	0.7209	16.04	190.60	46.00	0.00800	-5.200
C_2H_6	0.0636	30.07	305.40	48.84	0.09800	-5.790
C_3H_8	0.0623	44.10	369.80	42.46	0.15200	-6.350
C_4H_{10}	0.0407	58.12	417.43	37.31	0.18530	-6.800
C_5H_{12}	0.0177	72.15	464.61	33.79	0.23800	-5.710
C_6H_{14}	0.0128	86.18	507.40	29.69	0.29600	1.390
PC-1	0.0264	104.57	596.05	31.02	0.16650	5.800
PC-2	0.0208	133.04	647.52	27.99	0.21590	15.870
PC-3	0.0156	176.65	717.59	24.72	0.29040	32.430
PC-4	0.0095	290.96	882.94	19.79	0.48110	81.380

Table 7C.3b : BIPs for PR EOS model from PnA characterization for fluid 3 in Table 7.2												
	N_2	CO_2	CH_4	C_2H_6	C_3H_8	C_4H_{10}	C_5H_{12}	C_6H_{14}	PC-1	PC-2	PC-3	PC-4
N_2	0.0000											
CO_2	0.0000	0.0000										
CH_4	0.1000	0.1000	0.0000									
C_2H_6	0.1000	0.1450	0.0420	0.0000								
C_3H_8	0.1000	0.1968	0.0420	0.0400	0.0000							
C_4H_{10}	0.1000	0.1718	0.0420	0.0400	0.0300	0.0000						
C_5H_{12}	0.1000	0.1463	0.0420	0.0400	0.0300	0.0116	0.0000					
C_6H_{14}	0.1000	0.1322	0.0420	0.0400	0.0300	0.0155	0.0058	0.0000				
PC-1	0.1300	0.0166	0.0500	0.0414	0.0320	0.0337	0.0186	0.0000	0.0000			
PC-2	0.1300	0.0417	0.0518	0.0416	0.0328	0.0418	0.0275	0.0000	0.0000	0.0000		
PC-3	0.1300	0.0731	0.0545	0.0419	0.0346	0.0510	0.0393	0.0000	0.0000	0.0000	0.0000	
PC-4	0.1300	0.1156	0.0617	0.0428	0.0419	0.0652	0.0620	0.0000	0.0000	0.0000	0.0000	0.0000

Table 7C.4a : PR EOS model from PnA characterization for fluid 4 in Table 7.2 Saturation pressure (dew point) for this fluid is 415.39 bars at 397.59 K.						
Components	Z	MW (g/mol)	T_C (K)	P_C (bars)	ω	C_{PEN} (CC/Mol)
N_2	0.0011	28.01	126.20	33.94	0.04000	-4.230
CO_2	0.0001	44.01	304.20	73.76	0.22500	-1.640
CH_4	0.6893	16.04	190.60	46.00	0.00800	-5.200
C_2H_6	0.0863	30.07	305.40	48.84	0.09800	-5.790
C_3H_8	0.0534	44.10	369.80	42.46	0.15200	-6.350
C_4H_{10}	0.0348	58.12	419.55	37.50	0.18740	-6.720
C_5H_{12}	0.0178	72.15	464.79	33.79	0.23850	-5.680
C_6H_{14}	0.0173	86.18	507.40	29.69	0.29600	1.390
PC-1	0.0370	106.56	595.23	31.83	0.18940	-1.010
PC-2	0.0286	137.96	646.62	28.91	0.24560	-2.710
PC-3	0.0213	185.04	738.16	24.96	0.35840	-5.720
PC-4	0.0129	304.96	898.70	20.73	0.57290	-13.360

Table 7C.4b : BIPs for PR EOS model from PnA characterization for fluid 4 in Table 7.2											
	N_2	CO_2	CH_4	C_2H_6	C_3H_8	C_4H_{10}	C_5H_{12}	C_6H_{14}	PC-1	PC-2	PC-3	PC-4
N_2	0.0000										
CO_2	0.0000	0.0000									
CH_4	0.1000	0.1000	0.0000								
C_2H_6	0.1000	0.1450	0.0420	0.0000							
C_3H_8	0.1000	0.2171	0.0420	0.0400	0.0000						
C_4H_{10}	0.1000	0.1877	0.0420	0.0400	0.0300	0.0000					
C_5H_{12}	0.1000	0.1574	0.0420	0.0400	0.0300	0.0116	0.0000				
C_6H_{14}	0.1000	0.1404	0.0420	0.0400	0.0300	0.0155	0.0058	0.0000			
PC-1	0.1300	0.0166	0.0500	0.0414	0.0320	0.0337	0.0186	0.0000	0.0000		
PC-2	0.1300	0.0417	0.0518	0.0416	0.0328	0.0418	0.0275	0.0000	0.0000	0.0000	
PC-3	0.1300	0.0814	0.0554	0.0420	0.0353	0.0534	0.0428	0.0000	0.0000	0.0000	0.0000
PC-4	0.1300	0.1183	0.0626	0.0429	0.0431	0.0663	0.0642	0.0000	0.0000	0.0000	0.0000	0.0000

Table 7C.5a : PR EOS model from PnA characterization for fluid 5 in Table 7.2
Saturation pressure (dew point) for this fluid is 360.23 bars at 424.82 K.

Components	Z	MW (g/mol)	T_C (K)	P_C (bars)	ω	C_{PEN} (CC/Mol)
N_2	0.0030	28.01	126.20	33.94	0.04000	-4.230
CO_2	0.0435	44.01	304.20	73.76	0.22500	-1.640
CH_4	0.6255	16.04	190.60	46.00	0.00800	-5.200
C_2H_6	0.0999	30.07	305.40	48.84	0.09800	-5.790
C_3H_8	0.0500	44.10	369.80	42.46	0.15200	-6.350
C_4H_{10}	0.0351	58.12	418.82	37.43	0.18670	-6.750
C_5H_{12}	0.0196	72.15	464.77	33.79	0.23840	-5.690
C_6H_{14}	0.0147	86.18	507.40	29.69	0.29600	1.390
PC-1	0.0422	111.44	592.24	30.33	0.14690	-0.800
PC-2	0.0312	150.51	667.06	25.93	0.21250	-2.290
PC-3	0.0224	209.99	753.43	22.13	0.29960	-4.730
PC-4	0.0129	364.76	954.99	16.87	0.52060	-12.200

Table 7C.5b : BIPs for PR EOS model from PnA characterization for fluid 5 in Table 7.2

	N_2	CO_2	CH_4	C_2H_6	C_3H_8	C_4H_{10}	C_5H_{12}	C_6H_{14}	PC-1	PC-2	PC-3	PC-4
N_2	0.0000											
CO_2	0.0000	0.0000										
CH_4	0.1000	0.1000	0.0000									
C_2H_6	0.1000	0.1450	0.0420	0.0000								
C_3H_8	0.1000	0.2605	0.0420	0.0400	0.0000							
C_4H_{10}	0.1000	0.2223	0.0420	0.0400	0.0300	0.0000						
C_5H_{12}	0.1000	0.1824	0.0420	0.0400	0.0300	0.0116	0.0000					
C_6H_{14}	0.1000	0.1597	0.0420	0.0400	0.0300	0.0155	0.0058	0.0000				
PC-1	0.1300	0.0166	0.0500	0.0414	0.0320	0.0337	0.0186	0.0000	0.0000			
PC-2	0.1300	0.0532	0.0527	0.0417	0.0334	0.0452	0.0317	0.0000	0.0000	0.0000		
PC-3	0.1300	0.0886	0.0563	0.0422	0.0360	0.0556	0.0461	0.0000	0.0000	0.0000	0.0000	
PC-4	0.1300	0.1259	0.0662	0.0434	0.0480	0.0702	0.0715	0.0000	0.0000	0.0000	0.0000	0.0000

Components	Z	MW (g/mol)	T_C (K)	P_C (bars)	ω	C_{PEN} (CC/Mol)
N_2	0.0343	28.01	126.20	33.94	0.04000	-4.230
CO_2	0.0275	44.01	304.20	73.76	0.22500	-1.640
CH_4	0.6783	16.04	190.60	46.00	0.00800	-5.200
C_2H_6	0.0449	30.07	305.40	48.84	0.09800	-5.790
C_3H_8	0.0267	44.10	369.80	42.46	0.15200	-6.350
C_4H_{10}	0.0268	58.12	419.52	37.50	0.18740	-6.720
C_5H_{12}	0.0185	72.15	465.37	33.79	0.24000	-5.620
C_6H_{14}	0.0203	86.18	507.40	29.69	0.29600	1.390
PC-1	0.0450	105.73	593.72	29.93	0.13560	-5.120
PC-2	0.0349	136.03	644.98	26.75	0.17580	-14.040
PC-3	0.0264	180.22	713.96	23.29	0.23640	-28.400
PC-4	0.0164	289.08	873.61	18.02	0.39170	-71.100

Table 7C.6a : PR EOS model from PnA characterization for fluid 6 in Table 7.2
Saturation pressure (dew point) for this fluid is 339.41 bars at 422.59 K.

Table 7C.6b : BIPs for PR EOS model from PnA characterization for fluid 6 in Table 7.2

	N_2	CO_2	CH_4	C_2H_6	C_3H_8	C_4H_{10}	C_5H_{12}	C_6H_{14}	PC-1	PC-2	PC-3	PC-4
N_2	0.0000											
CO_2	0.0000	0.0000										
CH_4	0.1000	0.1000	0.0000									
C_2H_6	0.1000	0.1450	0.0420	0.0000								
C_3H_8	0.1000	0.2566	0.0420	0.0400	0.0000							
C_4H_{10}	0.1000	0.2192	0.0420	0.0400	0.0300	0.0000						
C_5H_{12}	0.1000	0.1801	0.0420	0.0400	0.0300	0.0116	0.0000					
C_6H_{14}	0.1000	0.1579	0.0420	0.0400	0.0300	0.0155	0.0058	0.0000				
PC-1	0.1300	0.0166	0.0500	0.0414	0.0320	0.0337	0.0186	0.0000	0.0000			
PC-2	0.1300	0.0417	0.0518	0.0416	0.0328	0.0418	0.0275	0.0000	0.0000	0.0000		
PC-3	0.1300	0.0731	0.0545	0.0419	0.0346	0.0510	0.0393	0.0000	0.0000	0.0000	0.0000	
PC-4	0.1300	0.1156	0.0617	0.0428	0.0419	0.0652	0.0620	0.0000	0.0000	0.0000	0.0000	0.0000

Table 7C.7a : PR EOS model from PnA characterization for fluid 7 in Table 7.2 Saturation pressure (dew point) for this fluid is 312.73 bars at 424.82 K.						
Components	Z	MW (g/mol)	T_C (K)	P_C (bars)	ω	C_{PEN} (CC/Mol)
N_2	0.0345	28.01	126.20	33.94	0.04000	-4.230
CO_2	0.0273	44.01	304.20	73.76	0.22500	-1.640
CH_4	0.5771	16.04	190.60	46.00	0.00800	-5.200
C_2H_6	0.1072	30.07	305.40	48.84	0.09800	-5.790
C_3H_8	0.0599	44.10	369.80	42.46	0.15200	-6.350
C_4H_{10}	0.0345	58.12	419.95	37.53	0.18780	-6.700
C_5H_{12}	0.0184	72.15	465.25	33.79	0.23970	-5.630
C_6H_{14}	0.0172	86.18	507.40	29.69	0.29600	1.390
PC-1	0.0453	108.21	594.94	30.51	0.15190	-1.650
PC-2	0.0353	138.84	646.31	27.41	0.19710	-3.300
PC-3	0.0267	183.71	715.87	24.05	0.26500	-4.940
PC-4	0.0166	294.82	878.50	18.96	0.43910	-6.590

Table 7C.7b : BIPs for PR EOS model from PnA characterization for fluid 7 in Table 7.2											
	N_2	CO_2	CH_4	C_2H_6	C_3H_8	C_4H_{10}	C_5H_{12}	C_6H_{14}	PC-1	PC-2	PC-3	PC-4
N_2	0.0000											
CO_2	0.0000	0.0000										
CH_4	0.1000	0.1000	0.0000									
C_2H_6	0.1000	0.1450	0.0420	0.0000								
C_3H_8	0.1000	0.2605	0.0420	0.0400	0.0000							
C_4H_{10}	0.1000	0.2223	0.0420	0.0400	0.0300	0.0000						
C_5H_{12}	0.1000	0.1824	0.0420	0.0400	0.0300	0.0116	0.0000					
C_6H_{14}	0.1000	0.1597	0.0420	0.0400	0.0300	0.0155	0.0058	0.0000				
PC-1	0.1300	0.0166	0.0500	0.0414	0.0320	0.0337	0.0186	0.0000	0.0000			
PC-2	0.1300	0.0417	0.0518	0.0416	0.0328	0.0418	0.0275	0.0000	0.0000	0.0000		
PC-3	0.1300	0.0731	0.0545	0.0419	0.0346	0.0510	0.0393	0.0000	0.0000	0.0000	0.0000	
PC-4	0.1300	0.1156	0.0617	0.0428	0.0419	0.0652	0.0620	0.0000	0.0000	0.0000	0.0000	0.0000

Table 7C.8a : PR EOS model from PnA characterization for fluid 8 in Table 7.2 Saturation pressure (dew point) for this fluid is 334.86 bars at 403.71 K.						
Components	Z	MW (g/mol)	T_C (K)	P_C (bars)	ω	C_{PEN} (CC/Mol)
N_2	0.0034	28.01	126.20	33.94	0.04000	-4.230
CO_2	0.0217	44.01	304.20	73.76	0.22500	-1.640
CH_4	0.7064	16.04	190.60	46.00	0.00800	-5.200
C_2H_6	0.1076	30.07	305.40	48.84	0.09800	-5.790
C_3H_8	0.0494	44.10	369.80	42.46	0.15200	-6.350
C_4H_{10}	0.0302	58.12	425.20	38.00	0.19300	-6.490
C_5H_{12}	0.0135	72.15	469.60	33.74	0.25100	-5.120
C_6H_{14}	0.0090	86.18	507.40	29.69	0.29600	1.390
PC-1	0.0211	106.55	595.72	30.81	0.16050	6.190
PC-2	0.0169	133.35	647.16	27.75	0.20820	15.490
PC-3	0.0129	174.58	717.07	24.44	0.27990	31.070
PC-4	0.0079	283.21	881.60	19.45	0.46380	78.030

Table 7C.8b : BIPs for PR EOS model from PnA characterization for fluid 8 in Table 7.2											
	N_2	CO_2	CH_4	C_2H_6	C_3H_8	C_4H_{10}	C_5H_{12}	C_6H_{14}	PC-1	PC-2	PC-3	PC-4
N_2	0.0000											
CO_2	0.0000	0.0000										
CH_4	0.1000	0.1000	0.0000									
C_2H_6	0.1000	0.1450	0.0420	0.0000								
C_3H_8	0.1000	0.2261	0.0420	0.0400	0.0000							
C_4H_{10}	0.1000	0.1948	0.0420	0.0400	0.0300	0.0000						
C_5H_{12}	0.1000	0.1625	0.0420	0.0400	0.0300	0.0116	0.0000					
C_6H_{14}	0.1000	0.1443	0.0420	0.0400	0.0300	0.0155	0.0058	0.0000				
PC-1	0.1300	0.0166	0.0500	0.0414	0.0320	0.0337	0.0186	0.0000	0.0000			
PC-2	0.1300	0.0417	0.0518	0.0416	0.0328	0.0418	0.0275	0.0000	0.0000	0.0000		
PC-3	0.1300	0.0731	0.0545	0.0419	0.0346	0.0510	0.0393	0.0000	0.0000	0.0000	0.0000	
PC-4	0.1300	0.1156	0.0617	0.0428	0.0419	0.0652	0.0620	0.0000	0.0000	0.0000	0.0000	0.0000

Table 7C.9a : PR EOS model from PnA characterization for fluid 9 in Table 7.2
Saturation pressure (dew point) for this fluid is 307.85 bars at 360.93 K.

Components	Z	MW (g/mol)	T_C (K)	P_C (bars)	ω	C_{PEN} (CC/Mol)
N_2	0.0000	28.01	126.20	33.94	0.04000	
CO_2	0.0073	44.01	304.20	73.76	0.22500	
CH_4	0.5832	16.04	190.60	46.00	0.00800	
C_2H_6	0.1355	30.07	305.40	48.84	0.09800	
C_3H_8	0.0761	44.10	369.80	42.46	0.15200	
C_4H_{10}	0.0403	58.12	425.20	38.00	0.19300	
C_5H_{12}	0.0241	72.15	469.60	33.74	0.25100	
C_6H_{14}	0.0190	86.18	595.85	28.89	0.17570	
PC-1	0.0457	120.97	595.85	28.92	0.17650	
PC-2	0.0329	167.96	663.85	25.11	0.24520	
PC-3	0.0230	239.86	755.43	21.11	0.35810	
PC-4	0.0129	428.15	946.05	16.05	0.63620	

Table 7C.9b : BIPs for PR EOS model from PnA characterization for fluid 9 in Table 7.2

	N_2	CO_2	CH_4	C_2H_6	C_3H_8	C_4H_{10}	C_5H_{12}	C_6H_{14}	PC-1	PC-2	PC-3	PC-4
N_2	0.0000											
CO_2	0.0000	0.0000										
CH_4	0.1000	0.1000	0.0000									
C_2H_6	0.1000	0.1450	0.0420	0.0000								
C_3H_8	0.1000	0.1720	0.0420	0.0400	0.0000							
C_4H_{10}	0.1000	0.1529	0.0420	0.0400	0.0300	0.0000						
C_5H_{12}	0.1000	0.1337	0.0420	0.0400	0.0300	0.0116	0.0000					
C_6H_{14}	0.1000	0.1232	0.0420	0.0400	0.0300	0.0155	0.0058	0.0000				
PC-1	0.1300	0.0294	0.0509	0.0415	0.0324	0.0380	0.0231	0.0000	0.0000			
PC-2	0.1300	0.0637	0.0536	0.0418	0.0339	0.0482	0.0356	0.0000	0.0000	0.0000		
PC-3	0.1300	0.1003	0.0581	0.0424	0.0378	0.0594	0.0521	0.0000	0.0000	0.0000	0.0000	
PC-4	0.1300	0.1314	0.0707	0.0439	0.0544	0.0738	0.0788	0.0000	0.0000	0.0000	0.0000	0.0000

Table 7C.10a : PR EOS model from PnA characterization for fluid 10 in Table 7.2 Saturation pressure (dew point) for this fluid is 389.90 bars at 406.45 K.						
Components	Z	MW (g/mol)	T_C (K)	P_C (bars)	ω	C_{PEN} (CC/Mol)
N_2	0.0082	28.01	126.20	33.94	0.04000	-4.230
CO_2	0.0143	44.01	304.20	73.76	0.22500	-1.640
CH_4	0.7985	16.04	190.60	46.00	0.00800	-5.200
C_2H_6	0.0840	30.07	305.40	48.84	0.09800	-5.790
C_3H_8	0.0319	44.10	369.80	42.46	0.15200	-6.350
C_4H_{10}	0.0146	58.12	418.17	37.38	0.18600	-6.490
C_5H_{12}	0.0056	72.15	464.84	33.79	0.23860	-5.120
C_6H_{14}	0.0041	86.18	507.40	29.69	0.29600	1.390
PC-1	0.0136	115.89	621.80	29.45	0.19260	5.890
PC-2	0.0112	141.58	646.89	28.04	0.21750	10.760
PC-3	0.0087	181.13	716.68	24.78	0.29260	19.900
PC-4	0.0055	285.20	880.60	19.86	0.48470	47.480

Table 7C.10b : BIPs for PR EOS model from PnA characterization for fluid 10 in Table 7.2												
	N_2	CO_2	CH_4	C_2H_6	C_3H_8	C_4H_{10}	C_5H_{12}	C_6H_{14}	PC-1	PC-2	PC-3	PC-4
N_2	0.0000											
CO_2	0.0000	0.0000										
CH_4	0.1000	0.1000	0.0000									
C_2H_6	0.1000	0.1450	0.0420	0.0000								
C_3H_8	0.1000	0.2303	0.0420	0.0400	0.0000							
C_4H_{10}	0.1000	0.1981	0.0420	0.0400	0.0300	0.0000						
C_5H_{12}	0.1000	0.1649	0.0420	0.0400	0.0300	0.0116	0.0000					
C_6H_{14}	0.1000	0.1461	0.0420	0.0400	0.0300	0.0155	0.0058	0.0000				
PC-1	0.1300	0.0294	0.0509	0.0415	0.0324	0.0380	0.0231	0.0000	0.0000			
PC-2	0.1300	0.0417	0.0518	0.0416	0.0328	0.0418	0.0275	0.0000	0.0000	0.0000		
PC-3	0.1300	0.0731	0.0545	0.0419	0.0346	0.0510	0.0393	0.0000	0.0000	0.0000	0.0000	
PC-4	0.1300	0.1156	0.0617	0.0428	0.0419	0.0652	0.0620	0.0000	0.0000	0.0000	0.0000	0.0000

Table 7C.11a : PR EOS model from PnA characterization for fluid 11 in Table 7.2
Saturation pressure (dew point) for this fluid is 362.66 bars at 374.81 K.

Components	Z	MW (g/mol)	T_C (K)	P_C (bars)	ω	C_{PEN} (CC/Mol)
N_2	0.0223	28.01	126.20	33.94	0.04000	-4.230
CO_2	0.0045	44.01	304.20	73.76	0.22500	-1.640
CH_4	0.6568	16.04	190.60	46.00	0.00800	-5.200
C_2H_6	0.1170	30.07	305.40	48.84	0.09800	-5.790
C_3H_8	0.0587	44.10	369.80	42.46	0.15200	-6.350
C_4H_{10}	0.0295	58.12	425.20	38.00	0.19300	-6.490
C_5H_{12}	0.0142	72.15	469.60	33.74	0.25100	-5.120
C_6H_{14}	0.0098	86.18	507.40	29.69	0.29600	1.390
PC-1	0.0334	109.59	592.96	30.17	0.14240	6.710
PC-2	0.0251	145.83	667.93	25.74	0.20590	19.410
PC-3	0.0182	201.62	754.90	21.91	0.29040	40.800
PC-4	0.0105	348.74	942.02	16.90	0.48660	103.970

Table 7C.11b : BIPs for PR EOS model from PnA characterization for fluid 11 in Table 7.2

	N_2	CO_2	CH_4	C_2H_6	C_3H_8	C_4H_{10}	C_5H_{12}	C_6H_{14}	PC-1	PC-2	PC-3	PC-4
N_2	0.0000											
CO_2	0.0000	0.0000										
CH_4	0.1000	0.1000	0.0000									
C_2H_6	0.1000	0.1450	0.0420	0.0000								
C_3H_8	0.1000	0.1872	0.0420	0.0400	0.0000							
C_4H_{10}	0.1000	0.1645	0.0420	0.0400	0.0300	0.0000						
C_5H_{12}	0.1000	0.1413	0.0420	0.0400	0.0300	0.0116	0.0000					
C_6H_{14}	0.1000	0.1285	0.0420	0.0400	0.0300	0.0155	0.0058	0.0000				
PC-1	0.1300	0.0166	0.0500	0.0414	0.0320	0.0337	0.0186	0.0000	0.0000			
PC-2	0.1300	0.0532	0.0527	0.0417	0.0334	0.0452	0.0317	0.0000	0.0000	0.0000		
PC-3	0.1300	0.0886	0.0563	0.0422	0.0360	0.0556	0.0461	0.0000	0.0000	0.0000	0.0000	
PC-4	0.1300	0.1244	0.0653	0.0433	0.0468	0.0693	0.0698	0.0000	0.0000	0.0000	0.0000	0.0000

Table 7C.12a : PR EOS model from PnA characterization for fluid 12 in Table 7.2
Saturation pressure (dew point) for this fluid is 214.78 bars at 435.93 K.

Components	Z	MW (g/mol)	T_C (K)	P_C (bars)	ω	C_{PEN} (CC/Mol)
N_2	0.0567	28.01	126.20	33.94	0.04000	-4.230
CO_2	0.0201	44.01	304.20	73.76	0.22500	-1.640
CH_4	0.4679	16.04	190.60	46.00	0.00800	-5.200
C_2H_6	0.1265	30.07	305.40	48.84	0.09800	-5.790
C_3H_8	0.0587	44.10	369.80	42.46	0.15200	-6.350
C_4H_{10}	0.0604	58.12	425.20	38.00	0.19300	-6.490
C_5H_{12}	0.0392	72.15	469.60	33.74	0.25100	-5.120
C_6H_{14}	0.0478	86.18	507.40	29.69	0.29600	1.390
PC-1	0.0423	107.64	570.11	30.50	0.15170	0.570
PC-2	0.0348	131.00	621.84	27.39	0.19670	1.310
PC-3	0.0276	164.93	670.10	25.02	0.24200	2.380
PC-4	0.0184	247.51	803.17	20.42	0.37490	5.510

Table 7C.12b : BIPs for PR EOS model from PnA characterization for fluid 12 in Table 7.2

	N_2	CO_2	CH_4	C_2H_6	C_3H_8	C_4H_{10}	C_5H_{12}	C_6H_{14}	PC-1	PC-2	PC-3	PC-4
N_2	0.0000											
CO_2	0.0000	0.0000										
CH_4	0.1000	0.1000	0.0000									
C_2H_6	0.1000	0.1450	0.0420	0.0000								
C_3H_8	0.1000	0.2807	0.0420	0.0400	0.0000							
C_4H_{10}	0.1000	0.2385	0.0420	0.0400	0.0300	0.0000						
C_5H_{12}	0.1000	0.1944	0.0420	0.0400	0.0300	0.0116	0.0000					
C_6H_{14}	0.1000	0.1691	0.0420	0.0400	0.0300	0.0155	0.0058	0.0000				
PC-1	0.1300	0.0166	0.0500	0.0414	0.0320	0.0337	0.0186	0.0000	0.0000			
PC-2	0.1300	0.0417	0.0518	0.0416	0.0328	0.0418	0.0275	0.0000	0.0000	0.0000		
PC-3	0.1300	0.0637	0.0536	0.0418	0.0339	0.0482	0.0356	0.0000	0.0000	0.0000	0.0000	
PC-4	0.1300	0.1050	0.0590	0.0425	0.0387	0.0610	0.0548	0.0000	0.0000	0.0000	0.0000	0.0000

Table 7C.13a : PR EOS model from PnA characterization for fluid 13 in Table 7.2 Saturation pressure (dew point) for this fluid is 208.58 bars at 435.93 K.						
Components	Z	MW (g/mol)	T_C (K)	P_C (bars)	ω	C_{PEN} (CC/Mol)
N_2	0.0567	28.01	126.20	33.94	0.04000	-4.230
CO_2	0.0226	44.01	304.20	73.76	0.22500	-1.640
CH_4	0.4574	16.04	190.60	46.00	0.00800	-5.200
C_2H_6	0.1147	30.07	305.40	48.84	0.09800	-5.790
C_3H_8	0.0759	44.10	369.80	42.46	0.15200	-6.350
C_4H_{10}	0.0638	58.12	425.20	38.00	0.19300	-6.490
C_5H_{12}	0.0431	72.15	469.60	33.74	0.25100	-5.120
C_6H_{14}	0.0592	86.18	507.40	29.69	0.29600	1.390
PC-1	0.0359	109.83	596.63	30.27	0.14520	8.210
PC-2	0.0300	131.36	648.16	27.14	0.18830	17.370
PC-3	0.0242	162.83	695.76	24.73	0.23160	30.580
PC-4	0.0164	239.95	804.52	20.67	0.33820	66.250

Table 7C.13b : BIPs for PR EOS model from PnA characterization for fluid 13 in Table 7.2												
	N_2	CO_2	CH_4	C_2H_6	C_3H_8	C_4H_{10}	C_5H_{12}	C_6H_{14}	PC-1	PC-2	PC-3	PC-4
N_2	0.0000											
CO_2	0.0000	0.0000										
CH_4	0.1000	0.1000	0.0000									
C_2H_6	0.1000	0.1450	0.0420	0.0000								
C_3H_8	0.1000	0.2807	0.0420	0.0400	0.0000							
C_4H_{10}	0.1000	0.2385	0.0420	0.0400	0.0300	0.0000						
C_5H_{12}	0.1000	0.1944	0.0420	0.0400	0.0300	0.0116	0.0000					
C_6H_{14}	0.1000	0.1691	0.0420	0.0400	0.0300	0.0155	0.0058	0.0000				
PC-1	0.1300	0.0166	0.0500	0.0414	0.0320	0.0337	0.0186	0.0000	0.0000			
PC-2	0.1300	0.0417	0.0518	0.0416	0.0328	0.0418	0.0275	0.0000	0.0000	0.0000		
PC-3	0.1300	0.0637	0.0536	0.0418	0.0339	0.0482	0.0356	0.0000	0.0000	0.0000	0.0000	
PC-4	0.1300	0.1003	0.0581	0.0424	0.0378	0.0594	0.0521	0.0000	0.0000	0.0000	0.0000	0.0000

Table 7C.14a : PR EOS model from PnA characterization for fluid 14 in Table 7.2 Saturation pressure (dew point) for this fluid is 333.00 bars at 387.59 K.						
Components	Z	MW (g/mol)	T_C (K)	P_C (bars)	ω	C_{PEN} (CC/Mol)
N_2	0.0162	28.01	126.20	33.94	0.04000	-4.230
CO_2	0.0014	44.01	304.20	73.76	0.22500	-1.640
CH_4	0.6306	16.04	190.60	46.00	0.00800	-5.200
C_2H_6	0.1135	30.07	305.40	48.84	0.09800	-5.790
C_3H_8	0.0601	44.10	369.80	42.46	0.15200	-6.350
C_4H_{10}	0.0331	58.12	418.12	37.37	0.18600	-6.490
C_5H_{12}	0.0177	72.15	465.33	33.79	0.23990	-5.120
C_6H_{14}	0.0102	86.18	507.40	29.69	0.29600	1.390
PC-1	0.0457	108.24	592.15	29.82	0.13230	0.230
PC-2	0.0336	147.22	666.95	25.31	0.19130	0.730
PC-3	0.0240	206.21	753.24	21.40	0.26970	1.550
PC-4	0.0138	358.66	954.44	15.96	0.46870	4.130

Table 7C.14b : BIPs for PR EOS model from PnA characterization for fluid 14 in Table 7.2												
	N_2	CO_2	CH_4	C_2H_6	C_3H_8	C_4H_{10}	C_5H_{12}	C_6H_{14}	PC-1	PC-2	PC-3	PC-4
N_2	0.0000											
CO_2	0.0000	0.0000										
CH_4	0.1000	0.1000	0.0000									
C_2H_6	0.1000	0.1450	0.0420	0.0000								
C_3H_8	0.1000	0.2032	0.0420	0.0400	0.0000							
C_4H_{10}	0.1000	0.1769	0.0420	0.0400	0.0300	0.0000						
C_5H_{12}	0.1000	0.1498	0.0420	0.0400	0.0300	0.0116	0.0000					
C_6H_{14}	0.1000	0.1347	0.0420	0.0400	0.0300	0.0155	0.0058	0.0000				
PC-1	0.1300	0.0166	0.0500	0.0414	0.0320	0.0337	0.0186	0.0000	0.0000			
PC-2	0.1300	0.0532	0.0527	0.0417	0.0334	0.0452	0.0317	0.0000	0.0000	0.0000		
PC-3	0.1300	0.0886	0.0563	0.0422	0.0360	0.0556	0.0461	0.0000	0.0000	0.0000	0.0000	
PC-4	0.1300	0.1259	0.0662	0.0434	0.0480	0.0702	0.0715	0.0000	0.0000	0.0000	0.0000	0.0000

Table 7C.15a : PR EOS model from PnA characterization for fluid 15 in Table 7.2
Saturation pressure (dew point) for this fluid is 471.50 bars at 394.00 K.

Components	Z	MW (g/mol)	T_C (K)	P_C (bars)	ω	C_{PEN} (CC/Mol)
N_2	0.0030	28.01	126.20	33.94	0.04000	-4.230
CO_2	0.0172	44.01	304.20	73.76	0.22500	-1.640
CH_4	0.7908	16.04	190.60	46.00	0.00800	-5.200
C_2H_6	0.0748	30.07	305.40	48.84	0.09800	-5.790
C_3H_8	0.0329	44.10	369.80	42.46	0.15200	-6.350
C_4H_{10}	0.0177	58.12	420.23	37.56	0.18810	-6.490
C_5H_{12}	0.0091	72.15	465.93	33.78	0.24140	-5.120
C_6H_{14}	0.0162	86.18	507.40	29.69	0.29600	1.390
PC-1	0.0135	132.14	644.61	28.13	0.22040	10.850
PC-2	0.0110	162.04	691.33	25.83	0.27120	18.540
PC-3	0.0085	208.06	755.74	23.27	0.34660	30.870
PC-4	0.0054	329.21	926.64	18.89	0.55900	68.400

Table 7C.15b : BIPs for PR EOS model from PnA characterization for fluid 15 in Table 7.2

	N_2	CO_2	CH_4	C_2H_6	C_3H_8	C_4H_{10}	C_5H_{12}	C_6H_{14}	PC-1	PC-2	PC-3	PC-4
N_2	0.0000											
CO_2	0.0000	0.0000										
CH_4	0.1000	0.1000	0.0000									
C_2H_6	0.1000	0.1450	0.0420	0.0000								
C_3H_8	0.1000	0.2120	0.0420	0.0400	0.0000							
C_4H_{10}	0.1000	0.1837	0.0420	0.0400	0.0300	0.0000						
C_5H_{12}	0.1000	0.1546	0.0420	0.0400	0.0300	0.0116	0.0000					
C_6H_{14}	0.1000	0.1383	0.0420	0.0400	0.0300	0.0155	0.0058	0.0000				
PC-1	0.1300	0.0417	0.0518	0.0416	0.0328	0.0418	0.0275	0.0000	0.0000			
PC-2	0.1300	0.0637	0.0536	0.0418	0.0339	0.0482	0.0356	0.0000	0.0000	0.0000		
PC-3	0.1300	0.0886	0.0563	0.0422	0.0360	0.0556	0.0461	0.0000	0.0000	0.0000	0.0000	
PC-4	0.1300	0.1226	0.0644	0.0431	0.0455	0.0684	0.0680	0.0000	0.0000	0.0000	0.0000	0.0000

Table 7C.16a : PR EOS model from PnA characterization for fluid 16 in Table 7.2 Saturation pressure (dew point) for this fluid is 388.00 bars at 428.15 K.						
Components	Z	MW (g/mol)	T_C (K)	P_C (bars)	ω	C_{PEN} (CC/Mol)
N_2	0.0060	28.01	126.20	33.94	0.04000	-4.230
CO_2	0.0334	44.01	304.20	73.76	0.22500	-1.640
CH_4	0.7416	16.04	190.60	46.00	0.00800	-5.200
C_2H_6	0.0790	30.07	305.40	48.84	0.09800	-5.790
C_3H_8	0.0415	44.10	369.80	42.46	0.15200	-6.350
C_4H_{10}	0.0215	58.12	419.55	37.50	0.18740	-6.490
C_5H_{12}	0.0119	72.15	465.50	33.78	0.24030	-5.120
C_6H_{14}	0.0081	86.18	507.40	29.69	0.29600	1.390
PC-1	0.0204	105.32	596.65	32.01	0.19450	0.130
PC-2	0.0163	131.67	648.17	29.12	0.25230	0.330
PC-3	0.0125	172.22	718.52	26.01	0.33920	0.650
PC-4	0.0077	279.05	865.50	21.80	0.53540	1.530

Table 7C.16b : BIPs for PR EOS model from PnA characterization for fluid 16 in Table 7.2											
	N_2	CO_2	CH_4	C_2H_6	C_3H_8	C_4H_{10}	C_5H_{12}	C_6H_{14}	PC-1	PC-2	PC-3	PC-4
N_2	0.0000											
CO_2	0.0000	0.0000										
CH_4	0.1000	0.1000	0.0000									
C_2H_6	0.1000	0.1450	0.0420	0.0000								
C_3H_8	0.1000	0.2664	0.0420	0.0400	0.0000							
C_4H_{10}	0.1000	0.2270	0.0420	0.0400	0.0300	0.0000						
C_5H_{12}	0.1000	0.1859	0.0420	0.0400	0.0300	0.0116	0.0000					
C_6H_{14}	0.1000	0.1624	0.0420	0.0400	0.0300	0.0155	0.0058	0.0000				
PC-1	0.1300	0.0166	0.0500	0.0414	0.0320	0.0337	0.0186	0.0000	0.0000			
PC-2	0.1300	0.0417	0.0518	0.0416	0.0328	0.0418	0.0275	0.0000	0.0000	0.0000		
PC-3	0.1300	0.0731	0.0545	0.0419	0.0346	0.0510	0.0393	0.0000	0.0000	0.0000	0.0000	
PC-4	0.1300	0.1126	0.0608	0.0427	0.0408	0.0639	0.0598	0.0000	0.0000	0.0000	0.0000	0.0000

Table 7C.17a : PR EOS model from PnA characterization for fluid 17 in Table 7.2 Saturation pressure (dew point) for this fluid is 451.27 bars at 358.78 K.						
Components	Z	MW (g/mol)	T_C (K)	P_C (bars)	ω	C_{PEN} (CC/Mol)
N_2	0.0012	28.01	126.20	33.94	0.04000	-4.230
CO_2	0.0024	44.01	304.20	73.76	0.22500	-1.640
CH_4	0.8804	16.04	190.60	46.00	0.00800	-5.200
C_2H_6	0.0461	30.07	305.40	48.84	0.09800	-5.790
C_3H_8	0.0154	44.10	369.80	42.46	0.15200	-6.350
C_4H_{10}	0.0081	58.12	417.38	37.30	0.18520	-6.490
C_5H_{12}	0.0041	72.15	464.89	33.79	0.23870	-5.120
C_6H_{14}	0.0031	86.18	507.40	29.69	0.29600	1.390
PC-1	0.0138	113.43	595.12	30.81	0.16040	15.530
PC-2	0.0112	139.77	646.51	27.75	0.20810	32.950
PC-3	0.0087	180.32	716.14	24.44	0.27980	62.370
PC-4	0.0055	287.04	879.22	19.44	0.46360	151.420

Table 7C.17b : BIPs for PR EOS model from PnA characterization for fluid 17 in Table 7.2												
	N_2	CO_2	CH_4	C_2H_6	C_3H_8	C_4H_{10}	C_5H_{12}	C_6H_{14}	PC-1	PC-2	PC-3	PC-4
N_2	0.0000											
CO_2	0.0000	0.0000										
CH_4	0.1000	0.1000	0.0000									
C_2H_6	0.1000	0.1450	0.0420	0.0000								
C_3H_8	0.1000	0.1698	0.0420	0.0400	0.0000							
C_4H_{10}	0.1000	0.1513	0.0420	0.0400	0.0300	0.0000						
C_5H_{12}	0.1000	0.1326	0.0420	0.0400	0.0300	0.0116	0.0000					
C_6H_{14}	0.1000	0.1225	0.0420	0.0400	0.0300	0.0155	0.0058	0.0000				
PC-1	0.1300	0.0166	0.0500	0.0414	0.0320	0.0337	0.0186	0.0000	0.0000			
PC-2	0.1300	0.0417	0.0518	0.0416	0.0328	0.0418	0.0275	0.0000	0.0000	0.0000		
PC-3	0.1300	0.0731	0.0545	0.0419	0.0346	0.0510	0.0393	0.0000	0.0000	0.0000	0.0000	
PC-4	0.1300	0.1156	0.0617	0.0428	0.0419	0.0652	0.0620	0.0000	0.0000	0.0000	0.0000	0.0000

Table 7C.18a : PR EOS model from PnA characterization for fluid 18 in Table 7.2
Saturation pressure (dew point) for this fluid is 539.52 bars at 378.15 K.

Components	Z	MW (g/mol)	T_C (K)	P_C (bars)	ω	C_{PEN} (CC/Mol)
N_2	0.0006	28.01	126.20	33.94	0.04000	-4.230
CO_2	0.0087	44.01	304.20	73.76	0.22500	-1.640
CH_4	0.8922	16.04	190.60	46.00	0.00800	-5.200
C_2H_6	0.0355	30.07	305.40	48.84	0.09800	-5.790
C_3H_8	0.0168	44.10	369.80	42.46	0.15200	-6.350
C_4H_{10}	0.0103	58.12	417.38	37.30	0.18520	-6.490
C_5H_{12}	0.0046	72.15	464.89	33.79	0.23870	-5.120
C_6H_{14}	0.0037	86.18	507.40	29.69	0.29600	1.390
PC-1	0.0093	115.89	622.55	31.79	0.26380	-20.530
PC-2	0.0078	138.16	647.69	30.53	0.29800	-35.400
PC-3	0.0063	172.40	717.83	27.64	0.40070	-62.910
PC-4	0.0041	262.40	844.00	24.18	0.60040	-131.640

Table 7C.18b : BIPs for PR EOS model from PnA characterization for fluid 18 in Table 7.2

	N_2	CO_2	CH_4	C_2H_6	C_3H_8	C_4H_{10}	C_5H_{12}	C_6H_{14}	PC-1	PC-2	PC-3	PC-4
N_2	0.0000											
CO_2	0.0000	0.0000										
CH_4	0.1000	0.1000	0.0000									
C_2H_6	0.1000	0.1450	0.0420	0.0000								
C_3H_8	0.1000	0.1912	0.0420	0.0400	0.0000							
C_4H_{10}	0.1000	0.1676	0.0420	0.0400	0.0300	0.0000						
C_5H_{12}	0.1000	0.1434	0.0420	0.0400	0.0300	0.0116	0.0000					
C_6H_{14}	0.1000	0.1300	0.0420	0.0400	0.0300	0.0155	0.0058	0.0000				
PC-1	0.1300	0.0294	0.0509	0.0415	0.0324	0.0380	0.0231	0.0000	0.0000			
PC-2	0.1300	0.0417	0.0518	0.0416	0.0328	0.0418	0.0275	0.0000	0.0000	0.0000		
PC-3	0.1300	0.0731	0.0545	0.0419	0.0346	0.0510	0.0393	0.0000	0.0000	0.0000	0.0000	
PC-4	0.1300	0.1091	0.0599	0.0426	0.0398	0.0625	0.0574	0.0000	0.0000	0.0000	0.0000	0.0000

Table 7C.19a : PR EOS model from PnA characterization for fluid 19 in Table 7.2 Saturation pressure (dew point) for this fluid is 355.77 bars at 357.59 K.						
Components	Z	MW (g/mol)	T_C (K)	P_C (bars)	ω	C_{PEN} (CC/Mol)
N_2	0.0008	28.01	126.20	33.94	0.04000	-4.230
CO_2	0.0035	44.01	304.20	73.76	0.22500	-1.640
CH_4	0.9189	16.04	190.60	46.00	0.00800	-5.200
C_2H_6	0.0183	30.07	305.40	48.84	0.09800	-5.790
C_3H_8	0.0121	44.10	369.80	42.46	0.15200	-6.350
C_4H_{10}	0.0088	58.12	417.78	37.34	0.18560	-6.490
C_5H_{12}	0.0046	72.15	464.75	33.79	0.23830	-5.120
C_6H_{14}	0.0039	86.18	507.40	29.69	0.29600	1.390
PC-1	0.0099	110.25	597.53	30.61	0.15480	14.010
PC-2	0.0083	131.86	649.14	27.52	0.20070	29.340
PC-3	0.0066	165.17	696.99	25.16	0.24690	52.150
PC-4	0.0043	252.65	827.73	20.59	0.38260	121.350

Table 7C.19b : BIPs for PR EOS model from PnA characterization for fluid 19 in Table 7.2												
	N_2	CO_2	CH_4	C_2H_6	C_3H_8	C_4H_{10}	C_5H_{12}	C_6H_{14}	PC-1	PC-2	PC-3	PC-4
N_2	0.0000											
CO_2	0.0000	0.0000										
CH_4	0.1000	0.1000	0.0000									
C_2H_6	0.1000	0.1450	0.0420	0.0000								
C_3H_8	0.1000	0.1687	0.0420	0.0400	0.0000							
C_4H_{10}	0.1000	0.1504	0.0420	0.0400	0.0300	0.0000						
C_5H_{12}	0.1000	0.1321	0.0420	0.0400	0.0300	0.0116	0.0000					
C_6H_{14}	0.1000	0.1221	0.0420	0.0400	0.0300	0.0155	0.0058	0.0000				
PC-1	0.1300	0.0166	0.0500	0.0414	0.0320	0.0337	0.0186	0.0000	0.0000			
PC-2	0.1300	0.0417	0.0518	0.0416	0.0328	0.0418	0.0275	0.0000	0.0000	0.0000		
PC-3	0.1300	0.0637	0.0536	0.0418	0.0339	0.0482	0.0356	0.0000	0.0000	0.0000	0.0000	
PC-4	0.1300	0.1050	0.0590	0.0425	0.0387	0.0610	0.0548	0.0000	0.0000	0.0000	0.0000	0.0000

Table 7C.20a : PR EOS model from PnA characterization for fluid 20 in Table 7.2
Saturation pressure (dew point) for this fluid is 441.61 bars at 364.22 K.

Components	Z	MW (g/mol)	T_C (K)	P_C (bars)	ω	C_{PEN} (CC/Mol)
N_2	0.0009	28.01	126.20	33.94	0.04000	-4.230
CO_2	0.0032	44.01	304.20	73.76	0.22500	-1.640
CH_4	0.9165	16.04	190.60	46.00	0.00800	-5.200
C_2H_6	0.0333	30.07	305.40	48.84	0.09800	-5.790
C_3H_8	0.0122	44.10	369.80	42.46	0.15200	-6.350
C_4H_{10}	0.0065	58.12	416.90	37.26	0.18470	-6.490
C_5H_{12}	0.0028	72.15	464.55	33.79	0.23780	-5.120
C_6H_{14}	0.0019	86.18	507.40	29.69	0.29600	1.390
PC-1	0.0076	114.82	597.79	32.49	0.20790	-3.370
PC-2	0.0064	135.14	649.41	29.65	0.26960	-6.750
PC-3	0.0052	166.40	697.34	27.51	0.33170	-10.120
PC-4	0.0035	248.47	828.48	23.44	0.51390	-13.500

Table 7C.20b : BIPs for PR EOS model from PnA characterization for fluid 20 in Table 7.2

	N_2	CO_2	CH_4	C_2H_6	C_3H_8	C_4H_{10}	C_5H_{12}	C_6H_{14}	PC-1	PC-2	PC-3	PC-4
N_2	0.0000											
CO_2	0.0000	0.0000										
CH_4	0.1000	0.1000	0.0000									
C_2H_6	0.1000	0.1450	0.0420	0.0000								
C_3H_8	0.1000	0.1754	0.0420	0.0400	0.0000							
C_4H_{10}	0.1000	0.1555	0.0420	0.0400	0.0300	0.0000						
C_5H_{12}	0.1000	0.1353	0.0420	0.0400	0.0300	0.0116	0.0000					
C_6H_{14}	0.1000	0.1243	0.0420	0.0400	0.0300	0.0155	0.0058	0.0000				
PC-1	0.1300	0.0166	0.0500	0.0414	0.0320	0.0337	0.0186	0.0000	0.0000			
PC-2	0.1300	0.0417	0.0518	0.0416	0.0328	0.0418	0.0275	0.0000	0.0000	0.0000		
PC-3	0.1300	0.0637	0.0536	0.0418	0.0339	0.0482	0.0356	0.0000	0.0000	0.0000	0.0000	
PC-4	0.1300	0.1050	0.0590	0.0425	0.0387	0.0610	0.0548	0.0000	0.0000	0.0000	0.0000	0.0000

Table 7C.21a : PR EOS model from PnA characterization for fluid 21 in Table 7.2
Saturation pressure (dew point) for this fluid is 334.05 bars at 355.37 K.

Components	Z	MW (g/mol)	T_C (K)	P_C (bars)	ω	C_{PEN} (CC/Mol)
N_2	0.0008	28.01	126.20	33.94	0.04000	-4.230
CO_2	0.0028	44.01	304.20	73.76	0.22500	-1.640
CH_4	0.9299	16.04	190.60	46.00	0.00800	-5.200
C_2H_6	0.0183	30.07	305.40	48.84	0.09800	-5.790
C_3H_8	0.0117	44.10	369.80	42.46	0.15200	-6.350
C_4H_{10}	0.0079	58.12	417.74	37.34	0.18560	-6.490
C_5H_{12}	0.0041	72.15	464.97	33.79	0.23890	-5.120
C_6H_{14}	0.0033	86.18	507.40	29.69	0.29600	1.390
PC-1	0.0070	112.01	598.91	31.08	0.16790	15.580
PC-2	0.0060	130.98	650.64	28.05	0.21780	30.020
PC-3	0.0049	160.21	698.87	25.74	0.26790	51.580
PC-4	0.0033	236.82	810.46	21.86	0.39120	111.710

Table 7C.21b : BIPs for PR EOS model from PnA characterization for fluid 21 in Table 7.2

	N_2	CO_2	CH_4	C_2H_6	C_3H_8	C_4H_{10}	C_5H_{12}	C_6H_{14}	PC-1	PC-2	PC-3	PC-4
N_2	0.0000											
CO_2	0.0000	0.0000										
CH_4	0.1000	0.1000	0.0000									
C_2H_6	0.1000	0.1450	0.0420	0.0000								
C_3H_8	0.1000	0.1665	0.0420	0.0400	0.0000							
C_4H_{10}	0.1000	0.1488	0.0420	0.0400	0.0300	0.0000						
C_5H_{12}	0.1000	0.1310	0.0420	0.0400	0.0300	0.0116	0.0000					
C_6H_{14}	0.1000	0.1214	0.0420	0.0400	0.0300	0.0155	0.0058	0.0000				
PC-1	0.1300	0.0166	0.0500	0.0414	0.0320	0.0337	0.0186	0.0000	0.0000			
PC-2	0.1300	0.0417	0.0518	0.0416	0.0328	0.0418	0.0275	0.0000	0.0000	0.0000		
PC-3	0.1300	0.0637	0.0536	0.0418	0.0339	0.0482	0.0356	0.0000	0.0000	0.0000	0.0000	
PC-4	0.1300	0.1003	0.0581	0.0424	0.0378	0.0594	0.0521	0.0000	0.0000	0.0000	0.0000	0.0000

Table 7C.22a : PR EOS model from PnA characterization for fluid 22 in Table 7.2 Saturation pressure (dew point) for this fluid is 408.38 bars at 367.59 K.						
Components	Z	MW (g/mol)	T_C (K)	P_C (bars)	ω	C_{PEN} (CC/Mol)
N_2	0.0009	28.01	126.20	33.94	0.04000	-4.230
CO_2	0.0059	44.01	304.20	73.76	0.22500	-1.640
CH_4	0.9164	16.04	190.60	46.00	0.00800	-5.200
C_2H_6	0.0352	30.07	305.40	48.84	0.09800	-5.790
C_3H_8	0.0131	44.10	369.80	42.46	0.15200	-6.350
C_4H_{10}	0.0069	58.12	417.82	37.34	0.18570	-6.490
C_5H_{12}	0.0032	72.15	465.03	33.79	0.23910	-5.120
C_6H_{14}	0.0023	86.18	507.40	29.69	0.29600	1.390
PC-1	0.0052	110.91	599.93	34.52	0.26550	34.610
PC-2	0.0045	127.41	626.35	33.15	0.30480	58.550
PC-3	0.0038	152.80	676.34	30.95	0.38390	98.510
PC-4	0.0026	219.17	791.23	27.46	0.58010	206.620

Table 7C.22b : BIPs for PR EOS model from PnA characterization for fluid 22 in Table 7.2											
	N_2	CO_2	CH_4	C_2H_6	C_3H_8	C_4H_{10}	C_5H_{12}	C_6H_{14}	PC-1	PC-2	PC-3	PC-4
N_2	0.0000											
CO_2	0.0000	0.0000										
CH_4	0.1000	0.1000	0.0000									
C_2H_6	0.1000	0.1450	0.0420	0.0000								
C_3H_8	0.1000	0.1790	0.0420	0.0400	0.0000							
C_4H_{10}	0.1000	0.1582	0.0420	0.0400	0.0300	0.0000						
C_5H_{12}	0.1000	0.1371	0.0420	0.0400	0.0300	0.0116	0.0000					
C_6H_{14}	0.1000	0.1256	0.0420	0.0400	0.0300	0.0155	0.0058	0.0000				
PC-1	0.1300	0.0166	0.0500	0.0414	0.0320	0.0337	0.0186	0.0000	0.0000			
PC-2	0.1300	0.0294	0.0509	0.0415	0.0324	0.0380	0.0231	0.0000	0.0000	0.0000		
PC-3	0.1300	0.0532	0.0527	0.0417	0.0334	0.0452	0.0317	0.0000	0.0000	0.0000	0.0000	
PC-4	0.1300	0.0949	0.0572	0.0423	0.0369	0.0576	0.0492	0.0000	0.0000	0.0000	0.0000	0.0000

Table 7C.23a : PR EOS model from PnA characterization for fluid 23 in Table 7.2
Saturation pressure (dew point) for this fluid is 237.36 bars at 366.48 K.

Components	Z	MW (g/mol)	T_C (K)	P_C (bars)	ω	C_{PEN} (CC/Mol)
N_2	0.0194	28.01	126.20	33.94	0.04000	-4.230
CO_2	0.0121	44.01	304.20	73.76	0.22500	-1.640
CH_4	0.6599	16.04	190.60	46.00	0.00800	-5.200
C_2H_6	0.0869	30.07	305.40	48.84	0.09800	-5.790
C_3H_8	0.0591	44.10	369.80	42.46	0.15200	-6.350
C_4H_{10}	0.0517	58.12	417.30	37.30	0.18510	-6.490
C_5H_{12}	0.0269	72.15	464.23	33.80	0.23700	-5.120
C_6H_{14}	0.0181	86.18	507.40	29.69	0.29600	1.390
PC-1	0.0226	102.22	596.85	30.03	0.13820	5.190
PC-2	0.0187	123.30	623.21	28.33	0.15870	12.280
PC-3	0.0149	155.09	672.62	25.57	0.19990	23.910
PC-4	0.0098	236.39	805.08	20.30	0.32200	60.100

Table 7C.23b : BIPs for PR EOS model from PnA characterization for fluid 23 in Table 7.2

	N_2	CO_2	CH_4	C_2H_6	C_3H_8	C_4H_{10}	C_5H_{12}	C_6H_{14}	PC-1	PC-2	PC-3	PC-4
N_2	0.0000											
CO_2	0.0000	0.0000										
CH_4	0.1000	0.1000	0.0000									
C_2H_6	0.1000	0.1450	0.0420	0.0000								
C_3H_8	0.1000	0.1778	0.0420	0.0400	0.0000							
C_4H_{10}	0.1000	0.1573	0.0420	0.0400	0.0300	0.0000						
C_5H_{12}	0.1000	0.1365	0.0420	0.0400	0.0300	0.0116	0.0000					
C_6H_{14}	0.1000	0.1252	0.0420	0.0400	0.0300	0.0155	0.0058	0.0000				
PC-1	0.1300	0.0166	0.0500	0.0414	0.0320	0.0337	0.0186	0.0000	0.0000			
PC-2	0.1300	0.0294	0.0509	0.0415	0.0324	0.0380	0.0231	0.0000	0.0000	0.0000		
PC-3	0.1300	0.0532	0.0527	0.0417	0.0334	0.0452	0.0317	0.0000	0.0000	0.0000	0.0000	
PC-4	0.1300	0.1003	0.0581	0.0424	0.0378	0.0594	0.0521	0.0000	0.0000	0.0000	0.0000	0.0000

Table 7C.24a : PR EOS model from PnA characterization for fluid 24 in Table 7.2 Saturation pressure (dew point) for this fluid is 278.87 bars at 365.37 K.						
Components	Z	MW (g/mol)	T_C (K)	P_C (bars)	ω	C_{PEN} (CC/Mol)
N_2	0.0058	28.01	126.20	33.94	0.04000	
CO_2	0.1166	44.01	304.20	73.76	0.22500	
CH_4	0.7533	16.04	190.60	46.00	0.00800	
C_2H_6	0.0544	30.07	305.40	48.84	0.09800	
C_3H_8	0.0249	44.10	369.80	42.46	0.15200	
C_4H_{10}	0.0127	58.12	419.58	37.50	0.18740	
C_5H_{12}	0.0068	72.15	465.14	33.79	0.23940	
C_6H_{14}	0.0041	86.18	507.40	29.69	0.29600	
PC-1	0.0069	100.34	577.63	35.93	0.22110	
PC-2	0.0060	115.02	631.61	32.90	0.29740	
PC-3	0.0050	137.65	657.38	31.71	0.33590	
PC-4	0.0035	196.75	755.73	28.29	0.49010	

Table 7C.24b : BIPs for PR EOS model from PnA characterization for fluid 24 in Table 7.2												
	N_2	CO_2	CH_4	C_2H_6	C_3H_8	C_4H_{10}	C_5H_{12}	C_6H_{14}	PC-1	PC-2	PC-3	PC-4
N_2	0.0000											
CO_2	0.0000	0.0000										
CH_4	0.1000	0.1000	0.0000									
C_2H_6	0.1000	0.1450	0.0420	0.0000								
C_3H_8	0.1000	0.1766	0.0420	0.0400	0.0000							
C_4H_{10}	0.1000	0.1564	0.0420	0.0400	0.0300	0.0000						
C_5H_{12}	0.1000	0.1359	0.0420	0.0400	0.0300	0.0116	0.0000					
C_6H_{14}	0.1000	0.1247	0.0420	0.0400	0.0300	0.0155	0.0058	0.0000				
PC-1	0.1300	0.0040	0.0491	0.0413	0.0317	0.0289	0.0141	0.0000	0.0000			
PC-2	0.1300	0.0294	0.0509	0.0415	0.0324	0.0380	0.0231	0.0000	0.0000	0.0000		
PC-3	0.1300	0.0417	0.0518	0.0416	0.0328	0.0418	0.0275	0.0000	0.0000	0.0000	0.0000	
PC-4	0.1300	0.0814	0.0554	0.0420	0.0353	0.0534	0.0428	0.0000	0.0000	0.0000	0.0000	0.0000

Table 7C.25a : PR EOS model from PnA characterization for fluid 25 in Table 7.2
Saturation pressure (dew point) for this fluid is 466.42 bars at 410.93 K.

Components	Z	MW (g/mol)	T_C (K)	P_C (bars)	ω	C_{PEN} (CC/Mol)
N_2	0.0031	28.01	126.20	33.94	0.04000	-4.230
CO_2	0.0237	44.01	304.20	73.76	0.22500	-1.640
CH_4	0.7319	16.04	190.60	46.00	0.00800	-5.200
C_2H_6	0.0780	30.07	305.40	48.84	0.09800	-5.790
C_3H_8	0.0355	44.10	369.80	42.46	0.15200	-6.350
C_4H_{10}	0.0216	58.12	419.58	37.50	0.18740	-6.490
C_5H_{12}	0.0132	72.15	465.14	33.79	0.23940	-5.120
C_6H_{14}	0.0109	86.18	507.40	29.69	0.29600	1.390
PC-1	0.0319	118.56	617.20	28.66	0.16880	0.008
PC-2	0.0236	159.73	688.00	24.82	0.23460	0.010
PC-3	0.0169	223.12	770.49	21.42	0.32130	0.012
PC-4	0.0097	390.34	979.53	16.32	0.55720	0.020

Table 7C.25b : BIPs for PR EOS model from PnA characterization for fluid 25 in Table 7.2

	N_2	CO_2	CH_4	C_2H_6	C_3H_8	C_4H_{10}	C_5H_{12}	C_6H_{14}	PC-1	PC-2	PC-3	PC-4
N_2	0.0000											
CO_2	0.0000	0.0000										
CH_4	0.1000	0.1000	0.0000									
C_2H_6	0.1000	0.1450	0.0420	0.0000								
C_3H_8	0.1000	0.2373	0.0420	0.0400	0.0000							
C_4H_{10}	0.1000	0.2037	0.0420	0.0400	0.0300	0.0000						
C_5H_{12}	0.1000	0.1689	0.0420	0.0400	0.0300	0.0116	0.0000					
C_6H_{14}	0.1000	0.1492	0.0420	0.0400	0.0300	0.0155	0.0058	0.0000				
PC-1	0.1300	0.0294	0.0509	0.0415	0.0324	0.0380	0.0231	0.0000	0.0000			
PC-2	0.1300	0.0637	0.0536	0.0418	0.0339	0.0482	0.0356	0.0000	0.0000	0.0000		
PC-3	0.1300	0.0949	0.0572	0.0423	0.0369	0.0576	0.0492	0.0000	0.0000	0.0000	0.0000	
PC-4	0.1300	0.1285	0.0680	0.0436	0.0506	0.0718	0.0746	0.0000	0.0000	0.0000	0.0000	0.0000

Table 7C.26a : PR EOS model from PnA characterization for fluid 26 in Table 7.2 Saturation pressure (dew point) for this fluid is 276.81 bars at 358.71 K.						
Components	Z	MW (g/mol)	T_C (K)	P_C (bars)	ω	C_{PEN} (CC/Mol)
N_2	0.0013	28.01	126.20	33.94	0.04000	0.0013
CO_2	0.0018	44.01	304.20	73.76	0.22500	0.0018
CH_4	0.6172	16.04	190.60	46.00	0.00800	0.6172
C_2H_6	0.1410	30.07	305.40	48.84	0.09800	0.1410
C_3H_8	0.0837	44.10	369.80	42.46	0.15200	0.0837
C_4H_{10}	0.0443	58.12	421.42	37.66	0.18920	0.0443
C_5H_{12}	0.0243	72.15	466.16	33.78	0.24200	0.0243
C_6H_{14}	0.0179	86.18	507.40	29.69	0.29600	0.0179
PC-1	0.0238	102.96	600.43	32.17	0.19880	0.0238
PC-2	0.0195	125.54	626.86	30.62	0.22830	0.0195
PC-3	0.0153	159.76	700.94	27.11	0.31720	0.0153
PC-4	0.0099	247.85	836.22	22.95	0.49160	0.0099

Table 7C.26b : BIPs for PR EOS model from PnA characterization for fluid 26 in Table 7.2											
	N_2	CO_2	CH_4	C_2H_6	C_3H_8	C_4H_{10}	C_5H_{12}	C_6H_{14}	PC-1	PC-2	PC-3	PC-4
N_2	0.0000											
CO_2	0.0000	0.0000										
CH_4	0.1000	0.1000	0.0000									
C_2H_6	0.1000	0.1450	0.0420	0.0000								
C_3H_8	0.1000	0.1698	0.0420	0.0400	0.0000							
C_4H_{10}	0.1000	0.1512	0.0420	0.0400	0.0300	0.0000						
C_5H_{12}	0.1000	0.1326	0.0420	0.0400	0.0300	0.0116	0.0000					
C_6H_{14}	0.1000	0.1225	0.0420	0.0400	0.0300	0.0155	0.0058	0.0000				
PC-1	0.1300	0.0166	0.0500	0.0414	0.0320	0.0337	0.0186	0.0000	0.0000			
PC-2	0.1300	0.0294	0.0509	0.0415	0.0324	0.0380	0.0231	0.0000	0.0000	0.0000		
PC-3	0.1300	0.0637	0.0536	0.0418	0.0339	0.0482	0.0356	0.0000	0.0000	0.0000	0.0000	
PC-4	0.1300	0.1050	0.0590	0.0425	0.0387	0.0610	0.0548	0.0000	0.0000	0.0000	0.0000	0.0000

Table 7C.27a : PR EOS model from PnA characterization for fluid 27 in Table 7.2 Saturation pressure (dew point) for this fluid is 471.05 bars at 436.70 K.						
Components	Z	MW (g/mol)	T_C (K)	P_C (bars)	ω	C_{PEN} (CC/Mol)
N_2	0.0056	28.01	126.20	33.94	0.04000	-4.230
CO_2	0.0264	44.01	304.20	73.76	0.22500	-1.640
CH_4	0.7416	16.04	190.60	46.00	0.00800	-5.200
C_2H_6	0.0768	30.07	305.40	48.84	0.09800	-5.790
C_3H_8	0.0352	44.10	369.80	42.46	0.15200	-6.350
C_4H_{10}	0.0215	58.12	419.71	37.51	0.18750	-6.490
C_5H_{12}	0.0126	72.15	465.51	33.78	0.24030	-5.120
C_6H_{14}	0.0093	86.18	507.40	29.69	0.29600	1.390
PC-1	0.0268	117.57	618.06	29.24	0.18630	5.720
PC-2	0.0204	154.28	666.52	26.58	0.23460	12.640
PC-3	0.0150	210.81	752.52	22.89	0.33090	24.930
PC-4	0.0088	359.86	952.28	17.81	0.57500	62.110

Table 7C.27b : BIPs for PR EOS model from PnA characterization for fluid 27 in Table 7.2											
	N_2	CO_2	CH_4	C_2H_6	C_3H_8	C_4H_{10}	C_5H_{12}	C_6H_{14}	PC-1	PC-2	PC-3	PC-4
N_2	0.0000											
CO_2	0.0000	0.0000										
CH_4	0.1000	0.1000	0.0000									
C_2H_6	0.1000	0.1450	0.0420	0.0000								
C_3H_8	0.1000	0.2822	0.0420	0.0400	0.0000							
C_4H_{10}	0.1000	0.2397	0.0420	0.0400	0.0300	0.0000						
C_5H_{12}	0.1000	0.1953	0.0420	0.0400	0.0300	0.0116	0.0000					
C_6H_{14}	0.1000	0.1698	0.0420	0.0400	0.0300	0.0155	0.0058	0.0000				
PC-1	0.1300	0.0294	0.0509	0.0415	0.0324	0.0380	0.0231	0.0000	0.0000			
PC-2	0.1300	0.0532	0.0527	0.0417	0.0334	0.0452	0.0317	0.0000	0.0000	0.0000		
PC-3	0.1300	0.0886	0.0563	0.0422	0.0360	0.0556	0.0461	0.0000	0.0000	0.0000	0.0000	
PC-4	0.1300	0.1259	0.0662	0.0434	0.0480	0.0702	0.0715	0.0000	0.0000	0.0000	0.0000	0.0000

Table 7C.28a : PR EOS model from PnA characterization for fluid 28 in Table 7.2 Saturation pressure (dew point) for this fluid is 344.72 bars at 393.20 K.						
Components	Z	MW (g/mol)	T_C (K)	P_C (bars)	ω	C_{PEN} (CC/Mol)
N_2	0.0102	28.01	126.20	33.94	0.04000	-4.230
CO_2	0.0108	44.01	304.20	73.76	0.22500	-1.640
CH_4	0.7394	16.04	190.60	46.00	0.00800	-5.200
C_2H_6	0.1019	30.07	305.40	48.84	0.09800	-5.790
C_3H_8	0.0568	44.10	369.80	42.46	0.15200	-6.350
C_4H_{10}	0.0266	58.12	419.03	37.45	0.18690	-6.490
C_5H_{12}	0.0114	72.15	465.16	33.79	0.23940	-5.120
C_6H_{14}	0.0063	86.18	507.40	29.69	0.29600	1.390
PC-1	0.0124	104.03	600.68	33.61	0.23960	8.770
PC-2	0.0104	124.06	627.11	32.17	0.27500	18.780
PC-3	0.0083	154.89	677.24	29.85	0.34650	34.890
PC-4	0.0055	235.89	815.07	25.61	0.55810	81.630

Table 7C.28b : BIPs for PR EOS model from PnA characterization for fluid 28 in Table 7.2											
	N_2	CO_2	CH_4	C_2H_6	C_3H_8	C_4H_{10}	C_5H_{12}	C_6H_{14}	PC-1	PC-2	PC-3	PC-4
N_2	0.0000											
CO_2	0.0000	0.0000										
CH_4	0.1000	0.1000	0.0000									
C_2H_6	0.1000	0.1450	0.0420	0.0000								
C_3H_8	0.1000	0.2108	0.0420	0.0400	0.0000							
C_4H_{10}	0.1000	0.1828	0.0420	0.0400	0.0300	0.0000						
C_5H_{12}	0.1000	0.1540	0.0420	0.0400	0.0300	0.0116	0.0000					
C_6H_{14}	0.1000	0.1378	0.0420	0.0400	0.0300	0.0155	0.0058	0.0000				
PC-1	0.1300	0.0166	0.0500	0.0414	0.0320	0.0337	0.0186	0.0000	0.0000			
PC-2	0.1300	0.0294	0.0509	0.0415	0.0324	0.0380	0.0231	0.0000	0.0000	0.0000		
PC-3	0.1300	0.0532	0.0527	0.0417	0.0334	0.0452	0.0317	0.0000	0.0000	0.0000	0.0000	
PC-4	0.1300	0.1003	0.0581	0.0424	0.0378	0.0594	0.0521	0.0000	0.0000	0.0000	0.0000	0.0000

Table 7C.29a : PR EOS model from PnA characterization for fluid 29 in Table 7.2 Saturation pressure (dew point) for this fluid is 396.48 bars at 377.60 K.						
Components	Z	MW (g/mol)	T_C (K)	P_C (bars)	ω	C_{PEN} (CC/Mol)
N_2	0.0050	28.01	126.20	33.94	0.04000	-4.230
CO_2	0.0206	44.01	304.20	73.76	0.22500	-1.640
CH_4	0.7617	16.04	190.60	46.00	0.00800	-5.200
C_2H_6	0.0774	30.07	305.40	48.84	0.09800	-5.790
C_3H_8	0.0357	44.10	369.80	42.46	0.15200	-6.350
C_4H_{10}	0.0196	58.12	425.20	38.00	0.19300	-6.490
C_5H_{12}	0.0113	72.15	469.60	33.74	0.25100	-5.120
C_6H_{14}	0.0102	86.18	507.40	29.69	0.29600	1.390
PC-1	0.0212	98.31	571.04	34.28	0.17780	24.040
PC-2	0.0171	122.22	625.18	30.98	0.23920	28.960
PC-3	0.0131	158.87	698.70	27.53	0.33240	36.360
PC-4	0.0082	254.91	831.41	23.46	0.51510	58.230

Table 7C.29b : BIPs for PR EOS model from PnA characterization for fluid 29 in Table 7.2											
	N_2	CO_2	CH_4	C_2H_6	C_3H_8	C_4H_{10}	C_5H_{12}	C_6H_{14}	PC-1	PC-2	PC-3	PC-4
N_2	0.0000											
CO_2	0.0000	0.0000										
CH_4	0.1000	0.1000	0.0000									
C_2H_6	0.1000	0.1450	0.0420	0.0000								
C_3H_8	0.1000	0.1906	0.0420	0.0400	0.0000							
C_4H_{10}	0.1000	0.1671	0.0420	0.0400	0.0300	0.0000						
C_5H_{12}	0.1000	0.1431	0.0420	0.0400	0.0300	0.0116	0.0000					
C_6H_{14}	0.1000	0.1298	0.0420	0.0400	0.0300	0.0155	0.0058	0.0000				
PC-1	0.1300	0.0040	0.0491	0.0413	0.0317	0.0289	0.0141	0.0000	0.0000			
PC-2	0.1300	0.0294	0.0509	0.0415	0.0324	0.0380	0.0231	0.0000	0.0000	0.0000		
PC-3	0.1300	0.0637	0.0536	0.0418	0.0339	0.0482	0.0356	0.0000	0.0000	0.0000	0.0000	
PC-4	0.1300	0.1050	0.0590	0.0425	0.0387	0.0610	0.0548	0.0000	0.0000	0.0000	0.0000	0.0000

Table 7C.30a : PR EOS model from PnA characterization for fluid 30 in Table 7.2 Saturation pressure (dew point) for this fluid is 283.35 bars at 377.60 K.						
Components	Z	MW (g/mol)	T_C (K)	P_C (bars)	ω	C_{PEN} (CC/Mol)
N_2	0.0054	28.01	126.20	33.94	0.04000	-4.230
CO_2	0.0314	44.01	304.20	73.76	0.22500	-1.640
CH_4	0.8354	16.04	190.60	46.00	0.00800	-5.200
C_2H_6	0.0663	30.07	305.40	48.84	0.09800	-5.790
C_3H_8	0.0268	44.10	369.80	42.46	0.15200	-6.350
C_4H_{10}	0.0121	58.12	425.20	38.00	0.19300	-6.490
C_5H_{12}	0.0055	72.15	469.60	33.74	0.25100	-5.120
C_6H_{14}	0.0025	86.18	507.40	29.69	0.29600	1.390
PC-1	0.0046	99.90	575.59	37.58	0.26440	-41.580
PC-2	0.0041	113.02	603.14	36.09	0.30980	-85.450
PC-3	0.0035	133.21	655.25	33.75	0.40180	-159.680
PC-4	0.0025	185.80	752.25	30.73	0.58620	-348.720

Table 7C.30b : BIPs for PR EOS model from PnA characterization for fluid 30 in Table 7.2												
	N_2	CO_2	CH_4	C_2H_6	C_3H_8	C_4H_{10}	C_5H_{12}	C_6H_{14}	PC-1	PC-2	PC-3	PC-4
N_2	0.0000											
CO_2	0.0000	0.0000										
CH_4	0.1000	0.1000	0.0000									
C_2H_6	0.1000	0.1450	0.0420	0.0000								
C_3H_8	0.1000	0.1906	0.0420	0.0400	0.0000							
C_4H_{10}	0.1000	0.1671	0.0420	0.0400	0.0300	0.0000						
C_5H_{12}	0.1000	0.1431	0.0420	0.0400	0.0300	0.0116	0.0000					
C_6H_{14}	0.1000	0.1298	0.0420	0.0400	0.0300	0.0155	0.0058	0.0000				
PC-1	0.1300	0.0040	0.0491	0.0413	0.0317	0.0289	0.0141	0.0000	0.0000			
PC-2	0.1300	0.0166	0.0500	0.0414	0.0320	0.0337	0.0186	0.0000	0.0000	0.0000		
PC-3	0.1300	0.0417	0.0518	0.0416	0.0328	0.0418	0.0275	0.0000	0.0000	0.0000	0.0000	
PC-4	0.1300	0.0814	0.0554	0.0420	0.0353	0.0534	0.0428	0.0000	0.0000	0.0000	0.0000	0.0000

Table 7C.31a : PR EOS model from PnA characterization for fluid 31 in Table 7.2
Saturation pressure (dew point) for this fluid is 471.04 bars at 377.04 K.

Components	Z	MW (g/mol)	T_C (K)	P_C (bars)	ω	C_{PEN} (CC/Mol)
N_2	0.0010	28.01	126.20	33.94	0.04000	-4.230
CO_2	0.0062	44.01	304.20	73.76	0.22500	-1.640
CH_4	0.8099	16.04	190.60	46.00	0.00800	-5.200
C_2H_6	0.0664	30.07	305.40	48.84	0.09800	-5.790
C_3H_8	0.0341	44.10	369.80	42.46	0.15200	-6.350
C_4H_{10}	0.0187	58.12	413.96	37.00	0.18180	-6.490
C_5H_{12}	0.0088	72.15	463.92	33.80	0.23620	-5.120
C_6H_{14}	0.0085	86.00	507.40	29.69	0.29600	1.390
PC-1	0.0164	108.23	596.12	32.33	0.20360	6.360
PC-2	0.0133	133.61	647.60	29.48	0.26400	14.670
PC-3	0.0103	172.69	717.70	26.43	0.35500	28.380
PC-4	0.0064	275.55	863.59	22.31	0.56030	65.350

Table 7C.31b : BIPs for PR EOS model from PnA characterization for fluid 31 in Table 7.2

	N_2	CO_2	CH_4	C_2H_6	C_3H_8	C_4H_{10}	C_5H_{12}	C_6H_{14}	PC-1	PC-2	PC-3	PC-4
N_2	0.0000											
CO_2	0.0000	0.0000										
CH_4	0.1000	0.1000	0.0000									
C_2H_6	0.1000	0.1450	0.0420	0.0000								
C_3H_8	0.1000	0.1899	0.0420	0.0400	0.0000							
C_4H_{10}	0.1000	0.1665	0.0420	0.0400	0.0300	0.0000						
C_5H_{12}	0.1000	0.1427	0.0420	0.0400	0.0300	0.0116	0.0000					
C_6H_{14}	0.1000	0.1295	0.0420	0.0400	0.0300	0.0155	0.0058	0.0000				
PC-1	0.1300	0.0166	0.0500	0.0414	0.0320	0.0337	0.0186	0.0000	0.0000			
PC-2	0.1300	0.0417	0.0518	0.0416	0.0328	0.0418	0.0275	0.0000	0.0000	0.0000		
PC-3	0.1300	0.0731	0.0545	0.0419	0.0346	0.0510	0.0393	0.0000	0.0000	0.0000	0.0000	
PC-4	0.1300	0.1126	0.0608	0.0427	0.0408	0.0639	0.0598	0.0000	0.0000	0.0000	0.0000	0.0000

Table 7C.32a : PR EOS model from PnA characterization for fluid 32 in Table 7.2
Saturation pressure (dew point) for this fluid is 399.40 bars at 392.10 K.

Components	Z	MW (g/mol)	T_C (K)	P_C (bars)	ω	C_{PEN} (CC/Mol)
N_2	0.0071	28.01	126.20	33.94	0.04000	
CO_2	0.0864	44.01	304.20	73.76	0.22500	
CH_4	0.7085	16.04	190.60	46.00	0.00800	
C_2H_6	0.0853	30.07	305.40	48.84	0.09800	
C_3H_8	0.0495	44.10	369.80	42.46	0.15200	
C_4H_{10}	0.0201	58.12	418.82	37.43	0.18670	
C_5H_{12}	0.0081	72.15	464.94	33.79	0.23890	
C_6H_{14}	0.0046	86.18	507.40	29.69	0.29600	
PC-1	0.0101	116.66	625.38	32.42	0.28270	
PC-2	0.0086	137.27	650.72	31.20	0.31940	
PC-3	0.0070	168.84	698.97	29.21	0.39290	
PC-4	0.0047	251.47	831.98	25.50	0.60890	

Table 7C.32b : BIPs for PR EOS model from PnA characterization for fluid 32 in Table 7.2

	N_2	CO_2	CH_4	C_2H_6	C_3H_8	C_4H_{10}	C_5H_{12}	C_6H_{14}	PC-1	PC-2	PC-3	PC-4
N_2	0.0000											
CO_2	0.0000	0.0000										
CH_4	0.1000	0.1000	0.0000									
C_2H_6	0.1000	0.1450	0.0420	0.0000								
C_3H_8	0.1000	0.2093	0.0420	0.0400	0.0000							
C_4H_{10}	0.1000	0.1816	0.0420	0.0400	0.0300	0.0000						
C_5H_{12}	0.1000	0.1532	0.0420	0.0400	0.0300	0.0116	0.0000					
C_6H_{14}	0.1000	0.1372	0.0420	0.0400	0.0300	0.0155	0.0058	0.0000				
PC-1	0.1300	0.0294	0.0509	0.0415	0.0324	0.0380	0.0231	0.0000	0.0000			
PC-2	0.1300	0.0417	0.0518	0.0416	0.0328	0.0418	0.0275	0.0000	0.0000	0.0000		
PC-3	0.1300	0.0637	0.0536	0.0418	0.0339	0.0482	0.0356	0.0000	0.0000	0.0000	0.0000	
PC-4	0.1300	0.1050	0.0590	0.0425	0.0387	0.0610	0.0548	0.0000	0.0000	0.0000	0.0000	0.0000

Components	Z	MW (g/mol)	T_C (K)	P_C (bars)	ω	C_{PEN} (CC/Mol)
N_2	0.0020	28.01	126.20	33.94	0.04000	
CO_2	0.0201	44.01	304.20	73.76	0.22500	
CH_4	0.6750	16.04	190.60	46.00	0.00800	
C_2H_6	0.0931	30.07	305.40	48.84	0.09800	
C_3H_8	0.0541	44.10	369.80	42.46	0.15200	
C_4H_{10}	0.0353	58.12	418.81	37.43	0.18660	
C_5H_{12}	0.0148	72.15	464.63	33.79	0.23800	
C_6H_{14}	0.0151	86.18	507.40	29.69	0.29600	
PC-1	0.0340	107.66	593.51	29.77	0.13090	
PC-2	0.0260	140.93	644.75	26.56	0.16980	
PC-3	0.0191	191.65	735.11	22.16	0.24770	
PC-4	0.0113	323.76	909.36	16.92	0.41340	

Table 7C.33a : PR EOS model from PnA characterization for fluid 33 in Table 7.2
Saturation pressure (dew point) for this fluid is 307.00 bars at 381.00 K.

Table 7C.33b : BIPs for PR EOS model from PnA characterization for fluid 33 in Table 7.2

	N_2	CO_2	CH_4	C_2H_6	C_3H_8	C_4H_{10}	C_5H_{12}	C_6H_{14}	PC-1	PC-2	PC-3	PC-4
N_2	0.0000											
CO_2	0.0000	0.0000										
CH_4	0.1000	0.1000	0.0000									
C_2H_6	0.1000	0.1450	0.0420	0.0000								
C_3H_8	0.1000	0.1948	0.0420	0.0400	0.0000							
C_4H_{10}	0.1000	0.1703	0.0420	0.0400	0.0300	0.0000						
C_5H_{12}	0.1000	0.1453	0.0420	0.0400	0.0300	0.0116	0.0000					
C_6H_{14}	0.1000	0.1314	0.0420	0.0400	0.0300	0.0155	0.0058	0.0000				
PC-1	0.1300	0.0166	0.0500	0.0414	0.0320	0.0337	0.0186	0.0000	0.0000			
PC-2	0.1300	0.0417	0.0518	0.0416	0.0328	0.0418	0.0275	0.0000	0.0000	0.0000		
PC-3	0.1300	0.0814	0.0554	0.0420	0.0353	0.0534	0.0428	0.0000	0.0000	0.0000	0.0000	
PC-4	0.1300	0.1206	0.0635	0.0430	0.0443	0.0674	0.0662	0.0000	0.0000	0.0000	0.0000	0.0000

Table 7C.34a : PR EOS model from PnA characterization for fluid 34 in Table 7.2 Saturation pressure (dew point) for this fluid is 359.00 bars at 381.00 K.						
Components	Z	MW (g/mol)	T_C (K)	P_C (bars)	ω	C_{PEN} (CC/Mol)
N_2	0.0023	28.01	126.20	33.94	0.04000	
CO_2	0.0212	44.01	304.20	73.76	0.22500	
CH_4	0.7315	16.04	190.60	46.00	0.00800	
C_2H_6	0.0939	30.07	305.40	48.84	0.09800	
C_3H_8	0.0486	44.10	369.80	42.46	0.15200	
C_4H_{10}	0.0180	58.12	418.97	37.45	0.18680	
C_5H_{12}	0.0109	72.15	464.54	33.80	0.23780	
C_6H_{14}	0.0093	86.18	507.40	29.69	0.29600	
PC-1	0.0235	111.00	594.60	30.36	0.14780	
PC-2	0.0185	141.05	645.94	27.24	0.19170	
PC-3	0.0139	187.12	737.04	22.97	0.27960	
PC-4	0.0085	307.85	895.95	18.30	0.44700	

Table 7C.34b : BIPs for PR EOS model from PnA characterization for fluid 34 in Table 7.2											
	N_2	CO_2	CH_4	C_2H_6	C_3H_8	C_4H_{10}	C_5H_{12}	C_6H_{14}	PC-1	PC-2	PC-3	PC-4
N_2	0.0000											
CO_2	0.0000	0.0000										
CH_4	0.1000	0.1000	0.0000									
C_2H_6	0.1000	0.1450	0.0420	0.0000								
C_3H_8	0.1000	0.1948	0.0420	0.0400	0.0000							
C_4H_{10}	0.1000	0.1703	0.0420	0.0400	0.0300	0.0000						
C_5H_{12}	0.1000	0.1453	0.0420	0.0400	0.0300	0.0116	0.0000					
C_6H_{14}	0.1000	0.1314	0.0420	0.0400	0.0300	0.0155	0.0058	0.0000				
PC-1	0.1300	0.0166	0.0500	0.0414	0.0320	0.0337	0.0186	0.0000	0.0000			
PC-2	0.1300	0.0417	0.0518	0.0416	0.0328	0.0418	0.0275	0.0000	0.0000	0.0000		
PC-3	0.1300	0.0814	0.0554	0.0420	0.0353	0.0534	0.0428	0.0000	0.0000	0.0000	0.0000	
PC-4	0.1300	0.1183	0.0626	0.0429	0.0431	0.0663	0.0642	0.0000	0.0000	0.0000	0.0000	0.0000

Table 7C.35a : PR EOS model from PnA characterization for fluid 35 in Table 7.2 Saturation pressure (dew point) for this fluid is 207.00 bars at 333.00 K.						
Components	Z	MW (g/mol)	T_C (K)	P_C (bars)	ω	C_{PEN} (CC/Mol)
N_2	0.0220	28.01	126.20	33.94	0.04000	
CO_2	0.0006	44.01	304.20	73.76	0.22500	
CH_4	0.7417	16.04	190.60	46.00	0.00800	
C_2H_6	0.1127	30.07	305.40	48.84	0.09800	
C_3H_8	0.0575	44.10	369.80	42.46	0.15200	
C_4H_{10}	0.0298	58.12	417.51	37.32	0.18540	
C_5H_{12}	0.0099	72.15	465.88	33.78	0.24130	
C_6H_{14}	0.0058	86.18	507.40	29.69	0.29600	
PC-1	0.0063	91.57	579.74	34.72	0.18940	
PC-2	0.0056	103.92	607.12	32.98	0.22190	
PC-3	0.0047	122.90	633.66	31.50	0.25480	
PC-4	0.0034	172.32	734.80	27.28	0.38710	

Table 7C.35b : BIPs for PR EOS model from PnA characterization for fluid 35 in Table 7.2											
	N_2	CO_2	CH_4	C_2H_6	C_3H_8	C_4H_{10}	C_5H_{12}	C_6H_{14}	PC-1	PC-2	PC-3	PC-4
N_2	0.0000										
CO_2	0.0000	0.0000									
CH_4	0.1000	0.1000	0.0000								
C_2H_6	0.1000	0.1450	0.0420	0.0000							
C_3H_8	0.1000	0.1481	0.0420	0.0400	0.0000						
C_4H_{10}	0.1000	0.1355	0.0420	0.0400	0.0300	0.0000					
C_5H_{12}	0.1000	0.1232	0.0420	0.0400	0.0300	0.0116	0.0000				
C_6H_{14}	0.1000	0.1167	0.0420	0.0400	0.0300	0.0155	0.0058	0.0000			
PC-1	0.1300	0.0040	0.0491	0.0413	0.0317	0.0289	0.0141	0.0000	0.0000		
PC-2	0.1300	0.0166	0.0500	0.0414	0.0320	0.0337	0.0186	0.0000	0.0000	0.0000	
PC-3	0.1300	0.0294	0.0509	0.0415	0.0324	0.0380	0.0231	0.0000	0.0000	0.0000	0.0000
PC-4	0.1300	0.0731	0.0545	0.0419	0.0346	0.0510	0.0393	0.0000	0.0000	0.0000	0.0000	0.0000

Table 7C.36a : PR EOS model from PnA characterization for fluid 36 in Table 7.2 Saturation pressure (dew point) for this fluid is 314.97 bars at 366.48 K.						
Components	Z	MW (g/mol)	T_C (K)	P_C (bars)	ω	C_{PEN} (CC/Mol)
N_2	0.0042	28.01	126.20	33.94	0.04000	
CO_2	0.0050	44.01	304.20	73.76	0.22500	
CH_4	0.6146	16.04	190.60	46.00	0.00800	
C_2H_6	0.1485	30.07	305.40	48.84	0.09800	
C_3H_8	0.0529	44.10	369.80	42.46	0.15200	
C_4H_{10}	0.0367	58.12	423.20	37.82	0.19100	
C_5H_{12}	0.0210	72.15	465.92	33.78	0.24140	
C_6H_{14}	0.0168	86.18	507.40	29.69	0.64960	
PC-1	0.0384	112.27	592.66	30.06	0.13920	
PC-2	0.0288	149.60	667.57	25.60	0.20120	
PC-3	0.0209	206.48	754.29	21.74	0.28380	
PC-4	0.0122	354.52	957.55	16.39	0.49310	

Table 7C.36b : BIPs for PR EOS model from PnA characterization for fluid 36 in Table 7.2												
	N_2	CO_2	CH_4	C_2H_6	C_3H_8	C_4H_{10}	C_5H_{12}	C_6H_{14}	PC-1	PC-2	PC-3	PC-4
N_2	0.0000											
CO_2	0.0000	0.0000										
CH_4	0.1000	0.1000	0.0000									
C_2H_6	0.1000	0.1450	0.0420	0.0000								
C_3H_8	0.1000	0.1778	0.0420	0.0400	0.0000							
C_4H_{10}	0.1000	0.1573	0.0420	0.0400	0.0300	0.0000						
C_5H_{12}	0.1000	0.1365	0.0420	0.0400	0.0300	0.0116	0.0000					
C_6H_{14}	0.1000	0.1252	0.0420	0.0400	0.0300	0.0155	0.0058	0.0000				
PC-1	0.1300	0.0166	0.0500	0.0414	0.0320	0.0337	0.0186	0.0000	0.0000			
PC-2	0.1300	0.0532	0.0527	0.0417	0.0334	0.0452	0.0317	0.0000	0.0000	0.0000		
PC-3	0.1300	0.0886	0.0563	0.0422	0.0360	0.0556	0.0461	0.0000	0.0000	0.0000	0.0000	
PC-4	0.1300	0.1259	0.0662	0.0434	0.0480	0.0702	0.0715	0.0000	0.0000	0.0000	0.0000	0.0000

Table 7C.37a : PR EOS model from PnA characterization for fluid 37 in Table 7.2 Saturation pressure (dew point) for this fluid is 857.75 bars at 399.82 K.						
Components	Z	MW (g/mol)	T_C (K)	P_C (bars)	ω	C_{PEN} (CC/Mol)
N_2	0.0019	28.01	126.20	33.94	0.04000	
CO_2	0.0102	44.01	304.20	73.76	0.22500	
CH_4	0.8673	16.04	190.60	46.00	0.00800	
C_2H_6	0.0248	30.07	305.40	48.84	0.09800	
C_3H_8	0.0127	44.10	369.80	42.46	0.15200	
C_4H_{10}	0.0108	58.12	413.96	37.00	0.18180	
C_5H_{12}	0.0034	72.15	463.92	33.80	0.23620	
C_6H_{14}	0.0019	86.18	507.40	29.69	0.29600	
PC-1	0.0276	179.23	697.92	22.39	0.20240	
PC-2	0.0192	257.57	802.18	17.93	0.30320	
PC-3	0.0131	377.36	914.50	14.65	0.42560	
PC-4	0.0072	690.90	1164.42	10.95	0.67670	

Table 7C.37b : BIPs for PR EOS model from PnA characterization for fluid 37 in Table 7.2											
	N_2	CO_2	CH_4	C_2H_6	C_3H_8	C_4H_{10}	C_5H_{12}	C_6H_{14}	PC-1	PC-2	PC-3	PC-4
N_2	0.0000											
CO_2	0.0000	0.0000										
CH_4	0.1000	0.1000	0.0000									
C_2H_6	0.1000	0.1450	0.0420	0.0000								
C_3H_8	0.1000	0.2203	0.0420	0.0400	0.0000							
C_4H_{10}	0.1000	0.1902	0.0420	0.0400	0.0300	0.0000						
C_5H_{12}	0.1000	0.1592	0.0420	0.0400	0.0300	0.0116	0.0000					
C_6H_{14}	0.1000	0.1418	0.0420	0.0400	0.0300	0.0155	0.0058	0.0000				
PC-1	0.1300	0.0731	0.0545	0.0419	0.0346	0.0510	0.0393	0.0000	0.0000			
PC-2	0.1300	0.1091	0.0599	0.0426	0.0398	0.0625	0.0574	0.0000	0.0000	0.0000		
PC-3	0.1300	0.1273	0.0671	0.0435	0.0493	0.0710	0.0731	0.0000	0.0000	0.0000	0.0000	
PC-4	0.1300	0.1384	0.0878	0.0460	0.0710	0.0810	0.0953	0.0000	0.0000	0.0000	0.0000	0.0000

Table 7C.38a : PR EOS model from PnA characterization for fluid 38 in Table 7.2
Saturation pressure (dew point) for this fluid is 241.72 bars at 377.04 K.

Components	Z	MW (g/mol)	T_C (K)	P_C (bars)	ω	C_{PEN} (CC/Mol)
N_2	0.0168	28.01	126.20	33.94	0.04000	
CO_2	0.0023	44.01	304.20	73.76	0.22500	
CH_4	0.5609	16.04	190.60	46.00	0.00800	
C_2H_6	0.1348	30.07	305.40	48.84	0.09800	
C_3H_8	0.0845	44.10	369.80	42.46	0.15200	
C_4H_{10}	0.0514	58.12	417.65	37.33	0.18550	
C_5H_{12}	0.0228	72.15	464.48	33.80	0.23760	
C_6H_{14}	0.0145	86.18	507.40	29.69	0.29600	
PC-1	0.0410	102.37	554.69	30.51	0.15180	
PC-2	0.0320	131.13	606.40	27.40	0.19690	
PC-3	0.0241	174.15	677.72	24.04	0.26480	
PC-4	0.0148	283.26	849.59	18.95	0.43880	

Table 7C.38b : BIPs for PR EOS model from PnA characterization for fluid 38 in Table 7.2

	N_2	CO_2	CH_4	C_2H_6	C_3H_8	C_4H_{10}	C_5H_{12}	C_6H_{14}	PC-1	PC-2	PC-3	PC-4
N_2	0.0000											
CO_2	0.0000	0.0000										
CH_4	0.1000	0.1000	0.0000									
C_2H_6	0.1000	0.1450	0.0420	0.0000								
C_3H_8	0.1000	0.1899	0.0420	0.0400	0.0000							
C_4H_{10}	0.1000	0.1665	0.0420	0.0400	0.0300	0.0000						
C_5H_{12}	0.1000	0.1427	0.0420	0.0400	0.0300	0.0116	0.0000					
C_6H_{14}	0.1000	0.1295	0.0420	0.0400	0.0300	0.0155	0.0058	0.0000				
PC-1	0.1300	0.0166	0.0500	0.0414	0.0320	0.0337	0.0186	0.0000	0.0000			
PC-2	0.1300	0.0417	0.0518	0.0416	0.0328	0.0418	0.0275	0.0000	0.0000	0.0000		
PC-3	0.1300	0.0731	0.0545	0.0419	0.0346	0.0510	0.0393	0.0000	0.0000	0.0000	0.0000	
PC-4	0.1300	0.1156	0.0617	0.0428	0.0419	0.0652	0.0620	0.0000	0.0000	0.0000	0.0000	0.0000

Table 7C.39a : PR EOS model from PnA characterization for fluid 39 in Table 7.2
Saturation pressure (dew point) for this fluid is 354.65 bars at 422.59 K.

Components	Z	MW (g/mol)	T_C (K)	P_C (bars)	ω	C_{PEN} (CC/Mol)
N_2	0.0349	28.01	126.20	33.94	0.04000	-4.230
CO_2	0.0270	44.01	304.20	73.76	0.22500	-1.640
CH_4	0.6507	16.04	190.60	46.00	0.00800	-5.200
C_2H_6	0.1050	30.07	305.40	48.84	0.09800	-5.790
C_3H_8	0.0497	44.10	369.80	42.46	0.15200	-6.350
C_4H_{10}	0.0282	58.12	419.44	37.49	0.18730	-6.490
C_5H_{12}	0.0155	72.15	465.03	33.79	0.23910	-5.120
C_6H_{14}	0.0125	86.18	507.40	29.69	0.29600	1.390
PC-1	0.0284	111.29	593.80	30.33	0.14690	0.780
PC-2	0.0220	143.49	668.94	25.93	0.21250	2.050
PC-3	0.0164	192.87	735.62	22.93	0.27800	3.960
PC-4	0.0098	322.24	910.74	17.87	0.46410	9.910

Table 7C.39b : BIPs for PR EOS model from PnA characterization for fluid 39 in Table 7.2

	N_2	CO_2	CH_4	C_2H_6	C_3H_8	C_4H_{10}	C_5H_{12}	C_6H_{14}	PC-1	PC-2	PC-3	PC-4
N_2	0.0000											
CO_2	0.0000	0.0000										
CH_4	0.1000	0.1000	0.0000									
C_2H_6	0.1000	0.1450	0.0420	0.0000								
C_3H_8	0.1000	0.2566	0.0420	0.0400	0.0000							
C_4H_{10}	0.1000	0.2192	0.0420	0.0400	0.0300	0.0000						
C_5H_{12}	0.1000	0.1801	0.0420	0.0400	0.0300	0.0116	0.0000					
C_6H_{14}	0.1000	0.1579	0.0420	0.0400	0.0300	0.0155	0.0058	0.0000				
PC-1	0.1300	0.0166	0.0500	0.0414	0.0320	0.0337	0.0186	0.0000	0.0000			
PC-2	0.1300	0.0532	0.0527	0.0417	0.0334	0.0452	0.0317	0.0000	0.0000	0.0000		
PC-3	0.1300	0.0814	0.0554	0.0420	0.0353	0.0534	0.0428	0.0000	0.0000	0.0000	0.0000	
PC-4	0.1300	0.1206	0.0635	0.0430	0.0443	0.0674	0.0662	0.0000	0.0000	0.0000	0.0000	0.0000

Table 7C.40a : PR EOS model from PnA characterization for fluid 40 in Table 7.2 Saturation pressure (dew point) for this fluid is 382.31 bars at 420.93 K.						
Components	Z	MW (g/mol)	T_C (K)	P_C (bars)	ω	C_{PEN} (CC/Mol)
N_2	0.0307	28.01	126.20	33.94	0.04000	-4.230
CO_2	0.0292	44.01	304.20	73.76	0.22500	-1.640
CH_4	0.6877	16.04	190.60	46.00	0.00800	-5.200
C_2H_6	0.0977	30.07	305.40	48.84	0.09800	-5.790
C_3H_8	0.0409	44.10	369.80	42.46	0.15200	-6.350
C_4H_{10}	0.0223	58.12	419.76	37.52	0.18760	-6.490
C_5H_{12}	0.0119	72.15	465.19	33.79	0.23950	-5.120
C_6H_{14}	0.0090	86.18	507.40	29.69	0.29600	1.390
PC-1	0.0261	112.99	593.77	30.45	0.15010	0.000
PC-2	0.0203	145.27	668.90	26.07	0.21710	0.000
PC-3	0.0151	194.74	735.57	23.08	0.28410	0.000
PC-4	0.0091	324.37	910.60	18.06	0.47410	0.000

Table 7C.40b : BIPs for PR EOS model from PnA characterization for fluid 40 in Table 7.2											
	N_2	CO_2	CH_4	C_2H_6	C_3H_8	C_4H_{10}	C_5H_{12}	C_6H_{14}	PC-1	PC-2	PC-3	PC-4
N_2	0.0000											
CO_2	0.0000	0.0000										
CH_4	0.1000	0.1000	0.0000									
C_2H_6	0.1000	0.1450	0.0420	0.0000								
C_3H_8	0.1000	0.2538	0.0420	0.0400	0.0000							
C_4H_{10}	0.1000	0.2169	0.0420	0.0400	0.0300	0.0000						
C_5H_{12}	0.1000	0.1785	0.0420	0.0400	0.0300	0.0116	0.0000					
C_6H_{14}	0.1000	0.1566	0.0420	0.0400	0.0300	0.0155	0.0058	0.0000				
PC-1	0.1300	0.0166	0.0500	0.0414	0.0320	0.0337	0.0186	0.0000	0.0000			
PC-2	0.1300	0.0532	0.0527	0.0417	0.0334	0.0452	0.0317	0.0000	0.0000	0.0000		
PC-3	0.1300	0.0814	0.0554	0.0420	0.0353	0.0534	0.0428	0.0000	0.0000	0.0000	0.0000	
PC-4	0.1300	0.1206	0.0635	0.0430	0.0443	0.0674	0.0662	0.0000	0.0000	0.0000	0.0000	0.0000

Table 7C.41a : PR EOS model from PnA characterization for fluid 41 in Table 7.2 Saturation pressure (dew point) for this fluid is 311.71 bars at 424.82 K.						
Components	Z	MW (g/mol)	T_C (K)	P_C (bars)	ω	C_{PEN} (CC/Mol)
N_2	0.0345	28.01	126.20	33.94	0.04000	-4.230
CO_2	0.0273	44.01	304.20	73.76	0.22500	-1.640
CH_4	0.5771	16.04	190.60	46.00	0.00800	-5.200
C_2H_6	0.1072	30.07	305.40	48.84	0.09800	-5.790
C_3H_8	0.0599	44.10	369.80	42.46	0.15200	-6.350
C_4H_{10}	0.0345	58.12	419.95	37.53	0.18780	-6.490
C_5H_{12}	0.0184	72.15	465.25	33.79	0.23970	-5.120
C_6H_{14}	0.0172	86.18	507.40	29.69	0.29600	1.390
PC-1	0.0471	107.91	592.54	29.78	0.13140	0.710
PC-2	0.0355	143.33	667.42	25.27	0.19000	2.140
PC-3	0.0259	196.25	733.38	22.18	0.24850	4.250
PC-4	0.0154	330.70	922.26	16.57	0.43200	11.230

Table 7C.41b : BIPs for PR EOS model from PnA characterization for fluid 41 in Table 7.2											
	N_2	CO_2	CH_4	C_2H_6	C_3H_8	C_4H_{10}	C_5H_{12}	C_6H_{14}	PC-1	PC-2	PC-3	PC-4
N_2	0.0000											
CO_2	0.0000	0.0000										
CH_4	0.1000	0.1000	0.0000									
C_2H_6	0.1000	0.1450	0.0420	0.0000								
C_3H_8	0.1000	0.2605	0.0420	0.0400	0.0000							
C_4H_{10}	0.1000	0.2223	0.0420	0.0400	0.0300	0.0000						
C_5H_{12}	0.1000	0.1824	0.0420	0.0400	0.0300	0.0116	0.0000					
C_6H_{14}	0.1000	0.1597	0.0420	0.0400	0.0300	0.0155	0.0058	0.0000				
PC-1	0.1300	0.0166	0.0500	0.0414	0.0320	0.0337	0.0186	0.0000	0.0000			
PC-2	0.1300	0.0532	0.0527	0.0417	0.0334	0.0452	0.0317	0.0000	0.0000	0.0000		
PC-3	0.1300	0.0814	0.0554	0.0420	0.0353	0.0534	0.0428	0.0000	0.0000	0.0000	0.0000	
PC-4	0.1300	0.1226	0.0644	0.0431	0.0455	0.0684	0.0680	0.0000	0.0000	0.0000	0.0000	0.0000

Table 7C.42a : PR EOS model from PnA characterization for fluid 42 in Table 7.2 Saturation pressure (dew point) for this fluid is 355.29 bars at 424.82 K.						
Components	Z	MW (g/mol)	T_C (K)	P_C (bars)	ω	C_{PEN} (CC/Mol)
N_2	0.0349	28.01	126.20	33.94	0.04000	-4.230
CO_2	0.0270	44.01	304.20	73.76	0.22500	-1.640
CH_4	0.6507	16.04	190.60	46.00	0.00800	-5.200
C_2H_6	0.1050	30.07	305.40	48.84	0.09800	-5.790
C_3H_8	0.0497	44.10	369.80	42.46	0.15200	-6.350
C_4H_{10}	0.0282	58.12	419.44	37.49	0.18730	-6.490
C_5H_{12}	0.0153	72.15	465.03	33.79	0.23910	-5.120
C_6H_{14}	0.0125	86.18	507.40	29.69	0.29600	1.390
PC-1	0.0285	111.82	593.80	30.36	0.14760	0.000
PC-2	0.0220	144.36	668.94	25.96	0.21350	0.000
PC-3	0.0164	194.23	735.62	22.96	0.27930	0.000
PC-4	0.0098	324.87	910.73	17.91	0.46620	0.000

Table 7C.42b : BIPs for PR EOS model from PnA characterization for fluid 42 in Table 7.2												
	N_2	CO_2	CH_4	C_2H_6	C_3H_8	C_4H_{10}	C_5H_{12}	C_6H_{14}	PC-1	PC-2	PC-3	PC-4
N_2	0.0000											
CO_2	0.0000	0.0000										
CH_4	0.1000	0.1000	0.0000									
C_2H_6	0.1000	0.1450	0.0420	0.0000								
C_3H_8	0.1000	0.2605	0.0420	0.0400	0.0000							
C_4H_{10}	0.1000	0.2223	0.0420	0.0400	0.0300	0.0000						
C_5H_{12}	0.1000	0.1824	0.0420	0.0400	0.0300	0.0116	0.0000					
C_6H_{14}	0.1000	0.1597	0.0420	0.0400	0.0300	0.0155	0.0058	0.0000				
PC-1	0.1300	0.0166	0.0500	0.0414	0.0320	0.0337	0.0186	0.0000	0.0000			
PC-2	0.1300	0.0532	0.0527	0.0417	0.0334	0.0452	0.0317	0.0000	0.0000	0.0000		
PC-3	0.1300	0.0814	0.0554	0.0420	0.0353	0.0534	0.0428	0.0000	0.0000	0.0000	0.0000	
PC-4	0.1300	0.1206	0.0635	0.0430	0.0443	0.0674	0.0662	0.0000	0.0000	0.0000	0.0000	0.0000

Table 7C.43a : PR EOS model from PnA characterization for fluid 43 in Table 7.2 Saturation pressure (dew point) for this fluid is 381.76 bars at 412.59 K.						
Components	Z	MW (g/mol)	T_C (K)	P_C (bars)	ω	C_{PEN} (CC/Mol)
N_2	0.0345	28.01	126.20	33.94	0.04000	-4.230
CO_2	0.0279	44.01	304.20	73.76	0.22500	-1.640
CH_4	0.7798	16.04	190.60	46.00	0.00800	-5.200
C_2H_6	0.0884	30.07	305.40	48.84	0.09800	-5.790
C_3H_8	0.0288	44.10	369.80	42.46	0.15200	-6.350
C_4H_{10}	0.0131	58.12	417.89	37.35	0.18570	-6.490
C_5H_{12}	0.0052	72.15	464.12	33.80	0.23670	-5.120
C_6H_{14}	0.0032	86.18	507.40	29.69	0.29600	1.390
PC-1	0.0062	120.53	625.23	33.56	0.31720	-24.600
PC-2	0.0054	138.88	650.56	32.40	0.35840	-37.610
PC-3	0.0045	167.03	698.76	30.54	0.44080	-58.860
PC-4	0.0031	240.57	810.26	27.54	0.64360	-114.380

Table 7C.43b : BIPs for PR EOS model from PnA characterization for fluid 43 in Table 7.2												
	N_2	CO_2	CH_4	C_2H_6	C_3H_8	C_4H_{10}	C_5H_{12}	C_6H_{14}	PC-1	PC-2	PC-3	PC-4
N_2	0.0000											
CO_2	0.0000	0.0000										
CH_4	0.1000	0.1000	0.0000									
C_2H_6	0.1000	0.1450	0.0420	0.0000								
C_3H_8	0.1000	0.2400	0.0420	0.0400	0.0000							
C_4H_{10}	0.1000	0.2058	0.0420	0.0400	0.0300	0.0000						
C_5H_{12}	0.1000	0.1704	0.0420	0.0400	0.0300	0.0116	0.0000					
C_6H_{14}	0.1000	0.1504	0.0420	0.0400	0.0300	0.0155	0.0058	0.0000				
PC-1	0.1300	0.0294	0.0509	0.0415	0.0324	0.0380	0.0231	0.0000	0.0000			
PC-2	0.1300	0.0417	0.0518	0.0416	0.0328	0.0418	0.0275	0.0000	0.0000	0.0000		
PC-3	0.1300	0.0637	0.0536	0.0418	0.0339	0.0482	0.0356	0.0000	0.0000	0.0000	0.0000	
PC-4	0.1300	0.1003	0.0581	0.0424	0.0378	0.0594	0.0521	0.0000	0.0000	0.0000	0.0000	0.0000

Table 7C.44a : PR EOS model from PnA characterization for fluid 44 in Table 7.2 Saturation pressure (dew point) for this fluid is 385.44 bars at 404.82 K.						
Components	Z	MW (g/mol)	T_C (K)	P_C (bars)	ω	C_{PEN} (CC/Mol)
N_2	0.0042	28.01	126.20	33.94	0.04000	
CO_2	0.0157	44.01	304.20	73.76	0.22500	
CH_4	0.7498	16.04	190.60	46.00	0.00800	
C_2H_6	0.0634	30.07	305.40	48.84	0.09800	
C_3H_8	0.0319	44.10	369.80	42.46	0.15200	
C_4H_{10}	0.0295	58.12	415.99	37.18	0.18380	
C_5H_{12}	0.0171	72.15	463.87	33.80	0.23600	
C_6H_{14}	0.0135	86.18	507.40	29.69	0.29600	
PC-1	0.0280	111.64	593.22	30.22	0.14360	
PC-2	0.0215	145.09	668.24	25.79	0.20770	
PC-3	0.0159	196.36	734.59	22.77	0.27180	
PC-4	0.0095	330.69	925.81	17.31	0.47240	

Table 7C.44b : BIPs for PR EOS model from PnA characterization for fluid 44 in Table 7.2												
	N_2	CO_2	CH_4	C_2H_6	C_3H_8	C_4H_{10}	C_5H_{12}	C_6H_{14}	PC-1	PC-2	PC-3	PC-4
N_2	0.0000											
CO_2	0.0000	0.0000										
CH_4	0.1000	0.1000	0.0000									
C_2H_6	0.1000	0.1450	0.0420	0.0000								
C_3H_8	0.1000	0.2278	0.0420	0.0400	0.0000							
C_4H_{10}	0.1000	0.1961	0.0420	0.0400	0.0300	0.0000						
C_5H_{12}	0.1000	0.1634	0.0420	0.0400	0.0300	0.0116	0.0000					
C_6H_{14}	0.1000	0.1450	0.0420	0.0400	0.0300	0.0155	0.0058	0.0000				
PC-1	0.1300	0.0166	0.0500	0.0414	0.0320	0.0337	0.0186	0.0000	0.0000			
PC-2	0.1300	0.0532	0.0527	0.0417	0.0334	0.0452	0.0317	0.0000	0.0000	0.0000		
PC-3	0.1300	0.0814	0.0554	0.0420	0.0353	0.0534	0.0428	0.0000	0.0000	0.0000	0.0000	
PC-4	0.1300	0.1226	0.0644	0.0431	0.0455	0.0684	0.0680	0.0000	0.0000	0.0000	0.0000	0.0000

Table 7C.45a : PR EOS model from PnA characterization for fluid 45 in Table 7.2
Saturation pressure (dew point) for this fluid is 362.68 bars at 374.82 K.

Components	Z	MW (g/mol)	T_C (K)	P_C (bars)	ω	C_{PEN} (CC/Mol)
N_2	0.0223	28.01	126.20	33.94	0.04000	-4.230
CO_2	0.0045	44.01	304.20	73.76	0.22500	-1.640
CH_4	0.6568	16.04	190.60	46.00	0.00800	-5.200
C_2H_6	0.1170	30.07	305.40	48.84	0.09800	-5.790
C_3H_8	0.0587	44.10	369.80	42.46	0.15200	-6.350
C_4H_{10}	0.0295	58.12	425.20	38.00	0.19300	-6.490
C_5H_{12}	0.0142	72.15	469.60	33.74	0.25100	-5.120
C_6H_{14}	0.0098	86.18	507.40	29.69	0.29600	1.390
PC-1	0.0331	110.54	592.92	30.15	0.14180	-5.150
PC-2	0.0251	145.98	667.87	25.72	0.20510	-14.400
PC-3	0.0183	200.28	754.80	21.87	0.28910	-30.000
PC-4	0.0107	342.54	941.75	16.86	0.48460	-76.180

Table 7C.45b : BIPs for PR EOS model from PnA characterization for fluid 45 in Table 7.2

	N_2	CO_2	CH_4	C_2H_6	C_3H_8	C_4H_{10}	C_5H_{12}	C_6H_{14}	PC-1	PC-2	PC-3	PC-4
N_2	0.0000											
CO_2	0.0000	0.0000										
CH_4	0.1000	0.1000	0.0000									
C_2H_6	0.1000	0.1450	0.0420	0.0000								
C_3H_8	0.1000	0.1873	0.0420	0.0400	0.0000							
C_4H_{10}	0.1000	0.1645	0.0420	0.0400	0.0300	0.0000						
C_5H_{12}	0.1000	0.1413	0.0420	0.0400	0.0300	0.0116	0.0000					
C_6H_{14}	0.1000	0.1285	0.0420	0.0400	0.0300	0.0155	0.0058	0.0000				
PC-1	0.1300	0.0166	0.0500	0.0414	0.0320	0.0337	0.0186	0.0000	0.0000			
PC-2	0.1300	0.0532	0.0527	0.0417	0.0334	0.0452	0.0317	0.0000	0.0000	0.0000		
PC-3	0.1300	0.0886	0.0563	0.0422	0.0360	0.0556	0.0461	0.0000	0.0000	0.0000	0.0000	
PC-4	0.1300	0.1244	0.0653	0.0433	0.0468	0.0693	0.0698	0.0000	0.0000	0.0000	0.0000	0.0000

Table 7C.46a : PR EOS model from PnA characterization for fluid 46 in Table 7.2
Saturation pressure (dew point) for this fluid is 254.57 bars at 352.59 K.

Components	Z	MW (g/mol)	T_C (K)	P_C (bars)	ω	C_{PEN} (CC/Mol)
N_2	0.0050	28.01	126.20	33.94	0.04000	
CO_2	0.0062	44.01	304.20	73.76	0.22500	
CH_4	0.7433	16.04	190.60	46.00	0.00800	
C_2H_6	0.0871	30.07	305.40	48.84	0.09800	
C_3H_8	0.0527	44.10	369.80	42.46	0.15200	
C_4H_{10}	0.0282	58.12	419.93	37.53	0.18780	
C_5H_{12}	0.0167	72.15	465.17	33.79	0.23940	
C_6H_{14}	0.0106	86.18	507.40	29.69	0.29600	
PC-1	0.0172	97.28	571.14	32.51	0.13150	
PC-2	0.0143	116.98	625.28	28.93	0.17680	
PC-3	0.0114	147.00	675.07	26.23	0.22280	
PC-4	0.0074	225.00	788.80	21.77	0.33660	

Table 7C.46b : BIPs for PR EOS model from PnA characterization for fluid 46 in Table 7.2

	N_2	CO_2	CH_4	C_2H_6	C_3H_8	C_4H_{10}	C_5H_{12}	C_6H_{14}	PC-1	PC-2	PC-3	PC-4
N_2	0.0000											
CO_2	0.0000	0.0000										
CH_4	0.1000	0.1000	0.0000									
C_2H_6	0.1000	0.1450	0.0420	0.0000								
C_3H_8	0.1000	0.1639	0.0420	0.0400	0.0000							
C_4H_{10}	0.1000	0.1469	0.0420	0.0400	0.0300	0.0000						
C_5H_{12}	0.1000	0.1298	0.0420	0.0400	0.0300	0.0116	0.0000					
C_6H_{14}	0.1000	0.1207	0.0420	0.0400	0.0300	0.0155	0.0058	0.0000				
PC-1	0.1300	0.0040	0.0491	0.0413	0.0317	0.0289	0.0141	0.0000	0.0000			
PC-2	0.1300	0.0294	0.0509	0.0415	0.0324	0.0380	0.0231	0.0000	0.0000	0.0000		
PC-3	0.1300	0.0532	0.0527	0.0417	0.0334	0.0452	0.0317	0.0000	0.0000	0.0000	0.0000	
PC-4	0.1300	0.0949	0.0572	0.0423	0.0369	0.0576	0.0492	0.0000	0.0000	0.0000	0.0000	0.0000

Table 7C.47a : PR EOS model from PnA characterization for fluid 47 in Table 7.2
Saturation pressure (dew point) for this fluid is 281.03 bars at 355.65 K.

Components	Z	MW (g/mol)	T_C (K)	P_C (bars)	ω	C_{PEN} (CC/Mol)
N_2	0.0008	28.01	126.20	33.94	0.04000	-4.230
CO_2	0.0244	44.01	304.20	73.76	0.22500	-1.640
CH_4	0.8210	16.04	190.60	46.00	0.00800	-5.200
C_2H_6	0.0578	30.07	305.40	48.84	0.09800	-5.790
C_3H_8	0.0287	44.10	369.80	42.46	0.15200	-6.350
C_4H_{10}	0.0179	58.12	413.96	37.00	0.18180	-6.490
C_5H_{12}	0.0112	72.15	463.92	33.80	0.23620	-5.120
C_6H_{14}	0.0072	86.00	507.40	29.69	0.29600	1.390
PC-1	0.0103	98.85	572.45	33.12	0.14730	19.780
PC-2	0.0088	116.53	626.55	29.63	0.19820	39.560
PC-3	0.0071	143.74	676.58	27.02	0.24960	59.330
PC-4	0.0048	215.15	791.69	22.72	0.37720	79.110

Table 7C.47b : BIPs for PR EOS model from PnA characterization for fluid 47 in Table 7.2

	N_2	CO_2	CH_4	C_2H_6	C_3H_8	C_4H_{10}	C_5H_{12}	C_6H_{14}	PC-1	PC-2	PC-3	PC-4
N_2	0.0000											
CO_2	0.0000	0.0000										
CH_4	0.1000	0.1000	0.0000									
C_2H_6	0.1000	0.1450	0.0420	0.0000								
C_3H_8	0.1000	0.1668	0.0420	0.0400	0.0000							
C_4H_{10}	0.1000	0.1490	0.0420	0.0400	0.0300	0.0000						
C_5H_{12}	0.1000	0.1312	0.0420	0.0400	0.0300	0.0116	0.0000					
C_6H_{14}	0.1000	0.1215	0.0420	0.0400	0.0300	0.0155	0.0058	0.0000				
PC-1	0.1300	0.0040	0.0491	0.0413	0.0317	0.0289	0.0141	0.0000	0.0000			
PC-2	0.1300	0.0294	0.0509	0.0415	0.0324	0.0380	0.0231	0.0000	0.0000	0.0000		
PC-3	0.1300	0.0532	0.0527	0.0417	0.0334	0.0452	0.0317	0.0000	0.0000	0.0000	0.0000	
PC-4	0.1300	0.0949	0.0572	0.0423	0.0369	0.0576	0.0492	0.0000	0.0000	0.0000	0.0000	0.0000

Table 7C.48a : PR EOS model from PnA characterization for fluid 48 in Table 7.2 Saturation pressure (dew point) for this fluid is 467.00 bars at 364.15 K.						
Components	Z	MW (g/mol)	T_C (K)	P_C (bars)	ω	C_{PEN} (CC/Mol)
N_2	0.0057	28.01	126.20	33.94	0.04000	-4.230
CO_2	0.0144	44.01	304.20	73.76	0.22500	-1.640
CH_4	0.6878	16.04	190.60	46.00	0.00800	-5.200
C_2H_6	0.0671	30.07	305.40	48.84	0.09800	-5.790
C_3H_8	0.0403	44.10	369.80	42.46	0.15200	-6.350
C_4H_{10}	0.0273	58.12	413.96	37.00	0.18180	-6.490
C_5H_{12}	0.0164	72.15	463.92	33.80	0.23620	-5.120
C_6H_{14}	0.0099	86.18	507.40	29.69	0.29600	1.390
PC-1	0.0524	113.11	590.22	30.67	0.15640	0.090
PC-2	0.0375	158.11	687.02	25.23	0.24960	0.280
PC-3	0.0263	225.23	768.82	21.89	0.34180	0.560
PC-4	0.0150	396.07	990.10	16.67	0.61130	1.450

Table 7C.48b : BIPs for PR EOS model from PnA characterization for fluid 48 in Table 7.2												
	N_2	CO_2	CH_4	C_2H_6	C_3H_8	C_4H_{10}	C_5H_{12}	C_6H_{14}	PC-1	PC-2	PC-3	PC-4
N_2	0.0000											
CO_2	0.0000	0.0000										
CH_4	0.1000	0.1000	0.0000									
C_2H_6	0.1000	0.1450	0.0420	0.0000								
C_3H_8	0.1000	0.1753	0.0420	0.0400	0.0000							
C_4H_{10}	0.1000	0.1554	0.0420	0.0400	0.0300	0.0000						
C_5H_{12}	0.1000	0.1353	0.0420	0.0400	0.0300	0.0116	0.0000					
C_6H_{14}	0.1000	0.1243	0.0420	0.0400	0.0300	0.0155	0.0058	0.0000				
PC-1	0.1300	0.0166	0.0500	0.0414	0.0320	0.0337	0.0186	0.0000	0.0000			
PC-2	0.1300	0.0637	0.0536	0.0418	0.0339	0.0482	0.0356	0.0000	0.0000	0.0000		
PC-3	0.1300	0.0949	0.0572	0.0423	0.0369	0.0576	0.0492	0.0000	0.0000	0.0000	0.0000	
PC-4	0.1300	0.1296	0.0689	0.0437	0.0519	0.0725	0.0761	0.0000	0.0000	0.0000	0.0000	0.0000

Table 7C.49a : PR EOS model from PnA characterization for fluid 49 in Table 7.2 Saturation pressure (bubble point) for this fluid is 455.38 bars at 354.82 K.						
Components	Z	MW (g/mol)	T_C (K)	P_C (bars)	ω	C_{PEN} (CC/Mol)
N_2	0.0088	28.01	126.20	33.94	0.04000	-4.230
CO_2	0.0018	44.01	304.20	73.76	0.22500	-1.640
CH_4	0.6801	16.04	190.60	46.00	0.00800	-5.200
C_2H_6	0.0740	30.07	305.40	48.84	0.09800	-5.790
C_3H_8	0.0475	44.10	369.80	42.46	0.15200	-6.350
C_4H_{10}	0.0276	58.12	420.80	37.61	0.18860	-6.490
C_5H_{12}	0.0175	72.15	466.13	33.78	0.24190	-5.120
C_6H_{14}	0.0135	86.18	507.40	29.69	0.29600	1.390
PC-1	0.0533	124.28	614.53	28.44	0.16205	0.890
PC-2	0.0369	179.57	705.57	23.55	0.24620	1.500
PC-3	0.0252	262.90	818.25	19.31	0.36889	2.600
PC-4	0.0139	477.66	1047.17	14.64	0.63035	3.500

Table 7C.49b : BIPs for PR EOS model from PnA characterization for fluid 49 in Table 7.2											
	N_2	CO_2	CH_4	C_2H_6	C_3H_8	C_4H_{10}	C_5H_{12}	C_6H_{14}	PC-1	PC-2	PC-3	PC-4
N_2	0.0000											
CO_2	0.0000	0.0000										
CH_4	0.1000	0.1000	0.0000									
C_2H_6	0.1000	0.1450	0.0420	0.0000								
C_3H_8	0.1000	0.1660	0.0420	0.0400	0.0000							
C_4H_{10}	0.1000	0.1484	0.0420	0.0400	0.0300	0.0000						
C_5H_{12}	0.1000	0.1308	0.0420	0.0400	0.0300	0.0116	0.0000					
C_6H_{14}	0.1000	0.1213	0.0420	0.0400	0.0300	0.0155	0.0058	0.0000				
PC-1	0.1300	0.0294	0.0509	0.0415	0.0324	0.0380	0.0231	0.0000	0.0000			
PC-2	0.1300	0.0731	0.0545	0.0419	0.0346	0.0510	0.0393	0.0000	0.0000	0.0000		
PC-3	0.1300	0.1091	0.0599	0.0426	0.0398	0.0625	0.0574	0.0000	0.0000	0.0000	0.0000	
PC-4	0.1300	0.1335	0.0734	0.0442	0.0581	0.0755	0.0823	0.0000	0.0000	0.0000	0.0000	0.0000

Table 7C.50a : PR EOS model from PnA characterization for fluid 50 in Table 7.2 Saturation pressure (bubble point) for this fluid is 315.62 bars at 425.93 K.						
Components	Z	MW (g/mol)	T_C (K)	P_C (bars)	ω	C_{PEN} (CC/Mol)
N_2	0.0065	28.01	126.20	33.94	0.04000	-4.230
CO_2	0.0019	44.01	304.20	73.76	0.22500	-1.640
CH_4	0.5318	16.04	190.60	46.00	0.00800	-5.200
C_2H_6	0.1156	30.07	305.40	48.84	0.09800	-5.790
C_3H_8	0.0762	44.10	369.80	42.46	0.15200	-6.350
C_4H_{10}	0.0500	58.12	419.01	37.45	0.18680	-6.490
C_5H_{12}	0.0260	72.15	465.32	33.79	0.23980	-5.120
C_6H_{14}	0.0199	86.18	507.40	29.69	0.29600	1.390
PC-1	0.0721	129.93	638.75	26.23	0.15890	4.860
PC-2	0.0488	192.13	725.30	21.76	0.23190	5.850
PC-3	0.0330	284.34	850.75	17.28	0.35420	7.350
PC-4	0.0181	518.05	1084.33	12.89	0.58450	11.770

Table 7C.50b : BIPs for PR EOS model from PnA characterization for fluid 50 in Table 7.2												
	N_2	CO_2	CH_4	C_2H_6	C_3H_8	C_4H_{10}	C_5H_{12}	C_6H_{14}	PC-1	PC-2	PC-3	PC-4
N_2	0.0000											
CO_2	0.0000	0.0000										
CH_4	0.1000	0.1000	0.0000									
C_2H_6	0.1000	0.1450	0.0420	0.0000								
C_3H_8	0.1000	0.2625	0.0420	0.0400	0.0000							
C_4H_{10}	0.1000	0.2238	0.0420	0.0400	0.0300	0.0000						
C_5H_{12}	0.1000	0.1836	0.0420	0.0400	0.0300	0.0116	0.0000					
C_6H_{14}	0.1000	0.1606	0.0420	0.0400	0.0300	0.0155	0.0058	0.0000				
PC-1	0.1300	0.0417	0.0518	0.0416	0.0328	0.0418	0.0275	0.0000	0.0000			
PC-2	0.1300	0.0814	0.0554	0.0420	0.0353	0.0534	0.0428	0.0000	0.0000	0.0000		
PC-3	0.1300	0.1156	0.0617	0.0428	0.0419	0.0652	0.0620	0.0000	0.0000	0.0000	0.0000	
PC-4	0.1300	0.1350	0.0761	0.0446	0.0615	0.0769	0.0854	0.0000	0.0000	0.0000	0.0000	0.0000

Table 7C.51a : PR EOS model from PnA characterization for fluid 51 in Table 7.2 Saturation pressure (bubble point) for this fluid is 302.67 bars at 408.70 K.						
Components	Z	MW (g/mol)	T_C (K)	P_C (bars)	ω	C_{PEN} (CC/Mol)
N_2	0.0000	28.01	126.20	33.94	0.04000	-4.230
CO_2	0.0584	44.01	304.20	73.76	0.22500	-1.640
CH_4	0.5043	16.04	190.60	46.00	0.00800	-5.200
C_2H_6	0.0965	30.07	305.40	48.84	0.09800	-5.790
C_3H_8	0.0875	44.10	369.80	42.46	0.15200	-6.350
C_4H_{10}	0.0589	58.12	418.35	37.39	0.18620	-6.490
C_5H_{12}	0.0295	72.15	464.67	33.79	0.23810	-5.120
C_6H_{14}	0.0229	86.18	507.40	29.69	0.29600	1.390
PC-1	0.0554	117.36	618.51	28.86	0.17470	-6.590
PC-2	0.0407	159.75	689.76	25.04	0.24280	-16.780
PC-3	0.0291	223.20	773.46	21.68	0.33250	-32.760
PC-4	0.0169	385.02	988.48	16.64	0.57660	-82.110

Table 7C.51b : BIPs for PR EOS model from PnA characterization for fluid 51 in Table 7.2												
	N_2	CO_2	CH_4	C_2H_6	C_3H_8	C_4H_{10}	C_5H_{12}	C_6H_{14}	PC-1	PC-2	PC-3	PC-4
N_2	0.0000											
CO_2	0.0000	0.0000										
CH_4	0.1000	0.1000	0.0000									
C_2H_6	0.1000	0.1450	0.0420	0.0000								
C_3H_8	0.1000	0.2338	0.0420	0.0400	0.0000							
C_4H_{10}	0.1000	0.2009	0.0420	0.0400	0.0300	0.0000						
C_5H_{12}	0.1000	0.1669	0.0420	0.0400	0.0300	0.0116	0.0000					
C_6H_{14}	0.1000	0.1476	0.0420	0.0400	0.0300	0.0155	0.0058	0.0000				
PC-1	0.1300	0.0294	0.0509	0.0415	0.0324	0.0380	0.0231	0.0000	0.0000			
PC-2	0.1300	0.0637	0.0536	0.0418	0.0339	0.0482	0.0356	0.0000	0.0000	0.0000		
PC-3	0.1300	0.0949	0.0572	0.0423	0.0369	0.0576	0.0492	0.0000	0.0000	0.0000	0.0000	
PC-4	0.1300	0.1285	0.0680	0.0436	0.0506	0.0718	0.0746	0.0000	0.0000	0.0000	0.0000	0.0000

Table 7C.52a : PR EOS model from PnA characterization for fluid 52 in Table 7.2
Saturation pressure (bubble point) for this fluid is 313.15 bars at 393.70 K.

Components	Z	MW (g/mol)	T_C (K)	P_C (bars)	ω	C_{PEN} (CC/Mol)
N_2	0.0011	28.01	126.20	33.94	0.04000	-4.230
CO_2	0.0214	44.01	304.20	73.76	0.22500	-1.640
CH_4	0.5559	16.04	190.60	46.00	0.00800	-5.200
C_2H_6	0.0870	30.07	305.40	48.84	0.09800	-5.790
C_3H_8	0.0589	44.10	369.80	42.46	0.15200	-6.350
C_4H_{10}	0.0405	58.12	419.46	37.49	0.18730	-6.490
C_5H_{12}	0.0253	72.15	465.35	33.79	0.23990	-5.120
C_6H_{14}	0.0197	86.18	507.40	29.69	0.29600	1.390
PC-1	0.0765	119.41	617.17	28.42	0.16160	-22.280
PC-2	0.0539	169.32	687.97	24.54	0.22450	-44.550
PC-3	0.0379	240.96	789.61	20.43	0.32780	-66.830
PC-4	0.0219	416.17	1011.00	15.43	0.56630	-89.100

Table 7C.52b : BIPs for PR EOS model from PnA characterization for fluid 52 in Table 7.2

	N_2	CO_2	CH_4	C_2H_6	C_3H_8	C_4H_{10}	C_5H_{12}	C_6H_{14}	PC-1	PC-2	PC-3	PC-4
N_2	0.0000											
CO_2	0.0000	0.0000										
CH_4	0.1000	0.1000	0.0000									
C_2H_6	0.1000	0.1450	0.0420	0.0000								
C_3H_8	0.1000	0.2115	0.0420	0.0400	0.0000							
C_4H_{10}	0.1000	0.1834	0.0420	0.0400	0.0300	0.0000						
C_5H_{12}	0.1000	0.1544	0.0420	0.0400	0.0300	0.0116	0.0000					
C_6H_{14}	0.1000	0.1381	0.0420	0.0400	0.0300	0.0155	0.0058	0.0000				
PC-1	0.1300	0.0294	0.0509	0.0415	0.0324	0.0380	0.0231	0.0000	0.0000			
PC-2	0.1300	0.0637	0.0536	0.0418	0.0339	0.0482	0.0356	0.0000	0.0000	0.0000		
PC-3	0.1300	0.1003	0.0581	0.0424	0.0378	0.0594	0.0521	0.0000	0.0000	0.0000	0.0000	
PC-4	0.1300	0.1306	0.0698	0.0438	0.0532	0.0732	0.0774	0.0000	0.0000	0.0000	0.0000	0.0000

Table 7C.53a : PR EOS model from PnA characterization for fluid 53 in Table 7.2 Saturation pressure (bubble point) for this fluid is 280.98 bars at 346.48 K.						
Components	Z	MW (g/mol)	T_C (K)	P_C (bars)	ω	C_{PEN} (CC/Mol)
N_2	0.0155	28.01	126.20	33.94	0.04000	-4.230
CO_2	0.0029	44.01	304.20	73.76	0.22500	-1.640
CH_4	0.5197	16.04	190.60	46.00	0.00800	-5.200
C_2H_6	0.1172	30.07	305.40	48.84	0.09800	-5.790
C_3H_8	0.0923	44.10	369.80	42.46	0.15200	-6.350
C_4H_{10}	0.0413	58.12	419.46	37.49	0.18730	-6.490
C_5H_{12}	0.0182	72.15	465.35	33.79	0.23990	-5.120
C_6H_{14}	0.0159	86.18	507.40	29.69	0.29600	1.390
PC-1	0.0713	114.89	591.65	30.33	0.14680	5.060
PC-2	0.0504	162.58	688.96	24.81	0.23420	10.120
PC-3	0.0352	232.31	791.52	20.75	0.34200	15.190
PC-4	0.0202	406.11	1000.67	16.05	0.57370	20.250

Table 7C.53b : BIPs for PR EOS model from PnA characterization for fluid 53 in Table 7.2											
	N_2	CO_2	CH_4	C_2H_6	C_3H_8	C_4H_{10}	C_5H_{12}	C_6H_{14}	PC-1	PC-2	PC-3	PC-4
N_2	0.0000											
CO_2	0.0000	0.0000										
CH_4	0.1000	0.1000	0.0000									
C_2H_6	0.1000	0.1450	0.0420	0.0000								
C_3H_8	0.1000	0.1585	0.0420	0.0400	0.0000							
C_4H_{10}	0.1000	0.1429	0.0420	0.0400	0.0300	0.0000						
C_5H_{12}	0.1000	0.1274	0.0420	0.0400	0.0300	0.0116	0.0000					
C_6H_{14}	0.1000	0.1191	0.0420	0.0400	0.0300	0.0155	0.0058	0.0000				
PC-1	0.1300	0.0166	0.0500	0.0414	0.0320	0.0337	0.0186	0.0000	0.0000			
PC-2	0.1300	0.0637	0.0536	0.0418	0.0339	0.0482	0.0356	0.0000	0.0000	0.0000		
PC-3	0.1300	0.1003	0.0581	0.0424	0.0378	0.0594	0.0521	0.0000	0.0000	0.0000	0.0000	
PC-4	0.1300	0.1296	0.0689	0.0437	0.0519	0.0725	0.0761	0.0000	0.0000	0.0000	0.0000	0.0000

Table 7C.54a : PR EOS model from PnA characterization for fluid 54 in Table 7.2 Saturation pressure (bubble point) for this fluid is 389.30 bars at 424.25 K.						
Components	Z	MW (g/mol)	T_C (K)	P_C (bars)	ω	C_{PEN} (CC/Mol)
N_2	0.0046	28.01	126.20	33.94	0.04000	-4.230
CO_2	0.0336	44.01	304.20	73.76	0.22500	-1.640
CH_4	0.6223	16.04	190.60	46.00	0.00800	-5.200
C_2H_6	0.0888	30.07	305.40	48.84	0.09800	-5.790
C_3H_8	0.0530	44.10	369.80	42.46	0.15200	-6.350
C_4H_{10}	0.0298	58.12	419.98	37.54	0.18780	-6.490
C_5H_{12}	0.0158	72.15	465.35	33.79	0.23990	-5.120
C_6H_{14}	0.0104	86.18	507.40	29.69	0.29600	1.390
PC-1	0.0584	117.59	615.12	28.02	0.14920	5.080
PC-2	0.0404	169.86	685.22	24.06	0.20740	14.220
PC-3	0.0276	248.61	802.47	19.25	0.32130	31.610
PC-4	0.0152	451.58	1038.65	14.09	0.56660	83.260

Table 7C.54b : BIPs for PR EOS model from PnA characterization for fluid 54 in Table 7.2											
	N_2	CO_2	CH_4	C_2H_6	C_3H_8	C_4H_{10}	C_5H_{12}	C_6H_{14}	PC-1	PC-2	PC-3	PC-4
N_2	0.0000											
CO_2	0.0000	0.0000										
CH_4	0.1000	0.1000	0.0000									
C_2H_6	0.1000	0.1450	0.0420	0.0000								
C_3H_8	0.1000	0.2595	0.0420	0.0400	0.0000							
C_4H_{10}	0.1000	0.2215	0.0420	0.0400	0.0300	0.0000						
C_5H_{12}	0.1000	0.1818	0.0420	0.0400	0.0300	0.0116	0.0000					
C_6H_{14}	0.1000	0.1592	0.0420	0.0400	0.0300	0.0155	0.0058	0.0000				
PC-1	0.1300	0.0294	0.0509	0.0415	0.0324	0.0380	0.0231	0.0000	0.0000			
PC-2	0.1300	0.0637	0.0536	0.0418	0.0339	0.0482	0.0356	0.0000	0.0000	0.0000		
PC-3	0.1300	0.1050	0.0590	0.0425	0.0387	0.0610	0.0548	0.0000	0.0000	0.0000	0.0000	
PC-4	0.1300	0.1329	0.0725	0.0441	0.0569	0.0749	0.0812	0.0000	0.0000	0.0000	0.0000	0.0000

Table 7C.55a : PR EOS model from PnA characterization for fluid 55 in Table 7.2 Saturation pressure (bubble point) for this fluid is 331.63 bars at 374.82 K.						
Components	Z	MW (g/mol)	T_C (K)	P_C (bars)	ω	C_{PEN} (CC/Mol)
N_2	0.0027	28.01	126.20	33.94	0.04000	-4.230
CO_2	0.0024	44.01	304.20	73.76	0.22500	-1.640
CH_4	0.6683	16.04	190.60	46.00	0.00800	-5.200
C_2H_6	0.0828	30.07	305.40	48.84	0.09800	-5.790
C_3H_8	0.0515	44.10	369.80	42.46	0.15200	-6.350
C_4H_{10}	0.0331	58.12	425.20	38.00	0.19300	-6.490
C_5H_{12}	0.0204	72.15	469.60	33.74	0.25100	-5.120
C_6H_{14}	0.0185	86.18	507.40	29.69	0.29600	1.390
PC-1	0.0470	116.43	617.57	27.79	0.14230	4.940
PC-2	0.0344	158.90	688.50	23.79	0.19780	12.960
PC-3	0.0246	222.46	771.33	20.24	0.27090	25.850
PC-4	0.0142	384.52	982.07	14.87	0.46980	67.660

Table 7C.55b : BIPs for PR EOS model from PnA characterization for fluid 55 in Table 7.2												
	N_2	CO_2	CH_4	C_2H_6	C_3H_8	C_4H_{10}	C_5H_{12}	C_6H_{14}	PC-1	PC-2	PC-3	PC-4
N_2	0.0000											
CO_2	0.0000	0.0000										
CH_4	0.1000	0.1000	0.0000									
C_2H_6	0.1000	0.1450	0.0420	0.0000								
C_3H_8	0.1000	0.1873	0.0420	0.0400	0.0000							
C_4H_{10}	0.1000	0.1645	0.0420	0.0400	0.0300	0.0000						
C_5H_{12}	0.1000	0.1413	0.0420	0.0400	0.0300	0.0116	0.0000					
C_6H_{14}	0.1000	0.1285	0.0420	0.0400	0.0300	0.0155	0.0058	0.0000				
PC-1	0.1300	0.0294	0.0509	0.0415	0.0324	0.0380	0.0231	0.0000	0.0000			
PC-2	0.1300	0.0637	0.0536	0.0418	0.0339	0.0482	0.0356	0.0000	0.0000	0.0000		
PC-3	0.1300	0.0949	0.0572	0.0423	0.0369	0.0576	0.0492	0.0000	0.0000	0.0000	0.0000	
PC-4	0.1300	0.1285	0.0680	0.0436	0.0506	0.0718	0.0746	0.0000	0.0000	0.0000	0.0000	0.0000

Table 7C.1a : PR EOS model from PnA characterization for oil 1 in Table 7.3						
Saturation pressure (bubble point) for this fluid is 96.90 bars at 374.85 K.						
Components	Z	MW (g/mol)	T_C (K)	P_C (bars)	ω	C_{PEN} (CC/Mol)
N_2	0.0018	28.01	126.20	33.94	0.04000	-4.230
CO_2	0.0082	44.01	304.20	73.76	0.22500	-1.640
CH_4	0.2292	16.04	190.60	46.00	0.00800	-5.200
C_2H_6	0.0721	30.07	305.40	48.84	0.09800	-5.790
C_3H_8	0.0737	44.10	369.80	42.46	0.15200	-6.350
C_4H_{10}	0.0681	58.12	421.23	37.65	0.18910	-6.490
C_5H_{12}	0.0585	72.15	466.06	33.78	0.24180	-5.120
C_6H_{14}	0.0484	86.00	507.40	29.69	0.29600	1.390
PC-1	0.1871	151.53	661.61	24.76	0.17250	7.100
PC-2	0.1207	234.84	781.28	19.31	0.27780	18.530
PC-3	0.0831	341.02	912.58	15.49	0.40760	35.930
PC-4	0.0491	577.74	1145.28	11.98	0.62340	77.260

Table 7C.1b : BIPs for PR EOS model from PnA characterization for oil 1 in Table 7.3												
	N_2	CO_2	CH_4	C_2H_6	C_3H_8	C_4H_{10}	C_5H_{12}	C_6H_{14}	PC-1	PC-2	PC-3	PC-4
N_2	0.0000											
CO_2	0.0000	0.0000										
CH_4	0.1000	0.1000	0.0000									
C_2H_6	0.1000	0.1450	0.0420	0.0000								
C_3H_8	0.1000	0.1873	0.0420	0.0400	0.0000							
C_4H_{10}	0.1000	0.1645	0.0420	0.0400	0.0300	0.0000						
C_5H_{12}	0.1000	0.1414	0.0420	0.0400	0.0300	0.0116	0.0000					
C_6H_{14}	0.1000	0.1286	0.0420	0.0400	0.0300	0.0155	0.0058	0.0000				
PC-1	0.1300	0.0532	0.0527	0.0417	0.0334	0.0452	0.0317	0.0000	0.0000			
PC-2	0.1300	0.1003	0.0581	0.0424	0.0378	0.0594	0.0521	0.0000	0.0000	0.0000		
PC-3	0.1300	0.1244	0.0653	0.0433	0.0468	0.0693	0.0698	0.0000	0.0000	0.0000	0.0000	
PC-4	0.1300	0.1368	0.0806	0.0451	0.0661	0.0788	0.0898	0.0000	0.0000	0.0000	0.0000	0.0000

Table 7C.2a : PR EOS model from PnA characterization for oil 2 in Table 7.3
Saturation pressure (bubble point) for this fluid is 117.70 bars at 372.05 K.

Components	Z	MW (g/mol)	T_C (K)	P_C (bars)	ω	C_{PEN} (CC/Mol)
N_2	0.0020	28.01	126.20	33.94	0.04000	-4.230
CO_2	0.0134	44.01	304.20	73.76	0.22500	-1.640
CH_4	0.2364	16.04	190.60	46.00	0.00800	-5.200
C_2H_6	0.0856	30.07	305.40	48.84	0.09800	-5.790
C_3H_8	0.0668	44.10	369.80	42.46	0.15200	-6.350
C_4H_{10}	0.0530	58.12	421.17	37.64	0.18900	-6.490
C_5H_{12}	0.0445	72.15	465.92	33.78	0.24140	-5.120
C_6H_{14}	0.0403	86.00	507.40	29.69	0.29600	1.390
PC-1	0.1954	149.10	662.72	25.82	0.20850	-3.930
PC-2	0.1252	232.78	783.69	20.61	0.33590	-10.240
PC-3	0.0863	337.73	902.06	17.34	0.47420	-18.690
PC-4	0.0512	569.16	1145.01	13.82	0.74120	-39.400

Table 7C.2b : BIPs for PR EOS model from PnA characterization for oil 2 in Table 7.3

	N_2	CO_2	CH_4	C_2H_6	C_3H_8	C_4H_{10}	C_5H_{12}	C_6H_{14}	PC-1	PC-2	PC-3	PC-4
N_2	0.0000											
CO_2	0.0000	0.0000										
CH_4	0.1000	0.1000	0.0000									
C_2H_6	0.1000	0.1450	0.0420	0.0000								
C_3H_8	0.1000	0.1840	0.0420	0.0400	0.0000							
C_4H_{10}	0.1000	0.1620	0.0420	0.0400	0.0300	0.0000						
C_5H_{12}	0.1000	0.1397	0.0420	0.0400	0.0300	0.0116	0.0000					
C_6H_{14}	0.1000	0.1274	0.0420	0.0400	0.0300	0.0155	0.0058	0.0000				
PC-1	0.1300	0.0532	0.0527	0.0417	0.0334	0.0452	0.0317	0.0000	0.0000			
PC-2	0.1300	0.1003	0.0581	0.0424	0.0378	0.0594	0.0521	0.0000	0.0000	0.0000		
PC-3	0.1300	0.1226	0.0644	0.0431	0.0455	0.0684	0.0680	0.0000	0.0000	0.0000	0.0000	
PC-4	0.1300	0.1365	0.0797	0.0450	0.0653	0.0784	0.0890	0.0000	0.0000	0.0000	0.0000	0.0000

Table 7C.3a : PR EOS model from PnA characterization for oil 3 in Table 7.3 Saturation pressure (bubble point) for this fluid is 255.60 bars at 387.35 K.						
Components	Z	MW (g/mol)	T_C (K)	P_C (bars)	ω	C_{PEN} (CC/Mol)
N_2	0.0045	28.01	126.20	33.94	0.04000	-4.230
CO_2	0.0164	44.01	304.20	73.76	0.22500	-1.640
CH_4	0.4585	16.04	190.60	46.00	0.00800	-5.200
C_2H_6	0.0715	30.07	305.40	48.84	0.09800	-5.790
C_3H_8	0.0674	44.10	369.80	42.46	0.15200	-6.350
C_4H_{10}	0.0395	58.12	421.56	37.68	0.18940	-6.490
C_5H_{12}	0.0268	72.15	466.06	33.78	0.24180	-5.120
C_6H_{14}	0.0252	86.00	507.40	29.69	0.29600	1.390
PC-1	0.1211	129.45	640.30	26.98	0.18330	-3.530
PC-2	0.0809	193.79	727.84	22.66	0.26740	-9.310
PC-3	0.0558	280.81	839.32	18.81	0.38900	-18.320
PC-4	0.0324	483.29	1072.22	14.48	0.64570	-42.450

Table 7C.3b : BIPs for PR EOS model from PnA characterization for oil 3 in Table 7.3											
	N_2	CO_2	CH_4	C_2H_6	C_3H_8	C_4H_{10}	C_5H_{12}	C_6H_{14}	PC-1	PC-2	PC-3	PC-4
N_2	0.0000											
CO_2	0.0000	0.0000										
CH_4	0.1000	0.1000	0.0000									
C_2H_6	0.1000	0.1450	0.0420	0.0000								
C_3H_8	0.1000	0.2029	0.0420	0.0400	0.0000							
C_4H_{10}	0.1000	0.1766	0.0420	0.0400	0.0300	0.0000						
C_5H_{12}	0.1000	0.1497	0.0420	0.0400	0.0300	0.0116	0.0000					
C_6H_{14}	0.1000	0.1346	0.0420	0.0400	0.0300	0.0155	0.0058	0.0000				
PC-1	0.1300	0.0417	0.0518	0.0416	0.0328	0.0418	0.0275	0.0000	0.0000			
PC-2	0.1300	0.0814	0.0554	0.0420	0.0353	0.0534	0.0428	0.0000	0.0000	0.0000		
PC-3	0.1300	0.1126	0.0608	0.0427	0.0408	0.0639	0.0598	0.0000	0.0000	0.0000	0.0000	
PC-4	0.1300	0.1341	0.0743	0.0444	0.0592	0.0760	0.0834	0.0000	0.0000	0.0000	0.0000	0.0000

Table 7C.4a : PR EOS model from PnA characterization for oil 4 in Table 7.3 Saturation pressure (bubble point) for this fluid is 320.20 bars at 388.15 K.						
Components	Z	MW (g/mol)	T_C (K)	P_C (bars)	ω	C_{PEN} (CC/Mol)
N_2	0.0035	28.01	126.20	33.94	0.04000	-4.230
CO_2	0.0314	44.01	304.20	73.76	0.22500	-1.640
CH_4	0.5426	16.04	190.60	46.00	0.00800	-5.200
C_2H_6	0.0857	30.07	305.40	48.84	0.09800	-5.790
C_3H_8	0.0572	44.10	369.80	42.46	0.15200	-6.350
C_4H_{10}	0.0321	58.12	421.15	37.64	0.18900	-6.490
C_5H_{12}	0.0195	72.15	466.06	33.78	0.24180	-5.120
C_6H_{14}	0.0153	86.00	507.40	29.69	0.29600	1.390
PC-1	0.0889	121.73	615.55	28.23	0.15580	-3.350
PC-2	0.0599	180.66	707.12	23.30	0.23670	-9.820
PC-3	0.0409	264.90	821.51	19.01	0.35460	-20.630
PC-4	0.0230	470.89	1056.93	14.28	0.60590	-50.990

Table 7C.4b : BIPs for PR EOS model from PnA characterization for oil 4 in Table 7.3												
	N_2	CO_2	CH_4	C_2H_6	C_3H_8	C_4H_{10}	C_5H_{12}	C_6H_{14}	PC-1	PC-2	PC-3	PC-4
N_2	0.0000											
CO_2	0.0000	0.0000										
CH_4	0.1000	0.1000	0.0000									
C_2H_6	0.1000	0.1450	0.0420	0.0000								
C_3H_8	0.1000	0.2040	0.0420	0.0400	0.0000							
C_4H_{10}	0.1000	0.1775	0.0420	0.0400	0.0300	0.0000						
C_5H_{12}	0.1000	0.1502	0.0420	0.0400	0.0300	0.0116	0.0000					
C_6H_{14}	0.1000	0.1350	0.0420	0.0400	0.0300	0.0155	0.0058	0.0000				
PC-1	0.1300	0.0294	0.0509	0.0415	0.0324	0.0380	0.0231	0.0000	0.0000			
PC-2	0.1300	0.0731	0.0545	0.0419	0.0346	0.0510	0.0393	0.0000	0.0000	0.0000		
PC-3	0.1300	0.1091	0.0599	0.0426	0.0398	0.0625	0.0574	0.0000	0.0000	0.0000	0.0000	
PC-4	0.1300	0.1335	0.0734	0.0442	0.0581	0.0755	0.0823	0.0000	0.0000	0.0000	0.0000	0.0000

Table 7C.5a : PR EOS model from PnA characterization for oil 5 in Table 7.3 Saturation pressure (bubble point) for this fluid is 145.80 bars at 394.25 K.						
Components	Z	MW (g/mol)	T_C (K)	P_C (bars)	ω	C_{PEN} (CC/Mol)
N_2	0.0045	28.01	126.20	33.94	0.04000	-4.230
CO_2	0.0207	44.01	304.20	73.76	0.22500	-1.640
CH_4	0.2658	16.04	190.60	46.00	0.00800	-5.200
C_2H_6	0.0789	30.07	305.40	48.84	0.09800	-5.790
C_3H_8	0.0673	44.10	369.80	42.46	0.15200	-6.350
C_4H_{10}	0.0538	58.12	420.48	37.58	0.18830	-6.490
C_5H_{12}	0.0444	72.15	465.59	33.78	0.24050	-5.120
C_6H_{14}	0.0335	86.00	507.40	29.69	0.29600	1.390
PC-1	0.1838	144.13	662.45	25.72	0.20530	-1.380
PC-2	0.1181	224.25	764.65	21.16	0.31020	-3.510
PC-3	0.0812	326.21	900.87	17.21	0.46700	-6.870
PC-4	0.0479	553.33	1128.92	13.80	0.71720	-14.360

Table 7C.5b : BIPs for PR EOS model from PnA characterization for oil 5 in Table 7.3												
	N_2	CO_2	CH_4	C_2H_6	C_3H_8	C_4H_{10}	C_5H_{12}	C_6H_{14}	PC-1	PC-2	PC-3	PC-4
N_2	0.0000											
CO_2	0.0000	0.0000										
CH_4	0.1000	0.1000	0.0000									
C_2H_6	0.1000	0.1450	0.0420	0.0000								
C_3H_8	0.1000	0.2123	0.0420	0.0400	0.0000							
C_4H_{10}	0.1000	0.1840	0.0420	0.0400	0.0300	0.0000						
C_5H_{12}	0.1000	0.1548	0.0420	0.0400	0.0300	0.0116	0.0000					
C_6H_{14}	0.1000	0.1385	0.0420	0.0400	0.0300	0.0155	0.0058	0.0000				
PC-1	0.1300	0.0532	0.0527	0.0417	0.0334	0.0452	0.0317	0.0000	0.0000			
PC-2	0.1300	0.0949	0.0572	0.0423	0.0369	0.0576	0.0492	0.0000	0.0000	0.0000		
PC-3	0.1300	0.1226	0.0644	0.0431	0.0455	0.0684	0.0680	0.0000	0.0000	0.0000	0.0000	
PC-4	0.1300	0.1362	0.0788	0.0449	0.0644	0.0781	0.0882	0.0000	0.0000	0.0000	0.0000	0.0000

Table 7C.6a : PR EOS model from PnA characterization for oil 6 in Table 7.3
Saturation pressure (bubble point) for this fluid is 172.90 bars at 383.15 K.

Components	Z	MW (g/mol)	T_C (K)	P_C (bars)	ω	C_{PEN} (CC/Mol)
N_2	0.0000	28.01	126.20	33.94	0.04000	-4.230
CO_2	0.0077	44.01	304.20	73.76	0.22500	-1.640
CH_4	0.3620	16.04	190.60	46.00	0.00800	-5.200
C_2H_6	0.0974	30.07	305.40	48.84	0.09800	-5.790
C_3H_8	0.0675	44.10	369.80	42.46	0.15200	-6.350
C_4H_{10}	0.0496	58.12	424.46	37.93	0.19230	-6.490
C_5H_{12}	0.0389	72.15	462.98	33.81	0.23370	-5.120
C_6H_{14}	0.0329	86.00	507.40	29.69	0.29600	1.390
PC-1	0.1429	132.44	640.32	26.53	0.16880	3.630
PC-2	0.0955	198.14	727.86	22.12	0.24630	9.360
PC-3	0.0664	284.84	856.51	17.71	0.37620	19.210
PC-4	0.0392	482.42	1072.36	13.74	0.59480	42.810

Table 7C.6b : BIPs for PR EOS model from PnA characterization for oil 6 in Table 7.3

	N_2	CO_2	CH_4	C_2H_6	C_3H_8	C_4H_{10}	C_5H_{12}	C_6H_{14}	PC-1	PC-2	PC-3	PC-4
N_2	0.0000											
CO_2	0.0000	0.0000										
CH_4	0.1000	0.1000	0.0000									
C_2H_6	0.1000	0.1450	0.0420	0.0000								
C_3H_8	0.1000	0.1975	0.0420	0.0400	0.0000							
C_4H_{10}	0.1000	0.1724	0.0420	0.0400	0.0300	0.0000						
C_5H_{12}	0.1000	0.1467	0.0420	0.0400	0.0300	0.0116	0.0000					
C_6H_{14}	0.1000	0.1325	0.0420	0.0400	0.0300	0.0155	0.0058	0.0000				
PC-1	0.1300	0.0417	0.0518	0.0416	0.0328	0.0418	0.0275	0.0000	0.0000			
PC-2	0.1300	0.0814	0.0554	0.0420	0.0353	0.0534	0.0428	0.0000	0.0000	0.0000		
PC-3	0.1300	0.1156	0.0617	0.0428	0.0419	0.0652	0.0620	0.0000	0.0000	0.0000	0.0000	
PC-4	0.1300	0.1341	0.0743	0.0444	0.0592	0.0760	0.0834	0.0000	0.0000	0.0000	0.0000	0.0000

Table 7C.7a : PR EOS model from PnA characterization for oil 7 in Table 7.3 Saturation pressure (bubble point) for this fluid is 153.90 bars at 393.15 K.						
Components	Z	MW (g/mol)	T_C (K)	P_C (bars)	ω	C_{PEN} (CC/Mol)
N_2	0.0000	28.01	126.20	33.94	0.04000	-4.230
CO_2	0.0213	44.01	304.20	73.76	0.22500	-1.640
CH_4	0.3128	16.04	190.60	46.00	0.00800	-5.200
C_2H_6	0.0751	30.07	305.40	48.84	0.09800	-5.790
C_3H_8	0.0693	44.10	369.80	42.46	0.15200	-6.350
C_4H_{10}	0.0626	58.12	424.46	37.93	0.19230	-6.490
C_5H_{12}	0.0474	72.15	462.98	33.81	0.23370	-5.120
C_6H_{14}	0.0437	86.00	507.40	29.69	0.29600	1.390
PC-1	0.1461	126.76	618.26	28.63	0.16770	-5.290
PC-2	0.1025	180.82	711.28	23.78	0.25480	-13.830
PC-3	0.0738	251.06	811.51	20.12	0.36120	-26.260
PC-4	0.0454	407.94	1003.21	16.01	0.57100	-57.050

Table 7C.7b : BIPs for PR EOS model from PnA characterization for oil 7 in Table 7.3												
	N_2	CO_2	CH_4	C_2H_6	C_3H_8	C_4H_{10}	C_5H_{12}	C_6H_{14}	PC-1	PC-2	PC-3	PC-4
N_2	0.0000											
CO_2	0.0000	0.0000										
CH_4	0.1000	0.1000	0.0000									
C_2H_6	0.1000	0.1450	0.0420	0.0000								
C_3H_8	0.1000	0.2108	0.0420	0.0400	0.0000							
C_4H_{10}	0.1000	0.1828	0.0420	0.0400	0.0300	0.0000						
C_5H_{12}	0.1000	0.1539	0.0420	0.0400	0.0300	0.0116	0.0000					
C_6H_{14}	0.1000	0.1378	0.0420	0.0400	0.0300	0.0155	0.0058	0.0000				
PC-1	0.1300	0.0294	0.0509	0.0415	0.0324	0.0380	0.0231	0.0000	0.0000			
PC-2	0.1300	0.0731	0.0545	0.0419	0.0346	0.0510	0.0393	0.0000	0.0000	0.0000		
PC-3	0.1300	0.1050	0.0590	0.0425	0.0387	0.0610	0.0548	0.0000	0.0000	0.0000	0.0000	
PC-4	0.1300	0.1296	0.0689	0.0437	0.0519	0.0725	0.0761	0.0000	0.0000	0.0000	0.0000	0.0000

Table 7C.8a : PR EOS model from PnA characterization for oil 8 in Table 7.3 Saturation pressure (bubble point) for this fluid is 245.70 bars at 373.75 K.						
Components	Z	MW (g/mol)	T_C (K)	P_C (bars)	ω	C_{PEN} (CC/Mol)
N_2	0.0027	28.01	126.20	33.94	0.04000	-4.230
CO_2	0.0293	44.01	304.20	73.76	0.22500	-1.640
CH_4	0.3828	16.04	190.60	46.00	0.00800	-5.200
C_2H_6	0.0722	30.07	305.40	48.84	0.09800	-5.790
C_3H_8	0.0574	44.10	369.80	42.46	0.15200	-6.350
C_4H_{10}	0.0511	58.12	419.95	37.53	0.18780	-6.490
C_5H_{12}	0.0411	72.15	469.50	33.74	0.25070	-5.120
C_6H_{14}	0.0315	86.18	507.40	29.69	0.29600	1.390
PC-1	0.1327	123.84	617.78	28.57	0.16600	-2.070
PC-2	0.0926	177.39	710.53	23.71	0.25220	-5.610
PC-3	0.0663	247.89	810.11	20.04	0.35750	-10.810
PC-4	0.0403	407.20	999.67	15.91	0.56510	-23.720

Table 7C.8b : BIPs for PR EOS model from PnA characterization for oil 8 in Table 7.3												
	N_2	CO_2	CH_4	C_2H_6	C_3H_8	C_4H_{10}	C_5H_{12}	C_6H_{14}	PC-1	PC-2	PC-3	PC-4
N_2	0.0000											
CO_2	0.0000	0.0000										
CH_4	0.1000	0.1000	0.0000									
C_2H_6	0.1000	0.1450	0.0420	0.0000								
C_3H_8	0.1000	0.2244	0.0420	0.0400	0.0000							
C_4H_{10}	0.1000	0.1935	0.0420	0.0400	0.0300	0.0000						
C_5H_{12}	0.1000	0.1616	0.0420	0.0400	0.0300	0.0116	0.0000					
C_6H_{14}	0.1000	0.1436	0.0420	0.0400	0.0300	0.0155	0.0058	0.0000				
PC-1	0.1300	0.0294	0.0509	0.0415	0.0324	0.0380	0.0231	0.0000	0.0000			
PC-2	0.1300	0.0731	0.0545	0.0419	0.0346	0.0510	0.0393	0.0000	0.0000	0.0000		
PC-3	0.1300	0.1050	0.0590	0.0425	0.0387	0.0610	0.0548	0.0000	0.0000	0.0000	0.0000	
PC-4	0.1300	0.1296	0.0689	0.0437	0.0519	0.0725	0.0761	0.0000	0.0000	0.0000	0.0000	0.0000

Table 7C.9a : PR EOS model from PnA characterization for oil 9 in Table 7.3
Saturation pressure (bubble point) for this fluid is 202.08 bars at 402.59 K.

Components	Z	MW (g/mol)	T_C (K)	P_C (bars)	ω	C_{PEN} (CC/Mol)
N_2	0.0027	28.01	126.20	33.94	0.04000	-4.230
CO_2	0.0293	44.01	304.20	73.76	0.22500	-1.640
CH_4	0.3828	16.04	190.60	46.00	0.00800	-5.200
C_2H_6	0.0722	30.07	305.40	48.84	0.09800	-5.790
C_3H_8	0.0574	44.10	369.80	42.46	0.15200	-6.350
C_4H_{10}	0.0511	58.12	419.95	37.53	0.18780	-6.490
C_5H_{12}	0.0411	72.15	469.50	33.74	0.25070	-5.120
C_6H_{14}	0.0315	86.18	507.40	29.69	0.29600	1.390
PC-1	0.1327	123.84	617.78	28.57	0.16600	-2.070
PC-2	0.0926	177.39	710.53	23.71	0.25220	-5.610
PC-3	0.0663	247.89	810.11	20.04	0.35750	-10.810
PC-4	0.0403	407.20	999.67	15.91	0.56510	-23.720

Table 7C.9b : BIPs for PR EOS model from PnA characterization for oil 9 in Table 7.3

	N_2	CO_2	CH_4	C_2H_6	C_3H_8	C_4H_{10}	C_5H_{12}	C_6H_{14}	PC-1	PC-2	PC-3	PC-4
N_2	0.0000											
CO_2	0.0000	0.0000										
CH_4	0.1000	0.1000	0.0000									
C_2H_6	0.1000	0.1450	0.0420	0.0000								
C_3H_8	0.1000	0.1860	0.0420	0.0400	0.0000							
C_4H_{10}	0.1000	0.1635	0.0420	0.0400	0.0300	0.0000						
C_5H_{12}	0.1000	0.1407	0.0420	0.0400	0.0300	0.0116	0.0000					
C_6H_{14}	0.1000	0.1281	0.0420	0.0400	0.0300	0.0155	0.0058	0.0000				
PC-1	0.1300	0.0417	0.0518	0.0416	0.0328	0.0418	0.0275	0.0000	0.0000			
PC-2	0.1300	0.0814	0.0554	0.0420	0.0353	0.0534	0.0428	0.0000	0.0000	0.0000		
PC-3	0.1300	0.1126	0.0608	0.0427	0.0408	0.0639	0.0598	0.0000	0.0000	0.0000	0.0000	
PC-4	0.1300	0.1341	0.0743	0.0444	0.0592	0.0760	0.0834	0.0000	0.0000	0.0000	0.0000	0.0000

Table 7C.10a : PR EOS model from PnA characterization for oil 10 in Table 7.3 Saturation pressure (bubble point) for this fluid is 246.00 bars at 368.15 K.						
Components	Z	MW (g/mol)	T_C (K)	P_C (bars)	ω	C_{PEN} (CC/Mol)
N_2	0.0027	28.01	126.20	33.94	0.04000	-4.230
CO_2	0.0079	44.01	304.20	73.76	0.22500	-1.640
CH_4	0.4562	16.04	190.60	46.00	0.00800	-5.200
C_2H_6	0.0609	30.07	305.40	48.84	0.09800	-5.790
C_3H_8	0.0443	44.10	369.80	42.46	0.15200	-6.350
C_4H_{10}	0.0313	58.12	420.46	37.58	0.18830	-6.490
C_5H_{12}	0.0236	72.15	465.87	33.78	0.24130	-5.120
C_6H_{14}	0.0210	86.18	507.40	29.69	0.29600	1.390
PC-1	0.1491	134.58	639.30	27.14	0.18850	-0.340
PC-2	0.0969	207.11	745.83	22.05	0.29640	-0.940
PC-3	0.0668	300.45	869.23	18.16	0.43970	-1.850
PC-4	0.0394	509.87	1090.03	14.44	0.69340	-3.970

Table 7C.10b : BIPs for PR EOS model from PnA characterization for oil 10 in Table 7.3												
	N_2	CO_2	CH_4	C_2H_6	C_3H_8	C_4H_{10}	C_5H_{12}	C_6H_{14}	PC-1	PC-2	PC-3	PC-4
N_2	0.0000											
CO_2	0.0000	0.0000										
CH_4	0.1000	0.1000	0.0000									
C_2H_6	0.1000	0.1450	0.0420	0.0000								
C_3H_8	0.1000	0.1797	0.0420	0.0400	0.0000							
C_4H_{10}	0.1000	0.1587	0.0420	0.0400	0.0300	0.0000						
C_5H_{12}	0.1000	0.1374	0.0420	0.0400	0.0300	0.0116	0.0000					
C_6H_{14}	0.1000	0.1258	0.0420	0.0400	0.0300	0.0155	0.0058	0.0000				
PC-1	0.1300	0.0417	0.0518	0.0416	0.0328	0.0418	0.0275	0.0000	0.0000			
PC-2	0.1300	0.0886	0.0563	0.0422	0.0360	0.0556	0.0461	0.0000	0.0000	0.0000		
PC-3	0.1300	0.1183	0.0626	0.0429	0.0431	0.0663	0.0642	0.0000	0.0000	0.0000	0.0000	
PC-4	0.1300	0.1350	0.0761	0.0446	0.0615	0.0769	0.0854	0.0000	0.0000	0.0000	0.0000	0.0000

Table 7C.11a : PR EOS model from PnA characterization for oil 11 in Table 7.3 Saturation pressure (bubble point) for this fluid is 22.10 bars at 344.26 K.						
Components	Z	MW (g/mol)	T_C (K)	P_C (bars)	ω	C_{PEN} (CC/Mol)
N_2	0.0034	28.01	126.20	33.94	0.04000	-4.230
CO_2	0.0025	44.01	304.20	73.76	0.22500	-1.640
CH_4	0.0407	16.04	190.60	46.00	0.00800	-5.200
C_2H_6	0.0311	30.07	305.40	48.84	0.09800	-5.790
C_3H_8	0.0488	44.10	369.80	42.46	0.15200	-6.350
C_4H_{10}	0.0567	58.12	425.20	38.00	0.19300	-6.490
C_5H_{12}	0.0551	72.15	469.60	33.74	0.25100	-5.120
C_6H_{14}	0.0551	86.18	507.40	29.69	0.29600	1.390
PC-1	0.2821	142.71	643.85	28.16	0.22130	-20.810
PC-2	0.1915	210.24	754.33	23.30	0.34800	-29.460
PC-3	0.1410	285.55	869.48	20.03	0.49320	-39.510
PC-4	0.0920	437.58	1057.62	16.96	0.72540	-56.770

Table 7C.11b : BIPs for PR EOS model from PnA characterization for oil 11 in Table 7.3												
	N_2	CO_2	CH_4	C_2H_6	C_3H_8	C_4H_{10}	C_5H_{12}	C_6H_{14}	PC-1	PC-2	PC-3	PC-4
N_2	0.0000											
CO_2	0.0000	0.0000										
CH_4	0.1000	0.1000	0.0000									
C_2H_6	0.1000	0.1450	0.0420	0.0000								
C_3H_8	0.1000	0.1566	0.0420	0.0400	0.0000							
C_4H_{10}	0.1000	0.1416	0.0420	0.0400	0.0300	0.0000						
C_5H_{12}	0.1000	0.1266	0.0420	0.0400	0.0300	0.0116	0.0000					
C_6H_{14}	0.1000	0.1186	0.0420	0.0400	0.0300	0.0155	0.0058	0.0000				
PC-1	0.1300	0.0694	0.0518	0.0416	0.0328	0.0418	0.0275	0.0000	0.0000			
PC-2	0.1300	0.1115	0.0563	0.0422	0.0360	0.0556	0.0461	0.0000	0.0000	0.0000		
PC-3	0.1300	0.1291	0.0617	0.0428	0.0419	0.0652	0.0620	0.0000	0.0000	0.0000	0.0000	
PC-4	0.1300	0.1376	0.0716	0.0440	0.0557	0.0744	0.0800	0.0000	0.0000	0.0000	0.0000	0.0000

Table 7C.12a : PR EOS model from PnA characterization for oil 12 in Table 7.3
Saturation pressure (bubble point) for this fluid is 142.00 bars at 394.00 K.

Components	Z	MW (g/mol)	T_C (K)	P_C (bars)	ω	C_{PEN} (CC/Mol)
N_2	0.0036	28.01	126.20	33.94	0.04000	-4.230
CO_2	0.0299	44.01	304.20	73.76	0.22500	-1.640
CH_4	0.2907	16.04	190.60	46.00	0.00800	-5.200
C_2H_6	0.0716	30.07	305.40	48.84	0.09800	-5.790
C_3H_8	0.0658	44.10	369.80	42.46	0.15200	-6.350
C_4H_{10}	0.0608	58.12	420.01	37.54	0.18780	-6.490
C_5H_{12}	0.0514	72.15	465.53	33.78	0.24040	-5.120
C_6H_{14}	0.0410	86.18	507.40	29.69	0.29600	1.390
PC-1	0.1552	128.84	616.91	28.14	0.15290	-2.930
PC-2	0.1071	186.78	730.04	22.27	0.25210	-8.270
PC-3	0.0764	261.80	825.88	18.87	0.34810	-15.470
PC-4	0.0466	429.35	1024.47	14.72	0.55130	-34.160

Table 7C.12b : BIPs for PR EOS model from PnA characterization for oil 12 in Table 7.3

	N_2	CO_2	CH_4	C_2H_6	C_3H_8	C_4H_{10}	C_5H_{12}	C_6H_{14}	PC-1	PC-2	PC-3	PC-4
N_2	0.0000											
CO_2	0.0000	0.0000										
CH_4	0.1000	0.1000	0.0000									
C_2H_6	0.1000	0.1450	0.0420	0.0000								
C_3H_8	0.1000	0.2120	0.0420	0.0400	0.0000							
C_4H_{10}	0.1000	0.1837	0.0420	0.0400	0.0300	0.0000						
C_5H_{12}	0.1000	0.1546	0.0420	0.0400	0.0300	0.0116	0.0000					
C_6H_{14}	0.1000	0.1383	0.0420	0.0400	0.0300	0.0155	0.0058	0.0000				
PC-1	0.1300	0.0294	0.0509	0.0415	0.0324	0.0380	0.0231	0.0000	0.0000			
PC-2	0.1300	0.0814	0.0554	0.0420	0.0353	0.0534	0.0428	0.0000	0.0000	0.0000		
PC-3	0.1300	0.1091	0.0599	0.0426	0.0398	0.0625	0.0574	0.0000	0.0000	0.0000	0.0000	
PC-4	0.1300	0.1314	0.0707	0.0439	0.0544	0.0738	0.0788	0.0000	0.0000	0.0000	0.0000	0.0000

Table 7C.13a : PR EOS model from PnA characterization for oil 13 in Table 7.3
Saturation pressure (bubble point) for this fluid is 328.50 bars at 444.26 K.

Components	Z	MW (g/mol)	T_C (K)	P_C (bars)	ω	C_{PEN} (CC/Mol)
N_2	0.0025	28.01	126.20	33.94	0.04000	
CO_2	0.0360	44.01	304.20	73.76	0.22500	
CH_4	0.5686	16.04	190.60	46.00	0.00800	
C_2H_6	0.0937	30.07	305.40	48.84	0.09800	
C_3H_8	0.0548	44.10	369.80	42.46	0.15200	
C_4H_{10}	0.0407	58.12	419.07	37.45	0.18690	
C_5H_{12}	0.0259	72.15	465.34	33.79	0.23990	
C_6H_{14}	0.0126	86.00	507.40	29.69	0.29600	
PC-1	0.0659	114.86	590.34	29.83	0.13250	
PC-2	0.0471	160.74	687.18	24.17	0.21150	
PC-3	0.0332	227.97	788.10	20.00	0.30880	
PC-4	0.0191	395.73	990.98	15.15	0.51800	

Table 7C.13b : BIPs for PR EOS model from PnA characterization for oil 13 in Table 7.3

	N_2	CO_2	CH_4	C_2H_6	C_3H_8	C_4H_{10}	C_5H_{12}	C_6H_{14}	PC-1	PC-2	PC-3	PC-4
N_2	0.0000											
CO_2	0.0000	0.0000										
CH_4	0.1000	0.1000	0.0000									
C_2H_6	0.1000	0.1450	0.0420	0.0000								
C_3H_8	0.1000	0.2968	0.0420	0.0400	0.0000							
C_4H_{10}	0.1000	0.2515	0.0420	0.0400	0.0300	0.0000						
C_5H_{12}	0.1000	0.2041	0.0420	0.0400	0.0300	0.0116	0.0000					
C_6H_{14}	0.1000	0.1768	0.0420	0.0400	0.0300	0.0155	0.0058	0.0000				
PC-1	0.1300	0.0166	0.0500	0.0414	0.0320	0.0337	0.0186	0.0000	0.0000			
PC-2	0.1300	0.0637	0.0536	0.0418	0.0339	0.0482	0.0356	0.0000	0.0000	0.0000		
PC-3	0.1300	0.1003	0.0581	0.0424	0.0378	0.0594	0.0521	0.0000	0.0000	0.0000	0.0000	
PC-4	0.1300	0.1296	0.0689	0.0437	0.0519	0.0725	0.0761	0.0000	0.0000	0.0000	0.0000	0.0000

Table 7C.14a : PR EOS model from PnA characterization for oil 14 in Table 7.3
Saturation pressure (bubble point) for this fluid is 327.81 bars at 366.48 K.

Components	Z	MW (g/mol)	T_C (K)	P_C (bars)	ω	C_{PEN} (CC/Mol)
N_2	0.0058	28.01	126.20	33.94	0.04000	
CO_2	0.0032	44.01	304.20	73.76	0.22500	
CH_4	0.5450	16.04	190.60	46.00	0.00800	
C_2H_6	0.0809	30.07	305.40	48.84	0.09800	
C_3H_8	0.0582	44.10	369.80	42.46	0.15200	
C_4H_{10}	0.0295	58.12	420.68	37.60	0.18850	
C_5H_{12}	0.0259	72.15	466.26	33.78	0.24230	
C_6H_{14}	0.0239	86.00	507.40	29.69	0.29600	
PC-1	0.0939	126.84	615.48	28.71	0.17010	
PC-2	0.0640	186.24	727.54	22.99	0.28040	
PC-3	0.0443	269.16	838.71	19.20	0.40780	
PC-4	0.0255	467.26	1056.28	15.11	0.66160	

Table 7C.14b : BIPs for PR EOS model from PnA characterization for oil 14 in Table 7.3

	N_2	CO_2	CH_4	C_2H_6	C_3H_8	C_4H_{10}	C_5H_{12}	C_6H_{14}	PC-1	PC-2	PC-3	PC-4
N_2	0.0000											
CO_2	0.0000	0.0000										
CH_4	0.1000	0.1000	0.0000									
C_2H_6	0.1000	0.1450	0.0420	0.0000								
C_3H_8	0.1000	0.1778	0.0420	0.0400	0.0000							
C_4H_{10}	0.1000	0.1573	0.0420	0.0400	0.0300	0.0000						
C_5H_{12}	0.1000	0.1365	0.0420	0.0400	0.0300	0.0116	0.0000					
C_6H_{14}	0.1000	0.1252	0.0420	0.0400	0.0300	0.0155	0.0058	0.0000				
PC-1	0.1300	0.0294	0.0509	0.0415	0.0324	0.0380	0.0231	0.0000	0.0000			
PC-2	0.1300	0.0814	0.0554	0.0420	0.0353	0.0534	0.0428	0.0000	0.0000	0.0000		
PC-3	0.1300	0.1126	0.0608	0.0427	0.0408	0.0639	0.0598	0.0000	0.0000	0.0000	0.0000	
PC-4	0.1300	0.1335	0.0734	0.0442	0.0581	0.0755	0.0823	0.0000	0.0000	0.0000	0.0000	0.0000

Table 7C.15a : PR EOS model from PnA characterization for oil 15 in Table 7.3
Saturation pressure (bubble point) for this fluid is 319.53 bars at 380.37 K.

Components	Z	MW (g/mol)	T_C (K)	P_C (bars)	ω	C_{PEN} (CC/Mol)
N_2	0.0000	28.01	126.20	33.94	0.04000	
CO_2	0.0000	44.01	304.20	73.76	0.22500	
CH_4	0.5039	16.04	190.60	46.00	0.00800	
C_2H_6	0.0882	30.07	305.40	48.84	0.09800	
C_3H_8	0.0591	44.10	369.80	42.46	0.15200	
C_4H_{10}	0.0417	58.12	421.55	37.68	0.18940	
C_5H_{12}	0.0223	72.15	465.72	33.78	0.24090	
C_6H_{14}	0.0136	86.18	507.40	29.69	0.29600	
PC-1	0.1201	140.90	636.43	27.04	0.18530	
PC-2	0.0748	226.19	758.77	21.20	0.31220	
PC-3	0.0492	344.09	902.17	16.93	0.48830	
PC-4	0.0271	625.69	1153.82	13.30	0.78180	

Table 7C.15b : BIPs for PR EOS model from PnA characterization for oil 15 in Table 7.3

	N_2	CO_2	CH_4	C_2H_6	C_3H_8	C_4H_{10}	C_5H_{12}	C_6H_{14}	PC-1	PC-2	PC-3	PC-4
N_2	0.0000											
CO_2	0.0000	0.0000										
CH_4	0.1000	0.1000	0.0000									
C_2H_6	0.1000	0.1450	0.0420	0.0000								
C_3H_8	0.1000	0.1940	0.0420	0.0400	0.0000							
C_4H_{10}	0.1000	0.1697	0.0420	0.0400	0.0300	0.0000						
C_5H_{12}	0.1000	0.1449	0.0420	0.0400	0.0300	0.0116	0.0000					
C_6H_{14}	0.1000	0.1311	0.0420	0.0400	0.0300	0.0155	0.0058	0.0000				
PC-1	0.1300	0.0417	0.0518	0.0416	0.0328	0.0418	0.0275	0.0000	0.0000			
PC-2	0.1300	0.0949	0.0572	0.0423	0.0369	0.0576	0.0492	0.0000	0.0000	0.0000		
PC-3	0.1300	0.1244	0.0653	0.0433	0.0468	0.0693	0.0698	0.0000	0.0000	0.0000	0.0000	
PC-4	0.1300	0.1375	0.0833	0.0455	0.0683	0.0797	0.0920	0.0000	0.0000	0.0000	0.0000	0.0000

Table 7C.16a : PR EOS model from PnA characterization for oil 16 in Table 7.3
Saturation pressure (bubble point) for this fluid is 314.71 bars at 423.71 K.

Components	Z	MW (g/mol)	T_C (K)	P_C (bars)	ω	C_{PEN} (CC/Mol)
N_2	0.0046	28.01	126.20	33.94	0.04000	
CO_2	0.0134	44.01	304.20	73.76	0.22500	
CH_4	0.4901	16.04	190.60	46.00	0.00800	
C_2H_6	0.0704	30.07	305.40	48.84	0.09800	
C_3H_8	0.0493	44.10	369.80	42.46	0.15200	
C_4H_{10}	0.0347	58.12	420.48	37.58	0.18830	
C_5H_{12}	0.0268	72.15	465.62	33.78	0.24060	
C_6H_{14}	0.0334	86.00	507.40	29.69	0.29600	
PC-1	0.1195	145.09	660.18	25.59	0.20080	
PC-2	0.0769	225.64	760.33	21.00	0.30340	
PC-3	0.0517	335.46	891.13	17.02	0.45670	
PC-4	0.0292	593.77	1140.82	13.23	0.73750	

Table 7C.16b : BIPs for PR EOS model from PnA characterization for oil 16 in Table 7.3

	N_2	CO_2	CH_4	C_2H_6	C_3H_8	C_4H_{10}	C_5H_{12}	C_6H_{14}	PC-1	PC-2	PC-3	PC-4
N_2	0.0000											
CO_2	0.0000	0.0000										
CH_4	0.1000	0.1000	0.0000									
C_2H_6	0.1000	0.1450	0.0420	0.0000								
C_3H_8	0.1000	0.2586	0.0420	0.0400	0.0000							
C_4H_{10}	0.1000	0.2207	0.0420	0.0400	0.0300	0.0000						
C_5H_{12}	0.1000	0.1813	0.0420	0.0400	0.0300	0.0116	0.0000					
C_6H_{14}	0.1000	0.1588	0.0420	0.0400	0.0300	0.0155	0.0058	0.0000				
PC-1	0.1300	0.0532	0.0527	0.0417	0.0334	0.0452	0.0317	0.0000	0.0000			
PC-2	0.1300	0.0949	0.0572	0.0423	0.0369	0.0576	0.0492	0.0000	0.0000	0.0000		
PC-3	0.1300	0.1226	0.0644	0.0431	0.0455	0.0684	0.0680	0.0000	0.0000	0.0000	0.0000	
PC-4	0.1300	0.1371	0.0815	0.0452	0.0669	0.0791	0.0906	0.0000	0.0000	0.0000	0.0000	0.0000

Table 7C.17a : PR EOS model from PnA characterization for oil 17 in Table 7.3
Saturation pressure (bubble point) for this fluid is 210.00 bars at 376.15 K.

Components	Z	MW (g/mol)	T_C (K)	P_C (bars)	ω	C_{PEN} (CC/Mol)
N_2	0.0092	28.01	126.20	33.94	0.04000	
CO_2	0.0032	44.01	304.20	73.76	0.22500	
CH_4	0.4125	16.04	190.60	46.00	0.00800	
C_2H_6	0.0868	30.07	305.40	48.84	0.09800	
C_3H_8	0.0727	44.10	369.80	42.46	0.15200	
C_4H_{10}	0.0490	58.12	420.42	37.58	0.18820	
C_5H_{12}	0.0289	72.15	465.24	33.79	0.23960	
C_6H_{14}	0.0429	86.18	507.40	29.69	0.29600	
PC-1	0.1160	122.65	618.55	28.70	0.17000	
PC-2	0.0826	172.17	711.71	23.87	0.25830	
PC-3	0.0597	238.35	793.15	20.82	0.34500	
PC-4	0.0365	389.37	988.75	16.39	0.56110	

Table 7C.17b : BIPs for PR EOS model from PnA characterization for oil 17 in Table 7.3

	N_2	CO_2	CH_4	C_2H_6	C_3H_8	C_4H_{10}	C_5H_{12}	C_6H_{14}	PC-1	PC-2	PC-3	PC-4
N_2	0.0000											
CO_2	0.0000	0.0000										
CH_4	0.1000	0.1000	0.0000									
C_2H_6	0.1000	0.1450	0.0420	0.0000								
C_3H_8	0.1000	0.1888	0.0420	0.0400	0.0000							
C_4H_{10}	0.1000	0.1657	0.0420	0.0400	0.0300	0.0000						
C_5H_{12}	0.1000	0.1422	0.0420	0.0400	0.0300	0.0116	0.0000					
C_6H_{14}	0.1000	0.1291	0.0420	0.0400	0.0300	0.0155	0.0058	0.0000				
PC-1	0.1300	0.0294	0.0509	0.0415	0.0324	0.0380	0.0231	0.0000	0.0000			
PC-2	0.1300	0.0731	0.0545	0.0419	0.0346	0.0510	0.0393	0.0000	0.0000	0.0000		
PC-3	0.1300	0.1003	0.0581	0.0424	0.0378	0.0594	0.0521	0.0000	0.0000	0.0000	0.0000	
PC-4	0.1300	0.1285	0.0680	0.0436	0.0506	0.0718	0.0746	0.0000	0.0000	0.0000	0.0000	0.0000

Table 7C.18a : PR EOS model from PnA characterization for oil 18 in Table 7.3 Saturation pressure (bubble point) for this fluid is 204.80 bars at 375.15 K.						
Components	Z	MW (g/mol)	T_C (K)	P_C (bars)	ω	C_{PEN} (CC/Mol)
N_2	0.0098	28.01	126.20	33.94	0.04000	0.0098
CO_2	0.0037	44.01	304.20	73.76	0.22500	0.0037
CH_4	0.4179	16.04	190.60	46.00	0.00800	0.4179
C_2H_6	0.0887	30.07	305.40	48.84	0.09800	0.0887
C_3H_8	0.0711	44.10	369.80	42.46	0.15200	0.0711
C_4H_{10}	0.0522	58.12	420.39	37.57	0.18820	0.0522
C_5H_{12}	0.0288	72.15	465.61	33.78	0.24060	0.0288
C_6H_{14}	0.0430	86.18	507.40	29.69	0.29600	0.0430
PC-1	0.1143	127.07	616.92	28.15	0.15330	0.1143
PC-2	0.0798	181.94	709.22	23.20	0.23290	0.0798
PC-3	0.0567	256.15	825.91	18.89	0.34890	0.0567
PC-4	0.0340	427.75	1024.54	14.74	0.55260	0.0340

Table 7C.18b : BIPs for PR EOS model from PnA characterization for oil 18 in Table 7.3											
	N_2	CO_2	CH_4	C_2H_6	C_3H_8	C_4H_{10}	C_5H_{12}	C_6H_{14}	PC-1	PC-2	PC-3	PC-4
N_2	0.0000											
CO_2	0.0000	0.0000										
CH_4	0.1000	0.1000	0.0000									
C_2H_6	0.1000	0.1450	0.0420	0.0000								
C_3H_8	0.1000	0.1876	0.0420	0.0400	0.0000							
C_4H_{10}	0.1000	0.1648	0.0420	0.0400	0.0300	0.0000						
C_5H_{12}	0.1000	0.1415	0.0420	0.0400	0.0300	0.0116	0.0000					
C_6H_{14}	0.1000	0.1287	0.0420	0.0400	0.0300	0.0155	0.0058	0.0000				
PC-1	0.1300	0.0294	0.0509	0.0415	0.0324	0.0380	0.0231	0.0000	0.0000			
PC-2	0.1300	0.0731	0.0545	0.0419	0.0346	0.0510	0.0393	0.0000	0.0000	0.0000		
PC-3	0.1300	0.1091	0.0599	0.0426	0.0398	0.0625	0.0574	0.0000	0.0000	0.0000	0.0000	
PC-4	0.1300	0.1314	0.0707	0.0439	0.0544	0.0738	0.0788	0.0000	0.0000	0.0000	0.0000	0.0000

Table 7C.19a : PR EOS model from PnA characterization for oil 19 in Table 7.3 Saturation pressure (bubble point) for this fluid is 339.90 bars at 379.15 K.						
Components	Z	MW (g/mol)	T_C (K)	P_C (bars)	ω	C_{PEN} (CC/Mol)
N_2	0.0069	28.01	126.20	33.94	0.04000	
CO_2	0.0038	44.01	304.20	73.76	0.22500	
CH_4	0.5941	16.04	190.60	46.00	0.00800	
C_2H_6	0.0815	30.07	305.40	48.84	0.09800	
C_3H_8	0.0499	44.10	369.80	42.46	0.15200	
C_4H_{10}	0.0371	58.12	419.90	37.53	0.18770	
C_5H_{12}	0.0197	72.15	465.07	33.79	0.23920	
C_6H_{14}	0.0317	86.18	507.40	29.69	0.29600	
PC-1	0.0692	120.91	617.61	28.63	0.16780	
PC-2	0.0498	168.21	688.55	24.78	0.23320	
PC-3	0.0355	236.06	790.73	20.72	0.34050	
PC-4	0.0208	401.52	998.44	16.01	0.57120	

Table 7C.19b : BIPs for PR EOS model from PnA characterization for oil 19 in Table 7.3												
	N_2	CO_2	CH_4	C_2H_6	C_3H_8	C_4H_{10}	C_5H_{12}	C_6H_{14}	PC-1	PC-2	PC-3	PC-4
N_2	0.0000											
CO_2	0.0000	0.0000										
CH_4	0.1000	0.1000	0.0000									
C_2H_6	0.1000	0.1450	0.0420	0.0000								
C_3H_8	0.1000	0.1925	0.0420	0.0400	0.0000							
C_4H_{10}	0.1000	0.1685	0.0420	0.0400	0.0300	0.0000						
C_5H_{12}	0.1000	0.1441	0.0420	0.0400	0.0300	0.0116	0.0000					
C_6H_{14}	0.1000	0.1305	0.0420	0.0400	0.0300	0.0155	0.0058	0.0000				
PC-1	0.1300	0.0294	0.0509	0.0415	0.0324	0.0380	0.0231	0.0000	0.0000			
PC-2	0.1300	0.0637	0.0536	0.0418	0.0339	0.0482	0.0356	0.0000	0.0000	0.0000		
PC-3	0.1300	0.1003	0.0581	0.0424	0.0378	0.0594	0.0521	0.0000	0.0000	0.0000	0.0000	
PC-4	0.1300	0.1296	0.0689	0.0437	0.0519	0.0725	0.0761	0.0000	0.0000	0.0000	0.0000	0.0000

Components	Z	MW (g/mol)	T_C (K)	P_C (bars)	ω	C_{PEN} (CC/Mol)
N_2	0.0000	28.01	126.20	33.94	0.04000	
CO_2	0.0000	44.01	304.20	73.76	0.22500	
CH_4	0.4270	16.04	190.60	46.00	0.00800	
C_2H_6	0.1250	30.07	305.40	48.84	0.09800	
C_3H_8	0.1020	44.10	369.80	42.46	0.15200	
C_4H_{10}	0.0620	58.12	425.20	38.00	0.19300	
C_5H_{12}	0.0380	72.15	469.60	33.74	0.25100	
C_6H_{14}	0.0330	86.18	507.40	29.69	0.29600	
PC-1	0.0841	120.96	619.70	29.19	0.18470	
PC-2	0.0604	168.39	691.36	25.43	0.25670	
PC-3	0.0431	236.03	796.10	21.49	0.37480	
PC-4	0.0254	400.07	1013.67	16.95	0.62870	

Table 7C.20a : PR EOS model from PnA characterization for oil 20 in Table 7.3
Saturation pressure (bubble point) for this fluid is 191.30 bars at 333.15 K.

Table 7C.20b : BIPs for PR EOS model from PnA characterization for oil 20 in Table 7.3

	N_2	CO_2	CH_4	C_2H_6	C_3H_8	C_4H_{10}	C_5H_{12}	C_6H_{14}	PC-1	PC-2	PC-3	PC-4
N_2	0.0000											
CO_2	0.0000	0.0000										
CH_4	0.1000	0.1000	0.0000									
C_2H_6	0.1000	0.1450	0.0420	0.0000								
C_3H_8	0.1000	0.1482	0.0420	0.0400	0.0000							
C_4H_{10}	0.1000	0.1356	0.0420	0.0400	0.0300	0.0000						
C_5H_{12}	0.1000	0.1232	0.0420	0.0400	0.0300	0.0116	0.0000					
C_6H_{14}	0.1000	0.1168	0.0420	0.0400	0.0300	0.0155	0.0058	0.0000				
PC-1	0.1300	0.0294	0.0509	0.0415	0.0324	0.0380	0.0231	0.0000	0.0000			
PC-2	0.1300	0.0637	0.0536	0.0418	0.0339	0.0482	0.0356	0.0000	0.0000	0.0000		
PC-3	0.1300	0.1003	0.0581	0.0424	0.0378	0.0594	0.0521	0.0000	0.0000	0.0000	0.0000	
PC-4	0.1300	0.1296	0.0689	0.0437	0.0519	0.0725	0.0761	0.0000	0.0000	0.0000	0.0000	0.0000

Table 7C.1a : PR EOS model from PnA characterization for oil 1 in Table 7.4
Saturation pressure (bubble point) for this fluid is 117.54 bars at 299.81 K.

Components	Z	MW (g/mol)	T_C (K)	P_C (bars)	ω	C_{PEN} (CC/Mol)
N_2	0.0003	28.01	126.20	33.94	0.04000	-4.230
CO_2	0.0002	44.01	304.20	73.76	0.22500	-1.640
CH_4	0.3825	16.04	190.60	46.00	0.00800	-5.200
C_2H_6	0.0086	30.07	305.40	48.84	0.09800	-5.790
C_3H_8	0.0036	44.10	369.80	42.46	0.15200	-6.350
C_4H_{10}	0.0018	58.12	425.20	38.00	0.19300	-6.490
C_5H_{12}	0.0006	72.15	469.60	33.74	0.25100	-5.120
C_6H_{14}	0.0020	86.18	507.40	29.69	0.29600	1.390
PC-1	0.2748	201.93	734.23	20.65	0.23870	13.200
PC-2	0.1560	355.66	897.81	15.03	0.41480	22.180
PC-3	0.1059	523.98	1036.19	12.37	0.56970	31.110
PC-4	0.0636	872.32	1263.45	10.23	0.76240	45.860

Table 7C.1b : BIPs for PR EOS model from PnA characterization for oil 1 in Table 7.4

	N_2	CO_2	CH_4	C_2H_6	C_3H_8	C_4H_{10}	C_5H_{12}	C_6H_{14}	PC-1	PC-2	PC-3	PC-4
N_2	0.0000											
CO_2	0.0000	0.0000										
CH_4	0.1000	0.1000	0.0000									
C_2H_6	0.1000	0.1450	0.0420	0.0000								
C_3H_8	0.1000	0.1313	0.0420	0.0400	0.0000							
C_4H_{10}	0.1000	0.1249	0.0420	0.0400	0.0300	0.0000						
C_5H_{12}	0.1000	0.1192	0.0420	0.0400	0.0300	0.0116	0.0000					
C_6H_{14}	0.1000	0.1166	0.0420	0.0400	0.0300	0.0155	0.0058	0.0000				
PC-1	0.1300	0.0886	0.0563	0.0422	0.0360	0.0556	0.0461	0.0000	0.0000			
PC-2	0.1300	0.1259	0.0662	0.0434	0.0480	0.0702	0.0715	0.0000	0.0000	0.0000		
PC-3	0.1300	0.1355	0.0770	0.0447	0.0625	0.0773	0.0864	0.0000	0.0000	0.0000	0.0000	
PC-4	0.1300	0.1397	0.0995	0.0474	0.0738	0.0835	0.1016	0.0000	0.0000	0.0000	0.0000	0.0000

Table 7C.2a : PR EOS model from PnA characterization for oil 2 in Table 7.4
Saturation pressure (bubble point) for this fluid is 227.20 bars at 347.15 K.

Components	Z	MW (g/mol)	T_C (K)	P_C (bars)	ω	C_{PEN} (CC/Mol)
N_2	0.0049	28.01	126.20	33.94	0.04000	-4.230
CO_2	0.0031	44.01	304.20	73.76	0.22500	-1.640
CH_4	0.4401	16.04	190.60	46.00	0.00800	-5.200
C_2H_6	0.0384	30.07	305.40	48.84	0.09800	-5.790
C_3H_8	0.0112	44.10	369.80	42.46	0.15200	-6.350
C_4H_{10}	0.0133	58.12	417.36	37.30	0.18520	-6.490
C_5H_{12}	0.0104	72.15	463.50	33.81	0.23510	-5.120
C_6H_{14}	0.0101	86.00	507.40	29.69	0.29600	1.390
PC-1	0.2019	141.88	637.91	27.30	0.19350	-2.470
PC-2	0.1260	227.35	779.98	20.88	0.34750	-7.450
PC-3	0.0874	327.83	894.67	17.64	0.49060	-13.530
PC-4	0.0530	540.80	1101.11	14.42	0.73990	-26.890

Table 7C.2b : BIPs for PR EOS model from PnA characterization for oil 2 in Table 7.4

	N_2	CO_2	CH_4	C_2H_6	C_3H_8	C_4H_{10}	C_5H_{12}	C_6H_{14}	PC-1	PC-2	PC-3	PC-4
N_2	0.0000											
CO_2	0.0000	0.0000										
CH_4	0.1000	0.1000	0.0000									
C_2H_6	0.1000	0.1450	0.0420	0.0000								
C_3H_8	0.1000	0.1591	0.0420	0.0400	0.0000							
C_4H_{10}	0.1000	0.1433	0.0420	0.0400	0.0300	0.0000						
C_5H_{12}	0.1000	0.1277	0.0420	0.0400	0.0300	0.0116	0.0000					
C_6H_{14}	0.1000	0.1193	0.0420	0.0400	0.0300	0.0155	0.0058	0.0000				
PC-1	0.1300	0.0417	0.0518	0.0416	0.0328	0.0418	0.0275	0.0000	0.0000			
PC-2	0.1300	0.1003	0.0581	0.0424	0.0378	0.0594	0.0521	0.0000	0.0000	0.0000		
PC-3	0.1300	0.1226	0.0644	0.0431	0.0455	0.0684	0.0680	0.0000	0.0000	0.0000	0.0000	
PC-4	0.1300	0.1358	0.0779	0.0448	0.0635	0.0777	0.0873	0.0000	0.0000	0.0000	0.0000	0.0000

| Table 7C.3a : PR EOS model from PnA characterization for oil 3 in Table 7.4 |||||||
| Saturation pressure (bubble point) for this fluid is 107.30 bars at 305.45 K. |||||||
Components	Z	MW (g/mol)	T_C (K)	P_C (bars)	ω	C_{PEN} (CC/Mol)
N_2	0.0105	28.01	126.20	33.94	0.04000	-4.230
CO_2	0.0006	44.01	304.20	73.76	0.22500	-1.640
CH_4	0.3050	16.04	190.60	46.00	0.00800	-5.200
C_2H_6	0.0003	30.07	305.40	48.84	0.09800	-5.790
C_3H_8	0.0002	44.10	369.80	42.46	0.15200	-6.350
C_4H_{10}	0.0005	58.12	425.20	38.00	0.19300	-6.490
C_5H_{12}	0.0008	72.15	469.60	33.74	0.25100	-5.120
C_6H_{14}	0.0033	86.00	507.40	29.69	0.29600	1.390
PC-1	0.3105	245.95	778.03	19.01	0.30990	-2.300
PC-2	0.1753	435.53	940.26	14.21	0.51870	-6.820
PC-3	0.1200	636.50	1080.81	11.97	0.69550	-13.600
PC-4	0.0730	1046.09	1285.03	10.41	0.85940	-28.400

Table 7C.3b : BIPs for PR EOS model from PnA characterization for oil 3 in Table 7.4												
	N_2	CO_2	CH_4	C_2H_6	C_3H_8	C_4H_{10}	C_5H_{12}	C_6H_{14}	PC-1	PC-2	PC-3	PC-4
N_2	0.0000											
CO_2	0.0000	0.0000										
CH_4	0.1000	0.1000	0.0000									
C_2H_6	0.1000	0.1450	0.0420	0.0000								
C_3H_8	0.1000	0.1332	0.0420	0.0400	0.0000							
C_4H_{10}	0.1000	0.1260	0.0420	0.0400	0.0300	0.0000						
C_5H_{12}	0.1000	0.1192	0.0420	0.0400	0.0300	0.0116	0.0000					
C_6H_{14}	0.1000	0.1160	0.0420	0.0400	0.0300	0.0155	0.0058	0.0000				
PC-1	0.1300	0.1050	0.0590	0.0425	0.0387	0.0610	0.0548	0.0000	0.0000			
PC-2	0.1300	0.1314	0.0707	0.0439	0.0544	0.0738	0.0788	0.0000	0.0000	0.0000		
PC-3	0.1300	0.1377	0.0842	0.0456	0.0690	0.0800	0.0927	0.0000	0.0000	0.0000	0.0000	
PC-4	0.1300	0.1403	0.1103	0.0488	0.0742	0.0849	0.1057	0.0000	0.0000	0.0000	0.0000	0.0000

Table 7C.4a : PR EOS model from PnA characterization for oil 4 in Table 7.4 Saturation pressure (bubble point) for 31.7% CO_2, 34.3% butane, and 34% oil mixture is 56.64 bars at 347.67 K.						
Components	Z	MW (g/mol)	T_C (K)	P_C (bars)	ω	C_{PEN} (CC/Mol)
N_2						
CO_2						
CH_4						
C_2H_6						
C_3H_8						
C_4H_{10}						
C_5H_{12}						
C_6H_{14}						
PC-1	0.4270	282.77	827.18	17.09	0.30450	
PC-2	0.2592	465.87	1025.15	12.62	0.49400	
PC-3	0.1891	638.54	1168.25	10.93	0.61380	
PC-4	0.1247	968.53	1399.00	9.51	0.74290	

Table 7C.4b : BIPs for PR EOS model from PnA characterization for oil 4 in Table 7.4												
	N_2	CO_2	CH_4	C_2H_6	C_3H_8	C_4H_{10}	C_5H_{12}	C_6H_{14}	PC-1	PC-2	PC-3	PC-4
N_2	0.0000											
CO_2	0.0000	0.0000										
CH_4	0.1000	0.1000	0.0000									
C_2H_6	0.1000	0.1450	0.0420	0.0000								
C_3H_8	0.1000	0.1595	0.0420	0.0400	0.0000							
C_4H_{10}	0.1000	0.1437	0.0420	0.0400	0.0300	0.0000						
C_5H_{12}	0.1000	0.1279	0.0420	0.0400	0.0300	0.0116	0.0000					
C_6H_{14}	0.1000	0.1194	0.0420	0.0400	0.0300	0.0155	0.0058	0.0000				
PC-1	0.1300	0.1126	0.0608	0.0427	0.0408	0.0639	0.0598	0.0000	0.0000			
PC-2	0.1300	0.1335	0.0734	0.0442	0.0581	0.0755	0.0823	0.0000	0.0000	0.0000		
PC-3	0.1300	0.1377	0.0842	0.0456	0.0690	0.0800	0.0927	0.0000	0.0000	0.0000	0.0000	
PC-4	0.1300	0.1401	0.1049	0.0481	0.0741	0.0842	0.1038	0.0000	0.0000	0.0000	0.0000	0.0000

Table 7C.5a : PR EOS model from PnA characterization for oil 5 in Table 7.4 Saturation pressure (bubble point) for 40.71% propane and 59.29% bitumen mixture is 10.82 bars at 333.15 K.						
Components	Z	MW (g/mol)	T_C (K)	P_C (bars)	ω	C_{PEN} (CC/Mol)
N_2						
CO_2						
CH_4						
C_2H_6						
C_3H_8						
C_4H_{10}						
C_5H_{12}						
C_6H_{14}						
PC-1	0.4001	345.52	917.92	14.34	0.34270	58.290
PC-2	0.2616	528.46	1105.49	11.22	0.48800	113.110
PC-3	0.1995	692.98	1258.72	9.83	0.58490	165.310
PC-4	0.1388	996.26	1490.02	8.67	0.67880	252.650

Table 7C.5b : BIPs for PR EOS model from PnA characterization for oil 5 in Table 7.4												
	N_2	CO_2	CH_4	C_2H_6	C_3H_8	C_4H_{10}	C_5H_{12}	C_6H_{14}	PC-1	PC-2	PC-3	PC-4
N_2	0.0000											
CO_2	0.0000	0.0000										
CH_4	0.1000	0.1000	0.0000									
C_2H_6	0.1000	0.1450	0.0420	0.0000								
C_3H_8	0.1000	0.1482	0.0420	0.0400	0.0000							
C_4H_{10}	0.1000	0.1356	0.0420	0.0400	0.0300	0.0000						
C_5H_{12}	0.1000	0.1232	0.0420	0.0400	0.0300	0.0116	0.0000					
C_6H_{14}	0.1000	0.1168	0.0420	0.0400	0.0300	0.0155	0.0058	0.0000				
PC-1	0.1300	0.1244	0.0653	0.0433	0.0468	0.0693	0.0698	0.0000	0.0000			
PC-2	0.1300	0.1355	0.0770	0.0447	0.0625	0.0773	0.0864	0.0000	0.0000	0.0000		
PC-3	0.1300	0.1384	0.0878	0.0460	0.0710	0.0810	0.0953	0.0000	0.0000	0.0000	0.0000	
PC-4	0.1300	0.1401	0.1067	0.0483	0.0741	0.0845	0.1044	0.0000	0.0000	0.0000	0.0000	0.0000

Table 7C.6a : PR EOS model from PnA characterization for oil 6 in Table 7.4
Saturation pressure (bubble point) for 21.83% methane and 78.17% bitumen mixture is 50.50 bars at 326.65 K.

Components	Z	MW (g/mol)	T_C (K)	P_C (bars)	ω	C_{PEN} (CC/Mol)
N_2						
CO_2						
CH_4						
C_2H_6						
C_3H_8						
C_4H_{10}						
C_5H_{12}						
C_6H_{14}						
PC-1	0.4001	330.22	865.14	14.20	0.30170	65.690
PC-2	0.2616	505.03	1001.44	10.98	0.42850	124.980
PC-3	0.1995	662.27	1113.86	9.40	0.52240	183.160
PC-4	0.1388	952.11	1268.28	8.15	0.61330	274.900

Table 7C.6b : BIPs for PR EOS model from PnA characterization for oil 6 in Table 7.4

	N_2	CO_2	CH_4	C_2H_6	C_3H_8	C_4H_{10}	C_5H_{12}	C_6H_{14}	PC-1	PC-2	PC-3	PC-4
N_2	0.0000											
CO_2	0.0000	0.0000										
CH_4	0.1000	0.1000	0.0000									
C_2H_6	0.1000	0.1450	0.0420	0.0000								
C_3H_8	0.1000	0.1439	0.0420	0.0400	0.0000							
C_4H_{10}	0.1000	0.1326	0.0420	0.0400	0.0300	0.0000						
C_5H_{12}	0.1000	0.1217	0.0420	0.0400	0.0300	0.0116	0.0000					
C_6H_{14}	0.1000	0.1161	0.0420	0.0400	0.0300	0.0155	0.0058	0.0000				
PC-1	0.1300	0.1226	0.0644	0.0431	0.0455	0.0684	0.0680	0.0000	0.0000			
PC-2	0.1300	0.1346	0.0752	0.0445	0.0604	0.0764	0.0844	0.0000	0.0000	0.0000		
PC-3	0.1300	0.1381	0.0860	0.0458	0.0701	0.0806	0.0940	0.0000	0.0000	0.0000	0.0000	
PC-4	0.1300	0.1400	0.1040	0.0480	0.0740	0.0841	0.1034	0.0000	0.0000	0.0000	0.0000	0.0000

| Table 7C.1a : PR EOS model from PnA characterization for oil 1 in Table 7.5 | | | | | | |
Saturation pressure (bubble point) for this fluid is 51.27 bars at 314.26 K.						
Components	Z	MW (g/mol)	T_C (K)	P_C (bars)	ω	C_{PEN} (CC/Mol)
N_2	0.0050	28.01	126.20	33.94	0.04000	0.0050
CO_2	0.0040	44.01	304.20	73.76	0.22500	0.0040
CH_4	0.1270	16.04	190.60	46.00	0.00800	0.1270
C_2H_6	0.0670	30.07	305.40	48.84	0.09800	0.0670
C_3H_8	0.0690	44.10	369.80	42.46	0.15200	0.0690
C_4H_{10}	0.0620	58.12	420.86	37.62	0.18870	0.0620
C_5H_{12}	0.0520	72.15	465.39	33.79	0.24000	0.0520
C_6H_{14}	0.0290	86.00	507.40	29.69	0.29600	0.0290
PC-1	0.2420	136.83	643.09	28.20	0.22266	0.2420
PC-2	0.1590	207.56	752.91	23.35	0.35009	0.1590
PC-3	0.1140	291.23	866.68	20.09	0.49613	0.1140
PC-4	0.0710	467.50	1082.97	16.67	0.76665	0.0710

Table 7C.1b : BIPs for PR EOS model from PnA characterization for oil 1 in Table 7.5												
	N_2	CO_2	CH_4	C_2H_6	C_3H_8	C_4H_{10}	C_5H_{12}	C_6H_{14}	PC-1	PC-2	PC-3	PC-4
N_2	0.0000											
CO_2	0.0000	0.0000										
CH_4	0.1000	0.1000	0.0000									
C_2H_6	0.1000	0.1450	0.0420	0.0000								
C_3H_8	0.1000	0.1370	0.0420	0.0400	0.0000							
C_4H_{10}	0.1000	0.1282	0.0420	0.0400	0.0300	0.0000						
C_5H_{12}	0.1000	0.1198	0.0420	0.0400	0.0300	0.0116	0.0000					
C_6H_{14}	0.1000	0.1157	0.0420	0.0400	0.0300	0.0155	0.0058	0.0000				
PC-1	0.1300	0.0417	0.0518	0.0416	0.0328	0.0418	0.0275	0.0000	0.0000			
PC-2	0.1300	0.0886	0.0563	0.0422	0.0360	0.0556	0.0461	0.0000	0.0000	0.0000		
PC-3	0.1300	0.1156	0.0617	0.0428	0.0419	0.0652	0.0620	0.0000	0.0000	0.0000	0.0000	
PC-4	0.1300	0.1335	0.0734	0.0442	0.0581	0.0755	0.0823	0.0000	0.0000	0.0000	0.0000	0.0000

Table 7C.2a : PR EOS model from PnA characterization for oil 2 in Table 7.5						
Saturation pressure (bubble point) for this fluid is 47.00 bars at 314.26 K.						
Components	Z	MW (g/mol)	T_C (K)	P_C (bars)	ω	C_{PEN} (CC/Mol)
N_2	0.0052	28.01	126.20	33.94	0.04000	
CO_2	0.0056	44.01	304.20	73.76	0.22500	
CH_4	0.1543	16.04	190.60	46.00	0.00800	
C_2H_6	0.0726	30.07	305.40	48.84	0.09800	
C_3H_8	0.0614	44.10	369.80	42.46	0.15200	
C_4H_{10}	0.0459	58.12	423.38	37.84	0.19120	
C_5H_{12}	0.0405	72.15	466.51	33.78	0.24290	
C_6H_{14}	0.0361	86.00	507.40	29.69	0.29600	
PC-1	0.2393	140.79	640.11	25.94	0.14960	
PC-2	0.1572	214.39	766.57	19.80	0.25200	
PC-3	0.1120	300.73	872.49	16.41	0.34880	
PC-4	0.0699	481.87	1070.39	12.74	0.52690	

Table 7C.2b : BIPs for PR EOS model from PnA characterization for oil 2 in Table 7.5												
	N_2	CO_2	CH_4	C_2H_6	C_3H_8	C_4H_{10}	C_5H_{12}	C_6H_{14}	PC-1	PC-2	PC-3	PC-4
N_2	0.0000											
CO_2	0.0000	0.0000										
CH_4	0.1000	0.1000	0.0000									
C_2H_6	0.1000	0.1450	0.0420	0.0000								
C_3H_8	0.1000	0.1370	0.0420	0.0400	0.0000							
C_4H_{10}	0.1000	0.1282	0.0420	0.0400	0.0300	0.0000						
C_5H_{12}	0.1000	0.1198	0.0420	0.0400	0.0300	0.0116	0.0000					
C_6H_{14}	0.1000	0.1157	0.0420	0.0400	0.0300	0.0155	0.0058	0.0000				
PC-1	0.1300	0.0417	0.0518	0.0416	0.0328	0.0418	0.0275	0.0000	0.0000			
PC-2	0.1300	0.0949	0.0572	0.0423	0.0369	0.0576	0.0492	0.0000	0.0000	0.0000		
PC-3	0.1300	0.1183	0.0626	0.0429	0.0431	0.0663	0.0642	0.0000	0.0000	0.0000	0.0000	
PC-4	0.1300	0.1341	0.0743	0.0444	0.0592	0.0760	0.0834	0.0000	0.0000	0.0000	0.0000	0.0000

Table 7C.3a : PR EOS model from PnA characterization for oil 3 in Table 7.5
Saturation pressure (bubble point) for this fluid is 63.85 bars at 313.70 K.

Components	Z	MW (g/mol)	T_C (K)	P_C (bars)	ω	C_{PEN} (CC/Mol)
N_2	0.0000	28.01	126.20	33.94	0.04000	
CO_2	0.0001	44.01	304.20	73.76	0.22500	
CH_4	0.1830	16.04	190.60	46.00	0.00800	
C_2H_6	0.0780	30.07	305.40	48.84	0.09800	
C_3H_8	0.0790	44.10	369.80	42.46	0.15200	
C_4H_{10}	0.0540	58.12	423.14	37.82	0.19090	
C_5H_{12}	0.0340	72.15	465.17	33.79	0.23950	
C_6H_{14}	0.0380	86.00	507.40	29.69	0.29600	
PC-1	0.2220	138.27	642.36	27.58	0.20280	
PC-2	0.1450	210.83	751.54	22.60	0.31880	
PC-3	0.1030	298.23	881.55	18.80	0.47290	
PC-4	0.0630	484.84	1091.63	15.49	0.71440	

Table 7C.3b : BIPs for PR EOS model from PnA characterization for oil 3 in Table 7.5

	N_2	CO_2	CH_4	C_2H_6	C_3H_8	C_4H_{10}	C_5H_{12}	C_6H_{14}	PC-1	PC-2	PC-3	PC-4
N_2	0.0000											
CO_2	0.0000	0.0000										
CH_4	0.1000	0.1000	0.0000									
C_2H_6	0.1000	0.1450	0.0420	0.0000								
C_3H_8	0.1000	0.1368	0.0420	0.0400	0.0000							
C_4H_{10}	0.1000	0.1280	0.0420	0.0400	0.0300	0.0000						
C_5H_{12}	0.1000	0.1197	0.0420	0.0400	0.0300	0.0116	0.0000					
C_6H_{14}	0.1000	0.1157	0.0420	0.0400	0.0300	0.0155	0.0058	0.0000				
PC-1	0.1300	0.0417	0.0518	0.0416	0.0328	0.0418	0.0275	0.0000	0.0000			
PC-2	0.1300	0.0886	0.0563	0.0422	0.0360	0.0556	0.0461	0.0000	0.0000	0.0000		
PC-3	0.1300	0.1183	0.0626	0.0429	0.0431	0.0663	0.0642	0.0000	0.0000	0.0000	0.0000	
PC-4	0.1300	0.1341	0.0743	0.0444	0.0592	0.0760	0.0834	0.0000	0.0000	0.0000	0.0000	0.0000

Table 7C.4a : PR EOS model from PnA characterization for oil 4 in Table 7.5 Saturation pressure (bubble point) for this fluid is 42.20 bars at 313.70 K.						
Components	Z	MW (g/mol)	T_C (K)	P_C (bars)	ω	C_{PEN} (CC/Mol)
N_2	0.0000	28.01	126.20	33.94	0.04000	
CO_2	0.0000	44.01	304.20	73.76	0.22500	
CH_4	0.1262	16.04	190.60	46.00	0.00800	
C_2H_6	0.0380	30.07	305.40	48.84	0.09800	
C_3H_8	0.0480	44.10	369.80	42.46	0.15200	
C_4H_{10}	0.0401	58.12	420.55	37.59	0.18840	
C_5H_{12}	0.0340	72.15	465.43	33.79	0.24010	
C_6H_{14}	0.0244	86.00	507.40	29.69	0.29600	
PC-1	0.2881	147.74	664.84	26.47	0.23100	
PC-2	0.1849	230.24	788.27	21.43	0.37208	
PC-3	0.1324	321.51	894.50	18.62	0.50445	
PC-4	0.0839	507.08	1111.46	15.41	0.76189	

Table 7C.4b : BIPs for PR EOS model from PnA characterization for oil 4 in Table 7.5												
	N_2	CO_2	CH_4	C_2H_6	C_3H_8	C_4H_{10}	C_5H_{12}	C_6H_{14}	PC-1	PC-2	PC-3	PC-4
N_2	0.0000											
CO_2	0.0000	0.0000										
CH_4	0.1000	0.1000	0.0000									
C_2H_6	0.1000	0.1450	0.0420	0.0000								
C_3H_8	0.1000	0.1368	0.0420	0.0400	0.0000							
C_4H_{10}	0.1000	0.1280	0.0420	0.0400	0.0300	0.0000						
C_5H_{12}	0.1000	0.1197	0.0420	0.0400	0.0300	0.0116	0.0000					
C_6H_{14}	0.1000	0.1157	0.0420	0.0400	0.0300	0.0155	0.0058	0.0000				
PC-1	0.1300	0.0532	0.0527	0.0417	0.0334	0.0452	0.0317	0.0000	0.0000			
PC-2	0.1300	0.1003	0.0581	0.0424	0.0378	0.0594	0.0521	0.0000	0.0000	0.0000		
PC-3	0.1300	0.1206	0.0635	0.0430	0.0443	0.0674	0.0662	0.0000	0.0000	0.0000	0.0000	
PC-4	0.1300	0.1350	0.0761	0.0446	0.0615	0.0769	0.0854	0.0000	0.0000	0.0000	0.0000	0.0000

Table 7C.5a : PR EOS model from PnA characterization for oil 5 in Table 7.5 Saturation pressure (bubble point) for this fluid is 39.02 bars at 313.70 K.						
Components	Z	MW (g/mol)	T_C (K)	P_C (bars)	ω	C_{PEN} (CC/Mol)
N_2	0.0040	28.01	126.20	33.94	0.04000	
CO_2	0.0297	44.01	304.20	73.76	0.22500	
CH_4	0.0861	16.04	190.60	46.00	0.00800	
C_2H_6	0.0739	30.07	305.40	48.84	0.09800	
C_3H_8	0.0764	44.10	369.80	42.46	0.15200	
C_4H_{10}	0.0722	58.12	422.95	37.80	0.19080	
C_5H_{12}	0.0543	72.15	466.91	33.77	0.24400	
C_6H_{14}	0.0406	86.00	507.40	29.69	0.29600	
PC-1	0.2324	138.61	644.14	28.07	0.21845	
PC-2	0.1539	209.40	754.86	23.19	0.34347	
PC-3	0.1092	295.15	870.52	19.90	0.48674	
PC-4	0.0673	478.67	1092.38	16.46	0.75214	

Table 7C.5b : BIPs for PR EOS model from PnA characterization for oil 5 in Table 7.5												
	N_2	CO_2	CH_4	C_2H_6	C_3H_8	C_4H_{10}	C_5H_{12}	C_6H_{14}	PC-1	PC-2	PC-3	PC-4
N_2	0.0000											
CO_2	0.0000	0.0000										
CH_4	0.1000	0.1000	0.0000									
C_2H_6	0.1000	0.1450	0.0420	0.0000								
C_3H_8	0.1000	0.1368	0.0420	0.0400	0.0000							
C_4H_{10}	0.1000	0.1280	0.0420	0.0400	0.0300	0.0000						
C_5H_{12}	0.1000	0.1197	0.0420	0.0400	0.0300	0.0116	0.0000					
C_6H_{14}	0.1000	0.1157	0.0420	0.0400	0.0300	0.0155	0.0058	0.0000				
PC-1	0.1300	0.0417	0.0518	0.0416	0.0328	0.0418	0.0275	0.0000	0.0000			
PC-2	0.1300	0.0886	0.0563	0.0422	0.0360	0.0556	0.0461	0.0000	0.0000	0.0000		
PC-3	0.1300	0.1156	0.0617	0.0428	0.0419	0.0652	0.0620	0.0000	0.0000	0.0000	0.0000	
PC-4	0.1300	0.1335	0.0734	0.0442	0.0581	0.0755	0.0823	0.0000	0.0000	0.0000	0.0000	0.0000

Table 7C.6a : PR EOS model from PnA characterization for oil 6 in Table 7.5 Saturation pressure (bubble point) for this fluid is 59.87 bars at 301.48 K.						
Components	Z	MW (g/mol)	T_C (K)	P_C (bars)	ω	C_{PEN} (CC/Mol)
N_2	0.0019	28.01	126.20	33.94	0.04000	
CO_2	0.0044	44.01	304.20	73.76	0.22500	
CH_4	0.2028	16.04	190.60	46.00	0.00800	
C_2H_6	0.0592	30.07	305.40	48.84	0.09800	
C_3H_8	0.0590	44.10	369.80	42.46	0.15200	
C_4H_{10}	0.0559	58.12	420.73	37.60	0.18860	
C_5H_{12}	0.0492	72.15	464.86	33.79	0.23860	
C_6H_{14}	0.0436	86.00	507.40	29.69	0.29600	
PC-1	0.2150	139.57	642.10	26.97	0.18282	
PC-2	0.1433	209.36	751.06	21.83	0.28746	
PC-3	0.1023	293.39	863.05	18.33	0.40737	
PC-4	0.0635	472.23	1074.09	14.63	0.62949	

Table 7C.6b : BIPs for PR EOS model from PnA characterization for oil 6 in Table 7.5												
	N_2	CO_2	CH_4	C_2H_6	C_3H_8	C_4H_{10}	C_5H_{12}	C_6H_{14}	PC-1	PC-2	PC-3	PC-4
N_2	0.0000											
CO_2	0.0000	0.0000										
CH_4	0.1000	0.1000	0.0000									
C_2H_6	0.1000	0.1450	0.0420	0.0000								
C_3H_8	0.1000	0.1318	0.0420	0.0400	0.0000							
C_4H_{10}	0.1000	0.1252	0.0420	0.0400	0.0300	0.0000						
C_5H_{12}	0.1000	0.1192	0.0420	0.0400	0.0300	0.0116	0.0000					
C_6H_{14}	0.1000	0.1164	0.0420	0.0400	0.0300	0.0155	0.0058	0.0000				
PC-1	0.1300	0.0417	0.0518	0.0416	0.0328	0.0418	0.0275	0.0000	0.0000			
PC-2	0.1300	0.0886	0.0563	0.0422	0.0360	0.0556	0.0461	0.0000	0.0000	0.0000		
PC-3	0.1300	0.1156	0.0617	0.0428	0.0419	0.0652	0.0620	0.0000	0.0000	0.0000	0.0000	
PC-4	0.1300	0.1335	0.0734	0.0442	0.0581	0.0755	0.0823	0.0000	0.0000	0.0000	0.0000	0.0000

Table 7C.7a : PR EOS model from PnA characterization for oil 7 in Table 7.5 Saturation pressure (bubble point) for this fluid is 30.82 bars at 316.48 K.						
Components	Z	MW (g/mol)	T_C (K)	P_C (bars)	ω	C_{PEN} (CC/Mol)
N_2	0.0038	28.01	126.20	33.94	0.04000	-4.230
CO_2	0.0135	44.01	304.20	73.76	0.22500	-1.640
CH_4	0.0694	16.04	190.60	46.00	0.00800	-5.200
C_2H_6	0.1006	30.07	305.40	48.84	0.09800	-5.790
C_3H_8	0.0739	44.10	369.80	42.46	0.15200	-6.350
C_4H_{10}	0.0771	58.12	422.54	37.76	0.19040	-6.490
C_5H_{12}	0.0631	72.15	466.46	33.77	0.24280	-5.120
C_6H_{14}	0.0545	86.00	507.40	29.69	0.29600	1.390
PC-1	0.2276	148.17	665.80	25.75	0.20634	-1.380
PC-2	0.1487	226.75	771.06	21.19	0.31175	-1.950
PC-3	0.1043	323.35	898.28	17.62	0.45059	-2.730
PC-4	0.0633	532.71	1135.18	14.11	0.69431	-4.300

Table 7C.7b : BIPs for PR EOS model from PnA characterization for oil 7 in Table 7.5												
	N_2	CO_2	CH_4	C_2H_6	C_3H_8	C_4H_{10}	C_5H_{12}	C_6H_{14}	PC-1	PC-2	PC-3	PC-4
N_2	0.0000											
CO_2	0.0000	0.0000										
CH_4	0.1000	0.1000	0.0000									
C_2H_6	0.1000	0.1450	0.0420	0.0000								
C_3H_8	0.1000	0.1381	0.0420	0.0400	0.0000							
C_4H_{10}	0.1000	0.1289	0.0420	0.0400	0.0300	0.0000						
C_5H_{12}	0.1000	0.1200	0.0420	0.0400	0.0300	0.0116	0.0000					
C_6H_{14}	0.1000	0.1156	0.0420	0.0400	0.0300	0.0155	0.0058	0.0000				
PC-1	0.1300	0.0532	0.0527	0.0417	0.0334	0.0452	0.0317	0.0000	0.0000			
PC-2	0.1300	0.0949	0.0572	0.0423	0.0369	0.0576	0.0492	0.0000	0.0000	0.0000		
PC-3	0.1300	0.1206	0.0635	0.0430	0.0443	0.0674	0.0662	0.0000	0.0000	0.0000	0.0000	
PC-4	0.1300	0.1355	0.0770	0.0447	0.0625	0.0773	0.0864	0.0000	0.0000	0.0000	0.0000	0.0000

Table 7C.8a : PR EOS model from PnA characterization for oil 8 in Table 7.5 Saturation pressure (bubble point) for this fluid is 55.35 bars at 307.60 K.						
Components	Z	MW (g/mol)	T_C (K)	P_C (bars)	ω	C_{PEN} (CC/Mol)
N_2	0.0048	28.01	126.20	33.94	0.04000	
CO_2	0.0011	44.01	304.20	73.76	0.22500	
CH_4	0.1630	16.04	190.60	46.00	0.00800	
C_2H_6	0.0403	30.07	305.40	48.84	0.09800	
C_3H_8	0.0297	44.10	369.80	42.46	0.15200	
C_4H_{10}	0.0365	58.12	423.51	37.85	0.19130	
C_5H_{12}	0.0373	72.15	465.70	33.78	0.24080	
C_6H_{14}	0.0332	86.00	507.40	29.69	0.29600	
PC-1	0.2648	140.17	642.41	27.67	0.20553	
PC-2	0.1767	210.11	751.65	22.70	0.32316	
PC-3	0.1290	287.66	864.20	19.33	0.45796	
PC-4	0.0836	444.23	1045.98	16.16	0.67352	

Table 7C.8b : BIPs for PR EOS model from PnA characterization for oil 8 in Table 7.5												
	N_2	CO_2	CH_4	C_2H_6	C_3H_8	C_4H_{10}	C_5H_{12}	C_6H_{14}	PC-1	PC-2	PC-3	PC-4
N_2	0.0000											
CO_2	0.0000	0.0000										
CH_4	0.1000	0.1000	0.0000									
C_2H_6	0.1000	0.1450	0.0420	0.0000								
C_3H_8	0.1000	0.1341	0.0420	0.0400	0.0000							
C_4H_{10}	0.1000	0.1264	0.0420	0.0400	0.0300	0.0000						
C_5H_{12}	0.1000	0.1193	0.0420	0.0400	0.0300	0.0116	0.0000					
C_6H_{14}	0.1000	0.1159	0.0420	0.0400	0.0300	0.0155	0.0058	0.0000				
PC-1	0.1300	0.0417	0.0518	0.0416	0.0328	0.0418	0.0275	0.0000	0.0000			
PC-2	0.1300	0.0886	0.0563	0.0422	0.0360	0.0556	0.0461	0.0000	0.0000	0.0000		
PC-3	0.1300	0.1156	0.0617	0.0428	0.0419	0.0652	0.0620	0.0000	0.0000	0.0000	0.0000	
PC-4	0.1300	0.1322	0.0716	0.0440	0.0557	0.0744	0.0800	0.0000	0.0000	0.0000	0.0000	0.0000

Table 7C.9a : PR EOS model from PnA characterization for oil 9 in Table 7.5						
Saturation pressure (bubble point) for this fluid is 60.21 bars at 307.60 K.						
Components	Z	MW (g/mol)	T_C (K)	P_C (bars)	ω	C_{PEN} (CC/Mol)
N_2	0.0029	28.01	126.20	33.94	0.04000	-4.230
CO_2	0.0119	44.01	304.20	73.76	0.22500	-1.640
CH_4	0.1756	16.04	190.60	46.00	0.00800	-5.200
C_2H_6	0.0992	30.07	305.40	48.84	0.09800	-5.790
C_3H_8	0.1257	44.10	369.80	42.46	0.15200	-6.350
C_4H_{10}	0.0793	58.12	421.40	37.66	0.18920	-6.490
C_5H_{12}	0.0507	72.15	465.73	33.78	0.24090	-5.120
C_6H_{14}	0.0377	86.00	507.40	29.69	0.29600	1.390
PC-1	0.1713	130.86	643.85	27.32	0.19420	1.820
PC-2	0.1157	193.74	733.63	23.06	0.28333	3.630
PC-3	0.0813	275.65	851.10	19.29	0.41216	5.450
PC-4	0.0487	460.10	1073.72	15.40	0.65271	7.260

Table 7C.9b : BIPs for PR EOS model from PnA characterization for oil 9 in Table 7.5												
	N_2	CO_2	CH_4	C_2H_6	C_3H_8	C_4H_{10}	C_5H_{12}	C_6H_{14}	PC-1	PC-2	PC-3	PC-4
N_2	0.0000											
CO_2	0.0000	0.0000										
CH_4	0.1000	0.1000	0.0000									
C_2H_6	0.1000	0.1450	0.0420	0.0000								
C_3H_8	0.1000	0.1341	0.0420	0.0400	0.0000							
C_4H_{10}	0.1000	0.1264	0.0420	0.0400	0.0300	0.0000						
C_5H_{12}	0.1000	0.1193	0.0420	0.0400	0.0300	0.0116	0.0000					
C_6H_{14}	0.1000	0.1159	0.0420	0.0400	0.0300	0.0155	0.0058	0.0000				
PC-1	0.1300	0.0417	0.0518	0.0416	0.0328	0.0418	0.0275	0.0000	0.0000			
PC-2	0.1300	0.0814	0.0554	0.0420	0.0353	0.0534	0.0428	0.0000	0.0000	0.0000		
PC-3	0.1300	0.1126	0.0608	0.0427	0.0408	0.0639	0.0598	0.0000	0.0000	0.0000	0.0000	
PC-4	0.1300	0.1329	0.0725	0.0441	0.0569	0.0749	0.0812	0.0000	0.0000	0.0000	0.0000	0.0000

Supporting Information

Table 3-S1. Fluid model for oil 3 developed using the new characterization method with 11 components.

Components	Mole Fractions	MW (gm/mol)	T_C (K)	P_C (bars)	V_C (cc/mol)	ω
N_2	0.0004	28.02	126.20	33.90	89.80	0.0400
CO_2	0.0216	44.01	304.20	73.80	94.00	0.2250
C_1	0.1992	16.04	190.60	46.00	99.00	0.0080
C_2	0.0011	30.07	305.40	48.84	148.00	0.0980
C_3	0.0002	44.10	369.80	42.46	203.00	0.1520
C_{4-5}	0.0010	67.94	453.70	35.12	283.50	0.2356
C_6	0.0021	86.18	508.00	30.31	370.00	0.3005
PC1	0.3389	275.45	1008.79	21.38	805.80	0.2038
PC2	0.2015	463.51	1080.01	14.92	1951.96	0.3963
PC3	0.1430	652.65	1109.47	11.70	3834.48	0.5677
PC4	0.0910	1025.86	1132.71	8.39	7984.38	0.8277
Temperature (K)	322.05					
Saturation Pressure (bars)	47.23					

Table 3-S2. Fluid model for oil 3 developed using the conventional characterization method with volume shift with 11 components.

Components	Mole Fractions	MW (gm/mol)	T_C (K)	P_C (bars)	V_C (cc/mol)	ω	C_{PEN} (cc/mol)
N_2	0.0004	28.02	126.20	33.90	89.80	0.0400	-4.23
CO_2	0.0216	44.01	304.20	73.80	94.00	0.2250	-1.64
C_1	0.1992	16.04	190.60	46.00	99.00	0.0080	-5.20
C_2	0.0011	30.07	305.40	48.84	148.00	0.0980	-5.79
C_3	0.0002	44.10	369.80	42.46	203.00	0.1520	-6.35
C_{4-5}	0.0010	67.94	453.70	35.12	283.50	0.2355	-5.53
C_6	0.0021	86.18	508.00	30.31	370.00	0.3004	1.39
PC1	0.4294	226.26	702.850	21.56	1212.59	0.3701	-96.76
PC2	0.1744	532.79	803.872	17.25	2357.30	0.4100	-405.20
PC3	0.1072	853.44	860.001	15.76	3754.90	0.4257	-753.83
PC4	0.0632	1450.93	841.495	14.80	6744.42	0.4330	-1458.94
Temperature (K)	322.05						
Saturation Pressure (bars)	47.23						

Table 3-S3. Fluid model for oil 6 developed using the new characterization method with 11 components.

Components	Mole Fractions	MW (gm/mol)	T_C (K)	P_C (bars)	V_C (cc/mol)	ω
N_2	0.0002	28.02	126.20	33.90	89.80	0.0400
CO_2	0.0096	44.01	304.20	73.80	94.00	0.2250
C_1	0.3203	16.04	190.60	46.00	99.00	0.0080
C_2	0.0349	30.07	305.40	48.84	148.00	0.0980
C_3	0.0039	44.10	369.80	42.46	203.00	0.1520
C_{4-5}	0.0120	64.08	440.95	36.27	283.50	0.2215
C_6	0.0053	86.18	508.00	30.31	370.00	0.3005
PC1	0.2472	175.93	911.66	29.75	358.31	0.2361
PC2	0.1640	265.30	995.42	22.55	867.96	0.3965
PC3	0.1217	357.55	1043.41	18.39	1704.61	0.5445
PC4	0.0810	537.28	1090.73	13.84	3550.33	0.7753
Temperature (K)	333.15					
Saturation Pressure (bars)	137.80					

Table 3-S4. Fluid model for oil 6 developed using the conventional characterization method with volume shift with 11 components.

Components	Mole Fractions	MW (gm/mol)	T_C (K)	P_C (bars)	V_C (cc/mol)	ω	C_{PEN} (cc/mol)
N_2	0.0002	28.02	126.20	33.90	89.80	0.0400	-4.23
CO_2	0.0096	44.01	304.20	73.80	94.00	0.2250	-1.64
C_1	0.3203	16.04	190.60	46.00	99.00	0.0080	-5.20
C_2	0.0349	30.07	305.40	48.84	148.00	0.0980	-5.79
C_3	0.0039	44.10	369.80	42.46	203.00	0.1520	-6.35
C_{4-5}	0.0120	64.08	440.95	36.27	283.50	0.2217	-5.91
C_6	0.0053	86.18	508.00	30.31	370.00	0.3005	1.39
PC1	0.2472	147.787	744.734	29.24	693.47	0.3917	-5.91
PC2	0.1640	289.608	871.316	23.07	1142.91	0.4496	-18.45
PC3	0.1217	449.077	944.574	20.15	1732.70	0.5371	-66.56
PC4	0.0810	759.664	1034.300	18.04	3134.73	0.5307	-130.90
Temperature (K)	333.15						
Saturation Pressure (bars)	137.80						
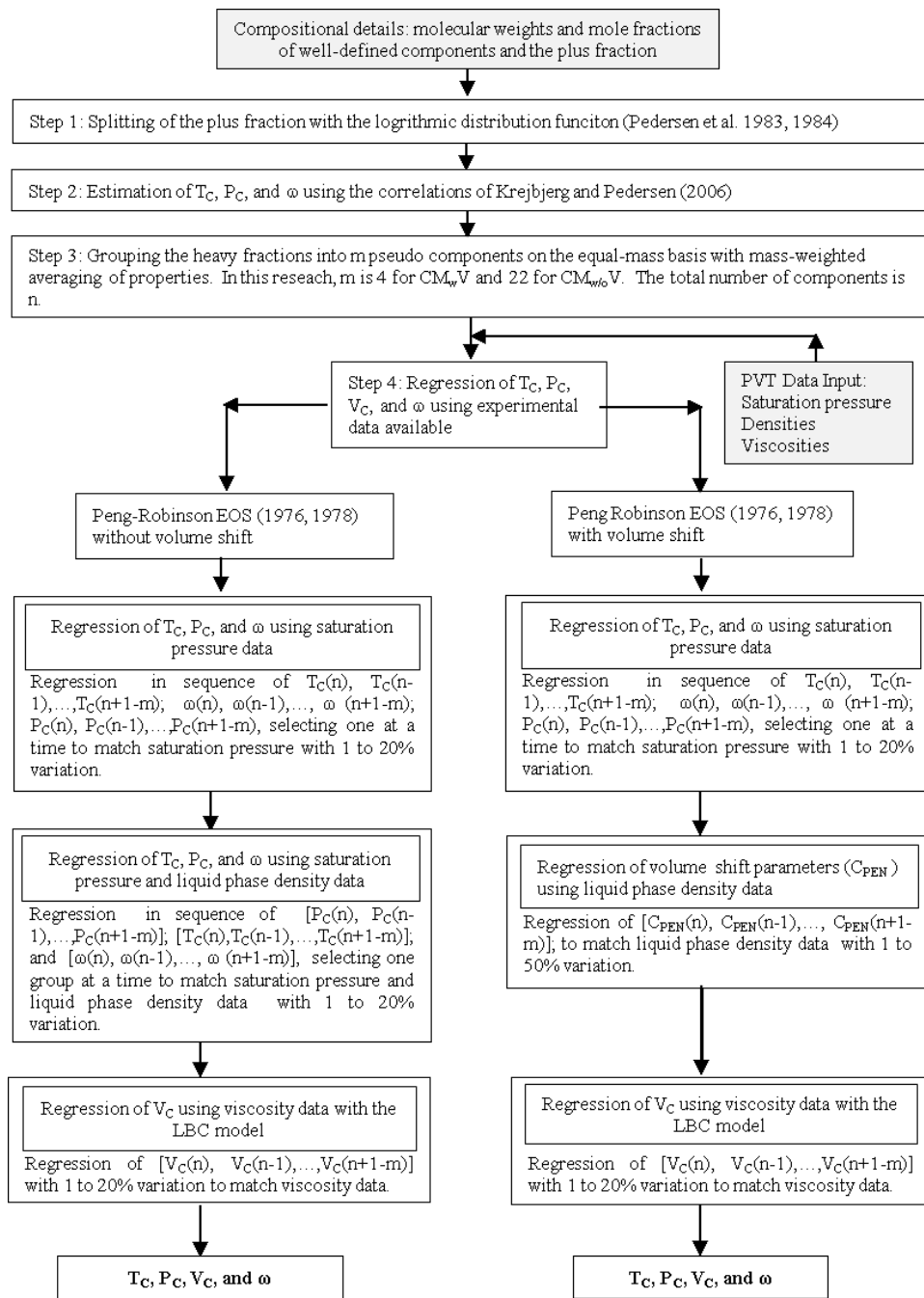
Figure 3-S1. Flow chart for the conventional characterization method (CM) in this research, which is based on Pedersen and Christensen (2007).

The shaded blocks show the input data. The CM with volume-shift parameters is referred to as the CM$_w$V (the right branch of the flow chart). The CM$_{w/o}$V is the CM without volume-shift parameters (the left branch of the flow chart). See the Introduction section for the definitions of steps 1-4.

377
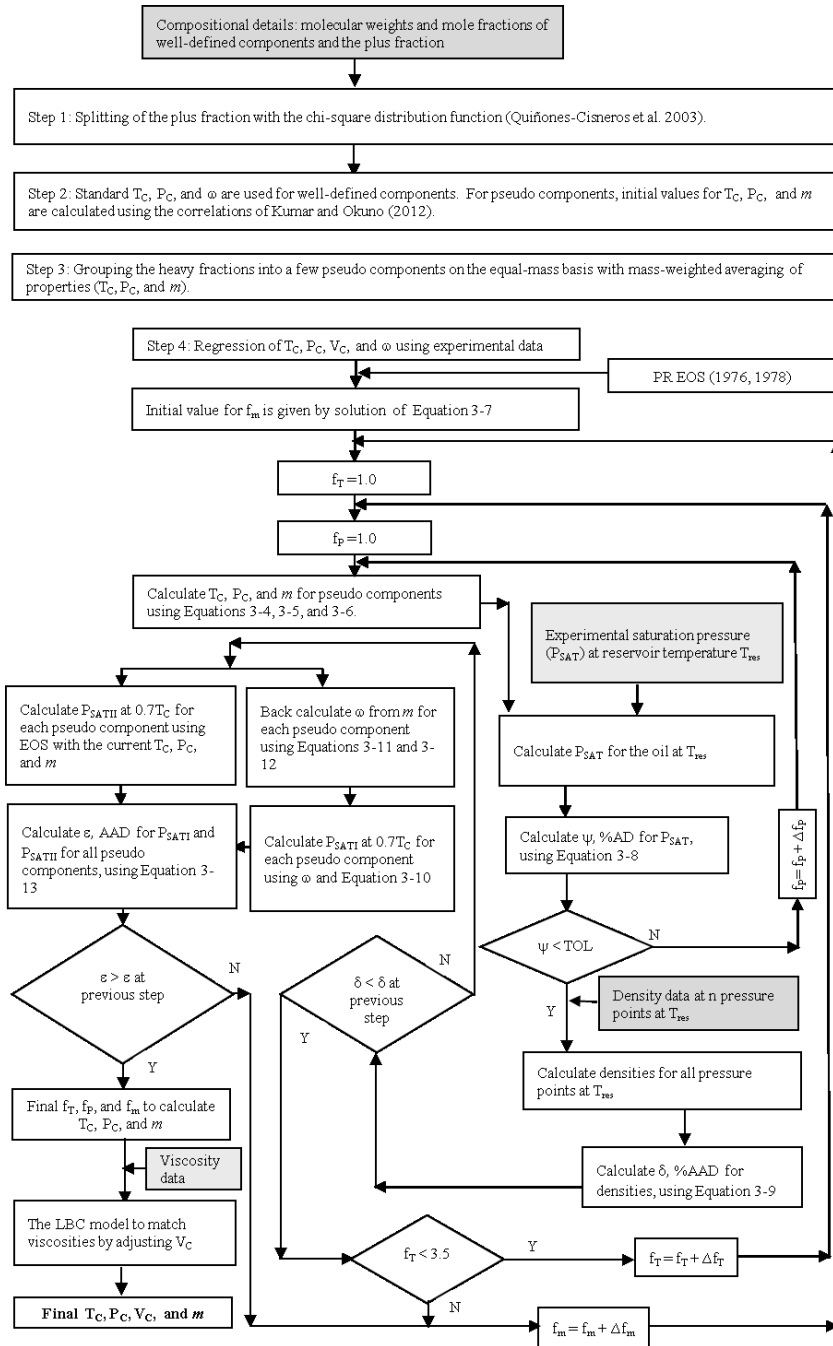
Figure 3-S2. Flow chart for the new characterization method (NM) developed in this research.

Section 3-S1: Summary of Step 4 of the New Characterization Method given in Figure 3-S2

1. The initial values for f_T and f_P are unity. The f_m parameter is initialized by solving Equation 3- 7.
2. The m parameters are calculated using Equation 3-6 and the current f_m for pseudocomponents.
3. T_C's are calculated using Equation 3-4 and the current f_T for pseudocomponents.
4. P_C's are calculated using Equation 3-5 and the current f_P for pseudocomponents.
5. Calculate the P_{SAT} at the reservoir temperature. If the function Ψ given in Equation 8 is greater than a tolerance (e.g., 10^{-4}), increase f_P by Δf_P (e.g., 10^{-6}) and go back to Item 4. If the function Ψ is less than the tolerance, go to item 6.
6. Calculate densities at pressures at the reservoir temperature. If the δ function given in Equation 3-9 is greater than a tolerance, set f_P to unity and increase f_T by Δf_T (e.g., 10^{-5}) and go to Item 3. If f_T exceeds 3.5 or the δ function at the current iteration is greater than that at the previous iteration, go to the ω loop.
7. For each pseudocomponent,
   a. Back calculate ω from the current m using Equations 3-11 and 3-12
   b. Calculate P_{SAT} at $0.7T_C$ using the current T_C, P_C and m.
8. Calculate the ε function given in Equation 3-13. If the ε function at the current iteration is smaller than that at the previous iteration, increase f_m by Δf_m (e.g., 10^{-3}) and go to Item 2. Each iteration in the ω loop starts with f_T of 1.0 and f_P of 1.0. The final set of f_T, f_P, and f_m is determined when the ε function becomes greater than that at the previous iteration.
9. The LBC model is used to match viscosity data by adjusting V_C.

Section 3-S2: Effects of Volume-Shift Parameter Regression on Phase Behavior Predictions

Table 3-S5 lists the composition and critical parameters for a ternary fluid characterized using the PR EOS with and without volume shift. Only three components are used to illustrate the impact of using volume shift in regression on phase behavior predictions using ternary diagrams. The saturation pressure of 196.48 bar at 330.4 K and density data at 276.3, 258.5, 223.6, 196.5, 175.2, 144.6, 103.0, 62.3, 41.0, and 7.1 bars at 330.4 K are matched using the CM_wV and $CM_{w/o}V$ as described in Figure 3-S1. The two characterizations have the same phase behavior predictions at the composition shown in Table 3-S5.

Equally spaced contour lines for the dimensionless Gibbs free energy change on mixing ($\Delta_{mix}\underline{G}/RT$) at 330.4 K and 196.48 bars are plotted for the two cases in Figures 3-S3 and 3-S4. The characterization without volume shift results in a deeper valley of the Gibbs free energy. Flash calculations on these Gibbs free energy surfaces result in two different phase envelopes as shown in Figure 3-S5 and 3-S6. The significant difference in the two-phase predictions results in a large difference in the minimum miscibility pressure (MMP) predictions. The MMP calculated at 330.4 K for the injection gas of 40% L and 60% I is 351.86 bars without volume shift and 250.75 bars with volume shift.

Table 3-S5. Ternary fluid using the conventional characterization method with/without volume shift in regression.									
			PR EOS with volume shift				PR EOS without volume shift		
Comp.	Mole Fractions	MW (gm/mol)	T_C (K)	P_C (bars)	ω	C_{PEN} (cc/mol)	T_C (K)	P_C (bars)	ω
L	0.4219	16.10	190.86	46.07	0.0089	-5.19	190.86	46.07	0.0089
I	0.0176	31.66	315.59	47.83	0.1065	-5.85	315.59	47.83	0.1065
H	0.5605	291.30	848.33	24.18	0.4373	-110.14	1022.44	19.48	0.5108
Temperature (K)		330.40							
Saturation Pressure (bars)		196.48							
$L = N_2 + CO_2 + C_1$, $I = C_2 + C_3$, $H = C_{4+}$									

Figure 3-S3. Dimensionless molar Gibbs free energy change on mixing for the ternary fluid given in Table 3-S5 at 330.4 K and 196.48 bars.
Contour lines are drawn with the interval of 0.05 between -0.85 to 2.0. The PR EOS is used without volume shift.
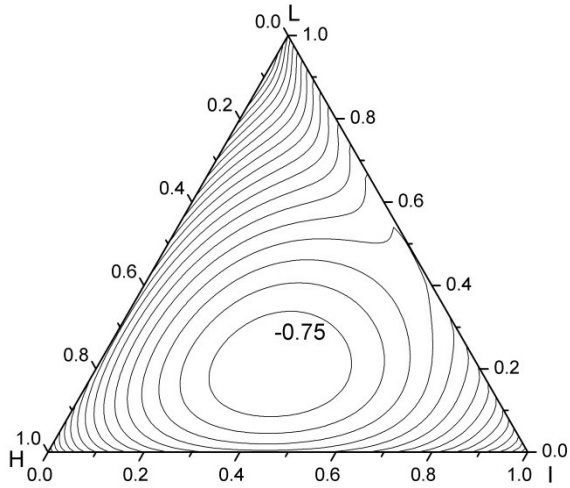
Figure 3-S4. Dimensionless molar Gibbs free energy change on mixing for the ternary fluid given in Table 3-S5 at 330.4 K and 196.48 bars.
Contour lines are drawn with the interval of 0.05 between -0.85 to 2.0. The PR EOS is used. Volume shift parameters are used in regression.
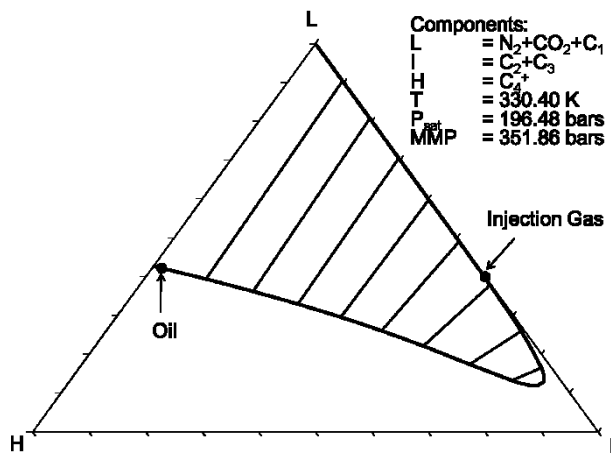
Figure 3-S5. Phase envelope for the ternary fluid given in Table 3-S5.
The PR EOS is used without volume shift. MMP calculated for the injection gas is 351.86 bars at 330.40 K.
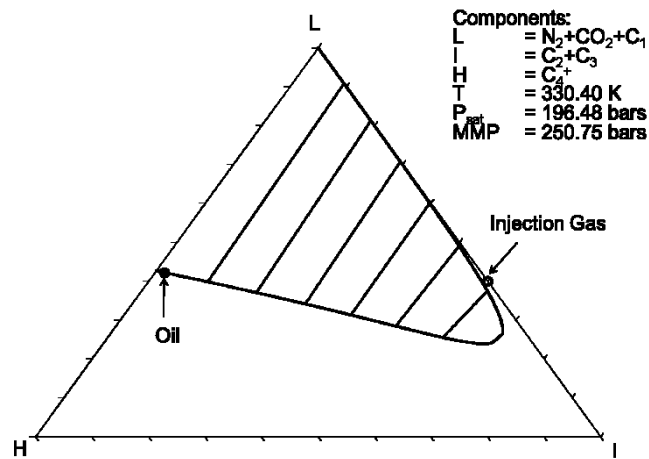
Figure 3-S6. Phase envelope for the ternary fluid given in Table 3-S5.
The PR EOS is used. Volume shift parameters are used in regression. Use of volume shift results in a two-phase envelope that is significantly smaller than that in Figure 3-3. MMP calculated for the injection gas is 250.75 bars 330.40 K.

Section 5-S1. Peng-Robinson Attraction and Covolume Parameters Optimized for n-Alkanes

This part presents a critical review for various sets of the attraction and covolume parameters presented in the literature. They are categorized into three types; i) the parameter sets that are based on estimated physical critical points, ii) the optimized parameter sets from Ting et al. (2003) and Voutsas et al. (2006), and iii) the optimized parameter set from Kumar and Okuno (2012). This part is concerned with the suitability of the optimized parameter set from Kumar and Okuno (2012) for use in the direct perturbation from n-alkanes (PnA) in this research.

The Peng-Robinson equation of state (PR EOS) used throughout this paper is given below.

$$p = \frac{RT}{v-b} - \frac{a}{v^2 + 2bv - b^2} \,, \tag{5-S1}$$

where $a = a_C \alpha(T_r)$ (5-S2)

$$a_C = \Omega_a \, (RT_C)^2 / P_C \tag{5-S3}$$

$$\alpha(T_r) = [1 + m(1 - (T/T_C)^{0.5})]^2 \tag{5-S4}$$

$$b = \Omega_b \, RT_C / P_C \tag{5-S5}$$

$$m = 0.37464 + 1.54226\omega - 0.26992\omega^2 \quad \text{for } \omega < 0.3984 \tag{5-S6}$$

$$m = 0.379642 + 1.48503\omega - 0.164423\omega^2 + 0.016666\omega^3 \quad \text{for } \omega \geq 0.3984 \tag{5-S7}$$

Critical points were measured for C_1 through n-C_{24}, n-C_{26}, n-C_{27}, n-C_{30}, and n-C_{36} (Nikitin et al. 1997). Although there are many correlations proposed for critical parameters, not all of them are reliably extrapolated to heavier n-alkanes. For example, the correlations of Gao et al. (2001), Riazi and Al-Sahhaf (1996) give a normal boiling point (T_b) that is greater than T_C of a given compound. The correlation of T_C by Joback and Reid (1987) yields physically absurd values; 32130 K for n-C_{73} and – 189113 K for n-C_{74}. Their correlation for T_b gives 2487.60 K for n-C_{100}. Kontogeorgis and Tassios (1997) presented a critical review of various correlations for critical points. They recommended Magoulos and Tassios (1990) for n-alkanes up to n-C_{40} and Constantinou and Gani (1994) for more general application to heavier n-alkanes. In this paper, the group-contribution method of Constantinou and Gani (1994) is used when physical critical points are required in phase behavior computations for n-alkanes from C_7 to C_{100}.

Kumar and Okuno (2012) optimized T_C, P_C, and m for n-alkanes from n-C_7 through n-C_{100} in terms of liquid densities and vapor pressures by use of the PR EOS. The optimized critical parameters deviate, to some extent, from the physically measured critical points, and give extended two-phase lines in P-T space. Therefore, a comprehensive analysis of the deviation and its impact on phase behavior prediction has been made by comparing with various estimations of physical critical points presented in the literature. **Table 5-S1** presents T_C and P_C of n-C_{100} from various sources in the literature. The optimized values by Kumar and Okuno (2012) are 1084 K and 4.01 bars, and are within the variation ranges (950 – 1215 K for T_C and 0.48 – 4.43 bars for P_C) presented in Table 5-S1. The deviation of the optimized T_C from the value of Constantinou and Gani (1994) is within the experimental uncertainty of

3% (Rowley et al. 2006). Compared to Constantinou and Gani (1994), the optimized T_C is lower for n-alkanes lighter than n-C_{15}, but becomes higher for heavier n-alkanes. The deviation from Constantinou and Gani (1994) in terms of P_C is higher than the experimental uncertainty of 25% (Rowley et al. 2006). The optimized P_C is higher than the value from Constantinou and Gani (1994) for all n-alkanes from n-C_7 to n-C_{100}. **Figure 5-S1** compares the two sets of the critical parameters and vapor pressures.

Densities calculated by the PR EOS tend to increase when values of critical parameters are increased. **Figure 5-S2** shows data and predictions for saturated liquid densities (ρ_L^S) and vapor pressures (P_{vap}) for n-C_{28}. The data were taken from Yaws (2010) and Riazi and AlQaheem (2010). The predictions were made by the PR EOS with two different sets of critical parameters; Constantinou and Gani (1994) and Kumar and Okuno (2012). The PR EOS underpredicts ρ_L^S when physical values from Constantinou and Gani (1994) are used. Figure 5-S2 clearly shows that ρ_L^S predictions are increased by use of higher T_C and P_C, and lower ω from Kumar and Okuno (2012). However, vapor pressure predictions are kept nearly the same along the data.

In this figure, the predictions with the parameter set of Constantinou and Gani (1994) deviate substantially from the density data (Yaws 2010), due to the well-known shortcoming of the PR EOS in liquid density predictions. However, they agree well with the vapor pressure data (Riazi and AlQaheem 2010). The availability of vapor pressure data for light n-alkanes allows for better fitting of the $\alpha(T_r)$ function (Equation 5-S4), which results in improved vapor pressure prediction.

Figure 5-S3 presents data and predictions for three isodensity curves in P-T space for n-C_{28}. The three curves represent P-T conditions at which measured densities are 0.78 g/cc, 0.76 g/cc, and 0.74 g/cc. The PR EOS gives density predictions along the three curves that depend significantly on the critical-parameter values used. They are respectively 0.74 g/cc, 0.73 g/cc, and 0.72 g/cc with Kumar and Okuno (2012), and 0.50 g/cc, 0.49 g/cc, and 0.48 g/cc with Constantinou and Gani (1994). The comparisons in Figures 5-S2 and 5-S3 show that the density predictions from the PR EOS are much improved by using the critical parameters of Kumar and Okuno (2012), as compared to the physical critical parameters estimated by Constantinou and Gani (1994).

The optimization of critical parameters for n-alkanes in Kumar and Okuno (2012) did not consider critical volume predictions. **Figure 5-S4** compares critical densities calculated with the PR EOS with the optimized critical parameters from Kumar and Okuno (2012) with those with the physical critical parameters from Constantinou and Gani (1994). It also shows estimated critical densities by use of the correlations of Teja et al. (1990), Tsonopoulos (1993), Constantinou and Gani (1994). Teja et al. (1990) and Tsonopoulos and Tan (1993) developed the correlations by use of experimental critical density data for n-alkanes up to n-C_{18} (Anselme et al. 1990, Ambrose and Tsonopoulos 1995). Critical densities estimated by Teja et al. (1990) tend to zero with increasing CN, which may be unlikely (Tsonopoulos and Tan 1993). Critical densities estimated by Constantinou and Gani (1994) do not follow the data trend; however, they are kept at the same level for higher CNs, unlike those from Teja et al. (1990). The correlation of Tsonopoulos and Tan (1993) is based on a modified Flory theory (Flory et al. 1964) of the

statistical thermodynamics for chain molecules applied to n-alkanes. The critical densities from the PR EOS with the optimized critical parameters from Kumar and Okuno (2012) exhibit a minimum. For large CNs, they remain nearly constant, and are close to the values estimated by Tsonopoulos and Tan (1993). The average absolute deviation (AAD) in the critical density predictions from the PR EOS with the critical parameters from Kumar and Okuno (2012) is less than 10%, compared to the available data. This is within the experimental uncertainty for critical density; for example, the experimental uncertainty is 14% for n-C_{18} (Ambrose and Tsonopoulos, 1995).

The review given above for the critical parameters of Kumar and Okuno (2012) showed how density predictions of the PR EOS can be improved while keeping vapor pressure predictions by adjusting T_C, P_C, and m. Ting et al. (2003) and Voutsas et al. (2006) also conducted the indirect optimization of the PR attraction and covolume parameters for n-alkanes by matching vapor pressures and liquid densities through T_C, P_C, and m. Voutsas et al. (2006) also presented correlations for a_C (Equation 5-S3) and covolumes. However, the CN range used by them does not cover many reservoir fluids. C_1, C_2, C_3, C_4, C_6, C_7, C_{10}, C_{16}, C_{18}, C_{20}, C_{24}, C_{30}, C_{36}, and C_{40} were considered in Ting et al. (2003) and Voutsas et al. (2006), while C_7 through C_{100} in Kumar and Okuno (2012). Nevertheless, these three publications commonly showed that phase equilibrium predictions for n-alkane mixtures were also improved when the optimized critical parameters were used with the PR EOS.

Here, a comparison is made between the optimized sets of Voutsas et al. (2006), Kumar and Okuno (2012). **Figure 5-S5** presents the a_C values based on three different sets of T_C, P_C, and m; two optimized sets from Kumar and Okuno (2012) and from Voutsas et al. (2006), and the other one from the method of Constantinou and Gani (1994) and Constantinou et al. (1995) as a physical-value set. The same comparison is presented for the covolume parameter in **Figure 5-S6** and for the attraction parameter at 350 K in **Figure 5-S7.** For each of the three parameters shown, the optimized set of Kumar and Okuno (2012) results in a value that is lower than when the physical-value set is used for a given MW. The parameters are well correlated with a linear function of MW. The small deviations between Kumar and Okuno (2012) and Voutsas et al. (2006) are likely due to the different ranges of n-alkanes used. The attraction parameter at 350 K from Voutsas et al. (2006) is greater than that from Kumar and Okuno (2012) for CNs higher than 40. The deviation becomes greater for higher CNs.

The m parameter (Equations 5-S6 and 5-S7) in the PR EOS is significant in vapor pressure prediction at sub-critical temperatures. **Figure 5-S8** compares the m parameter estimated by the method of Constantinou et al. (1995) with the optimized m parameters by Voutsas et al. (2006) and by Kumar and Okuno (2012). The optimized m parameter of Kumar and Okuno (2012) is approximately equal to the estimated physical value up to n-C_{21}. For higher CNs, the optimized m parameter is smaller than the estimated physical value for each CN. The trends from Voutsas et al. (2006), Kumar and Okuno (2012) start deviating from each other approximately at the MW of 550 g/mol. This is likely attributed to the fact that Voutsas et al. (2006) only considered n-alkanes up to n-C_{40}, which corresponds to a MW of 563 g/mol.

The attraction and covolume parameters calculated based on Voutsas et al. (2006) may not be satisfactory for predictions of vapor pressures and liquid phase densities for CNs higher than 40. **Figure 5-S9** presents a comparative analysis of predictive capabilities of Voutsas et al. (2006), and Kumar and Okuno (2012) for n-C_{100}. Saturated liquid density data were taken from Yaws (2010), and vapor pressure data were reproduced using the correlation of Raizi and AlQaheem (2010). Use of the parameter set from Voutsas et al. (2006) results in significant overprediction of the vapor pressures and underprediction of the saturated liquid densities. Use of the parameter set from Kumar and Okuno (2012) results in good agreement with data. **Figure 5-S10** shows isodensity curves with liquid phase density values of 0.74 g/cc and 0.76 g/cc for n-C_{100} in P-T space. The density predictions based on Kumar and Okuno (2012) and Voutsas et al. (2006) are widely apart from each other.

Figure 5-S11 shows the normal boiling points for n-alkanes based on the parameter set of Voutsas et al. (2006) and that of Kumar and Okuno (2012). The comparison with data indicates that the parameter set of Voutsas et al. (2006) is not satisfactory for normal boiling point predictions for CNs 7 through 11 and 40 and higher. The trends of the parameters from Voutsas et al. (2006), and Kumar and Okuno (2012) are qualitatively similar and quantitatively close to each other for CNs lower than 40. However, the small differences in the parameters can result in significant differences in phase behavior predictions.

This part presented a critical review for three different types of the PR attraction and covolume parameters available in the literature; i.e., i) the physical parameter sets, ii) the optimized parameter sets from Ting et al. (2003) and Voutsas et al. (2006), and iii) the optimized parameter set from Kumar and Okuno (2012). The first type is not suitable for the direct PnA method primarily because they do not give accurate density predictions. As explained in Kumar and Okuno (2013, 2014), use of volume shift as adjustment parameters in reservoir fluid characterization can result in erroneous phase behavior predictions at the thermodynamic conditions that the available phase behavior data do not cover. The first type also showed less accurate phase equilibrium predictions for n-alkane mixtures in comparison with the optimized parameters from Kumar and Okuno (2012), as shown in Kumar and Okuno (2012) and Figures 5-16 and 5-17 in the current paper. The second type was not satisfactory for phase behavior predictions for CNs higher than 40, as discussed previously in this section. That is, this is not suitable for use in characterization of reservoir fluids, many of which contain hydrocarbons heavier than C_{40}. Therefore, the direct PnA method is applied with the optimized parameter set from Kumar and Okuno (2012) in this research.

Table 5-S1. Estimated physical critical points for n-C$_{100}$. The critical points from Kumar and Okuno (2012) are optimized ones with the PR EOS.		
	T$_C$ (K)	P$_C$ (bars)
Gao et al. 2001	966.26	0.50
Riazi and Al-Sahhaf 1996	963.20	0.69
Yaws 2010	1215.25	1.51
Ambrose 1978	1049.30	2.66
Constantinou and Gani 1994	1058.70	2.10
Magoulos and Tassios 1990	950.30	0.48
Tsonopoulos and Tan 1993	989.31	4.43
Kumar and Okuno 2012	1084.00	4.01
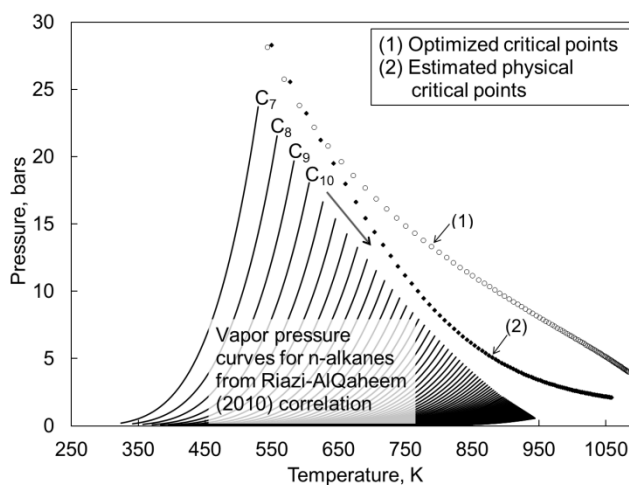
Figure 5-S1. Comparison of optimized and physical critical parameters.
Comparison of optimized critical parameters (Kumar and Okuno 2012) is presented with the estimated physical critical parameters from Constantinou and Gani (1994) for n-alkanes from n-C$_7$ through n-C$_{100}$. Vapor pressure curves for n-C$_7$ through n-C$_{100}$ are drawn using the correlations of Raizi-AlQaheem (2010).
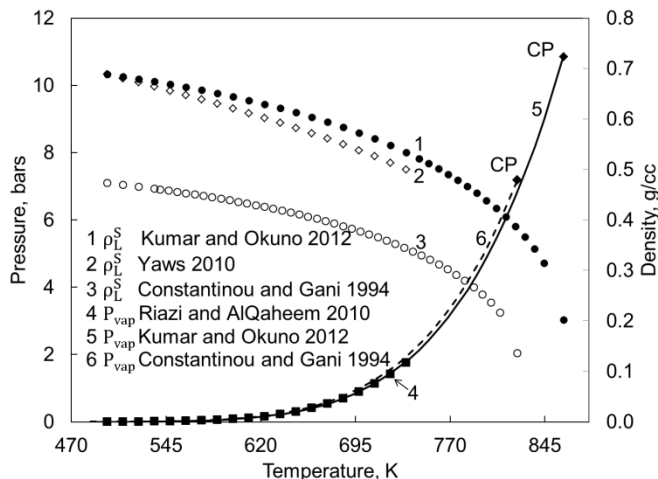
Figure 5-S2. Comparison of vapor pressure curves and saturated liquid densities predicted with optimized and physical critical parameters for n-C₂₈.

Vapor pressures and saturated liquid densities predicted for n-C₂₈ by use of the optimized critical parameters from Kumar and Okuno (2012) and the physical critical parameters from Constantinou and Gani (1994). The optimized T_C and P_C are higher than the estimated physical values. Use of the optimized parameters increases the saturated liquid density curve systematically, while keeping the vapor pressure curve along the vapor pressure data, which are shown by the filled squares.
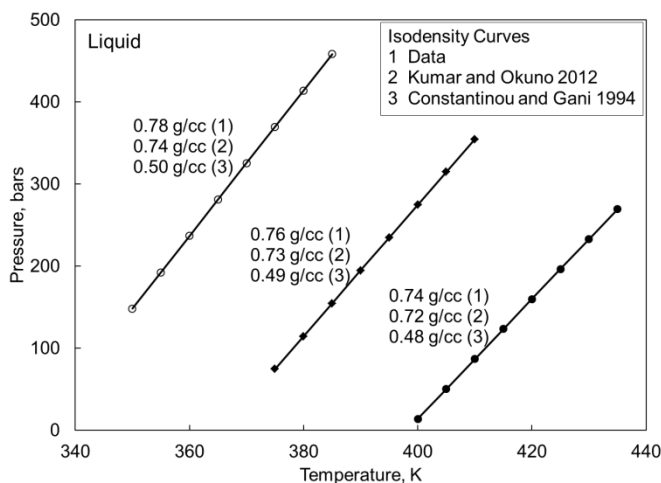
Figure 5-S3. Comparison of predicted isodensity curves with PR EOS with data (Dutour et al. 2001). Liquid-phase isodensity curves for n-C₂₈ from experimental data (Dutour et al. 2001) and from the PR EOS with the optimized (Kumar and Okuno 2012) and estimated physical critical parameters (Constantinou and Gani 1994). The three isodensity curves represent different density values. Along the left-most isodensity curve, for example, the measured value is 0.78 g/cc (1), but the PR EOS gives 0.74 g/cc with the critical parameters of Kumar and Okuno (2012) and 0.50 g/cc with the critical parameters of Constantinou and Gani (1994).

389
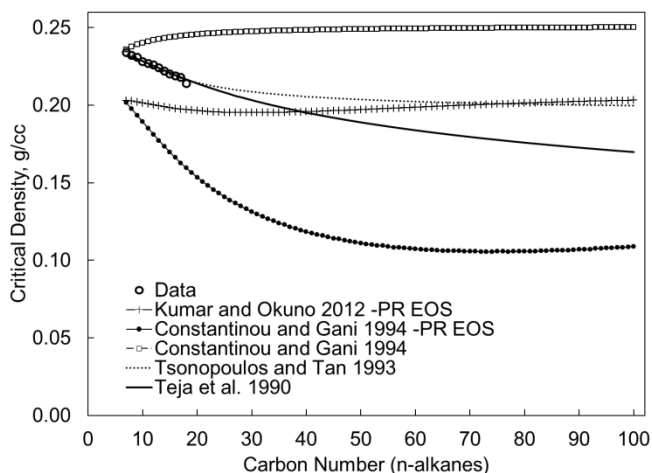
Figure 5-S4. Comparison of critical densities from different correlations.
Critical densities of n-alkanes from three correlations (Teja et al. 1990, Constantinou and Gani 1994, and Tsonopoulos and Tan 1993) and the PR EOS with two sets of critical parameters (Kumar and Okuno 2012, and Constantinou and Gani 1994). Data were taken from Ambrose and Tsonopoulos (1995). The critical densities calculated by the PR EOS with the parameters of Kumar and Okuno are in good agreement with Tsonopoulos and Tan (1993) for extended CNs.
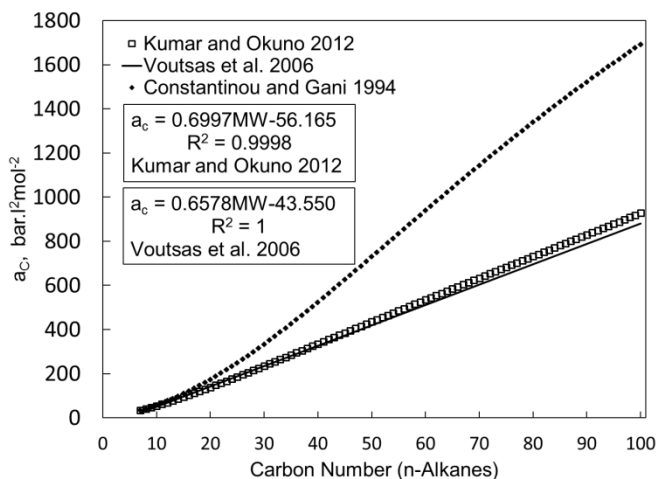
Figure 5-S5. Comparison of a_c for PR EOS from optimized and physical critical parameters.
The figure presents comparison of aC for the PR EOS using two sets of optimized critical parameters; one from Kumar and Okuno (2012) and the other from Voutsas et al. (2006). The values calculated with the physical critical parameters from Constantinou and Gani (1994) are also presented. For a given CN, the optimized aC values are smaller than that from the estimated physical critical parameters. The optimized aC values are well correlated with linear functions of MW. The optimized aC parameter from Voutsas et al. (2006) starts deviating from that from Kumar and Okuno (2012) at CN 40.

390
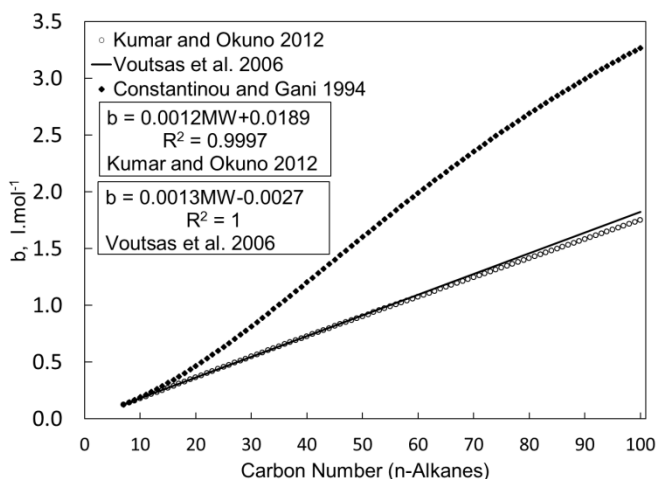
Figure 5-S6. Comparison of b parameter for PR EOS from optimized and physical critical parameters. Comparison is presented for the covolume parameters using two sets of optimized critical parameters; one from Kumar and Okuno (2012) and the other from Voutsas et al. (2006). The values calculated with the physical critical parameters from Constantinou and Gani (1994) are also presented. For a given CN, the optimized covolume values are smaller than that from the estimated physical critical parameters. The optimized covolume values are well correlated with linear functions of MW. The optimized covolume parameter from Voutsas et al. (2006) starts deviating from that from Kumar and Okuno (2012) at CN 40.
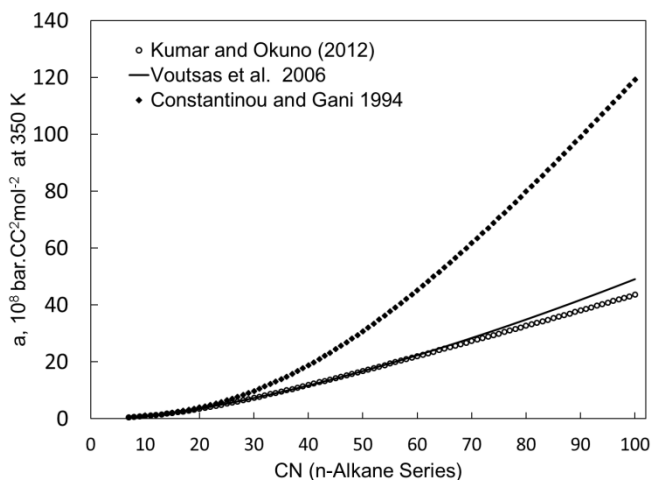
Figure 5-S7. Comparison of a parameter for PR EOS from optimized and physical critical parametes. Comparison is presented for the PR attraction parameters at 350 K using two sets of optimized critical parameters; one from Kumar and Okuno (2012) and the other from Voutsas et al. (2006). The values calculated with the physical critical parameters from Constantinou and Gani (1994) are also presented. For a given CN, the optimized attraction parameters are smaller than that from the estimated physical critical parameters. The optimized attraction parameter from Voutsas et al. (2006) starts deviating from that from Kumar and Okuno (2012) at CN 40.

391
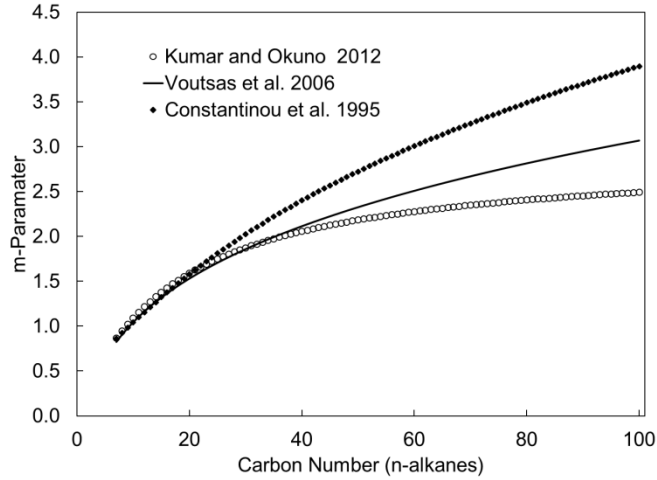
Figure 5-S8. Comparison of optimized and physical m-parameters.
The optimized m parameters from Kumar and Okuno (2012) and from Voutsas et al. (2006) are plotted along with the estimated physical values from Constantinou et al. (1995). The optimized m parameter from Kumar and Okuno (2012) is approximately equal to the estimated physical value up to n-C$_{21}$. For higher CNs, the optimized m parameter is smaller than the estimated physical value. The trends from Voutsas et al. (2006) and Kumar and Okuno (2012) start deviating from each other approximately at the MW of 550 g/mol.
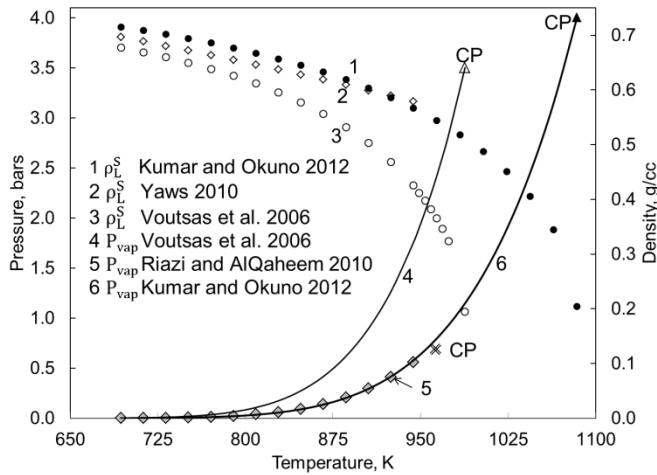
Figure 5-S9. Vapor pressures and saturated liquid densities predicted for n-C$_{100}$ by use of two sets of optimized critical parameters; one from Voutsas et al. (2006) and the other Kumar and Okuno (2012). Use of the optimized critical parameters of Kumar and Okuno (2012) results in more accurate predictions of densities and vapor pressures for n-C$_{100}$.
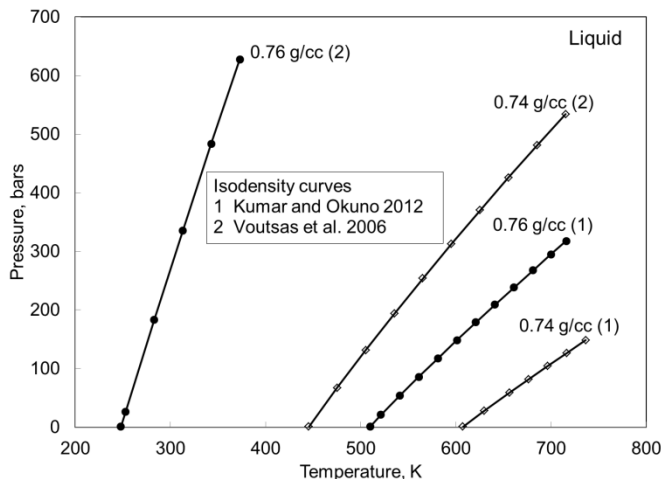
Figure 5-S10. Two liquid-phase isodensity curves (0.74 g/cc and 0.76 g/cc) in P-T space predicted for n-C$_{100}$ using the PR EOS.

The two sets of optimized critical parameters used are from Kumar and Okuno (2012) and Voutsas et al. (2006). Large differences are observed between the sets of predictions.
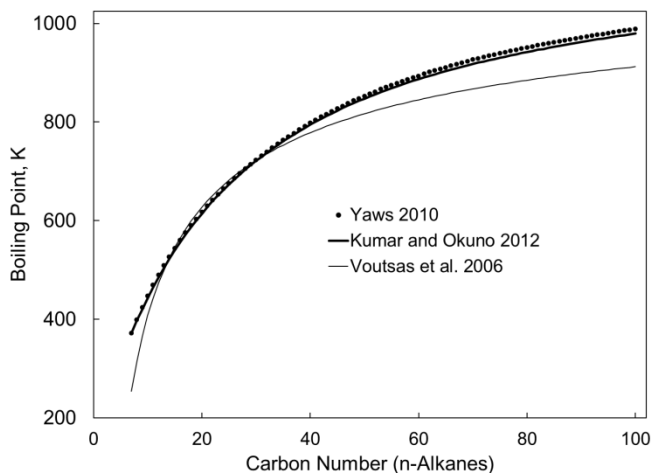
Figure 5-S11. Comparison of normal boiling points from PR EOS with optimized and physical critical parameters.

Normal boiling points predicted for n-alkanes by use of the PR EOS with the optimized critical parameters from Kumar and Okuno (2012) and from Voutsas et al. (2006). Data were taken from Yaws (2010). Use of the optimized critical parameters from Kumar and Okuno (2012) gives good agreement with the data. Voutsas et al. (2006) optimized the critical parameters for up to n-C40. They correlated the aC and covolume parameters as linear functions of MW. However, these linear correlations may not be accurate when extrapolated to higher CNs.

Section 5-S2. Effect of Aromaticity on Attraction and Covolume Parameters

Kumar and Okuno (2013) presented the effect of aromaticity on the parameters and proper interrelationship between the attraction and covolume parameters. Considering the importance of these points in the current paper, they are briefly summarized here. **Figure 5-S12** reproduces the trend curves of Yarborough (1979) for the standard specific gravity (SG) as a function of CN and aromaticity. The standard SG increases with CN and aromaticity. Kumar and Okuno (2013) used these curves to explain how perturbation of parameters should be done in different CN ranges. They fitted the PR EOS to the SG trend curves for CNs from 8 to 40 by perturbation of T_C, P_C, and m from the n-alkane values using the following equations:

$$T_C = 1154.35 - 844.83(1.0 + 1.7557 \times 10^{-3} f_T MW)^{-2.0} \tag{5-S8}$$

$$P_C = 559.93 \left(\frac{MW}{f_P}\right)^{-0.638} - 1.49 \tag{5-S9}$$

$$m = 0.4707 + 2.4831(f_m\ MW)^{-\left(\frac{39.933}{f_m\ MW}\right)}\ , \tag{5-S10}$$

where f_T, f_P, and f_m are the perturbation parameters. Equations 5-S8 through 5-S10 reduce to the correlations of Kumar and Okuno (2012) if the perturbation parameters are all unity.

Figures 5-S13 and **5-S14** show the attraction and covolume parameters, respectively, for three levels of aromaticity, 0, 10, and 60. Figure 5-S15 presents the ψ parameter based on the values for covolume parameters given in Figures 5-S14 and attraction parameters calculated at 370.15 K. The ψ trends for the lighter and heavier model fluids are presented. The two model trends are shown to be linear for simplicity. The lighter model fluid has all pseudocomponents within the range of C_7 through C_{20}. The heavier model fluid has all pseudocomponents heavier than C_{20}. The lighter model fluid has a CN range for pseudocomponents that is much narrower than the heavier model fluid as can be expected from Figure 5-S16, which shows the chi-squared distributions (Quinones-Cisneros et al. 2004) for different p values;

$$f_{dis} = 2^{-\frac{p}{2}} e^{-\frac{S}{2}} S^{\left(\frac{p}{2}-1\right)} / \Gamma\left(\frac{p}{2}\right). \tag{5-S11}$$

In the CN range higher than approximately 20, the ψ parameter decreases with CN for a given level of aromaticity, and is insensitive to the level of aromaticity. Therefore, the decreasing ψ trend with respect to CN is considered for the heavier model fluid. In the CN range lower than approximately 20, the ψ parameter is sensitive to the level of aromaticity within the narrow CN range. Therefore, the increasing ψ trend with respect to CN is considered for the lighter model fluid. For many real reservoir fluids, the CN range of pseudocomponents contains the boundary of the two distinct regions, which is approximately C_{20}. For these fluids, the ψ parameter is expected to exhibit combinations of these two model trends depending on the CN range of their pseudocomponents and their average aromaticity.
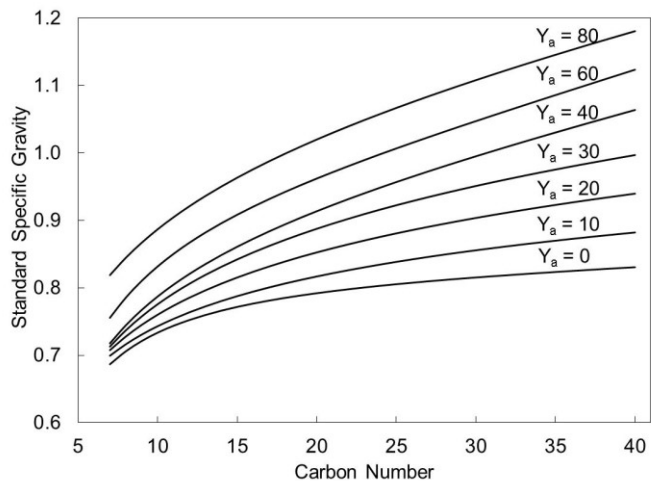
Figure 5-S12. Trend curves of Yarborough (1979) for standard specific gravity with respect to CN of single CN fractions at different aromaticity levels.

The aromaticity parameter Y_a was defined as the percentage of total carbon atoms in a molecule which are within the benzene ring.
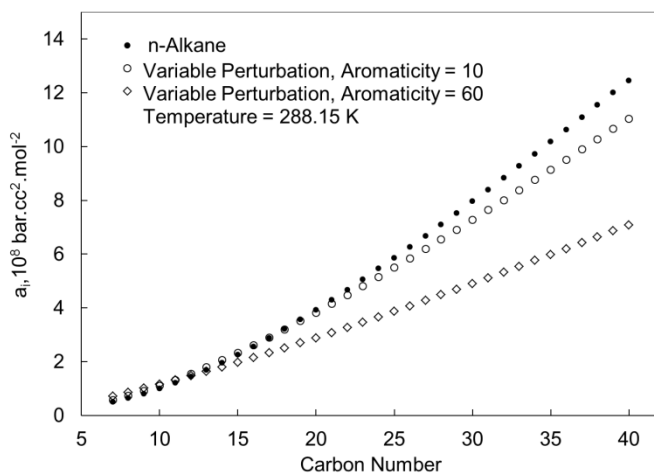
Figure 5-S13. Trend of attraction (a) parameters with carbon number of single carbon number fraction for three levels of aromaticity 0, 10, and 60.

The correlations of Kumar and Okuno (2012) are used for n-alkanes (i.e., zero aromaticity). The f_T, f_P, and f_m values (Equations 5-S8, 5-S9, and 5-S10) fitted to Yarborough's trend curves are used for the aromaticity levels 10 and 60. Temperature is 288.15 K.
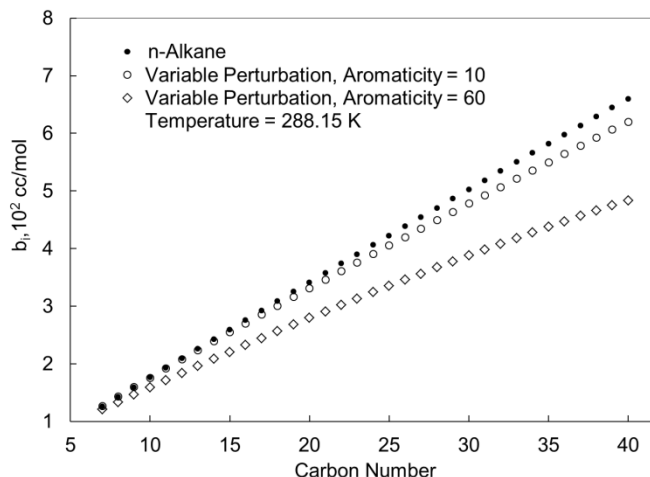
Figure 5-S14. Trend of covolume (b) parameters with carbon number of single carbon number fraction for three levels of aromaticity 0, 10, and 60.

The correlations of Kumar and Okuno (2012) are used for n-alkanes (i.e., zero aromaticity). The f_T, f_P, and f_m values (Equations 5-S8, 5-S9, and 5-S10) fitted to Yarborough's trend curves are used for the aromaticity levels 10 and 60.
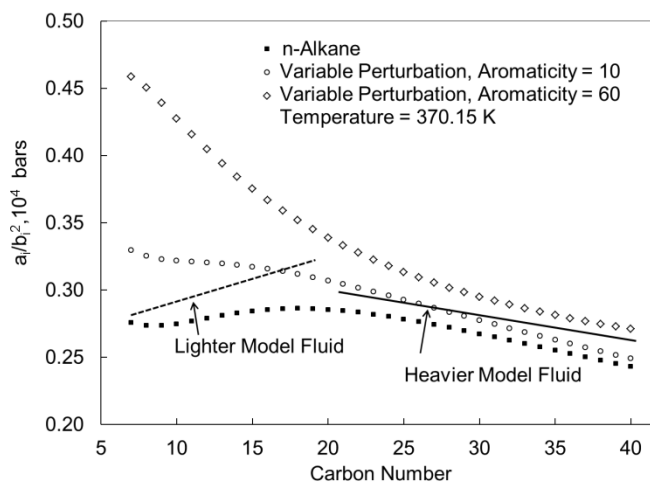
Figure 5-S15. Trend of ψ parameters (ψ = a/b^2) with single carbon number fractions for three levels of aromaticity at 370.15 K (Kumar and Okuno 2013).

All critical parameters and acentric factors are the same as those used in Figures 5-A2 and 5-A3. The ψ parameter changes its sensitive to aromaticity around the CN of 20. Trend curves are given for the lighter and heavier model fluids. For the model trends, the physical trend is also considered that heavier fractions are relatively more naphthenic and aromatic than lighter fractions.

The figure shows chi-squared distributions plotted as f_{dis} versus S Parameter, with curves labeled for different p values. The equation shown is:

$$f_{dis} = \frac{2^{-\frac{p}{2}} e^{-\frac{S}{2}} S^{\left(\frac{p}{2}-1\right)}}{\Gamma\left(\frac{p}{2}\right)}$$

Curves labeled: p = 2.5, p = 3.5, p = 5.0, p = 7.0, p = 9.0, p = 10.0, with an arrow indicating "Increasing API gravity".
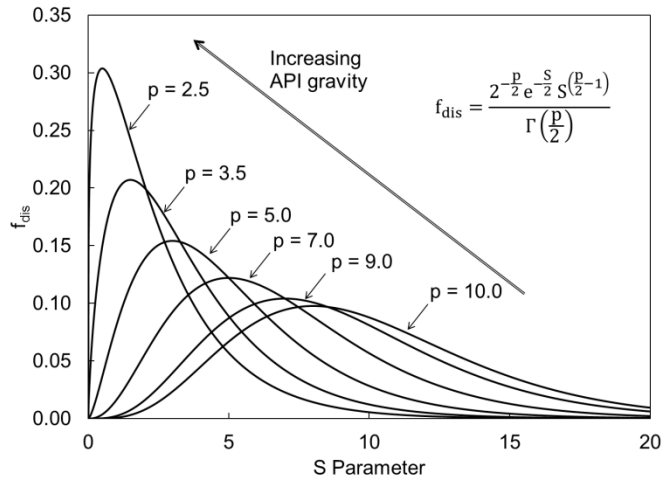
Figure 5-S16. Chi-squared distributions for different p values.
The p parameter controls the degree of skew and the size of effective composition space. The p-value for a fluid decreases with increasing API gravity (or decreasing standard specific gravity). For light fluids, the effective CN (or MW) range is small compared to heavy oils.